# FROM FUNCTIONAL GENOMICS TO BIOTECHNOLOGY IN ORNAMENTAL PLANTS

EDITED BY: Swee-Suak Ko, Akira Kanno, Raquel Sánchez-Pérez, Hsin-Hung Yeh, Annette Hohe and Mariana Mondragón-Palomino

PUBLISHED IN: Frontiers in Plant Science

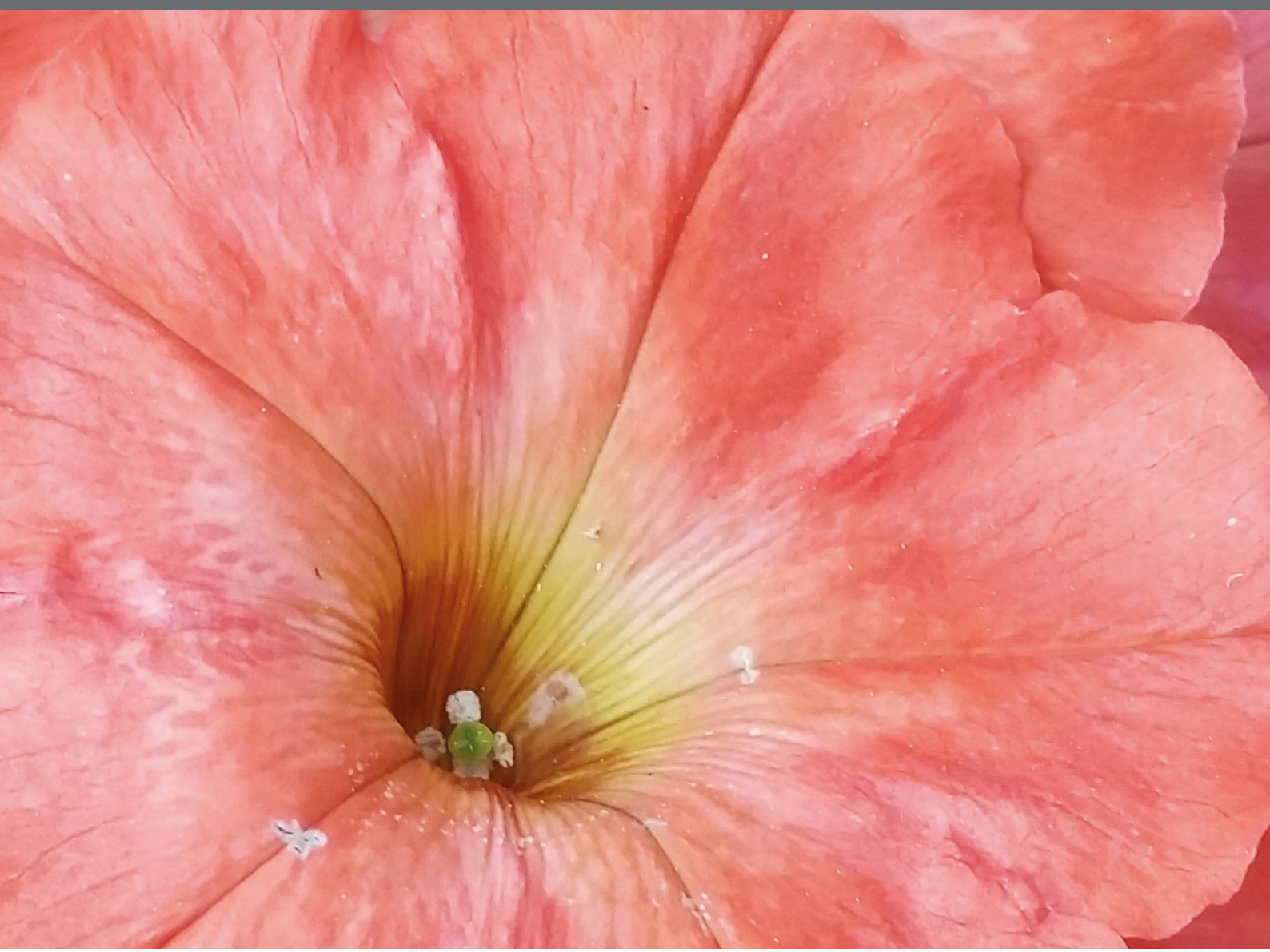

frontiers Research Topics

ISSN 1664-8714
ISBN 978-2-88945-906-3
DOI 10.3389/978-2-88945-906-3

## About Frontiers

Frontiers is more than just an open-access publisher of scholarly articles: it is a pioneering approach to the world of academia, radically improving the way scholarly research is managed. The grand vision of Frontiers is a world where all people have an equal opportunity to seek, share and generate knowledge. Frontiers provides immediate and permanent online open access to all its publications, but this alone is not enough to realize our grand goals.

## Frontiers Journal Series

The Frontiers Journal Series is a multi-tier and interdisciplinary set of open-access, online journals, promising a paradigm shift from the current review, selection and dissemination processes in academic publishing. All Frontiers journals are driven by researchers for researchers; therefore, they constitute a service to the scholarly community. At the same time, the Frontiers Journal Series operates on a revolutionary invention, the tiered publishing system, initially addressing specific communities of scholars, and gradually climbing up to broader public understanding, thus serving the interests of the lay society, too.

## Dedication to Quality

Each Frontiers article is a landmark of the highest quality, thanks to genuinely collaborative interactions between authors and review editors, who include some of the world's best academicians. Research must be certified by peers before entering a stream of knowledge that may eventually reach the public - and shape society; therefore, Frontiers only applies the most rigorous and unbiased reviews.
Frontiers revolutionizes research publishing by freely delivering the most outstanding research, evaluated with no bias from both the academic and social point of view. By applying the most advanced information technologies, Frontiers is catapulting scholarly publishing into a new generation.

## What are Frontiers Research Topics?

Frontiers Research Topics are very popular trademarks of the Frontiers Journals Series: they are collections of at least ten articles, all centered on a particular subject. With their unique mix of varied contributions from Original Research to Review Articles, Frontiers Research Topics unify the most influential researchers, the latest key findings and historical advances in a hot research area! Find out more on how to host your own Frontiers Research Topic or contribute to one as an author by contacting the Frontiers Editorial Office: researchtopics@frontiersin.org

# FROM FUNCTIONAL GENOMICS TO BIOTECHNOLOGY IN ORNAMENTAL PLANTS

Topic Editors:
**Swee-Suak Ko,** Academia Sinica Biotechnology Center in Southern Taiwan, Taiwan
**Akira Kanno,** Tohoku University, Japan
**Raquel Sánchez-Pérez,** CEBAS-CSIC, Murcia, Spain
**Hsin-Hung Yeh,** Agricultural Biotechnology Research Center, Academia Sinica, Taiwan
**Annette Hohe,** University of Applied Sciences Erfurt, Germany
**Mariana Mondragón-Palomino,** University of Regensburg, Germany

Petunia × hybrida cv. Viva Orange
Image by Heidi Halbwirth

For centuries plants of a broad taxonomical background have been bred and commercialized because of the beauty of their flowers. However, until recently genomic analyses of ornamentals remained a challenge because of their large genome sizes and high ploidy levels. In the last decade, increasingly affordable sequencing technologies and powerful bioinformatic approaches resulted in the complete

sequencing of several horticultural species genomes and the characterization of their transcriptomes.

These developments enabled research on many challenging topics.

This Research Topic gives you a primer into them by featuring a broad range of original research contributions on some of the most active areas of ornamental plant research: the genetic basis of flower morphology, scent, and color, the genetic regulation of physiology as well as the epigenetic factors affecting vegetative development. In this context, one of the most significant hurdles to functional genetic studies in ornamentals is achieving efficient genetic transformation. Several articles in this Research Topic describe strategies to tackle this challenge and present insights into the way transgene activity renders novel flower phenotypes.

**Citation:** Ko, S.-S., Kanno, A., Sánchez-Pérez, R., Yeh, H.-H., Hohe, A., Mondragón-Palomino, M., eds. (2019). From Functional Genomics to Biotechnology in Ornamental Plants. Lausanne: Frontiers Media. doi: 10.3389/978-2-88945-906-3

# Table of Contents


06 ***Editorial: From Functional Genomics to Biotechnology in Ornamental Plants***
Swee-Suak Ko, Akira Kanno, Raquel Sánchez-Pérez, Hsin-Hung Yeh, Annette Hohe and Mariana Mondragón-Palomino

**SECTION 1**
**FLOWER MORPHOLOGY, COLOR AND SCENT**

09 ***The Greenish Flower Phenotype of* Habenaria radiata *(Orchidaceae) is Caused by a Mutation in the* SEPALLATA*-Like MADS-Box Gene* HrSEP-1**
Mai Mitoma and Akira Kanno

21 ***Long-Lasting Corolla Cultivars in Japanese Azaleas: A Mutant* AP3/DEF *Homolog Identified in Traditional Azalea Cultivars From More Than 300 Years ago***
Kyeong-Seong Cheon, Akira Nakatsuka, Keisuke Tasaki and Nobuo Kobayashi

31 ***Genetic Analysis of Floral Symmetry Transition in African Violet Suggests the Involvement of Trans-acting Factor for* CYCLOIDEA *Expression Shifts***
Hui-Ju Hsu, Cheng-Wen He, Wen-Hsi Kuo, Kuan-Ting Hsin, Jing-Yi Lu, Zhao-Jun Pan and Chun-Neng Wang

50 ***A Dual Repeat* Cis*-Element Determines Expression of* GERANYL DIPHOSPHATE SYNTHASE *for Monoterpene Production in* Phalaenopsis *Orchids***
Yu-Chen Chuang, Yi-Chu Hung, Chi-Yu Hsu, Chuan-Ming Yeh, Nobutaka Mitsuda, Masaru Ohme-Takagi, Wen-Chieh Tsai, Wen-Huei Chen and Hong-Hwa Chen

64 ***Overexpression of* LiDXS *and* LiDXR *From Lily (*Lilium *'Siberia') Enhances the Terpenoid Content in Tobacco Flowers***
Tengxun Zhang, Ming Sun, Yanhong Guo, Xuejun Shi, Yongjuan Yang, Juntong Chen, Tangchun Zheng, Yu Han, Fei Bao and Sagheer Ahmad

76 ***A Novel AP2/ERF Transcription Factor CR1 Regulates the Accumulation of Vindoline and Serpentine in* Catharanthus roseus**
Jiaqi Liu, Fangyuan Gao, Juansheng Ren, Xianjun Lu, Guangjun Ren and Rui Wang

87 ***Great Cause—Small Effect: Undeclared Genetically Engineered Orange Petunias Harbor an Inefficient Dihydroflavonol 4-Reductase***
Christian Haselmair-Gosch, Silvija Miosic, Daria Nitarska, Barbara L. Roth, Benjamin Walliser, Renate Paltram, Rares C. Lucaciu, Lukas Eidenberger, Thomas Rattei, Klaus Olbricht, Karl Stich and Heidi Halbwirth

**SECTION 2**
**EPIGENETIC FACTORS BEHIND PLANT MORPHOLOGY**

99 ***Epigenetic Variance, Performing Cooperative Structure With Genetics, is Associated With Leaf Shape Traits in Widely Distributed Populations of Ornamental Tree* Prunus mume**
Kaifeng Ma, Lidan Sun, Tangren Cheng, Huitang Pan, Jia Wang and Qixiang Zhang

## SECTION 3

### REGULATION OF PLANT PHYSIOLOGY


114 ***Expression Profiles of Phosphoenolpyruvate Carboxylase and Phosphoenolpyruvate Carboxylase Kinase Genes in* Phalaenopsis*, Implications for Regulating the Performance of Crassulacean Acid Metabolism***

Chia-Yun Ping, Fure-Chyi Chen, Teen-Chi Cheng, Huey-Ling Lin, Tzong-Shyan Lin, Wen-Ju Yang and Yung-I Lee

124 ***Immunolocalization and Changes of Hydroxyproline-Rich Glycoproteins During Symbiotic Germination of* Dendrobium officinale**

Yuan-Yuan Li, Xiao-Mei Chen, Ying Zhang, Yu-Hsiu Cho, Ai-Rong Wang, Edward C. Yeung, Xu Zeng, Shun-Xing Guo and Yung-I Lee

137 ***Increased Expression of 9-*Cis*-Epoxycarotenoid Dioxygenase,* PtNCED1*, Associated With Inhibited Seed Germination in a Terrestrial Orchid,* Phaius tankervilliae**

Yung-I. Lee, Ming-Chuan Chen, Li Lin, Mei-Chu Chung and Wei-Ming Leu


## SECTION 4

### APPROACHES TO GENETIC TRANSFORMATION


150 ***Embryogenic Callus as Target for Efficient Transformation of* Cyclamen persicum *Enabling Gene Function Studies***

Svenja Ratjens, Samuel Mortensen, Antje Kumpf, Melanie Bartsch and Traud Winkelmann

165 ***A Protoplast Transient Expression System to Enable Molecular, Cellular, and Functional Studies in* Phalaenopsis *Orchids***

Hsiang-Yin Lin, Jhun-Chen Chen and Su-Chiung Fang

frontiers in Plant Science

EDITORIAL
published: 16 April 2019
doi: 10.3389/fpls.2019.00463

# Editorial: From Functional Genomics to Biotechnology in Ornamental Plants

*Swee-Suak Ko[1†], Akira Kanno[2], Raquel Sánchez-Pérez[3], Hsin-Hung Yeh[4], Annette Hohe[5] and Mariana Mondragón-Palomino[6*]*

[1] Academia Sinica, ABRC/BCST, Taipei, Taiwan, [2] Graduate School of Life Sciences, Tohoku University, Aoba-Ku, Sendai, Japan, [3] CEBAS-CSIC, Murcia, Spain, [4] Academia Sinica, ABRC, Taipei, Taiwan, [5] Faculty of Landscaping, Horticulture and Forestry, University of Applied Sciences Erfurt, Erfurt, Germany, [6] Department of Cell Biology and Plant Biochemistry, University of Regensburg, Regensburg, Germany

**Keywords: ornamental plant, functional genomics, flower development, flower scent, flower color, genetic transformation, RNA-seq, CAM**

OPEN ACCESS

***Edited by:***
*Jianjun Chen,*
*University of Florida, United States*

***Reviewed by:***
*Neil O. Anderson,*
*University of Minnesota Twin Cities, United States*
*Yi Li,*
*University of Connecticut, United States*

****Correspondence:***
*Mariana Mondragón-Palomino*
*mariana.mondragon@biologie.uni-regensburg.de;*
*m.mondragonpalomino@gmail.com*
*orcid.org/0000-0002-9468-6335*

*[†]Swee-Suak Ko*
*orcid.org/0000-0002-7515-4077*

***Specialty section:***
*This article was submitted to Plant Breeding, a section of the journal Frontiers in Plant Science*

***Received:*** *07 February 2019*
***Accepted:*** *28 March 2019*
***Published:*** *16 April 2019*

***Citation:***
*Ko S-S, Kanno A, Sánchez-Pérez R, Yeh H-H, Hohe A and Mondragón-Palomino M (2019) Editorial: From Functional Genomics to Biotechnology in Ornamental Plants. Front. Plant Sci. 10:463. doi: 10.3389/fpls.2019.00463*

### Editorial on the Research Topic

### From Functional Genomics to Biotechnology in Ornamental Plants

> "*Among roses there are many differences, in the number of petals, in roughness, in beauty of color, and in sweetness of scent. Most have five petals, but some have twelve or twenty, and some a great many more than these; for there are some, they say, which are even called 'hundred-petalled.'*"
> (Theophrastus, ca. 350 B.C.)

Ancient civilizations around the world already selected, cultivated and exchanged plants because of their distinctive or unusual flowers. This interest motivated, for instance, the domestication of *Dahlia* species by the Aztecs (Treviño de Castro et al., 2007) as well as the breeding of peonies in Imperial China and tulips in the Ottoman Empire (Kingsbury, 2009). Ornamental plant breeding experienced significant advances during the seventeenth and eighteenth centuries after the mechanisms of plant reproduction and hybridization were understood and commercial routes exchanged plants and their products around the globe. Scientific advances and international floriculture trade also drive the most recent breakthrough in ornamental plant sciences: The complete sequencing of the genomes of *Rosa chinensis*, *Aquilegia coerulea*, *Petunia* as well as *Phalaenopsis* and several other orchids (Cai et al., 2015; Bombarely et al., 2016; Chao et al., 2018; Filiault et al., 2018; Raymond et al., 2018), facilitate both basic scientific research and motivate the development of a biotechnological tool-kit for functional genomics. In this Research Topic, we present a primer into the changing face of this area and its new applications to floriculture in the twenty-first century.

## FLOWER MORPHOLOGY, COLOR AND SCENT

Most of the 13 Original Research Articles in this Research Topic test hypotheses on the role of specific genes in flower organ development and organization or in the synthesis of flower scent and perianth color. Because genetic transformation is not feasible in most ornamental species, the three studies dealing with flower development tap on a diverse repertoire of morphological mutants. This strategy is not only helpful for developing biotechnological approaches in plant breeding, but it also offers fascinating insights into plant developmental biology and phylogeny.

In their article, Mitoma and Kanno analyzed the developmental genetics of *Habenaria radiata* "Ryokusei" (Orchidaceae), a mutant bearing greenish flowers and greenish sepaloid organs in place of the reproductive organs. Comparison of the patterns of expression of class C and class E MADS-box genes between flowers of *H. radiata* wild-type and the mutant suggest the suppressed expression of *HrSEP-1* might cause the unusual flower morphology. Further analyses of the mutant revealed a retrotransposon insertion on the first exon of *HrSEP-1*, which possibly explains its phenotype and suggests an essential role of this gene in the development of petals and labellum. Similarly to the study of Mitoma and Kanno; Cheon et al. associated the sepal-like petal phenotype of old ornamental azalea cultivars (*Rhododendron*, Ericaceae), to the insertion of an LTR-retrotransposon in a class B MADS-box gene. The authors found out that this insertion abolished the wild-type mRNA sequences of the *AP3*/*DEF* homologs, thus conferring these evergreen azaleas their sepaloid phenotype.

African violet (*Saintpaulia ionantha*) is characterized by bilateral flower symmetry. Hsu et al. investigated the molecular developmental genetics of perianth symmetry in this species by comparing the patterns of expression of *SiCYC1A* and *SiCYC1B*, orthologs of the transcription factor *CYCLOIDEA* (*CYC*), in the wild-type and each of two peloric forms with dorsalized actinomorphy (DA) or ventralized actinomorphy (VA). The authors showed heterotopic expression shifts of *SiCYC1A*/*1B* correlated with DA, whereas reduced expression of *SiCYC1A*/*1B* is associated with VA. The authors suggest the expression shifts might be caused by the activity of upstream trans-acting factors or epigenetic regulatory mechanisms, similar to those acting on *CYC* in the peloric mutant of *Linaria vulgaris* (Cubas et al., 1999).

Scent is a key determinant of the commercial value of pot and cut ornamental flowers. In this Research Topic, two contributions investigate the genes encoding enzymes mediating the synthesis of terpenes, volatile organic compounds that contribute to floral fragrance and herbivore inhibition. Chuang et al. compared the promoter fragments of geranyl diphosphate synthase (*GDPS*), a key enzyme for monoterpene biosynthesis, in 12 *Phalaenopsis* species or hybrids, to identify the genetic regulatory mechanisms behind floral scent. The authors concluded that in scented orchids the integrity of a dual repeat motif in the *GDPS* promoter is crucial for its activity. These findings are essential for the development of molecular markers needed to accelerate breeding of scented orchids and to study the genetic basis of scent-mediated orchid-pollinator co-evolution. In lily (*Lilium* "Siberia"), Zhang et al. investigated the contribution of rate-delimiting enzymes 1-deoxy-D-xylulose-5-phosphate synthase (LiDXS) and 1-deoxy-D-xylulose-5-phosphate reductoisomerase (LiDXR), to the synthesis of terpenes via the MEP pathway. The authors demonstrated via transgenic overexpression of these enzymes in tobacco flowers that they participate in the synthesis of mono- and diterpenes.

Besides their role in the composition of flower scent, naturally occurring terpenes and their derivatives have important pharmaceutical applications. Specifically, terpenoid indole alkaloids (TIAs), like vindoline are substrates for synthesis of drugs used in chemotherapy. Employing an approach based on RNA-seq, Liu et al. identified a novel AP2/ERF transcription factor gene (*CR1*) from *Catharanthus roseus* (rose periwinkle, Apocynaceae), which is involved in the regulation of TIAs synthesis. Functional gene analysis of *CR1* via virus-induced gene silencing (VIGS) demonstrated its downregulation increases the accumulation of vindoline and serpentine. The authors propose this finding could be applied to increase TIAs production.

Ornamentals with unusual flower colors have been selected and bred for centuries. However, the genetics of each species limits the palette of possible shades that can be obtained by hybridization and mutagenesis. The transfer of genes of interest between different species through genetic engineering (GE), already enabled the production of transgenic blue roses and carnations (Tanaka et al., 2010). Before any GE ornamental variety is commercialized, it must meet regulatory requirements involving molecular characterization and risk assessment (Chandler and Brugliera, 2011). In this number, Haselmair-Gosch et al. present detailed genetic, transcriptomic and biochemical analyses of orange flowering GE Petunias carrying a maize dihydroflavonol 4-reductase gene (*A1*). These cultivars had to be recalled after it was discovered they originated from transgenic parental lines. The study points out at one possible source of the transgenic construct as well as the fact that the *A1* gene involved encodes a lowly expressed enzyme with a low substrate acceptance. Thus, the unusual orange color results from the formation of pelargonidin in the context of a flavonol synthase and B-ring hydroxylation enzymes with strongly reduced activities.

## EPIGENETIC FACTORS BEHIND PLANT MORPHOLOGY

Understanding the contribution of epigenetic factors to plant phenotypic variance is essential to optimize molecular breeding and cultivation strategies and assess the impact of climate change in plant health and productivity. Ma et al. investigate the relationships between epigenetic and genetic variances, environmental factors and leaf dimensions of *Prunus mume* (ornamental prune, Rosaceae). Statistical analyses of genetic and epigenetic markers showed that epigenetic diversity was higher than genetic diversity and the increase or decrease of DNA methylation level might affect the expression of genes that determine leaf development and metabolism. The markers characterized facilitate considering epigenetic factors in molecular plant breeding.

## REGULATION OF PLANT PHYSIOLOGY

*Phalaenopsis* was the first CAM species with a completely sequenced genome. In their contribution, Ping et al. investigated the genetic causes behind the different types of photosynthesis along the development of *Phalaenopsis aphrodite* (moth orchid). During tissue culture, the young seedling performs C3

photosynthesis and when leaves mature switches to CAM. The authors found that the gene encoding phosphoenolpyruvate carboxylase kinase (*PPCK*), is associated with the distinct performance of CAM photosynthesis during seedling ontogeny. This knowledge is relevant to optimize the micropropagation of this genus.

In this issue, two contributions focus on the molecular physiology of orchid seed germination. Mycorrhizal symbiosis is essential for the germination of orchid seeds, including those of *Dendrobium officinale*. Li et al. revealed the role of cell wall structural hydroxyproline-rich glycoproteins (HRGPs). The authors showed HRGPs are highly upregulated in symbiotically germinated protocorms of *D. officinale* and inhibition of their biosynthesis resulted in uncontrolled hyphae growth in protocorms, suggesting a relevant role in the regulation of symbiotic fungal colonization and compartmentalization.

Abscisic acid (ABA) has been shown to regulate stress responses, seed dormancy, and seed germination. Lee et al. characterized the expression of *PtNCED1* (9-cis-epoxycarotenoid dioxygenase), a candidate regulator of ABA biosynthesis, in orchid *Phaius tankervilliae*. This study revealed a relationship between *PtNCED1* expression and biosynthesis of ABA in developing orchid seeds, thus suggesting a link with the rate of germination and the content of ABA in seeds. This association is useful to further investigate the role of *PtNCED1* in seed dormancy.

## APPROACHES TO GENETIC TRANSFORMATION

In this Research Topic, two studies describe techniques of genetic transformation which open up new possibilities for functional genomic analyses of *Cyclamen* (Primulaceae) and *Phalaenopsis in planta* or in cellular culture. Specifically, Ratjens et al. employed embryogenic callus cultures for *Agrobacterium*-mediated transformation of *Cyclamen persicum* and achieved transformation rates of up to 43%. Besides, the study generated fluorophore-based marker lines useful to follow the localization of auxin and reactive oxygen species concentrations during somatic embryogenesis. In order to gain an insight into genetic regulation in Orchidaceae, Lin et al. developed and tested a method of transient gene expression based on protoplast from *Phalaenopsis aphrodite* flowers. The feasibility of this approach was demonstrated by testing multiple hypotheses on gene regulation, protein-protein interactions, and subcellular localization.

## AUTHOR CONTRIBUTIONS

MM-P provided the idea of the editorial and wrote the manuscript with contributions from S-SK, AK, RS-P, H-HY, and AH. All authors critically reviewed and approved the final manuscript.

## REFERENCES


Bombarely, A., Moser, M., Amrad, A., Bao, M., Bapaume, L., Barry, C. S., et al. (2016). Insight into the evolution of the Solanaceae from the parental genomes of *Petunia hybrida*. *Nat. Plants* 2, 16074. doi: 10.1038/nplants.2016.74

Cai, J., Liu, X., Vanneste, K., Proost, S., Tsai, W. C., Liu, K. W., et al. (2015). The genome sequence of the orchid *Phalaenopsis equestris*. *Nat. Genet.* 47, 65–72. doi: 10.1038/ng.3149

Chandler, S. F., and Brugliera, F. (2011). Genetic modification in floriculture. *Biotechnol. Lett*. 33, 207–214. doi: 10.1007/s10529-010-0424-4

Chao, Y. T., Chen, W. C., Chen, C. Y., Ho, H. Y., Yeh, C. H., Kuo, Y. T., et al. (2018). Chromosome-level assembly, genetic and physical mapping of *Phalaenopsis aphrodite* genome provides new insights into species adaptation and resources for orchid breeding. *Plant Biotechnol. J.* 16, 2027–2041. doi: 10.1111/pbi.12936

Cubas, P., Vincent, C., and Coen, E. (1999). An epigenetic mutation responsible for natural variation in floral symmetry. *Nature* 401, 157–161. doi: 10.1038/43657

Filiault, D. L., Ballerini, E. S., Mandáková, T., Aköz, G., Derieg, N. J., Schmutz, J., et al. (2018). The *Aquilegia* genome provides insight into adaptive radiation and reveals an extraordinarily polymorphic chromosome with a unique history. *Elife* 7:e36426. doi: 10.7554/eLife.36426

Kingsbury, N. (2009). *Hybrid: The History An Science Of Plant Breeding*. Chicago: The University of Chicago Press.

Raymond, O., Gouzy, J., Just, J., Badouin, H., Verdenaud, M., Lemainque, A., et al. (2018). The *Rosa* genome provides new insights into the domestication of modern roses. *Nat. Genet.* 50, 772–777. doi: 10.1038/s41588-018-0110-3

Tanaka, Y., Brugliera, F., Kalc, G., Senior, M., Dyson, B., Nakamura, N., et al. (2010). Flower color modification by engineering of the flavonoid biosynthetic pathway: practical perspectives. *Biosci. Biotechnol., Biochem*. 74, 1760–1769. doi: 10.1271/bbb.100358

Theophrastus (ca. 350 B.C.). *Enquiry into Plants*. Available online at: www.loebclassics.com/view/theophrastus-enquiry_plants/1916/pb_LCL079.39.xml.

Treviño de Castro, G., Mera Ovando, L. M., Bye Boettler, R., Mejía Muñoz, J. M., and Laguna Cerda, A. (2007). *Historia de la dalia (Acocoxóchitl). La flor nacional de México*. Chapingo: Publicación de difusión 1. SNICS-SAGARPA.


**Conflict of Interest Statement:** The authors declare that the research was conducted in the absence of any commercial or financial relationships that could be construed as a potential conflict of interest.

frontiers in Plant Science

ORIGINAL RESEARCH
published: 19 June 2018
doi: 10.3389/fpls.2018.00831

# The Greenish Flower Phenotype of *Habenaria radiata* (Orchidaceae) Is Caused by a Mutation in the *SEPALLATA*-Like MADS-Box Gene *HrSEP-1*

*Mai Mitoma and Akira Kanno**

*Graduate School of Life Sciences, Tohoku University, Sendai, Japan*

In *Arabidopsis thaliana*, the E-class *SEPALLATA* (*SEP*) genes are generally expressed across all floral whorls. These genes play fundamental roles in floral organ fate determination during development by interacting with other MADS-box gene products, such as those from A-, B-, and C-class genes. However, the function of *SEP* genes in orchid remains obscure. Here, we analyzed a mutant orchid cultivar with greenish flowers in *Habenaria radiata* and found that this phenotype is caused by the absence of SEP function. Wild type *H. radiata* flowers contain a column and two perianth whorls consisting of three greenish sepals, two white petals, and a lip (labellum). By contrast, the flowers of *H. radiata* cultivar 'Ryokusei' appear greenish, with three normal sepals in whorl 1, two greenish petals and a lip in whorl 2, and several sepaloid organs and a ventral column in whorls 3 and 4. We isolated two *SEP*-like genes (*HrSEP-1* and *HrSEP-2*) and two *AGAMOUS*-like genes (*HrAG-1* and *HrAG-2*) from wild type *H. radiata* and compared their expression in the wild type vs. the mutant cultivar. *HrAG-1* and *HrAG-2* were expressed in the column in the wild type, whereas these genes were expressed in the ventral column and in sepaloid organs that had been converted from a column in 'Ryokusei.' *HrSEP-1* and *HrSEP-2* were expressed in all floral organs in the wild type. However, in the mutant cultivar, *HrSEP-2* was expressed in all floral organs, while *HrSEP-1* expression was not detected. Thus, we analyzed the genomic structures of *HrSEP-1* in the wild type and 'Ryokusei' and identified a retrotransposon-like element in its first exon in 'Ryokusei.' Yeast two-hybrid assays demonstrated that HrSEP-1 interacts with HrDEF, HrAG-1, and HrAG-2. These results indicate that the mutant phenotype of 'Ryokusei' flowers is caused by the loss of function of *HrSEP-1*. Therefore, this gene plays an important role in column, lip, and petal development in *H. radiata* flowers.

**Keywords: greenish flower, floral homeotic mutant, *SEPALLATA*-like gene, MADS-box gene, retrotransposon, Orchidaceae**

OPEN ACCESS

***Edited by:***
*Elena M. Kramer,*
*Harvard University, United States*

***Reviewed by:***
*Fure-Chyi Chen,*
*National Pingtung University of Science and Technology, Taiwan*
*Xianzhong Feng,*
*Northeast Institute of Geography and Agroecology (CAS), China*

***Correspondence:**
*Akira Kanno*
*kanno@ige.tohoku.ac.jp*

***Specialty section:***
*This article was submitted to Plant Evolution and Development, a section of the journal Frontiers in Plant Science*

***Received:*** *17 March 2018*
***Accepted:*** *29 May 2018*
***Published:*** *19 June 2018*

***Citation:***
*Mitoma M and Kanno A (2018) The Greenish Flower Phenotype of Habenaria radiata (Orchidaceae) Is Caused by a Mutation in the SEPALLATA-Like MADS-Box Gene HrSEP-1. Front. Plant Sci. 9:831. doi: 10.3389/fpls.2018.00831*

## INTRODUCTION

The ABC model of floral organ identity determination was established based on genetic studies in *Arabidopsis thaliana* and *Antirrhinum majus* (Carpenter and Coen, 1990; Bowman et al., 1991; Schwarz-Sommer et al., 1992). According to this model, the activity of A-, B-, and C-class genes, alone or in combination, specifies the formation of the distinct organs of the four floral

whorls. The A function specifies sepal formation in whorl 1, co-expression of the A and B functions specifies petal formation in whorl 2, B and C genes together determine stamen development in whorl 3, and C genes specify carpel development in whorl 4 (Coen and Meyerowitz, 1991; Weigel and Meyerowitz, 1994). The A-class MADS-box gene *APETALA1* (*AP1*)-like is required for the establishment of floral meristem and for specifying sepal and petal identity. The B-class floral homeotic genes, which are responsible for specifying petal and stamen identity, form two major clades: *DEFICIENS* (*DEF*)- and *GLOBOSA*-like genes. The C-class *AGAMOUS* (*AG*) genes play a central role in stamen and carpel development (Yanofsky et al., 1990).

*SEPALLATA* (*SEP*) genes are E-class MADS-box genes. SEP proteins form higher-order complexes together with A-, B-, and C-class gene products. *A. thaliana* contains four *SEP* genes: *SEP1*, *SEP2*, *SEP3*, and *SEP4*. The flowers of a triple mutant of three *SEP* genes (*sep1/sep2/sep3*) consist entirely of sepal-like organs (Pelaz et al., 2000), whereas in *sep1 sep2 sep3 sep4* quadruple mutants, all floral organs are converted into leaf-like organs (Ditta et al., 2004). Therefore, the four *A. thaliana SEP* genes function redundantly and are important for the activities of B- and C-function genes in petal, stamen, and carpel development (Honma and Goto, 2001; Theissen and Saedler, 2001). *SEP*-like genes have been isolated from many dicots, such as petunia (Ferrario et al., 2003; Vandenbussche et al., 2003; Matsubara et al., 2008) and tomato (Pnueli et al., 1991; Ampomah-Dwamena et al., 2002), as well as monocots such as rice (Arora et al., 2007) and maize (Lid et al., 2004). Phylogenetic analyses suggested that *SEP*-like genes are monophyletic and that they form two subclades, the SEP1/2/4-like clade (AGL2/3/4 clade) and the SEP3-like clade (AGL9 clade) (Zahn et al., 2005). Functional analyses of *SEP* orthologs have been conducted in several plants by disrupting RNA expression. The petunia *fbp2* mutant (a *SEP3* ortholog) exhibits greenish petals and ectopic inflorescences originating from the third floral whorl, while the *fbp5* mutant (a *SEP1/2* ortholog) exhibits no significant morphological changes (Vandenbussche et al., 2003). Double mutants of these two genes show significant changes, with the conversion of floral organs to leaf-like organs (Vandenbussche et al., 2003). In the monocot rice, simultaneous knockdown of the four *SEP*-like genes (*OsMADS1*, *OsMADS5*, *OsMADS7*, and *OsMADS8*) caused the transformation of all floral organs except the lemma into leaf-like structures. These findings indicate that the *SEP* orthologs are required for petal, stamen, and carpel formation in both dicots and monocots (Cui et al., 2010).

Orchidaceae is the largest family of flowering plants. Many orchids are highly valued for their elaborate flowers and unique organ structures. The floral organs of many Orchidaceae plants comprise three sepals in whorl 1, two petals and a lip in whorl 2, and a column (fused stamen and carpel) in whorls 3 and 4. Orchid B-, C/D-, and E-class MADS-box genes have been characterized, and gene duplications in each group have been analyzed (Tsai and Chen, 2006; Aceto and Gaudio, 2011; Mondragón-Palomino, 2013). To date, several *SEP*-like genes have been identified from a few orchid species, including *AdOM1* in *Aranda* (Lu et al., 1993), *DOMADS1* and *DOMADS3* in *Dendrobium* grex Madame Thong-In (Yu and Goh, 2000), *DcOSEP-1* in *Dendrobium crumenatum* (Xu et al., 2006), *OMADS6* and *OMADS11* in *Oncidium* Gower Ramsey (Chang et al., 2009), *PeSEP1-4* in *Phalaenopsis equestris* (Pan et al., 2014) and *CgSEP1-4* in *Cymbidium goeringii* Rchb.f (Xiang et al., 2017). Expression analysis of orchid *SEP*-like genes showed that *SEP3* orthologs (*DOMADS1*, *DcOSEP1*, *PeSEP1*, *PeSEP3,* and *OMADS6*) are expressed in sepals, petals, lips, and columns during flower development, whereas *CgSEP1, CgSEP3,* and *AdOM1* are rarely expressed in columns (Lu et al., 1993; Xiang et al., 2017). By contrast, the expression patterns of *SEP1/2* orthologs (*DOMADS3*, *PeSEP2*, *PeSEP4*, *OMADS11*, *CgSEP2*, and *CgSEP4*) vary among species. For example, in *Phalaenopsis*, *PeSEP2* is expressed in all floral organs, whereas *PeSEP4* is expressed at extremely low levels in all floral organs (Pan et al., 2014).

Studies involving ectopic expression in *Arabidopsis* and virus-induced gene silencing (VIGS) in *Phalaenopsis* were carried out to investigate the functions of *Phalaenopsis* SEPs in determining floral organ identity (Pan et al., 2014). Transgenic *35S:PeSEP3 Arabidopsis* plants exhibited early flowering and much smaller flowers than the wild type, whereas transgenic *35S:PeSEP1 Arabidopsis* plants showed no phenotypic changes compared with the wild type. The flowers of *PeSEP3*- and *PeSEP2/3*-silenced plants (obtained by VIGS) showed partial leaf-like structures in whorls 1 and 2, and epidermis identity as well as anthocyanin and chlorophyll contents were altered in these flowers. Although the functions of orchid *SEP*-like genes have been investigated via heterogenic transformation and VIGS, *sep* mutants have thus far not been identified in orchid. Such mutants would be very useful for analyzing the functions of *SEP* genes in orchid.

The genus *Habenaria* contains approximately 800 species, representing one of the largest genera in Orchidaceae (Yokota, 1990). *Habenaria* species are distributed throughout the world, with the highest concentrations in the tropical regions of Africa and Southeast Asia (Yokota, 1990). *H. radiata* is one of the most famous orchids in Japan. This small terrestrial orchid lives in wetlands in East Asia. *H. radiata* flowers have greenish sepals in whorl 1, two white petals and a lip in whorl 2, and a column in whorls 3 and 4. There are some mutant cultivars of *H. radiata*. One of these cultivars, 'Hishou,' has flowers with a white petaloid organ instead of a greenish dorsal sepal and two greenish lateral sepals replacing the lip-like organs (Kim et al., 2007).

We previously suggested that the floral phenotypes of 'Hishou' appear to be caused by the expanded expression of the *DEF*-like gene, *HrDEF*, which belongs to DEF clade 3 (Kim et al., 2007). In the current study, we characterized a mutant cultivar of *H. radiata* named 'Ryokusei.' This cultivar has greenish flowers, and its column has been converted into greenish sepaloid organs. We isolated C- and E-class genes in wild type *H. radiata* and compared the expression of these genes in the wild type and 'Ryokusei,' finding that the expression of the *SEP*-like gene, *HrSEP-1*, was suppressed in 'Ryokusei'. We compared the genomic structures of *HrSEP-1* in the wild type and

'Ryokusei' and found that this mutant character is caused by the insertion of a retrotransposon in *HrSEP-1*. Our findings suggest that *HrSEP-1* plays an important role in floral development in *H. radiata*.

# MATERIALS AND METHODS

## Plant Materials

*Habenaria radiata* 'Aoba' (the wild type) and 'Ryokusei' (a mutant with greenish flowers) were used in this study. These cultivars were obtained from a garden shop and cultivated in a greenhouse at the Graduate School of Life Sciences, Tohoku University, Japan. Floral buds (0.7–1.0 cm) were collected and stored at −80°C for subsequent RNA extraction. Sepals, petals, and columns (fused stamens and carpel) were dissected from 5 to 10 flowers and used for expression analysis.

## Isolation of MADS-Box Genes From *H. radiata*

Total RNA was prepared from whole floral buds of 'Aoba' using an RNeasy Plant Mini Kit (QIAGEN). Poly A-tailed mRNA was separated from total RNA using a Dynabeads mRNA Purification Kit (Life Technologies). cDNA was synthesized from mRNA using oligo dT primer P019HA with AMV Reverse Transcriptase following the manufacturer's instructions (Roche). cDNA fragments were isolated from MADS-box genes by 3′ rapid amplification of cDNA ends (RACE) using MADS-box-specific degenerate primers alongside a species-specific adaptor primer. The PCR products were electrophoresed on agarose gels, extracted using a QIAquick Gel Extraction Kit (QIAGEN), and cloned into pGEM-T Easy Vector (Promega). Upstream sequences of the MADS-box genes were isolated by 5′RACE using a 5′/3′RACE Kit, 2nd Generation (Roche), according to the manufacturer's protocol. The primers used in this study are shown in **Supplementary Table S1**. The sequences of the HrAGs and HrSEPs isolated in this study were submitted to GenBank under accession numbers LC369631–LC369634.

## Phylogenetic Analysis of *HrAGs* and *HrSEPs*

Phylogenetic analysis was conducted using MEGA v7.0.26 software (Kumar et al., 2016). Predicted amino acid sequences of known MADS-box genes were obtained from the EMBL/DDBJ/GenBank DNA database (**Supplementary Tables S2**, **S3**). Full-length amino acid sequences were used to construct the phylogenetic trees and aligned using Clustal W. JTT + G was selected and used to construct a neighbor-joining tree, with 1000 bootstrap replicates. In the case of AG-like genes, non-conserved C-regions were excluded.

## Expression Analysis via Semi-Quantitative and Quantitative RT-PCR

Semi-quantitative reverse-transcription PCR (semi-qRT-PCR) and quantitative RT-PCR (RT-qPCR) were performed to examine the expression levels of the *DEF*, *AG*, and *SEP* genes. Total RNA was extracted from sepals, petals, lips, and columns ('Aoba') or sepaloid organs converted from dorsal and ventral columns ('Ryokusei'). cDNA was synthesized as described above, using oligo dT primers P019HA and P019HR for 'Aoba' and 'Ryokusei,' respectively. RT-qPCR was conducted using a MiniOpticon Real-time PCR Detection System with CFX Manager software (Bio-Rad). The cycling program was as follows: one cycle at 95°C for 3 min followed by 40 cycles of 95°C (10 s) and 64°C (1 min), with plate reading after each cycle. Gene-specific primers were designed for *HrDEF*, *HrSEP-1*, *HrSEP-2*, *HrAG-1*, and *HrAG-2* (**Supplementary Table S1**). The transcript levels of these five genes were determined using three experimental replicate PCRs for each cDNA sample. The *eEF1A* (*eukaryotic translation elongation factor 1A*) gene was used as an internal control for standardization.

## Isolation of the *HrSEP-1* Promoter From the Wild Type and 'Ryokusei' by DNA Walking

Genomic DNA was isolated from *H. radiata* leaves using a modified CTAB (hexadecyl trimethyl-ammonium bromide) method (Porebski et al., 1997). The genomic DNA was digested at 37°C overnight with four different blunt-end restriction enzymes (DraI, EcoRV, PvuII, and StuI). The digested DNA was ligated to a custom-designed adaptor from a Genome Walker kit at 16°C overnight. The constructed libraries were used as templates for two-step PCR. The primary PCR was performed using the outer adaptor primer (AP1) provided in the kit and a specific primer for *HrSEP-1* (GSP1). The secondary PCR was performed using the nested adaptor primer (AP2) and a nested specific primer for *HrSEP-1* (GSP2), using the primary PCR products as template. The secondary PCR products were cloned and sequenced as described above.

## Identification of Insertion Sequence in *HrSEP-1* Gene

Genomic DNAs were extracted from the leaves of wild type and 'Ryokusei' as described above. Transposon PCR amplifications were performed on leaf genomic DNA of 'Ryokusei,' using primers to specifically amplify between promoter and exon 1 of *HrSEP-1* (**Supplementary Table S1**). Purified PCR product was further sequenced. Retrotransposon-like insertion isolated in this study, designated as *Hret1*, were submitted to GenBank under accession numbers LC382365.

To confirm the insertion of retrotransposon-like structure, we performed genomic PCR. We used genomic DNA from the leaves of wild type and 'Ryokusei' after adjusting the concentration as 100 ng/μl. PCR was conducted in a 25 μL reaction mixture containing 50 ng total DNA, Tks Gflex DNA Polymerase (TaKaRa Bio Inc.), using the primers (50 pmol of each primer) P1 + P4 and P2 + P3, which are specific for the gene and retrotransposon, respectively. PCR amplification was performed in a TaKaRa PCR Thermal Cycler Dice (TaKaRa Bio Inc.). The following PCR cycling condition was used: denaturation for 1 min at 94°C,

followed by 30 cycles of 10 s at 98°C, 15 s at 62°C, and 3 min at 68°C.

## Yeast Two-Hybrid Assays

Yeast two-hybrid analysis to investigate protein–protein interactions among B-class (HrDEF), C-class (HrAGs), and E-class (HrSEPs) proteins was performed using the GAL4 system. Full-length cDNA from HrDEF, HrSEP-1, and the two HrAGs was amplified by PCR using primers containing the attB sequence site to facilitate full-length cDNA cloning, whereas for HrSEP-2, the C-region was deleted to prevent autoactivation. The PCR fragments were ligated into both the prey vector pDEST22 and the bait vector pDEST32 using the Gateway system (Life Technologies). Bait and prey constructs were transformed into yeast strains PJ69-4α and PJ69-4A, respectively, using the lithium acetate method. The yeast transformations were screened on selection medium according to the manufacturer's instructions (de Folter and Immink, 2011). To test for autoactivation, all PJ69-4α strains were plated on SD/-Leu -Trp -His medium, and 5 mM 3-amino-1,2,4-triazole (3-AT) was added to suppress background signals due to autoactivation. All interaction experiments were conducted in triplicate, and yeast growth was scored after 7 days of incubation at 20°C.

# RESULTS

## Floral Morphology of 'Aoba' (Wild Type) and 'Ryokusei' (Greenish Flower Mutant)

Wild type 'Aoba' flowers contain three greenish sepals in whorl 1, two white petals and a white lip in whorl 2, and a column in whorls 3 and 4 (**Figure 1A**). By contrast, 'Ryokusei' flowers appear greenish overall and are smaller than wild type flowers (**Figures 1B,C**). In the 'Ryokusei' perianth, two petals have been converted into greenish sepaloid structures and the lip is greenish and smaller than that of the wild type, although there are no notable differences in the three (greenish) sepals between flowers (**Figures 1D–G**). In whorls 3 and 4, the dorsal column (stamen-like organ) has been converted into several sepaloid organs, with degenerated pollinium-like organs on the edges of these organs (**Figures 1B,F**). The form of the ventral column (carpel-like organ) is almost the same as that of the wild type, and 'Ryokusei' flowers contain stigma-like structures, although this cultivar is sterile (**Figure 1G**).

'Ryokusei' was derived from a *H. radiata* strain found in Shodoshima Island, Japan (Mitsuhashi, 1988). Since the floral morphology of the wild type and 'Ryokusei' is very different, we analyzed the sequences of the nuclear ribosomal internal transcribed spacer (ITS) regions from 'Ryokusei' and various *Habenaria* species to confirm the origin of this mutant cultivar (**Supplementary Figure S1**). We designed a primer set based on the ITS region and amplified this region in 'Aoba' and 'Ryokusei.' We obtained PCR products of approximately 500 bp and determined the sequences of the ITS regions. We compared the ITS sequence of 'Ryokusei' with that of other *Habenaria* species (*H. propinquior*, *H. arenaria*, *H. laevigata*, *H. clavata*, and *H. lithophila*), finding that the ITS sequence of 'Ryokusei' is completely identical to that of *H. radiata* 'Aoba.' Phylogenetic analysis confirmed that 'Ryokusei' is classified in *H. radiata* (**Supplementary Figure S1**).

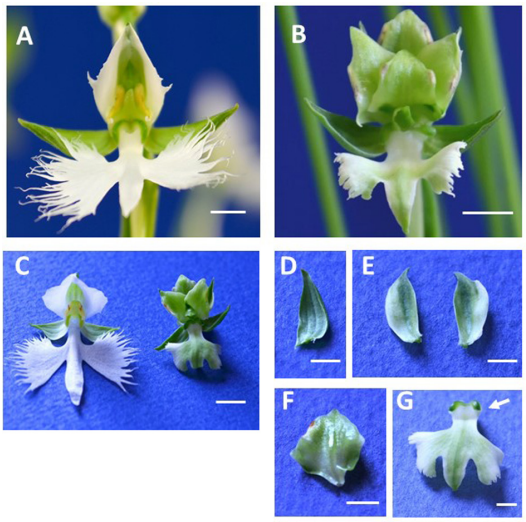


**FIGURE 1 |** Flower morphology of *Habenaria radiata* 'Aoba' (wild type) and 'Ryokusei' (greenish flower mutant). **(A)** Wild type flower. The flower has three greenish sepals in whorl 1, two white petals and one white lip in whorl 2, and a column in whorls 3 and 4. **(B)** Flower of the greenish flower mutant 'Ryokusei.' The mutant has three normal sepals in whorl 1, two greenish petals and a lip in whorl 2, and sepaloid organs and a ventral column in whorls 3 and 4. **(C)** Wild type and 'Ryokusei' flowers before dissection. **(D–G)** Dissected 'Ryokusei' flower, with a sepal **(D)**, petals **(E)**, a sepaloid organ instead of a dorsal column **(F)**, and a greenish lip with a ventral column **(G)**. Arrow indicates the stigma-like structure **(G)**. Scale bars: 0.5 cm **(A–C)** and 0.25 cm **(D–G)**.

## cDNA Cloning of *AG*- and *SEP*-Like Genes From *H. radiata*

We isolated four cDNA clones of MADS-box genes from *H. radiata* 'Aoba' by RACE using MADS-box-specific degenerate primers. After cloning and sequencing the cDNA fragments, BLAST searches (TBLASTN) revealed that two of these clones shared high sequence similarity with *SEP*-like genes, and two were highly similar to *AG*-like genes. After obtaining the 5′-regions of the cDNAs by 5′RACE, we isolated full-length cDNA clones by PCR using gene-specific primers. Phylogenetic analysis classified the four genes into two major groups according to gene lineage: the SEP-like and AG-like clades (**Figures 2–4**).

We designated the two *AG*-like genes from wild type *H. radiata* as *HrAG-1* and *HrAG-2* (**Figure 2**). The 687 bp full-length *HrAG-1* cDNA encodes a 228 aa protein, and the 702 bp full-length *HrAG-2* cDNA encodes a 233 aa protein. These genes consist of a MADS-box domain, an I-region, a K-domain, and a C-region. In addition, both HrAG-1 and HrAG-2 contain AG motifs I and II at their C-terminal ends. HrAG-1 shares 83.8% identity with HrAG-2 on the amino acid level. HrAG-1 and HrAG-2 share high homology with the *Phalaenopsis* protein, PhalAG1 (93 and 91% identity, respectively).

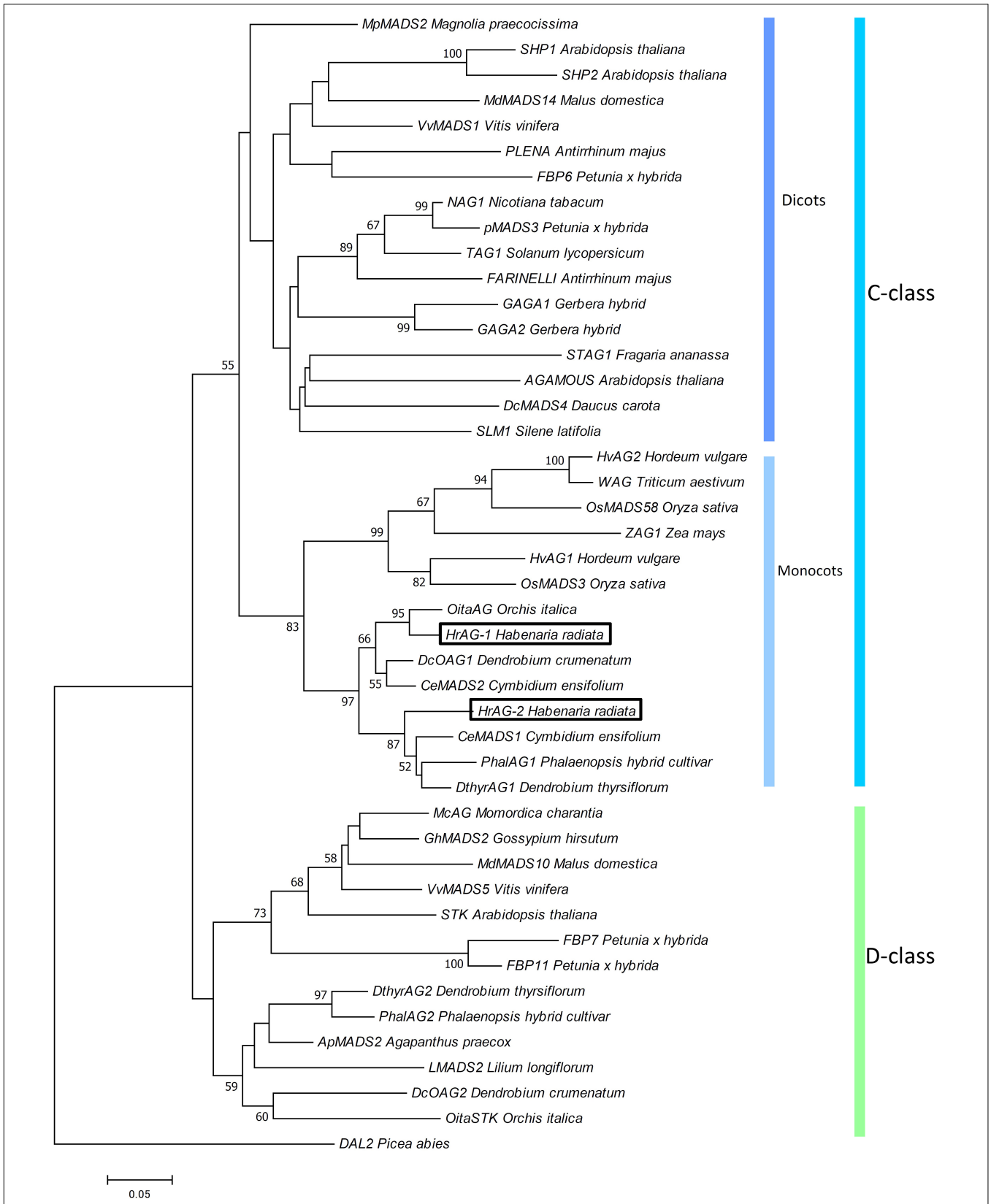


**FIGURE 2 |** Phylogenetic analysis of AG-like genes. The phylogenetic tree was constructed using the neighbor-joining method with the JTT + G model. The genes isolated from *H. radiata* are boxed. Bootstrap values greater than 50% from 1000 replicates are shown on the nodes.

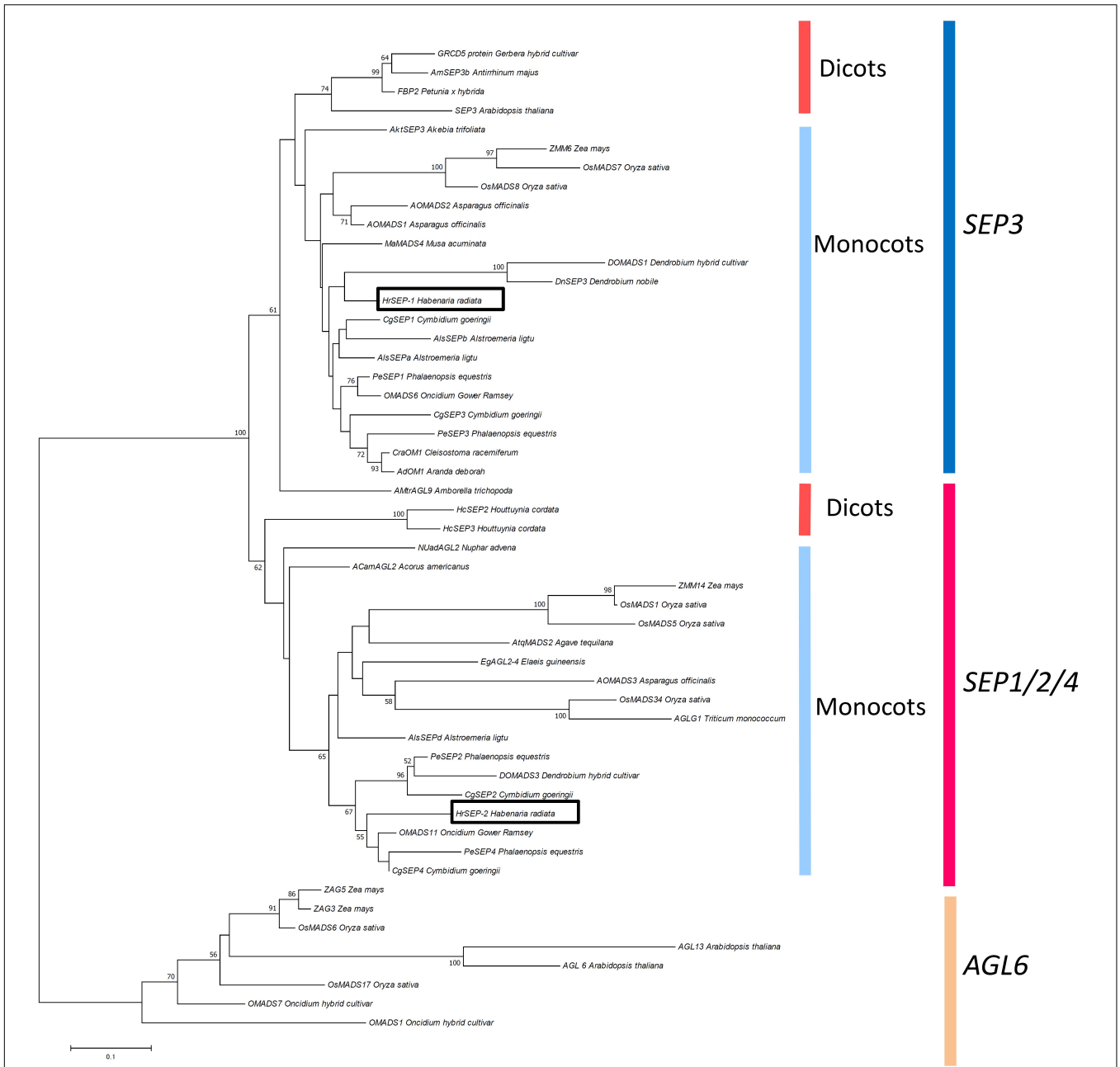


**FIGURE 3 |** Phylogenetic analysis of SEP-like genes. The phylogenetic tree was constructed using the neighbor-joining method with the JTT + G model. The genes isolated from *H. radiata* are boxed. Bootstrap values greater than 50% from 1000 replicates are shown on the nodes.

The two *SEP*-like genes from *H. radiata* were designated *HrSEP-1* and *HrSEP-2* (**Figure 3**). The 657 bp full-length *HrSEP-1* cDNA encodes a 218 aa protein, and the 735 bp full-length *HrSEP-2* cDNA encodes a 244 aa protein. HrSEP-1 and HrSEP-2 contain a MADS-domain, an I-region, and a K-domain. Although HrSEP-2 has SEP-I and SEP-II motifs at its C-terminal region, the C-terminal region of HrSEP-1 lacks a SEP-II motif. The deduced amino acid sequences of HrSEP-1 and HrSEP-2 share 58.8% identity. A comparison of published SEP amino acid sequences with that of HrSEP-1 showed that it shares 88% identity with DOSEP1 from *Dendrobium* and 87% identity with PeSEP 1 from *Phalaenopsis*. HrSEP-2 shares high homology (79% sequence identity) with DOMADS3 from *Dendrobium* and 81% identity with PeSEP 2 from *Phalaenopsis*.

## Expression Analysis of *DEF-*, *AG-*, and *SEP*-Like Genes From *H. radiata*

We performed semi-quantitative and quantitative RT-PCR to analyze the expression patterns of the *DEF*-like gene (*HrDEF*),

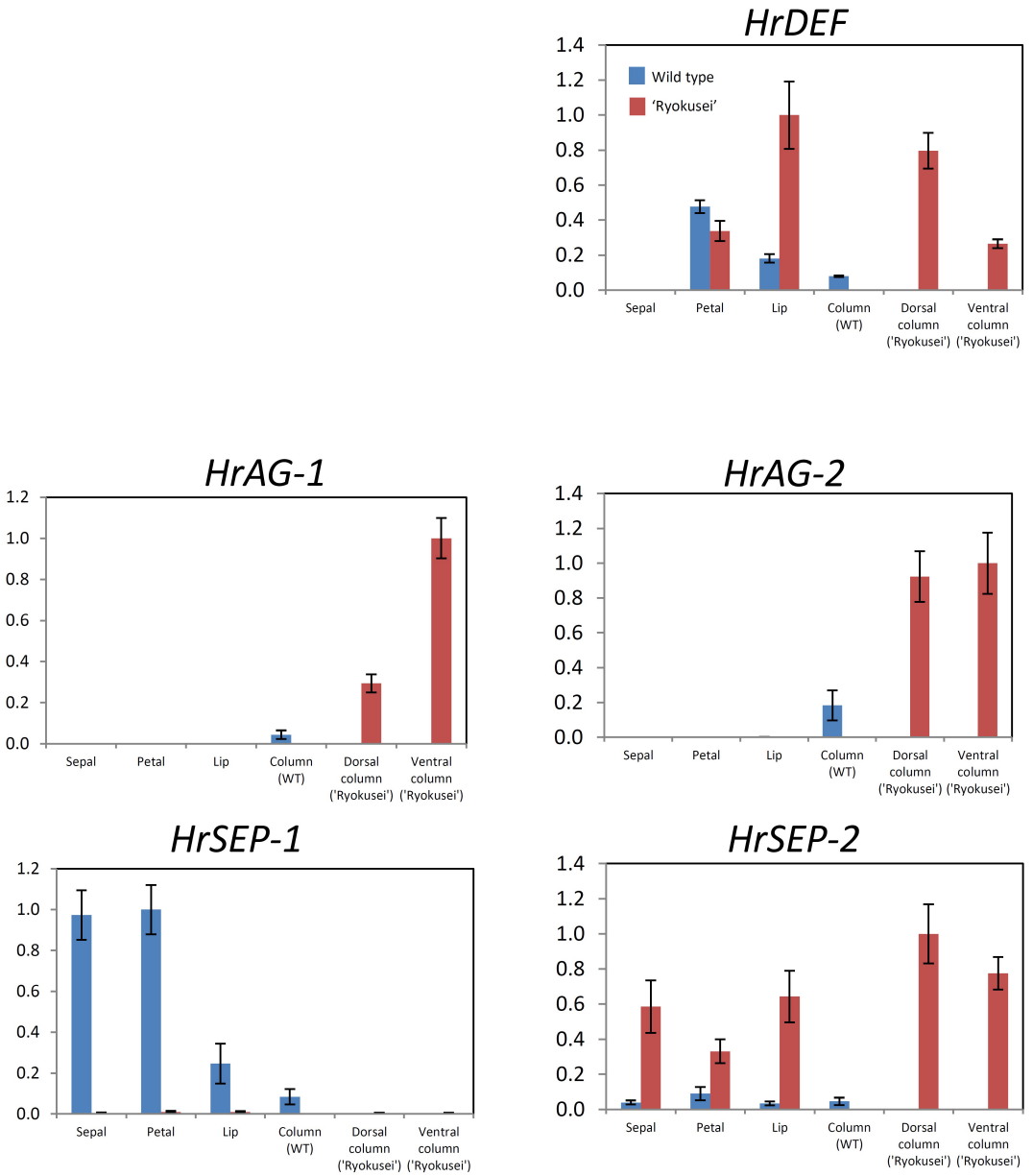


**FIGURE 4 |** Quantitative RT-PCR analysis of MADS-box genes in sepal, petal, lip, and column tissue from wild type *H. radiata* flowers and sepal, greenish petal, greenish lip, and sepaloid tissue in whorls 3 and 4 (dorsal and ventral column) from 'Ryokusei.' Error bars represent the standard error from three experimental replicates.

two *SEP*-like genes (*HrSEP-1*, *HrSEP-2*), and two *AG*-like genes (*HrAG-1*, *HrAG-2*) using dissected floral organs from wild type (sepal, petal, lip, and column) and 'Ryokusei' (sepal, petal, lip, and dorsal and ventral columns) in *H. radiata* (**Supplementary Figure S2** and **Figure 4**). These experiments were repeated three times, with each replicate revealing the same expression patterns.

In the wild type, *HrDEF* was expressed in petals, lips, and columns, whereas *HrDEF* transcript was not detected in sepals. The expression patterns of *HrDEF* in the wild type were consistent with those of other orchid species and generally fit the 'orchid code' for organ identity in the orchid perianth. In 'Ryokusei,' *HrDEF* expression was detected in the petal and lip, as well as the dorsal and ventral column. In 'Ryokusei,' the expression level of this gene was higher in lip and dorsal and ventral column tissue and lower in petal tissue compared with the wild type. These results indicate that the expression patterns of *HrDEF* differed in the wild type vs. 'Ryokusei.'

In the wild type, *HrAG-1* and *HrAG-2* were expressed only in columns, which matches the expression patterns of their orthologs in other orchid species. In 'Ryokusei,' these genes were expressed only in dorsal and ventral columns, as in the wild type. However, *HrAG-1* and *HrAG-2* were expressed at higher levels

in the dorsal and ventral columns of 'Ryokusei' compared with wild type columns. In addition, *HrAG-1* was expressed at higher levels in the ventral vs. the dorsal column. Thus, the expression patterns of *HrAG-1* and *HrAG-2* in the wild type and 'Ryokusei' were similar, whereas the expression level of these genes differed strongly among lines.

*HrSEP-1* and *HrSEP-2* transcripts were widely detected throughout all floral organs in the wild type. However, in 'Ryokusei,' *HrSEP-2* was strongly upregulated in all floral organs (**Supplementary Figure S2** and **Figure 4**), whereas *HrSEP-1* expression was significantly suppressed in all floral organs. These results suggest that the suppressed expression of *HrSEP-1* in 'Ryokusei' might be the cause of greenish flower formation in this cultivar.

## A Retrotransposon Insertion Is Detected in the First Exon of *HrSEP-1* in 'Ryokusei'

As mentioned above, *HrSEP-1* expression was strongly suppressed in all floral organs of 'Ryokusei.' To clarify the molecular mechanism involving the suppressed expression of this gene, we compared the gene structures of *HrSEP-1* in the wild type vs. 'Ryokusei.' In both plants, *HrSEP-1* consists of seven exons and six introns. The size of each exon is identical in both plants, except the first exon (**Figure 5A**). We also isolated the promoter region of *HrSEP-1* by Genome Walker PCR and detected 140 bp promoter regions with identical sequences in the wild type and 'Ryokusei.' To confirm the structure of the first exon of *HrSEP-1* in the wild type and 'Ryokusei,' we performed PCR amplification with primers designed based on the sequence of promoter region and first exon (P1 and P2 primers; **Figure 5B**). The P1 and P2 primer pair amplified a PCR product of approximately 250 bp from the wild type, whereas the size of the PCR product from 'Ryokusei' was approximately 4,800 bp (**Figure 5B**). We cloned and sequenced these PCR products and found that the first exon of *HrSEP-1* from 'Ryokusei' contained an insertion sequence. This insertion sequence has typical features of a LTR-retrotransposon, and was therefore designated *Hret1* (*Habenaria* retrotransposon 1). *Hret1* is 4,534 bp long, with 5 bp of target site duplication (TSD) [213 bp of a long terminal repeat (LTR) – 407 bp of group-specific antigen (GAG) – 284 bp of integrase (IN) – 728 bp of reverse transcriptase (RT) – 425 bp of ribonuclease H (RH) – 213 bp of LTR] – 5 bp of TSD, indicating that *Hret1* is a *Ty1/Copia*-type retrotransposon. *Hret1* is inserted in the first exon with reverse orientation to *Hret1* transcript. To confirm the insertion of *Hret1* in the first exon of *HrSEP-1* gene in 'Ryokusei,' we performed PCR amplification with primers specific for the gene and retrotransposon. Using the primers of P1 + P4 and P2 + P3, which are specific for the gene and retrotransposon, respectively, DNA fragment was amplified in 'Ryokusei,' but not in wild type. This data clearly showed the insertion of retrotransposon in *HrSEP-1* gene of 'Ryokusei.' We obtained a PCR product of approximately 2000 bp with P3 and P4 primer pair from both wild type and 'Ryokusei,' indicating that *Hret1* exist in wild type plant as well as 'Ryokusei' cultivar.

## Protein–Protein Interactions of HrSEP-1 With Other MADS-Box Proteins in *H. radiata*

To investigate whether HrSEP-1 forms protein complexes with other MADS-box proteins, we performed a GAL4-based yeast two-hybrid assay. Specifically, we assessed protein complex formation with HrSEP-1 in a GAL4-based yeast two-hybrid assay for HrDEF, two AG proteins (HrAG-1 and HrAG-2), and one SEP protein (HrSEP-2). Autoactivation tests revealed no background signals for yeast strains containing bait only (data not shown), except for HrSEP-2. For HrSEP-2, we used truncated HrSEP-2 protein containing the MADS-domain, I-region, and K-domain. HrSEP-1 protein interacted with B-class HrDEF protein and C-class HrAG-1, HrAG-2, and HrSEP-1 proteins. As shown in **Figure 6**, heterodimerization of HrSEP-1/HrDEF, HrSEP-1/HrAG-1, and HrSEP-1/HrAG-2 was detected even when the bait and prey constructs were switched. A HrSEP-1/HrSEP-2 interaction was detected when HrSEP-1 was used as bait, whereas this interaction was not detected when HrSEP-1 was used as prey, suggesting it is likely that HrSEP-1/HrSEP-2 interact weakly. These results suggest that heterodimers of HrSEP-1/HrDEF, HrSEP-1/HrAG-1, and HrSEP-1/HrAG-2 bind stably to each other, unlike HrSEP-1/HrSEP-2 (**Figure 6**).

# DISCUSSION

## A Retrotransposon Insertion Is Present in *HrSEP-1* in 'Ryokusei'

In this study, we investigated the cause of greenish flower formation in the mutant *H. radiata* cultivar 'Ryokusei.' Instead of the white flowers of the wild type, 'Ryokusei' flowers have an overall greenish color. Although the petals, lip, and column have been converted into sepaloid structures in this mutant orchid, the sepals in whorl 1 are unaffected. The dorsal column has also been converted into sepaloid organs that are thick and partially yellow at both ends. In addition, the number of sepaloid organs derived from the column varies from three to five. The floral morphology of 'Ryokusei' appears to resemble that of indeterminate flowers, suggesting that this phenotype is caused by a mutation in an *AG*-like gene. Thus, we isolated two *AG*-like genes (*HrAG-1* and *HrAG-2*) from *H. radiata* (**Figure 4**). However, these genes were highly expressed in the column-derived, greenish sepaloid structures in 'Ryokusei' (**Figure 4**). These results suggest that the floral phenotype of 'Ryokusei' is not caused by the mutation of *AG*-like genes.

The morphological changes in *Arabidopsis ag* mutants are restricted to male and female reproductive organs (Bowman et al., 1989), whereas in 'Ryokusei,' we also detected morphogenetic changes in the lip and petal in whorl 2, as well as the column in whorls 3 and 4 (**Figure 1**). This phenotype is similar to that of a rice *OsMADS7/8* knockdown line (Cui et al., 2010): the knockdown of *OsMADS7* and *OsMADS8* in rice led to significant morphological changes in the organs of the three innermost whorls (Cui et al., 2010). Thus, we isolated two *SEP*-like genes (*HrSEP-1* and *HrSEP-2*) from wild type

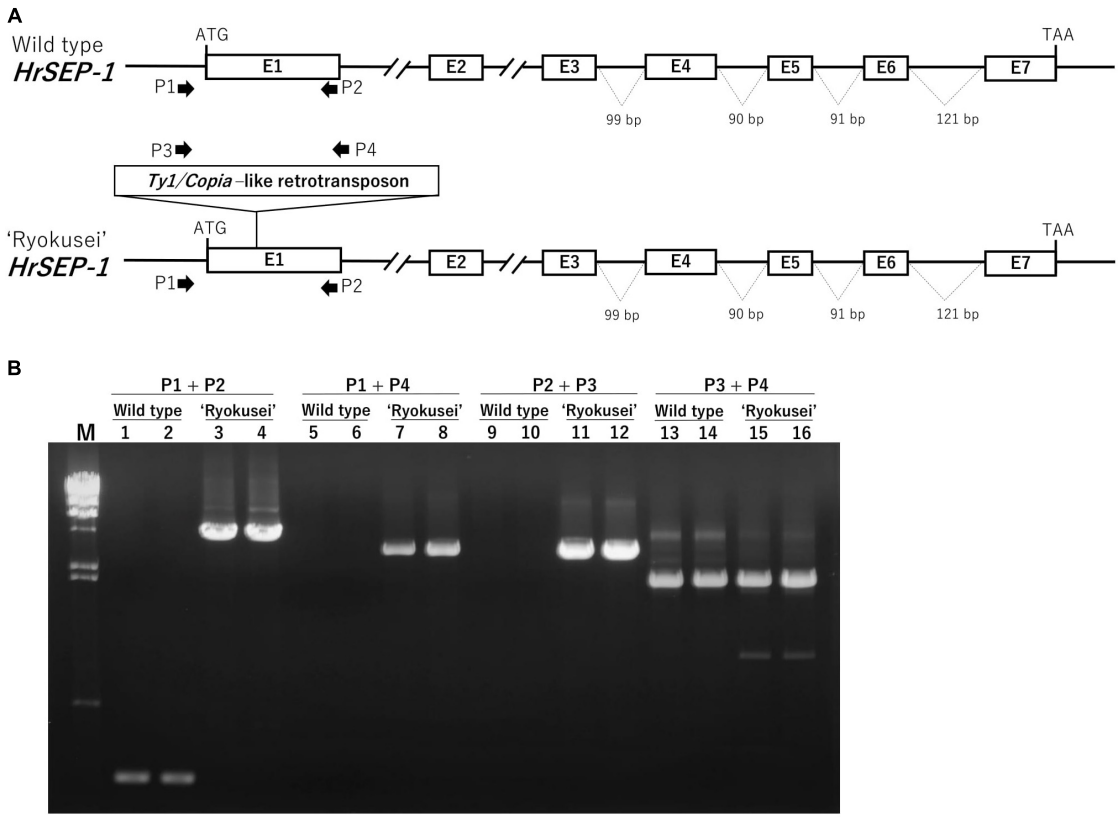


**FIGURE 5 |** Genomic structure of *HrSEP-1* from wild type and 'Ryokusei' in *H. radiata*. **(A)** Schematic diagrams of the genomic structures of *HrSEP-1* from the wild type and 'Ryokusei.' White boxes indicate exons; the ATG start codons and TAA stop codons are also shown. 'Ryokusei' has a *Ty1/Copia*-like retrotransposon in the first exon of *HrSEP-1*. **(B)** PCR analysis of *HrSEP-1* from the wild type and 'Ryokusei.' PCR was performed using primer sets specific for *HrSEP-1* gene (P1 and P2) and retrotransposon (P3 and P4), as shown in **(A)**.

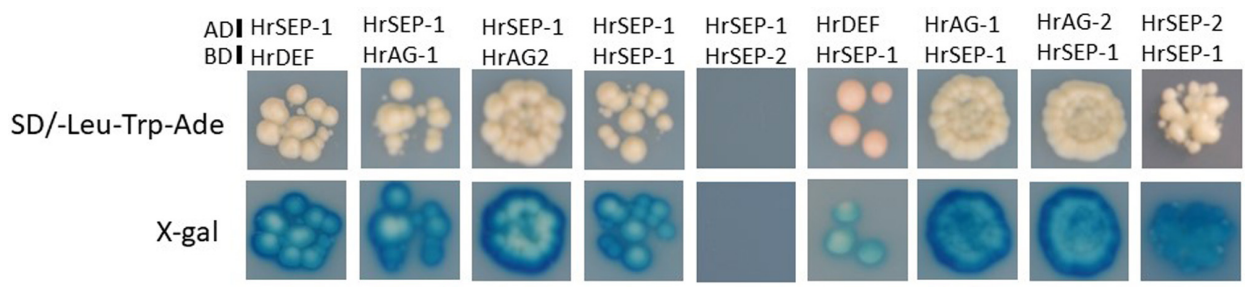


**FIGURE 6 |** Analysis of protein-protein interactions between HrSEP-1 and other MADS-box proteins in *H. radiata* by GAL4 yeast two-hybrid analysis. Baits were expressed as GAL4 DNA-BD fusion proteins in pDEST32 and transformed into the PJ69-4α yeast strain, and preys were expressed as GAL4 AD fusion proteins in pDEST22 and transformed into the PJ69-4A yeast strain. Activation of ADE was determined on SD selection medium (SD/-Leu-Trp-Ade), and activation of *lacZ* is indicated by *X*-gal staining. Full-length amino acid sequences were used in this study, except for HrSEP-2; to avoid autoactivation, the C-region was removed from HrSEP-2.

*H. radiata* and analyzed their expression patterns. These genes were expressed in all floral organs of the wild type, matching the expression patterns of other orchid *SEP* genes from *Cymbidium*, *Oncidium*, and *Phalaenopsis* (Chang et al., 2009; Pan et al., 2014; Xiang et al., 2017). By contrast, *HrSEP-1* transcript was not detected in 'Ryokusei', although *HrSEP-2* was expressed in all floral organs (**Figure 4**). These results suggested that a deletion or structural rearrangement might have occurred in *HrSEP-1* in 'Ryokusei.' Thus, we isolated genomic clones of *HrSEP-1* from the wild type and 'Ryokusei' and compared their gene structures. As shown in **Figure 6**, we detected a retrotransposon insertion in the first exon of *HrSEP-1* from 'Ryokusei.' BLAST analysis demonstrated that this retrotransposon insertion is a *Ty1/Copia*-like retrotransposon, which we named *Hret1*. PCR analysis using

a primer set flanking to this insertion showed that 'Ryokusei' contains the mutant gene and not the wild type gene, indicating that the mutant allele of *HrSEP-1* containing *Hret1* is present in the homozygous state (**Figure 6**). Thus, the *Hret1* insertion likely leads to the formation of greenish flowers, and this mutation is likely to be recessive.

A functional analysis of *SEP*-like genes was previously carried out in *Phalaenopsis* using VIGS (Pan et al., 2014). The tepals of *PeSEP3*-silenced flowers with off-target silencing of *PeSEP1* and *PeSEP2* were converted into leaf-like organs, but column formation was not affected in these plants (Pan et al., 2014). The morphological differences in the columns of 'Ryokusei' vs. *PeSEP3*-silenced *Phalaenopsis* might have been due to residual activity of the *Phalaenopsis SEP3* ortholog. In other words, 'Ryokusei' showed the same phenotype as null mutants of *SEP3*-like genes, whereas residual expression of *PeSEP3* and *PeSEP1* might have helped maintain column formation in the *Phalaenopsis* VIGS line.

## HrSEP-1 Is Essential for Petal, Lip, and Column Development

In the perianths of 'Ryokusei' flowers, lips and petals were converted into sepaloid organs, whereas there were no morphological changes in sepals (**Figure 1**). These findings indicate that *HrSEP-1* plays an important role in the development of petals and lips, but not sepals. In 'Ryokusei,' the dorsal column was converted into sepaloid organs, indicating that *HrSEP-1* is also essential for column development (**Figure 1**). The dorsal column was converted into three to five sepaloid organs, suggesting that *HrSEP-1* likely functions in the transition of meristem activity from indeterminate to determinate growth in *H. radiata* flowers.

*Arabidopsis thaliana* contains four *SEP* genes whose functions are largely redundant (Pelaz et al., 2000, 2001; Ditta et al., 2004). On the other hand, in the current study, loss of function of *HrSEP-1* caused significant morphological changes in floral organs, even though *HrSEP-2* was highly expressed in the 'Ryokusei' mutant. These results indicate that *HrSEP-1* and *HrSEP-2* are not functionally redundant. In *Phalaenopsis*, downregulating *PeSEP3* by VIGS also had a significant effect on floral morphology (Pan et al., 2014). Meanwhile, silencing of *PeSEP2* had only minor effects on floral phenotype, even though the expression of *PeSEP2* was strongly downregulated in these plants. Therefore, although both *HrSEP-1* and *PeSEP3* belong to the SEP3 clade, as shown in **Figure 3**, orchid SEP3 and the SEP1/2/4 orthologs might not be functionally redundant.

According to the quartet model (Theissen and Saedler, 2001) in *A. thaliana*, the floral organ identity is specified by combinational protein interactions of ABCE-class MADS-domain transcription factors (Theissen, 2001). These quartets control gene expression by binding to the DNA of their target genes (Theissen, 2001). Sepal identity is determined by a complex of two A (AP1) class proteins and two E (SEP) class proteins, petal identity is controlled by a complex of one AP1 and one SEP protein together with one of each of the B class proteins APETALA3 (AP3) and PISTILLATA (PI), stamen identity is specified by a complex of one SEP, one AP3, one PI protein and the C (AG) class protein, and carpel identity is determined by a complex of two SEP proteins together with two AG proteins. Therefore, E class genes are essential for quaternary complexes. As shown in **Figure 6**, yeast two hybrid experiments demonstrated that HrSEP-1 interact with B and C class proteins. Suppressed expression of *HrSEP-1* gene in 'Ryokusei' is likely to affect the construction of quaternary complexes with SEP and B/C proteins, and this might be the cause of the greenish phenotype of this mutant.

In the 'Ryokusei' cultivar, B-, C-, and E-class genes were upregulated in the ventral column and in sepaloid organs that had been converted from the dorsal column in whorls 3 and 4 (**Figure 4**). If HrSEP-1 and other MADS-box genes interact via positive feedback loops, the expression levels of MADS proteins interacting with HrSEP-1 would likely decrease in the absence of HrSEP-1 function. In 'Ryokusei,' HrSEP-1 was not expressed, but B (HrDEF)-, C (HrAGs)-, and E (HrSEP-2)-class genes were upregulated compared with the wild type (**Figure 4**). Based on the studies in *A. thaliana*, SEP3 is involved in positive and negative cross-control of AG via complex formation. The AG/SEP3 complex undergoes positive autoregulation to coordinately regulate and maintain its own expression in whorls 3 and 4 (Gomez-Mena et al., 2005). SEU/LUG/SEP3 prevent AG transcription in all four floral whorls via negative regulation (Sridhar et al., 2006), but this negative regulation in the whorls 3 and 4 is antagonized by the activities of LFY, WUS and the positive autoregulatory AG/SEP3 complexes (Sridhar et al., 2006). Our expression results suggested that the upregulated expression of *HrAGs* in column of 'Ryokusei' may be caused by loss of negative control of SEU/LUG/SEP3.

According to the orchid code and P-code model, clade 3 *DEF*-like genes play an important role in lip development in orchid (Mondragón-Palomino and Theißen, 2011; Hsu et al., 2015). The clade 3 *DEF*-like gene is highly expressed in lips but is also weakly expressed in columns (Hsu et al., 2015). In 'Ryokusei,' the clade 3 *DEF*-like gene *HrDEF* was highly upregulated in sepaloid organs that had been converted from a dorsal column (**Figure 4**). Therefore, the homeotic conversion of the dorsal column to sepaloid organs in 'Ryokusei' is likely associated with the upregulated expression of *HrDEF* in the dorsal column. Meanwhile, there are no noticeable changes in sepal of 'Ryokusei,' even though the expression of *HrSEP-1* was downregulated. This indicates that *HrSEP-1* may not be necessary for sepal development in *H. radiata.* Another possibility is that other *SEP*-like gene which has redundant function of *HrSEP-1* might exist in *H. radiata*. Some orchids (e.g., *C. goeringii*, *Erycina Pusilla,* and *P. equestris*) have four *SEP*-like genes (Pan et al., 2014; Dirks-Mulder et al., 2017; Xiang et al., 2017), however, we have isolated only two *SEP*-like genes from *H. radiata*. So, there might be a few of undetected *SEP*-like genes in *H. radiata* and exhibit redundant functions in the floral organ identity.

Our findings demonstrate that the mutant phenotype of 'Ryokusei' is caused by the insertion of a retrotransposon in *HrSEP-1*. In addition, we demonstrated that this gene is essential for petal, lip, and column development and that it appears

to function in floral meristem determination. 'Ryokusei' is a spontaneous mutant that was first found in Shodoshima Island in Japan. Since 'Ryokusei' is a homozygous mutant of *HrSEP-1*, this mutant might have been selected from self-pollinated progeny containing a heterozygous retrotransposon insertion. Although 'Ryokusei' is sterile, this cultivar can be maintained by vegetative (bulb) propagation, like other *H. radiata* cultivars. Since a null mutant of *SEP*-like genes has not yet been identified in orchid, 'Ryokusei' is highly important for further analyzing the role of SEP in orchid.

## AUTHOR CONTRIBUTIONS

MM and AK: experimental design and manuscript preparation. MM: experiments. MM: data analysis. AK: supervision, funding, and reagents.

## FUNDING

This study was financially supported through a Grant-in-Aid for Scientific Research (KAKENHI Nos. 19380016, 22380018, and 25292018) from the Japan Society for the Promotion of Science (JSPS).

## ACKNOWLEDGMENTS

We gratefully thank Drs. John C. Cushman and Yuichi Uno for providing the yeast strains. We also thank Ms. Yoko Kakimoto for her help with *Habenaria* orchid cultivation.

## SUPPLEMENTARY MATERIAL

The Supplementary Material for this article can be found online at: https://www.frontiersin.org/articles/10.3389/fpls.2018.00831/full#supplementary-material

**FIGURE S1 |** Phylogenetic tree of 'Ryokusei' and *Habenaria* species derived based on ITS sequences. Numbers on the nodes represent bootstrap values greater than 50% from 1000 replicates.

**FIGURE S2 |** Expression analysis of *HrDEF*, *HrAG-1*, *HrAG-2*, *HrSEP-1*, and *HrSEP*-2 using semi-qRT-PCR. **(A)** Wild type. **(B)** 'Ryokusei'. *eEF1A* was used as a positive control. Se, sepals; Pe, petals; Li, lip; Co, columns; Dco, dorsal column; Vco, ventral column.

**TABLE S1 |** List of primers used in the present study.

**TABLE S2 |** Accession numbers for the AG-like genes isolated in the present study and the genes used in the phylogenetic analysis.

**TABLE S3 |** Accession numbers for the SEP-like genes isolated in the present study and the genes used in the phylogenetic analysis.

## REFERENCES

Aceto, S., and Gaudio, L. (2011). The MADS and the beauty: genes involved in the development of orchid flowers. *Curr. Genomics* 12, 342–356. doi: 10.2174/1389202 11796429754

Ampomah-Dwamena, C., Morris, B. A., Sutherland, P., Veit, B., and Yao, J. L. (2002). Down-regulation of TM29, a tomato SEPALLATA homolog, causes parthenocarpic fruit development and floral reversion. *Plant Physiol.* 130, 605–617. doi: 10.1104/pp.005223

Arora, R., Agarwal, P., Ray, S., Singh, A., Singh, V., Tyagi, A. K., et al. (2007). MADS-box gene family in rice: genome-wide identification, organization and expression profiling during reproductive development and stress. *BMC Genomics* 8:242. doi: 10.1186/1471-2164-8-242

Bowman, J. L., Drews, G. N., and Meyerowitz, E. M. (1991). Expression of the Arabidopsis floral homeotic gene AGAMOUS is restricted to specific cell types late in flower development. *Plant Cell* 3, 749–758. doi: 10.1105/tpc.3.8.749

Bowman, J. L., Smyth, D. R., and Meyerowitz, E. M. (1989). Genes directing flower development in *Arabidopsis*. *Plant Cell* 1, 37–52. doi: 10.1105/tpc.1.1.37

Carpenter, R., and Coen, E. S. (1990). Floral homeotic mutations produced by transposon-mutagenesis in *Antirrhinum majus*. *Genes Dev.* 4, 1483–1493. doi: 10.1101/gad.4.9.1483

Chang, Y. Y., Chiu, Y. F., Wu, J. W., and Yang, C. H. (2009). Four orchid (*Oncidium* 'Gower Ramsey') *AP1/AGL9*-like MADS box genes show novel expression patterns and cause different effects on floral transition and formation in *Arabidopsis thaliana*. *Plant Cell Physiol.* 50, 1425–1438. doi: 10.1093/pcp/pcp087

Coen, E. S., and Meyerowitz, E. M. (1991). The war of the whorls: genetic interactions controlling flower development. *Nature* 353, 31–37. doi: 10.1038/353031a0

Cui, R., Han, J., Zhao, S., Su, K., Wu, F., Du, X., et al. (2010). Functional conservation and diversification of class E floral homeotic genes in rice (*Oryza sativa*). *Plant J.* 61, 767–781. doi: 10.1111/j.1365-313X.2009.04101.x

de Folter, S., and Immink, R. G. (2011). "Yeast protein-protein interaction assays and screens," in *Plant Transcription Factors. Methods and Protocols (Methods in Molecular Biology)*, eds L. Yuan and S. E. Perry (New York, NY: Springer), 145–165. doi: 10.1007/978-1-61779-154-3_8

Ditta, G., Pinyopich, A., Robles, P., Pelaz, S., and Yanofsky, M. F. (2004). The *SEP4* gene of *Arabidopsis thaliana* functions in floral organ and meristem identity. *Curr. Biol.* 14, 1935–1940. doi: 10.1016/j.cub.2004.10.028

Dirks-Mulder, A., Butôt, R., van Schaik, P., Wijnands, J. W., van den Berg, R., Krol, L., et al. (2017). Exploring the evolutionary origin of floral organs of *Erycina pusilla*, an emerging orchid model system. *BMC Evol. Biol.* 17:89. doi: 10.1186/s12862-017-0938-7

Ferrario, S., Immink, R. G., Shchennikova, A., Busscher-Lange, J., and Angenent, G. C. (2003). The MADS box gene *FBP2* is required for SEPALLATA function in petunia. *Plant Cell* 15, 914–925. doi: 10.1105/tpc.010280

Gomez-Mena, C., de Folter, S., Costa, M. M., Angenent, G. C., and Sablowski, R. (2005). Transcriptional program controlled by the floral homeotic gene *AGAMOUS* during early organogenesis. *Development* 132, 429–438. doi: 10.1242/dev.01600

Honma, T., and Goto, K. (2001). Complexes of MADS-box proteins are sufficient to convert leaves into floral organs. *Nature* 409, 525–529. doi: 10.1038/35054083

Hsu, H. F., Hsu, W. H., Lee, Y. I., Mao, W. T., Yang, J. Y., Li, J. Y., et al. (2015). Model for perianth formation in orchids. *Nat. Plants* 1:15046. doi: 10.1038/nplants.2015.46

Kim, S. Y., Yun, P. Y., Fukuda, T., Ochiai, T., Yokoyama, J., Kameya, T., et al. (2007). Expression of a *DEFICIENS*-like gene correlates with the differentiation between sepal and petal in the orchid, *Habenaria radiata* (Orchidaceae). *Plant Sci.* 172, 319–326. doi: 10.1016/j.plantsci.2006.09.009

Kumar, S., Stecher, G., and Tamura, K. (2016). MEGA7: molecular evolutionary genetics analysis version 7.0 for bigger datasets. *Mol. Biol. Evol.* 3, 1870–1874. doi: 10.1093/molbev/msw054

Lid, S., Meeley, R., Min, Z., Nichols, S., and Olsen, O. A. (2004). Knock-out mutants of two members of the AGL2 subfamily of MADS-box genes expressed during maize kernel development. *Plant Sci.* 167, 575–582. doi: 10.1016/j.plantsci.2004.04.031

Lu, Z. X., Wu, M., Loh, C. S., Yeong, C. Y., and Goh, C. J. (1993). Nucleotide sequence of a flower-specific MADS box cDNA clone from orchid. *Plant Mol. Biol.* 23, 901–904. doi: 10.1007/BF00021545

Matsubara, K., Shimamura, K., Kodama, H., Kokubun, H., Watanabe, H., Basualdo, I. L., et al. (2008). Green corolla segments in a wild *Petunia* species caused by

a mutation in *FBP2*, a *SEPALLATA*-like MADS box gene. *Planta* 228, 401–409. doi: 10.1007/s00425-008-0744-y

Mitsuhashi, S. (1988). *Mezurashii Yasei no Ran (Rare Wild Orchid, Written in Japanese)*. Tokyo: Ikedashoten, 21.

Mondragón-Palomino, M. (2013). Perspectives on MADS-box expression during orchid flower evolution and development. *Front. Plant Sci.* 4:377. doi: 10.3389/fpls.2013.00377

Mondragón-Palomino, M., and Theißen, G. (2011). Conserved differential expression of paralogous *DEFICIENS*- and *GLOBOSA*-like MADS-box genes in the flowers of Orchidaceae: refining the 'orchid code'. *Plant J.* 66, 1008–1019. doi: 10.1111/j.1365-313X.2011.04560.x

Pan, Z. J., Chen, Y. Y., Du, J. S., Chen, Y. Y., Chung, M. C., Tsai, W. C., et al. (2014). Flower development of *Phalaenopsis* orchid involves functionally divergent *SEPALLATA*-like genes. *New Phytol.* 202, 1024–1042. doi: 10.1111/nph.12723

Pelaz, S., Ditta, G. S., Baumann, E., Wisman, E., and Yanofsky, M. F. (2000). B and C floral organ identity functions require SEPALLATA MADS-box genes. *Nature* 405, 200–203. doi: 10.1038/35012103

Pelaz, S., Tapia-Lopez, R., Alvarez-Buylla, E. R., and Yanofsky, M. F. (2001). Conversion of leaves into petals in *Arabidopsis*. *Curr. Biol.* 11, 182–184. doi: 10.1016/S0960-9822(01)00024-0

Pnueli, L., Abu-Abeid, M., Zamir, D., Nacken, W., Schwarz-Sommer, Z., and Lifschitz, E. (1991). The MADS box gene family in tomato: temporal expression during floral development, conserved secondary structures and homology with homeotic genes from *Antirrhinum* and *Arabidopsis*. *Plant J.* 1, 255–266. doi: 10.1111/j.1365-313X.1991.00255.x

Porebski, S., Bailey, L. G., and Baum, B. R. (1997). Modification of a CTAB DNA extraction protocol for plants containing high polysaccharide and polyphenol components. *Plant Mol. Biol. Rep.* 15, 8–15. doi: 10.1007/BF02772108

Schwarz-Sommer, Z., Hue, I., Huijser, P., Flor, P. J., Hansen, R., Tetens, F., et al. (1992). Characterization of the *Antirrhinum* floral homeotic MADS-box gene deficiens: evidence for DNA binding and autoregulation of its persistent expression throughout flower development. *EMBO J.* 11, 251–263. doi: 10.1002/j.1460-2075.1992.tb05048.x

Sridhar, V. V., Surendrarao, A., and Liu, Z. (2006). *APETALA1* and *SEPALLATA3* interact with *SEUSS* to mediate transcription repression during flower development. *Development* 133, 3159–3166. doi: 10.1242/dev.02498

Theissen, G., and Saedler, H. (2001). Plant biology. Floral quartets. *Nature* 409, 469–471. doi: 10.1038/35054172

Theissen, G. (2001). Development of floral organ identity: stories from the MADS house. *Curr. Opin. Plant Biol.* 4, 75–85. doi: 10.1016/S1369-5266(00)00139-4

Tsai, W. C., and Chen, H. H. (2006). The orchid MADS-box genes controlling floral morphogenesis. *ScientificWorldJournal* 6, 1933–1944. doi: 10.1100/tsw.2006.321

Vandenbussche, M., Zethof, J., Souer, E., Koes, R., Tornielli, G. B., Pezzotti, M., et al. (2003). Toward the analysis of the petunia MADS box gene family by reverse and forward transposon insertion mutagenesis approaches: B, C, and D floral organ identity functions require *SEPALLATA*-like MADS box genes in petunia. *Plant Cell* 15, 2680–2693. doi: 10.1105/tpc.017376

Weigel, D., and Meyerowitz, E. M. (1994). The ABCs of floral homeotic genes. *Cell* 78, 203–209. doi: 10.1016/0092-8674(94)90291-7

Xiang, L., Chen, Y., Chen, L., Fu, X., Zhao, K., Zhang, J., et al. (2017). B and E MADS-box genes determine the perianth formation in *Cymbidium goeringii* Rchb.f. *Physiol. Plant* 162, 353–369. doi: 10.1111/ppl.12647

Xu, Y., Teo, L. L., Zhou, J., Kumar, P. P., and Yu, H. (2006). Floral organ identity genes in the orchid *Dendrobium crumenatum*. *Plant J.* 46, 54–68. doi: 10.1111/j.1365-313X.2006.02669.x

Yanofsky, M. F., Ma, H., Bowman, J. L., Drews, G. N., Feldmann, K. A., and Meyerowitz, E. M. (1990). The protein encoded by the *Arabidopsis* homeotic gene agamous resembles transcription factors. *Nature* 346, 35–39. doi: 10.1038/346035a0

Yokota, M. (1990). Karyomorphological studies of *Habenaria*, Orchidaceae, and allied genera from Japan. *J. Sci. Hiroshima Univ. B Division 2 Bot.* 23, 53–161.

Yu, H., and Goh, C. J. (2000). Identification and characterization of three orchid MADS-box genes of the AP1/AGL9 subfamily during floral transition. *Plant Physiol.* 123, 1325–1336. doi: 10.1104/pp.123.4.1325

Zahn, L. M., Kong, H., Leebens-Mack, J. H., Kim, S., Soltis, P. S., Landherr, L. L., et al. (2005). The evolution of the *SEPALLATA* subfamily of MADS-box genes: a preangiosperm origin with multiple duplications throughout angiosperm history. *Genetics* 169, 2209–2223. doi: 10.1534/genetics.104.037770

**Conflict of Interest Statement:** The authors declare that the research was conducted in the absence of any commercial or financial relationships that could be construed as a potential conflict of interest.

frontiers in Plant Science

ORIGINAL RESEARCH
published: 09 January 2018
doi: 10.3389/fpls.2017.02239

# Long-lasting Corolla Cultivars in Japanese Azaleas: A Mutant *AP3/DEF* Homolog Identified in Traditional Azalea Cultivars from More Than 300 Years Ago

*Kyeong-Seong Cheon[1,2], Akira Nakatsuka[1], Keisuke Tasaki[1,3] and Nobuo Kobayashi[1]**

[1] Faculty of Life and Environmental Science, Shimane University, Matsue, Japan, [2] Genomics Division, National Institute of Agricultural Sciences, Rural Development Administration, Jeonju, South Korea, [3] Iwate Biotechnology Research Center, Kitakami, Japan

Floral shape in higher plants typically requires genetic regulation through MADS transcription factors. In Japan, hundreds of azalea cultivars including flower shape mutations have been selected from the diversity of endogenous species and natural hybrids since the early 17th century, the Edo era (1603–1867). The long-lasting trait, known as "Misome-shō" in Japanese, has been identified in several species and cultivar groups of evergreen azaleas (*Rhododendron* L.) from three hundred years ago in Japan. However, the natural mutation conferring the long-lasting trait in azalea remains unknown. Here, we showed MADS-box gene mutations in long-lasting flowers, *R. kaempferi* 'Nikkō-misome,' *R. macrosepalum* 'Kochō-zoroi,' *R. indicum* 'Chōjyu-hō,' and *R.* × *hannoense* 'Amagi-beni-chōjyu.' All of the long-lasting flowers exhibited small-sized corollas with stomata during long blooming. In the long-lasting flowers, transcript of the *APETALA3 (AP3)/DEFICIENS (DEF)* homolog was reduced, and an LTR-retrotransposon was independently inserted into exons 1, 2, and 7 or an unknown sequence in exon 1 in gDNA of each cultivar. This insertion apparently abolished the normal mRNA sequence of the *AP3/DEF* homolog in long-lasting flowers. Also, long-lasting flowers were shown from F2 hybrids that had homozygous *ap3/def* alleles. Therefore, we concluded that the loss of function of the *AP3/DEF* homolog through a transposable element insertion may confer a stable long-lasting mutation in evergreen azaleas.

**Keywords: long-lasting flower, corolla mutant, *AP3/DEF* homolog, transcriptional factors, retrotransposon, evergreen azalea**

OPEN ACCESS

***Edited by:***
*Akira Kanno,*
*Tohoku University, Japan*

***Reviewed by:***
*Chaoying He,*
*State Key Laboratory of Systematic and Evolutionary Botany, Institute of Botany, Chinese Academy of Sciences, China*
*Masaru Nakano,*
*Niigata University, Japan*

****Correspondence:***
*Nobuo Kobayashi*
*nkobayashi@life.shimane-u.ac.jp*

***Specialty section:***
*This article was submitted to Plant Breeding, a section of the journal Frontiers in Plant Science*

***Received:*** *06 November 2017*
***Accepted:*** *20 December 2017*
***Published:*** *09 January 2018*

***Citation:***
*Cheon K-S, Nakatsuka A, Tasaki K and Kobayashi N (2018) Long-lasting Corolla Cultivars in Japanese Azaleas: A Mutant AP3/DEF Homolog Identified in Traditional Azalea Cultivars from More Than 300 Years Ago. Front. Plant Sci. 8:2239. doi: 10.3389/fpls.2017.02239*

## INTRODUCTION

Species of the genus *Rhododendron* (Ericaceae), subgenus *Tsutsusi*, section *Tsutsusi* are important genetic resources for evergreen azalea cultivars used as ornamental shrubs or potted azaleas in many regions worldwide, including Asia, Europe, and America. Japan has many wild evergreen azalea species, and hundreds of azalea cultivars have been selected from natural populations of endogenous azalea species and hybrids since the Edo era (1603–1867) (Yamazaki, 1996).

A monograph on azaleas, "Kinshū-makura" (**Figure 1A**), edited in 1692, described more than 300 azalea cultivars, and several of the cultivars described in this monograph still exist and have unique flower and leaf characteristics (Ito, 1984). This monograph provided the first description of 'Misome-guruma' (**Figure 1B**), a cultivar possessing small light-red flowers, long stamens, and a long blooming season, with the flowers turning greenish in June (Ito, 1984). The 'Misome-guruma' has been defined as "Misome-shō," a long-lasting trait in Japanese, and "Misome-shō" species have been identified in several azalea cultivars. The long-lasting flower mechanisms remain largely unknown; however, the trait is characterized by a temporal color change and a long-lasting corolla (**Figures 1C–E**) that is smaller than other evergreen azaleas and may be derived from the sepaloid corolla (Kobayashi et al., 2010; Gobara et al., 2017). In genetic analysis by crossing of azaleas, normal flowers were shown from all F1 progenies between normal and long-lasting flowers, and long-lasting flowers were detected from 1/3 F2 progenies. Therefore, long-lasting flower was shown as recessive trait to normal flower and was controlled by single gene (Gobara et al., 2017).

The corolla mutant of long-lasting flowers is likely associated with the ABC model. Flower development has been studied using *Arabidopsis* and *Antirrhinum* as model plants (Coen and Meyerowitz, 1991). In these model plants, floral homeotic mutant have been described converting to other organs. Most of these mutants have been found from different mutant alleles including one or more MADS-box gene encoding putative transcription factors (Weigel and Meyerowitz, 1994). The floral homeotic MADS-box genes have been classified into three classes by different function according to ABC model (Coen and Meyerowitz, 1991; Weigel and Meyerowitz, 1994). In summary, for *Arabidopsis*, the A-class gene *APETALA1* (*AP1*) controls sepal formation in whorl 1; *AP1* and two B-class genes [*APETALA3* (*AP3*) and *PISTILLATA* (*PI*)] together control petal formation in whorl 2; the B-class genes and the C-class gene *AGAMOUS* (*AG*) together control stamen formation in whorl 3; and *AG* alone control carpel formation in whorl 4. The B-class *PI* and *AP3* proteins are functional partners and form a heterodimer for petal formation (Yang et al., 2003). A loss-of-function mutation in either *PI* or *AP3* produces sepals in two outer whorls of flowers (Jack et al., 1992). Also, in case of *Antirrhinum majus*, similar mutant phenotypes are described for mutation of the gene *GLOBOSA* (*GLO*) and/or *DEFICIENS* (*DEF*), homologs to *PI* and *AP3*, respectively (Sommer et al., 1990; Tröbner et al., 1992). In B-class gene mutants, B-class loss-of-function mutants have sepal or sepaloid petal instead of petals in the second whorl in model and horticultural plants (Sommer et al., 1990; Tröbner et al., 1992; Weigel and Meyerowitz, 1994; De Byzova et al., 2004; Vandenbussche et al., 2004; Drea et al., 2007; Hirai et al., 2010; Gong et al., 2017). In B-class genes, the natural corolla mutation of long-lasting azaleas might be associated with the *AP3/DEF* gene, as the sepaloid petals or sepals in whorl 2 were produced from artificial *ap3/def* and/or the *pi/glo* mutant (Vandenbussche et al., 2004), whereas the stamens in whorl 3 were not observed in artificial and natural *pi/glo* mutants in horticulture plants (Yao et al., 2001; Vandenbussche et al., 2004). Thus, we postulated that the long-lasting flower is due to mutation homologs of *AP3/DEF* in the azalea.

In a previous study, we isolated two full-length sequences of *PI/GLO* from *R. obtusum* (Cheon et al., 2016) and a partial length of the *AP3/DEF* homolog from *R. pulchrum* (Cheon et al., 2011) and reported that *PI/GLO* and *AP3/DEF* homologs participated in corolla development in the evergreen azaleas (Tasaki et al., 2012a; Cheon et al., 2016). In this study, to further characterize long-lasting flowers in evergreen azaleas, including *R. kaempferi* 'Nikkō-misome,' *R. macrosepalum* 'Kochō-zoroi,' *R. indicum* 'Chōjyu-hō,' and *R.* × *hannoense* 'Amagi-beni-chōjyu,' and to understand how mutant genes result in long-lasting flowers, we investigated the floral morphologies and B-class genes using the cultivars and progenies from a cross between normal and long-lasting flowers.

# MATERIALS AND METHODS

## Plant Materials

The normal-flower azaleas *R. kaempferi* (**Figure 2A**), *R. macrosepalum* (**Figure 2B**), and *R. indicum* 'Ōsakazuki' (**Figure 2C**), Kurume hybrid 'Wakakaede,' and *R. oldhamii*, the long-lasting flower azaleas *R. kaempferi* 'Nikkō-misome' (**Figures 1C**, **2D**), *R. macrosepalum* 'Kochō-zoroi' (**Figure 2E**), *R. indicum* 'Chōjyu-hō' (**Figure 2F**), and *R.* × *hannoense* 'Amagi-beni-chōjyu' (**Figure 2G**), and several progenies between normal and long-lasting flowers used in this study were obtained from the azalea resources collection of the Plant Breeding Laboratory of the Faculty of Life and Environmental Sciences of Shimane University (**Figure 1**). For the extraction of genomic DNA (gDNA) and total RNA, three leaves, ten floral buds, and five flowers were collected from plant materials. These samples were immediately frozen in liquid nitrogen and stored at −80°C until the extraction of gDNAs and total RNAs.

## Flower Morphological Investigation

The length of the corolla and the width of the corolla lobe were measured in 3–10 fully expanded flowers per individual plant (Hang et al., 2010; Gobara et al., 2017). The observation of abaxial epidermal cells was performed using a Scanning Electron Microscope (*HITACHI TM3000*) (Cheon et al., 2016). The stomatal density of abaxial surface in the corolla was determined using Suzuki's Universal Microprinting Method (*SUMP; SUMP Laboratory*) and a light microscope (*Nikon*) (Tasaki et al., 2012b). The date of flower opening and abscission was investigated in both the stock and the flower (Gobara et al., 2017).

## mRNA Analysis of *AP3/DEF* Homologs

Ten floral buds from each plant and five flowers from wild type and cultivar of *R. kaempferi* were collected and used for RNA extraction, *AP3/DEF* homolog isolation, semi-quantitative reverse transcription-PCR (semi-qRT-PCR), and RT-qPCR. Total RNA was extracted by RNeasy plant mini kit (*Qiagen*) and treated with DNase I (*Promega*) as previously described (Cheon et al., 2011). These RNA samples were subjected to semi-qRT-PCR and RT-qPCR using ReverTra-Ace (*TOYOBO*)


**FIGURE 1 |** Information of long-lasting trait in Japanese azalea. **(A,B)** Photograph of "Kinshū-makura" **(A)** and 'Misome-guruma' **(B)**, edited in 1692. **(C–E)** Flower photos of *Rhododendron kaempferi* 'Nikkō-misome' after just flowering **(C)**, approximately 50 days **(D)**, and approximately 100 days **(E)**.

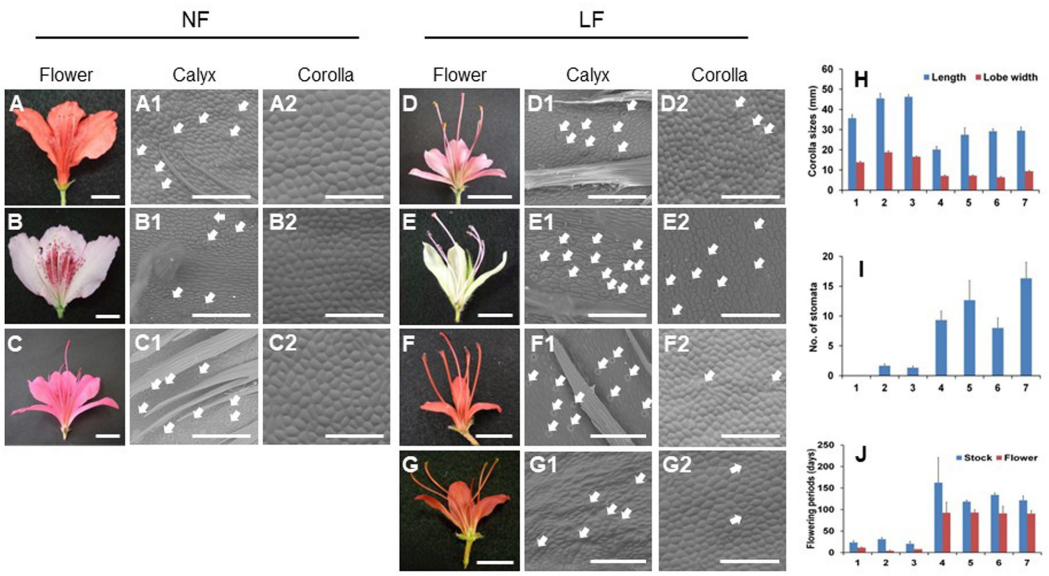


**FIGURE 2 |** Floral morphological analysis of normal (NF) and long-lasting flowers (LF). **(A–G2)** Photos of flowers **(A–G)** and abaxial epidermal cells of calyx **(A1–G1)** and corollas **(A2–G2)** in normal **(A–C)** and long-lasting flowers **(D–G)**. **(H–J)** Analyses of floral phenotypes, such as corolla sizes (mm) **(H)**, number of stomata **(I)**, and flowering periods (days) **(J)**. The bars for flowers and abaxial epidermal cells indicate 1 cm and 250 μm, respectively. Closed arrows indicate stomata. The error bars indicate the mean ± SE of three biological replicates. The following numbers indicate the azaleas cultivars; 1, *R. kaempferi* **(A–A2)**; 2, *R. macrospalum* **(B–B2)**; 3, *R. indicum* 'Ōsakazuki' **(C–C2)**; 4, *R. kaempferi* 'Nikkō-misome' **(D–D2)**; 5, *R. macrosepalum* 'Kochō-zoroi' **(E–E2)**; 6, *R. indicum* 'Chōjyu-hō' **(F–F2)**; 7, *R.* × *hannoense* 'Amagi-beni-chōjyu' **(G–G2)**.

according to the manufacturer's instructions. The *R. kaempferi* total RNA sample and the 5′-Full RACE Core Set (*TaKaRa*) was used for 5′ RACE PCR with the partial sequence of the *AP3/DEF* homolog (Cheon et al., 2011). The primers of full-length *AP3/DEF* homolog, from 5′ untranslated region (UTR) to 3′ UTR, were P1-F (TCTCTTCCTCAACCGAGATCTG) and P1-R (GGTTCTACAACATCACAAGTGC) (**Supplementary Figure S1A**). PCR analysis was used to identify the full-length *AP3/DEF* homolog in the cDNA of *R. kaempferi*. Each 10 μl reaction mixture contained 1 × Ex Taq buffer, 200 μM dNTPs, 0.2 μM of each primer, 1.25 U Ex Taq (*Takara*), and 25 ng cDNA template. The reaction conditions were as follows: preheating at 94°C for 1 min; 35 cycles of denaturation at 94°C for 30 s, annealing at 60°C for 30 s, and extension at 72°C for 30 s; and final extension at 72°C for 1 min. The fragments were cloned into the pGEM-T easy vector (*Promega*), transformed into DH5α (*Nippon gene*) and subsequently sequenced using the BigDye Terminator version 3.1 Cycle Sequencing Kit (*Applied Biosystems*) and an ABI 3130 genetic analyser (*Applied Biosystems*). The deduced amino acid sequences were aligned by the NCBI BLASTp function and Genetyx ver.10 (*Software Development Co.*).

For expression analysis, semi-qRT-PCR was performed for B-class genes. For *AP3/DEF* homolog, each 10 μl reaction mixture contained 1 × Ex Taq buffer, 200 μM dNTPs, 0.2 μM of each primer, 1.25 U Ex-Taq (*Takara*), and 2.5 ng cDNA template. The primer sets were P1-F and P1-R for set 1, P1-F and P2-R for set 2, P3-F and P3-R for set 3, P4-F and P4-R for set 4, and P5-F and P1-R for set 5 (**Supplementary Figure S1A**). The reaction conditions were as follows: preheating at 94°C for 1 min; 35 cycles of denaturation at 94°C for 10 s/30 s, annealing at 61°C or 63°C for 10 s/30 s, and extension at 72°C for 10 s/30 s; and final extension at 72°C for 1 min. Also, expression analysis of *AP3/DEF* and *PI/GLO* homologs in each floral organ was performed according to previous study (Tasaki et al., 2012a). RT-qPCR with one biological and three technical replicates was performed using the Thermal Cycler Dice Real-Time System, SYBR Premix Ex Taq II (*TaKaRa*) and primers (**Supplementary Table S1**). The housekeeping gene *ACTIN* was used to normalize the RT-qPCR output (Cheon et al., 2011).

## Genomic DNA Analysis of the *AP3/DEF* Homolog

gDNAs were extracted from the young leaves of plants using the modified CTAB method (Kobayashi et al., 1998). P-F1 and P-R1 primers were used for *AP3/DEF* homolog isolation in gDNA of *R. kaempferi*. However, because the homolog was not amplified by these primers in each long-lasting cultivar, inverse PCR (Ochman et al., 1988) was performed after digesting *R. kaempferi* gDNA with *Hin*dIII. Finally, the full-sized *AP3/DEF* homolog, including the 5′ upstream region, was isolated from the gDNAs of *R. kaempferi* and long-lasting flowers. Each 10 μl reaction mixture contained 1 × PrimeSTAR GXL buffer, 200 μM dNTPs, 0.2 μM of each primer, 1.25 U PrimeSTAR GXL DNA polymerase, and 25 ng gDNA in *R. kaempferi* or each 25 μl reaction mixture contained 50 ng gDNA template of long-lasting flowers with 5P-F1 (TTCCGACCCAACTCACATAC) and/or 5P-F2 (CGCAAGTCCCAACTCACATA), and P1-R primers. The conditions for *R. kaempferi* and long-lasting flowers were as follows: preheating at 98°C for 10 min; 30–35 cycles of denaturation at 98°C for 10 s, annealing at 60°C for 15 s, and extension at 68°C for 3–12 min; and final extension at 68°C for 15 min. The PCR products were amplified with PrimeSTAR GXL DNA polymerase (*TaKaRa*) and acquired from overhanging dA at the 3′-ends using an A-overhang mixture from the Mighty TA-cloning Reagent Set for PrimeSTAR, followed by sequencing as described above. For analysis of mutant region in azalea *AP3/DEF* sequences, *R. kaempferi* mRNA and gDNA sequences of *AP3/DEF* homologs were used as reference. After exon and intron positions of *AP3/DEF* homologs were analyzed using mRNA and gDNA sequences of *R. kaempferi*, the isolated *AP3/DEF* sequences from gDNAs of *R. kaempferi*, *R. kaempferi* 'Nikkō-misome,' *R. macrosepalum* 'Kochō-zoroi,' *R. indicum* 'Chōjyu-hō,' and *R.* × *hannoense* 'Amagi-beni-chōjyu' were aligned by Genetyx ver.10 (*Software Development Co.*). PCR analysis for mutant allele was performed using Ex-taq (*TaKaRa*) and primers (**Supplementary Table S1**).

# RESULTS

## Corolla Mutations Develop to Long-lasting Flowers

To analyze the floral phenotype of long-lasting flowers, we investigated several corolla morphologies (**Figure 2**). Each floral organ of long-lasting flowers existed in each whorl as normal flowers (**Figures 2A–G**). The abaxial epidermal cells of corollas in long-lasting flowers were smaller compared with normal flowers and were similar to the abaxial epidermal cells of calyx (**Figures 2A1–G2**). However, the length and lobe width of the corollas in long-lasting flowers were also smaller compared with normal flowers (**Figure 2H**), and a higher number of stomata were observed on the abaxial surface of the corollas in long-lasting flowers compared with normal flowers (**Figures 2A2–G2,I**). The flowering periods, which facilitate corolla maintenance after flowering, were longer in long-lasting flowers than in normal flowers (**Figure 2J**). Thus, based on these observations of floral morphologies, we confirmed that long-lasting flowers have small-sized corollas with stomata during long blooming period and that the corollas of long-lasting flowers show the conversion of normal corollas to sepaloid corollas, whereas the stamens remain unaffected.

## Isolation of *AP3/DEF* Homolog from *R. kaempferi*

We cloned the azalea *AP3/DEF* homolog using a PCR approach. Based on a partial *RpAP3* sequence, the region from MADS domain to 3′ UTRs, in previously study (Cheon et al., 2011), the 5′ UTR were further amplified by using two nested PCR primers (**Supplementary Table S1**). Ten clones containing the 5′ UTR fragments were sequenced. Subsequently, when we cloned the azalea *AP3/DEF* homolog by using a PCR approach

with a P1 primer set, two clones were detected from *R. kaempferi* (**Supplementary Figure S1A**). These cloned mRNA sequences involved a MADS-domain, a K-box, and the C-terminal region (Sommer et al., 1990); and showed 76% amino sequence identity with the DEF genes of *A. majus* (**Supplementary Figure S1B**). The putative azalea *AP3/DEF* homologs were named *RkAP3a* (approximately 824 bp, DDBJ accession number AB853117) and *RkAP3b* (approximately 826 bp, DDBJ Acc. No. AB853118), respectively.

## Abnormal Sequences of *AP3/DEF* Homologs Affected to Reduce Expression in Long-lasting Flowers

PCR analyses were carried out to investigate the mRNA structure and expression level of the azalea *AP3/DEF* and *PI/GLO* homolog in floral buds and organs (**Figure 3**). In PCR products of primer set 1, P1-F and P1-R (**Figure 3A** and **Supplementary Figure S1A**), the PCR product predicted for the full-size sequence (approximately 800-bp) was detected from all normal flowers (**Figure 3B**). However, the normal sized band was not detected from long-lasting flowers and multi-bands were detected from *R. indicum* 'Chōjyu-hō' in especially (**Figure 3B**). When we analyzed the sequences of multi bands, insertion and deletion of sequences were detected from five clones, which have 1340-, 874-, 742-, 642-, and 168-bp sizes, of *AP3/DEF* homolog in *R. indicum* 'Chōjyu-hō' (**Figure 4**). Moreover, PCR analysis was carried out to investigate why the full-sized *AP3/DEF* homolog was not amplified (**Figure 3C**). The amplified PCR product (approximately 250 bp) of primer set 2, P1-F and P2-R, was not detected from *R. macrosepalum* 'Kochō-zoroi' or *R.* × *hannoense* 'Amagi-beni-chōjyu,' and the PCR product

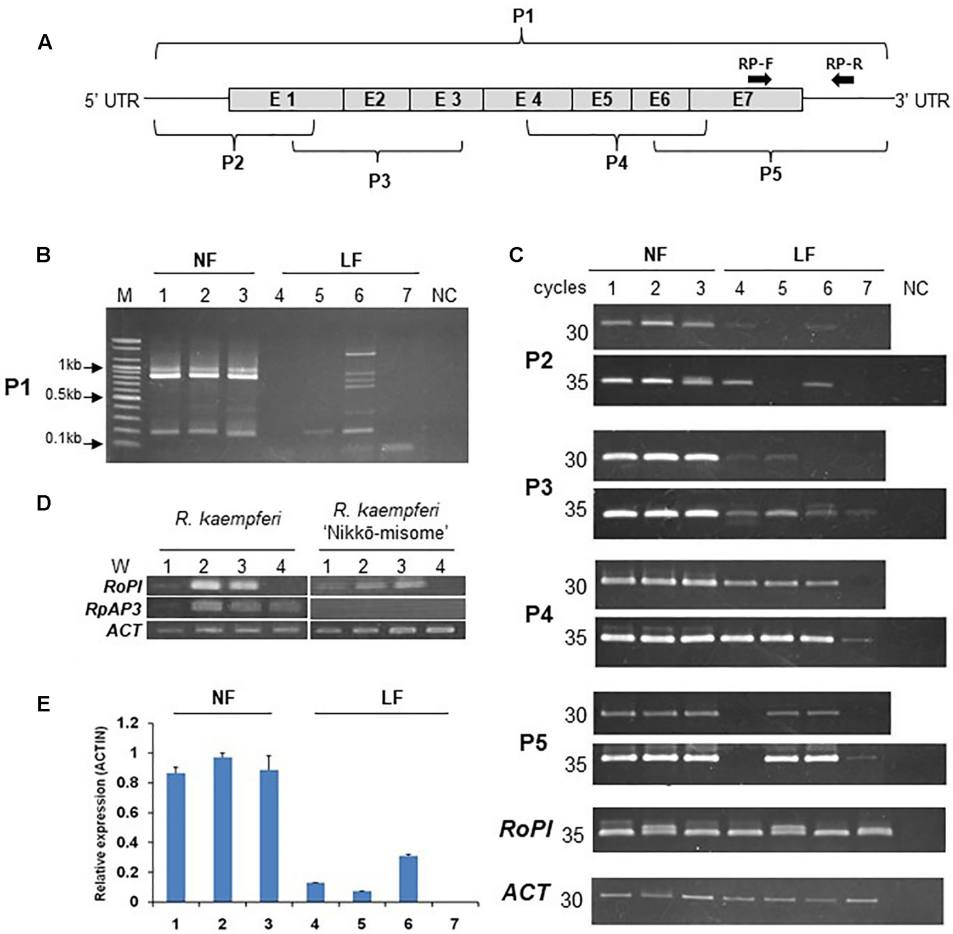


**FIGURE 3 |** Expression and structure analysis of the *AP3/DEF* homolog in the cDNA of floral buds and organs in normal (NF) and long-lasting flowers (LF). **(A)** Schematic diagram of the *AP3/DEF* homolog sequences according to **Supplementary Figure S1A**. P1–5 and RP-F and -R indicate primer set in this study. **(B,C)** Analysis of PCR amplification using semi-qRT-PCR; analysis of *AP3/DEF* homolog using P1-F and -R primer set **(B)** and other primers **(C)**. M and NC indicate 100 bp DNA ladder (*Bioneer*) and negative control, respectively. **(D)** Expression analysis of *RoPI* and *RkAP3* genes using semi-qRT-PCR in floral organs of *R. kaempferi* and its cultivar 'Nikkō-misome.' W1–4 indicate calyx, corolla, stamens, and carpels, respectively. **(E)** Expression analysis of the *AP3/DEF* homolog using RT-qPCR. The error bars indicate the mean ± SE of three technical replicates. The numbers correspond to the plant materials; normal flowers *R. kaempferi* (1), *R. macrospalum* (2), and *R. indicum* 'Ōsakazuki' (3) and long-lasting flowers *R. kaempferi* 'Nikkō-misome' (4), *R. macrosepalum* 'Kochō-zoroi' (5), *R. indicum* 'Chōjyu-hō' (6), and *R.* × *hannoense* 'Amagi-beni-chōjyu' (7).

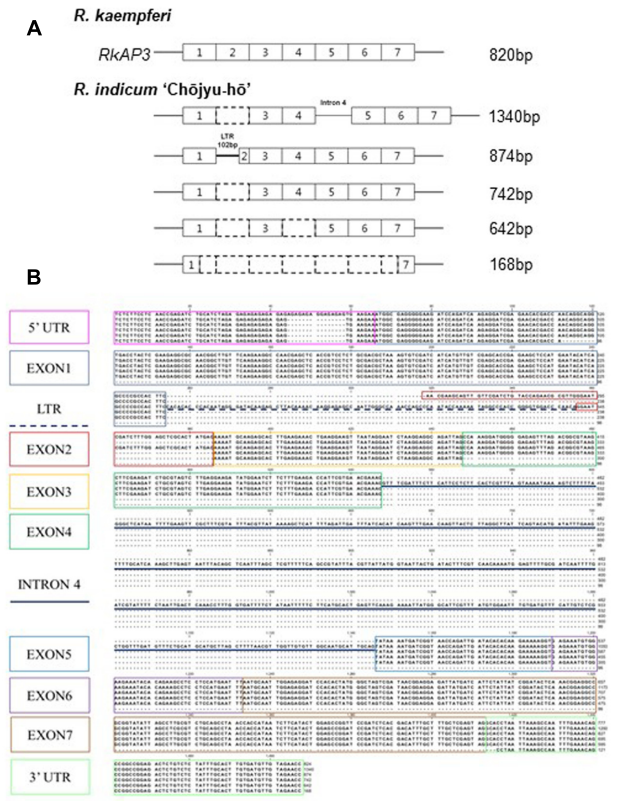


**FIGURE 4 |** Sequence analysis of the *AP3/DEF* homolog transcript variants in *R. indicum* 'Chōjyu-hō' (**Figure 3B**). **(A)** Schematic diagrams of *AP3/DEF* homolog sequences in *R. indicum* 'Chōjyu-hō.' **(B)** Sequences of transcript variants. The colored boxes indicate the region of mRNA sequences corresponding to the same color lines.

(approximately 135 bp) expression of primer set 3, P3-F and P3-R, in long-lasting flowers were lower than in normal flowers. The PCR product (approximately 260 bp) of primer set 4, P4-F and P4-R, was detected from the cDNA of floral buds in all plant materials. The PCR product (approximately 284 bp) of primer set 5, P5-F and P1-R, was not detected from *R. kaempferi* 'Nikkō-misome.' In floral organs, *PI/GLO* homolog was mainly expressed from corolla and stamen in both normal and long-lasting flowers, whereas *AP3/DEF* homolog was not expressed from all floral organs in long-lasting flowers (**Figure 3D**). In addition to semi-qRT-PCR, the results of RT-qPCR showed that the expression of the *AP3/DEF* homolog in floral buds of long-lasting cultivars was lower than that in floral buds of normal cultivars (**Figure 3E**).

## Insertion Mutation Detected in *AP3/DEF* Homolog of Long-lasting Flowers

To analyze evidence of abnormal mRNA sequences, *AP3/DEF* homologs were isolated from gDNA samples of *R. kaempferi* and all long-lasting flowers (**Figure 5**). For isolation of *AP3/DEF* homolog gDNA sequences, PCR amplifications were performed using 5P-F1, 5P-F2, and P1-R primers, which designed on 5′ upstream region in *R. kaempferi*. Approximately 3.5-, 4-, and 5-kb sized bands were detected from normal flowers, *R. macrosepalum* 'Kochō-zoroi,' and *R. indicum* 'Chōjyu-hō,' respectively, and over 10-kb sized bands were detected from *R. kaempferi* 'Nikkō-misome' and *R.* × *hannoense* 'Amagi-beni-chōjyu' (**Figure 5A**). PCR products of 5P-F1 and 5P-F2 primers were used for cloning of *AP3/DEF* homolog in *R. kaempferi*. However, PCR products of either 5P-F1 and/or 5P-F2 primers were used to analyze *AP3/DEF* gDNA sequences in long-lasting flowers, because too large-sized bands were detected from gDNAs of long-lasting flowers. The length of the *RkAP3a* and *RkAP3b* sequences, including the 5′ upstream region, seven exons, and six introns, was 3,772 (DDBJ Acc. No. AB861603) and 3,804 bp (DDBJ Acc. No. AB861604), respectively (**Supplementary Figure S1C**). The sequence analysis in long-lasting flowers predicted full-length sequences of the *AP3/DEF* homolog region from *R. kaempferi* 'Nikkō-misome,' *R. macrosepalum* 'Kochō-zoroi,' *R. indicum* 'Chōjyu-hō,' and *R.* × *hannoense* 'Amagi-beni-chōjyu' as approximately 17,102 bp (*RkAP3NM*, DDBJ Acc. No. AB861605), 4,507 bp (*RmAP3KZ*, DDBJ Acc. No. AB861606), 6,887 bp (*RiAP3CH*, DDBJ Acc. No. AB861607), and 17,070 bp (*RhAP3AC*, DDBJ Acc. No. AB861608), respectively (**Figure 5B**).

## Insertion Sequences in Azalea *AP3/DEF* Homolog Are LTR-Retrotransposon or Unknown Sequence

Inserted sequences and regions were revealed by sequence comparison among isolated sequences (**Figure 5B**). The inserted *RkAP3NM* sequence in was approximately 13,488 bp and located in exon 7. This sequence contained both 688-bp long-terminal repeats (LTRs) in the same orientation. The inset in *RhAP3AC* was approximately 13,420 bp and located in exon 1. This sequence contained both 690-bp LTRs in the same orientation. The LTR-retrotransposon in both *RkAP3NM* and *RhAP3AC* had similar sequences, but the inserted sequence in *RkAP3NM* was oriented in the opposite direction from *RhAP3AC*. In addition, the insert in *RiAP3CH* was 3,206 bp and located in exon 2. This insert contained the same 359-bp LTRs on both the left and right sides. The other insert in *RmAP3KZ* was 815 bp and located in exon 1. Although this inserted sequence did not correspond to the LTRs of *RkAP3NM* and *RiAP3CH*, the inserted sequence in *RmAP3KZ* was predicted as an LTR, reflecting the presence of TA and CA sequences, which are start and stop sequences (Kumar and Bennetzen, 1999), respectively, in other LTR-retrotransposons. Compared with part of the primer binding (PBS) site and polypurine tract (PPT) among other transposable elements (TEs) (Smyth et al., 1989; Kumekawa et al., 1999), we proposed that the TE in both *RkAP3NM* and *RhAP3AC* were *Ty1-copia* type and the TE in *RiAP3CH* was a *Ty3-gypsy* type (**Figure 5C**).

Moreover, to confirm the mutant gene status in long-lasting flowers, we searched the gDNA of long-lasting flowers using multiplex-PCR with three primers (**Figure 5B** and **Supplementary Table S1**) designed on exon and putative TE sequences. The PCR product obtained using the EP1 primer

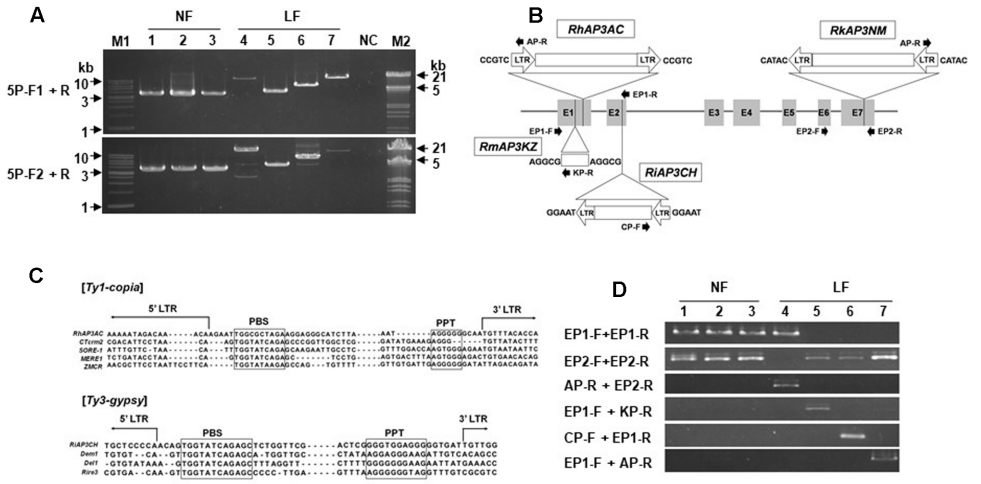


**FIGURE 5 |** The *AP3/DEF* homolog analysis in gDNA from normal (NF) and long-lasting flowers (LF). **(A)** gDNA fragments were amplified from normal and long-lasting flowers by using primers 5P-F1, 5P-F2, and P1-R. M1, M2, and NC indicate hyperladder1 kb (*Bioline*) and lambda DNA/*Eco*RI+*Hin*dIII conventional DNA digest marker (*Promega*), and negative control, respectively. **(B)** Schematic diagram of the structures of the *AP3/DEF* homolog in long-lasting flowers. E1–7 and lines indicate each exon and each intron, respectively. The open arrows and boxes indicate insertions of TEs. The five nucleotides indicate TSD sequences. The closed arrows indicate primers for TE analysis. **(C)** Comparison among the sequences of LTR-retrotransposons. The boxes indicate the sequences of the PBS and PPT regions. The names of LTR-retrotransposons included *RhAP3AC*, *Rhododendron* × *hannoense* 'Amagi-beni-chōjyu'; *CTerm2*, *Malus* × *domestica*; *SORE-1*, *Glycine max*; *MERE1*, *Medicago truncatula*; *ZMCR*, *Zea mays*; *RiAP3CH*, *R. indicum* 'Chōjyu-hō'; *Dem1*, *Malus* × *domestica*; *Del1*, *Lilium henryi*; and *Rire3*, *Oryza sativa*. **(D)** PCR analysis for TE confirmation. Normal flowers *R. kaempferi* (1), *R. macrospalum* (2), and *R. indicum* 'Ōsakazuki' (3) and long-lasting flowers *R. kaempferi* 'Nikkō-misome' (4), *R. macrosepalum* 'Kochō-zoroi' (5), *R. indicum* 'Chōjyu-hō' (6), and *R.* × *hannoense* 'Amagi-beni-chōjyu' (7).

set was amplified in normal and *RkAP3NM* samples, and the PCR product obtained using the EP2 primer set was amplified from all of the samples, except *RkAP3NM*. In addition, the PCR products of the other primer sets were amplified from each region containing a TE insertion (**Figure 5D**). The long-lasting flower contained the mutant gene, but not the normal gene, suggesting that the TE insertion likely leads to long-lasting flowers and that the long-lasting flowers likely carry homozygous mutant genes.

## Long-lasting Mutant Was Caused by *ap3/def* Alleles

To determine whether the mutant allele is essential for long-lasting flowers, we investigated floral phenotypes and genotypes using cultivars ($n = 4$) and individual progenies ($n = 12$) through multiplex-PCR with three primers (**Supplementary Table S1**) that were used to distinguish each *ap3/def* mutant allele in evergreen azaleas based on differences in the TE insertion regions (**Figure 6**). All of the F1 progenies resulting from the cross between normal and long-lasting flowers showed normal flowers, whereas F2 progenies showed normal and long-lasting flowers (**Figures 6A–C**). Consistent with the observed phenotypes, normal genes were detected in all of the F1 progenies and one F2 progeny, and only mutant alleles, both *RiAP3CH* and *RmAP3KZ*, were detected from the two F2 progenies with long-lasting flowers, whereas normal and mutant genes, *RiAP3CH* or *RmAP3KZ*, were detected from the F2 progenies with normal flowers (**Figure 6D**). As heterozygous alleles, combination of normal and mutant flowers, in F1 and F2 leads to normal flower development and the homozygous mutant alleles permit long-lasting flower development in F2, we concluded that long-lasting flowers are conferred through homozygous *ap3/def* mutant alleles.

# DISCUSSION

Our investigation of floral morphology and molecular characters in long-lasting flowers showed that the characteristics of evergreen azaleas with flowers, including long-lasting, small-sized, and sepaloid corollas, are unique to these species and are rarely found in other horticultural plants.

We have shown that azalea *AP3/DEF* homolog has functions similar to those of *Antirrhinum DEF* gene in regulation of long-lasting flower development (Schwarz-Sommer et al., 1992). The *Antirrhinum def* mutants have several phenotypes as *chlorantha* and *nicotianoides* flowers that are smaller and their petals show green color indicating sepaloid features. In addition, *gloifera* petals are morphologically indistinguishable from sepals, except that these sepaloid whorl 2 organs are larger than sepals in the whorl 1 and that their position in the mature mutant flower resembles the position of wild type petals of the upper and lower lobes. In analysis of *Antirrhinum GLO* and *DEF* expressions, *DEF* gene is lowly expressed than *GLO* gene expression in *chlorantha* and *nicotianoides* flowers, both genes were not detected from *gloifera* flower buds (Sommer et al., 1990; Schwarz-Sommer et al., 1992; Tröbner et al., 1992). In other plants, an investigation of the relationship between the observed phenotype and *PhDEF* gene expression

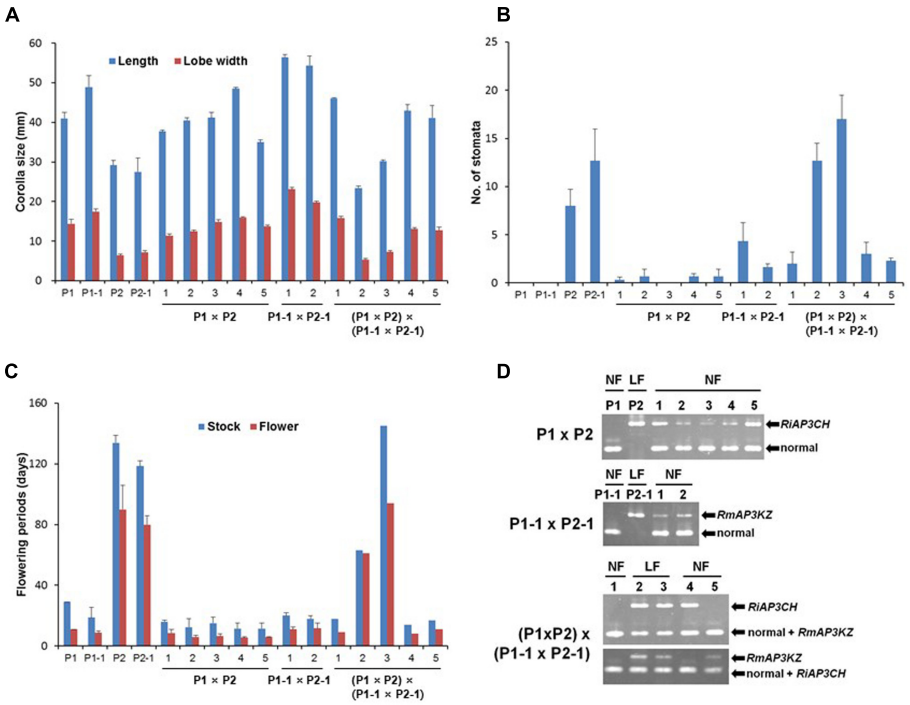


**FIGURE 6 |** Investigation of floral morphology and mutant gene in progenies resulting from a cross between normal (NF) and long-lasting flowers (LF). **(A–C)** Analysis of floral morphology, such as corolla sizes (mm) **(A)**, number of stomata **(B)**, and flowering periods (days) **(C)**. **(D)** Mutant allele analysis using PCR and mutant gene-specific primers (**Supplementary Table S1**). P1, Kurume hybrid 'Wakakaede'; P1-1, *R. oldhamii*; P2, *R. indicum* 'Chōjyu-hō'; P2-1, *R. macroseplaum* 'Kochō-zoroi'; F1, P1 × P2; F1-1, P1-1 × P2-1; F2, (P1 × P2) × (P1-1 × P2-1).

in the *Petunia hybrid* artificial *phdef* mutants showed that the corolla was converted to sepals in the whorl 2, where *PhDEF* gene expression was found to be significantly reduced (Vandenbussche et al., 2004). When *AP3* homolog expression is repressed in oilseed rape (*Brassica napus*) and poppies (*Papaver somniferum*) flower mutants, petals of the transformed plants are converted to sepaloid petals, which are smaller than normal petals; furthermore, in these mutant plants, stomata grow from the sepaloid petal in the same manner as the sepal (De Byzova et al., 2004; Drea et al., 2007). Also, Hirai et al. (2010) suggested that the reduced expressions of *TGDEFA* and *TGDEFB* are associated in the floral development of the viridiflora tulip ('White Dream' and 'Spring Green'), which is partially composed of sepaloid tepals in the first and second whorl. As case of herbaceous peony (*Paeonia lactiflora*), spontaneous corolla mutant in natural condition was closely associated with selective expression alterations of duplicated *AP3* and *PI* genes, because down-regulation of duplicated B-class genes might result in reduction of *AP3-PI* heterodimer in sepaloid corolla (Gong et al., 2017). Although phenotype is different, *Malus* × *domestica PI* (*MdPI*) mutant, which inserted retrotransposon in natural condition, was weakly expressed in mutant plant; some apples produce parthenocarpic fruit, resulting in LTR-retrotransposon insertion in the *MdPI* MADS transcription factor; Intron 4 of *MdPI* has insertions in 'Rae Ime,' and intron 6 has insertions in 'Spencer Seedless' and 'Wellington Bloomless.' In these mutant cultivars, flowers have no petals or stamens but two whorls of five sepals and an increased number of styles and carpels (Yao et al., 2001), due to insertion into the common MADS transcription factor. In this study, long-lasting flowers have functional stamens (**Figure 6**) and azalea *AP3/DEF* homolog was expressed in floral buds of plant materials, except *R.* × *hannoense* 'Amagi-beni-chojyu' in RT-qPCR, but results of semi-qRT-PCR and sequence analysis indicated that the abnormal mRNA sequence of azalea *AP3/DEF* exist in floral buds of all long-lasting cultivars (**Figures 3**, **4**). Moreover, TE or unknown sequences were detected from gDNA sequences in *AP3/DEF* homologs of long-lasting flowers (**Figure 5**). Thus, the loss-of-function of the *AP3/DEF* homolog in long-lasting flowers were caused by the insertion of a retrotransposon or putative LTR sequence, and these inserted sequences might be affected by mRNA splicing of the *AP3/DEF* homolog in long-lasting flowers, because gene expression or the structure encoded proteins can be occurred by mutations due to TE insertions in or near genes (Kumar and Bennetzen, 1999; Lisch, 2013).

The original species of four long-lasting flowers were distributed at different site and the original species have been recorded since 17th century in Japan (Ito, 1984; Yamazaki, 1996). The geographic origin of the azalea species indicates the possibility of independent events of mutation, because azalea cultivars were selected from natural hybrid population and the selected cultivars have been propagated by cutting (Kobayashi, 2013). We have

analyzed azalea *AP3/DEF* gDNA sequences of four flower mutants and found insertions in all four cultivars; 'Nikkō-misome' and 'Amagi-beni-chōjyu' have the nearly same insertion sequence in exon 7 and exon 1, respectively, but 'Kochō-zoroi' and 'Chōjyu-hō' have different insertion sequence in exon 1 and exon 2, respectively (**Figure 5B**). The different TE insertion regions at same gene are good evidence that *ap3/def* mutant is included in the development of long-lasting flower in these azaleas. In addition, when we analyzed normal and mutant alleles from individual azalea cultivars and its progenies, the non-functional *AP3/DEF* mutant gene was detected from long-lasting flowers but normal allele was not detected (**Figures 5D**, **6**). The results corresponded to petal loss plant in apetalous mutant of Nigella; the mutant was recessive trait that indeed caused by the TE insertion in *AP3-3* gene, and the non-functional *AP3-3* gene was existed as homozygous for petal loss (Zhang et al., 2013). In previous study of azalea, long-lasting flower was shown as recessive trait to normal corollas and was controlled by single gene (Gobara et al., 2017). From this, the results of mutant allele investigation in cultivars and progenies suggest that whereas all long-lasting flowers are homozygous for the *ap3/def* mutant alleles, normal flowers are either heterozygous (normal allele/mutant allele) or homozygous (normal alleles). Despite the phenotypic similarity of *Antirrhinum def* mutants (Sommer et al., 1990), it is still difficult to conclude that azalea *AP3/DEF* homolog was participated to long-lasting flower development. A difference between azalea *ap/def* homolog and *Antirrhinum DEF* mutants is that the azalea long-lasting flowers produce corollas, which have long maintenance period. Phenotypic and molecular evidence show that corollas in long-lasting flowers are related to mutations in azalea mutant allele. The corolla persisting period of long-lasting flower after flowering was long, approximately 100 days (**Figures 1C–E**, **2J**,**6C**). When we analyzed normal and mutant allele from individual azalea cultivars and its progenies, the non-functional azalea *ap3/def* mutant allele was detected from long-lasting flowers but normal allele was not detected (**Figures 5D**, **6D**). The sepaloid corolla of long-lasting flowers may affect flower longevity, because the period of sepal persisting is longer than the period of petal persisting after flowering in evergreen azaleas. Although the maintenance of *PeMADS6*, which might have the function of *GLO/PI*-like genes in *Phalaenopsis* in orchids, transcripts in flower through flowering to senescence corresponds to the long-lasting flower longevity in orchids; transgenic plants overexpressing *PeMADS6* or *PI*, respectively, had a 3.4- or 2.1-fold higher flower longevity than wild-type *Arabidopsis* plants (Tsai et al., 2005), the relationship of *AP3/DEF*-like gene and flower longevity has not been reported. Thus, the results in this study showed that the long-lasting flower would be derived from the sepaloid corolla in long-lasting flowers and would be caused by a mutation of the *AP3/DEF* homolog, although more experiments are needed to clarify mechanism of long flower longevity.

The flower quality of the current long-lasting flowers is a desirable trait (Kobayashi et al., 2010; Kobayashi, 2013). To breed long-lasting trait into commercial azalea cultivars, azalea breeding have attempted. However, the breeding process is slow when traditional crossing methods are used in wood plants because of the long juvenile period required. With the identification of the *AP3/DEF* homolog sequence, genetic transformation could be used to generate high-quality, long-lasting flowers by the down-regulation of *AP3/DEF* homolog expression using RNAi techniques together with transgenic systems developed for azalea cultivars. This study firstly revealed LTR-retrotransposons in azalea cultivars and the TEs into *AP3/DEF* homolog may also be used as a gene base marker for the selection of the long-lasting trait at the juvenile period in evergreen azalea breeding. Collectively, our results increase the current understanding of long-lasting flowers. With regard to the nature of the mutation at azalea *AP3/DEF* homolog, this naturally occurring TE-induced phenotypic change may be especially important for variety flower in horticultural plants, as it affects an essential trait for adaptive plant evolution. From more than 300 years ago, unique mutant flowers have been collected from natural population, reflecting the natural selection and maintenance of TE-induced mutant flowers, and Japanese people have been enjoyed mutant flowers as ornamental plant.

## AUTHOR CONTRIBUTIONS

Experimental design: NK, AN, and K-SC. Experiments: K-SC and KT. Data analysis: K-SC, AN, and KT. Manuscript preparation: K-SC, KT, AN, and NK. Supervision, funding, and reagents: NK and AN.

## FUNDING

This study was financially supported through a Grant-in-Aid for Scientific Research (KAKENHI Nos. 23241076 and 26292017) from the Japan Society for the Promotion of Science (JSPS).

## SUPPLEMENTARY MATERIAL

The Supplementary Material for this article can be found online at: https://www.frontiersin.org/articles/10.3389/fpls.2017.02239/full#supplementary-material

**FIGURE S1 |** Sequence and structure information for *RkAP3a* and *RkAP3b*. **(A)** The cDNA sequences of *RkAP3a* and *RkAP3b* isolated from *R. kaempferi* are shown in the top and bottom lines, respectively. The dots and boxes indicate sequence identity and different sequences between *RkAP3a* and *RkAP3b* mRNA sequences, respectively. The M and asterisk indicate the start and stop codons, respectively. Primers and directions are indicated with horizontal arrows. The intron positions are indicated with vertical arrows. **(B)** Comparison of the amino acids among AP3, DEF, RkAP3a, and RkAP3b. The box indicates the amino acid sequence of the euAP3 motif. **(C)** The gDNA structure of *RkAP3a* and *RkAP3b*. Dotted lines, bold lines, thin lines, and gray boxes indicate the 5′ upstream region, 5′ and 3′ UTR, introns, and exons, respectively.

**TABLE S1 |** Primers used for the sequence and mutant gene analysis in normal and long-lasting flower types.

## REFERENCES


Cheon, K.-S., Nakatsuka, A., and Kobayashi, N. (2011). Isolation and expression pattern of genes related to flower initiation in the evergreen azalea, *Rhododendron* × *pulchrum* 'Oomurasaki'. *Sci. Hortic.* 130, 906–912. doi: 10.1016/j.scienta.2011.09.001

Cheon, K.-S., Nakatsuka, A., and Kobayashi, N. (2016). Mutant *PI/GLO* homolog confers the hose-in-hose flower phenotype in Kurume azaleas. *Hort. J.* 85, 380–387. doi: 10.2503/hortj.MI-138

Coen, E. S., and Meyerowitz, E. M. (1991). The war of the whorls: genetic interactions controlling flower development. *Nature* 353, 31–37. doi: 10.1038/353031a0

De Byzova, M., Verduyn, C., De Brouwer, D., and De Block, M. (2004). Transforming petals into sepaloid organs in *Arabidopsis* and oilseed rape: implementation of the hairpin RNA-mediated gene silencing technology in an organ-specific manner. *Planta* 218, 379–387. doi: 10.1007/s00425-003-1117-1

Drea, S., Hileman, L. C., De Martino, G., and Irish, V. F. (2007). Functional analyses of genetic pathways controlling petal specification in poppy. *Development* 134, 4157–4166. doi: 10.1242/dev.013136

Gobara, Y., Nakatska, A., Cheon, K.-S., and Kobayashi, N. (2017). Floral morphology and inheritance of the long-lasting flower trait (misome-sho) in Japanese evergreen azalea cultivars. *Hort. Res.* 16, 383–390. doi: 10.2503/hrj.16.383

Gong, P., Ao, X., Liu, G., Cheng, F., and He, C. (2017). Duplication and whorl-specific down-regulation of the obligate AP3–PI heterodimer genes explain the origin of *Paeonia lactiflora* plants with spontaneous corolla mutation. *Plant Cell Physiol.* 58, 411–425. doi: 10.1093/pcp/pcw204

Hang, N. T. T., Miyajima, I., Ureshino, K., Masuda, J.-I., and Okubo, H. (2010). Comparison of morphological characteristics of *Rhododendron simsii* planch. Distributed in Vietnam and Japan. *J. Fac. Agric. Kyushu Univ.* 55, 233–237.

Hirai, M., Ochiai, T., and Kanno, A. (2010). The expression of two *DEFICIENS*-like genes was reduced in the sepaloid tepals of viridiflora tulips. *Breed. Sci.* 60, 110–120. doi: 10.1270/jsbbs.60.110

Ito, I. (1984). *A Brocade Pillow: Azaleas of Old Japan*. New York, NY: Weatherhill, Inc.

Jack, T., Brockman, L. L., and Meyerowitz, E. M. (1992). The homeotic gene *APETALA3* of *Arabidopsis thaliana* encodes a MADS box and is expressed in petals and stamens. *Cell* 68, 683–697. doi: 10.1016/0092-8674(92)90144-2

Kobayashi, N. (2013). Evaluation and application of evergreen azalea resources of Japan. *Acta Hortic.* 990, 213–219. doi: 10.17660/ActaHortic.2013.990.24

Kobayashi, N., Horikoshi, T., Katsuyama, H., Handa, T., and Takayanagi, K. (1998). A simple and efficient DNA extraction method for plants, especially woody plants. *Plant Tissue Cult. Biotechnol.* 4, 76–80.

Kobayashi, N., Ishihara, M., Ohtani, M., Nakatsuka, A., Cheon, K. S., Mizuta, D., et al. (2010). Evaluation and application of the long-lasting flower trait (Misome-sho) of azalea cultivars. *Acta Hortic.* 855, 165–168. doi: 10.17660/ActaHortic.2010.855.23

Kumar, A., and Bennetzen, J. L. (1999). Plant retrotransposons. *Annu. Rev. Genet.* 33, 479–532. doi: 10.1146/annurev.genet.33.1.479

Kumekawa, N., Ohtsubo, H., Horiuchi, T., and Ohtsubo, E. (1999). Identification and characterization of novel retrotransposons of the *gypsy* type in rice. *Mol. Gen. Genet.* 260, 593–602. doi: 10.1007/s004380050933

Lisch, D. (2013). How important are transposons for plant evolution? *Nat. Rev. Genet.* 14, 49–61. doi: 10.1038/nrg3374

Ochman, H., Gerber, A. S., and Hart, D. L. (1988). Genetic applications of an inverse polymerase chain reaction. *Genetics* 120, 621–623.

Schwarz-Sommer, Z., Hue, I., Huijser, P., Flor, P. J., Hansen, R., Tetens, F., et al. (1992). Characterization of the *Antirrhinum* floral homeotic MADS-box gene deficiens: evidence for DNA binding and autoregulation of its persistent expression throughout flower development. *EMBO J.* 11, 251–263.

Smyth, D. R., Kalitsis, P., Joseph, J. L., and Sentry, J. W. (1989). Plant retrotransposon from *Lilium henryi* is related to *Ty3* of yeast and the gypsy group of *Drosophila*. *Proc. Natl. Acad. Sci. U.S.A.* 86, 5015–5019. doi: 10.1073/pnas.86.13.5015

Sommer, H., Beltrán, J. P., Huijser, P., Pape, H., Lönnig, W. E., Saedler, H., et al. (1990). *Deficiens*, a homeotic gene involved in the control of flower morphogenesis in *Antirrhinum majus*: the protein shows homology to transcription factors. *EMBO J.* 9, 605–613.

Tasaki, K., Nakatsuka, A., Cheon, K.-S., Koga, M., and Kobayashi, N. (2012a). Morphological and expression analyses of MADS genes in Japanese traditional narrow- and/or staminoid-petaled cultivars of *Rhododendron kaempferi* planch. *Sci. Hortic.* 134, 191–199. doi: 10.1016/j.scienta.2011.11.013

Tasaki, K., Nakatsuka, A., and Kobayashi, N. (2012b). Morphological analysis of narrow-petaled cultivars of *Rhododendron macrosepalum* maxim. *J. Japan. Soc. Hortic. Sci.* 81, 72–79. doi: 10.2503/jjshs1.81.72

Tröbner, W., Ramirez, L., Motte, P., Hue, I., Huijser, P., Lönnig, W. E., et al. (1992). *GLOBOSA*: a homeotic gene which interacts with *DEFICIENS* in the control of *Antirrhinum* floral organogenesis. *EMBO J.* 11, 4693–4704.

Tsai, W. C., Lee, P. F., Chen, H. I., Hsiao, Y. Y., Wei, W. J., Pan, Z. J., et al. (2005). *PeMADS6*, a *GLOBOSA/PISTILLATA*-like gene in *Phalaenopsis equestris* involved in petaloid formation, and correlated with flower longevity and ovary development. *Plant Cell Physiol.* 46, 1125–1139. doi: 10.1093/pcp/pci125

Vandenbussche, M., Zethof, J., Royaert, S., Weterings, K., and Gerats, T. (2004). The duplicated B-class heterodimer model: whorl-specific effects and complex genetic interactions in *Petunia hybrida* flower development. *Plant Cell* 16, 741–754. doi: 10.1105/tpc.019166

Weigel, D., and Meyerowitz, E. M. (1994). The ABCs of floral homeotic genes. *Cell* 78, 203–209. doi: 10.1016/0092-8674(94)90291-7

Yamazaki, T. (1996). *A Revision of the Genus Rhododendron in Japan, Taiwan, Korea, and Sakhalin*. Tokyo: Tsumura Laboratory.

Yang, Y., Fanning, L., and Jack, T. (2003). The K domain mediates heterodimerization of the *Arabidopsis* floral organ identity proteins, APETALA3 and PISTILLATA. *Plant J.* 33, 47–59. doi: 10.1046/j.0960-7412.2003.01473.x

Yao, J.-L., Dong, Y.-H., and Morris, B. A. M. (2001). Parthenocarpic apple fruit production conferred by transposon insertion mutations in a MADS-box transcription factor. *Proc. Natl. Acad. Sci. U.S.A.* 98, 1306–1311. doi: 10.1073/pnas.98.3.1306

Zhang, R., Guo, C., Zhang, W., Wang, P., Li, L., Duan, X., et al. (2013). Disruption of the petal identity gene *APETALA3-3* is highly correlated with loss of petals within the buttercup family (Ranunculaceae). *Proc. Natl. Acad. Sci. U.S.A.* 110, 5074–5079. doi: 10.1073/pnas.1219690110


**Conflict of Interest Statement:** The authors declare that the research was conducted in the absence of any commercial or financial relationships that could be construed as a potential conflict of interest.

frontiers in Plant Science

ORIGINAL RESEARCH
published: 15 August 2018
doi: 10.3389/fpls.2018.01008

# Genetic Analysis of Floral Symmetry Transition in African Violet Suggests the Involvement of Trans-acting Factor for *CYCLOIDEA* Expression Shifts

*Hui-Ju Hsu*[1†], *Cheng-Wen He*[1†], *Wen-Hsi Kuo*[1†], *Kuan-Ting Hsin*[1†], *Jing-Yi Lu*[2], *Zhao-Jun Pan*[2†] *and Chun-Neng Wang*[1,2*]

[1] *Institute of Ecology and Evolutionary Biology, National Taiwan University, Taipei, Taiwan,* [2] *Department of Life Science, National Taiwan University, Taipei, Taiwan*

OPEN ACCESS

**Edited by:**
*Swee-Suak Ko,*
*Academia Sinica, Taiwan*

**Reviewed by:**
*Maria Manuela Ribeiro Costa,*
*University of Minho, Portugal*
*Xianzhong Feng,*
*Northeast Institute of Geography and Agroecology (CAS), China*

***Correspondence:**
*Chun-Neng Wang*
*leafy@ntu.edu.tw*

[†]*These authors have contributed equally to this work*

**Specialty section:**
*This article was submitted to Plant Evolution and Development, a section of the journal Frontiers in Plant Science*

**Received:** *10 April 2018*
**Accepted:** *21 June 2018*
**Published:** *15 August 2018*

**Citation:**
*Hsu H-J, He C-W, Kuo W-H, Hsin K-T, Lu J-Y, Pan Z-J and Wang C-N (2018) Genetic Analysis of Floral Symmetry Transition in African Violet Suggests the Involvement of Trans-acting Factor for CYCLOIDEA Expression Shifts. Front. Plant Sci. 9:1008. doi: 10.3389/fpls.2018.01008*

With the growing demand for its ornamental uses, the African violet (*Saintpaulia ionantha*) has been popular owing to its variations in color, shape and its rapid responses to artificial selection. Wild type African violet (WT) is characterized by flowers with bilateral symmetry yet reversals showing radially symmetrical flowers such as dorsalized actinomorphic (DA) and ventralized actinomorphic (VA) peloria are common. Genetic crosses among WT, DA, and VA revealed that these floral symmetry transitions are likely to be controlled by three alleles at a single locus in which the levels of dominance are in a hierarchical fashion. To investigate whether the floral symmetry gene was responsible for these reversals, orthologs of *CYCLOIDEA* (*CYC*) were isolated and their expressions correlated to floral symmetry transitions. Quantitative RT-PCR and *in situ* results indicated that dorsal-specific *SiCYC1s* expression in WT *S. ionantha* (*SCYC1A* and *SiCYC1B*) shifted in DA with a heterotopically extended expression to all petals, but in VA, *SiCYC1s'* dorsally specific expressions were greatly reduced. Selection signature analysis revealed that the major high-expressed copy of *SCYC1A* had been constrained under purifying selection, whereas the low-expressed helper *SiCYC1B* appeared to be relaxed under purifying selection after the duplication into *SCYC1A* and *SiCYC1B*. Heterologous expression of *SCYC1A* in *Arabdiopsis* showed petal growth retardation which was attributed to limited cell proliferation. While expression shifts of *SCYC1A* and *SiCYC1B* correlate perfectly to the resulting symmetry phenotype transitions in F1s of WT and DA, there is no certain allelic combination of inherited *SiCYC1s* associated with specific symmetry phenotypes. This floral transition indicates that although the expression shifts of *SCYC1A/1B* are responsible for the two contrasting actinomorphic reversals in African violet, they are likely to be controlled by upstream trans-acting factors or epigenetic regulations.

**Keywords: *CYCLOIDEA*, *Saintpaulia ionantha*, zygomorphy, actinomorphy, *RADIALIS*, genotype–phenotype association, gene duplication, bilateral symmetry**

## INTRODUCTION

Variation in floral symmetry in horticultural species provides a great opportunity to study the molecular genetics of floral symmetry transition. Peloric mutations, the acquisition of actinomorphy (radial symmetry) by zygomorphic (with dorsiventral asymmetry) plants, have provided precious opportunities to examine the developmental genetics of floral symmetry transition. The African violet, *Saintpaulia ionantha* (Gesneriaceae), is ancestrally zygomorphic with a long cultivation history and is also famous for a great variety of reversion to actinomorphy cultivars. The zygomorphic wild type (WT) of *S ionantha* ssp. *velutina* (B.L. Burtt) I. Darbysh has flowers with two dorsal (adaxial) petals (dp) smaller than the three petals in lateral (lp) and ventral (abaxial) (vp) positions, (**Figures 1B,K**). It has only two stamens (positioned abaxially), while the adaxial and lateral stamens have been reduced to staminodes. One peloric (actinomorphic) cultivar *S. ionantha* ssp. *velutina* "little rick" (**Figure 1C**) of African violet arose in cultivation during the early 1950s as a single gene recessive (Reed, 1961). This peloric form differs from WT in having all five petals identical in shape and size, and all five stamens are fully functional (although the dorsal and lateral stamens are marginally smaller than the ventral ones) (**Figure 1F**). All five petals in this peloric form are mostly similar to the ventral petals of the wild type, and thus the peloric flowers appear to have lost their dorsal identity or acquired ventral identity (abbreviated as VA, ventralized actinomorphy, hereafter). Recently in flower markets, another peloric cultivar *S. ionantha* ssp. *gortei* (Engl.) I. Darbysh."no stamen" has begun to grow in popularity owing to its numerous small-sized flowers and fused petals which form a somewhat unusually tubular corolla in a fully upright actinomorphy (**Figure 1A**). Interestingly, this peloria has all stamens aborted in mature flowers but it exists in cultivation as African violets can be easily propagated through leaf cuttings. This peloric cultivar differs from WT and VA in having all five petals similar to the small-sized dorsal petals of WT. "no stamen" is therefore a dramatically different peloria of African violet with dorsalized actinomorphy (abbreviated as DA, hereafter). With these cultivars, we can explore the flexibility of genetic control on floral symmetry transitions exerted by artificial selection.

The rise of two different peloric phenotypes, DA and VA, from the zygomorphic WT implies that the genes controlling dorsal and ventral identity may have been involved. In *Antirrhinum majus* (Snapdragon) and other zygomorphic flowering plants, *CYCLOIDEA* (*CYC*) gene is necessary to establish the dorsiventral flower axis (Luo et al., 1996, 1999). This *CYC* has been known to regulate cell proliferation (cell division) and cell expansion (Costa et al., 2005). In *Antirrhinum*, *CYC* is restricted to express in the dorsal part of the flower and is therefore responsible for the growth promotion of dorsal petals and growth retardation of the dorsal staminode (Luo et al., 1996; Clark and Coen, 2002). DICHOTOMA (*DICH*) is also expressed in the dorsal part of the flower, but its expression is largely confined to the inner half of each dorsal petal (Luo et al., 1999). Mutant phenotypes of *DICH*, therefore, only have slightly altered dorsal petal shape. This indicates that *CYC* has a stronger effect on altering dorsal petal morphology than *DICH* does. Mutation of both *CYC/DICH* results in actinomorphy, in which all petals switch to ventral identity (Coen and Nugent, 1994; Luo et al., 1996).

Floral symmetry transition has independently evolved among major angiosperm lineages and has been demonstrated to correlate with the shifts of *CYC* expression (Rosin and Kramer, 2009; reviewed in Busch and Zachgo, 2009; Hileman, 2014a). Most common mechanisms for floral symmetry transitions could be summarized into the spatial and temporal shifts in *CYC* expression (Spencer and Kim, 2018). Similar to *Antirrhinum,* reversals to actinomorphy attributable to a loss of dorsal-specific or asymmetrical expression of *CYC* were reported in *Tradescantia* (Commelinaceae, monocot, Preston and Hileman, 2012), in three Oleaceae species (early diverging Lamiales, Zhong and Kellogg, 2015), in two pollinator shifting Malpighiaceae lineages (Zhang et al., 2013), in *Lotus japonicas* double mutant (Fabaceae, Feng et al., 2006), and in tubular mutants of sunflower (Asteraceae, Chapman et al., 2012). In these cases, they are ventralized as all petals acquired ventral identity attributable to the loss of dorsal-specific *CYC*. On the other hand, reversals into DA attributable to the extension of *CYC* expression into all petals to acquire dorsal identity has been reported in *Cadia* (Fabaceae, Citerne et al., 2006), in two parallel Malpighiaceae lineages (Zhang et al., 2013), in petal-indistinct wind pollinated *Plantago lanceolata* (Reardon et al., 2009; Plantaginaceae, Preston et al., 2011), and in radially symmetrical Viburnum (Dipsacles, Howarth et al., 2011). The existence of both DA and VA in many angiosperm lineages indicates that the regulation of *CYC* can be very diverse.

Among Gesneriaceae species, reversals to actinomorphy from dorsalization and ventralization have both been described. Ventralized actinomorphy (VA) attributable to mutated *CYC* or loss of expression of *CYC* in the late petal development stage has been reported in *Sinningia speciosa*, and *Bournea* (Zhou et al., 2008; Hsu et al., 2015, 2017). On the other hand, DA has been reported in *Tengia* and occasionally in *Petrocosmea* hybrids in which *CYC* expression has extended to all petals (Pang et al., 2010; Yang et al., 2015).

It is worth mentioning that temporal (heterochronic) changes of *CYC* expression also trigger floral symmetry transition. The transient only dorsal expression of *TCP1* (*CYC*) in the early floral meristem stage, yet not persisting into later organogenesis stages, make it unable to trigger *Arabidopsis* and *Bournea* to develop zygomorphy (Cubas et al., 2001; Zhou et al., 2008). Another genetic mechanism involved in creating a peloric phenotype is epigenetic silencing caused by gene methylation. In the peloric form of *Linaria vulgaris* (toadflax), there were no *CYC* mRNA transcripts that could be detected in the flower (Cubas et al., 1999b), attributable to hyper-methylation of the gene. If this is the situation in African violet, we would expect an entire loss of *CYC* expression in flower buds.

Möller et al. (1999) first isolated partial *CYC* homologs from several Gesneriaceae species. In *Saintpaulia*, the *CYC* homologs exist as a pair of recently duplicated *CYC* paralogs (*SiCYC1A*, *SiCYC1B*) and both are direct orthologs

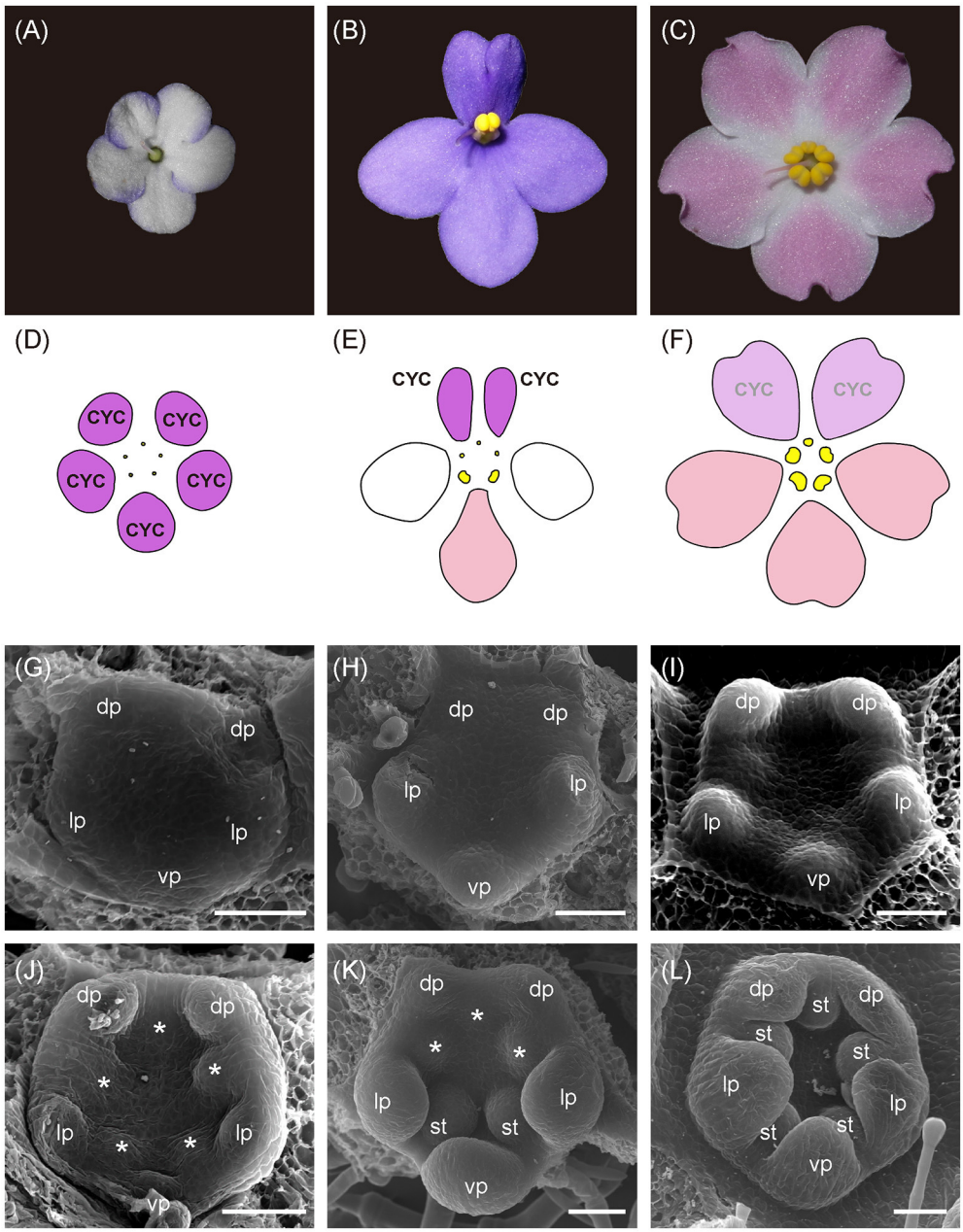


**FIGURE 1 |** The photos, floral diagram, and SEM photos of flowers between zygomorphic wild type (WT) and its two actinomorphic mutants, dorsalized (DA) and ventralized peloria (VA). **(A,D)** The flower of DA is actinomorphic in that all five petals are small, similar to the size of dorsal petals (color in purple) in WT. No mature stamens can be seen; **(B,E)** In WT, two dorsal petals (purple) are smaller than the lateral (white) and ventral ones (pink). Two stamens are located in the ventral side between lateral and ventral petals; **(C,F)** The flower of VA is also actinomorphic in that all five petals are of larger size, similar to lateral and ventral petals of WT. Five mature stamens were developed in VA although the dorsal one is smaller. The SEM images of DA, WT, and VA flowers during petal initiation (**G–I**, stage 5) and stamen initiation (**J–L**, stage 6) stages. dp, dorsal petal; lp, lateral petal; vp, ventral petal; st, stamen; *, staminode (aborted stamen). Bars = 50 μm.

of *Antirrhinum CYC* and *DICH* (Citerne et al., 2000; Wang et al., 2004a). Phylogenetic analysis indicated that *SiCYC1A* and *SiCYC1B* were recently duplicated in the lineage leading to the genus *Streptocarpus/Saintpaulia* complex. Whether or not *SiCYC1A* and *SiCYC1B* are involved in the establishment of zygomorphy and responsible for floral symmetry transitions in DA and VA peloria of African violet remains to be studied.

Paralogs of duplicated genes can evolve subfunctions or neofunctions through sequence and regulatory changes. In Gesneriaceae *CYC* (*GCYC*), duplication events were found to be exceptionally high (Citerne et al., 2000; Wang et al., 2004a;

Zhong and Kellogg, 2015). Certain *GCYC* duplications were found that can either predate or postdate the divergence of the family, tribe, and genus level (Smith et al., 2004, 2006; Wang et al., 2004a). After gene duplication, different selective pressure may be exerted on each duplicate that thus generate functional specializations (Gao et al., 2008). For example, relaxed purifying selection (estimated by dN/dS, the ratio of non-synonymous to synonymous substitutions) was detected in TCP domains of *DICH* along the lineage along the snapdragon, but *CYC* was detected, persisting on purifying selection to maintain the function (Hileman and Baum, 2003). Other studies, however, reported that while one copy of *CYC* might have been positively selected after duplications, the other copy remained under purifying selection (Chapman et al., 2008; Zhong and Kellogg, 2015). Therefore, gene duplication of *CYC* is prevailing in many angiosperm lineages and perhaps diversifying selection on each copy may lead to their functional divergence (Bello et al., 2017). Indeed, duplicated *CYC* paralogs have been found differentiating their expression levels and patterns both spatially and temporally (Chapman et al., 2008; Jabbour et al., 2014; Zhong and Kellogg, 2015). Moreover, differential expressions of *CYC* after duplications have been found to be associated with multiple independent reversals to actinomorphy in Malpighiaceae species (Zhang et al., 2013). It would therefore be essential to know whether the *SiCYC* duplications in African violet have exerted heterogenous selection on each paralog and created expressional differentiation contributing to the transitions in floral symmetry.

Previous studies therefore suggest that the peloric forms of African violet could have arisen either by (1) a loss of function of *CYC*: gene mutations in coding sequence or the regulatory region thus the dorsally specific expression pattern of *SiCYC1s* (*SiCYC1A* and *SiCYC1B*) in the flower is lost, or (2) a gain of function of *CYC*: a shift in spatial or temporal expression thus *SiCYC1s* are symmetrically expressed along the flower's dorsiventral axis. To investigate the cause, we compared expression patterns of *SiCYC1s* in petals of wild type and both peloric forms (DA and VA) via quantitative real-time RT-PCR (qRT-PCR). We further use RNA *in-situ* hybridization (ISH) to detect any spatial shift of *SiCYC1s* mRNA transcripts within the early stages of flower buds.

The aim of this study is therefore to compare flower development between WT and two pelorias DA and VA, to characterize the expression differences of *SiCYC1s* in flowers of these cultivars, to detect signature of *SiCYC1s* selection following gene duplications, to investigate *SiCYC1s* functions by ectopically expressing them in *Arabidopsis*, and to validate the association between *SiCYC1s* genotypes and their corresponding floral symmetry phenotypes among F1s from genetic crossings between WT, DA, and VA. Together we shall realize whether various genetic mechanisms are involved in these two contrasting actinomorphic reversals within African violet.

# MATERIALS AND METHODS

## Plant Materials

African violet WT, DA, and VA cultivars were propagated by leaf cuttings to maintain the same genetic unity. The original plants of WT and DA were provided by Dr. Cecilia Koo Botanic Conservation Center, Pingtung, Taiwan. At ChienKuo Holiday Flower Market, Taipei, Taiwan, VA were originally purchased. All materials were cultivated at continuously 24°C under 16 h light and 8 h darkness. Ploidy levels of all cultivars were checked by flow cytometry and the results showed that G1 peaks of all three cultivars are in relatively the same position. Hence all cultivars, WT, DA, and VA, perhaps share the same ploidy level (**Figure S1**).

## Flower Development and Petal Cell Measurement

Inflorescences of WT, DA, and VA were partially dissected to separate flower buds into stages of varying sizes (stage 1–7, **Table S1**, **Figure S2**). Buds were fixed in FAA (3.7% formaldehyde, 5% acetic acid, 50% ethanol in water) overnight and dehydrated through an ethanol/acetone series into 100% acetone dried. Material was then dried in a Hitachi HCP-2 critical point dryer. Dried buds were mounted with carbon conductive tape on 1.25 cm aluminum stubs, and further dissected. Stubs were sputter coated with gold-palladium using a Hitachi E101. Specimens were viewed using a scanning electron microscope (SEM, FEI Inspect S), and operating at 15 kV.

To compare the morphology of petal epidermal cell between WT, DA, and VA and transgenic *Arabidopsis* plants, petals of fully open flowers (stage 16, **Table S1**, **Figure S3**) were examined. Fresh tissues were mounted with carbon conductive tape on 1.25 cm aluminum stubs, then the stubs were dipped in liquid nitrogen and viewed using a Cryogenic scanning electron microscopy (Cryo-SEM) that was operating at 5 kV.

## Isolation of *CYC*-Like Genes Homologs and Reconstructed Phylogeny

Parts of the *Saintpaulia SiCYC 1A* and *1B* sequences were first amplified with DNA and cDNA using primer pairs FS (5′-ATG CTA GGT TTC GAC AAG CC-3′) and R (5′-ATG AAT TTG TGC TGA TCC AAA ATG-3′) designed from highly conserved TCP and R domain as in Möller et al. (1999). This primer pair has been demonstrated to efficiently amplify all *CYC* copies from all major Gesneriaceae lineages (Wang et al., 2004a). Partial sequences obtained were then cloned for the identity of *SiCYC1A* and *SiCYC1B.* To get full length sequence of these *SiCYC1s*, we used the genome walking technique to amplify the remaining 5′-end upstream flanking region and 3′ RACE for 3′-end sequences, as previously described (Wang et al., 2004b).

For phylogeny reconstruction, the nucleotide sequences of available Genbank *GCYC* sequences (**Table S2**) and those from *Antirrhinum* were isolated and aligned with *SiCYC1s* based on their amino acid sequences using MAFFT (https://mafft.cbrc.jp/alignment/server/) and manually adjusted. The maximum likelihood (ML) analysis was conducted in RAxML version 8 (Stamatakis, 2014). Twenty heuristic searches under the General Time Reversible (GTR) + $\gamma$ nucleotide substitution model with no partition were performed and the congruence was checked manually. One thousand bootstrap trees were calculated and consensus values >70% were

mapped to the best tree. The Bayesian inference (BI) tree was reconstructed by BEAST2 (Bouckaert et al., 2014) under the same substitution model with 100,000,000 generations with the samplings every 5,000 generations. The stability of final posterior probability (ESS state) was confirmed in Tracer 1.6 software. If the BI tree topology was congruous with the ML tree, the posterior probabilities >0.80 were mapped to the backbone of ML tree at the corresponding nodes.

## RNA Extraction and Quantitative Real-Time RT-PCR

Total RNA of dorsal, lateral, and ventral petals of stage 9, 12, and 15 of flowers was separately extracted using Trizol (Invitrogen, Carlsbad, CA, USA). Additional phase separation step by acid phenol: chloroform: IAA (25: 24: 1, pH 4.5) was added before the precipitation step to aid the removal of DNA. The MMLV reverse transcriptase (Invitrogen) was used to synthesize cDNA from total RNA with a mixture of oligo dT primers (5′-TTT TTT TTT TTT TTT TTV-3′) and random hexamer. Quantitative real-time PCR (qPCR) was performed with the KAPA SYBR FAST qPCR kit (KAPA Biosystems, Woburn, MA, USA) in Bio-Rad CFX real-time PCR machine (Bio-Rad, Hercules, CA, USA). qPCR primers for each *SiCYC1s* copy are listed in **Table S3**. The melting curve and the obtained threshold cycle (Ct) values were analyzed in CFX Manager 3.0 (BioRad, 2013). All the reactions were performed in triplicate and had NTC (no template control) and NRC (no reverse transcription control) to exclude contamination from chemicals and DNA contamination from RNA samples, respectively. Housekeeping genes in African violet for the purpose of internal control to calibrate equal amounts of RNA as reference were *18S rRNA* (for WT, DA, and VA comparison) or *β-actin* (actin 7) (for comparison in flowers of F1 hybrids between WT × DA). The expression amount was calculated by the formula: $E^{ct}_{ref}$/E $E^{ct}_{exp}$ (E = 1 + efficiency value). The efficiency value of each primer pair was calculated from the slope of the standard curve using the formula: efficiency value $=10^{-1/\text{slope}}$. The reason why the internal control was switched to *β-actin* in F1 hybrids is due to the *SiCYCs* expression levels being low, the 18S expression levels being too high, and thus causing difficulty in the quantification of *SiCYCs*' relative expression amount.

## *In situ* Hybridization for *SiCYC1s*

mRNA ISH was carried out by the following methods by Wang et al. (2008). To synthesize gene-specific RNA probes, the partial sequence of *SiCYC1A* (252 bps in R domain) was cloned into the pGEM-T easy vector system (Promega, Fitchburg, WI, USA), using primers pSiCYC1A_DFA_F1 (5′-GAT CCA GCA CAG AGT GCA TCA AC-3′) andpSiCYC1A_HQS_R1 (5′-CGA CTG GTG GTG CCT CAG-3′). These plasmids were then digested with SpeI (Thermo Fisher Scientific Inc., Waltham, MA, USA). Digoxigenin (DIG)-labeled antisense RNA probes and sense RNA probes were synthesized with DIG-dNTP (Roche Diagnostics GmbH, Basel, Schwelz) by T7 RNA polymerase and SP6 RNA polymerase, separately, using digested plasmid as the template. The plant material was fixed in 4% paraformaldehyde and processed for paraffin embedding and sectioning. The sections were hybridized with RNA probes and hybridization signals were detected by Anti-DIG-AP (Roche Diagnostics GmbH) with NBT/BCIP as the substrate. Hybridization was visible as purple to blue signals. The sections were observed under a BX51 (Olympus) bright field microscope. Sense RNA probes were used for negative control.

## Detection of Selective Pressure Differences Between *SiCYC1A* and *SiCYC1B*

To elucidate whether different selective pressures has affected the evolution of *SiCYC1A* and *SiCYC1B* after their duplication, molecular evolution of *GCYC* duplicates in Gesneriaceae was investigated with codeml from the PAML package v.4.4 (Yang, 2007). From previous *GCYC* phylogeny (Wang et al., 2004a) and our study (**Figure 2**), *SiCYC1A* and *SiCYC1B* each is grouped with other *GCYC1A* and *GCYC1B* genes, respectively, from *Streptocarpus*/*Saintpaulia* species. Therefore, *SiCYC1A* and *SiCYC1B* from African violet were aligned with available *Streptocarpus GCYC1A* and *GCYC1B* from NCBI (accession numbers in **Table S4**). *GCYC1C* genes from Gesneriaceae species were selected as the outgroup on account of their closest relationship with *GCYC1A* and *GCYC1B* (Wang et al., 2004a).

To find evidence of divergent or positive selection along *GCYC1A* (*SiCYC1A*) and *GCYC1B* (*SiCYC1B*) lineages, models of different evolutionary scenarios of selective pressures were analyzed. The tree topology was thereafter unrooted and applied to the evaluation of selective pressure at molecular level by ω value ($K_N/K_S$) using CODEML in PAML v4.0 (Yang, 2007). We especially focused on detecting whether selective pressure changes before and post duplication event occurred. To achieve this goal, we modified the duplication ML model from Bielawski and Yang (2003) to test the change in selective regime before and after gene duplication. All gaps in the sequence alignment were treated as missing data (marked as "?" in the alignment in CODEML) to retain the information from these sites. Branch models allowing ω values varying on different lineages were designed according to evolutionary scenarios. Thus, *GCYC1A* and *GCYC1B* were separately assigned as foreground in two-ratio branch models for testing shifts in selective pressures (ω values) along each duplicate (**Table 1**). All the two-ratio models were tested against the general one-ratio null model of constant selective pressures. A branch site three ratio model was further compared with *GCYC1A* and *GCYC1B* as different foregrounds in the same model to test the hypothesis of lineage-specific selection. The three-ratio model was tested against the "post-duplication" model. Site model was set up for testing the selective pressures acting on certain portions of sites. Branch-site models were also implemented to increase the detectability in previous scenarios in branch models with the consideration of site proportion. Two Clade Model C models with the foreground as *GCYC1A* and post-duplication lineages were tested against the null model m2a_rel (Weadick

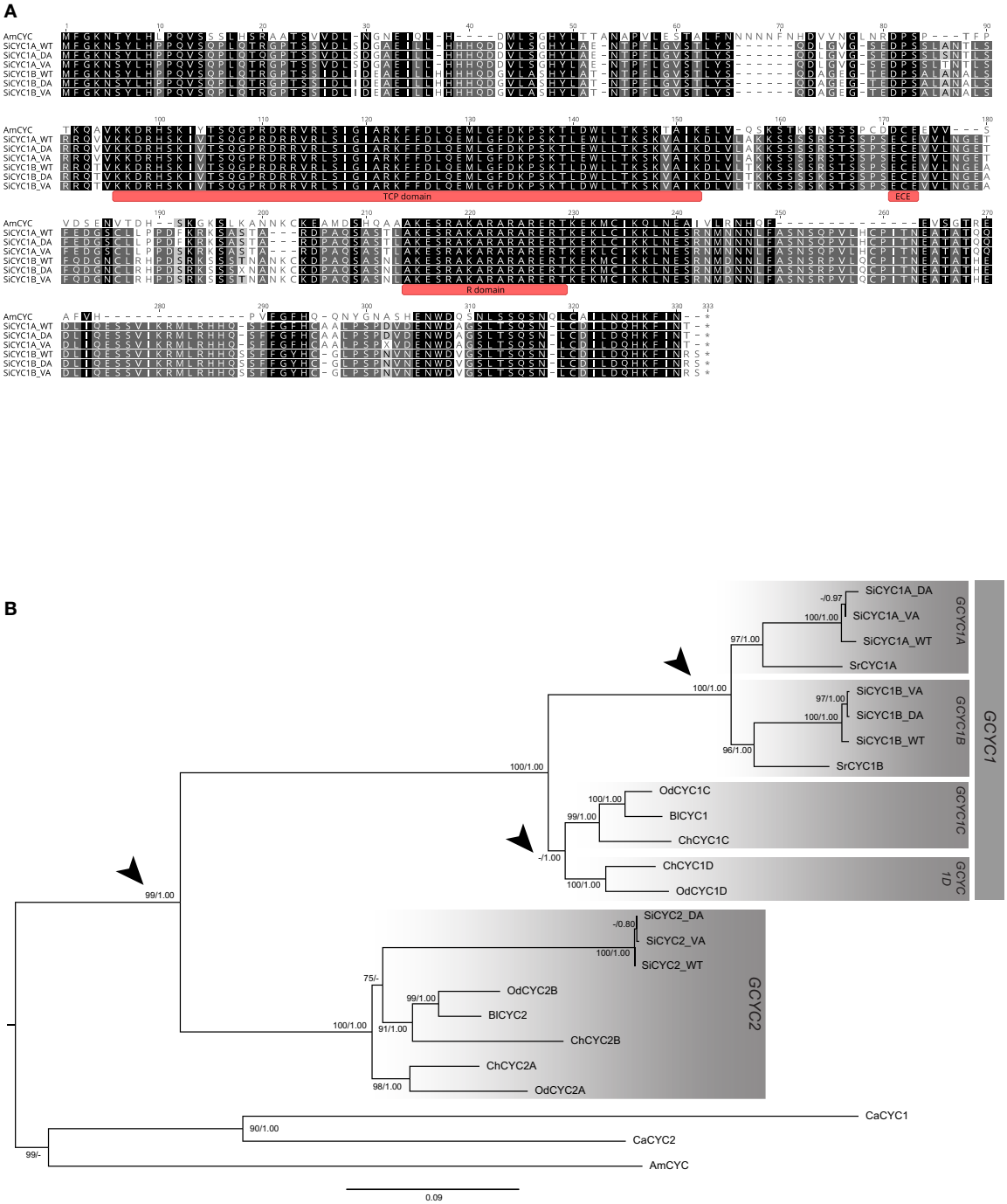


**FIGURE 2 |** Alignment and the phylogeny of African violet SiCYC1A and *SiCYC1B* with selected Gesneriaceae GCYC homologs. **(A)** The alignment of *SiCYC1A* and *SiCYC1B* with *AmCYC* (snapdragon), with TCP, ECE, and R domains is indicated. **(B)** The ML tree with *AmCYC* as outgroup. The topology indicates that the evolution of Gesneriaceae *GCYC* homologs contains multiple duplication events (arrow heads). In particular, the duplication before the divergence of genus *Streptocarpus* (including African violet) which gave rise to *GCYC1A* (*SiCYC1A*) and *GCYC1B* (*SiCYC1B*) becomes the major paralogs involving floral symmetry transitions in African violet. ML bootstrap supports (> 70%) and BI posterior probabilities ( > 0.80) are labeled.

and Chang, 2011). The further "lineage-specific" model was compared to the "post-duplication" model to determine whether the two duplicate lineages have difference in selective pressure (**Table 1**).

## Genotyping *SiCYC* Alleles by PCR-RFLP

To find out the association between *SiCYC1A* and *SiCYC1B* alleles and floral symmetry phenotypes among F1 individuals, PCR-based restriction fragment length polymorphism (RFLP)

**TABLE 1 |** Parameter estimates and likelihood scores of the nested branch and branch-sites models for detecting selective constrains between *GCYC1A* and *GCYC1B*.

| Clade | Model | n.p. | Log Likelihood (lnL) | 2ΔL[a] | *P*-value[b] | Estimates of ω value |
|---|---|---|---|---|---|---|
| **BRANCH MODEL** | | | | | | |
| Null | One-ratio | 39 | −2898.3994 | | | $\omega_0 = 0.3690$ |
| *GCYC1A* as foreground | Two-ratio | 40 | −2895.4538 | 5.8911 | **0.015*** | $\omega_0 = 0.4168$, $\omega_{GCYC1A} = 0.2083$ |
| *GCYC1B* as foreground | Two-ratio | 40 | −2898.3696 | 0.05958 | 0.8 | $\omega_0 = 0.3640$, $\omega_{GCYC1B} = 0.3884$ |
| *GCYC1A* + *GCYC1B* as foreground (post-duplication) | Two-ratio | 40 | −2896.9931 | 2.8125 | 0.094 | $\omega_0 = 0.4262$, $\omega_{post-duplication} = 0.2943$ |
| *GCYC1A* , *GCYC1B* as foreground (lineage-specific) | Three-ratio | 41 | −2895.4048 | 3.1769 | 0.075 | $\omega_0 = 0.4260$, $\omega_{GCYC1A} = 0.2085$, $\omega_{GCYC1B} = 0.3909$ |
| **BRANCH-SITE MODEL (CLADE MODEL C)** | | | | | | |
| M2a_rel (null) | One-ratio | 42 | −2883.5782 | | | $P1 = 0.3177$, $\omega_{P1} = 0.0182$; $P2 = 0.1128$, $\omega_{P2} = 1.0000$; $P3 = 0.4789$, $\omega_{P3} = 0.4789$ |
| *GCYC1A* as foreground | Two-ratio | 43 | −2879.2689 | 8.6185 | **0.0033***** | $P1 = 0.5190$, $\omega_0 = 0.1030$, $\omega_{GCYC1A} = 0.1030$; $P2 = 0.0473$, $\omega_0 = 1.0000$, $\omega_{GCYC1A} = 1.0000$; $P3 = 0.4338$, $\omega_0 = 0.8369$, $\omega_{GCYC1A} = 0.2075$ |
| *GCYC1A* + *GCYC1B* as foreground (post-duplication) | Two-ratio | 43 | −2880.7007 | 5.755 | **0.016*** | $P1 = 0.5148$, $\omega_0 = 0.1108$, $\omega_{post-duplication} = 0.1108$; $P2 = 0.2042$, $\omega_0 = 1.0000$, $\omega_{post-duplication} = 1.0000$; $P3 = 0.2811$, $\omega_0 = 0.9178$, $\omega_{post-duplication} = 0.1472$ |
| *GCYC1A* , *GCYC1B* as foreground (lineage-specific) | Three-ratio | 44 | −2879.1924 | 8.7715 | **0.012*** | $P1 = 0.5081$, $\omega_0 = 0.0990$, $\omega_{GCYC1A} = 0.0990$, $\omega_{GCYC1B} = 0.0990$; $P2 = 0.5081$, $\omega_0 = 1.0000$, $\omega_{GCYC1A} = 1.0000$, $\omega_{GCYC1B} = 1.0000$; $P3 = 0.4241$, $\omega_0 = 0.8520$, $\omega_{GCYC1A} = 0.1784$, $\omega_{GCYC1B} = 0.7077$ |

[a] *Models were compared by the double value of the difference in likelihood (2ΔL). Each likelihood ratio was calculated in comparison of alternative models and the suitable null model described in the main text.*

[b] *The statistical significance of models were tested by Likelihood Ratio Test (LRT). P-values were calculated from the 2ΔL of each comparison in the Chi-Square distribution with the degree of freedom equals to difference of parameters (n.p.) between compared models. Significant p-value is highlighted in bold. * <0.05; ** <0.01; *** <0.001.*

was conducted. This PCR-RFLP procedure was divided into 4 parts: (1) isolation of genomic DNA, (2) performing a standard PCR, (3) digestion with appropriate enzymes, and (4) resolution digest of PCR products. The enzymes used for digesting *SiCYC1A* and *SiCYC1B* PCR product were *Aat*II (#ER0991, Thermo) and *Pst*I(#ER0611, Thermo), respectively. The two chosen enzymes were determined by the allelic variation of DA *SiCYC1A* and *SiCYC1B*. The protocol for digestion of PCR products after amplification followed the manufacturer's instructions.

## Construction of *SiCYC1A* Transgenic Plants in *Arabidopsis*

The overexpression construct of *SiCYC1A*WT allele, p35S::*SiCYC1A*$^{W}$:c-Myc (hereinafter referred to as *35S::SiCYC1A*$^{W}$), and *SiCYC1A*VA allele, p35S::*SiCYC1A*$^{V}$:c-Myc (hereinafter referred to as *35S::SiCYC1A*$^{V}$) was engineered to pK2GW7.0 from the Gateway® system. Firstly, the sequences of *SiCYC1A* were amplified from cDNA by KAPA HiFi PCR Kits (KAPA biosystems, KK2501). The A-tailing PCR products were cloned into pGEM®-T Easy Vector (Promega, A1360). Using the extracted plasmid as the template, the secondary PCR reaction with c-Myc fusion primers was carried out by KAPA HiFi PCR Kits. The products were further purified for cloning into pCR®8/GW/TOPO® TA Cloning Kit. Owing to the fact that both pCR®8/GW/TOPO® Donor vector and pK2GW7.0 Destination vector contain the same resistant gene (spectinomycin), the Donor vector must be linearized by Pvu I to destroy the self-replication ability in *E. coli* cells. The gel purified products were then ready for LR reaction using LR Clonase™ II Enzyme Mix (Invitrogen) and the products were subsequently transformed into *E. coli* for amplification. The inserts in *E. coli* plasmids were cut by a restriction enzyme for gel validation, the correct size of the vectors, and the desired insertion size. The interchangeable regions, flanked by attB1 and attB2 sites, were sequenced to avoid any mutation or frame shift. The sequence confirmed vectors were then transformed into *Agrobacterium tumefaciens* GV3101 by electroporation for subsequent *Arabidopsis* transformation.

The *Arabidopsis* floral dip transformation protocol was followed by Clough and Bent (1988). The floral dip procedure was repeated once within the 8 days for obtaining more transformed seeds. Putative transgenic *Arabidopsis thaliana* T1 seedlings were selected by antibiotic kanamycin and PCR confirmed with T-DNA insertion primers *SiCYC1A*-F/R (5′-ATG TTT GGC AAG AAC TCG TAC CTT C-3′/5′-TTA CGT ATT GAT GAA TTT GTGCTG ATC C-3′) and NPTII-F/R (5′-TCA GAA GAA CTC GT CAA GAA-3′/5′-AAC AAG ATG GAT TGC ACG CA-3′). The transformed seedlings (T1) were selfed into T2 plants to document the phenotypic effect of each construct. For each allele construct, 3–7 independent T2 transgenic individuals of overexpressing *SiCYC1A*$^{W}$ and *SiCYC1A*$^{V}$, together with T1 plants, were summarized for the phenotypic effects on petal morphology. The mRNA expression level of *SiCYC1A* in T1 and T2 transgenic plants was verified by RT-PCR.

# RESULTS

## Developmental Transitions to Actinomorphy Occurred Early at Petal and Stamen Initiation Stages

To figure out the developmental differences of floral symmetry between *Saintpaulia* cultivars, the flower buds from early to late stages of WT, DA, and VA were examined by SEM. The stage definitions of flower development in African violet (**Table S1**) basically followed the work by Harrison et al. (1999). The SEM results showed that the floral symmetry transitions between actinomorphic cultivars and wild type were evident as early as petal and stamen primordia initiation stages. In WT flowers, dorsal petals and adaxial stamen primordia initiated late and smaller than lateral and ventral ones (stages 5–6, **Figures 1H,K**; **Figures S2Q,T**). Along the developmental stages, dorsal petals always retained smaller than lateral and ventral petal primordia (**Figures S2W, S3B**). This contributes to the development of flower zygomorphy with two smaller dorsal petals and three larger lateral and ventral petals (**Figure 1B**). The three adaxial-side staminodes also retained smaller than the two abaxial stamens (**Figures S2T,Z**) and finally aborted thus only two abaxial stamens matured (**Figures 1B,E**). The petal aestivation showed that two lateral petals enfold the dorsal and ventral petals (**Figure S2W**).

However, in DA, all petal and staminode primordia were initiated at the same time (**Figures 1G,J**; **Figures S2P,S**) and the whole bud remained in small size when compared to other cultivars along floral development (**Figures S2V, S3A**). Eventually all 5 staminodes were completely aborted (**Figures 1A,D**). On the other hand, in VA all petal and stamen primordia also initiated together at the same time (**Figures 1I,L**; **Figures S2R,U**) but they enlarged faster along floral development (**Figures S2X, S3C**). All 5 stamens were fully developed when mature although there is a residual zygomorphy where the adaxial stamen is slightly smaller in size than the two lateral ones whereas the ventral two are the largest (**Figures 1C,F**). The aestivation of both DA and VA cultivars was random (**Figures S2V,X**).

## Cell Proliferation but Not Cell Growth Cause Dorsiventral Petal Size Difference in African Violet

To clarify whether the dorsiventral petal size (area) difference was caused by differential cell proliferation or cell growth, epidermal cell size and morphology between dorsal, lateral, and ventral petals in WT, DA, and VA were compared at anthesis (stage 16) via SEM (**Figure S4**). The SEM photos showed that the size and morphology of petal cells between all petals and all cultivars (WT, DA, and VA) were not obviously different. This raises the possibility that the dorsiventral petal size difference was perhaps not owing to cell growth differences but cell proliferations.

We further measured the petal area ($mm^2$) and cell size from SEM photos through ImageJ software. Both petal area and cell size were converted to a ratio between ventral petal and dorsal petal (V/D, **Table S5**). In WT, the petal area of ventral petals was 2.16 times larger than dorsal petals. But in DA and VA, the ratios of petal area between ventral and dorsal petals was close to 1 (1.07 and 1.11, respectively). When comparing cell size differences between ventral and dorsal petals, the ratios (V/D) are about the same (0.87–1.17) across all cultivars, no matter where the samples were selected from proximal or distal petal parts. Given the fact that cell size has no difference between ventral/dorsal petals of all cultivars, the larger dorsal petal area in WT must be the result of the difference of cell number (cell proliferation) rather than that of cell size (cell growth).

## *CYC* Homologs Identified and Duplications Revealed From Phylogeny

To identify putative genes involved in floral symmetry in African violet, *CYC*-like genes (*SiCYC1A*, *SiCYC1B*, *SiCYC2*) were isolated in WT, DA, and VA (**Figure 2A**). Maximum likelihood (ML) and BI trees were reconstructed to identify the putative *CYC*-like homologs (**Figure 2B**). Sequences from actinomorphic peloric cultivars, DA and VA, were not found to have any frameshift mutation (all indels were in multiples of three nucleotides) or stop codons.

Three *CYC* homologous (*GCYC1A*, *GCYC1B*, and *GCYC2*) were isolated from WT, DA, and VA of African violet (**Figure 2A**). The full length ORFs are 954 bp (*SiCYC1A*) and 969 bp (*SiCYC1B*), and the length is conserved between the WT, DA, and VA peloria except some single-nucleotide polymorphism (SNP) sites exists between them (**Figure 2A**). The divergence between *SiCYC1A* and *SiCYC1B* are 12.8% at the amino acid level and 9.7% at the nucleotide level. *SiCYC1A* and *SiCYC1B* contain an apparent TCP domain (**Figure 2A)** and an additional *CYC/TB1* R domain (Cubas et al., 1999a). The 58 amino acid TCP domain contains a basic-Helix-Loop-Helix (bHLH) structure predicted from PSIPRED protein structure analysis. This indicates *SiCYC1A* and *SiCYC1B* are putative transcription factors utilizing bHLH structure in the TCP domain to facilitate DNA binding with downstream genes or involving dimerization. The cultivars of WT and VA are homozygous for *SiCYC1A* and *SiCYC1B*. The alleles of WT are denoted as $SiCYC1A^{WT}$ and $SiCYC1B^{WT}$, for VA, $SiCYC1A^{VA}$, and $SiCYC1B^{VA}$ (**Figure 2A**). However, DA cultivar is heterozygous for *SiCYC1A* and *SiCYC1B*, containing one allele specific to DA ($SiCYC1A^{DA}$ and $SiCYC1B^{DA}$) with another allele from WT ($SiCYC1A^{WT}$ and $SiCYC1B^{WT}$). The allelic divergence of *SiCYC1A* between WT, DA and VA is small, that is, 0.9% at the amino acid level (3 of 318 are different) with 12 nucleotide substitutions in 954 bp (including some synonymous substitutions). The allelic divergence of *SiCYC1B* between WT, DA, and VA are even minute, that is, 0.3% at the amino acid level (1 of 323 are different) with 7 nucleotide substitutions in 954 bp (synonymous substitutions included as well).

In the Bayesian phylogenetic tree with *Antirrihinum CYC* as the outgroup including available old world Gesneriaceae, *GCYCs* from GenBank, *SiCYC1A*, and *SiCYC1B* (together with *SrCYCs* from *Streptocarpus rexii*) were nested in their own clade with strong branch support ($BS = 100\%$) (**Figure 2B**). In fact, when we added more available genus *Streptocarpus/Saintpaulia GCYC*

sequences in, every species contains both *GCYC1A* and *GCYC1B* clade duplicates (see below). These indicate that *SiCYC1A* and *SiCYC1B* are duplicated paralogs (*GCYC1A* and *GCYC1B*) that predated the origin of *Streptocarpus*/*Saintpaulia* species.

## Expression Shifts of *SiCYC1s* Correlates to Developmental Reversals to Actinomorphy in DA and VA Peloria

The expression patterns of these *SiCYCs* were compared between petal parts (i.e., dorsal, lateral, and ventral) among all cultivars in trying to associate the possible expression shifts to the transitions of floral symmetry. The quantitative (q)RT-PCR results revealed that the expression of *SiCYC1s*, *SiCYC1A*, and *SiCYC1B* were shifted corresponding to apparent floral symmetry reversals in DA and VA pelorias. In zygomorphic WT, expressions of *SiCYC1A* and *SiCYC1B* were both restricted to the dorsal petals (**Figure 3**, middle panel). But in DA peloria, expression of both *SiCYC1A* and *SiCYC1B* extended to all dorsal, lateral, and ventral petals (**Figure 3**, left panel). This *CYC* ubiquitous expression correlates with the development of 5 small-sized petals and growth retardation of all stamens in DA. On the other hand, in VA peloria, although *SiCYC1A* and *SiCYC1B* expressions are 50% lower than those in WT their expressions are still restricted to dorsal petals (**Figure 3**, right panel). The reduced expression of *SiCYC1s* in VA correlates with its 5 equal sized enlarged petals and fully developed stamens. Besides, the transcript levels of *SiCYC1A* (**Figure 3**, top row) were always higher than those of *SiCYC1B* (**Figure 3**, bottom row). The changes of expression patterns in both *SiCYC1A* and *SiCYC1B* among WT, DA, and VA were most evident at stage 9 (the petal whorl starts to enlarge as the size of sepal whorl, **Figure S3**). The transcripts of both *SiCYC1A* and *SiCYC1B* were declined during later flower development toward anthesis (stage 15) in all cultivars (**Figure 3**). The expression patterns of *SiCYC2* were not examined since the transcript of *SiCYC2* could not be detected in any part of the inflorescence along different stages.

## *SiCYC1s* Expression Shifts Also Observed in Early Bud Stages of Peloria by ISH

We further used RNA ISH to determine the exact *SiCYC1s* transcript locations within flower buds in early flower development (floral meristem, petal and stamen primordia initiation, and early differentiation stages) between WT, DA, and VA. Owing to the high similarity of nucleotide sequences between *SiCYC1A* and *SiCYC1B* (93.7% identity, 16 sites differences in 252 bps probe), we could not rule out that the anti-sense probe for *SiCYC1A* may also have hybridized to *SiCYC1B*. Nonetheless, *SiCYC1s* transcripts locations within the flower buds detected by ISH showed similar patterns as qRT-PCR results did.

From ISH result, the expression pattern shifts between WT, DA, and VA could be traced back to petal primodia initiation (stage 5, **Figure S2**). In zygomorphic WT, *SiCYC1s* expressions were restricted to the dorsal petal primodia (**Figure 4E**) and dorsal petals tips (**Figure 4H**). In DA peloira, *SiCYC1s* expressions were not restricted to the dorsal part of the flower, but on both dorsal and ventral petal primodia (**Figure 4D**), and later in all petals (dorsal, lateral, and ventral, **Figure 4G**). *SiCYC1s* started to express as early as the floral meristem stage both in WT and DA (**Figures 4A,B**). However, in VA peloria, *SiCYC1s* expression could not be detected in the floral meristem initiation stage (**Figure 4C**). *SiCYC1s* signals were detected on the tips of both dorsal and ventral petal primodia (**Figures 4F,I**), but they were obviously weaker than the signals in the wild type (**Figures 4E,H**).

We also found *SiCYC1s* expressions on both dorsal staminode and ventral stamen primodia in flower buds of all three cultivars (**Figures 4D–I**). However, this was also evident in sense controls (**Figures 4J–L**), so we could not be sure whether *SiCYC1s* expressed on staminode/stamens or not. The cross sections of ISH were all shown in **Figure S5**.

## Change of Selective Pressures After the Duplication of *GCYC1A* and *GCYC1B*

Our expression results suggest that *SiCYC1A* and *SiCYC1B* are expressed in different levels within the flower, implying that they are under a divergent selective regime. To test this hypothesis, we designed a series of branch models and branch site models to investigate the pattern of selection at the molecular level focusing on predating and postdating duplication events (**Figure 5**). Our ingroups were comprised with all available *Streptocarpus* *GCYC1A* and *GCYC1B* sequences (accession numbers listed in **Table S4**). Our analysis revealed that the evolution of *GCYC1A* (*SiCYC1A*) is obviously constrained by purifying selection but *GCYC1B* (*SiCYC1B*) showed relaxation from selection. The paml branch model results showed that *GCYC1A* clade experienced a relatively stronger purifying selection ($\omega_{GCYC1A} = 0.2083$, **Figure 5C**) than background branches ($\omega_0 = 0.4168$) with statistic support whereas other models received no support (**Table 1**). When applying branch site model (clade model C), we further confirmed that almost half ($P3 = 0.4338$) of the *GCYC1A* sites were under purifying selection ($\omega_{GCYC1A} = 0.2075$). In addition, relative stronger purifying selection signal was detected after the duplication of *GCYC1A* and *GCYC1B* under post duplication scenario ($\omega_{\text{Post}-\text{duplication}} = 0.1472$, $p = 0.016$). However, lineage-specific model is statistically most significant ($p = 0.012$) when compared to the post-duplication senario in branch-site analysis and further support that these *GCYC1A* and *GCYC1B* clades experienced divergent selection signals after their duplication. *GCYC1A* experienced purifying selection ($\omega_{GCYC1A} = 0.1784$) whereas *GCYC1B* is relaxed from selective constraint ($\omega_{GCYC1B} = 0.7077$) (**Figure 5E**, **Table 1**).

## Inheritance of Floral Symmetry in African Violet

The genetics of floral symmetry in African violet can be revealed by genetic crosses between floral symmetry types. Crossings between WT and VA, VA and DA, also DA and WT were conducted to determine how the floral symmetry phenotypes were inherited. Selfing of WT and VA each produced phenotypes corresponding to the parent implying WT and VA are pure lines. The "No stamens" cultivar, DA however, could not be selfed owing to the lack of stamens. The crosses between WT and

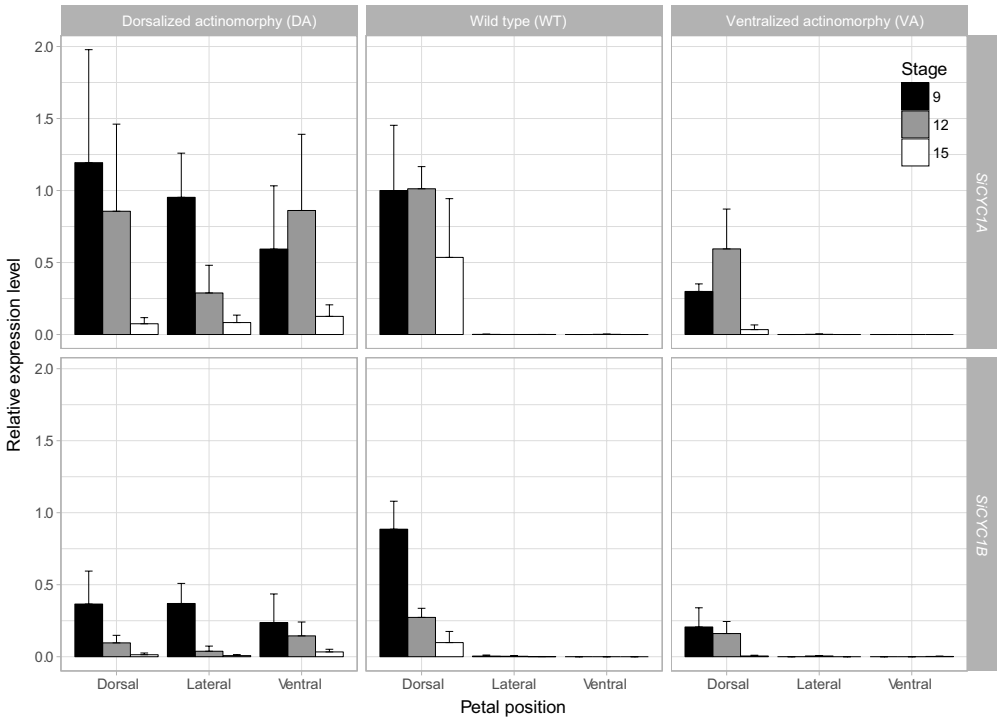


**FIGURE 3 |** qRT-PCR expression of *SiCYC1A* and *SiCYC1B* in dissected petals of African violet. The expressions levels are compared between dorsal, lateral, and ventral petals at stage 9 (black bar), 12 (gray bar), and 15 (white bar) of DA, WT, and VA. *SiCYC1A* and *SiCYC1B* both express in all petals (dorsal, lateral, and ventral) of DA, but in WT their expressions are restricted to dorsal petals. *SiCYC1A* and *SiCYC1B* expressions are weak in VA but are still confined to dorsal petals. Each bar represents three biological repeats (mean ± SD). The relative expression levels are normalized to *18S rRNA*, and the fold change of expressions are calculated relative to *SiCYC1A* expression level of stage 9 dorsal petals of WT.

VA resulted in all F1 offsprings in zygomorphic WT (**Figure 6**). If assuming *SiCYC1s* (either *SiCYC1A* or *SiCYC1B*, or both) is the responsible locus for floral symmetry transitions, this implies that *CYC* allele of WT ($SiCYC1^W$) is dominant to that of VA ($SiCYC1^V$). Interestingly, the crossing between VA and DA resulted in 1:1 ratio of two phenotypes, actinomorphic DA and unexpectedly zygomorphic WT. This suggests the *SiCYC1s* allele ($SiCYC1^D$) of DA is also dominant to VA ($SiCYC1^V$) but DA is probably a heterozygote. This idea is further supported by the crossing between DA and WT in which the floral symmetry phenotypes of F1 hybrids were segregated into 1:1 of DA and WT, exactly corresponding to their parents (**Figure 6**). Thus DA ($SiCYC1^{D/W}$) could be inferred as a heterozygote of $SiCYC1^D$ and $SiCYC1^W$, whereas WT could be referred as $SiCYC1^{W/W}$. As WT is dominant to VA, pure line VA can be inferred as $SiCYC1^{V/V}$. The level of dominance follows a hierarchical fashion in which $SiCYC1^D > SiCYC1^W > SiCYC1^V$.

## Genetic Association Analysis of *SiCYC1s* to Floral Symmetry

To further confirm whether these *SiCYC1s* alleles are responsible for the genetic change of floral symmetry transition, genotype–phenotype associations between *SiCYC1A* and *SiCYC1B* alleles with floral symmetry phenotypes were examined among F1 hybrids of WT and DA. Among 117 F1 individuals, their phenotypes were segregated into 1:1 ratio (61 vs. 56) of WT and DA. *SiCYC1A* and *SiCYC1B* alleles of each cultivar WT, DA, and VA were cloned and sequenced to identify their segregation sites. From segregation sites sequences we recognized restriction enzymes to distinguish *SiCYC1A* and *SiCYC1B* alleles of WT and DA (**Figure S6A**). Here we use A to denote *SiCYC1A* and B to denote *SiCYC1B*, and thus the allelic identity of WT is $A^{W/W}B^{W/W}$ (WT is homozygous for both *SiCYC1A* and *SiCYC1B*) and DA is $A^{D/W}B^{D/W}$ (DA is heterozygous for both *SiCYC1A* and *SiCYC1B*, see results above) (**Figure S6B**). To genotype *SiCYC1s* alleles of each F1 individual, PCR-based RFLP was then performed. Genotype frequency test confirmed that there is no segregation distortion of these alleles among F1 hybrids (**Table 2**). However, when correlating genotypes to phenotypes among F1s, there is no clear association of inherited alleles ($A^{D/W}$, $A^{W/W}$, $B^{D/W}$, $B^{W/W}$) with corresponding traits (zygomorphy, dorsalized actinomorphy) (**Figure S6B**).

## Expression of *SiCYC1s* Alleles Correlates to Floral Symmetry Phenotypes Among F1s but Not to Their Inherited Genotypes

To examine whether these *SiCYC1A* and *SiCYC1B* alleles displayed distinct expression patterns correlating with floral symmetry phenotypes in F1s between WT and DA, we detected their expression level differences between dorsal, lateral, and

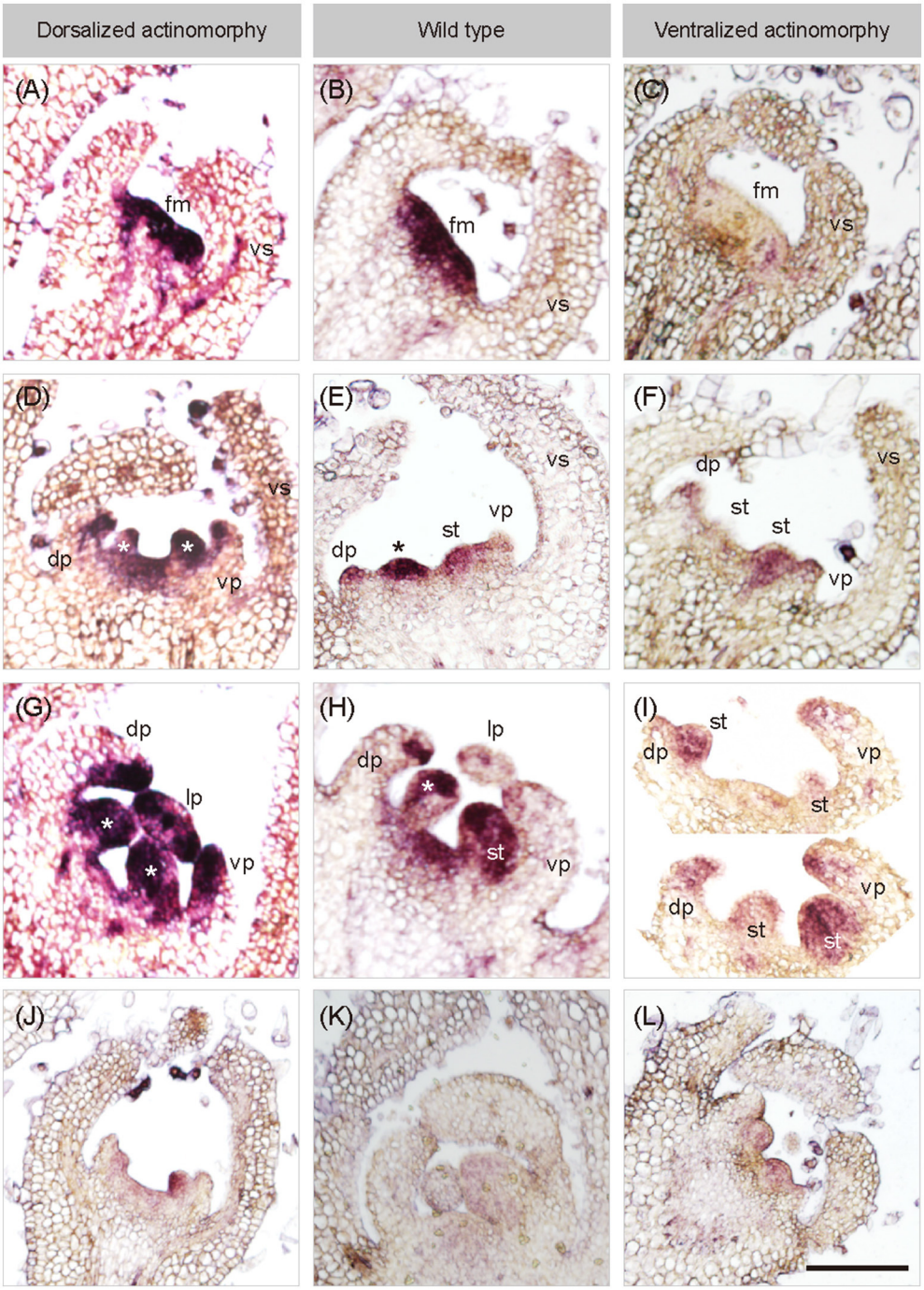


**FIGURE 4 |** *In situ* hybridization of *SiCYC1A* in flower buds of African violet. Longitudinal sections on early flowering stages of all cultivars hybridized with antisense probes of *SiCYC1A:* stage 4 **(A–C)**, stage 5 **(D–F)** and stage 6 **(G–I)**. The purple color represents the *in-situ* signals of *SiCYC1A* mRNA. *SiCYC1A* has early expression in the entire floral meristem of DA and WT **(A,B)** but is absent in VA **(C)**. During floral organ initiation **(D–F)**, *SiCYC1A* persists in inner whorls of the flower including the dorsal (dp) and ventral petal primordia (vp) of DA **(D)**. **(E)** But in zygomorphic WT, *SiCYC1A* confines more to the dorsal petal primordia (dp) than the ventral one. **(F)** In VA, weak *SiCYC1A* signals start to acuminate at tips of both dorsal and ventral petal primordia. **(G)** Later in floral organ differentiation, *SiCYC1A* can be detected in all petals (dp, lp and vp) of DA. **(H)** But in WT, *SiCYC1A* is largely restricted to dorsal petals (dp). **(I)** In the petal whorl of VA, a weak but slightly stronger *SiCYC1A* is evident in dorsal petals (dp) when compared to ventral petals (vp). The sense probe controls were shown in **(J–L)**. The cross sections of *ISH* are shown in **Figure S5**. **fm**, floral meristem; **vs**, ventral sepal; **dp**, dorsal petal; **lp**, lateral petal; **vp**, ventral petal; **st**, stamen. *, staminode. Scale bar = 100 μm.

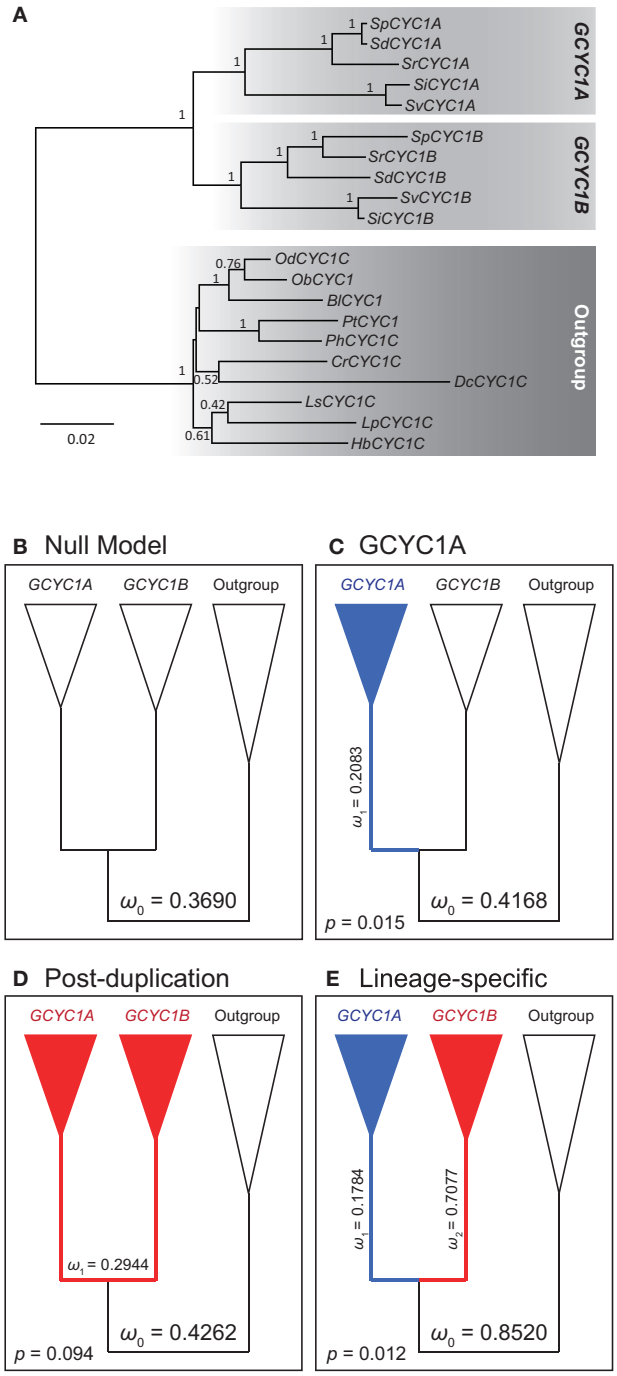


**FIGURE 5 |** Phylogeny and Nested models (branch and branch-site) to detect selective constraint shifts between GCYC1A and GCYC1B. **(A)** Phylogeny of Generiaceae *GCYC1* by Bayesian inference was used for inference of molecular evolution by PAML. Posterior probabilities are labeled on the branches **(B–E)** Evolutionary scenarios of different models; **(B)** One-ratio null model with constant ω value; **(C)** Two-ratio model with a distinct selective pressure on *GCYC1A*; **(D)** Two-ratio model with a post-duplication alteration of selective pressure; **(E)** Lineage-specific selective pressures on *GCYC1A* and *GCYC1B* lineages estimated from clade model **C**. The ω value values follow the results in **Table 1**.

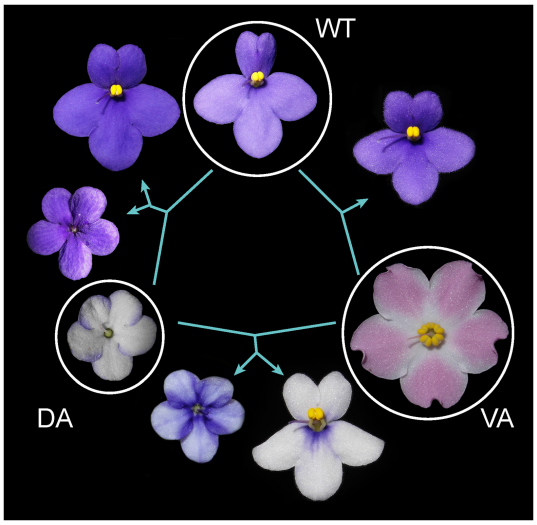


**FIGURE 6 |** Genetic crossing designs among DA, WT, and VA. Crossings between WT and VA resulted in all F1s similar to zygomorphic WT. Crossing between two peloria VA and DA, resulted in F1s in 1:1 of zygomorphic WT and DA. Crossing between DA and WT segregated into 1:1 of DA and WT. Thus floral symmetry transitions are likely to be controlled by three alleles at a single locus in which the DA allele is dominant to WT and WT is dominant to VA. See main text for inferring their dominance hierarchy.

ventral petals via quantitative RT-PCR. The expression patterns of these F1 *SiCYC1s* alleles correlate with the resulting floral symmetry phenotypes but do not necessarily follow their inherited genotype. For example, as shown in **Figure 7**, those four zygomorphic F1 individuals shared the same *SiCYC1A* and *SiCYC1B* expressions in the dorsal petal only, yet their *SiCYC1s* allele combinations appeared in all four equally probable ways (F1_84: $A^{D/W}B^{D/W}$, F1_104: $A^{D/W}B^{W/W}$, F1_136: $A^{W/W}B^{D/W}$, F1_144: $A^{W/W}B^{W/W}$). Similarly, those four dorsalized actinomorphy individuals all showed that *SiCYC1A* and *SiCYC1B* ubiquitously expressed to all petals, but their *SiCYC1s* allelic combinations were comparably the same in four equally probable ways as those in zygomorphic ones (F1_31: $A^{D/W}B^{D/W}$, F1_58: $A^{D/W}B^{W/W}$, F1_92: $A^{W/W}B^{D/W}$, F1_15: $A^{W/W}B^{W/W}$) (**Figure 7**). The cDNA products of these *SiCYC1s* alleles were further confirmed for their genotypes by sequencing. Thus, the expression shifts of these *SiCYC1A* and *SiCYC1B* alleles correlate nicely with the resulting F1 symmetry phenotype, but there lacks a specific allelic combination associating with certain symmetry phenotype.

## Heterologous Expression and Phenotypes of *SiCYC1A*$^W$ and *SiCYC1A*$^V$ in *Arabidopsis*

To elucidate what phenotypic effects of *SiCYC1s* are present on flower morphology, the complete coding sequences of WT allele *SiCYC1A*$^w$ and VA peloric allele *SiCYC1A*$^V$ were ectopically expressed into *Arabidopsis*. We did not further examine the over expression phenotype of *SiCYC1A*$^D$ since the overexpression phenotypes of *SiCYC1A*$^w$ and *SiCYC1A*$^V$ in *Arabidopsis* were

almost identical, and the allelic difference between *SiCYC1A*$^D$ to *SiCYC1A*$^w$ and *SiCYC1A*$^V$ is in just one non-synonymous amino acid substitution. In particular, this single non-synonymous amino acid substitution (position 86 in alignment of **Figure 2A**) in *SiCYC1A*$^D$ is not on important domains such as TCP, ECE, or R.

Overexpression of *SiCYC1As* in *Arabidopsis* affects the flower size and leaf growth with smaller petals and leaf recurving (**Figure 8**, **Figure S7**). The *SiCYC1A*$^W$ and *SiCYC1A*$^V$ T2 transgenic plants generally produced smaller and narrower petals than those in WT *Arabidopsis* and empty vector control. To further understand whether the reduction of the petal size by *SiCYC1A*$^W$ and *SiCYC1A*$^V$ is caused by reduction of cell proliferation or cell expansion, petal size and cell size of T2 plants were measured by the following procedures as stated above. The measurements were averaged by 20 petals from five flowers per individual, three individuals of each construct. The average size of *Arabidopsis* wild-type petals and empty vector control was measured to be 2.4 mm$^2$ ($\pm$0.21) and 2.3 mm$^2$ ($\pm$0.18), respectively. However, petals of $T_2$ plants of *SiCYC1A*$^W$ and *SiCYC1A*$^V$ had a reduced petal size of 1.6 to 1.4 mm$^2$ ($\pm$0.17$\sim$0.26) therefore were 1.5-fold to 2.0-fold smaller than *Arabidopsis* WT petals (**Figure 8B**) [ANOVA test, $F_{(3,150)} = 150.6$, $p < 0.001$].

The cell sizes (including distal and proximal regions) differences between each construct were further compared (**Figure 8C**). Both in *SiCYC1A*$^W$ and *SiCYC1A*$^V$ $T_2$ transgenic plants, the cell size in the proximal petal region (615.10 $\pm$ 94.55 $\mu$m, 531.30 $\pm$ 96.41 $\mu$m, respectively) showed no difference to that in the wild type (573.54 $\pm$ 111.33 $\mu$m). Similarly, no cell size difference could be found in the distal petal region among $T_2$ plants and wild type. Together, these suggest that the reduction of petal size by *SiCYC1A*$^W$and *SiCYC1A*$^V$ in *Arabidopsis* T2 transgenic plants is caused by reduced cell proliferation rather than cell size changes, similar to that in African violet. This is evident from SEM pictures that there is no conspicuous morphological difference on petal epidermal cell among wildtype, *35S::SiCYC1A*$^W$, and *35::SiCYC1A*$^V$ transgenic plants. The distal side petal cells in transgenic T2 looks normal as conical cells and at the proximal side cells are long and columnar, resembling those of the wild type (**Figure S8**). For leaf morphology, the *SiCYC1A*$^W$ and *SiCYC1A*$^V$ $T_2$ transgenic plants had thicker and more curly leaves than that in wild type and empty vector control (**Figure S7**). And this effect was more severe in *SiCYC1A*$^V$ $T_2$ transgenic plants than it was in *SiCYC1A*$^W$ $T_2$ transgenic plants.

# DISCUSSION

## Divergent Expression Shifts of *SiCYC1s* Associate With Reversions to Actinomorphy

We have demonstrated that *SiCYC1*s (*SiCYC1A* and *SiCYC1B*), similar to *CYC* and *DICH* in snapdragon, have a dorsal petal-specific expression pattern in floral meristems (*RNA in-situ*) and late petal development stages (qRT-PCR) of WT (**Figures 3**, **4**). The expression of *SiCYC1*s correlates to smaller dorsal petal size observed in WT. The extended *SiCYC1*s expression to all petals in DA also correlates with the fact that all five petals are small in size and all five stamens are aborted. The much reduced *SiCYC1*s expression in VA, although still dorsal specific, correlates positively with enlarged dorsal petals similar to the size of lateral and ventral petals. Therefore, the shifts of *SiCYC1*s expression correlate to floral symmetry transitions in both DA and VA.

From our study, it is unique that the petal homeotic transformation into dorsal and ventral identity both evolved in African violet peloria. In Gesneriaceae, dorsalized actinomorphy has been reported in *Tengia* and occasionally in *Petrocosmea* hybrids (Pang et al., 2010; Yang et al., 2015). On the other hand, ventralized actinomorphy attributable to mutated *CYC* or cessation of expression of *CYC* in late petal development stage has been reported in *Sinningia speciosa* and *Bournea* (Zhou et al., 2008; Hsu et al., 2015, 2017). Other than Gesneriaceae, the evolutionary reversals to dorsalized actinomorphy attributable to the extension of *CYC* into all petals have been reported in *Cadia* (Leguminosae), parallel Malpighiaceae lineages (Citerne et al., 2006; Zhang et al., 2010, 2012, 2013). But reversals to actinomorphy owing to loss of asymmetrical *CYC* expression or transient expression only are more frequently observed such asin *Tradescantia* (Commelinaceae, monocot), in *Plantago lanceolate* (Plantaginaceae, eudicots), in pollinator shifted Malpighiaceae lineages and in *Arabidopsis* (Cubas et al., 2001; Reardon et al., 2009; Preston et al., 2011; Preston and Hileman, 2012; Zhang et al., 2013).

It is worth mentioning that the shifts of *CYC* expression have also been demonstrated to correlate with patterns of stamen arrest. In *Mohavea confertiflora* (Plantaginaceae), expansion of *CYC* expression into lateral stamen primordia correlates with the abortion into sterile staminodes (Hileman et al., 2003). Our finding clearly indicates that *SiCYC1A / 1B* are still weakly expressed in the dorsal part of the ventralized actinomorphic flower (VA) and this may explain why the VA peloria shows some residual asymmetry in having the dorsal stamen slightly reduced in size when compared to lateral and ventral ones (**Figures 1C,F, Figure S2AA**). On the other hand, ubiquitous expression of *CYC* in the entire flower bud, as in DA of African violet, may retard all stamen development (**Figure S2Y**). However, the function of *CYC* may not be necessary to link to petal growth and stamen development in all cases. In dorsalized actinomorphy of *Tengia* and *Cadia*, the whole flower expression of *CYC* apparently does not contribute to stamen arrest (Citerne et al., 2006; Pang et al., 2010). Therefore, the regulation shifts of *CYC* expression correlating to floral symmetry transition, by means of controlling petal and stamen development in different parts of the flower, could be far more complicated and diverse than one could imagine.

## *SiCYC1s* Gene Duplication Resulted in Divergence of Gene Expression and Divergent Selection

Gene duplication is usually accompanied by increased gene expression diversity. Our results clearly indicate that *SiCYC1A* acts as the major expressed copy whereas *SiCYC1B* as the weakly

**TABLE 2 |** Association of *SiCYC1A* and *SiCYC1B* alleles to floral symmetry phenotypes in F1 hybrids (WT × DA).

| Phenotype \ Genotype[a] | $A^{D/W}B^{D/W}$ | $A^{D/W}B^{W/W}$ | $A^{W/W}B^{D/W}$ | $A^{W/W}B^{W/W}$ | $\chi^2$-value | *P*-value |
|---|---|---|---|---|---|---|
| Bilateral symmetry | 14 | 17 | 10 | 16 | – | – |
| Dorsalized actinomorphy | 11 | 8 | 16 | 14 | – | – |
| | 25 | 25 | 26 | 30 | 0.6415 | 0.8868 |

[a]*The null hypothesis of genotype frequency is 1:1:1:1. $A^{D/W}$ denotes F1s with heterozygote SiCYC1A: A combination of one allele from DA, SiCYC1A$^D$ and another allele from WT, SiCYC1A$^W$. Similarly, $B^{D/W}$ denotes F1s with heterozygous SiCYC1B: A combination of one allele from DA, SiCYC1B$^D$ and another allele from WT, SiCYC1B$^W$. The parent DA is a heterozygote for SiCYC1A and SiCYC1B ($A^{D/W}B^{D/W}$), while parent WT is homozygous for both locus ($A^{W/W}B^{W/W}$).*

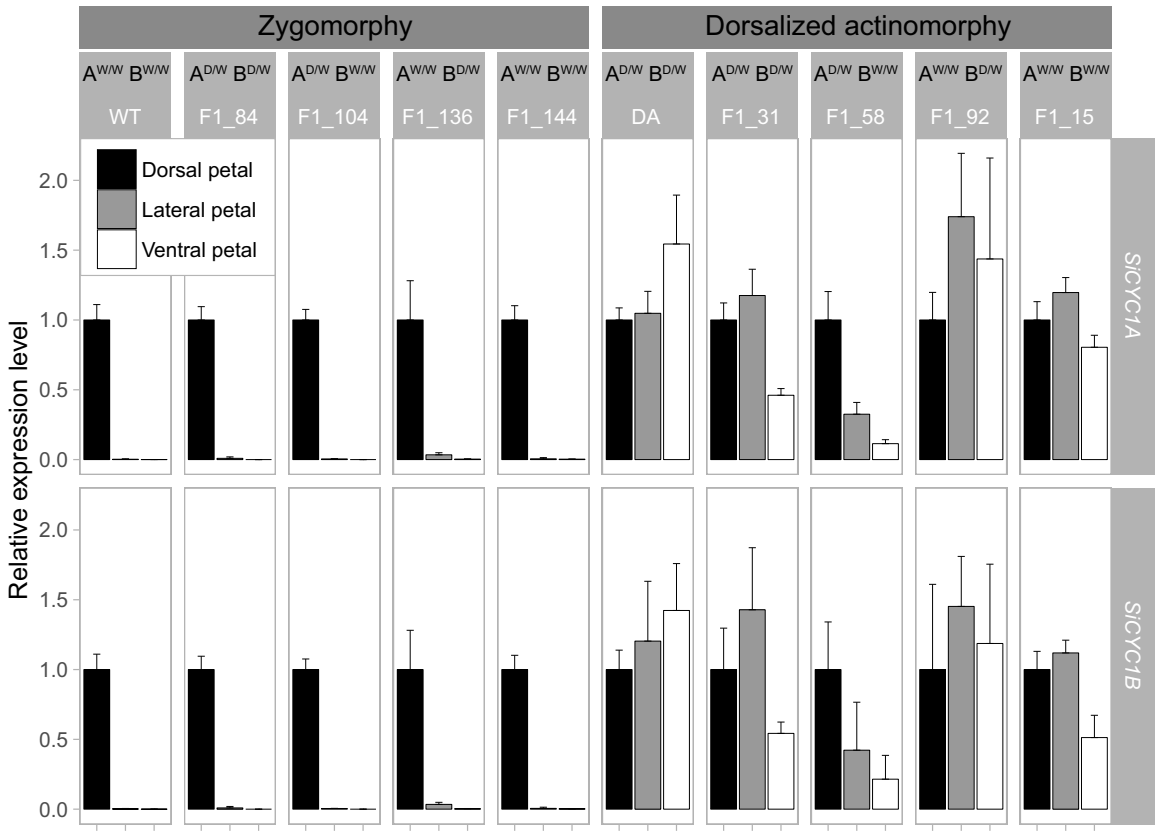


**FIGURE 7 |** qRT-PCR expression patterns of *SiCYC1A* and *SiCYC1B* in dissected petals at stage 12 of F1 hybrids (WT × DA). This figure summarized expression patterns of *SiCYC1A* and *SiCYCB* among F1 individuals with all possible combinations of genotypes ($A^{D/W}B^{D/W}$, $A^{D/W}B^{W/W}$, $A^{W/W}B^{D/W}$, $A^{W/W}B^{W/W}$) and their phenotypes (zygomorphy, actinomorphy). For genotype abbreviation, A denotes *SiCYC1A* and B denotes *SiCYC1B*. Those F1s in zygomorphic phenotype (F1_136, F1_104, F1_84, F1_144) all share the same *SiCYC1A* and *SiCYC1B* expression pattern as their WT parent, but their inherited genotypes (allelic combinations) are in all four equally probable ways. Those F1s in dorsalized actinomorphy revealed the same phenomena in that (F1_31, F1_58, F1_92, F1_15) also share the same *SiCYC1A* and *SiCYC1B* expression pattern as their DA parent but is not confined to a certain inherited genotype. See text for the explanation. Each facet represents a biological repeat with three technical repeats (mean ± SD). The relative expression levels were normalized to *Actin* and *SiCYC1A/SiCYC1B* of the dorsal petals.

expressed one in all studied floral tissues (**Figure 3**). Given the evidence that *SiCYC1A* and *SiCYC1B* are apparently recently duplicated paralogues and their amino acid sequence similarity is as high as 87% (**Figure 2**, see also Wang et al., 2004a), *SiCYC1A* and *SiCYC1B* thus act redundantly. This is reminiscent of *Antirrhinum* in that *CYC* expressed stronger when compared to weaker *DICH* expression in the dorsal part of the flower (Luo et al., 1996, 1999).

Consistent with previous findings (Wang et al., 2004a), an ancient *GCYC* duplication event (*GCYC1* vs. *GCYC2*) was also uncovered from our analysis (**Figure 2B**). This duplication seems to predate the origin of all Gesneriaceae species owing to the fact that every species contains both *GCYC1* and *GCYC2* copies including our African violet cultivars. Certain old world Gesneriaceae, particularly Didymocarpoideae species, also contain another subfamily level duplication of *GCYC1* into

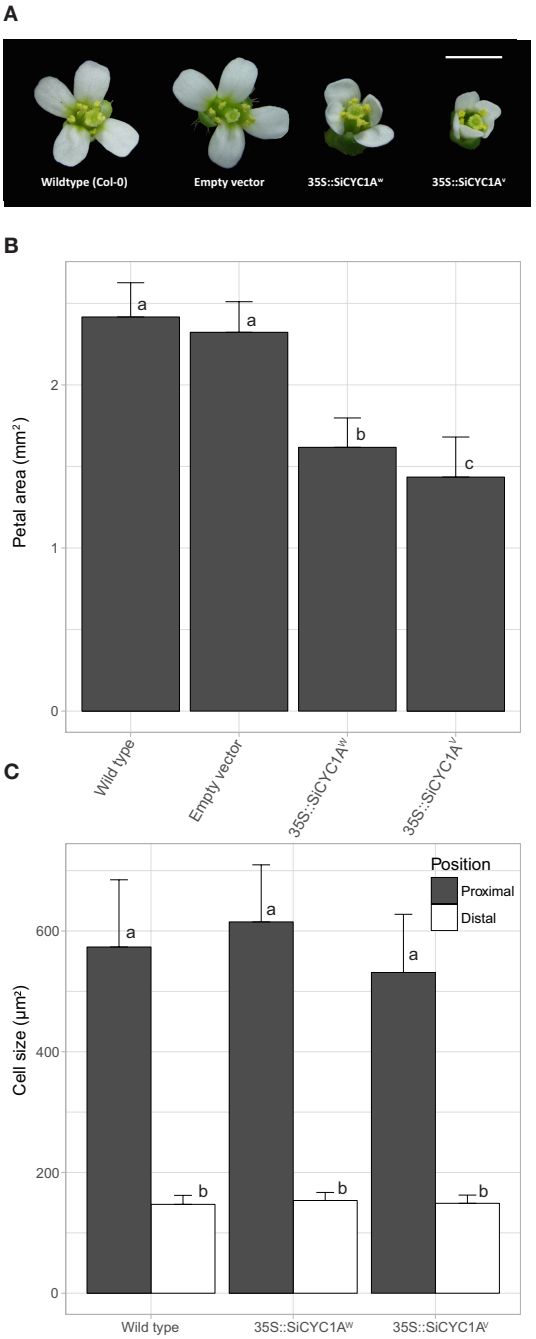


**FIGURE 8 |** Flower morphology of Arabidopsis T2 transgenic plants. **(A)** Constitutive expression of different alleles of *SiCYC1A* in *Arabidopsis* represses petal size. Flower morphology of $T_2$ transgenic plants were measured at fully open stage. Scale bar = 1.5 mm. **(B)** Petal size (mean ± SD) decreases in *SiCYC1A* overexpression $T_2$ transgenic plants [$F_{(3,150)} = 150.6$, $p < 0.001$]. **(C)** Cell size (mean ± SD) in petals of $T_2$ transgenic plants are not different to the wild type. Thus *SiCYC1A* has effects on reducing cell proliferation to repress petal size. The significance was analyzed by ANOVA test and grouped by Turkey *post hoc* test (significant level = 0.05). See **Figure S8** for cell morphology in scanning electronic microscope.

*GCYC1C* and *GCYC1D* (Wang et al., 2004a), which is also revealed in our *GCYC* phylogeny tree. Whether or not these various levels of *GCYC* duplication resulted in a diversified expression pattern remains to be investigated.

Gene duplication may lead to the conservation of major function in one copy but allow a variation in the other copy. Analysis of our *GCYC1A* / *1B* gene dataset suggests a purifying selection constraint on the major high-expressed copy, *GCYC1A* (*SiCYC1A*), whereas the weakly expressed *GCYC1B* (*SiCYC1B*) showed relaxation of purifying selection since their duplication, in a lineage-specific manner (**Figure 5E**). Hileman and Baum (2003) also detected a relaxed purifying selection along the *DICH* linage whereas *CYC* lineage remains under strong genetic constraint. They hypothesized that duplication of *CYC*/*DICH* in *Antirrhinum* occurred in three stages: (1) duplication; (2) relaxed selection in one of the duplicated genes allowing to acquire sub or new function; and (3) purifying selection to stabilize both duplicated genes to maintain evolved functions.

Frequent *CYC* duplications followed by their diverse expression patterns have been proposed as a driving force for their functional divergence (Zhong and Kellogg, 2015). In *Lupinus*, positive selection acting at few *LEGCYC1B* sites were correlated with petal size changes in *L. densiflorus* (Ree et al., 2004), suggesting neo-functionalization of this *CYC* duplicate. In *Helianthus*, divergent expression patterns of *CYC* duplicates were correlated to residues in the conserved domains under positive selection following gene duplication (Chapman et al., 2008). Bello et al. (2017) has uncovered that each *CYC/TB1* duplicate has evolved either purifying or episodic positive selection among Asteraceae species thus allowing retention of multiple copies of *CYC* for generating flower shape diversity. To conclude, the rapid evolution through gene duplications and sub-functionalization among diversified copies could be a common regime for *CYC* evolution.

## Genetic Analysis Reveals Trans-acting Factors of *SiCYC1s* Required for Floral Symmetry Transition

Cis-regulatory changes, trans-regulatory changes, and a combination of both have been shown to contribute to the expression differentiation between *CYC* duplicates in Gesneriaceae species (Yang et al., 2012, 2015). *CYCs* in Generiaceae species can positively auto-regulate themselves (cis regulatory effect) and cross-regulate each other (trans regulatory effect) (Yang et al., 2012). Thus the shifts of *SiCYC1s* expression and the resulting floral symmetry transitions in African violet could be attributable to the difference in efficiency of positive auto- and cross- feedback for maintenance of expression between *SiCYC1s* alleles. For example, the low expression level of $SiCYC1A^V$ in VA flower when compared to higher $SiCYC1A^W$ in WT could be attributable to a mutation on auto- or cross-regulatory feedback loop of $SiCYC1A^V$ thus resulting in poor maintenance of its expression level.

From supposed dominance or recessiveness of allelic relationship inferred from our crossing design results, we expect that F1s of WT x DA with dorsalized actinomorphy phenotype should have inherited at least one DA allele (*SiCYC1A*$^{D}$ or *SiCYC1B*$^{D}$) from the DA parent (**Figure 6**, **Figure S6B**). To our surprise, from F1s genotyping results, there is an equal association of DA or WT allele (*SiCYC1A*$^{W}$ or *SiCYC1B*$^{W}$) to dorsalized actinomorphy (**Table 2**). The same conclusion also applies to those F1s with zygomorphic phenotype. Even though there is no clear association of certain *SiCYC1s* alleles to particular floral symmetry phenotypes in F1s, expression patterns of these alleles, however, match perfectly with their resulting phenotypes (**Figure 7**). Allelic sequences of *SiCYC1s* are highly similar to each other among cultivars (<1% divergence at amino acid level) and thus unlikely to evolve into new phenotypic functions. Adding to the fact that ectopically expressing CDS of either *SiCYC1A*$^{W}$ or *SiCYC1A*$^{V}$ gives the same phenotypic effect on *Arabidopsis* petal morphology, the function of *SiCYC1s* alleles from different African violet cultivars is perhaps identical. Thus, the shifts of *SiCYC1s* expression and the resulting floral symmetry transitions are more likely controlled by trans-acting factors upstream of *SiCYC1s* rather than their own cis-elements.

Several recent studies also suggest the possibility that other dorsiventral asymmetrically expressed genes rather than *CYC* could be the actual controlling factors of zygomorphy. This is evident in *Aristolochia*, Proteaceae, and Fumarioideae species where *CYC* differential expression along the dorsiventral axis in flower was observed only after the perianth zygomorphy had already been established (Damerval et al., 2013; Horn et al., 2015; Citerne et al., 2017). Trans-acting (upstream) factors other than *CYC* could therefore be the other possibility accounting for the shifts of *CYC* expression by either promoting or repressing the transcription of *CYC* in certain parts of the flower.

Although there are no reports on what *CYC* trans-acting (upstream) regulators should be, B class genes which specify petal and stamen identity were possible candidates. Only few studies ever managed to test this hypothesis yet their interaction remains unclear. In *Antirrhinum*, B class gene (*DEFICIENS*) activity is required for maintenance of *CYC* in petal whorl (Clark and Coen, 2002). Preston and Hileman (2012) when compared to *B* class (*DEF* and *GLO*) and *CYC* (*TB1*) expressions in zygomorphic *Commelina* and actinomorphic *Tradescantia* species (Commelinaceae). They found *CYC* expressed more in ventral parts (inner tepals and stamens) of the flowers but B class exclusively more in dorsal parts. B class genes especially *AP3-2* and *AGL6-2* have been found in orchids involving lip formation since their expressions are concentrated in the flower's ventral part, namely the lip (Pan et al., 2011; Hsu et al., 2015). This asymmetrical expression pattern thus helps to create zygomorphy in *Oncidium* and *Phalenopsis* orchids. Further works on whether B-class genes and *CYC* interact with each other shall resolve their regulation relationship.

## Epigenetic Regulation of *SiCYC1s* May Explain Floral Symmetry Transition in African Violet

DNA epigenetic mutation on *CYC*, although rarely reported, is also a plausible mechanism to account for the shifts of *CYC* expression in generating floral symmetry transition. *CYC* was transcriptionally silent and found to be extensively methylated in peloric mutant but not in the zygomorphic wildtype of *Linaria vulgaris* (Cubas et al., 1999b). Flowers from peloria in *L. vulgaris* show somatic instability and later develop reversely to zygomorphy, correlating with the demethylation and restoration of *CYC* expression. Epigenetic regulation is more likely the reason for the shifts of *SiCYC1s* expression in African violet since we also observed that F1 hybrids with dorsalized actinomorphy phenotypically reverts into zygomorphic WT within the same inflorescence (**Figure S9**). African violet is not alone. Among hybrids of two zygomorphic *Petrocosmea* species, individuals reversed to dorsalized actinomorphy with all stamens aborted can sometimes be observed (Yang et al., 2015). Therefore, the changes of epigenetic regulation on *CYC* could be a more widespread scenario but was previously neglected. Although not yet reported in *CYC*, a 4.9 fold increase in histone acetylation level has been reported for B class gene (PeMADS4) in the lip of *Phalaenopsis* orchid, correlating to its high expression in lip specifically (Hsu et al., 2014). Further works on checking the DNA methylations and histone acetylation levels among *SiCYC1s* alleles from flower parts between different cultivars are needed to prove this.

## *SiCYC1A* Function to Retard Petal Growth via Reduced Cell Proliferation and Higher Expression

*CYC* duplicates appear to evolve into a diverse phenotypic effect on petal morphology. In Gesneriaceae species, including our results, the high expression copy, *SiCYC1A*, appears to have a major role in restricting petal size of dorsal petals in African violet and in petals of transformed *Arabidopsis*. Similarly, two *Petrocosmea* species have their *CYC1C* and *CYC1D* expressing restrictively in dorsal petals (Yang et al., 2015). But both copies showed much higher expression in *one* species, *P. glabristoma*, in correlating to its smaller dorsal petal size, whereas a weaker expression in another species, *P. sinensis*, was associated to its larger dorsal petal size. Through genetic association studies, *CYC* mutation has been associated with the enlargement of the entire flower and petal in artificially selected VA of *Sinningia speciosa* (Hsu et al., 2015). From corolla 3D geometric morphometric analysis, *SsCYC* has been demonstrated as associating with the outward curvature of dorsal petals and petal size, again, a strong support that *CYC* affects diverse parts of petal morphology (Wang et al., 2015; Hsu et al., 2017).

The function of *SiCYC1A* in retarding African violet petal growth was further confirmed by their phenotypes in *Arabidopsis* transformants with apparently reduced petal size (**Figure 8**). This petal retarding effect is congruent with the ectopic expression phenotypes of *CYC1C* from *Primulina heterotricha* and *TCP1* genes from *Iberis amara* in *Arabidopsis* (Busch and Zachgo, 2007;

Yang et al., 2012). In contrast with that, however, *Antirrhinum CYC* promotes petal growth in *Arabidopsis* (Costa et al., 2005). This demonstrates that *CYC* genes in diverse lineages have evolved contrasting function on petal growth although their major roles in floral symmetry remain unchanged.

While looking in detail on whether the *CYC* effects on petal growth was achieved by regulating cell proliferation or expansion, different conclusions were drawn. From petal epidermal picture in African violet cultivars and in *Arabidopsis* transformants, it appears that the effect of *SiCYC1A* on petal size is attributable to reduced cell proliferation (cell division) rather than reduced cell growth (**Figures S4, S8**). This is again a different observation when compared to the effect of *CYC1C* from *Primulina heterotricha* and *CYC* from *Antirrhinum CYC*, in which they retard cell growth (reduced size of cells) but not cell proliferation (Costa et al., 2005; Yang et al., 2012). These facts imply that the regulation of *CYC* on petal morphology is far more complicated than we thought and they may evolve different modified functions independently in various flowering plant lineages.

### Homologs of *RADIALIS* and *DIVARICATA* Isolated From African Violet but Their Expressions Showed No Dorsiventral Asymmetric Patterns

In *Antirrhinum CYC* regulates a downstream MYB-like protein *RADIALIS* (*RAD*) to establish zygomorphy (Galego and Almeida, 2002; Corley et al., 2005; Costa et al., 2005). *CYC* protein directly binds to the *RAD* promoter in the dorsal part of the flower, allowing RAD protein to antagonistically compete with another MYB gene family *DIVARICATA* (DIV) protein for other two downstream MYB-like proteins to prevent DIV activity in dorsal regions (Costa et al., 2005; Raimundo et al., 2013; Hileman, 2014b). *rad* $^{-}$mutants of *Antirrhinum* have enhanced ventral identity but retained the dorsal identity (Carpenter and Coen, 1990). A ventralized peloric phenotype could therefore also result from a knock-out *RAD* mutation.

We also isolated putative *RAD* and *DIV* homologs from WT, DA and VA (**Figures S10, S11**, detailed methods please see **Supplementary Materials**). The (q)RT-PCR expression patterns of *RAD* (*SiRAD1* and *SiRAD2*) and *DIV* (*SiDIV1A* and *SiDIV1B*) (**Figures S12**, **S13**), however, were not correlated with *SiCYC1s* expression shifts in these cultivars. One could argue that our PCR cloning process may not isolate all possible homologs of *RAD* and *DIV*, given they belong to part of multigenic *MYB* families. It is therefore not clear whether *RAD* and *DIV* are associated with floral symmetry transitions in *S. ionantha*. Detailed results of this section were provided in the **Supplementary Material** and the findings were briefly discussed there.

## AUTHOR CONTRIBUTIONS

C-NW designed the research and carried out the main writing. The experiments were conceived and conducted by H-JH, C-WH, and W-HK. Experimental strategies were designed by Z-JP and C-NW. Gene selection analysis was performed and interpreted by K-TH, J-YL, and C-NW. All authors prepared and commented on the manuscript.

## FUNDING

The main funding from the Ministry of Science and Technology of Taiwan MOST-106-2313-B-002-035-MY3 and the National Science Council of Taiwan 95-2311-B-002-014-MY3 were granted to C-NW.

## ACKNOWLEDGMENTS

We thank Mr. Chun-Ming Chen at Dr. Cecilia Koo Botanic Conservation Center, Taiwan for providing African violet plants, Ms. Hsin-Rou Wang at the National Taiwan University for diagram drawing, Shiang-Jiuun Chen from Technology Common (College of Life Science, National Taiwan University, Taiwan) for SEM service, Michael Moeller at the Royal Botanic Garden Edinburgh and Quentin Cronk at the University of British Columbia for comments on initial experimental designs. We thank both reviewers for their constructive comments and suggestions.

## SUPPLEMENTARY MATERIAL

The Supplementary Material for this article can be found online at: https://www.frontiersin.org/articles/10.3389/fpls.2018.01008/full#supplementary-material

## REFERENCES

Bello, M. A., Cubas, P., Alvarez, I., Sanjuanbenito, G., and Fuertes-Aguilar, J. (2017). Evolution and expression patterns of CYC/TB1 genes in anacyclus: phylogenetic insights for floral symmetry genes in asteraceae. *Front. Plant Sci.* 8:589. doi: 10.3389/fpls.2017.00589

Bielawski, J. P., and Yang, Z. (2003) Maximum likelihood methods for detecting adaptive evolution after gene duplication. *J. Struct. Funct. Genomics* 3, 201–212. doi: 10.1023/A:1022642807731

Bouckaert, R., Heled, J., Kühnert, D., Vaughan, T., Wu, C. H., Xie, D., et al. (2014). BEAST 2: a software platform for bayesian evolutionary analysis. *PLoS Comput. Biol.* 10:e1003537. doi: 10.1371/journal.pcbi.1003537

Busch, A., and Zachgo, S. (2007). Control of corolla monosymmetry in the Brassicaceae Iberis amara. *Proc. Natl. Acad. Sci. U.S.A.* 104, 16714–16719. doi: 10.1073/pnas.0705338104

Busch, A., and Zachgo, S. (2009). Flower symmetry evolution: towards understanding the abominable mystery of angiosperm radiation. *Bioessays* 31, 1181–1190. doi: 10.1002/bies.200900081

Carpenter, R., and Coen, E. S. (1990). Floral homeotic mutations produced by transposon-mutagenesis in *Antirrhinum majus*. *Genes Dev.* 4, 1483–1493. doi: 10.1101/gad.4.9.1483

Chapman, M. A., Leebens-Mack, J. H., and Burke, J. M. (2008). Positive selection and expression divergence following gene duplication in the sunflower CYCLOIDEA gene family. *Mol. Biol. Evol.* 25, 1260–1273. doi: 10.1093/molbev/msn001

Chapman, M. A., Tang S., Draeger, D., Nambeesan, S., Shaffer, H., Barb, J. G., et al. (2012). Genetic analysis of floral symmetry in Van Gogh's sunflowers reveals independent recruitment of CYCLOIDEA genes in the Asteraceae. *PLoS Genet*. 8:e1002628. doi: 10.1371/journal.pgen.1002628

Citerne, H., Moller, M., and Cronk, Q. C. B. (2000). Diversity of cycloidea -like genes in gesneriaceae in relation to floral symmetry. *Ann. Bot.* 86, 167–176. doi: 10.1006/anbo.2000.1178

Citerne, H. L., Pennington, R. T., and Cronk, Q. C. (2006). An apparent reversal in floral symmetry in the legume Cadia is a homeotic transformation. *Proc. Natl. Acad. Sci. U.S.A.* 103, 12017–12020. doi: 10.1073/pnas.0600986103

Citerne, H. L., Reyes, E., Le Guilloux, M., Delannoy, E., Simonnet, F., Sauquet, H., et al. (2017). Characterization of CYCLOIDEA-like genes in Proteaceae, a basal eudicot family with multiple shifts in floral symmetry. *Ann. Bot.* 119, 367–378. doi: 10.1093/aob/mcw219

Clark, J. I., and Coen, E. S. (2002) The *cycloidea* gene can response to a common dorsoventral prepattern in *Antirrhinum*. *Plant J.* 30, 639–648. doi: 10.1046/j.1365-313X.2002.01310.x

Clough, S. J., and Bent, A. F. (1988). Floral dip: a simplified method for *Agrobacterium*-mediated transformation of *Arabidopsis thaliana*. *Plant J.* 16, 735–743. doi: 10.1046/j.1365-313x.1998.00343.x

Coen, E. S., and Nugent, J. M. (1994) Evolution of flowers and inflorescences. *Development* 1994(Suppl.), 107–116.

Corley, S. B., Carpenter, R., Copsey, L., and Coen, E. (2005). Floral asymmetry involves an interplay between TCP and MYB transcription factors in Antirrhinum. *Proc. Natl. Acad. Sci. U.S.A.* 102, 5068–5073. doi: 10.1073/pnas.0501340102

Costa, M. M., Fox, S., Hanna, A. I., Baxter, C., and Coen, E. (2005). Evolution of regulatory interactions controlling floral asymmetry. *Development* 132, 5093–5101. doi: 10.1242/dev.02085

Cubas, P., Coen, E., and Zapater, J. M. (2001). Ancient asymmetries in the evolution of flowers. *Curr. Biol.* 11, 1050–1052. doi: 10.1016/s0960-9822(01)00295-0

Cubas, P., Lauter, N., Doebley, J., and Coen, E. (1999a). The TCP domain: a motif found in proteins regulating plant growth and development. *Plant J.* 18, 215–222. doi: 10.1046/j.1365-313X.1999.00444.x

Cubas, P., Vincent, C., and Coen, E. (1999b). An epigenetic mutation responsible for natural variation in floral symmetry. *Nature* 401, 157–161. doi: 10.1038/43657

Damerval, C., Citerne, H., Le Guilloux, M., Domenichini, S., Dutheil, J., Ronse De Craene, L., et al. (2013). Asymmetric morphogenetic cues along the transverse plane: shift from disymmetry to zygomorphy in the flower of Fumarioideae. *Am. J. Bot.* 100, 391–402. doi: 10.3732/ajb.1200376

Feng, X., Zhao, Z., Tian, Z., Xu, S., Luo, Y., Cai, Z., et al. (2006). Control of petal shape and floral zygomorphy in *Lotus japonicus*. *Proc. Natl. Acad. Sci. U.S.A.* 103, 4970–4975. doi: 10.1073/pnas.0600681103

Galego, L., and Almeida, J. (2002). Role of DIVARICATA in the control of dorsoventral asymmetry in *Antirrhinum* flowers. *Genes Dev.* 16, 880–891. doi: 10.1101/gad.221002

Gao, Q., Tao, J. H., Yan, D., Wang, Y. Z., and Li, Z. Y. (2008). Expression differentiation of CYC-like floral symmetry genes correlated with their protein sequence divergence in *Chirita* heterotricha (Gesneriaceae). *Dev. Genes Evol.* 218, 341–351. doi: 10.1007/s00427-008-0227-y

Harrison, C., Moller, M., and Cronk, Q. C. B. (1999). Evolution and development of floral diversity in *Streptocarpus* and *Saintpaulia*. *Ann. Bot.* 84, 49–60. doi: 10.1006/anbo.1999.0887

Hileman, L. C. (2014a). Trends in flower symmetry evolution revealed through phylogenetic and developmental genetic advances. *Philos. Trans. R. Soc. Lond. B Biol. Sci.* 369: 20130348. doi: 10.1098/rstb.2013.0348

Hileman, L. C. (2014b). Bilateral flower symmetry–how, when and why? *Curr. Opin. Plant Biol.* 17, 146–152. doi: 10.1016/j.pbi.2013.12.002

Hileman, L. C., and Baum, D. A. (2003). Why do paralogs persist? Molecular evolution of CYCLOIDEA and related floral symmetry genes in Antirrhineae (Veronicaceae). *Mol. Biol. Evol.* 20, 591–600. doi: 10.1093/molbev/msg063

Hileman, L. C., Kramer, E. M., and Baum, D. A. (2003). Differential regulation of symmetry genes and the evolution of floral morphologies. *Proc. Natl. Acad. Sci. U.S.A.* 100, 12814–12819. doi: 10.1073/pnas.1835725100

Horn, S., Pabón-Mora, N., Theuß, V. S., Busch, A., and Zachgo, S. (2015). Analysis of the CYC/TB1 class of TCP transcription factors in basal angiosperms and magnoliids. *Plant J.* 81, 559–571. doi: 10.1111/tpj.12750

Howarth, D. G., Martins, T., Chimney, E., and Donoghue, M. J. (2011). Diversification of CYCLOIDEA expression in the evolution of bilateral flower symmetry in *Caprifoliaceae* and *Lonicera* (Dipsacales). *Ann. Bot.* 107, 1521–1532. doi: 10.1093/aob/mcr049

Hsu, C. C., Wu, P. S., Chen, T. C., Yu, C. W., Tsai, W. C., Wu, K., et al. (2014). Histone acetylation accompanied with promoter sequences displaying differential expression profiles of B-class MADS-box genes for phalaenopsis floral morphogenesis. *PLoS ONE* 9:e106033. doi: 10.1371/journal.pone.0106033

Hsu, H. C., Chen, C. Y., Lee, T. K., Weng, L. K., Yeh, D. M., Lin, T. T., et al. (2015). Quantitative analysis of floral symmetry and tube dilation in an F2 cross of Sinningia speciosa. *Sci. Hortic.* 188, 71–77. doi: 10.1016/j.scienta.2015.03.019

Hsu, H. C., Wang, C. N., Liang, C. H., Wang, C. C., and Kuo, Y. F. (2017). Association between petal form variation and CYC2-like genotype in a hybrid line of *Sinningia speciosa*. *Front. Plant Sci.* 8:558. doi: 10.3389/fpls.2017.00558

Jabbour, F., Cossard, G., Le Guilloux, M., Sannier, J., Nadot, S., and Damerval, C. (2014). Specific duplication and dorsoventrally asymmetric expression patterns of Cycloidea-like genes in zygomorphic species of *Ranunculaceae*. *PLoS ONE* 9:e95727. doi: 10.1371/journal.pone.0095727

Luo, D., Carpenter, R., Copsey, L.,Vincent, C., Clark, J., and Coen, E. (1999).Control of organ asymmetry in flowers of *Antirrhinum*. *Cell* 99, 367–376. doi: 10.1016/S0092-8674(00)81523-8

Luo, D., Carpenter, R., Vincent, C., Copsey, L., and Coen, E. (1996). Origin of floral asymmetry in *Antirrhinum*. *Nature* 383, 794–799. doi: 10.1038/383794a0

Möller, M., Clokie, M., Cubas, P., and Cronk, Q. C. B. (1999) "Integrating molecular and developmental genetics: a Gesneriaceae case study," in *Molecular Systematics and Plant Evolution*, eds P. M. Hollingsworth, R. M. Bateman, and R. J. Gornall (London: Taylor and Francis), 375–402.

Pan, Z. J., Cheng, C. C., Tsai, W. C., Chung, M. C., Chen, W. H., Hu, J. M., et al. (2011). The duplicated B-class MADS-box genes display dualistic characters in orchid floral organ identity and growth. *Plant Cell Physiol.* 52, 1515–1531. doi: 10.1093/pcp/pcr092

Pang, H. B., Sun, Q. W., He, S. Z., and Wang, Y. Z. (2010). Expression pattern of *CYC*-like genes relating to a dorsalized actinomorphic flower in Tengia (Gesneriaceae). *J. Syst. Evol.* 48, 309–317. doi: 10.1111/j.1759-6831.2010.00091.x

Preston, J. C., and Hileman, L. C. (2012). Parallel evolution of TCP and B-class genes in Commelinaceae flower bilateral symmetry. *Evodevo* 3:6. doi: 10.1186/2041-9139-3-6

Preston, J. C., Martinez, C. C., and Hileman, L. C. (2011). Gradual disintegration of the floral symmetry gene network is implicated in the evolution of a wind-pollination syndrome. *Proc. Natl. Acad. Sci. U.S.A.* 108, 2343–2348. doi: 10.1073/pnas.1011361108

Raimundo, J., Sobral, R., Bailey, P., Azevedo, H., Galego, L., Almeida, J., et al. (2013). A subcellular tug of war involving three MYB-like proteins underlies a molecular antagonism in Antirrhinum flower asymmetry. *Plant J.* 75, 527–538. doi: 10.1111/tpj.12225

Reardon, W., Fitzpatrick, D. A., Fares, M. A., and Nugent, J. M. (2009). Evolution of flower shape in Plantago lanceolata. *Plant Mol. Biol.* 71, 241–250. doi: 10.1007/s11103-009-9520-z

Ree, R. H., Citerne, H. L., Lavin, M., and Cronk, Q. C. (2004). Heterogeneous selection on LEGCYC paralogs in relation to flower morphology and the phylogeny of Lupinus (Leguminosae). *Mol. Biol. Evol.* 21, 321–331. doi: 10.1093/molbev/msh022

Reed, S. C. (1961). Genetic check-list. *Afr. Violet Magaz.* 14, 104–106.

Rosin, F. M., and Kramer, E. M. (2009). Old dogs, new tricks: regulatory evolution in conserved genetic modules leads to novel morphologies in plants. *Dev. Biol.* 332, 25–35. doi: 10.1016/j.ydbio.2009.05.542

Smith, J. F., Funke, M. M., and Woo, V. L. (2006). A duplication of gcyc predates divergence within tribe Coronanthereae (*Gesneriaceae*): phylogenetic analysis and evolution. *Plant Syst. Evol.* 261, 245–256. doi: 10.1007/s00606-006-0445-6

Smith, J. F., Hileman, L. C., Powell, M. P., and Baum, D. A. (2004). Evolution of GCYC, a Gesneriaceae homolog of CYCLOIDEA, within

Gesnerioideae (*Gesneriaceae*). *Mol. Phylogenet. Evol.* 31, 765–779. doi: 10.1016/j.ympev.2003.09.012

Spencer, V., and Kim, M. (2018). Re"CYC"ling molecular regulators in the evolution and development of flower symmetry. *Semin. Cell Dev. Biol.* 79, 16–26. doi: 10.1016/j.semcdb.2017.08.052

Stamatakis, A. (2014). RAxML version 8: a tool for phylogenetic analysis and post-analysis of large phylogenies. *Bioinformatics* 30, 1312–1313. doi: 10.1093/bioinformatics/btu033

Wang, C. N., Chen, Y. J., Chang, Y. C., and Wu, C. H. (2008). A step-by-step optimization guide for applying tissue specific RNA in-situ hybridization to non-model plant species. *Taiwania* 53, 383–393. doi: 10.6165/tai.2008.53(4).383

Wang, C. N., Hsu, H. C., Wang, C. C., Lee, T. K., and Kuo, Y. F. (2015). Quantifying floral shape variation in 3D using microcomputed tomography: a case study of a hybrid line between actinomorphic and zygomorphic flowers. *Front. Plant Sci.* 6:724. doi: 10.3389/fpls.2015.00724

Wang, C. N., Moller, M., and Cronk, Q. C. B. (2004a). Phylogenetic position of *Titanotrichum oldhamii* (Gesneriaceae) inferred from four different gene regions. *Syst. Bot.* 29, 407–418. doi: 10.1600/036364404774195593

Wang, C. N., Moller, M., and Cronk, Q. C. B. (2004b). Altered expression of GFLO, the Gesneriaceae homologue of *FLORICAULA/LEAFY*, is associated with the transition to bulbil formation in *Titanotrichum oldhamii*. *Dev. Genes Evol.* 214, 122–127. doi: 10.1007/s00427-004-0388-2

Weadick, C. J., and Chang, B. S. (2011). An improved likelihood ratio test for detecting site-specific functional divergence among clades of protein-coding genes. *Mol. Biol. Evol* 29, 1297–300. doi: 10.1093/molbev/msr311

Yang, X., Pang, H. B., Liu, B. L., Qiu, Z. J., Gao, Q., Wei, L., et al. (2012). Evolution of double positive autoregulatory feedback loops in *CYCLOIDEA2* clade genes is associated with the origin of floral zygomorphy. *Plant Cell* 24, 1834–1847. doi: 10.1105/tpc.112.099457

Yang, X., Zhao, X. G., Li, C. Q., Liu, J., Qiu, Z. J., Dong, Y., et al. (2015). Distinct regulatory changes underlying differential expression of teosinte branched1-cycloidea-proliferating cell factor genes associated with petal variations in zygomorphic flowers of petrocosmea spp. of the family gesneriaceae. *Plant Physiol.* 169, 2138–2151. doi: 10.1104/pp.15.01181

Yang, Z. (2007). PAML 4: phylogenetic analysis by maximum likelihood. *Mol. Biol. Evol.* 24, 1586–91. doi: 10.1093/molbev/msm088

Zhang, W., Kramer, E. M., and Davis, C. C. (2010). Floral symmetry genes and the origin and maintenance of zygomorphy in a plant-pollinator mutualism. *Proc. Natl. Acad. Sci. U.S.A.* 107, 6388–6393. doi: 10.1073/pnas.0910155107

Zhang, W., Kramer, E. M., and Davis, C. C. (2012). Similar genetic mechanisms underlie the parallel evolution of floral phenotypes. *PLoS ONE* 7:e36033. doi: 10.1371/journal.pone.0036033

Zhang, W., Steinmann, V. W., Nikolov, L., Kramer, E. M., and Davis, C. C. (2013). Divergent genetic mechanisms underlie reversals to radial floral symmetry from diverse zygomorphic flowered ancestors. *Front. Plant Sci.* 4:302. doi: 10.3389/fpls.2013.00302

Zhong, J., and Kellogg, E. A. (2015). Duplication and expression of CYC2-like genes in the origin and maintenance of corolla zygomorphy in Lamiales. *New Phytol.* 205, 852–868. doi: 10.1111/nph.13104

Zhou, X. R., Wang, Y. Z., Smith, J. F., and Chen, R. (2008). Altered expression patterns of TCP and MYB genes relating to the floral developmental transition from initial zygomorphy to actinomorphy in Bournea (*Gesneriaceae*). *New Phytol.* 178, 532–543. doi: 10.1111/j.1469-8137.2008.02384.x

**Conflict of Interest Statement:** The authors declare that the research was conducted in the absence of any commercial or financial relationships that could be construed as a potential conflict of interest.

frontiers in Plant Science

ORIGINAL RESEARCH
published: 05 June 2018
doi: 10.3389/fpls.2018.00765

# A Dual Repeat *Cis*-Element Determines Expression of *GERANYL DIPHOSPHATE SYNTHASE* for Monoterpene Production in *Phalaenopsis* Orchids

*Yu-Chen Chuang[1], Yi-Chu Hung[1], Chi-Yu Hsu[1], Chuan-Ming Yeh[2], Nobutaka Mitsuda[3], Masaru Ohme-Takagi[2,3], Wen-Chieh Tsai[4], Wen-Huei Chen[5] and Hong-Hwa Chen[1,4,5]**

[1] Department of Life Sciences, National Cheng Kung University, Tainan, Taiwan, [2] Division of Strategic Research and Development, Graduate School of Science and Engineering, Saitama University, Saitama, Japan, [3] Bioproduction Research Institute, National Institute of Advanced Industrial Science and Technology, Tsukuba, Japan, [4] Institute of Tropical Plant Sciences, National Cheng Kung University, Tainan, Taiwan, [5] Orchid Research and Development Center, National Cheng Kung University, Tainan, Taiwan

OPEN ACCESS

**Edited by:**
Swee-Suak Ko,
Academia Sinica, Taiwan

**Reviewed by:**
Dinesh A. Nagegowda,
Central Institute of Medicinal and Aromatic Plants (CIMAP), India
Tariq Akhtar,
University of Guelph, Canada

***Correspondence:**
Hong-Hwa Chen
hhchen@mail.ncku.edu.tw

**Specialty section:**
This article was submitted to Plant Breeding, a section of the journal Frontiers in Plant Science

**Received:** 09 March 2018
**Accepted:** 17 May 2018
**Published:** 05 June 2018

**Citation:**
Chuang Y-C, Hung Y-C, Hsu C-Y, Yeh C-M, Mitsuda N, Ohme-Takagi M, Tsai W-C, Chen W-H and Chen H-H (2018) A Dual Repeat Cis-Element Determines Expression of GERANYL DIPHOSPHATE SYNTHASE for Monoterpene Production in Phalaenopsis Orchids. Front. Plant Sci. 9:765. doi: 10.3389/fpls.2018.00765

*Phalaenopsis bellina* is a scented orchid emitting large amount of monoterpenes. GERANYL DIPHOSPHATE SYNTHASE (PbGDPS) is the key enzyme for monoterpene biosynthesis, and shows concomitant expression with the emission of monoterpenes during flower development in *P. bellina*. Here, we identified a dual repeat *cis*-element in the *GDPS* promoter that is critical for monoterpene biosynthesis in *Phalaenopsis* orchids. A strong correlation between the dual repeat and the monoterpene production was revealed by examination of the *GDPS* promoter fragments over 12 *Phalaenopsis* species. Serial-deletion of the 2-kb *GDPS* promoter fragments demonstrated that the integrity of the dual repeat was crucial for its promoter activities. By screening the *Arabidopsis* transcription factors (TFs) cDNA library using yeast one-hybrid assay, AtbZIP18, a member of group I of bZIP TFs, was identified to be able to bind the dual repeat. We then identified *PbbZIP4* in the transcriptome of *P. bellina*, showing 83% identity in the DNA binding region with that of AtbZIP18, and the expression level of *PbbZIP4* was higher in the scented orchids. In addition, PbbZIP4 transactivated the *GDPS* promoter fragment containing the dual repeat in dual luciferase assay. Furthermore, transient ectopic expression of *PbbZIP4* induced a 10-fold production of monoterpenoids in the scentless orchid. In conclusion, these results indicate that the dual repeat is a real TF-bound *cis*-element significant for *GDPS* gene expression, and thus subsequent monoterpene biosynthesis in the scented *Phalaenopsis* orchids.

**Keywords: *cis*-element, floral scent, monoterpene, orchid, *Phalaenopsis*, promoter, transcription factor, yeast-one hybrid screening**

**Abbreviations:** bZIP, basic leucine zipper; DMADP, dimethylallyl diphosphate; GDPS, geranyl diphosphate synthase; IDP, isopentenyl diphosphate; *P.*, *Phalaenopsis*; TFs, transcription factors; Y1H, yeast one-hybrid.

## INTRODUCTION

*Phalaenopsis* species are widespread in the tropical Asia regions and includes approximately 56 native species (Christenson, 2001). Numerous *Phalaenopsis* cultivars with diverse floral appearance are obtained via breeding and have become popular orchids due to their outstanding floral display and longevity (Hsiao et al., 2011a). In addition, some of the *Phalaenopsis* cultivars with pleasant fragrance improve their ornamental value in the floriculture market. However, breeding scented orchid cultivars under traditional breeding is difficult compared to other favorable traits (Yeh et al., 2014). The bottlenecks include long generation time (Hsiao et al., 2011a), cross-incompatibility due to the differences in genome size and chromosome size among species (Hsiao et al., 2011a,b; Yeh et al., 2014), and negative correlation between floral scent and other favorable traits (Hsiao et al., 2011b), which is also occurred in other modern floriculture varieties (Vainstein et al., 2001; Dudareva and Negre, 2005). In such circumstances, alternative approaches to facilitate scented orchid breeding are needed.

The majorities of *Phalaenopsis* orchids are scentless but some do emit scent volatile organic compounds (VOCs) (Kaiser, 1993). These scented species have been extensively used as breeding parents for production of scent cultivars, such as *P. amboinensis*, *P. bellina*, *P. javanica*, *P. lueddemanniana*, *P. schilleriana*, *P. stuartiana*, *P. venosa*, and *P. violace* (Hsiao et al., 2011b; Yeh et al., 2014). Both *P. bellina* and *P. violacea* are two very close species popular in breeding scented phenotype and emits similar but distinct floral VOCs. *P. bellina* emits mainly monoterpenoids, including citronellol, geraniol, linalool, myrcene, nerol, and ocimene (Hsiao et al., 2006, 2011b), while *P. violacea* emits monoterpenoids accompanied with a phenylpropanoid, cinnamyl alcohol (Kaiser, 1993). The VOCs of *P. schilleriana* contain monoterpenoids as well, including citronellol, nerol and neryl acetate (Awano et al., 1997).

Monoterpenoids, the most abundant constituent in volatile terpenoids (Knudsen and Gershenzon, 2006; Nagegowda et al., 2010), are involved in specialized interactions with other organisms and surrounding environment (Tholl, 2015), for example, to function as attractants for pollinators (Byers et al., 2014), as antibacterial and antifungal compounds (Hammer et al., 2003; Yamasaki et al., 2007; Marei et al., 2012; Mirzaei-Najafgholi et al., 2017), and for defense against herbivores (Paré and Tumlinson, 1999; Mumm et al., 2008; Huang et al., 2018). Apart from their roles in nature, monoterpenoids are widely used in flavor, cosmetics, and perfumery industries due to their unique and pleasant fragrance characteristics (Schwab et al., 2008). In addition, they are exploited as health-promoting compounds and have potential to be applied in cancer therapeutics because of their anti-cancer activities (Gould, 1997; Crowell, 1999; Carnesecchi et al., 2001; Jun et al., 2006; Murthy et al., 2012; Cho et al., 2016; Nakayama et al., 2017).

The precursors of monoterpenoids, IDP and its isomer, DMADP, are produced from the methylerythritol phosphate (MEP) pathway in the plastid. The short-chain prenyltransferases, GDPS, is responsible for the head-to-tail condensation of IDP and DMADP to generate the direct substrate GDP for monoterpene synthases (Dudareva et al., 2004). In *Phalaenopsis* orchids, PbGDPS is characterized as the key enzyme to provide precursors for monoterpene biosynthesis in *P. bellina* (Hsiao et al., 2008). Interestingly, recombinant PbGDPS possesses dual prenyltransferase activities for the production of both GDP and farnesyl diphosphate (FDP), the precursor for monoterpeneoids, and sesquiterpenoids, respectively (Hsiao et al., 2008). Expression of *PbGDPS* is concomitant with the emission of monoterpenoids during flower developments, peaked on day 5 post anthesis (D + 5) (Hsiao et al., 2008).

To date, promoters of the genes in the terpenoid biosynthesis pathway have been investigated and functionally assayed in several species. The vascular-specific expression of a hydroxymethylbutenyl 4-diphosphate synthase gene (*HDS*) promoter is identified from the MEP pathway in *Catharanthus roseus* (Ginis et al., 2012). The leaf-specific expression of a geranylgeranyl diphosphate synthase gene (*SmGGPPs*) promoter is analyzed in *Salvia miltiorrhiza* (Hua et al., 2012). The vegetative organ-specific expression of a mevalonate diphosphate decarboxylase (*GbMVD*) from MVA pathway is examined in *Ginkgo biloba* (Liao et al., 2016). For defense responses, the promoters of four sesquiterpene synthase genes for β-caryophyllene (*CPS*), epi-cedrol (*ECS*), β-farnesene (*FS*), and amorpha-4,11-diene synthase (*ADS*), and one monoterpene synthase gene (*LIS*) are studied in *Artemisia annua* (Wang et al., 2013, 2014). In addition, a number of *cis*-acting elements on the promoters of terpenoid biosynthesis pathway genes have been identified. A W-box palindrome is identified in the promoter of a cotton sesquiterpene synthase gene (*CAD1-A*) for GaWRKY1 binding (Xu et al., 2004). The E-box on the promoters of two *Arabidopsis* sesquiterpene synthase genes *TPS21* and *TPS11* is recognized by MYC2 involved in gibberellin and jasmonate induction (Hong et al., 2012). The NAC binding sites are found in the promoter of a monoterpene synthase gene (*AaTPS1*) in the scented kiwifruit *Actinidia arguta* for AaNAC2, 3 and 4 binding, which are mutated in the scentless *A. chinensis* (Nieuwenhuizen et al., 2015). The GCC-box is identified in the promoter of the terpene synthase gene (*TPS10*) for ZmEREB58 binding in *Zea mays* (Li et al., 2015), and in the promoter of *CitTPS16* for CitERF71 in *Citrus* fruit (Li et al., 2017).

In this study, we reported that a dual repeat in the upstream promoter fragments of *GDPS* is essential for its transcriptional activation in *Phalaenopsis* orchids. The full dual repeat was present only in the *Phalaenopsis* orchids emitting monoterpenes, and its integrity showed strong association with the transactivation of a bZIP TF, bZIP4. As this dual repeat was closely related to the monoterpene production in *Phalaenopsis* orchids, it could be developed as a promising molecular marker for early detection of monoterpene phenotype in the offspring and thus facilitate scented orchid breeding in future.

# MATERIALS AND METHODS

## Plant Materials and Growth Condition

Ten native and two cultivar hybrids were used in the study (Supplementary Figure 1), including *P. amboinensis* var. *yellow* (abbreviated as *P. amboinensis*), *P. aphrodite* subsp. *formosana* (abbreviated as *P. aphrodite*), *P. bellina*, *P. cornu-cervi* var. *red* (abbreviated as *P. cornu-cervi*), *P. equestris* 'RO-5', *P. equestris* 'WY-7', *P. javanica*, *P. lueddemanniana*, *P. mannii*, *P. schilleriana*, *P.* I-Hsin Venus 'KHM2212' (abbreviated as *P.* I-Hsin Venus), and *P.* Meidarland Bellina Age 'LM128' (abbreviated as *P.* Meidarland Bellina Age). These individual plants were collected from various orchid nurseries across Taiwan (details in Supplementary Table 1). Both *P.* I-Hsin Venus and *P.* Meidarland Bellina Age are commercial scented cultivars with monoterpenes as their major scent compounds (Chuang et al., 2017), whose ancestries contain multiple scent species as the following: *P.* I-Hsin Venus - *P. amboinensis* (25%), *P. equestris* (25%), *P. venosa* (18.75%), *P. violacea* (15.63%), *P. lueddemanniana* (3.13%); *P.* Meidarland Bellina Age - *P. bellina* (50%), *P. violacea* (24.22%), *P. venosa* (15.63%), *P. amboinensis* (3.91%), *P. lueddemanniana* (3.13%) via ORCHIDEYA.CA[1]. All the plant materials were grown in the greenhouse at National Cheng Kung University (NCKU) under natural light and surrounding temperature from 27 to 30°C in spring and summer with 75–85% humidity.

## Gas Chromatographic Analysis of Floral Volatiles

Analysis of the floral VOCs of 12 *Phalaenopsis* orchids was carried out according to the previous studies (Hsiao et al., 2006; Chuang et al., 2017). The VOCs were collected during the most emitted scent period (from 10:00 to 16:00) by using solid phase extraction system (DSC-Si and DCS-18, Supelco, United States) as described (Chuang et al., 2017), and the compounds were then identified by using gas chromatography/high-resolution mass spectrometry (GC/HRMS) at the NCKU Instrument Center (Hsiao et al., 2006). To assess the amounts of each compound, 1 μg of ethyl myristate was recruited as the internal standard (Fluka, Honeywell, United States).

## Detection of *GDPS* Gene Sequence, Upstream Regulatory Fragment and the Dual Repeat Region in 12 Orchid Genomes

To detect the *GDPS* gene and its upstream regulatory fragment, the genomic DNA of 12 *Phalaenopsis* orchids were extracted by using Plant Genomic DNA Purification Kit (Bio-GPD50, Biokit, Taiwan). Standard PCRs were applied to amplify the N-terminal region of *GDPS* (∼400-bp) with the primer designed based on *PbGDPS* genomic sequence (all the primers used here and thereafter were listed in Supplementary Table 2) since *PbGDPS* is an intronless gene (Hsiao et al., 2008). The 1-kb upstream promoter fragments of *GDPS* were also isolated from the 12 *Phalaenopsis* orchids using the designed primers based on the genomic DNA of *P. bellina* (Chuang et al., 2017). The dual repeat region was then amplified and cloned with ZeroBack Fast Ligation Kit (TIANGEN, China). Six to eight colonies were selected randomly for sequencing. The presence of the *cis*-elements in the dual repeats was predicted using PlantPAN (Chow et al., 2015), with 100% similar score accepted as the predicted results.

[1]http://www.orchideya.ca/

## Quantitative Real-Time RT-PCR

Total RNA was extracted from the flowers on D + 5 stage of the 12 *Phalaenopsis* orchids following the protocol of Plant Total RNA Miniprep Purification Kit (TR02, GeneMark, Taiwan). Reverse transcription to cDNA involved use of SuperScript III (Thermo Fisher Scientific, United States). Primers were designed by using Primer Express 3.0 (Thermo Fisher Scientific, United States). Quantitative RT-PCR (qRT-PCR) was performed by using the ABI StepOne Plus Quantitative real-time PCR instrument and SYBR Green kit (Applied Biosystems, United States) as described (Hsu et al., 2015). All expression results were normalized to the reference gene, *PbActin1* (Chuang et al., unpublished). Mean and standard error were calculated from triplicate repeats.

## Plasmid Construction

The 2-kb promoter fragment upstream from the translation start site of *PbGDPS* (denoted as *Pb*Gp-2010) and its nine serial deletion fragments (*Pb*Gp-1076, *Pb*Gp-859, *Pb*Gp-784, *Pb*Gp-710, *Pb*Gp-584, *Pb*Gp-410, *Pb*Gp-354, *Pb*Gp-297, *Pb*Gp-216) (**Figure 4A**) were amplified from the genomic DNA of *P. bellina*. Further serial-deletion fragments (*Pb*Gp-836, *Pb*Gp-822, *Pb*Gp-760, *Pb*Gp-747, *Pb*Gp-729) (**Figure 4B**) were amplified for detail analysis of the region between −836 bp to −710 bp. Specific primers with the restriction endonuclease sites of *Bam*H I and *Nco* I were designed to amplify these truncated fragments. The amplified fragments were double-digested with the restriction enzyme *Bam*H I and *Nco* I, and cloned into the corresponding enzyme digestion sites of pJD301(f) to drive the firefly (*Photinus pyralis*) luciferase gene (Hsu et al., 2014). All constructs were verified by DNA sequencing. The promoter-*LUC* constructs were schematically presented in **Figure 4**.

## Transactivation Assay of *PbGDPS* Promoter Fragments *in Planta*

The promoter-*LUC* constructs were bombarded into the floral tissues of *P.* I-Hsin Venus with an internal control plasmid, pJD301(R), containing the *Renilla* luciferase gene driven by cauliflower mosaic virus (CaMV) 35S promoter. For normalization, the luciferase activity of the reporter construct was divided by that of the internal control. The involvement of internal control reduced experimental variability resulted from differential bombardment efficiency and transformation efficiency among various experimental groups. The amount of the reporter plasmid and the internal control was 10 and 0.1 μg, respectively. At least six individual flowers of *P.* I-Hsin Venus were employed for replicates. Luciferase activity of each sample was measured (Hsu et al., 2014). For statistics analysis between

two groups, pairwise comparisons were performed by using Tukey's honestly significant difference test at $\alpha = 0.05$.

## Yeast One-Hybrid (Y1H) Library Screening

Systematic screening of Y1H TF library composed of approximately 1,350 *Arabidopsis* TFs (Mitsuda et al., 2010) was performed in yeast strain YM4271 to identify the TFs that are able to bind the dual repeat. For construction of bait plasmid, the dual repeat was amplified from the genomic DNA of *P. bellina* by using appropriate primers with the restriction endonuclease site of *Xma* I and *Xba* I, cloned into pHisi2, and integrated it into the yeast genome. The Y1H assay was performed as previously described (Mitsuda et al., 2010). In the screenings of *Arabidopsis* TF library, the degree of positive interaction between a prey TF and a bait sequences is scored between 0 and 3 in each screening according to the yeast growth status under selective media so that each TF has its own "sticky score" as the sum of this score. The sticky score of AtbZIP29 and AtbZIP30 was 50 and 24, respectively, among 247 TFs isolated so far in 105 screenings including this study and therefore were considered as sticky TFs in this Y1H system.

## Identification of bZIP Group I TFs in *Phalaenopsis* Transcriptome

The bZIP group I TFs was identified in the *P. bellina* transcriptomic data of four floral development stages at anthesis day (Dd), D + 3, D + 5, and D + 7, which corresponds to the four periods of the floral monoterpene emission pattern, including onset, increase, peak and decline (Chuang et al., unpublished), by using those in *Arabidopsis* as queries with *E*-value cutoff of $1e^{-5}$ (Jakoby et al., 2002; Pyo et al., 2006). The expression level of each individual TF gene was presented by fragments per kilobase of transcript per million mapped reads (FPKM). FPKM values of the *P. bellina* transcriptome were transformed by log 3.22 to achieve equivalent expression levels of reference genes as those in the transcriptomic data of *P. aphrodite* (Su et al., 2013b), including *Actin4* (Chen et al., 2005; Hsieh et al., 2013; Pan et al., 2014; Hsu et al., 2015), *Actin9* (Hsiao et al., 2008; Pan et al., 2011, 2014; Hsu et al., 2015), and *Ubiquitin10* (Lu et al., 2007; Hsiao et al., 2008) (Chuang et al., unpublished). A multiple sequence alignment of bZIP domains was generated by using Clustal Omega[2] and displayed by using BOXSHADE[3]. The phylogenetic tree was built with the neighbor-joining method with 1000 bootstrap trials by using MEGA6 (Tamura et al., 2013).

## Examination of the Transactivation of PbbZIP4 and PbbZIP26

Promoter fragments of *PbGDPS* and *PaGDPSpA*/*PaGDPSpB* were isolated from *P. bellina* and *P. aphrodite* genomic DNA, respectively (Chuang et al., unpublished). After sequence confirmation, these promoter fragments were cloned into pJD301(f) to drive the firefly luciferase gene. Coding sequences for both *PbbZIP4* and *PbbZIP26* were amplified with gene-specific primers from full-bloom flowers of *P. bellina* and cloned into pBI221 and under the control of CaMV 35S promoter. Three separate plasmids, including pBI221 with *PbbZIP4/26*, pJD301(f) with promoter fragments, and internal control pJD301(R), were co-bombarded into *P. aphrodite* floral tissues at a ratio of 1.5: 1.5: 0.15 (total 3.15 μg) as described previously (Hsu et al., 2014). The luciferase activity of each sample was measured after 20 h post bombardment. The relative fold change in activity was calculated by the comparison to the control assay with *GUS* in pBI221 for at least triplicate biological repeats. For statistics analysis between two groups, pairwise comparisons were performed by using Tukey's honestly significant difference test at $\alpha = 0.05$.

## Transient Ectopic Expression of *PbbZIP4* in the Scentless Orchid

The coding sequence of *PbbZIP4* was isolated from the pBI221 plasmid containing *PbbZIP4* described above, and cloned into the p1304NhXb vector under a duplicated CaMV 35S promoter. The *Agrobacterium tumefaciens* EHA105 cells taking the resulting plasmids were infiltrated into the perianths of *P. aphrodite* at the Dd stages (Hsu et al., 2015). The empty plasmid vector containing *GUS* served as a negative control. Three individual flowers of *P. aphrodite* were employed for replicates. The volatiles of infiltrated flowers were collected on day 4 post infiltration for 6 hr (from 10:00 to 16:00) and the compounds were identified by GC/HRMS as described above. Total RNA was isolated from the infiltrated tissues following the protocol of RNeasy Plant Mini Kit (QIAGEN, Germany). Reverse transcription to cDNA and quantitative RT-PCR was performed as described above.

# RESULTS

## Isolation of a Dual Repeat in the *GDPS* Upstream Promoter

Previously, two individual 1-kb fragments of *GDPS* promoters were isolated from the scentless *P. aphrodite*, namely *PaGDPS*pA and *PaGDPS*pB (Chuang et al., unpublished). Compared to the *GDPS* promoter from the scented *P. bellina* (*PbGDPS*p), two *GDPS* promoters identified from *P. aphrodite*, *PaGDPS*pA and *PaGDPS*pB contained an 11-bp deletion and a 75-bp deletion, respectively (**Figure 1**). *PaGDPS*pB also had two 14-bp insertions in addition to numerous nucleotide substitutions. By performing the luciferase promoter assays *in planta*, *PaGDPS*pA showed the similar promoter activity as *PbGDPS*p either in scented or scentless flowers, while *PaGDPS*pB revealed very low promoter activity even in the scented *P. bellina* floral tissues. These results indicated that the lack of the 75-bp region in the *PaGDPS*pB is detrimental for its activity (Chuang et al., unpublished). Further sequence analysis of the *PbGDPS* promoter showed that a second 75-bp repeat is present downstream from the original 75-bp repeat and formed a dual repeat consisted of the two 75-bp units. The first and second 75-bp units were then denoted as 'R1', and 'R2', respectively, located from −859 to −710 nt upstream from the ATG (**Figure 1**).

[2]http://www.ebi.ac.uk/Tools/msa/clustalo/

[3]https://embnet.vital-it.ch/software/BOX_form.html

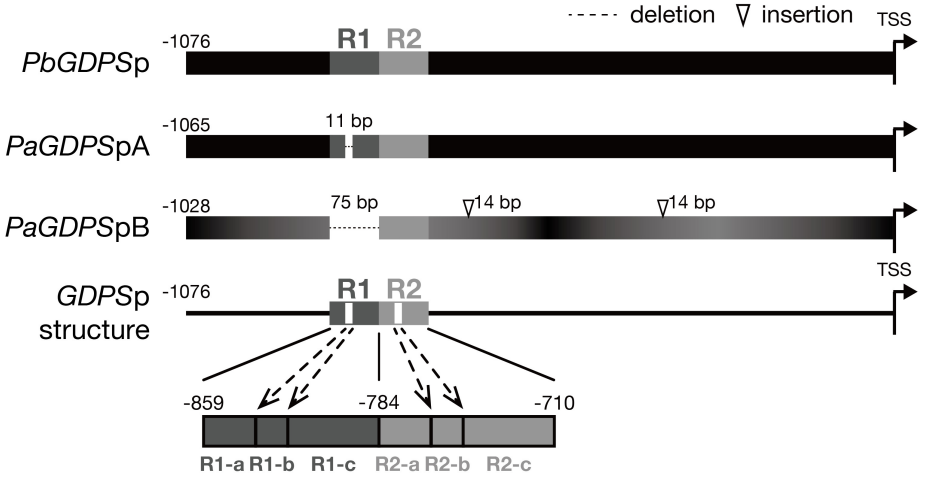


**FIGURE 1 |** Promoter structure of *GDPS*. Promoter structure of *GDPS* was revealed by the comparison of three sequences of *PbGDPS*p, *PaGDPS*pA, and *PaGDPS*pB. Two repeats located from –859 to –710 of *PbGDPS*p were named as R1 and R2. The repeat was further dissected into three subunits based on 11-bp deletion located in the center of R1. This deletion was referred as R1-b, and the sequences prior to and behind R1-b was R1-a and R1-c, respectively. The corresponding dissection in R2 was R2-a, R2-b, and R2-c. TSS indicates the translation start site (ATG). Black color gradient in *PaGDPS*pB indicated its numerous substitutions compared to *PbGDPS*p.

The *PaGDPS*pB lacked the entire R1 unit, and *PaGDPS*pA harbored a 11-bp deletion in the center of R1, which was defined as R1-b subunit (**Figure 1**). The region (25-bp) prior to the R1-b was denoted as R1-a, and those (39-bp) behind was R1-c, and the corresponding divisions in R2 were denoted as R2-a, R2-b and R2-c (**Figure 1**). The dual repeat structure was schematically represented in **Figure 1**, and the sequence of the dual repeat is in Supplementary Figure 2. The difference between the *GDPS* promoters of the scent *P. bellina* and the scentless *P. aphrodite* resided in the dual repeat, and this is well correlated with the monoterpene phenotype.

## Concomitance of the Integrity of the Dual Repeat With the Monoterpene Production

According to the promoter analysis results of *PaGDPS* and *PbGDPS* from scented and scentless *Phalaenopsis* orchids, we hypothesized that the dual repeat is associated with the monoterpene production. To confirm this, another 10 frequently used breeding parents of *Phalaenopsis* orchids (Supplementary Figure 1) were recruited and assessed for the correlation analysis between the dual repeat and the monoterpene production.

We first examined the floral scent profile (Supplementary Table 3) and found that four orchids emitted monoterpenoids, including *P.* Meidarland Bellina Age, *P. bellina*, *P.* I-Hsin Venus, and *P. lueddemanniana*. In contrast, the major VOCs of *P. javanica* and *P. amboinensis* were sesquiterpenoids and benzenoids, and that of *P. mannii* was phenylpropanoids and fatty acid derivatives (Supplementary Table 3). *P. schilleriana* emitted trace amounts of benzenoids. *P. aphrodite*, *P. cornu-cervi*, *P. equestris* 'RO-5', and *P. equestris* 'WY-7' were considered as "scentless" since no scent compounds were detected (Supplementary Table 3). For brief, the relative amounts of monoterpenoids emitted from these *Phalaenopsis* orchids were symbolized in **Figure 2A**.

The presence of the *GDPS* gene and its promoter sequence in the 12 *Phalaenopsis* orchids were then analyzed (**Figure 3**). Intriguingly, the *GDPS* gene was present in all of these orchids regardless of being scent or scentless phenotype (**Figure 3**). It is plausible that the defects are resided in the promoter region (*GDPS*p, **Figure 3**). We then amplified the dual repeat on *GDPS*p and a polymorphism of the dual repeat fragment length was detected among the 12 *Phalaenopsis* orchids (**Figure 3**). The four scented orchids with monoterpene production contain the complete dual repeat (**Figure 3**, the black arrowheads). In contrast, the amplified dual repeat fragments of the other orchids were reduced to various extents with various deletions in the dual repeat region. These 12 fragments were cloned and sequenced. Deletions in the dual repeats were detected between nucleotides 11 and 110, which appear to cause defects in *GDPS* promoter activities in the orchids without monoterpene production (**Figures 2A,B**). Strikingly, most defects occurred in the R1 region (**Figure 2B**).

We then examined the expression levels of *GDPS* for 12 *Phalaenopsis* orchids (**Figure 2C**). The four orchids emitting monoterpenoids especially both *P.* Meidarland Bellina Age and *P. bellina* showed higher *GDPS* expression levels than the others (**Figure 2C**). Taken together, we concluded that the integrity of the dual repeat in the *GDPS* promoter is strongly correlated with its elevated expression and thus the monoterpene production.

## The Dual Repeat Is Crucial for *GDPS* Promoter Activity

To investigate the role of the dual repeat in the promoter activity of *GDPS*, the ∼2-kb promoter fragment (denoted *Pb*Gp-2010)

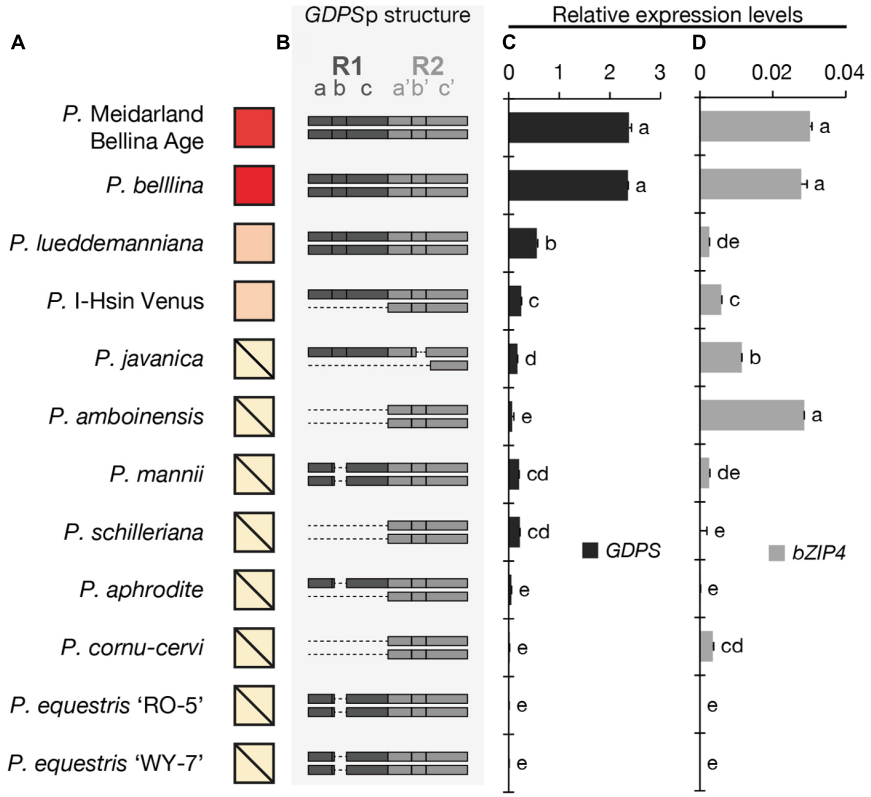


**FIGURE 2 |** The analysis of the floral volatiles, dual-repeat and gene expression in 12 *Phalaenopsis* orchids. **(A)** The relative amounts of floral volatiles were represented by a red color gradient. The block with a diagonal line indicates that no monoterpenoid is identified in this orchid. **(B)** The dual repeat structure of *GDPS* promoter. **(C,D)** The expression levels of *GDPS* **(C)**, and *bZIP4* **(D)**. Expression level was normalized to that of *PbActin1* by real-time RT-PCR. Data are mean ± SE from triplicate measurements. Statistic tests were performed by using Tukey's honestly significant difference test at $\alpha = 0.05$.

upstream from the start site of *PbGDPS* was isolated and subjected to serial deletions. The activity of *Pb*Gp-2010 and the nine truncated promoter fragments were evaluated in *P.* I-Hsin Venus flowers via particle bombardment for dual luciferase assays. It was legitimate that we should examine *PbGDPS* promoter activity in the original species *P. bellina*. However, the supply of *P. bellina* flowers fell short of demand for experiments as *P. bellina* commonly produces only one flower per 20 days. Instead, *P.* I-Hsin Venus, the offspring of *P. bellina* emitting similar scents, was micropropagated to large quantities with the identical genetic background and would help to reduce variation.

The highest luciferase activity was observed for *Pb*Gp-859, which showed approximately threefold increase as compared to that *Pb*Gp-784, and fivefold increase as compared to that of *Pb*Gp-710 (**Figure 4A**). Thus, the *cis*-element responsible for high promoter activity was between nucleotide (nt) −859 and nt −710 (150-bp), in which the dual repeat located. Further dissection of *Pb*Gp-710 to generate *Pb*Gp-584, *Pb*Gp-410, *Pb*Gp-354, *Pb*Gp-297, and *Pb*Gp-216 showed that no extra enhancers were present at the downstream of the dual repeat (**Figure 4A**). Compared with *Pb*Gp-859, the promoter activity of *Pb*Gp-2010 and P*b*Gp-1076 was much decreased (**Figure 4A**), suggesting the presence of repressor elements at the upstream region of *Pb*Gp-859. These results verified that the dual repeat plays a crucial role for *PbGDPS* promoter activity.

To further define the *cis*-element in the 150-bp dual repeat region for transcriptional regulation, a more detailed analysis was performed based on the subunit division, namely R1a, R1b, R1c, R2a, R2b, and R2c. These subunits were serial deleted to generate a series of truncated promoter constructs. The luciferase activities were reduced further with gradual deletions of the subunit, indicating the essential nature of the complete dual repeat for full promoter activity of *PbGDPS* (**Figure 4B**).

## Yeast One-Hybrid Screening of the Transcription Factor Bound Onto the Dual Repeat

To identify the candidate upstream *trans*-activators, Y1H screening was performed using *P. bellina* floral cDNA as preys. However, the dual repeat bait produced extensive background growth of yeast, and it could not be eliminated even under the addition of inhibitor 3-Amino-1,2,4-triazole (3-AT). Alternatively, Y1H screening against prey library composed of approximately 1,350 TFs of *Arabidopsis thaliana* was performed

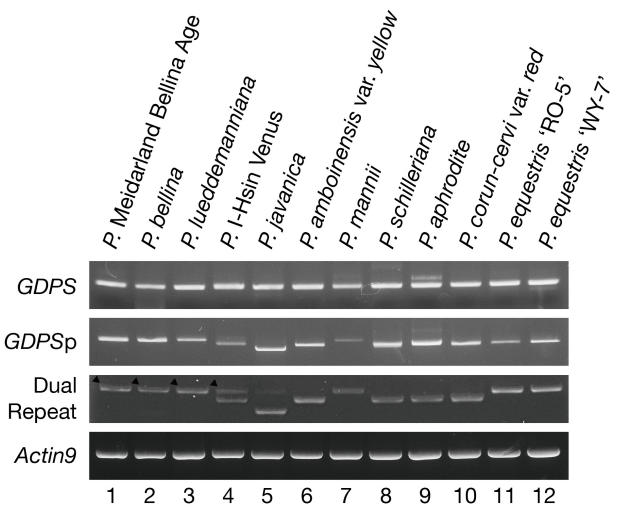


**FIGURE 3 |** PCR Amplification of the *GDPS* gene, its 1-kb promoter fragment and the dual repeat in the genomic DNA of 12 *Phalaenopsis* orchids. Actin was used as a control. Amplification of 1-kb promoter and dual repeat showed polymorphisms.

(Mitsuda et al., 2010). The dual repeat was amplified from *P. bellina* genomic DNA and fused to a minimal promoter of *HISTIDINE SYNTHASE3* (Supplementary Figure 3A). In this approach, the leaky expression of the reporter gene could be overcome by the addition of 4 mM 3-AT (Supplementary Figure 3B). Total four positive TFs were obtained from this screening (**Table 1**) and three of them encoded bZIP family proteins including AtbZIP18, AtbZIP29, and AtbZIP30. The other one candidate AtAGL81, a MADS-box TF, failed to be isolated from *P. bellina* floral transcriptome.

The three bZIP TFs belong to the group I of bZIP family composed of a conserved bZIP domain for DNA binding and a leucine zipper motif for dimerization (Jakoby et al., 2002). The *P. bellina* floral transcriptomic data (Chuang et al., unpublished) showed nine proteins belong to group I, and can be divided into three subgroups (i, ii, and iii) according to their phylogenetic relationship with the *Arabidopsis* ones (**Figure 5A**). We selected subgroup i including AtbZIP18 for further analysis since AtbZIP29 and AtbZIP30 (subgroup ii) were repeatedly isolated in other unrelated screenings and therefore considered as sticky factors in the Y1H system. No PbbZIPs were classified into subgroup iii (**Figure 5A**). Multiple alignments showed that five PbbZIPs namely PbbZIP4, PbbZIP10, PbbZIP26, PbbZIP29, and PbbZIP32 in the subgroup i shared 83–86% identity with AtbZIP18 in the basic region (**Figure 5B**).

Previously, we found that the promoter activity of *GDPS* was much higher in the scented *P. bellina* than in the scentless *P. aphrodite*. In addition, *PaGDPS*pA was a functional promoter since it showed similar promoter activity as *PbGDPS*p in the scented *P. bellina* flower tissues (Chuang et al., unpublished). Both results indicated that the down-regulation of the corresponding upstream activators of *GDPS* was responsible for the extremely low *GDPS* expression in *P. aphrodite* (**Figure 5C**).

The possibility of the five bZIPs regulating *GDPS* was evaluated by comparing their gene expression between *P. bellina* and *P. aphrodite* (**Figure 5C**). Among them, *bZIP4*, *bZIP26*, *bZIP29*, and *bZIP32* showed higher expression in *P. bellina* than in *P. aphrodite*. However, both *bZIP29* and *bZIP32* also expressed in floral bud of *P. aphrodite* but still *GDPS* did not express (**Figure 5C**), suggesting that both *bZIP29* and *bZIP32* did not transactivate *PaGDPSpA* promoter. Both PbbZIP29 and PbbZIP32 thus were excluded for further analysis.

## PbbZIP4 Was Able to Distinguish the Promoter Containing the Dual Repeat

Previously, we have shown that PbbZIP4 was able to transactivate *PbGDPS* promoter (Chuang et al., unpublished). Here, to further examine the transactivating ability of PbbZIP4 and PbbZIP26 on various *GDPS* promoters, dual luciferase assay was performed in the floral tissues of the scentless *P. aphrodite*. In the presence of PbbZIP4, it enhanced the promoter activities of both *PbGDPS*p and *PaGDPS*pA, but revealed no effects on *PaGDPS*pB (**Figure 6**). This was consistent with the previous results, in which the activities of both *PbGDPS*p and *PaGDPS*pA were higher than *PaGDPS*pB in the scented *P. bellina* floral tissues (Chuang et al., unpublished). In contrast, PbbZIP26 did not transactivate *PbGDPS*p, *PaGDPS*pA, or *PaGDPS*pB (**Figure 6**). These results indicated that PbbZIP4 was able to distinguish the *GDPS* promoter containing the full dual repeat (*PbGDPS*p), or near full-dual-repeat (*PaGDPS*pA), from the solely one repeat unit (*PaGDPS*pB).

## The Close Association Between the *Trans*-Factor and the *Cis*-Element for Monoterpene Phenotype

The *cis*-element and *trans*-factor for *GDPS* promoter were both identified in the scented *P. bellina*. To investigate how these two factors affected the monoterpene phenotype among the 12 *Phalaenopsis* orchids, we examined the expression levels of *bZIP4* (**Figure 2D**) to establish its correlation with the presence of the dual repeat on *GDPS* promoter (**Figure 2B**) and *GDPS* expression levels (**Figure 2C**) for monoterpene production (**Figure 2A**). Interestingly, *bZIP4* expressed to various extents among these orchids (**Figure 2D**). Strikingly, only the orchid plants concomitantly harbored *bZIP4* expression and the dual repeat on *GDPS* promoter exhibited high *GDPS* expression, and thus produced monoterpenes, including *P.* Meidarland Bellina Age, *P. bellina*, *P. lueddemanniana*, and *P.* I-Hsin Venus (**Figure 2**).

However, orchid species with similar or even higher *bZIP4* expression levels but without the dual repeat showed low *GDPS* expression, and thus did not emit monoterpenes, including *P. javanica*, *P. amboinensis*, *P. mannii*, and *P. cornu-cervi* (**Figure 2**). In contrast, another four species with extremely low expression levels of *bZIP4*, together with their incomplete

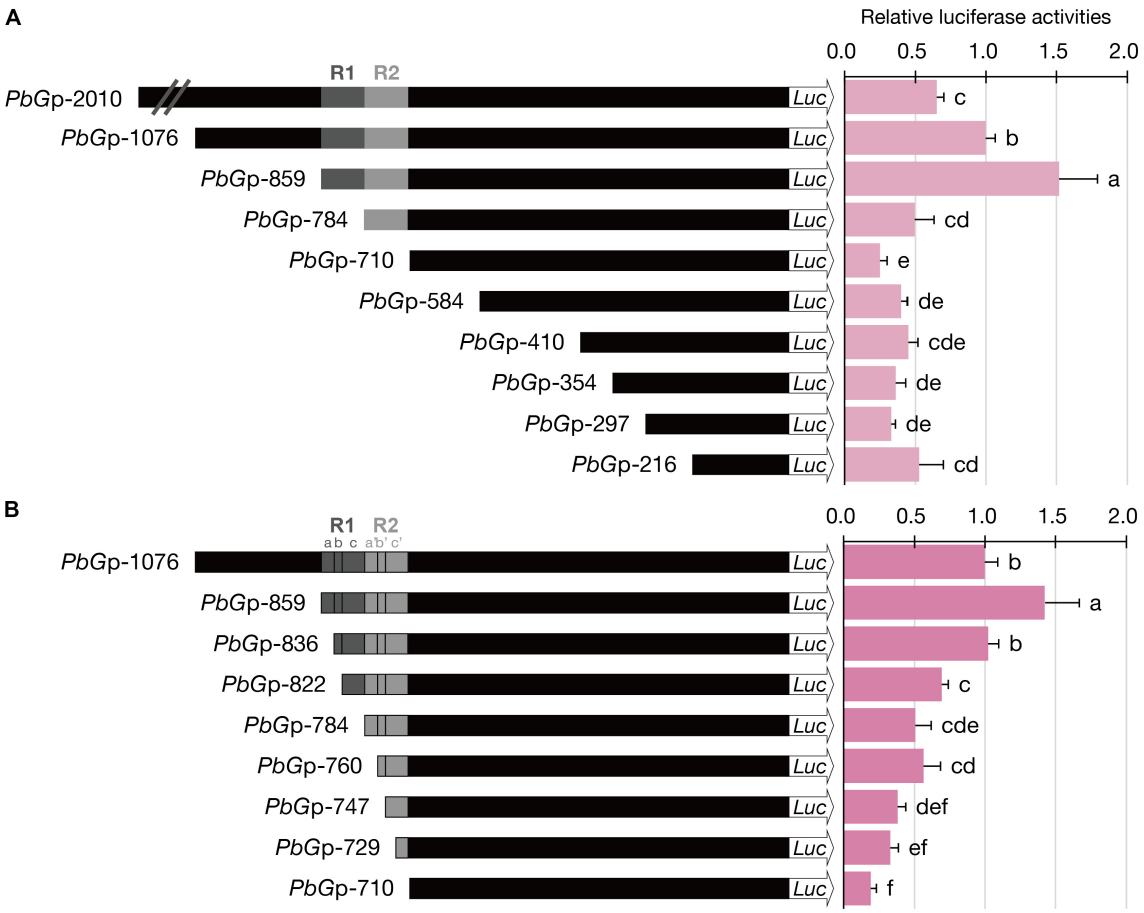


**FIGURE 4 |** Luciferase activities of dissected *PbGDPS* promoters in *P.* I-Hsin Venus by particle bombardment. **(A)** Serial deletion of *PbGDPS* promoter to analyze the putative *cis*-element. **(B)** Identification of the subunit of the dual repeat responsible for promoter driving abilities. Activation level was given by the ratio of Luc/RLuc and the level of *PbGp*-1076 was set as 1. Experiments are based on at least sextuplicate biological replicate. Statistic tests were performed by using Tukey's honestly significant difference test at $\alpha = 0.05$.

**TABLE 1 |** Transcription factors binding to the dual repeat by screening of yeast one-hybrid libraries.

| Screening of Y1H library | Isolated TF | | TF family | Interaction strength | Homology gene in *P. bellina* floral transcriptome |
|---|---|---|---|---|---|
| | Locus | Name | | | |
| *Arabidopsis* | AT2G21230 | AtbZIP30[a] | bZIP | Weak | — |
| | AT2G40620 | AtbZIP18 | bZIP | Weak | Yes |
| | AT4G38900 | AtbZIP29[a] | bZIP | Strong | — |
| | AT5G39750 | AGL81 | MADS | Strong | No |

[a]*AtbZIP29 and AtbZIP30 were excluded for following analysis due to their sticky feature in the system.*

dual repeat, contributed to their scentless phenotype, including *P. schilleriana*, *P. aphrodite*, *P. equestris* 'RO-5', and *P. equestris* 'WY-7' (**Figure 2**). Collectively, these results indicated that not only the dual repeat in *GDPS* promoter but also the TFs are crucial for monoterpene production in *Phalaenopsis* orchids.

## Transient Ectopic Expression of *PbbZIP4* in the Scentless *P. aphrodite*

So far, the stable genetic transformation for *Phalaenopsis* orchids is with low efficiency. In addition, *Phalaenopsis* orchids have a long-life cycle with the regeneration time is about 2–3 years, especially if we want to examine the floral phenotype. Instead, the transient ectopic expression system in floral tissues has been successfully established for the study of three MYB TFs regulating the pigmentation patterning in *Phalaenopsis* orchids (Hsu et al., 2015). Thus, to confirm the role of PbbZIP4 *in planta*, we performed a transient assay by infiltrating the Agrobacterium into the flower tissues of the scentless *P. aphrodite*. We analyzed the volatile terpenes emitted from *PbbZIP4*-expressing *P. aphrodite* flowers and detected a 10-fold induction of α-terpineol (a monoterpenoid) as compared to the *GUS* control (**Figures 7A,B**). Furthermore, the raise in the levels of monoterpenes in the infiltrated tissues was indeed resulted from the large increase of *PbbZIP4* transcripts (**Figure 7C**). Therefore, we concluded that PbbZIP4 was involved in the scent production in *Phalaenopsis* orchids.

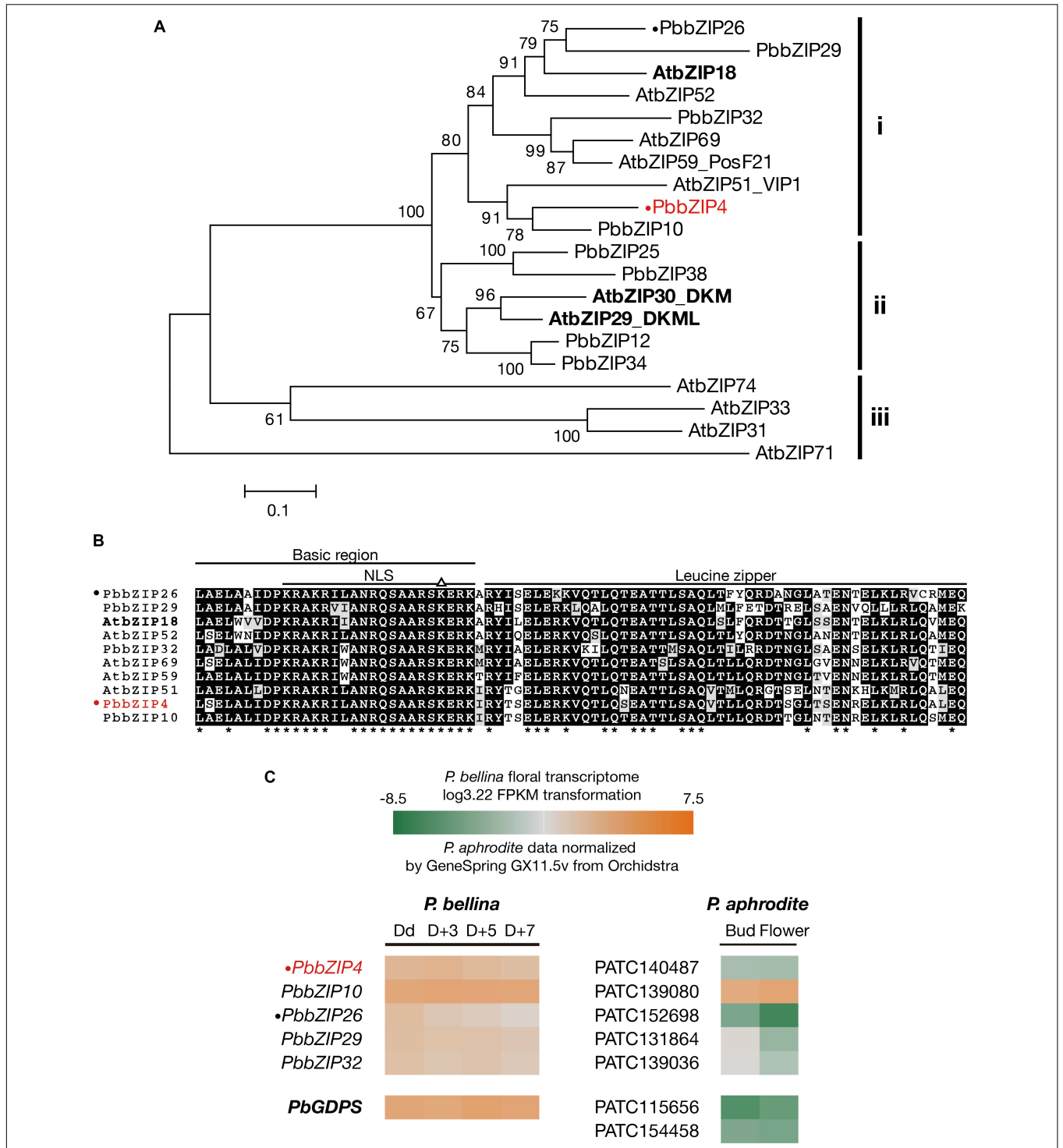


**FIGURE 5 |** Analysis of bZIP group I TFs in *P. bellina* floral transcriptome. **(A)** Phylogenetic tree inferred from the amino sequences of the nine bZIP group I TFs with the ones in *Arabidopsis*. The three subgroups were divided based on their phylogenetic relationship. Three AtbZIPs isolated by Y1H screening were seen in bold. **(B)** Amino acid sequence alignment of subgroup i proteins in **(A)**. Asterisks (*) below the alignment indicate the consensus residues in all sequences. The triangle (△) above the alignment indicates the lysine replacement of the conserved arginine residue in the basic region of group I of bZIP family. **(C)** Comparison of the expression levels of five bZIP TFs between two *Phalaenopsis* transcriptomes. Gene expression levels in *P. bellina* transcriptomes were transformed by log3.22 FPKM in four floral developmental stages, including Dd, D + 3, D + 5, and D + 7 (Chuang et al., unpublished), while the levels of two floral stages of flower bud and flower in *P. aphrodite* transcriptomes were analyzed via microarray experiments stored in Orchidstra (Su et al., 2013a). Expression levels of putative genes are represented by a color gradient from orange to gray to green. Two PbbZIPs for transient assays, PbbZIP4 and PbbZIP26, are labeled with a dot (•). PbbZIP4 was especially shown in red. The expression levels of *PbGDPS* (in bold) was also included for comparison.

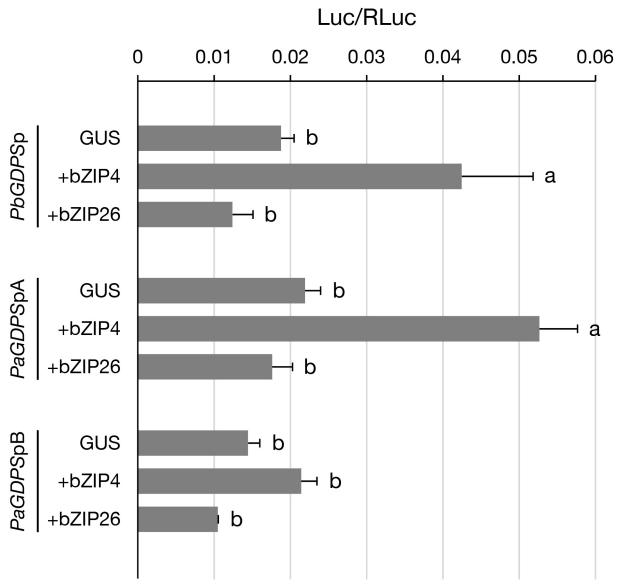


**FIGURE 6 |** Transient assay for analyzing the transactivation ability of PbbZIP4 and PbbZIP26 on *PbGDPS*p, *PaGDPS*pA, and *PaGDPS*pB. The promoter structure of *PbGDPS*p, *PaGDPS*pA, and *PaGDPS*pB was schematically represented in **Figure 1**. Activation level was given by the ratio of Luc/RLuc. GUS indicated that the assay was performed without the transcription factor. Experiments were based on at least three biological replicates. Statistic tests were performed by using Tukey's honestly significant difference test at $\alpha = 0.05$.

# DISCUSSION

## The Key Role of the Repeat Unit in the *GDPS* Promoter Activity

In this study, we studied the molecular mechanism determining the scent phenotype in *Phalaenopsis* orchids. We found that a dual repeat of *cis*-element on the *GDPS* promoter played a vital role for floral monoterpene production. The orchids without monoterpene production harbored defective dual repeat and noticeably, most occurring in the R1 region. Serial deletion analysis showed that the removal of R1 unit decreased the promoter activity by 67%, and the further deletion of R2 unit caused an additional 16% reduction, which implies that the R1 unit is crucial for high levels of *GDPS* promoter activity and that the R2 unit is required for the 100% transactivation activity.

## The Evolutionarily Conserved *GDPS* Promoter Sequences Among *Phalaenopsis* Orchids

The *GDPS* promoter fragments isolated from the 10 native *Phalaenopsis* species shared extremely high similarities (90–100% identities, data not shown), which indicates the conservation of the *GDPS* promoter sequences among the *Phalaenopsis* orchids. The 10 native *Phalaenopsis* orchids belong to two-pollinia *Polychilos* and subgenus *Phalaenopsis* (Supplementary Table 4) (Christenson, 2001). According to the evolutionary trend deduced by pollinia number, molecular evidences and biogeography, the four-pollinia basal subgenus *Aphyllae* in South China and Indochina is developed into two-pollina groups during the dispersal into Southeast Asia, including subgenus *Polychilos* in Indonesia and Malaysia, and subgenus *Phalaenopsis* in the Philippines, respectively (Tsai, 2003, 2011; Tsai et al., 2010). As both two-pollina subgenus shared similar *GDPS* promoter sequences, it is possible that this conserved *GDPS* promoter was inherited from their common ancestor of four-pollinia basal group.

## Possible Origin of the Dual Repeats

Repetitive DNA is accounting for a substantial proportion in the whole genomic DNA in most eukaryotes. A number of genetic diseases are related to the large copy number of repetitive sequences, such as Huntington's disease, fragile X syndrome, and myotonic dystrophy (Pelley, 2007). There are two main classes of repetitive DNA, interspersed repeats dispersed throughout the genome, and tandem repeats located in one area of DNA (also known as satellite DNA) (Bhagavan and Ha, 2011). The interspersed repeats include short interspersed nuclear elements (100- to 500-bp in length) and long interspersed nuclear elements (6000- to 7000-bp in length), and both belong to transposons (Pelley, 2007). On the other hand, satellite DNA is divided into three groups based on the length of the repeat unit, including macrosatellites, minisatellites, and microsatellites. Minisatellites are consisted of repeat sequences ranged from 9 bp to 80 bp (Bhagavan and Ha, 2011), and the size normally ranged from 1-kb to 20-kb. In cauliflower, a Harbinger DNA transposon in the promoter of an R2R3-MYB TF, *purple*, leads to an increase in the gene expression and produces the purple phenotype (Chiu et al., 2010). Two reports have described that a minisatellite-like structure on the promoter of an anthocyanin-regulating TF, *MYB10*, is required for the red color formation in the fruit flesh and leaves in apple and crabapple, respectively (Espley et al., 2009; Tian et al., 2017).

The 150-bp dual repeat identified here consisted of two 75-bp repeat units adjacent to each other, and thus was not considered as a transposon but defined as a minisatellite-like structure. Indeed, this dual repeat did not respond to any known transposon sequences by BLAST against the repetitive sequence database of RepBase (Jurka, 1998; Bao et al., 2015). We speculate that this dual repeat was generated by a tandem duplication event, and have not undergone additional mutation yet for multiple copies.

Six out of 10 *Phalaenopsis* orchids had the dual repeat or near-full dual repeat, including *P. bellina* and *P. luddemanian*, and *P. javanica*, *P. mannii*, *P. aphrodite*, and *P. equestris*, respectively. These six orchids either belong to subgenus *Polychilos* or subgenus *Phalaenopsis* (Supplementary Table 4), suggesting that the dual repeat was retained from their common predecessors, subjected to further mutation, and became defective in the orchids without monoterpene production. As two species of the basal four-pollina subgenus *Aphyllae* (Tsai et al., 2010), *P. hainanensis* and *P. wilsonii*, also emits fragrance (information from http://www.orchid.url.tw/), it will be interesting to study whether they have the dual repeat as well, just similar to the cases

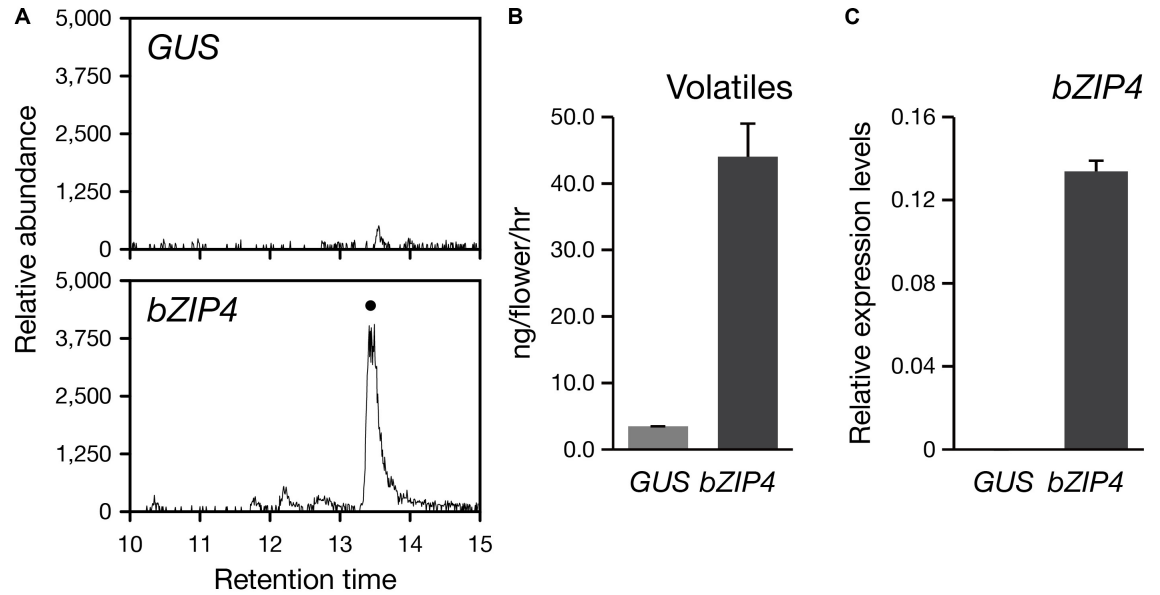


**FIGURE 7 |** Transient expression of *PbbZIP4* in the scentless *P. aphrodite* flowers induced the production of monoterpeneoids. **(A)** Selected ion (m/z 136) GC-MS profiles of volatiles detected from *GUS*- and *PbZIP4*-expression flowers. The peak with a dot indicates α-terpineol. The products were confirmed by comparing the mass spectra of the indicated peak with the one of the library hit. **(B)** The levels of volatiles emitted from the flowers infiltrated with *GUS* (gray) and *PbbZIP4* (dark-gray). **(C)** Relative expression levels of *PbbZIP4* of the flowers infiltrated with *GUS* (gray) and *PbbZIP4* (dark-gray). Error bars on each column represent ± SE from three biological replicates.

in *Capsella* (Brandvain et al., 2013; Sas et al., 2016) and *Petunia* genus (Amrad et al., 2016) describing the loss of the floral scent during the shift of pollinator types.

## Tandem Repeats Correlated to Transcriptional Regulation

In *Phalaenopsis* orchids, the dual repeat on *PbGDPS* promoter is required for its 100% promoter activity. Several studies have also shown that the increasing number of tandem repeats lead to a stepwise increase in promoter activity, and subsequently in gene expression levels. In citrus, three copies of a 20-bp enhancer element on the promoter of lycopene β-cyclases (*CsLCYb1*), an enzyme representing a branch point for carotenoid biosynthesis, are important for its promoter activity (Lu et al., 2016). In *C. roseus*, the copy number of a simple sequence repeats (CT) on the promoter of *Tryptophan decarboxylase*, the first step in the indole alkaloids biosynthesis pathway, is strongly associated its expression levels (Kumar and Bhatia, 2016). Furthermore, the copy number of the *cis*-elements even determines a specific phenotype. For instance, in apple, five direct tandem repeats on the promoter of *MYB10*, an anthocyanin-regulating TF, is only present in the red-fleshed apple varieties, and cause itself autoregulation (Espley et al., 2009). In cotton, two 228-bp tandem repeats on the promoter of an anthocyanin-regulating TF, Red Leaf Cotton 1, is critical for its promoter activity, and only present in the red leaf variety (Gao et al., 2013). Similarly, in our study, the dual repeat is essential for the monoterpene production in *Phalaenopsis* orchids.

## The Dual Repeat Could Be a Novel *Cis*-Acting Sequence

We performed Y1H screening to identify the TFs binding to the dual repeat, and member of bZIP, and MADS-box TFs were isolated. Here, we excluded the possibility of AtAGL81 (MADS-box TF) to interact with *PbGDPS* promoter since it was failed to be isolated from *P. bellina* floral transcriptome in *E*-value cutoff of $1e^{-5}$. Moreover, we were not able to isolate the similar sequences to AtAGL81 from *P. aphrodite* transcriptome, whose transcript profiles were analyzed in leaf, root, flower bud, and fully open flower (Orchidstra 2.0) (Chao et al., 2017) and *P. equestris* genome (Cai et al., 2015).

The presence of *cis*-elements on the dual repeat was examined by PlantPan analysis (Chow et al., 2015). Several types of TFs were predicted to interact with the dual repeat, including MYB-related, Dof zinc finger protein, GATA, zinc-finger homeodomain protein, squamosa promoter binding protein, and nuclear TF Y subunit beta. Interestingly, we did not find any bZIP-binding *cis*-elements, suggesting that the dual repeat could be a novel *cis*-acting sequence. As the length of the dual repeat is 150-bp, it is possible that other types of TFs may be involved in the scent regulating phenotype, and it awaits further analysis.

## Application for Molecular Marker-Assisted Breeding

The molecular markers to distinguish scent traits have been well developed in rice (Garland et al., 2000; Cordeiro et al., 2002; Jin et al., 2003; Bradbury et al., 2005; Shi et al., 2008; Sakthivel et al., 2009; Myint et al., 2012), and also in other crops, such as

soybean (Arikit et al., 2011; Juwattanasomran et al., 2011, 2012), sorghum (Yundaeng et al., 2013), cucumber (Pramnoi et al., 2013; Yundaeng et al., 2015), coconut (Vongvanrungruang et al., 2016), and winter melon (Ruangnam et al., 2017). Just like other modern floriculture cultivars, negative correlation between floral scent and other favorable traits resulted in the difficulty in the scented orchids breeding. The introduction of the scent trait to a well-commercialized cultivar is an alternative approach (Hsiao et al., 2011b). However, the long duration from seedling to first blooming for confirming the floral traits are time consuming and cost inefficient under conventional breeding.

Here, PCR amplification of the dual repeat showed fragment length polymorphism. The two native *Phalaenopsis* orchids and two cultivars emitting monoterpenes showed the 150-bp fragment length of dual repeat, which indicates its potential to be developed as a molecular marker for scent trait. After the link between the dual repeat and the monoterpene emission further verified in more *Phalaenopsis* species and cultivars, the dual repeat could be applied as a molecular marker for early characterization of the scent phenotype in the seedlings and thus benefiting the breeding of scented *Phalaenopsis* orchids.

## AUTHOR CONTRIBUTIONS

Y-CC, W-CT, W-HC, and H-HC conceived the research plans. Y-CC performed most of the experiment, analyzed the data, and wrote the article with contributions of all the authors. Y-CH and C-YH assisted in the identification of the dual repeat and the analysis in the gene expression and scent compounds in *Phalaenopsis* orchids. C-MY, NM, and MO-T performed the yeast one hybrid screening analysis and provided valuable comments on the manuscript. H-HC supervised and complemented the writing. All authors read and approved the submitted version.

## FUNDING

This work was supported by grant no. MOST-102-2313-B-006-001-MY3 from the Ministry of Science and Technology, Taiwan, and partly supported by KAKENHI (grant no. 25113001 to NM) from the Ministry of Education, Culture, Sports, Science and Technology (MEXT), Japan.

## ACKNOWLEDGMENTS

We thank Dr. Tuan-Hua David Ho and Dr. Shu-Hsing Wu (Institute of Plant and Microbial Biology, Academia Sinica, Taiwan), and Dr. Yu-Yun Hsiao (Orchid Research and Development Center, NCKU, Taiwan) for helpful discussions. We thank Ya-Lan Chang (Department of Life Sciences, NCKU, Taiwan) for the assistance in the statistics analysis, and Dr. Chia-Chi Hsu (Department of Life Sciences, NCKU, Taiwan) for the transposon analysis. We also thank Pei-Han Lai (Department of Life Sciences, NCKU, Taiwan) and Ms. Fumie Tobe (AIST, Japan) for their technical help.

## SUPPLEMENTARY MATERIAL

The Supplementary Material for this article can be found online at: https://www.frontiersin.org/articles/10.3389/fpls.2018.00765/full#supplementary-material

## REFERENCES

Amrad, A., Moser, M., Mandel, T., de Vries, M., Schuurink, R. C., Freitas, L., et al. (2016). Gain and loss of floral scent production through changes in structural genes during pollinator-mediated speciation. *Curr. Biol.* 26, 3303–3312. doi: 10.1016/j.cub.2016.10.023

Arikit, S., Yoshihashi, T., Wanchana, S., Tanya, P., Juwattanasomran, R., Srinives, P., et al. (2011). A PCR-based marker for a locus conferring aroma in vegetable soybean (*Glycine max* L.). *Theor. Appl. Genet.* 122, 311–316. doi: 10.1007/s00122-010-1446-y

Awano, K., Honda, T., Ogawa, T., Suzuki, S., and Matsunaga, Y. (1997). Volatile components of *Phalaenopsis schilleriana* Rehb. f. *Flav. Frag. J.* 12, 341–344. doi: 10.1002/(SICI)1099-1026(199709/10)12:5<341::AID-FFJ657>3.0.CO;2-L

Bao, W., Kojima, K. K., and Kohany, O. (2015). Repbase Update, a database of repetitive elements in eukaryotic genomes. *Mob. DNA* 6:11. doi: 10.1186/s13100-015-0041-9

Bhagavan, N., and Ha, C.-E. (2011). "Structure and properties of DNA," in *Essentials of Medical Biochemistry: With Clinical Cases*, eds C.-E. Ha and N. Bhagavan (Cambridge, MA: Academic Press).

Bradbury, L. M., Henry, R. J., Jin, Q., Reinke, R. F., and Waters, D. L. (2005). A perfect marker for fragrance genotyping in rice. *Mol. Breed.* 16, 279–283. doi: 10.1007/s11032-005-0776-y

Brandvain, Y., Slotte, T., Hazzouri, K. M., Wright, S. I., and Coop, G. (2013). Genomic identification of founding haplotypes reveals the history of the selfing species *Capsella rubella*. *PLoS Genet.* 9:e1003754. doi: 10.1371/journal.pgen.1003754

Byers, K. J., Bradshaw, H., and Riffell, J. A. (2014). Three floral volatiles contribute to differential pollinator attraction in monkeyflowers (*Mimulus*). *J. Exp. Biol.* 217, 614–623. doi: 10.1242/jeb.092213

Cai, J., Liu, X., Vanneste, K., Proost, S., Tsai, W. C., Liu, K. W., et al. (2015). The genome sequence of the orchid *Phalaenopsis equestris*. *Nat. Genet.* 47, 65–72. doi: 10.1038/ng.3149

Carnesecchi, S., Schneider, Y., Ceraline, J., Duranton, B., Gosse, F., Seiler, N., et al. (2001). Geraniol, a component of plant essential oils, inhibits growth and polyamine biosynthesis in human colon cancer cells. *J. Pharmacol. Exp. Ther.* 298, 197–200.

Chao, Y.-T., Yen, S.-H., Yeh, J.-H., Chen, W.-C., and Shih, M.-C. (2017). Orchidstra 2.0-A transcriptomics resource for the orchid family. *Plant Cell Physiol.* 58:e9. doi: 10.1093/pcp/pcw220

Chen, Y. H., Tsai, Y. J., Huang, J. Z., and Chen, F. C. (2005). Transcription analysis of peloric mutants of *Phalaenopsis* orchids derived from tissue culture. *Cell Res.* 15, 639–657. doi: 10.1038/sj.cr.7290334

Chiu, L.-W., Zhou, X., Burke, S., Wu, X., Prior, R. L., and Li, L. (2010). The purple cauliflower arises from activation of a MYB transcription factor. *Plant Physiol.* 154, 1470–1480. doi: 10.1104/pp.110.164160

Cho, M., So, I., Chun, J. N., and Jeon, J.-H. (2016). The antitumor effects of geraniol: modulation of cancer hallmark pathways. *Int. J. Oncol.* 48, 1772–1782. doi: 10.3892/ijo.2016.3427

Chow, C. N., Zheng, H. Q., Wu, N. Y., Chien, C. H., Huang, H. D., Lee, T. Y., et al. (2015). PlantPAN 2.0: an update of plant promoter analysis navigator for reconstructing transcriptional regulatory networks in plants. *Nucleic Acids Res.* 44, D1154–D1160. doi: 10.1093/nar/gkv1035

Christenson, E. A. (2001). *Phalaenopsis: A Monograph*. Portland, OR: Timber Press.

Chuang, Y.-C., Lee, M.-C., Chang, Y.-L., Chen, W.-H., and Chen, H.-H. (2017). Diurnal regulation of the floral scent emission by light and circadian rhythm in the *Phalaenopsis* orchids. *Bot. Stud.* 58:50. doi: 10.1186/s40529-017-0204-8

Cordeiro, G. M., Christopher, M. J., Henry, R. J., and Reinke, R. F. (2002). Identification of microsatellite markers for fragrance in rice by analysis of the rice genome sequence. *Mol. Breed.* 9, 245–250. doi: 10.1023/A:1020350725667

Crowell, P. L. (1999). Prevention and therapy of cancer by dietary monoterpenes. *J. Nutr.* 129, 775S–778S. doi: 10.1093/jn/129.3.775S

Dudareva, N., and Negre, F. (2005). Practical applications of research into the regulation of plant volatile emission. *Curr. Opin. Plant Biol.* 8, 113–118. doi: 10.1016/j.pbi.2004.11.007

Dudareva, N., Pichersky, E., and Gershenzon, J. (2004). Biochemistry of plant volatiles. *Plant Physiol.* 135, 1893–1902. doi: 10.1104/pp.104.049981

Espley, R. V., Brendolise, C., Chagné, D., Kutty-Amma, S., Green, S., Volz, R., et al. (2009). Multiple repeats of a promoter segment causes transcription factor autoregulation in red apples. *Plant Cell* 21, 168–183. doi: 10.1105/tpc.108.059329

Gao, Z., Liu, C., Zhang, Y., Li, Y., Yi, K., Zhao, X., et al. (2013). The promoter structure differentiation of a MYB transcription factor RLC1 causes red leaf coloration in empire red leaf cotton under light. *PLoS One* 8:e77891. doi: 10.1371/journal.pone.0077891

Garland, S., Lewin, L., Blakeney, A., Reinke, R., and Henry, R. (2000). PCR-based molecular markers for the fragrance gene in rice (*Oryza sativa*. L.). *Theor. Appl. Genet.* 101, 364–371. doi: 10.1007/s001220051492

Ginis, O., Courdavault, V., Melin, C., Lanoue, A., Giglioli-Guivarc'h, N., St-Pierre, B., et al. (2012). Molecular cloning and functional characterization of *Catharanthus roseus* hydroxymethylbutenyl 4-diphosphate synthase gene promoter from the methyl erythritol phosphate pathway. *Mol. Biol. Rep.* 39, 5433–5447. doi: 10.1007/s11033-011-1343-8

Gould, M. N. (1997). Cancer chemoprevention and therapy by monoterpenes. *Environ. Health Perspect.* 105(Suppl. 4), 977. doi: 10.1289/ehp.97105s4977

Hammer, K., Carson, C., and Riley, T. (2003). Antifungal activity of the components of *Melaleuca alternifolia* (tea tree) oil. *J. Appl. Microbiol.* 95, 853–860. doi: 10.1046/j.1365-2672.2003.02059.x

Hong, G.-J., Xue, X.-Y., Mao, Y.-B., Wang, L.-J., and Chen, X.-Y. (2012). Arabidopsis MYC2 interacts with DELLA proteins in regulating sesquiterpene synthase gene expression. *Plant Cell* 24, 2635–2648. doi: 10.1105/tpc.112.098749

Hsiao, Y. Y., Jeng, M. F., Tsai, W. C., Chuang, Y. C., Li, C. Y., Wu, T. S., et al. (2008). A novel homodimeric geranyl diphosphate synthase from the orchid *Phalaenopsis bellina* lacking a DD *(X)* $_{2-4}$D motif. *Plant J.* 55, 719–733. doi: 10.1111/j.1365-313X.2008.03547.x

Hsiao, Y.-Y., Pan, Z.-J., Hsu, C.-C., Yang, Y.-P., Hsu, Y.-C., Chuang, Y.-C., et al. (2011a). Research on orchid biology and biotechnology. *Plant Cell Physiol.* 52, 1467–1486. doi: 10.1093/pcp/pcr100

Hsiao, Y. Y., Tsai, W. C., Chen, W. H., and Chen, H. H. (2011b). "Biosynthetic regulation of floral scent in *Phalaenopsis*," in *Orchid Biotechnology II*, eds W. H. Chen and H. H. Chen (Singapore: World Scientific), 145–180.

Hsiao, Y. Y., Tsai, W. C., Kuoh, C. S., Huang, T. H., Wang, H. C., Wu, T. S., et al. (2006). Comparison of transcripts in *Phalaenopsis bellina* and *Phalaenopsis equestris* (Orchidaceae) flowers to deduce monoterpene biosynthesis pathway. *BMC Plant Biol.* 6:14. doi: 10.1186/1471-2229-6-14

Hsieh, M.-H., Pan, Z.-J., Lai, P.-H., Lu, H.-C., Yeh, H.-H., Hsu, C.-C., et al. (2013). Virus-induced gene silencing unravels multiple transcription factors involved in floral growth and development in Phalaenopsis orchids. *J. Exp. Bot.* 64, 3869–3884. doi: 10.1093/jxb/ert218

Hsu, C.-C., Chen, Y.-Y., Tsai, W.-C., Chen, W.-H., and Chen, H.-H. (2015). Three R2R3-MYB transcription factors regulate distinct floral pigmentation patterning in *Phalaenopsis* spp. *Plant Physiol.* 168, 175–191. doi: 10.1104/pp.114.254599

Hsu, C. C., Wu, P. S., Chen, T. C., Yu, C. W., Tsai, W. C., Wu, K., et al. (2014). Histone acetylation accompanied with promoter sequences displaying differential expression profiles of B-class MADS-box genes for *Phalaenopsis* floral morphogenesis. *PLoS One* 9:e106033. doi: 10.1371/journal.pone.0106033

Hua, W., Song, J., Li, C., and Wang, Z. (2012). Molecular cloning and characterization of the promoter of SmGGPPs and its expression pattern in *Salvia miltiorrhiza*. *Mol. Biol. Rep.* 39, 5775–5783. doi: 10.1007/s11033-011-1388-8

Huang, X. Z., Xiao, Y. T., Köllner, T. G., Jing, W. X., Kou, J. F., Chen, J. Y., et al. (2018). The terpene synthase gene family in *Gossypium hirsutum* harbors a linalool synthase GhTPS12 implicated in direct defense responses against herbivores. *Plant Cell Environ.* 41, 261–274. doi: 10.1111/pce.13088

Jakoby, M., Weisshaar, B., Dröge-Laser, W., Vicente-Carbajosa, J., Tiedemann, J., Kroj, T., et al. (2002). bZIP transcription factors in Arabidopsis. *Trends Plant Sci.* 7, 106–111. doi: 10.1016/S1360-1385(01)02223-3

Jin, Q., Waters, D., Cordeiro, G. M., Henry, R. J., and Reinke, R. F. (2003). A single nucleotide polymorphism (SNP) marker linked to the fragrance gene in rice (*Oryza sativa* L.). *Plant Sci.* 165, 359–364. doi: 10.1016/S0168-9452(03)00195-X

Jun, M., Jeong, W., and Ho, C. (2006). Health promoting properties of natural flavor substances. *Food Sci. Biotechnol.* 15, 329–338.

Jurka, J. (1998). Repeats in genomic DNA: mining and meaning. *Curr. Opin. Struct. Biol.* 8, 333–337. doi: 10.1016/S0959-440X(98)80067-5

Juwattanasomran, R., Somta, P., Chankaew, S., Shimizu, T., Wongpornchai, S., Kaga, A., et al. (2011). A SNP in GmBADH2 gene associates with fragrance in vegetable soybean variety "Kaori" and SNAP marker development for the fragrance. *Theor. Appl. Genet.* 122, 533–541. doi: 10.1007/s00122-010-1467-6

Juwattanasomran, R., Somta, P., Kaga, A., Chankaew, S., Shimizu, T., Sorajjapinun, W., et al. (2012). Identification of a new fragrance allele in soybean and development of its functional marker. *Mol. Breed.* 29, 13–21. doi: 10.1007/s11032-010-9523-0

Kaiser, R. (1993). *The Scent of Orchids: Olfactory and Chemical Investigations*. Amsterdam: Elsevier. doi: 10.1021/bk-1993-0525.ch018

Knudsen, J. T., and Gershenzon, J. (2006). "The chemical diversity of floral scent," in *Biology of Floral Scent*, eds N. Dudareva, and E. Pichersky (Boca Raton, FL: CRC Press), 27–52.

Kumar, S., and Bhatia, S. (2016). A polymorphic (GA/CT) *n*-SSR influences promoter activity of *Tryptophan decarboxylase* gene in *Catharanthus roseus* L. Don. *Sci. Rep.* 6:33280. doi: 10.1038/srep33280

Li, S., Wang, H., Li, F., Chen, Z., Li, X., Zhu, L., et al. (2015). The maize transcription factor EREB58 mediates the jasmonate-induced production of sesquiterpene volatiles. *Plant J.* 84, 296–308. doi: 10.1111/tpj.12994

Li, X., Xu, Y., Shen, S., Yin, X., Klee, H., Zhang, B., et al. (2017). Transcription factor CitERF71 activates the terpene synthase gene CitTPS16 involved in the synthesis of E-geraniol in sweet orange fruit. *J. Exp. Bot.* 68, 4929–4938. doi: 10.1093/jxb/erx316

Liao, Y., Xu, F., Huang, X., Zhang, W., Cheng, H., Wang, X., et al. (2016). Characterization and transcriptional profiling of Ginkgo biloba mevalonate diphosphate decarboxylase gene (GbMVD) promoter towards light and exogenous hormone treatments. *Plant Mol. Biol. Rep.* 34, 566–581. doi: 10.1007/s11105-015-0947-x

Lu, H.-C., Chen, H.-H., Tsai, W.-C., Chen, W.-H., Su, H.-J., Chang, D. C.-N., et al. (2007). Strategies for functional validation of genes involved in reproductive stages of orchids. *Plant Physiol.* 143, 558–569. doi: 10.1104/pp.106.092742

Lu, S., Zhang, Y., Zheng, X., Zhu, K., Xu, Q., and Deng, X. (2016). Isolation and functional characterization of a lycopene β-cyclase gene promoter from citrus. *Front. Plant Sci.* 7:1367. doi: 10.3389/fpls.2016.01367

Marei, G. I. K., Rasoul, M. A. A., and Abdelgaleil, S. A. (2012). Comparative antifungal activities and biochemical effects of monoterpenes on plant pathogenic fungi. *Pestic. Biochem. Physiol.* 103, 56–61. doi: 10.1016/j.pestbp.2012.03.004

Mirzaei-Najafgholi, H., Tarighi, S., Golmohammadi, M., and Taheri, P. (2017). The effect of citrus essential oils and their constituents on growth of *Xanthomonas citri* subsp. *citri*. *Molecules* 22:E591. doi: 10.3390/molecules22040591

Mitsuda, N., Ikeda, M., Takada, S., Takiguchi, Y., Kondou, Y., Yoshizumi, T., et al. (2010). Efficient yeast one-/two-hybrid screening using a library composed only of transcription factors in *Arabidopsis thaliana*. *Plant Cell Physiol.* 51, 2145–2151. doi: 10.1093/pcp/pcq161

Mumm, R., Posthumus, M. A., and Dicke, M. (2008). Significance of terpenoids in induced indirect plant defence against herbivorous arthropods. *Plant Cell Environ.* 31, 575–585. doi: 10.1111/j.1365-3040.2008.01783.x

Murthy, K. N. C., Jayaprakasha, G. K., and Patil, B. S. (2012). D-limonene rich volatile oil from blood oranges inhibits angiogenesis, metastasis and cell death in human colon cancer cells. *Life Sci.* 91, 429–439. doi: 10.1016/j.lfs.2012.08.016

Myint, K. M., Arikit, S., Wanchana, S., Yoshihashi, T., Choowongkomon, K., and Vanavichit, A. (2012). A PCR-based marker for a locus conferring the aroma in Myanmar rice (*Oryza sativa* L.). *Theor. Appl. Genet.* 125, 887–896. doi: 10.1007/s00122-012-1880-0

Nagegowda, D. A., Rhodes, D., and Dudareva, N. (2010). "The role of the methyl-erythritol-phosphate (MEP) pathway in rhythmic emission of volatiles," in *The Chloroplast: Basics and Application*, eds C. A. Rebeiz, C. Benning, H. J. Bohnert, H. Daniell, J. K. Hoober, H. K. Lichtenthaler et al. (Dordrecht: Springer), 139–154.

Nakayama, K., Murata, S., Ito, H., Iwasaki, K., Villareal, M. O., Zheng, Y. W., et al. (2017). Terpinen-4-ol inhibits colorectal cancer growth via reactive oxygen species. *Oncol. Lett.* 14, 2015–2024. doi: 10.3892/ol.2017.6370

Nieuwenhuizen, N. J., Chen, X., Wang, M. Y., Matich, A. J., Perez, R. L., Allan, A. C., et al. (2015). Natural variation in monoterpene synthesis in kiwifruit: transcriptional regulation of terpene synthases by NAC and ETHYLENE-INSENSITIVE3-like transcription factors. *Plant Physiol.* 167, 1243–1258. doi: 10.1104/pp.114.254367

Pan, Z. J., Chen, Y. Y., Du, J. S., Chen, Y. Y., Chung, M. C., Tsai, W. C., et al. (2014). Flower development of *Phalaenopsis* orchid involves functionally divergent *SEPALLATA*-like genes. *New Phytol.* 202, 1024–1042. doi: 10.1111/nph.12723

Pan, Z. J., Cheng, C. C., Tsai, W. C., Chung, M. C., Chen, W. H., Hu, J. M., et al. (2011). The duplicated B-class MADS-box genes display dualistic characters in orchid floral organ identity and growth. *Plant Cell Physiol.* 52, 1515–1531. doi: 10.1093/pcp/pcr092

Paré, P. W., and Tumlinson, J. H. (1999). Plant volatiles as a defense against insect herbivores. *Plant Physiol.* 121, 325–332. doi: 10.1104/pp.121.2.325

Pelley, J. W. (2007). "Organization, synthesis, and repair of DNA," in *Elsevier's Integrated Biochemistry*, ed. J. W. Pelley (Philadelphia, PA: Mosby).

Pramnoi, P., Somta, P., Chankaew, S., Juwattanasomran, R., and Srinives, P. (2013). A single recessive gene controls fragrance in cucumber (*Cucumis sativus* L.). *J. Genet.* 92, 147–149. doi: 10.1007/s12041-013-0228-0

Pyo, H., Demura, T., and Fukuda, H. (2006). Vascular cell expression patterns of *Arabidopsis* bZIP group I genes. *Plant Biotechnol.* 23, 497–501. doi: 10.5511/plantbiotechnology.23.497

Ruangnam, S., Wanchana, S., Phoka, N., Saeansuk, C., Mahatheeranont, S., de Hoop, S. J., et al. (2017). A deletion of the gene encoding amino aldehyde dehydrogenase enhances the "pandan-like" aroma of winter melon (*Benincasa hispida*) and is a functional marker for the development of the aroma. *Theor. Appl. Genet.* 130, 2557–2565. doi: 10.1007/s00122-017-2976-3

Sakthivel, K., Rani, N. S., Pandey, M. K., Sivaranjani, A., Neeraja, C., Balachandran, S., et al. (2009). Development of a simple functional marker for fragrance in rice and its validation in Indian Basmati and non-Basmati fragrant rice varieties. *Mol. Breed.* 24, 185–190. doi: 10.1007/s11032-009-9283-x

Sas, C., Müller, F., Kappel, C., Kent, T. V., Wright, S. I., Hilker, M., et al. (2016). Repeated inactivation of the first committed enzyme underlies the loss of benzaldehyde emission after the selfing transition in *Capsella*. *Curr. Biol.* 26, 3313–3319. doi: 10.1016/j.cub.2016.10.026

Schwab, W., Davidovich-Rikanati, R., and Lewinsohn, E. (2008). Biosynthesis of plant-derived flavor compounds. *Plant J.* 54, 712–732. doi: 10.1111/j.1365-313X.2008.03446.x

Shi, W., Yang, Y., Chen, S., and Xu, M. (2008). Discovery of a new fragrance allele and the development of functional markers for the breeding of fragrant rice varieties. *Mol. Breed.* 22, 185–192. doi: 10.1007/s11032-008-9165-7

Su, C.-L., Chao, Y.-T., Yen, S.-H., Chen, C.-Y., Chen, W.-C., Chang, Y.-C. A., et al. (2013a). Orchidstra: an integrated orchid functional genomics database. *Plant Cell Physiol.* 54:e11. doi: 10.1093/pcp/pct004

Su, C.-L., Chen, W.-C., Lee, A.-Y., Chen, C.-Y., Chang, Y.-C. A., Chao, Y.-T., et al. (2013b). A modified ABCDE model of flowering in orchids based on gene expression profiling studies of the moth orchid *Phalaenopsis aphrodite*. *PLoS One* 8:e80462. doi: 10.1371/journal.pone.0080462

Tamura, K., Stecher, G., Peterson, D., Filipski, A., and Kumar, S. (2013). MEGA6: molecular evolutionary genetics analysis version 6.0. *Mol. Biol. Evol.* 30, 2725–2729. doi: 10.1093/molbev/mst197

Tholl, D. (2015). "Biosynthesis and biological functions of terpenoids in plants," in *Biotechnology of Isoprenoids*, eds J. Schrader, and J. Bohlmann (Cham: Springer), 63–106.

Tian, J., Li, K.-T., Zhang, S.-Y., Zhang, J., Song, T.-T., Zhu, Y.-J., et al. (2017). The structure and methylation level of the *McMYB10* promoter determine the leaf color of *Malus* Crabapple. *HortScience* 52, 520–526. doi: 10.21273/HORTSCI11563-16

Tsai, C., Chiang, Y., Huang, S., Chen, C., and Chou, C. (2010). Molecular phylogeny of *Phalaenopsis* Blume (Orchidaceae) on the basis of plastid and nuclear DNA. *Plant Syst. Evol.* 288, 77–98. doi: 10.1007/s00606-010-0314-1

Tsai, C. C. (2003). *Molecular phylogeny, biogeography, and evolutionary trends of the genus Phalaenopsis (Orchidaceae)*. Ph.D. thesis, National Sun Yat-sen University, Kaohsiung.

Tsai, C.-C. (2011). "Molecular phylogeny and biogeography of *Phalaenopsis* species," in *Orchid Biotechnology II*, eds W.-H. Chen, and H. H. Chen (Singapore: World Scientific), 1–24.

Vainstein, A., Lewinsohn, E., Pichersky, E., and Weiss, D. (2001). Floral fragrance. New inroads into an old commodity. *Plant Physiol.* 127, 1383–1389. doi: 10.1104/pp.010706

Vongvanrungruang, A., Mongkolsiriwatana, C., Boonkaew, T., Sawatdichaikul, O., Srikulnath, K., and Peyachoknagul, S. (2016). Single base substitution causing the fragrant phenotype and development of a type-specific marker in aromatic coconut (*Cocos nucifera*). *Genet. Mol. Res.* 15. doi: 10.4238/gmr.15038748

Wang, H., Han, J., Kanagarajan, S., Lundgren, A., and Brodelius, P. E. (2013). Studies on the expression of sesquiterpene synthases using promoter-β-Glucuronidase fusions in transgenic *Artemisia annua* L. *PLoS One* 8:e80643. doi: 10.1371/journal.pone.0080643

Wang, H., Kanagarajan, S., Han, J., Hao, M., Yang, Y., Lundgren, A., et al. (2014). Studies on the expression of linalool synthase using a promoter-β-glucuronidase fusion in transgenic *Artemisia annua*. *J. Plant Physiol.* 171, 85–96. doi: 10.1016/j.jplph.2013.09.019

Xu, Y.-H., Wang, J.-W., Wang, S., Wang, J.-Y., and Chen, X.-Y. (2004). Characterization of GaWRKY1, a cotton transcription factor that regulates the sesquiterpene synthase gene (+)-δ-cadinene synthase-A. *Plant Physiol.* 135, 507–515. doi: 10.1104/pp.104.038612

Yamasaki, Y., Kunoh, H., Yamamoto, H., and Akimitsu, K. (2007). Biological roles of monoterpene volatiles derived from rough lemon (*Citrus jambhiri* Lush) in citrus defense. *J. Gen. Plant Pathol.* 73, 168–179. doi: 10.1007/s10327-007-0013-0

Yeh, Y.-C., Tsay, Y.-S., Shih, C.-T., and Huang, P. (2014). Selection and breeding of scented *Phalaenopsis* varieties. *Agric. Policy Agric. Situation* 267, 97.

Yundaeng, C., Somta, P., Tangphatsornruang, S., Chankaew, S., and Srinives, P. (2015). A single base substitution in BADH/AMADH is responsible for fragrance in cucumber (*Cucumis sativus* L.), and development of SNAP markers for the fragrance. *Theor. Appl. Genet.* 128, 1881–1892. doi: 10.1007/s00122-015-2554-5

Yundaeng, C., Somta, P., Tangphatsornruang, S., Wongpornchai, S., and Srinives, P. (2013). Gene discovery and functional marker development for fragrance in sorghum (*Sorghum bicolor* (L.) Moench). *Theor. Appl. Genet.* 126, 2897–2906. doi: 10.1007/s00122-013-2180-z

**Conflict of Interest Statement:** The authors declare that the research was conducted in the absence of any commercial or financial relationships that could be construed as a potential conflict of interest.

frontiers in Plant Science

ORIGINAL RESEARCH
published: 09 July 2018
doi: 10.3389/fpls.2018.00909

# Overexpression of *LiDXS* and *LiDXR* From Lily (*Lilium* 'Siberia') Enhances the Terpenoid Content in Tobacco Flowers

*Tengxun Zhang, Ming Sun*, Yanhong Guo, Xuejun Shi, Yongjuan Yang, Juntong Chen, Tangchun Zheng, Yu Han, Fei Bao and Sagheer Ahmad*

*Beijing Key Laboratory of Ornamental Plants Germplasm Innovation & Molecular Breeding, National Engineering Research Center for Floriculture, Beijing Laboratory of Urban and Rural Ecological Environment, Key Laboratory of Genetics and Breeding in Forest Trees and Ornamental Plants of Ministry of Education, School of Landscape Architecture, Beijing Forestry University, Beijing, China*

*Lilium*, the famous and significant cut flower, emits a variety of volatile organic compounds, which mainly contain monoterpenes, such as myrcene, (E)-β-ocimene, and linalool. To understand the molecular mechanism of monoterpene synthesis in *Lilium*, we cloned two potential genes in the methylerythritol 4-phosphate pathway, namely *LiDXS* and *LiDXR*, from the strong-flavored oriental *Lilium* 'Siberia' using a homology-based PCR strategy. The expression levels of *LiDXS* and *LiDXR* were consistent with the emission and accumulation of monoterpenes in different floral organs and during the floral development, indicating that these two genes may play key roles in monoterpene synthesis. Subcellular localization demonstrated that LiDXS and LiDXR are expressed in the chloroplasts. Ectopic expression in transgenic tobacco suggested that the flowers of *LiDXS* and *LiDXR* transgenic lines accumulated substantially more diterpene, sclareol, compared to the plants transformed with empty vector. Surprisingly, increased content of the monoterpene, linalool and sesquiterpene, caryophyllene, were detected in the *LiDXR* transgenic lines, whereas the emission of caryophyllene, increased in one of the *LiDXS* transgenic tobacco lines, indicating that these two genes play significant roles in the synthesis of floral volatiles in the transgenic plants. These results demonstrate that *LiDXR* can contribute to monoterpene biosynthesis in *Lilium* 'Siberia'; however, the role of *LiDXS* in the biosynthesis of monoterpenes needs further study.

**Keywords: *Lilium*, *LiDXS*, *LiDXR*, monoterpenes biosynthesis, floral scent, volatile**

OPEN ACCESS

***Edited by:***
*Raquel Sánchez-Pérez, University of Copenhagen, Denmark*

***Reviewed by:***
*Sun-Hwa Ha, Kyung Hee University, South Korea*
*Yongzhen Pang, Institute of Botany (CAS), China*

****Correspondence:***
*Ming Sun*
*sunmingbjfu@163.com*

***Specialty section:***
*This article was submitted to Plant Breeding, a section of the journal Frontiers in Plant Science*

***Received:*** *13 February 2018*
***Accepted:*** *08 June 2018*
***Published:*** *09 July 2018*

***Citation:***
*Zhang T, Sun M, Guo Y, Shi X, Yang Y, Chen J, Zheng T, Han Y, Bao F and Ahmad S (2018) Overexpression of LiDXS and LiDXR From Lily (Lilium 'Siberia') Enhances the Terpenoid Content in Tobacco Flowers. Front. Plant Sci. 9:909. doi: 10.3389/fpls.2018.00909*

## INTRODUCTION

Fragrance is a significant and important character of horticultural plants that provides pleasure and enhances the ornamental value of flowers. Moreover, the aromatic compounds and essential oils present in flowers determine their economic value (Feng et al., 2014). Floral scent is produced by volatile organic compounds (VOCs) with low molecular weight (Pichersky et al., 2006), which are categorized into three major groups, namely terpenoids, phenylpropanoids/benzenoids, and fatty acid derivatives, according to their biosynthetic origin (Muhlemann et al., 2014). Floral VOCs are signals between plants and insects (Piechulla and Pott, 2003; Reinhard et al., 2004;

Cseke et al., 2007), and they play vital roles in attracting the pollinators (Pellmyr and Thien, 1986) and in defending against pathogens (Ramak et al., 2014). Among the three major groups of VOCs, benzenoids are used mainly for attracting pollinators, whereas terpenoids and benzenoids protect plants from pathogens (Schiestl, 2010). Terpenoids are the largest class of floral volatiles derived from two common and interconvertible five-carbon precursors, isopentenyl diphosphate (IPP) and dimethylallyl diphosphate (DMAPP) (McGarvey and Croteau, 1995). Unlike most other organisms, plants use at least two metabolic pathways to synthesize IPP and DMAPP. These include the cytosolic mevalonate (MVA) pathway, which occurs in the cytoplasm and the 2-C-methyl-D-erythritol-4-phosphate (MEP) pathway, which operates in the plastids (Jadaun et al., 2017). It has been shown that volatile monoterpenes and diterpenes, carotenoids, and chlorophylls are all formed by the MEP pathway, whereas the MVA pathway is mainly responsible for the synthesis of volatile sesquiterpenes and triterpenes (Lichtenthaler, 1999; Eisenreich et al., 2004; Chaurasiya et al., 2012; Yadav et al., 2014).

The MEP pathway involves seven enzymatic reactions, starting with the condensation of D-glyceraldehyde-3-phosphate (G3P) and pyruvate, which results in the formation of 1-deoxy-D-xylulose-5-phosphate (DXP) and is catalyzed by DXP synthase (DXS) with the assistance of thiamine pyrophosphate (TPP) and $Mg^{2+}$ (Rodriguez-Concepcion and Boronat, 2002). In the second step, DXP reductoisomerase (DXR) synthesizes the intermediate product, MEP, from DXP in the presence of NADPH and $Mn^{2+}$ or $Mg^{2+}$ (Takahashi et al., 1998). Therefore, the conversion from DXP to MEP is considered the committed step in the formation of IPP, an important intermediate substrate in these two pathways.

Many researchers have proposed that DXS and DXR are the potential control points in the synthesis of isopentenes (Harker and Bramley, 1999; Kuzuyama et al., 2000; Carretero-Paulet et al., 2006). To date, multiple *DXS* and *DXR* genes have been isolated and characterized. The *DXS* genes have been reported frequently not only from the model plant, *Arabidopsis thaliana* (Carretero-Paulet et al., 2006), but also from ornamental plants like *Lavandula latifolia* (Munoz-Bertomeu et al., 2006), *Pelargonium* spp.(Jadaun et al., 2017), *Catharanthus roseus* (Chahed et al., 2000), and *Aquilaria sinensis* (Xu et al., 2014) and from crop plants, such as *Solanum lycopersicum* (Lois et al., 2000), *Zea mays* (Cordoba et al., 2011), *Aconitum balfourii* (Sharma et al., 2016), *Tripterygium wilfordii* (Tong et al., 2015), and *Salvia miltiorrhiza* (Zhou et al., 2016). Because of their relationship in catalyzing a subsequent step in the MEP pathway, the *DXRs* are always illustrated together with the *DXS* genes in *A. thaliana* (Carretero-Paulet et al., 2006), *Dendrobium officinale* (Fan et al., 2016), *Rosa rugosa* (Feng et al., 2014), *L. latifolia* (Mendoza-Poudereux et al., 2014), *Osmanthus fragrans* (Zeng et al., 2016), and other plants. However, detailed studies are required for understanding whether the *DXS* and *DXR* genes play key roles in monoterpene biosynthesis of essential oils. In *Ocimum basilicum*, the expression levels of *DXS* and *DXR* genes were positively correlated with the yield of monoterpenes (Xie et al., 2008). In spike lavender, *DXS* was reported to play a crucial role in the biosynthesis of the monoterpene precursor, whereas *DXR* was not found to be the rate-limiting enzyme in this pathway (Mendoza-Poudereux et al., 2014). In the flowers of *R. rugosa*, the *RrDXR* gene might play a key role in the biosynthesis of volatile monoterpenes, but *RrDXS* might not be a key gene (Feng et al., 2014). Surprisingly, the abundance of *DXS* and *DXR* transcripts in *O. fragrans* flowers was inconsistent with the emission of monoterpenes (Zeng et al., 2016). Whether *DXS* and *DXR* genes play important roles in monoterpene synthesis in lily, needs further investigation.

Lily, a popular and commercially important cut flower, emits significant amounts of VOCs, consisting mainly of monoterpenes (Hu et al., 2017; Kong et al., 2017). Although the floral scents of the oriental *Lilium* hybrids are flowery and sweet, it is not liked by people owing to the emission of large amounts of volatile compounds (Johnson et al., 2016). To improve this aspect and to produce new *Lilium* varieties with fragrance emission within the acceptable range, it is important to understand the biosynthesis of monoterpenes in *Lilium* in detail. However, until date the molecular mechanism of monoterpene biosynthesis in lily is poorly understood.

In the present study, we investigated the two potential rate-limiting enzymes, *LiDXS* and *LiDXR*, in the strong-scented oriental lily, *Lilium* 'Siberia', to improve our understanding of the process of synthesis volatile compounds in floral organs. Considering the fact that *Lilium* is a model plant used for understanding the molecular pathway related to floral scents (Johnson et al., 2016), our elucidation of the monoterpene metabolic pathway in lily provides the theoretical basis for future improvement of its flowering traits through genetic engineering, and lays a foundation for genetic improvement and molecular breeding for floral traits of ornamental plants.

## MATERIALS AND METHODS

### Plant Material

*Lilium* 'Siberia' was collected from Xiaotangshan, Beijing. Healthy buds of consistent size, prior to the budding stage, were cut and water-cultured in a condition-stable phytotron at 25 ± 1°C under 55% relative humidity and a photoperiod of 16 h light and 8 h dark.

### RNA Extraction and Gene Cloning

The inner petals from at least three flowers in full-bloom on day 2 were collected at 9:00 h and were immediately frozen in liquid nitrogen and stored in a −80°C freezer for RNA extraction. The total RNA was extracted using Trizol reagent (Invitrogen, Carlsbad, CA, United States) according to the manufacturer's instructions. The total RNA was digested at 37°C with RQ1 RNase-free DNase (Promega, United States) to eliminate the residual genomic DNA. To synthesize the first-strand cDNA, 5 μg total RNA was transcribed using GoScript™ Reverse Transcription System (Promega, United States) as per the prescribed protocol. To obtain an intermediate nucleotide fragment of *LiDXS*, a pair of degenerate primers, DXS-F1 and DXS-R1, was designed by aligning the conserved domains of different DXS protein sequences retrieved from National

Center for Biotechnology Information (NCBI) (Accession Nos. BAD43377.1, ACF60511.1, NP_001234672.1, ACT32136.1, and AEZ53173.1). We obtained the first-strand cDNA for 3′- and 5′-rapid amplification of cDNA ends (RACE) as per the procedure described in the user manual of SMARTer® RACE 5′/3′ Kit, and designed the gene-specific primers, 3′ GSP and 5′ GSP for amplifying the 3′- and 5′-ends. The intermediate fragment and the 3′- and 5′-ends were assembled to determine the full-length sequence of *LiDXS*. Subsequently, we designed another pair of primers, DXS-F2 and DXS-R2, to amplify the open reading frame (ORF) sequence.

The ORF of *DXR* was amplified using the primers, DXR-F and DXR-R, designed on the basis of the sequence of this gene from *Lilium longiflorum* (Accession No. KF765491). All the PCR products were sub-cloned into pCloneEZ-*TOPO* vector; the recombinant vector was transformed into *Escherichia coli* DH5α and the positive clones were screened by sequencing. The sequences of the primers used in this study are listed in Supplementary Table 1.

## Bioinformatics Analysis

The ClustalX 2.0 (Larkin et al., 2007) software was used for alignment of the sequences from *L.* 'Siberia' and other monocot, eudicot, and protist species. The multiple alignments of sequences were edited using the BioEdit 7.0 (Hall, 1999). MEGA 5.0 was used to construct the phylogenetic tree using the protein sequences from different species based on the neighbor-joining method with 1000 bootstrap replicates. The subcellular localization of the two potential genes was conducted using Plant-mPLoc, ChloroP, and WoLF PSORT online tools.

## Subcellular Localization

The vector construction was done using the In-Fusion® HD Cloning Kit (Clontech, Japan) following the recommended protocol. The ORFs of *LiDXS* and *LiDXR* were amplified using gene-specific primers (Supplementary Table 1) with 15-bp homologous sequences with plant expression vector *pSuper1300::GFP* containing the recognition sites for *Xba*I and *Spe*I. The vector *pSuper1300::GFP* was linearized by digestion with *Xba*I and *Spe*I. The targeted gene fragments and vectors were ligated by the In-fusion enzyme to construct the recombinant plasmids, *pSuper1300::LiDXS::GFP* and *pSuper1300::LiDXR::GFP*, driven by the CaMV-35S promoter. The recombinants were transformed into *Agrobacterium tumefaciens* GV3101 using freeze-thaw method for further study. The final $OD_{600}$ of the *Agrobacterium* cells transformed with the construct re-suspended in 5 mL of infiltration buffer (10 mM $MgCl_2$, 10 mM MES-KOH; pH 5.6–5.7) was adjusted to 0.5. The *Agrobacterium* solution containing 1/1000 volume of acetosyringone (150 mM) was incubated without shaking at 28°C for 2 h before injecting the leaves. The underside of the leaves of *Nicotiana benthamiana* was injected using a syringe and the infected leaves were exposed to long daylight for 48–56 h. The labeled pieces of leaves (1 cm in diameter) were placed on the glass slide. The expression of green fluorescent protein (GFP) was observed under the confocal laser scanning microscope, Leica TCS SP8 (Leica, Germany).

## Gene Expression Analysis

To determine the levels of the *LiDXS* and *LiDXR* transcripts during the flowering stages and in different floral tissues, quantitative real-time PCR (qRT-PCR) was performed using the PikoReal real-time PCR system (Thermo Fisher Scientific, China). Each sample was pooled in at least three replicates and the three pools served as the three biological replicates; for each replicate, qRT-PCR was performed thrice. Only the inner petals were collected from 13:00 to 15:00 h at every stage. RNA extraction was performed as described above and the cDNA was synthesized according to the instructions in the manual of PrimeScript™ RT reagent Kit with gDNA Eraser (Perfect Real Time) (TaKaRa, Japan). The PCRs were carried out using cDNA diluted 30-times with the SYBR® Premix Ex Taq™ Mix II (TaKaRa, Japan). The procedure for qRT-PCR was the classical three-step method and the relative transcript levels were computed using the $2^{-\Delta\Delta Ct}$ method, as described previously (Zhang et al., 2017). The *Actin* gene (Accession number: AB438963) was used as the internal reference, as described by earlier (Zhang et al., 2017). The sequences of all the gene-specific primers are listed in Supplementary Table 1.

## Transformation and Screening of Tobacco

The *pSuper1300::LiDXR* and *pSuper1300::LiDXS* constructs used for the stable transformation of tobacco were generated as described above except for the linearized plant expression vector, *pSuper1300*, without the GFP label.

They were transformed into wild type tobacco (*Nicotiana tabacum* 'NC89') leaf disks through *A. tumefaciens* GV3101-mediated freeze-thaw transformation. For obtaining the transgenic lines, *Agrobacterium*-mediated transformation of tobacco leaf disks was performed as described previously (Burow et al., 1990). The positive transgenic plants were screened on Murashige and Skoog's (MS) medium supplemented with 50 mg/L hygromycin, and were identified through PCR. The T1 and T2 transgenic seeds were collected. All the T2 seeds (T3) were generally transgenic and could be used for the determining the content of the floral volatiles. All the transgenic plants were cultured under the same conditions with 16 h light at 24°C /8 h night at 18°C.

For analyzing the expression levels of *LiDXS* and *LiDXR* in the transformed tobacco plants, we collected the flowers at 9:00 h on the first day of flowering. For each line, at least three petals from the transgenic tobacco flowers were pooled and real-time PCR was performed following the steps described above using *NtEFα1* as the endogenous control gene. The expression levels of endogenous *NtDXS* and *NtDXR* genes in tobacco were detected as well. The sequences of all the gene-specific primers are listed in Supplementary Table 1.

## Terpenoid Quantification in Tobacco

The floral volatiles in the transgenic tobacco plants were detected mainly by using headspace solid-phase microextraction (HS-SPME). Each sample, collected from three tobacco flowers, was put in the headspace bottle, and the samples from each line

were taken in triplicates. The fiber (50/30 μm DVB/CAR/PDMS) was conditioned for 2 h at 250°C in the gas chromatography inlet before the first volatile extraction. The sample was equilibrated for 3 h at 25°C and collection was done at 50°C for 30 min using the extractor inserted into the upper side of the vial. Immediately after extraction, the fibers were desorbed for 5 min at 250°C in the injection port and then gas chromatography-mass spectrometry (GC/MS) analysis was performed. GC/MS was carried out using Shimadzu CGMS-QP2010 (Shimadzu, Kyoto, Japan) equipped with a DB-5MS capillary column (30 m × 0.25 mm × 0.25 μm, Shimadzu). The chromatography program started at 40°C for 2 min, and the temperature was increased to 200°C at a rate of 5°C/min and held at this temperature for 6 min; the inlet temperature was set at 200°C, total flow was 27.5 mL/min, and the split ratio was 20. The carrier gas used was helium. The parameters for mass spectrometer were as follows: the electron potential was set to 1 KV, the mass scan range (m/z) was 30–300 amu, and the ion source temperature was set to 250°C. The volatile compounds in the flowers were identified by comparison with the compounds present in the National Institute of Standards and Technology (NIST) 11 library using GC/MS Postrun Analysis software. The relative content of each compound was calculated based on the peak area normalization method.

## Statistical Analysis

The statistical significance was determined with SPSS 22.0 (SPSS, Inc., Chicago, IL, United States) using one-way ANOVA. The standard deviation was calculated using triplicate samples and significant differences ($p < 0.05$) between the transformed lines and transgenic tobacco transformed with the empty vector were compared. The bar charts representing the data were drawn with Origin Pro 8.0 (Northampton, MA, United States).

# RESULTS

## Characterization of *LiDXS* and *LiDXR*

To identify the function of *LiDXS* and *LiDXR* in terpene biosynthesis, we isolated their ORFs using homologous cloning from *L.* 'Siberia.' The full-length cDNA sequence of *LiDXS* (Accession No. MF078467) was found to be 2479 bp, containing an ORF of 2199 bp encoding 732 amino acids. The alignment of the protein sequences of DXS from different sources using Clustal X and BioEdit showed that LiDXS was weakly conserved in the N-terminal and contained the typical WDVGHM and IAEQHA domains (**Figure 1A**), which are believed to be closely related to the catalytic function. The phylogenetic analysis was performed based on the selected DXS protein sequences. The results showed that the phylogenetic tree consisted of three clades. In addition, LiDXS belonged to the DXS type-2 (DXS2) clade and had higher homology to DXS2 from *Z. mays* (**Figure 1B**). The ORF length of *LiDXR* (Accession No. MF078468) was 1419 bp, encoding 472 amino acids. The blastp analysis showed that LiDXR contains two putative domains: DXP_reductoisom (78–206 amino acid), which is present on the C-terminus of the pfam02670 domain in bacterial and plant proteins, and DXP_redisom_C (28–472 amino acid). Moreover, the alignment of DXR sequences from eukaryotes and prokaryotes revealed that the DXRs were highly homologous and shared a conserved P(P/Q)PAWPG(R/T) motif (**Figure 1C**), which was not present in the DXR sequences from protists and regarded as a signature for DXR proteins in all plants (Devi et al., 2015). The sequence was not conserved at the N-terminal end (positions 1–54), whereas the extended region (55–77 amino acids) and the C-terminal region were strongly conserved. The phylogenetic tree of DXR sequences revealed that they were organized into four groups: cluster I comprised eudicots, monocots formed cluster II, gymnosperm formed cluster III, and cluster IV comprised protists; the phylogenetic tree revealed the evolutionary relationship among the different species (**Figure 1D**). In lily, the DXR sequence was conserved; for example, the sequence of LiDXR was highly similar to that of DXR from another monocot, *L. longiflorum*.

LiDXR and LiDXS were predicted to be localized to the chloroplasts using the online softwares, Plant-mPLoc, WoLF POST, and ChloroP. To determine the intracellular localization and roles of LiDXR and LiDXS, construct vectors and empty vector were transformed into the leaves of *N. benthamiana*. We found that the GFP signal from the empty vector was obtained from the nucleus and cytoplasm, whereas when LiDXS and LiDXR were fused to GFP, the signal was localized in the chloroplasts (**Figure 2**).

## *LiDXS* and *LiDXR* Expression in Floral Organs and Developmental Stages

To investigate the possible role of *LiDXS* and *LiDXR* in monoterpene production, the expression profiles of these genes was determined in different floral organs and during four flowering stages using qRT-PCR. We gathered the whole flowers on the first day of the full-bloom stage, and divided them into four parts: petals, filaments, anthers, and stigma (**Figure 3A**). The process of flowering was divided into four stages: (FS1) budding stage, (FS2) initial flowering stage, (FS3) full-blooming stage, (FS4) wilting stage (**Figure 3D**). The results indicated that the expression levels of *LiDXS* and *LiDXR* were consistently higher in petals as compared with those in the remaining organs (**Figures 3B,C**). Their expression levels increased from the budding stage to the full-bloom stage and then decreased during the withering stage (**Figures 3E,F**), consistent with the release of floral volatiles in *Lilium* (Hu et al., 2017).

## Overexpression of *LiDXS* and *LiDXR* in Tobacco Affects the Accumulation of Terpenoids

*LiDXS* and *LiDXR* might be the crucial genes contributing to the biosynthesis of monoterpenes (linalool, (E)-β-ocimene, and myrcene), as revealed by real-time PCR (**Figure 3**). The stably transformed tobacco plants were obtained by infecting leaf disks with *A. tumefaciens* GV3101 carrying *pSuper1300::LiDXR* and *pSuper1300::LiDXS*. At least 30 transgenic tobacco plants (T1)

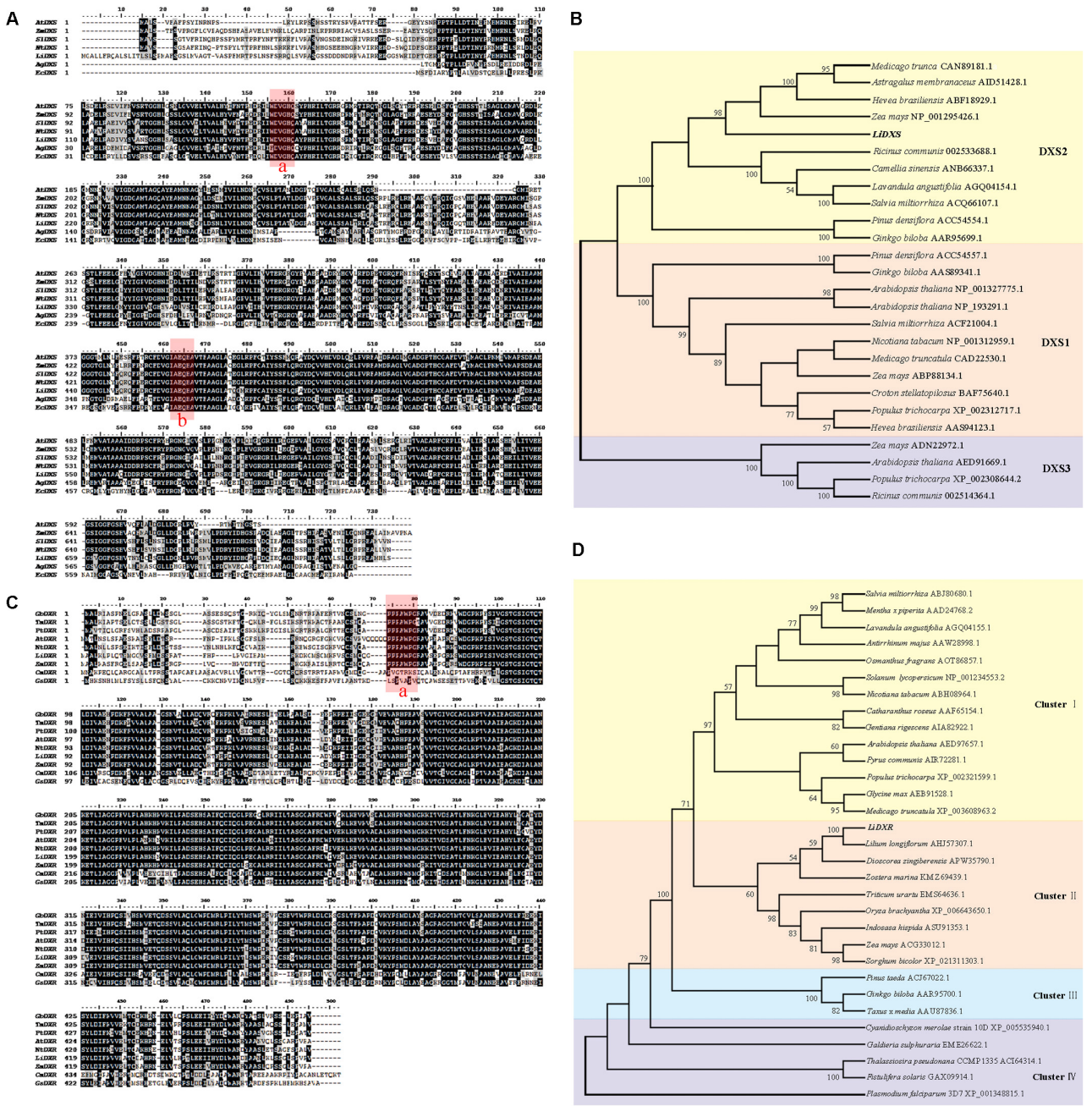


**FIGURE 1 |** Multiple alignment and phylogenetic analysis of protein sequence of DXS and DXR from different species. **(A)** Alignment of deduced amino acid sequences of DXS proteins performed using Cluster X and DNAMAN 7.0. Species abbreviations in gene names are as follows: At: *Arabidopsis thaliana*, Zm: *Zea mays*, Sl: *Solanum lycopersicum*, Nt: *Nicotiana tabacum*, Ag: *Agrobacterium tumefaciens* (AIC32317.1), Ec: *Escherichia coli* (EGT70614.1). Their accession numbers were in parallel with DXS2 protein in **(B)**. Identical amino acid residues are shaded black, and the similar ones are shaded gray. The highly conserved domains were marked red: box a is WDVGHM motif, box b is IAEQHA motif. **(B,D)** Phylogenetic tree of DXSs and DXRs proteins, respectively, using neighbor-joining method with 1000 bootstrap replicates and showing values more than 50%. Accession numbers of the amino acid sequences accession numbers registered in NCBI were listed after the species names. **(C)** Alignment of amino acid sequences of LiDXR and DXRs proteins from other species. Species abbreviations in gene names are as follows: Gb: *Ginkgo biloba*, Tm, *Taxus* × *media*, Pt: *Pinus taeda*, At: *Arabidopsis thaliana*, Nt: *Nicotiana tabacum*, Zm: *Zea mays*, Cm: *Cyanidioschyzon merolae* strain 10D, Gs: *Galdieria sulphuraria*. The assession number of these species were the same as that in part D. The P(P/Q)PAWPG(R/T) motif was labeled in box a.

were obtained for each of the target genes. The transformed lines were confirmed by hygromycin resistance and the presence of the target genes in the transgenic plants was determined by PCR. The seeds of T1 plants (T2 seeds) were screened on MS medium containing hygromycin. Two positive transgenic lines harboring *LiDXS* (S1 and S6) and three lines harboring

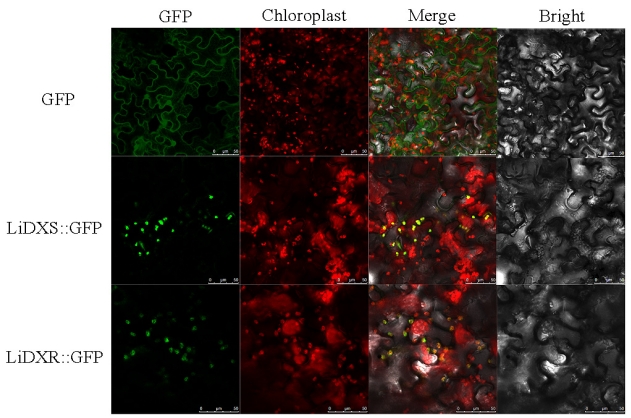


**FIGURE 2 |** Subcellular localization of LiDXS and LiDXR. The fusion proteins (LiDXS::GFP and LiDXR::GFP) and GFP as a control protein were observed under the confocal laser scanning microscope. The first panel was constructed in the green fluorescence channel. The second panel was the chloroplast autofluorescence channel. The merged images were formed from the first two panels. Bar = 10 μm.

*LiDXR* (R3, R4, and R8) were selected using RT-PCR. These were all provided in Supplementary Figure 1. The floral scent in all these transgenic plants were obviously increased without any changes in the phenotypic characters, such as flower color and shape (Supplementary Figure 2). The transgenic tobacco plants transformed with the empty vector were treated as control. The endogenous and heterogenous expression levels of the transgenes were further confirmed by qRT-PCR. The results showed that the ecpotic expression levels of both the genes were significantly increased in the transgenic lines compared to their levels in the control plants (**Figures 4A,E**). Meanwhile, the endogenous *NtDXS* and *NtDXR* genes in tobacco were expressed stably (Supplementary Figure 3). The floral volatiles in all the lines were examined by HS-SPME-GC-MS. There were no differences in the contents of the volatile compounds between the control and transgenic lines; however, terpenoids were enhanced differently in the transgenic lines (**Figure 5**). In the S1 and S6 lines, the amounts of linalool (a monoterpene) were enhanced slightly but no obvious changes were noticed compared to the level in the control (**Figure 4B**). The content of caryophyllene (a sesquiterpene) was strongly increased in S6, whereas no significant difference was detected in S1 (**Figure 4C**). The content of sclareol (a diterpenoid) was sharply increased in the S1 and S6 lines, and there were significant differences in the content compared to control (**Figure 4D**). The overexpression of *LiDXR* resulted in apparent changes in the contents of different compounds in the transgenic lines. The content of linalool was significantly increased in R3, R4, and R8 lines by 1.6–2.1 times compared to the content in the control plants (**Figure 4F**), and obvious changes in the content of caryophyllene were observed (**Figure 4G**). The content of sclareol was also significantly enhanced in the R3 and R4 lines, whereas no change was detected in the R8 line (**Figure 4H**).

## DISCUSSION

To elucidate the functions of LiDXS and LiDXR, we analyzed these sequences at first. The blastp analysis showed that LiDXS belonged to highly conserved transketolase-like enzyme family, in which the C-terminal domain serves as a regulatory binding site. Both, LiDXS and transketolase, contain histidine residues, which are thought to be involved in proton transport during the reaction (Lois et al., 1998). In addition, they contain a typical conserved motif for the binding of TPP, which acts as a cofactor (Jadaun et al., 2017). The phylogenetic tree of LiDXS revealed that these genes evolved during the evolution of the most advanced angiosperms. The distance of PiDXS from *Pinus densiflora* and GbDXS from *Ginkgo biloba* were the closest; both these plants are gymnosperms. LaDXS, from *Lavandula angustifolia*, clustered together with SaDXS from *S. miltiorrhiza*, both of which belong to Labiatae. LiDXS was next to ZmDXS from *Z. mays*, a monocot. The DXS is reported to be usually encoded by a small family of genes (Walter et al., 2002; Phillips et al., 2008; Cordoba et al., 2009, 2011) and there are many DXS homologs in plants, such as *Z. mays* (Cordoba et al., 2011), *Hedychium coronarium* (Yue et al., 2015), and *S. lycopersicum* (Zhou et al., 2016). The three clades of the gene family are differently expressed during plant development and in specific organs (Cordoba et al., 2011), and play different roles in plant development. The first group of *DXS* genes mainly functions as a housekeeping gene (Kim et al., 2005); the second clade is mainly involved in the secondary metabolism of plants (Walter et al., 2002). The third type synthesizes some substances derived from the isoprene pathway, which are necessary but have lesser demand in the plants, such as gibberellins and abscisic acid (Rohmer et al., 1996; Lichtenthaler, 1999). Moreover, in this phylogenetic tree, the proteins are organized into different clades according to their functions, among which the DXS2 clade is involved in the isoprene synthesis pathway; for example, CrDXS participates in the biosynthesis of the monoterpene indole alkaloids in *C. roseus* (Burlat et al., 2004). However, the phylogenetic analysis of LiDXR indicates the evolutionary relationship among the DXRs and their diversification, and suggests that the DXRs might have evolved from an ancestral gene (Tong et al., 2015) by parallel duplication (Devi et al., 2015). In lily, LiDXS belonged to the DXS2 clade, suggesting that it might function in the synthesis of monoterpenes.

The enzymes of the MEP pathway were demonstrated to be localized in chloroplasts in soybean, as well as in maize (Cordoba et al., 2011) and *Arabidopsis* (Hsieh et al., 2008), using GFP labeling (Wright et al., 2014). In plant cells, the movement of genes from the photosynthetic endo-symbiont (plastid) to the nucleus mandates that the encoded plastidal proteins must have a transit peptide that can translocate them to their site of function. The plastid localization signals in the DXS and DXR proteins were present on the N-terminus and were not found to be conserved in different species (**Figures 1A,C**). Moreover, the signal peptide was found to be absent in the bacterial DXS and DXR (Carretero-Paulet et al., 2002; Rodriguez-Concepcion and Boronat, 2002). Both LiDXS and LiDXR were predicted to

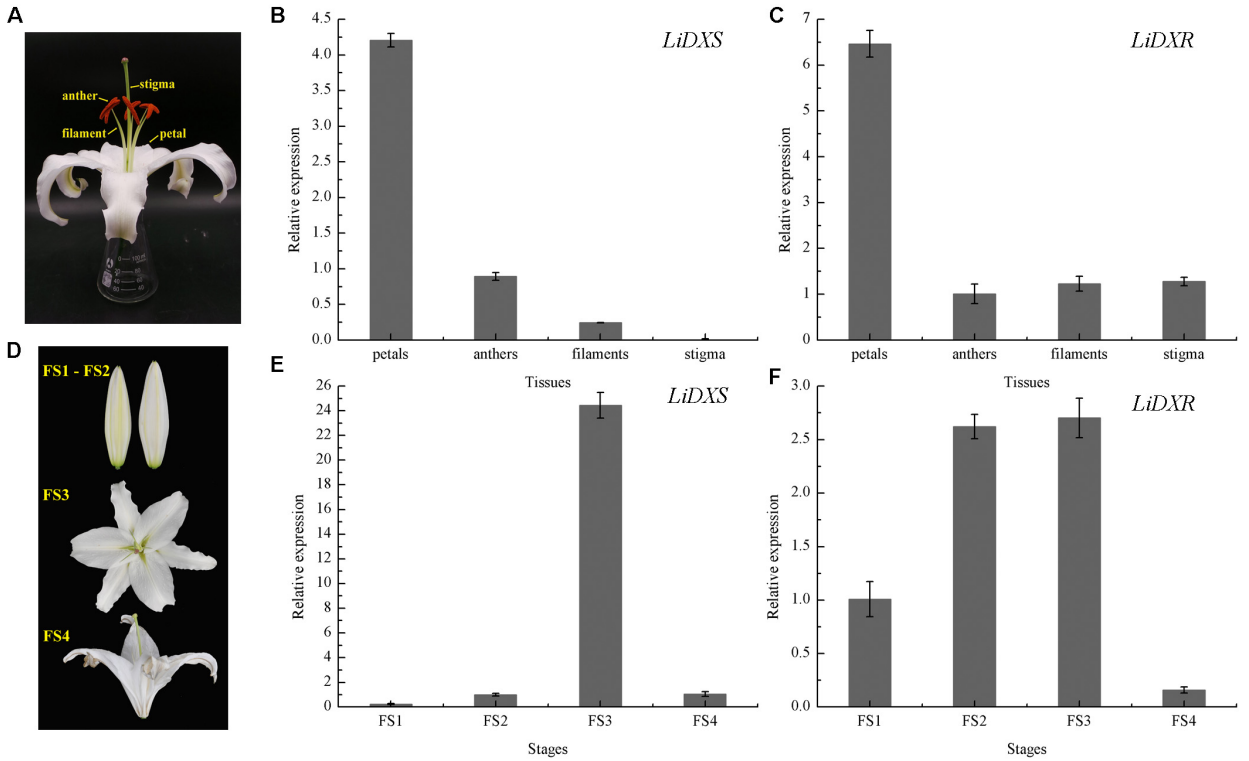


**FIGURE 3 |** The relative expression levels of *LiDXS* and *LiDXR* genes. **(A)** Petal, filament, anther, and stigma of a flower. **(B,C)** Expression levels of *LiDXS* and *LiDXR* genes in different flower parts at the first full-blooming day, respectively. **(D)** Flower development stages: FS1–FS4. **(E,F)** Expression patterns of *LiDXS* and *LiDXR* genes, respectively, during flower development stages.

contain a chloroplast transit peptide, respectively, 53 and 48 amino acids in length. The plant DXS proteins contain a typical plastid transit peptide sequence, which determines the plastidal localization of these proteins (Bouvier et al., 1998; Lois et al., 2000). All the enzymatic reactions of the MEP pathway are carried out in the chloroplast and control the metabolic flux in the cells (Hsieh et al., 2008). In the plastid-localized MEP pathway, the DXS enzyme has been demonstrated to be the rate-limiting step; investigations on *Arabidopsis CLA1* mutant, showed that dysfunction of *cla1* (DXS-like gene) results in the lack of isoprenoids leading to albinism (Mandel et al., 1996). The DXS proteins in maize, concluding dxs1, dxs2, and dxs3, were only observed in the chloroplasts (Cordoba et al., 2011). And SmDXS1 and SmDXS2 in *S. miltiorrhiza* were located in the chloroplasts, in agreement with the plastidal operation of the MEP pathway (Zhou et al., 2016). Similar results about DXR genes were found in some plants, such as *Arabidopsis* (Carretero-Paulet et al., 2002) and *Glycine max* (Zhang et al., 2012), providing evidence of plastid localization of plant DXRs. In this study, LiDXS and LiDXR were localized to the chloroplasts providing credence to the proposed roles of LiDXS and LiDXR in the MEP pathway in lily.

Previous studies have shown that the expression of genes for the rate-limiting enzymes controlling the MEP pathway also has features that correspond to the spatial and temporal rhythm of fragrance. For instance, the expression profile of *VvDXS* positively correlates with the accumulation of monoterpenes in *Moscato Bianco* berries (Battilana et al., 2011). Petals are the main organs that release distinct aroma compounds in many plants (Feng et al., 2014). As reported by Feng, the main aromatic components of *R. rugosa* are emitted from petals and stamens. The expression of *RrDXR* in petals was found to be the highest compared to its expression in other organs, such as stamens, pistils, calyxes, and receptacles, whereas the expression of *RrDXS* was lower in petals than in receptacles. This suggests that the isolated *RrDXS* belonged to the DXS1 clade and might not play the main function in the biosynthesis of monoterpenes, whereas *RrDXR* might be playing a key role in the MEP pathway. Here, the expression of *LiDXS* and *LiDXR* were significantly higher in the petals than in the other tissues; this result was consistent with the report that the amounts of volatile compounds from petals were similar to that in the whole detached flower of *L.* 'Siberia' (Hu et al., 2017).

The amounts of the emitted floral volatiles exhibited rhythmic patterns during the flowering stages. The analysis of the floral scents from *H. coronarium* indicated that the emission of monoterpenes was gradually enhanced from D1–D3 (budding stage) to D4 (full flowering stage) stage, in which the expression was highest. In addition, transcriptome analysis of samples from different stages, revealed that the expression levels of genes responsible for key enzymes (including *HcDXS2A*, *HcGPPS*, *HcTPS7*, and *HcTPS8*) were the highest at the full flowering

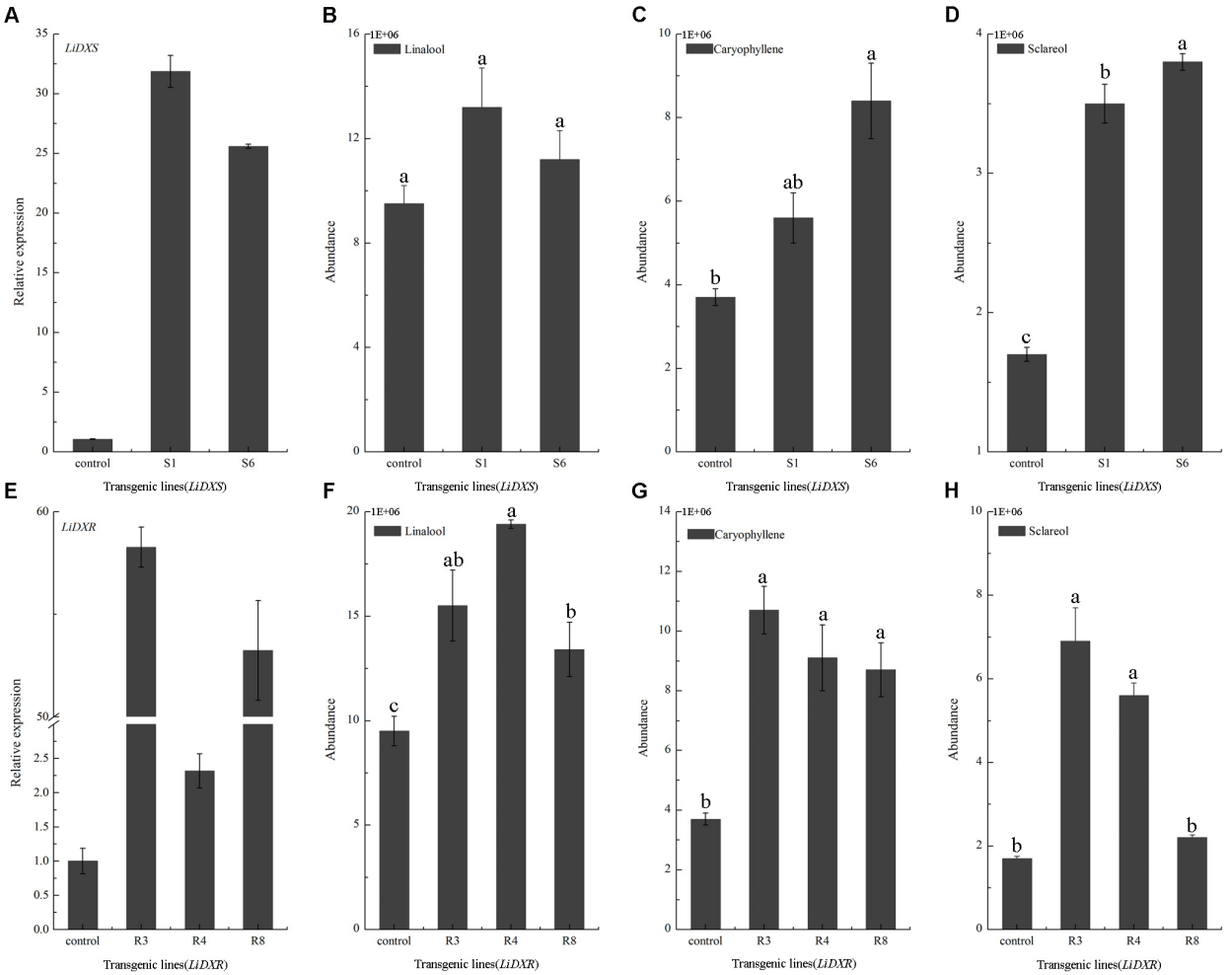


**FIGURE 4 |** Gene expression levels and volatiles emission amounts in transgenic plants. **(A,E)** The expression levels of *LiDXS* and *LiDXR* genes in different transgenic lines determined by qRT-PCR. *NtEFα1* gene was used as the endogenous control. **(B–D)** Relative emission amounts of linalool, caryophyllene, sclareol in *LiDXS* transgenic lines. **(F–H)** Relative emission amounts of linalool, caryophyllene, and sclareol in *LiDXR* transgenic lines. The columns represent average values for each line, and error bars show the standard deviation of three biological replicates. Duncan statistical analysis at the was used for testing significance of the observed differences level of at the $p < 0.05$ level.

stage, indicating that these genes might be involved in the synthesis of floral metabolites (Yue et al., 2015). In our study, the expression levels of *LiDXS* and *LiDXR* were initially lower at the budding stage and were apparently increased at the full flowering stage; subsequently, they were decreased at the wilting stage, as observed in a recent report, in which the terpenoid components peaked at the flowering stage (Hu et al., 2017). The expression levels of *LiDXS* and *LiDXR* were positively correlated with the emission of volatile compounds in *L.* 'Siberia', suggesting these two genes might play significant roles in the biosynthesis of monoterpenes.

The DXS and DXR proteins have been proposed to be the key and rate-limiting enzymes of terpenoid biosynthesis in many plants, such as *A. thaliana* (Carretero-Paulet et al., 2006) and *T. wilfordii* (Tong et al., 2015). Increased expression of *DXS* and *DXR* could alter the accumulation of MEP-derived isoprenoids (e.g., chlorophylls and carotenoids) in *A. thaliana* (Carretero-Paulet et al., 2006). *TwDXS1*, *TwDXS2*, and *TwDXR* from *T. wilfordii* promoted the accumulation lycopene in an *E. coli* strain as determined through color complementation assays, indicating that these genes could function in controlling the terpenoid biosynthetic flux (Tong et al., 2015). The overexpression and down-regulation of *SmDXS2* resulted in obvious increase and decrease in the content of tanshinone in transgenic roots of *S. miltiorrhiza* (Zhou et al., 2016). Several studies supported the view that DXS and DXR are crucial enzymes in regulating the metabolic flux through the MEP-pathway. In the present study, the high levels of ectopic expression of *LiDXS* and *LiDXR* was responsible for the induction of sclareol biosynthesis. These findings were consistent with a previous study (Morrone et al., 2010), which reported that the overexpression of three genes (*idi*, *dxs*, and *dxr*) led to the greatest increase in the yield of this diterpene. The ectopic expression *AtDXS* gene from *A. thaliana* in *L. latifolia*

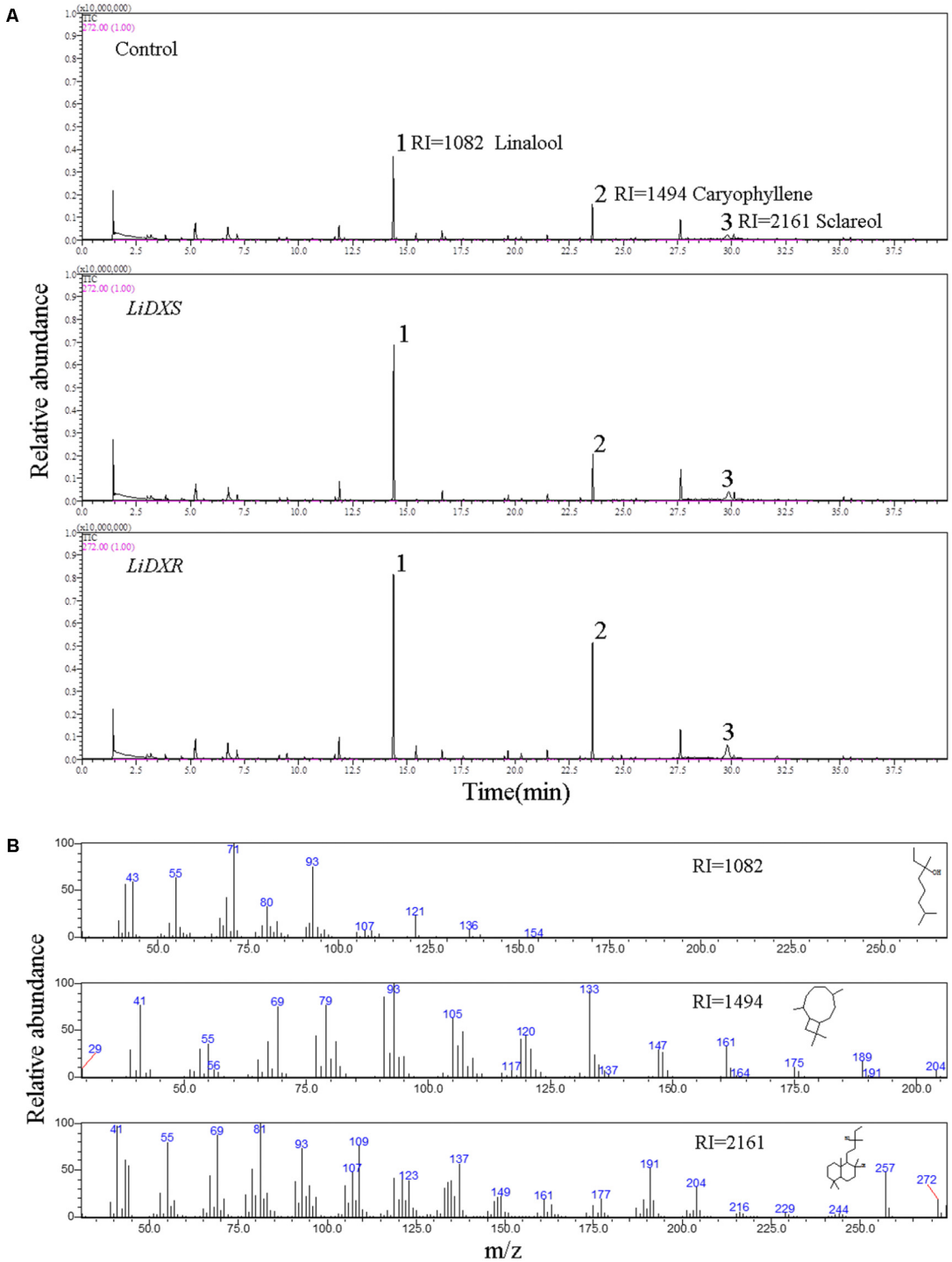


**FIGURE 5 |** The identification of flower volatiles from transgenic *N. tabacum*. **(A)** GC trace of flower of transgenic *N. tabacum* plants. **(B)** Mass spectra of linalool, caryophyllene, and sclareol. The products were identified by comparison with compounds in the library NIST11.

significantly altered the content of monoterpenes in transgenic lavender, without causing changes in growth characteristics and ecological habits (Munoz-Bertomeu et al., 2006). The analysis of the metabolites showed that the content of essential oil (geraniol, linalool, and citronellol) increased in the leaves of rose-scented geranium transiently expressing *LiDXS*. Interestingly, the amount of sesquiterpenes content increased as compared with that in the control (Jadaun et al., 2017), which consistent

with the findings in our transgenic lines. The content of caryophyllene was enhanced in the R3, R4, R8, and S6 lines. The tobacco plants transformed with *LiDXR* also accumulated substantial amount of linalool without any changes in the composition of plant volatiles with respect to the plants with empty vector. Similar results have been reported in transgenic peppermint (*Mentha* × *piperita*) (Mahmoud and Croteau, 2001). Because floral volatile compounds in lily mainly comprise of monoterpenes, such as linalool, (E)-β-ocimene and myrcene (Hu et al., 2017), *LiDXR* is a crucial gene associated with the synthesis of monoterpenes, even more terpenoids, and the function of *LiDXS* in this process needs to be verified.

## CONCLUSION

This is the first report on the cloning of *LiDXS* and *LiDXR* from oriental *Lilium* 'Siberia' based on an approach using homologous cloning and RACE. The expression patterns of *LiDXS* and *LiDXR* were consistent with the emission amounts of volatile compounds, indicating the potential roles of these genes in the biosynthesis of monoterpenes. The subcellular localization revealed that these two crucial enzymes are located in the plastids. Moreover, *LiDXR* was identified to play effective roles in the regulation of flower scents. However, we did not produce sufficient evidence regarding the regulatory role of *LiDXS* in monoterpene biosynthesis in the present study. Therefore, more research is needed to verify the function of *LiDXS*. Our results provide important background information on monoterpene biosynthesis in *Lilium*.

## AUTHOR CONTRIBUTIONS

TxZ and MS conceived and designed the experiments. YG, YY, and JC prepared the plant materials. TxZ, YG, and XS performed the experiments. TxZ analyzed the data and wrote the paper. YH and TcZ played important roles in interpreting the results. FB provided the vector *pSuper 1300* plasmid and revised the manuscript. SA and TxZ revised the manuscript. MS read and approved the final manuscript.

## FUNDING

This study was financially supported by the National Natural Science Foundation of China (Project No. 31501797), the Fundamental Research Funds for the Central Universities (Grant No. 2015ZCQ-YL-03), and the Special Fund for Beijing Common Construction Project.

## SUPPLEMENTARY MATERIAL

The Supplementary Material for this article can be found online at: https://www.frontiersin.org/articles/10.3389/fpls.2018.00909/full#supplementary-material

## REFERENCES

Battilana, J., Emanuelli, F., Gambino, G., Gribaudo, I., Gasperi, F., Boss, P. K., et al. (2011). Functional effect of grapevine 1-deoxy-D-xylulose 5-phosphate synthase substitution K284N on Muscat flavour formation. *J. Exp. Bot.* 62, 5497–5508. doi: 10.1093/jxb/err231

Bouvier, F., Harlingue, A., Suire, C., Backhaus, R. A., and Camara, B. (1998). Dedicated roles of plastid transketolases during the early onset of isoprenoid biogenesis in pepper fruits. *Plant Physiol.* 117, 1423–1431. doi: 10.1104/pp.117.4.1423

Burlat, V., Oudin, A., Courtois, M., Rideau, M., and St-Pierre, B. (2004). Co-expression of three MEP pathway genes and geraniol 10-hydroxylase in internal phloem parenchyma of *Catharanthus roseus* implicates multicellular translocation of intermediates during the biosynthesis of monoterpene indole alkaloids and isoprenoid-derived primary metabolites. *Plant J.* 38, 131–141. doi: 10.1111/j.1365-313X.2004.02030.x

Burow, M., Chlan, C., Sen, P., Lisca, A., and Murai, N. (1990). High-frequency generation of transgenic tobacco plants after modified leaf disk cocultivation with *Agrobacterium tumefaciens*. *Plant Mol. Biol. Rep.* 8, 124–139. doi: 10.1007/BF02669766

Carretero-Paulet, L., Ahumada, I., Cunillera, N. O., Rodríguez-Concepción, M., Ferrer, A., Boronat, A., et al. (2002). Expression and molecular analysis of the Arabidopsis DXR gene encoding 1-deoxy-D-xylulose 5-phosphate reductoisomerase, the first committed enzyme of the 2-*C*-methyl-D-erythritol 4-phosphate pathway. *Plant Physiol.* 129, 1581–1591. doi: 10.1104/pp.003798

Carretero-Paulet, L., Cairo, A., Botella-Pavia, P., Besumbes, O., Campos, N., Boronat, A., et al. (2006). Enhanced flux through the methylerythritol 4-phosphate pathway in Arabidopsis plants overexpressing deoxyxylulose 5-phosphate reductoisomerase. *Plant Mol. Biol.* 62, 683–695. doi: 10.1007/s11103-006-9051-9

Chahed, K., Clastre, M., Oudin, A., Guivarch, N., Hamdi, S., Chénieux, J. C., et al. (2000). 1-Deoxy-D-xylulose 5-phosphate synthase from periwinkle: cDNA identification and induced gene expression in terpenoid indole alkaloid-producing cells. *Plant Physiol.* 38, 559–566. doi: 10.1016/S0981-9428(00)00781-6

Chaurasiya, N. D., Sangwan, N. S., Sabir, F., Misra, L., and Sangwan, R. S. (2012). Withanolide biosynthesis recruits both mevalonate and DOXP pathways of isoprenogenesis in Ashwagandha *Withania somnifera* L. (Dunal). *Plant Cell Rep.* 31, 1889–1897. doi: 10.1007/s00299-012-1302-4

Cordoba, E., Porta, H., Arroyo, A., Roman, C. S., Medina, L., Rodriguez-Concepcion, M., et al. (2011). Functional characterization of the three genes encoding 1-deoxy-D-xylulose 5-phosphate synthase in maize. *J. Exp. Bot.* 62, 2023–2038. doi: 10.1093/jxb/erq393

Cordoba, E., Salmi, M., and Leon, P. (2009). Unravelling the regulatory mechanisms that modulate the MEP pathway in higher plants. *J. Exp. Bot.* 60, 2933–2943. doi: 10.1093/jxb/erp190

Cseke, L. J., Kaufman, P. B., and Kirakosyan, A. (2007). The biology of essential oils in the pollination of flowers. *Nat. Prod. Commun.* 2, 1317–1336.

Devi, K., Dehury, B., Phukon, M., Modi, M. K., and Sen, P. (2015). Novel insights into structure–function mechanism and tissue-specific expression profiling of full-length dxr gene from *Cymbopogon winterianus*. *FEBS Open Bio* 5, 325–334. doi: 10.1016/j.fob.2015.04.005

Eisenreich, W., Bacher, A., Arigoni, D., and Rohdich, F. (2004). Biosynthesis of isoprenoids via the non-mevalonate pathway. *Cell. Mol. Life Sci.* 61, 1401–1426. doi: 10.1007/s00018-004-3381-z

Fan, H. H., Wu, Q. J., Wang, X., Wu, L. S., Cai, Y. P., and Lin, Y. (2016). Molecular cloning and expression of 1-deoxy-D-xylulose-5-phosphate synthase and 1-deoxy-D-xylulose-5-phosphate reductoisomerase in *Dendrobium officinale*. *Plant Cell Tissue Org.* 125, 381–385. doi: 10.1007/s11240-016-0945-1

Feng, L. G., Chen, C., Li, T. L., Wang, M., Tao, J., Zhao, D. Q., et al. (2014). Flowery odor formation revealed by differential expression of monoterpene biosynthetic genes and monoterpene accumulation in rose (*Rosa rugosa* Thunb.). *Plant Physiol. Biochem.* 75, 80–88. doi: 10.1016/j.plaphy.2013.12.006

Hall, T. A. (1999). BioEdit: a user-friendly biological sequence alignment editor and analysis program for Windows 95/98/NT. *Nucleic Acids Symp. Ser.* 41, 95–98.

Harker, M., and Bramley, P. M. (1999). Expression of prokaryotic 1-deoxy-D-xylulose-5-phosphatases in *Escherichia coli* increases carotenoid and ubiquinone biosynthesis. *FEBS Lett.* 448, 115–119. doi: 10.1016/S0014-5793(99)00360-9

Hsieh, M. H., Chang, C. Y., Hsu, S. J., and Chen, J. J. (2008). Chloroplast localization of methylerythritol 4-phosphate pathway enzymes and regulation of mitochondrial genes in *ispD* and *ispE* albino mutants in Arabidopsis. *Plant Mol. Biol.* 66, 663–673. doi: 10.1007/s11103-008-9297-5

Hu, Z. H., Tang, B., Wu, Q., Zheng, J., Leng, P. S., and Zhang, K. Z. (2017). Transcriptome sequencing analysis reveals a difference in monoterpene biosynthesis between scented *Lilium* 'Siberia' and Unscented *Lilium* 'Novano'. *Front. Plant. Sci.* 8:1351. doi: 10.3389/fpls.2017.01351

Jadaun, J. S., Sangwan, N. S., Narnoliya, L. K., Singh, N., Bansal, S., Mishra, B., et al. (2017). Over-expression of *DXS* gene enhances terpenoidal secondary metabolite accumulation in rose-scented geranium and *Withania somnifera*: active involvement of plastid isoprenogenic pathway in their biosynthesis. *Physiol. Plant.* 159, 381–400. doi: 10.1111/ppl.12507

Johnson, T. S., Schwieterman, M. L., Kim, J. Y., Cho, K. H., Clark, D. G., and Colquhoun, T. A. (2016). Lilium floral fragrance: a biochemical and genetic resource for aroma and flavor. *Phytochemistry* 122, 103–112. doi: 10.1016/j.phytochem.2015.11.010

Kim, B. R., Kim, S. U., and Chang, Y. J. (2005). Differential expression of three 1-deoxy-D-xylulose-5-phosphate synthase genes in rice. *Biotechnol. Lett.* 27, 997–1001. doi: 10.1007/s10529-005-7849-1

Kong, Y., Bai, J. R., Lang, L. X., Bao, F., Dou, X. Y., Wang, H. A., et al. (2017). Variation in floral scent compositions of different lily hybrid groups. *J. Am. Soc. Hort. Sci.* 142, 175–183. doi: 10.21273/Jashs03934-16

Kuzuyama, T., Takagi, M., Takahashi, S., and Seto, H. (2000). Cloning and characterization of 1-deoxy-D-xylulose 5-phosphate synthase from *Streptomyces* sp. strain CL190, which uses both the mevalonate and nonmevalonate pathways for isopentenyl diphosphate biosynthesis. *J. Bacteriol.* 182, 891–897. doi: 10.1128/JB.182.4.891-897.2000

Larkin, M. A., Blackshields, G., Brown, N. P., Chenna, R., McGettigan, P. A., McWilliam, H., et al. (2007). Clustal W and Clustal X version 2.0. *Bioinformatics* 23, 2947–2948. doi: 10.1093/bioinformatics/btm404

Lichtenthaler, H. K. (1999). The 1-deoxy-D-xylulose-5-phosphate pathway of isoprenoid biosynthesis in plants. *Annu. Rev. Plant Physiol. Plant Mol. Biol.* 50, 47–65. doi: 10.1146/annurev.arplant.50.1.47

Lois, L. M., Campos, N., Rosa-Putra, S., Danielsen, K., Rohmer, M., and Boronat, A. (1998). Cloning and characterization of a gene from *Escherichia coli* encoding a transketolase-like enzyme that catalyzes the synthesis of D-1-deoxyxylulose 5-phosphate, a common precursor for isoprenoid, thiamin, and pyridoxol biosynthesis. *Proc. Natl. Acad. Sci. U.S.A.* 95, 2105–2110. doi: 10.1073/pnas.95.5.2105

Lois, L. M., Rodríguez-Concepción, M., Gallego, F., Campos, N., and Boronat, A. (2000). Carotenoid biosynthesis during tomato fruit development, regulatory role of 1-deoxy-D-xylulose-5-phosphate synthase. *Plant J.* 22, 503–513. doi: 10.1046/j.1365-313x.2000.00764.x

Mahmoud, S. S., and Croteau, R. B. (2001). Metabolic engineering of essential oil yield and composition in mint by altering expression of deoxyxylulose phosphate reductoisomerase and menthofuran synthase. *Proc. Natl. Acad. Sci. U.S.A.* 98, 8915–8920. doi: 10.1073/pnas.141237298

Mandel, M. A., Feldmann, K. A., Herrera-Estrella, L., Rocha-Sosa, M., and León, P. (1996). CLA1, a novel gene required for chloroplast development, is highly conserved in evolution. *Plant J.* 9, 649–658. doi: 10.1046/j.1365-313X.1996.9050649.x

McGarvey, D. J., and Croteau, R. (1995). Terpenoid metabolism. *Plant Cell* 7, 1015–1026. doi: 10.1105/tpc.7.7.1015

Mendoza-Poudereux, I., Muñoz-Bertomeu, J., Arrillaga, I., and Segura, J. (2014). Deoxyxylulose 5-phosphate reductoisomerase is not a rate-determining enzyme for essential oil production in spike lavender. *J. Plant Physiol.* 171, 1564–1570. doi: 10.1016/j.jplph.2014.07.012

Morrone, D., Lowry, L., Determan, M. K., Hershey, D. M., Xu, M., and Peters, R. J. (2010). Increasing diterpene yield with a modular metabolic engineering system in *E. coli*: comparison of MEV and MEP isoprenoid precursor pathway engineering. *Appl. Microbiol. Biotechnol.* 85, 1893–1906. doi: 10.1007/s00253-009-2219-x

Muhlemann, J. K., Klempien, A., and Dudareva, N. (2014). Floral volatiles: from biosynthesis to function. *Plant Cell Environ.* 37, 1936–1949. doi: 10.1111/pce.12314

Munoz-Bertomeu, J., Arrillaga, I., Ros, R., and Segura, J. (2006). Up-regulation of 1-deoxy-D-xylulose-5-phosphate synthase enhances production of essential oils in transgenic spike lavender. *Plant Physiol.* 142, 890–900. doi: 10.1104/pp.106.086355

Pellmyr, O., and Thien, L. B. (1986). Insect reproduction and floral fragrances: keys to the evolution of the angiosperms. *Taxon* 35, 76–85. doi: 10.2307/1221036

Phillips, M. A., Leon, P., Boronat, A., and Rodriguez-Concepcion, M. (2008). The plastidial MEP pathway: unified nomenclature and resources. *Trends Plant Sci.* 13, 619–623. doi: 10.1016/j.tplants.2008.09.003

Pichersky, E., Noel, J. P., and Dudareva, N. (2006). Biosynthesis of plant volatiles: nature's diversity and ingenuity. *Science* 311, 808–811. doi: 10.1126/science.1118510

Piechulla, B., and Pott, M. B. (2003). Plant scents - mediators of inter- and intraorganismic communication. *Planta* 217, 687–689. doi: 10.1007/s00425-003-1047-y

Ramak, P., Osaloo, S. K., Sharifi, M., Ebrahimzadeh, H., and Behmanesh, M. (2014). Biosynthesis, regulation and properties of plant monoterpenoids. *J. Med. Plant Res.* 8, 983–991. doi: 10.5897/JMPR2012.387

Reinhard, J., Srinivasan, M. V., and Zhang, S. W. (2004). Olfaction: scent-triggered navigation in honeybees. *Nature* 427, 411–411. doi: 10.1038/427411a

Rodriguez-Concepcion, M., and Boronat, A. (2002). Elucidation of the methylerythritol phosphate pathway for isoprenoid biosynthesis in bacteria and plastids. A metabolic milestone achieved through genomics. *Plant Physiol.* 130, 1079–1089. doi: 10.1104/pp.007138

Rohmer, M., Seemann, M., Horbach, S., BringerMeyer, S., and Sahm, H. (1996). Glyceraldehyde 3-phosphate and pyruvate as precursors of isoprenic units in an alternative non-mevalonate pathway for terpenoid biosynthesis. *J. Am. Chem. Soc.* 118, 2564–2566. doi: 10.1021/ja9538344

Schiestl, F. P. (2010). The evolution of floral scent and insect chemical communication. *Ecol. Lett.* 13, 643–656. doi: 10.1111/j.1461-0248.2010.01451.x

Sharma, E., Pandey, S., and Gaur, A. K. (2016). Identification and expression analysis of DXS1 gene isolated from *Aconitum balfourii* Stapf. *Acta Physiol. Plant* 38:233. doi: 10.1007/s11738-016-2239-y

Takahashi, S., Kuzuyama, T., Watanabe, H., and Seto, H. (1998). A 1-deoxy-D-xylulose 5-phosphate reductoisomerase catalyzing the formation of 2-*C*-methyl-D-erythritol 4-phosphate in an alternative nonmevalonate pathway for terpenoid biosynthesis. *Proc. Natl. Acad. Sci. U.S.A.* 95, 9879–9884. doi: 10.1073/pnas.95.17.9879

Tong, Y. R., Su, P., Zhao, Y. J., Zhang, M., Wang, X. J., Liu, Y. J., et al. (2015). Molecular cloning and characterization of *DXS* and *DXR* genes in the terpenoid biosynthetic pathway of *Tripterygium wilfordii*. *Int. J. Mol. Sci.* 16, 25516–25535. doi: 10.3390/ijms161025516

Walter, M. H., Hans, J., and Strack, D. (2002). Two distantly-related genes encoding 1-deoxy-D-xylulose 5-phosphate synthases: differential regulation in shoots and apocarotenoid-accumulating mycorrhizal roots. *Plant J.* 31, 243–254. doi: 10.1046/j.1365-313X.2002.01352.x

Wright, L. P., Rohwer, J. M., Ghirardo, A., Hammerbacher, A., Ortiz-Alcaide, M., Raguschke, B., et al. (2014). Deoxyxylulose 5-phosphate synthase controls flux through the methylerythritol 4-phosphate pathway in Arabidopsis. *Plant Physiol.* 165, 1488–1504. doi: 10.1104/pp.114.245191

Xie, Z., Kapteyn, J., and Gang, D. R. (2008). Asystems biology investigation of the MEP/terpenoid and shikimate/phenylpropanoid pathways points to multiple levels of metabolic control in sweet basil glandular trichomes. *Plant J.* 54, 349–361. doi: 10.1111/j.1365-313X.2008.03429.x

Xu, Y. H., Liu, J., Liang, L., Yang, X., Zhang, Z., Gao, Z. H., et al. (2014). Molecular cloning and characterization of three cDNAs encoding 1-deoxy-D-xylulose-5-phosphate synthase in *Aquilaria sinensis* (Lour.) Gilg. *Plant Physiol. Biochem.* 82, 133–141. doi: 10.1016/j.plaphy.2014.05.013

Yadav, R. K., Sangwan, R. S., Sabir, F., Srivastava, A. K., and Sangwan, N. S. (2014). Effect of prolonged water stress on specialized secondary metabolites, peltate glandular trichomes, and pathway gene expression in *Artemisia annua* L. *Plant Physiol. Biochem.* 74, 70–83. doi: 10.1016/j.plaphy.2013.10.023

Yue, Y. C., Yu, R. C., and Fan, Y. P. (2015). Transcriptome profiling provides new insights into the formation of floral scent in *Hedychium coronarium*. *BMC Genomics* 16:470. doi: 10.1186/s12864-015-1653-7

Zeng, X. L., Liu, C., Zheng, R. R., Cai, X., Luo, J., Zou, J. J., et al. (2016). Emission and accumulation of monoterpene and the key terpene synthase (TPS) associated with monoterpene biosynthesis in *Osmanthus fragrans* Lour. *Front. Plant Sci.* 6:1232. doi: 10.3389/fpls.2015.01232

Zhang, M., Li, K., Liu, J. Y., and Yu, D. Y. (2012). Identification and differential expression of two isogenes encoding 1-deoxy-D-xylulose 5-phosphate reductoisomerase in *Glycine max*. *Plant Biotechnol. Rep.* 6, 363–371. doi: 10.1007/s11816-012-0233-4

Zhang, T. X., Sun, M., Li, L. L., Guo, Y. H., Xie, X. H., and Hu, B. W. (2017). Molecular cloning and expression analysis of a monoterpene synthase gene involved in floral scent production in lily (*Lilium* 'Siberia'). *Russ. J. Plant Physiol.* 64, 600–607. doi: 10.1134/S1021443717040203

Zhou, W., Huang, F. F., Li, S., Wang, Y., Zhou, C. C., Shi, M., et al. (2016). Molecular cloning and characterization of two 1-deoxy-D-xylulose-5-phosphate synthase genes involved in tanshinone biosynthesis in *Salvia miltiorrhiza*. *Mol. Breed.* 36:124. doi: 10.1007/s11032-016-0550-3

**Conflict of Interest Statement:** The authors declare that the research was conducted in the absence of any commercial or financial relationships that could be construed as a potential conflict of interest.

frontiers in Plant Science

ORIGINAL RESEARCH
published: 06 December 2017
doi: 10.3389/fpls.2017.02082

# A Novel AP2/ERF Transcription Factor CR1 Regulates the Accumulation of Vindoline and Serpentine in *Catharanthus roseus*

*Jiaqi Liu, Fangyuan Gao, Juansheng Ren, Xianjun Lu, Guangjun Ren and Rui Wang**

*Crop Research Institute, Sichuan Academy of Agricultural Sciences, Chengdu, China*

As one type of the most important alkaloids in the world, terpenoid indole alkaloids (TIAs) show a wide range of pharmaceutical activities that are beneficial for clinical treatments. *Catharanthus roseus* produces approximately 130 identified TIAs and is considered to be a model plant to study TIA biosynthesis. In order to increase the production of high medical value metabolites whose yields are extremely low in *C. roseus*, genetic engineering combined with transcriptional regulation has been applied in recent years. By using bioinformatics which is based on RNA sequencing (RNA-seq) data from methyl jasmonate (MeJA)-treated *C. roseus* as well as phylogenetic analysis, the present work aims to screen candidate genes that may be involved in the regulation of TIA biosynthesis, resulting in a novel AP2/ERF transcription factor, CR1 (Catharanthus roseus 1). Subsequently, virus-induced gene silencing (VIGS) of *CR1* was carried out to identify the involvement of CR1 in the accumulations of several TIAs and quantitative real-time PCR (qRT-PCR) was then applied to detect the expression levels of 7 genes in the related biosynthetic pathway in silenced plants. The results show that all the 7 genes were upregulated in *CR1*-silenced plants. Furthermore, metabolite analyses indicate that silencing *CR1* could increase the accumulations of vindoline and serpentine in *C. roseus*. These results suggest a novel negative regulator which may be involved in the TIAs biosynthetic pathway.

**Keywords: terpenoid indole alkaloids, RNA-seq, phylogenetic analysis, AP2/ERF, VIGS, qRT-PCR, metabolite analysis, *Catharanthus roseus***

OPEN ACCESS

***Edited by:***
*Swee-Suak Ko,*
*Academia Sinica, Taiwan*

***Reviewed by:***
*Rita Sharma,*
*Jawaharlal Nehru University, India*
*Sailendra Nath Sarkar,*
*University of Calcutta, India*

***Correspondence:**
*Rui Wang*
*wangray1987@163.com*

***Specialty section:***
*This article was submitted to Plant Biotechnology, a section of the journal Frontiers in Plant Science*

***Received:*** *18 July 2017*
***Accepted:*** *21 November 2017*
***Published:*** *06 December 2017*

***Citation:***
*Liu J, Gao F, Ren J, Lu X, Ren G and Wang R (2017) A Novel AP2/ERF Transcription Factor CR1 Regulates the Accumulation of Vindoline and Serpentine in Catharanthus roseus. Front. Plant Sci. 8:2082. doi: 10.3389/fpls.2017.02082*

## INTRODUCTION

Plants produce a vast number of secondary metabolites, when they adapt themselves to variable ecological environment during long-term evolution. Secondary metabolites are usually derived from primary metabolites and have their own unique metabolic pathways and different properties. They are generally classified into three major groups: phenols, terpenoids and alkaloids. As one type of the most important alkaloids in the world, terpenoid indole alkaloids (TIAs) show a wide range of pharmaceutical activities that are beneficial for clinical treatments (Van Der Heijden et al., 2004; Wasternack, 2014). Most TIAs are produced from the plants of Apocynaceae, Loganiaceae and Rubiaceae. One from Apocynaceae, *Catharanthus roseus*, produces approximately 130 identified TIAs and is considered to be a model plant to study TIA biosynthesis. Most of the TIAs produced by *C. roseus*, such as ajmaline, serpentine and catharanthine, show significant clinical medical values,

moreover, vinblastine and vincristine, which are recognized to be the most valuable antineoplastic agents, have been widely used in the world. However, the yields of these high medical value metabolites are extremely low (Guéritte and Fahy, 2005).

During a long time, chemical synthesis, plant tissue, microbiological culture and other efforts have been done to increase the production of valuable secondary metabolites. But these methods still need to be optimized because of the excessive costs and low production. In recent years, genetic engineering has been applied in an attempt to increase TIAs yields, for example, transcriptionally regulating some specific genes in hairy root or cell suspension cultures to change the accumulations of specific TIAs (Papon et al., 2004; Runguphan et al., 2009; Peebles et al., 2011; Cui et al., 2015), while few great break-through have been made through these strategies. The major reasons could be: (1) few candidate genes involved in the accumulation of TIAs have been identified; (2) the limited effects on comprehensive TIAs synthetic pathway by single candidate gene. Hence, it is critical to find new candidate genes which could greatly facilitate TIAs production and the researches of TIA biosynthesis regulation.

Lots of studies suggest that genes in the TIAs synthetic pathway are under tight transcriptional regulations. It has been revealed that transcription factors are able to increase the production of TIAs via regulating the expression of multiple genes in the synthetic pathway. ORCA2 and ORCA3 are firstly identified AP2/ERF transcription factors in *C. roseus* which are involved in the TIAs synthetic pathway (Menke et al., 1999; Van der Fits and Memelink, 2000). Overexpressing either ORCA2 or ORCA3 in *C. roseus* suspension cells or hairy roots could change the expression of several key genes in the TIAs biosynthetic pathway (Van der Fits and Memelink, 2000; Pan et al., 2012; Li et al., 2013; Sun and Peebles, 2016). In addition, ORCA3 could be regulated by many inducers, such as jasmonic acid, artemisinic acid and fungal endophytes (Peebles et al., 2009; Pandey et al., 2016; Wang et al., 2016). Another two AP2/ERF members, ORCA4 and ORCA5, were cloned recently. They formed a cluster with ORCA3 and also can be induced by jasmonic acid, ORCA4 could act on the transcripts levels of genes in both tryptophan pathway and seco-iridoid pathway (Paul et al., 2016). In 2011, CrMYC2 in bHLH (basic helix-loop-helix) family, isolated by a yeast one-hybrid screening, could regulate the expression of ORCAs and also had a strong effect on the accumulation of catharanthine and tabersonine (Montiel et al., 2011; Zhang et al., 2011). WRKY transcription factor CrWRKY1 regulates several key genes in the TIAs synthetic pathway, especially TDC (tryptophan decarboxylase). Overexpressing CrWRKY1 in the hairy root of *C. roseus* caused significantly increased accumulation of serpentine (Suttipanta et al., 2011; Yang et al., 2013).

The genomic and transcriptomic information of *C. roseus* are not completely uncovered as many model plants like tobacco, Arabidopsis and rice. Hence, the studies aiming to excavate and functionally identify important transcription factors in *C. roseus* are not comprehensive. RNA sequencing is a widespread high-throughput technology in recent years (Mortazavi et al., 2008), which offers a holistic view of the transcriptome expression profiles of selected plant tissues or cells and provides an efficient way to identify transcripts involved in specific biological processes (Cloonan et al., 2008; Wilhelm et al., 2010). Therefore, excavating relative transcription factors combined with transcriptome sequencing data and understanding of the mechanism of transcriptional regulation during the overall TIAs biosynthetic pathway may promote our ability to break through the synthetic bottleneck (Aito et al., 2008; Saito and Matsuda, 2010; Guo et al., 2013; Verma et al., 2014; Yang et al., 2017).

In this study, three candidate AP2/ERF transcription factors were selected based on transcriptome sequencing data from *C. roseus* with methyl jasmonate (MeJA) treatment, and their responses to MeJA were verified by quantitative real-time PCR (qRT-PCR). After phylogenetic tree analysis of the three candidate genes with known AP2/ERF transcription factors involved in secondary metabolite biosynthetic pathway, CR1, which forms a cluster with OpERF2, was chosen for further study. Subsequently, Virus-induced gene silencing (VIGS) of *CR1* combined with metabolite analyses of silenced plants was performed to identify the involvement of CR1 in the accumulations of several TIAs. The results show that silencing *CR1* could increase the accumulations of vindoline and serpentine in *C. roseus*.

# MATERIALS AND METHODS

## Plant Growth Conditions and RNA-Seq

Seeds of *C. roseus* cv. Rose Red were germinated in a greenhouse at 28°C, 16/8 h photoperiod on MS plates. After 4 weeks, seedlings with two to three pairs of true leaves were transferred to soil. Samples were collected from 1-month-old plants which were treated with MeJA for 0, 1 or 4 h. The MeJA experiment was with three replicates. Three plants were combined from each replicate time sample. MeJA treatment consisted of spraying 100 μM MeJA then placing plants under a clear plastic dome sealed with tape. Leaves of the plants were harvested and then frozen in liquid nitrogen.

Total RNA extracted from each material were subjected to cDNA library preparation and sequenced at Novogene Bioinformatics Institute (China) on Illumina HiSeq$^{TM}$ 2000 sequencer (Illumina Inc., United States). Clean reads were aligned based on the reference genome (Medicinal Plant Genomics Resource, MPGR) (Kellner et al., 2015), transcript abundant estimation and expression level in fragment per kilobase exon per million mapped fragment (FPKM) were performed as described by Chen et al. (2017).

## Phylogenetic Analysis

Full-length amino acid sequences of candidate transcription factor as well as the AP2/ERFs which are potentially involved in secondary metabolite biosynthesis were aligned by ClustalW program. The neighbor-joining phylogeny was generated using MEGA 6 with bootstrap analysis of 1,000 replicates.

## Virus-Induced Gene Silencing

Seeds of *C. roseus* cv. Rose Red were germinated in a greenhouse at 28°C, 16/8 h photoperiod. Four weeks later, plants with

two to three pairs of true leaves were used for VIGS. The genomic DNA of *C. roseus* cv. Rose Red was used as template to amplify *CR1* with specific primers (**Table 1**). The PCR-generated fragment was then introduced into the terminal vector pTRV2 by *Bam*H I and *Xho* I digestion. Catharanthus phytoene desaturase (PDS) involved in chlorophyll biosynthesis produces visible photo bleaching and serves as a useful marker for determining the best time to collect samples for testing. The purified plasmid DNA pTRV2-CR1, pTRV2 (negative control), pTRV2-PDS were respectively transformed into *Agrobacterium tumefaciens* strain GV3101 by electroporation. Three kinds of strains and GV3101 harboring pTRV1 were cultured overnight at 28°C in 300 ml Luria-Bertani medium containing 10 Mm MES, 20 μM acetosyringone and 50 μg/mL kanamycin. These bacterial pellets were collected and then resuspended in 5 ml infiltration buffer (10 mM MES, 200 μM acetosyringone and 1 mM $MgCl_2$), and further incubated at 28°C for 3 h with shaking. The suspension of strain harboring pTRV1 was mixed with pTRV2-CR1, pTRV2 or pTRV2-PDS in equal volume just before the infection. The leaves of the seedlings were injected by a needle less syringe to fill the whole leaf with the bacteria, and each seedling was injected with 2–4 leaves. After injection, the plants were cultured in a constant temperature incubator. The PDS phenotype was observed 3 weeks after inoculation of leaves, and the other two sample plants were harvested at this stage. After recording the fresh weights of harvested materials, the samples were frozen in liquid nitrogen, one member of a leaf pair was used for RNA extraction, while the other was used for metabolite analysis.

## Expression Analysis by Quantitative Real-Time PCR

Total RNAs of *CR1*-silenced plants and control were extracted and reverse-transcribed as described previously (Wang et al., 2015), and qRT-PCR was performed according to the same reference. The primers of *CR1*, *CR2* and *CR3* as well as 7 genes whose expression levels were detected in our work are shown in **Table 1**. Relative expression levels were determined using $2^{-\Delta\Delta C_T}$ method (Livak and Schmittgen, 2001). All qRT-PCR analyses were performed with three independent biological replicates.

## Metabolite Analyses

The selected samples were quickly pulverized in liquid nitrogen. Precisely weighed 0.3 g powder, mixed with 2 mL methanol, then subjected to extraction using the ultrasonic for 20 min, the supernatant was obtained after centrifugation. Repeatedly extracted with methanol for three times, then combined supernatant extract and compressed to dry, diluted to 2 mL with methanol, finally, filtrated with 0.45 μm microporous membrane before metabolite analyses by MS. The three standards catharanthine, vindoline and vinblastine were configured as a reserve solution of 10 ng/L with methanol, stored at −20°C,

**TABLE 1 |** Polymerase chain reaction (PCR) primers used in this study.

| Primer name | Primer sequence (5′ to 3′)[a] | Purpose |
|---|---|---|
| CR1-vigs-F | GGATCCGGATTATCAACAGGCTGATTC | Target fragment clone |
| CR1-vigs-R | CTCGAGGCAAGAGAGGCAAGGCATTT | Target fragment clone |
| CR1-F | GCTGCACTCAGGTTCAGAGG | Target gene in qRT-PCR |
| CR1-R | GCAAGAGAGGCAAGGCATTT | Target gene in qRT-PCR |
| CR2-F | CAAACCACTATACCCGCCGT | Target gene in qRT-PCR |
| CR2-R | GAAGAATCCGTTGCGTCAGC | Target gene in qRT-PCR |
| CR3-F | GCCGTCGAAAAGAAAAACCCA | Target gene in qRT-PCR |
| CR3-R | GCGGTGTCAAATGTTCCCAA | Target gene in qRT-PCR |
| STR-F | GCCTTCACCTTCGATTCAACTG | Target gene in qRT-PCR |
| STR-R | GTGGCTAGTTGTGTGGCATACC | Target gene in qRT-PCR |
| G10H-F | GCTCACAATCAATTCAAATTCTCCGT | Target gene in qRT-PCR |
| G10H-R | CAACCGCTTCTCCGCTCTGGCTATTT | Target gene in qRT-PCR |
| TDC-F | GGTCGAGGATGACGTGGCGGCCGG | Target gene in qRT-PCR |
| TDC-R | ACTCAGACTCAGTGAGTCAACTCGTT | Target gene in qRT-PCR |
| PRX1-F | GCGATTCATCAGTGCTGCTGGTGGGA | Target gene in qRT-PCR |
| PRX1-R | GTGGAAGGTTTGCTATTGTGTCTGCC | Target gene in qRT-PCR |
| SLS-F | CTTCACTCTTGAGAAACTAAAGTCAA | Target gene in qRT-PCR |
| SLS-R | AGTCAATTGTGAGATCCATGAGTT | Target gene in qRT-PCR |
| DAT-F | CTTCTTCTCATCACGTACCAACTC | Target gene in qRT-PCR |
| DAT-R | ATACCAAACTCAACGGCCTTAG | Target gene in qRT-PCR |
| SGD-F | CATTGGTGAACCGTGCTATG | Target gene in qRT-PCR |
| SGD-R | AGATTGTAGAGTCCAGATGGAACA | Target gene in qRT-PCR |
| RPS9-F | GCGTTTGGATGCTGAGTTGAAG | Endogenous reference gene |
| RPS9-R | GGCGCTCAAGGAAGTTCTCTAC | Endogenous reference gene |

[a]*The underlined letters indicate the restriction enzyme sites.*

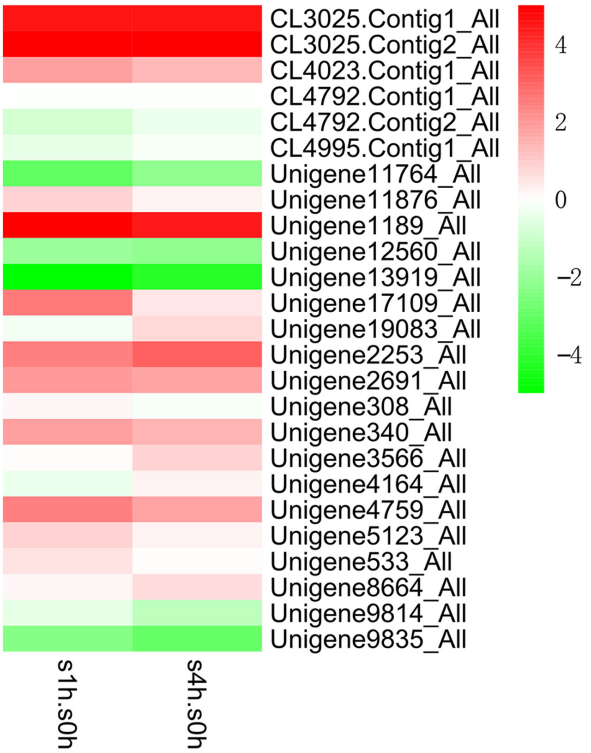


**FIGURE 1 |** Expression patterns ($log_2$ of FPKM) of AP2/ERF family in *C. roseus* at 1-h (s1h.s0h) and 4-h (s4h.s0h) after MeJA treatment. The expression levels are illustrated in green-red scale shown on the right. Green indicates lower expression and red indicates higher expression. Figure taken from Liu et al. (2017).

diluted to 10 ng/mL working fluid at the same time for testing purposes. ESI/MS/MS was used to detect the catharanthine, vindoline and vinblastine; using time-of-flight mass spectrometry (TOF-MS) to detect the serpentine.

# RESULTS

## Three Candidate AP2/ERF Genes Were Selected Based on RNA-seq Data

MeJA is identified as an important signaling molecule in TIA biosynthetic pathway in many plants (De Geyter et al., 2012). In order to excavate candidate transcription factors that may be involved in the regulation of TIA biosynthesis, we collected the leaves of 1-month-old *C. roseus* with MeJA treatment and extracted their RNA to generate the transcriptome sequencing data using Illumina platform. Subsequently, the expression profiles of different transcription factor families in *C. roseus* after MeJA treatment were analyzed. The expression profile of AP2/ERF family indicated that the expression levels of many AP2/ERF genes were changed obviously at 1-h and 4-h after MeJA treatment (their annotated gene names are shown in Supplementary Table S1). Three candidate AP2/ERF genes with different representative response to MeJA were selected for further studies (**Figure 1**). The expression level of Unigene9835_ALL (here designated as *CR1*) gradually decreased along the treatment. The expression level of Unigene2253_ALL (here designated as *CR2*) gradually increased after MeJA treatment. The transcript of Unigene1189_All (here designated as *CR3*) was up-regulated dramatically at 1-h and 4-h after MeJA treatment, while the expression level at 4-h was slightly lower than at 1-h. The expression pattern suggested that *CR3* is sharply induced by MeJA in a short time, and its expression level might gradually restore to the initial level. Above genes show different responses to MeJA treatment, and may be involved in the regulation of TIAs synthesis in *C. roseus*.

In order to determine the accuracy of the RNA-seq data, the expression levels of three candidate genes at different time point after MeJA treatment were confirmed by qRT-PCR. **Figure 2** shows that after MeJA treatment, the expression level of *CR1* decreased gradually with time; *CR2* showed gradually increased transcript along MeJA treatment; the expression level of *CR3* was up-regulated rapidly and reached a peak at 2-h, then gradually declined. According to the results, expression patterns of three candidate genes under MeJA treatment were consistent with the RNA-seq data. Hence, the above candidate genes were subjected to further study.

## Phylogenetic Analysis

A phylogenetic tree was constructed based on the protein sequences of the three candidate transcription factors (for their sequences, see Supplementary Table S2), together with the previously reported AP2/ERF transcription factors which are potentially involved in secondary metabolite biosynthesis, to analyze their evolutionary relationships (**Figure 3**). CR1 was classified to the same group with CR2, CR3 and OpERF2. Besides, CR1 showed the closest relationship with OpERF2 which was identified recently to be involved in the regulation of specialized metabolism in *Ophiorrhiza pumila* (Udomsom et al., 2016), while CR2 and CR3 form the same cluster. The divergent clusters as well as the opposite response to MeJA between CR1 and CR2 or CR3 suggest the different molecular functions between CR1 and the other two. ORCA2 and ORCA3 involved in MIA biosynthesis in *C. roseus*; NbERF1, NtERF189 and NtORC1 regulating nicotine alkaloids biosynthesis; AaERF1, AaERF2 and AaORA regulating terpenoid biosynthesis in *Artemisia annua*, all of them showed more distant relationship with three candidate transcription factors than OpERF2 (Van der Fits and Memelink, 2001; Rushton et al., 2008; Shoji et al., 2010; Todd et al., 2010; De Boer et al., 2011; Yu et al., 2012; Lu et al., 2013; Thagun et al., 2016). Since CR1 showed a close phylogenetic relationship with other secondary metabolite-regulating AP2/ERFs, which suggested that CR1 may be a potential regulator in TIA biosynthesis, we selected CR1 for further functional characterization.

## CR1 Negatively Regulates 7 Key Genes in the TIAs Synthetic Pathway

Virus-induced gene silencing is a technique used for functional analysis of genes, which can be effectively applied in plants

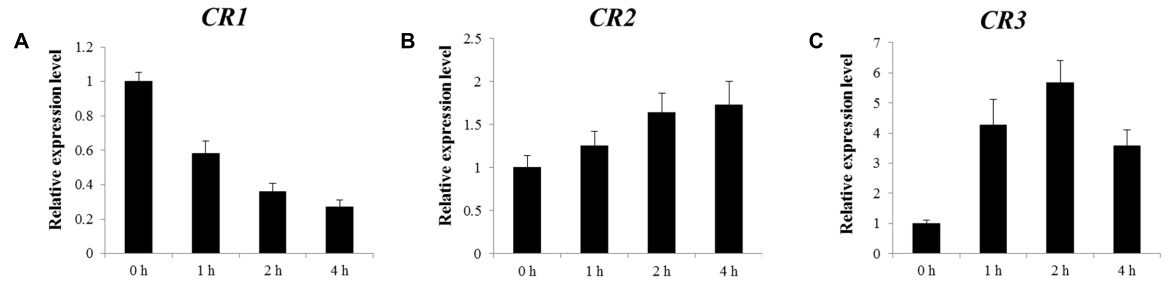


**FIGURE 2 |** Relative expression levels of *CR1* **(A)**, *CR2* **(B)**, and *CR3* **(C)** responding to MeJA treatment. Figure taken from Liu et al. (2017).

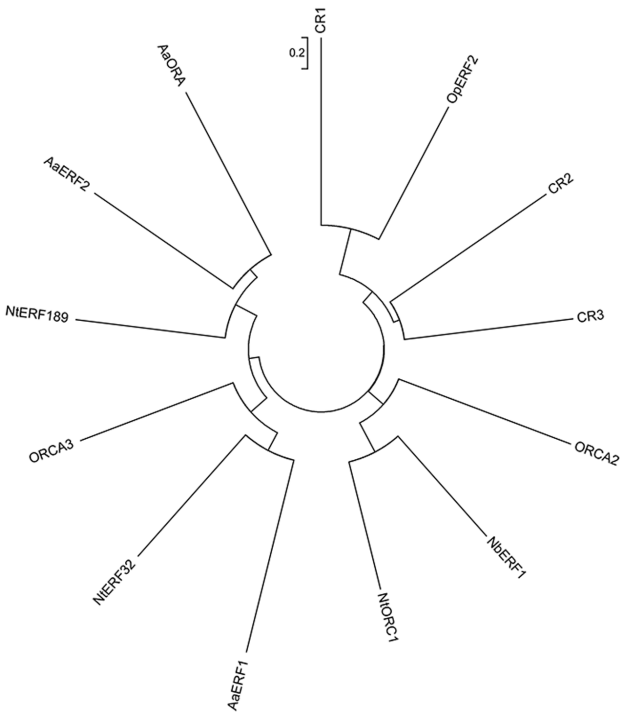


**FIGURE 3 |** Phylogenetic analysis of three candidate AP2/ERF transcription factors and previously reported AP2/ERF transcription factors which are potentially involved in secondary metabolite biosynthetic pathway. ORCA2 (CAB93940.1), *Catharanthus roseus*; ORCA3 (ABW77571.1), *Catharanthus roseus*; AaERF1 (AEQ93554.1), *Artemisia annua*; AaERF2 (AEQ93555.1), *Artemisia annua*; AaORA (AGB07586.1), *Artemisia annua*; NbERF1 (ADH04266.1), *Nicotiana benthamiana*; NtERF32 (NP_001311965.1), *Nicotiana tabacum*; NtERF189 (NP_001312507.1), *Nicotiana tabacum*; NtORC1 (XP_016478305.1), *Nicotiana tabacum*; OpERF2 (LC171328.1), *Ophiorrhiza pumila*. Figure taken from Liu et al. (2017).

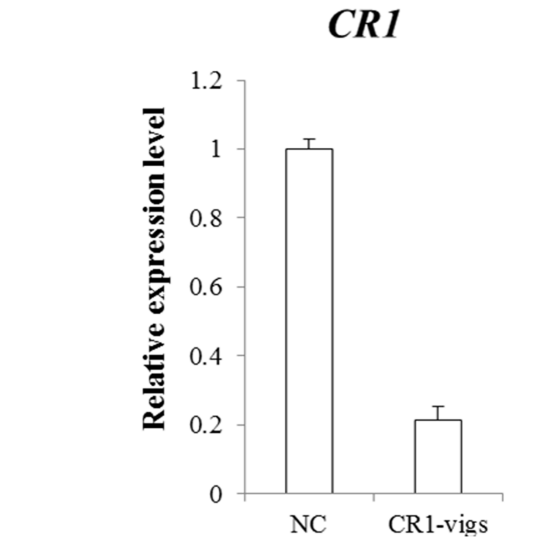


**FIGURE 4 |** Effect of silencing *CR1* in *C. roseus*. The expression level of *CR1* in plants containing pTRV2-CR1 was detected by qRT-PCR to confirm the fold change of transcript levels from individual plants expressing the silenced gene compared to negative control (NC) containing pTRV2 empty vector. Error bars indicate standard error based on three independent biological replicates from three individual VIGS lines. Figure taken from Liu et al. (2017).

with long growth cycle and low conversion efficiency. The utility of this approach has been successful in exploring new genes that were involved in iridoid biosynthesis (Geu-Flores et al., 2012) and MIA biosynthesis (Liscombe and O'Connor, 2011) in *C. roseus*. In order to identify the function of CR1, we selected VIGS technology with the pTRV vector system (Dinesh-Kumar et al., 2003; Burch-Smith et al., 2004; Velásquez et al., 2009).

Transcript analysis of *CR1* monitored by qRT-PCR revealed that the transcript level decreased by approximately 78% in *CR1*-silenced plants compared with the negative control (**Figure 4**). Subsequently, expression analysis of 7 genes (*G10H*, *SLS*, *TDC*, *STR*, *SGD*, *DAT* and *PRX*) which are representative in the TIAs synthetic pathway (**Figure 5**) in *CR1*-silenced plants was carried out. Their GenBank accession numbers are as follows: KF561461.1, L10081.1, X67662.1, X53602.1, EU072423.1, AF053307.1 and AM236087.1. The results indicated that silencing *CR1* in *C. roseus* could result in obvious changes in the expression levels of these genes. The expression levels of *G10H*, *SLS*, *TDC*, *STR*, *SGD*, *DAT* and *PRX* showed significant up-regulation (**Figure 6**). According to the previous results which suggest that the expression level of *CR1* is down-regulated in response to MeJA treatment, it can be inferred that CR1 may be a new negative regulatory transcription factor in the pathway of TIA biosynthesis.

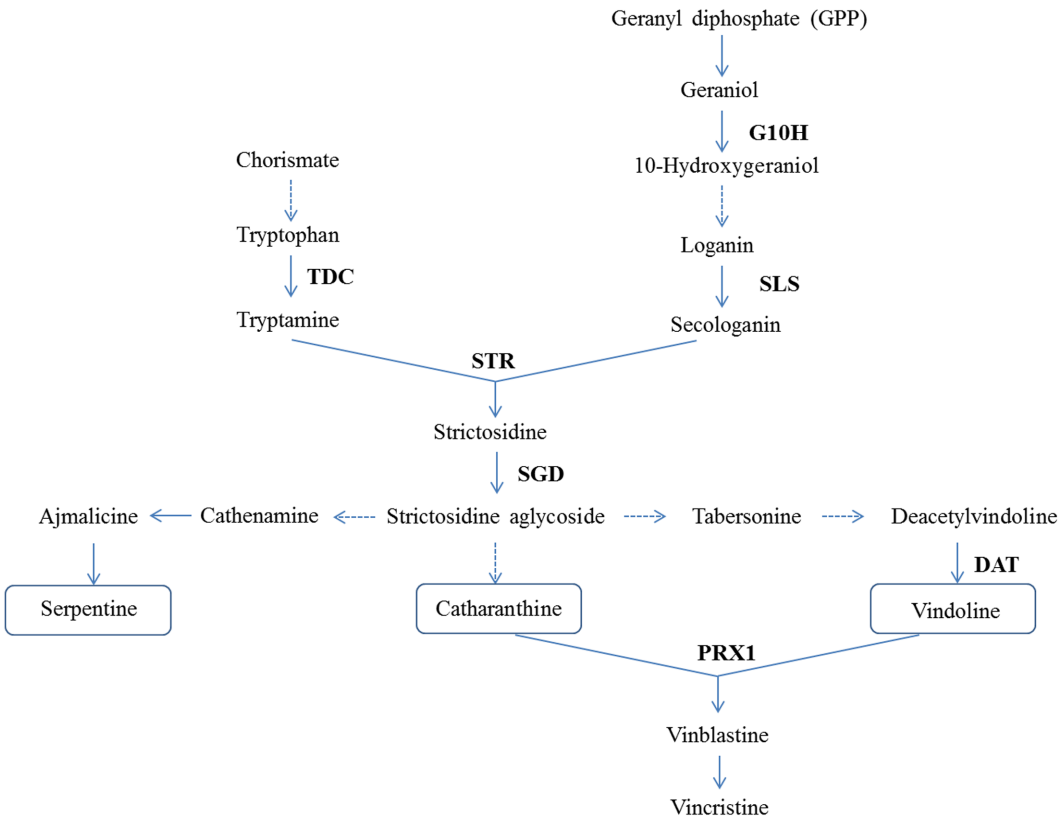


**FIGURE 5 |** Seven genes (indicated in bold) which are representative in the TIAs synthetic pathway were subjected to expression analysis. G10H, geraniol 10-hydroxylase; SLS, secologanin synthase; TDC, tryptophan decarboxylase; STR, strictosidine synthase; SGD, strictosidine β-D-glucosidase; DAT, acetyl CoA: deacetylvindoline 4-O-acetyltransferase; PRX1, a-3′, 4′-anhydrovinblastine synthase. Figure taken from Liu et al. (2017).

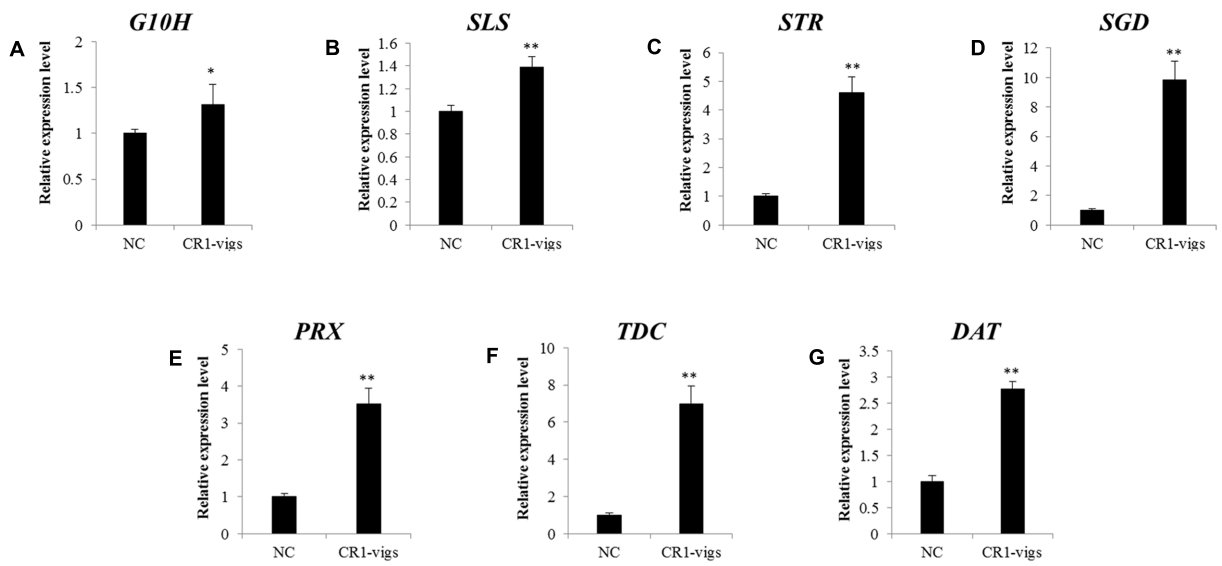


**FIGURE 6 |** Relative expression levels of **(A–G)** *G10H*, *SLS*, *TDC*, *STR*, *SGD*, *DAT* and *PRX1* in TIA biosynthesis in *CR1*-silenced plants (CR1-vigs) compared to negative control (NC). *Indicates statistically significant differences ($P < 0.05$); **indicates highly statistically significant differences ($P < 0.01$). Error bars indicate standard error based on three independent biological replicates from three individual VIGS lines. Figure taken from Liu et al. (2017).

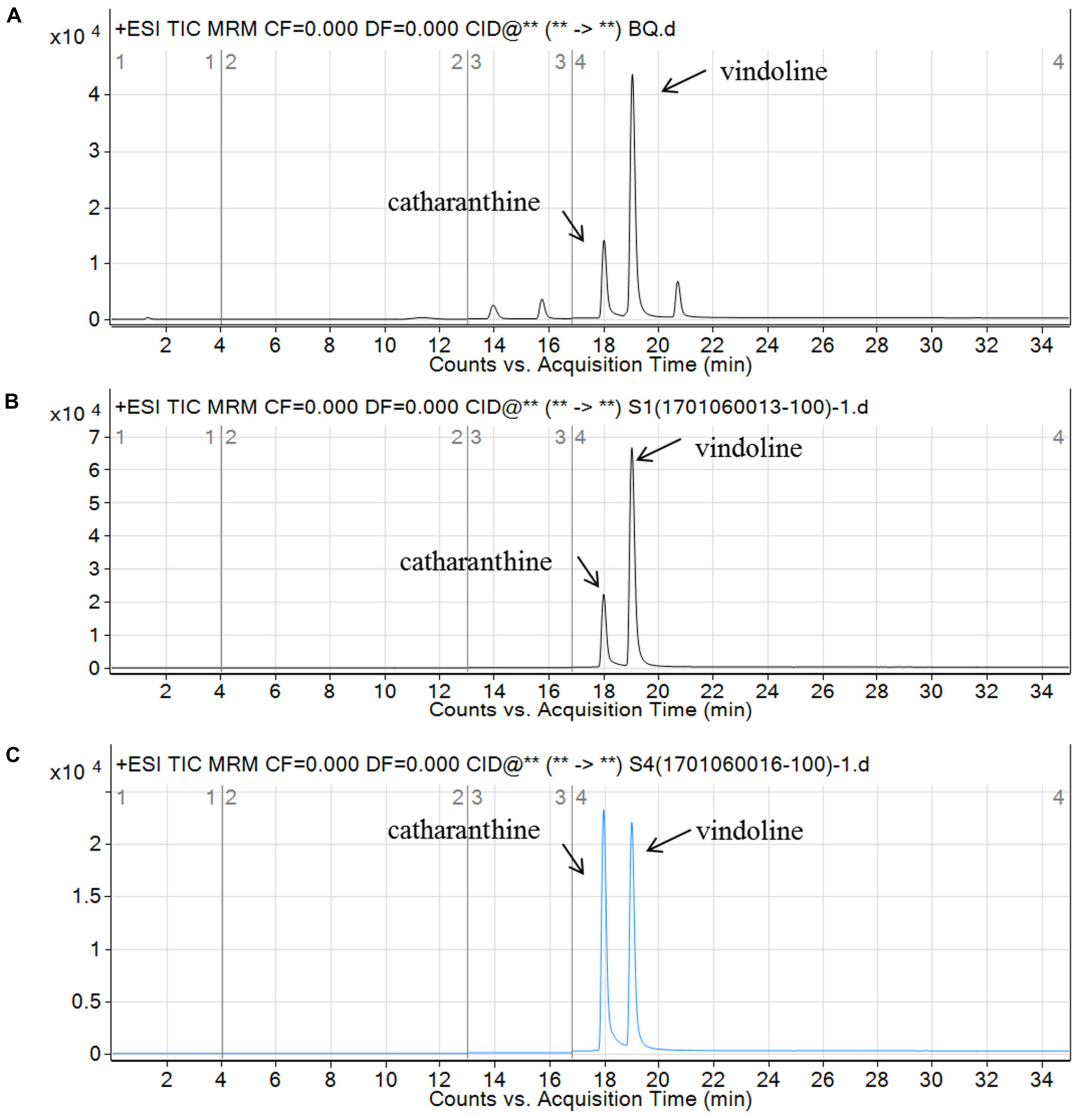


**FIGURE 7 |** Vindoline and catharanthine component analysis in the leaves of *C. roseus* by ESI/MS/MS. **(A)** ESI Tandem Mass spectrogram for the vindoline and catharanthine standard; **(B)** vindoline and catharanthine ion current in the leaves of *CR1*-silenced plants shown by ESI/MS/MS. The two peaks are vindoline (m/z 457, RT 19.039) and catharanthine (m/z 337, RT 18.01); **(C)** vindoline and catharanthine ion current in the leaves of negative control shown by ESI/MS/MS. The two peaks are vindoline (m/z 457, RT 19.004) and catharanthine (m/z 337, RT 17.979). Figure taken from Liu et al. (2017).

## Accumulations of Vindoline and Serpentine Were Increased in *CR1*-Silenced Plants

ESI/MS/MS was used to detect the catharanthine and vindoline levels; time-of-flight mass spectrometry (TOF-MS) was applied to detect the serpentine. The accumulations of catharathine and vindoline in the leaves of *CR1*-silenced plants were 0.191 nmol/L and 0.153 nmol/L, compared to 0.198 nmol/L and 0.046 nmol/L in negative control plants (**Figure 7**). According to the results, silencing *CR1* could increase the accumulation of vindoline, but not catharanthine. Based on the peak area of serpentine detected by TOF-MS (**Figure 8**), we found that the accumulation of serpentine in *CR1*-silenced samples was higher than that in negative control. These results are consistent with the changes of the expression levels of related genes in *CR1*-silenced plants, which confirmed the inference that CR1 could regulate the synthesis of TIAs with negatively regulatory function in *C. roseus*.

## DISCUSSION

It is well known that *C. roseus* which produces approximately 130 identified TIAs is considered to be a model plant to study TIA biosynthesis. Most of the TIAs produced by *C. roseus*, such as ajmaline, serpentine and catharanthine, show significant clinical medical value, moreover, vinblastine and vincristine, which are

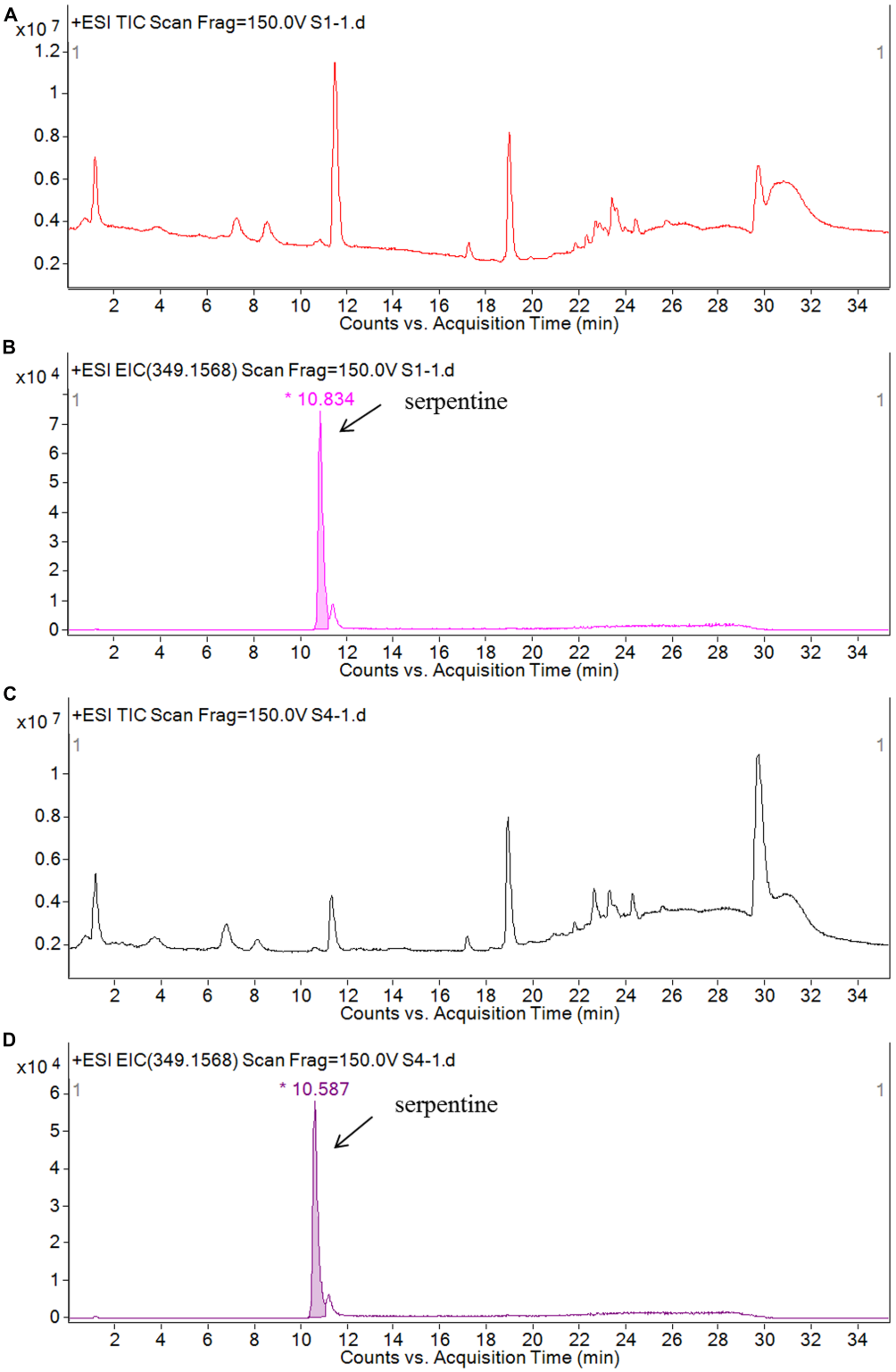


**FIGURE 8 |** Serpentine component analysis in the leaves of *C. roseus* by TOF/MS/MS. **(A)** Total ion current in the leaves of *CR1*-silenced plants; **(B)** corresponding peak of serpentine (m/z 349 RT 10. 834) component in total ion current in the leaves of *CR1*-silenced plants; **(C)** total ion current in the leaves of negative control; **(D)** corresponding peak of serpentine (m/z 349 RT 10. 587) component in total ion current in the leaves of negative control. Figure taken from Liu et al. (2017).

recognized to be the most valuable antineoplastic agents, have been widely used in the world. However, the yields of these high medical value metabolites are extremely low through traditional approach. Therefore, it is critical to find new ways which could greatly facilitate TIAs production, such as genetic engineering. Nowadays, bioinformatics has been widely used in many medicinal plants such as *Dioscorea nipponica* (Sun et al., 2017), *Panax ginseng C. A. Meyer* (Zhang et al., 2017), *Taxus chinensis* (Li et al., 2012; Meng et al., 2017), and *Ginkgo biloba* (Lin et al., 2011; He et al., 2015). High-throughput data such as transcriptome, proteome and metabolome could help us to gain an insight into the process of secondary metabolism in many non-model plants. The availability of several *C. roseus* transcriptomic databases, such as Medicinal Plant Genomics Resource (MPGR)[1] (Kellner et al., 2015); PhytoMetaSyn[2] (Facchini et al., 2012; Xiao et al., 2013) could greatly facilitate the studies on either biochemical pathways or transcriptional regulation in *C. roseus*. Our study utilized RNA sequencing combined with MPGR to compensate for the insufficiency of the genomic information as well as gene expression information in the discovery of candidate transcription factors involved in TIA biosynthesis regulation. By integrating bioinformatic analysis and a series of experimental methods, a novel negatively regulatory transcription factor, CR1, is identified.

The results of expression analysis of *CR1*-silenced plants suggested that CR1 could regulate several key genes in TIA biosynthesis, not only the genes upstream to the central precursor strictosidine which derive all the TIAs in *C. roseus* (G10H, SLS, TDC and STR), but the genes downstream to it (SGD, DAT and PRX1). ORCA2 and ORCA3 are the earliest found AP2/ERF transcription factors in *C. roseus* which play important roles in TIA biosynthesis. They mainly regulate the downstream genes in the seco-iridoid pathway (Menke et al., 1999; Van der Fits and Memelink, 2000; Pan et al., 2012; Li et al., 2013; Sun and Peebles, 2016), while ORCA4 is functionally overlapping but divergent with ORCA3, regulating the genes in both tryptophan pathway and seco-iridoid pathway (Paul et al., 2016). Combining these cases with our results, it can be inferred that CR1 may function together with other AP2 transcription factors as a negative feedback model to keep balance of TIA biosynthesis. Therefore, CR1 could be used in cooperation with other AP2/ERF such as ORCA3 to further increase the accumulations of target TIAs.

The suppression of *CR1* could promote the synthesis of vindoline and serpentine, but not catharathine, which may suggest that the genes in the catharathine-specific pathway can not be regulated by CR1. Vindoline and catharathine are the precursors of vinblastine and vincristine, the most valuable dimeric TIAs in *C. roseus* which have been used clinically to treat cancers since 1950s (Leveque and Jeh, 2007). If the accumulations of vindoline and catharathine are both increased, the biosynthesis of vinblastine and vincristine might be also promoted. Therefore, CR1 could be co-utilized with other transcription factors to increase the accumulations of vindoline and catharathine simultaneously. Overall, our study combined RNA sequencing and VIGS of the target gene as well as expression and metabolite analyses of silenced plants to discover an AP2/ERF transcription factor involved in TIA biosynthesis in *C. roseus*.

## AUTHOR CONTRIBUTIONS

RW conceived and designed the experiments. JL and RW performed the experiments. RW and FG performed the data analysis. RW and JL wrote the paper. RW, FG, JR, XL, and GR revised the paper. RW secured the funds to support this research.

## FUNDING

This research was supported by the National Natural Science Foundation of China.

## ACKNOWLEDGMENT

The authors thank Junjun Cai (West China Hospital, Sichuan University) for language improvement.

## SUPPLEMENTARY MATERIAL

The Supplementary Material for this article can be found online at: https://www.frontiersin.org/articles/10.3389/fpls.2017.02082/full#supplementary-material

[1] http://medicinalplantgenomics.msu.edu/

[2] http://www.phytometasyn.ca/index.php/

## REFERENCES

Aito, K., Hirai, M. Y., and Yonekura-Sakakibara, K. (2008). Decoding genes with coexpression networks and metabolomics - Majority report by precogs. *Trends Plant Sci.* 13, 36–43.

Burch-Smith, T. M., Anderson, J. C., Martin, G. B., and Dinesh-Kumar, S. P. (2004). Applications and advantages of virus-induced gene silencing for gene function studies in plants. *Plant J.* 9, 734–746.

Chen, T., Wu, H., Wu, J., Fan, X., Li, X., and Lin, Y. (2017). Absence of *OsβCA1* causes a CO2 deficit and affects leaf photosynthesis and the stomatal response to CO2 in rice. *Plant J.* 90, 344–357. doi: 10.1111/tpj.13497

Cloonan, N., Forrest, A. R., Kolle, G., Gardiner, B. B., Faulkner, G. J., Brown, M. K., et al. (2008). Stem cell transcriptome profiling via massive-scale mRNA sequencing. *Nat. Methods* 5, 613–619. doi: 10.1038/nmeth.1223

Cui, L., Ni, X., Ji, Q., Teng, X., Yang, Y., Wu, C., et al. (2015). Co-overexpression of geraniol-10-hydroxylase and strictosidine synthase improves anti-cancer drug camptothecin accumulation in *Ophiorrhiza pumila*. *Sci. Rep.* 5:8227. doi: 10.1038/srep08227

De Boer, K., Tilleman, S., Pauwels, L., Vanden Bossche, R., De Sutter, V., Vanderhaeghen, R., et al. (2011). APETALA2/ETHYLENE RESPONSE FACTOR and basic helix-loop-helix tobacco transcription factors cooperatively mediate jasmonate-elicited nicotine biosynthesis. *Plant J.* 66, 1053–1065. doi: 10.1111/j.1365-313X.2011.04566.x

De Geyter, N., Gholami, A., Goormachtig, S., and Goossens, A. (2012). Transcriptional machineries in jasmonate-elicited plant secondary metabolism. *Trends Plant Sci.* 17, 349–359. doi: 10.1016/j.tplants.2012.03.001

Dinesh-Kumar, S. P., Anandalakshmi, R., Marathe, R., Schiff, M., and Liu, Y. (2003). Virus-induced gene silencing. *Methods Mol. Biol.* 236, 287–294.

Facchini, P. J., Bohlmann, J., Covello, P. S., De Luca, V., Mahadevan, R., Page, J. E., et al. (2012). Synthetic biosystems for the production of high-value plant metabolites. *Trends Biotechnol.* 30, 127–131. doi: 10.1016/j.tibtech.2011.10.001

Geu-Flores, F., Sherden, N. H., Courdavault, V., Burlat, V., Glenn, W. S., Wu, C., et al. (2012). An alternative route to cyclic terpenes by reductive cyclization in iridoid biosynthesis. *Nature* 492, 138–142. doi: 10.1038/nature11692

Guéritte, F., and Fahy, J. (2005). "The vinca alkaloids," in *Anticancer Agents from Natural Products*, eds G. M. L. Cragg, D. Kingston, and D. J. Newman (Boca Raton, Fla: CRC Press), 123–136.

Guo, X., Li, Y., Li, C., Luo, H., Wang, L., Qian, J., et al. (2013). Analysis of the *Dendrobium officinale* transcriptome reveals putative alkaloid biosynthetic genes and genetic markers. *Gene* 527, 131–138. doi: 10.1016/j.gene.2013.05.073

He, B., Gu, Y., Xu, M., Wang, J., Cao, F., and Xu, L. A. (2015). Transcriptome analysis of *Ginkgo biloba* kernels. *Front. Plant Sci.* 6:819. doi: 10.3389/fpls.2015.00819

Liu, J., Cai, J., Wang, R., and Yang S. (2017). Transcriptional regulation and transport of terpenoid indole alkaloid in *Catharanthus roseus*: exploration of new research directions. *Int. J. Mol. Sci.* 18:53. doi: 10.3390/ijms18010053

Kellner, F., Kim, J., Clavijo, B. J., Hamilton, J. P., Childs, K. L., Vaillancourt, B., et al. (2015). Genome-guided investigation of plant natural product biosynthesis. *Plant J.* 82, 680–692. doi: 10.1111/tpj.12827

Leveque, D., and Jeh, F. (2007). Molecular pharmacokinetics of catharanthus (vinca) alkaloids. *J. Clin. Pharmacol.* 47, 579–588.

Li, C. Y., Leopold, A. L., Sander, G. W., Shanks, J. V., Zhao, L., and Gibson, S. I. (2013). The *ORCA2* transcription factor plays a key role in regulation of the terpenoid indole alkaloid pathway. *BMC Plant Biol.* 13:155. doi: 10.1186/1471-2229-13-155

Li, S. T., Zhang, P., Zhang, M., Fu, C. H., Zhao, C. F., Dong, Y. S., et al. (2012). Transcriptional profile of *Taxus chinensis* cells in response to methyl jasmonate. *BMC Genomics* 13:295. doi: 10.1186/1471-2164-13-295

Lin, X., Zhang, J., Li, Y., Luo, H., Wu, Q., Sun, C., et al. (2011). Functional genomics of a living fossil tree. Ginkgo, based on next-generation sequencing technology. *Physiol. Plant.* 143, 207–218. doi: 10.1111/j.1399-3054.2011.01500.x

Liscombe, D. K., and O'Connor, S. E. (2011). A virus-induced gene silencing approach to understanding alkaloid metabolism in *Catharanthus roseus*. *Phytochemistry* 72, 1969–1977. doi: 10.1016/j.phytochem.2011.07.001

Livak, K. J., and Schmittgen, T. D. (2001). Analysis of relative gene expression data using real-time quantitative PCR and the $2^{-\Delta\Delta C_T}$ method. *Methods* 25, 402–408.

Lu, X., Zhang, L., Zhang, F., Jiang, W., Shen, Q., Zhang, L., et al. (2013). AaORA, a trichome-specific AP2/ERF transcription factor of *Artemisia annua*, is a positive regulator in the artemisinin biosynthetic pathway and in disease resistance to *Botrytis cinerea*. *New Phytol.* 198, 1191–1202. doi: 10.1111/nph.12207

Meng, D., Yu, X., Ma, L., Hu, J., Liang, Y., Liu, X., et al. (2017). Transcriptomic response of Chinese yew (*Taxus chinensis*) to cold stress. *Front. Plant Sci.* 8:468. doi: 10.3389/fpls.2017.00468

Menke, F. L., Champion, A., Kijne, J. W., and Memelink, J. (1999). A novel jasmonate-and elicitor-responsive element in the periwinkle secondary metabolite biosynthetic gene Str interacts with a jasmonate-and elicitor-inducible AP2-domain transcription factor, *ORCA2. EMBO J.* 18, 4455–4463.

Montiel, G., Zarei, A., Korbes, A. P., and Memelink, J. (2011). The jasmonate-responsive element from the *ORCA3* promoter from *Catharanthus roseus* is active in arabidopsis and is controlled by the transcription factor ATMYC2. *Plant Cell Physiol.* 52, 578–587. doi: 10.1093/pcp/pcr016

Mortazavi, A., Williams, B. A., McCue, K., Schaeffer, L., and Wold, B. (2008). Mapping and quantifying mammalian transcriptomes by RNA-Seq. *Nat. Methods* 5, 621–628. doi: 10.1038/nmeth.1226

Pan, Q., Wang, Q., Yuan, F., Xing, S., Zhao, J., Choi, Y. H., et al. (2012). Overexpression of *ORCA3* and G10h in *Catharanthus roseus* plants regulated alkaloid biosynthesis and metabolism revealed by NMR-metabolomics. *PLOS ONE* 7:e43038. doi: 10.1371/journal.pone.0043038

Pandey, S. S., Singh, S., Babu, C. S., Shanker, K., Srivastava, N. K., Shukla, A. K., et al. (2016). Fungal endophytes of *Catharanthus roseus* enhance vindoline content by modulating structural and regulatory genes related to terpenoid indole alkaloid biosynthesis. *Sci. Rep.* 6:26583. doi: 10.1038/srep26583

Papon, N., Vansiri, A., Gantet, P., Chenieux, J. C., Rideau, M., and Creche, J. (2004). Histidine-containing phosphotransfer domain extinction by RNA interference turns off a cytokinin signalling circuitry in *Catharanthus roseus* suspension cells. *FEBS Lett.* 558, 85–88.

Paul, P., Singh, S. K., Patra, B., Sui, X., Pattanaik, S., and Yuan, L. (2016). A differentially regulated AP2/ERF transcription factor gene cluster acts downstream of a MAP kinase cascade to modulate terpenoid indole alkaloid biosynthesis in *Catharanthus roseus*. *New Phytol.* 213, 1107–1123. doi: 10.1111/nph.14252

Peebles, C. A., Hughes, E. H., Shanks, J. V., and San, K. Y. (2009). Transcriptional response of the terpenoid indole alkaloid pathway to the overexpression of *ORCA3* along with jasmonic acid elicitation of *Catharanthus roseus* hairy roots over time. *Metab. Eng.* 11, 76–86. doi: 10.1016/j.ymben.2008.09.002

Peebles, C. A., Sander, G. W., Hughes, E. H., Peacock, R., Shanks, J. V., and San, K. Y. (2011). The expression of 1-deoxy-D-xylulose synthase and geraniol-10-hydroxylase or anthranilate synthase increases terpenoid indole alkaloid accumulation in *Catharanthus roseus* hairy roots. *Metab. Eng.* 13, 234–240. doi: 10.1016/j.ymben.2010.11.005

Runguphan, W., Maresh, J. J., and O'Connor, S. E. (2009). Silencing of tryptamine biosynthesis for production of nonnatural alkaloids in plant culture. *Proc. Natl. Acad. Sci. U.S.A.* 106, 13673–13678. doi: 10.1073/pnas.0903393106

Rushton, P. J., Bokowiec, M. T., Han, S., Zhang, H., Brannock, J. F., Chen, X., et al. (2008). Tobacco transcription factors: novel insights into transcriptional regulation in the Solanaceae. *Plant Physiol.* 147, 280–295. doi: 10.1104/pp.107.114041

Saito, K., and Matsuda, F. (2010). Metabolomics for functional genomics, systems biology, and biotechnology. *Annu. Rev. Plant Biol.* 61, 463–489. doi: 10.1146/annurev.arplant.043008.092035

Shoji, T., Kajikawa, M., and Hashimoto, T. (2010). Clustered transcription factor genes regulate nicotine biosynthesis in tobacco. *Plant Cell* 22, 3390–3409. doi: 10.1105/tpc.110.078543

Sun, J., and Peebles, C. A. (2016). Engineering overexpression of *ORCA3* and strictosidine glucosidase in *Catharanthus roseus* hairy roots increases alkaloid production. *Protoplasma* 253, 1255–1264. doi: 10.1007/s00709-015-0881-7

Sun, W., Wang, B., Yang, J., Wang, W., Liu, A., Leng, L., et al. (2017). Weighted gene co-expression network analysis of the dioscin rich medicinal plant *Dioscorea nipponica*. *Front. Plant Sci.* 8:789. doi: 10.3389/fpls.2017.00789

Suttipanta, N., Pattanaik, S., Kulshrestha, M., Patra, B., Singh, S. K., and Yuan, L. (2011). The transcription factor CrWRKY1 positively regulates the terpenoid indole alkaloid biosynthesis in *Catharanthus roseus*. *Plant Physiol.* 157, 2081–2093. doi: 10.1104/pp.111.181834

Thagun, C., Imanishi, S., Kudo, T., Nakabayashi, R., Ohyama, K., Mori, T., et al. (2016). Jasmonate-responsive ERF transcription factors regulate steroidal glycoalkaloid biosynthesis in tomato. *Plant Cell Physiol.* 57, 961–975. doi: 10.1093/pcp/pcw067

Todd, A. T., Liu, E., Polvi, S. L., Pammett, R. T., and Page, J. E. (2010). A functional genomics screen identifies diverse transcription factors that regulate alkaloid biosynthesis in *Nicotiana benthamiana*. *Plant J.* 62, 589–600. doi: 10.1111/j.1365-313X.2010.04186.x

Udomsom, N., Rai, A., Suzuki, H., Okuyama, J., Imai, R., Mori, T., et al. (2016). Function of AP2/ERF transcription factors involved in the regulation of specialized metabolism in *Ophiorrhiza pumila* revealed by transcriptomics and metabolomics. *Front. Plant Sci.* 7:1861. doi: 10.3389/fpls.2016.01861

Van der Fits, L., and Memelink, J. (2000). *ORCA3*, a jasmonate-responsive transcriptional regulator of plant primary and secondary metabolism. *Science* 289, 295–297.

Van der Fits, L., and Memelink, J. (2001). The jasmonate-inducible AP2/ERF-domain transcription factor *ORCA3* activates gene expression via interaction with a jasmonate-responsive promoter element. *Plant J.* 25, 43–53.

Van Der Heijden, R., Jacobs, D., Snoeijer, W., Hallard, D., and Verpoorte, R. (2004). The *Catharanthus* alkaloids: pharmacognosy and biotechnology. *Curr. Med. Chem.* 11, 607–628.

Velásquez, A. C., Chakravarthy, S., and Martin, G. B. (2009). Virus-induced gene silencing (VIGS) in *Nicotiana benthamiana* and tomato. *J. Vis. Exp.* 10:1292. doi: 10.3791/1292

Verma, M., Ghangal, R., Sharma, R., Sinha, A. K., and Jain, M. (2014). Transcriptome analysis of *Catharanthus roseus* for gene discovery and expression profiling. *PLOS ONE* 9:e103583. doi: 10.1371/journal.pone.0103583

Wang, M., Zi, J., Zhu, J., Chen, S., Wang, P., Song, L., et al. (2016). Artemisinic acid serves as a novel *ORCA3* inducer to enhance biosynthesis of terpenoid indole alkaloids in *Catharanthus roseus* cambial meristematic cells. *Nat. Prod. Commun.* 11, 715–717.

Wang, R., Lu, L., Pan, X., Hu, Z., Ling, F., Yan, Y., et al. (2015). Functional analysis of OsPGIP1 in rice sheath blight resistance. *Plant Mol. Biol.* 87, 181–191. doi: 10.1007/s11103-014-0269-7

Wasternack, C. (2014). Action of jasmonates in plant stress responses and development-applied aspects. *Biotechnol. Adv.* 32, 31–39. doi: 10.1016/j.biotechadv.2013.09.009

Wilhelm, B. T., Marguerat, S., Goodhead, I., and Bahler, J. (2010). Defining transcribed regions using RNA-seq. *Nat. Protoc.* 5, 255–266. doi: 10.1038/nprot.2009.229

Xiao, M., Zhang, Y., Chen, X., Lee, E. J., Barber, C. J., Chakrabarty, R., et al. (2013). Transcriptome analysis based on next-generation sequencing of non-model plants producing specialized metabolites of biotechnological interest. *J. Biotechnol.* 166, 122–134. doi: 10.1016/j.jbiotec.2013.04.004

Yang, M., You, W., Wu, S., Fan, Z., Xu, B., Zhu, M., et al. (2017). Global transcriptome analysis of *Huperzia serrata* and identification of critical genes involved in the biosynthesis of huperzine A. *BMC Genomics* 18:245. doi: 10.1186/s12864-017-3615-8

Yang, Z., Patra, B., Li, R., Pattanaik, S., and Yuan, L. (2013). Promoter analysis reveals *cis*-regulatory motifs associated with the expression of the WRKY transcription factor CrWRKY1 in *Catharanthus roseus*. *Planta* 238, 1039–1049. doi: 10.1007/s00425-013-1949-2

Yu, Z. X., Li, J. X., Yang, C. Q., Hu, W. L., Wang, L. J., and Chen, X. Y. (2012). The jasmonate-responsive AP2/ERF transcription factors AaERF1 and AaERF2 positively regulate artemisinin biosynthesis in *Artemisia annua* L. *Mol. Plant* 5, 353–365. doi: 10.1093/mp/ssr087

Zhang, H., Hedhili, S., Montiel, G., Zhang, Y., Chatel, G., Pré, M., et al. (2011). The basic helix-loop-helix transcription factor CrMYC2 controls the jasmonate-responsive expression of the *ORCA* genes that regulate alkaloid biosynthesis in *Catharanthus roseus*. *Plant J.* 67, 61–71. doi: 10.1111/j.1365-313X.2011.04575.x

Zhang, J. J., Su, H., Zhang, L., Liao, B. S., Xiao, S. M., Dong, L. L., et al. (2017). Comprehensive characterization for ginsenosides biosynthesis in ginseng root by integration analysis of chemical and transcriptome. *Molecules* 22:E889. doi: 10.3390/molecules22060889

**Conflict of Interest Statement:** The authors declare that the research was conducted in the absence of any commercial or financial relationships that could be construed as a potential conflict of interest.

frontiers in Plant Science

ORIGINAL RESEARCH
published: 28 February 2018
doi: 10.3389/fpls.2018.00149

# Great Cause—Small Effect: Undeclared Genetically Engineered Orange Petunias Harbor an Inefficient Dihydroflavonol 4-Reductase

*Christian Haselmair-Gosch[1], Silvija Miosic[1], Daria Nitarska[1], Barbara L. Roth[1], Benjamin Walliser[1], Renate Paltram[1], Rares C. Lucaciu[2], Lukas Eidenberger[1], Thomas Rattei[2], Klaus Olbricht[3], Karl Stich[1] and Heidi Halbwirth[1]**

[1] Institute of Chemical, Environmental and Bioscience Engineering, Technische Universität Wien, Vienna, Austria, [2] Department of Microbiology and Ecosystem Science, University of Vienna, Vienna, Austria, [3] Thaer-Institute of Agricultural and Horticultural Sciences Humboldt University Berlin, Berlin, Germany

OPEN ACCESS

**Edited by:**
*Mariana Mondragón-Palomino, University of Regensburg, Germany*

**Reviewed by:**
*Teemu Heikki Teeri, University of Helsinki, Finland*
*Xiang Gao, Key Laboratory of Molecular Epigenetics of MOE, Northeast Normal University, Changchun, China*
*Michal Oren-Shamir, Agricultural Research Organization, Israel*

***Correspondence:**
*Heidi Halbwirth*
*heidrun.halbwirth@tuwien.ac.at*

**Specialty section:**
*This article was submitted to Plant Biotechnology, a section of the journal Frontiers in Plant Science*

**Received:** *11 September 2017*
**Accepted:** *29 January 2018*
**Published:** *28 February 2018*

**Citation:**
*Haselmair-Gosch C, Miosic S, Nitarska D, Roth BL, Walliser B, Paltram R, Lucaciu RC, Eidenberger L, Rattei T, Olbricht K, Stich K and Halbwirth H (2018) Great Cause—Small Effect: Undeclared Genetically Engineered Orange Petunias Harbor an Inefficient Dihydroflavonol 4-Reductase. Front. Plant Sci. 9:149. doi: 10.3389/fpls.2018.00149*

A recall campaign for commercial, orange flowering petunia varieties in spring 2017 caused economic losses worldwide. The orange varieties were identified as undeclared genetically engineered (GE)-plants, harboring a maize dihydroflavonol 4-reductase (*DFR, $A_1$*), which was used in former scientific transgenic breeding attempts to enable formation of orange pelargonidin derivatives from the precursor dihydrokaempferol (DHK) in petunia. How and when the $A_1$ cDNA entered the commercial breeding process is unclear. We provide an in-depth analysis of three orange petunia varieties, released by breeders from three countries, with respect to their transgenic construct, transcriptomes, anthocyanin composition, and flavonoid metabolism at the level of selected enzymes and genes. The two possible sources of the $A_1$ cDNA in the undeclared GE-petunia can be discriminated by PCR. A special version of the $A_1$ gene, the $A_1$ type 2 allele, is present, which includes, at the 3′-end, an additional 144 bp segment from the non-viral transposable *Cin4-1* sequence, which does not add any functional advantage with respect to DFR activity. This unequivocally points at the first scientific GE-petunia from the 1980s as the $A_1$ source, which is further underpinned e.g., by the presence of specific restriction sites, parts of the untranslated sequences, and the same arrangement of the building blocks of the transformation plasmid used. Surprisingly, however, the GE-petunia cannot be distinguished from native red and blue varieties by their ability to convert DHK in common *in vitro* enzyme assays, as DHK is an inadequate substrate for both the petunia and maize DFR. Recombinant maize DFR underpins the low DHK acceptance, and, thus, the strikingly limited suitability of the $A_1$ protein for a transgenic approach for breeding pelargonidin-based flower color. The effect of single amino acid mutations on the substrate specificity of DFRs is demonstrated. Expression of the $A_1$ gene is generally lower than the petunia *DFR* expression despite being under the control

of the strong, constitutive p*35S* promoter. We show that a rare constellation in flavonoid metabolism—absence or strongly reduced activity of both flavonol synthase and B-ring hydroxylating enzymes—allows pelargonidin formation in the presence of DFRs with poor DHK acceptance.

**Keywords: *Petunia* × *hybrida, Zea mays,* dihydroflavonol 4-reductase, $A_1$ type 2 allele, anthocyanin, pelargonidin, orange flower color, transgenic plant**

## INTRODUCTION

The color of anthocyanin pigments is determined by their B-ring hydroxylation pattern (**Figure 1**), ranging from orange to bright red (one hydroxy group), dark red to magenta (two hydroxy groups), and violet to blue (three hydroxy groups; Halbwirth, 2010). This basically depends on two factors, which have both been exploited by biotechnological methods to influence flower color (Meyer et al., 1986; Tanaka et al., 2009, 2010): the presence of enzymes introducing hydroxy groups vicinal to that in position 4′ [flavonoid 3′-hydroxylase (F3′H) and flavonoid 3′5′-hydroxylase (F3′5′H)], and the substrate specificity of DFR (Winkel-Shirley, 2001).

Important ornamental plants such as petunia, African violet and cyclamen do not naturally produce orange/bright-red flowers (Johnson et al., 1999) because they lack the ability to synthesize pelargonidin-type anthocyanin pigments. This is based on the presence of a substrate specific dihydroflavonol 4-reductase (DFR) enzyme, which does not accept the essential precursor, dihydrokaempferol (DHK), as a substrate.

DFR is an oxidoreductase (EC 1.1.1.219) that catalyzes the NADPH dependent stereospecific reduction of the keto group of (+)-(*2R,3R*)-dihydroflavonols in position 4 to the respective (*2R,3S,4S*)-flavan-2,3-*trans*-3,4-*cis*-diols (leucoanthocyanidins), as well as the reverse reaction in the presence of $NADP^+$ (Halbwirth et al., 2006; Petit et al., 2007). DFR is the first of the so-called "late" enzymes of the flavonoid pathway which shows a major impact on the formation of anthocyanin pigments, flavan 3-ols and flavonols. DFR provides the immediate precursors for the formation of anthocyanidins and flavan 3-ols, the building blocks of condensed tannins. On the formation of flavonols, DFR has an indirect effect. DFR competes with flavonol synthase (FLS), which opens a side branch of the anthocyanin pathway, for common substrates (Winkel-Shirley, 2001; **Figure 1**). Several DFRs can convert dihydroflavonols irrespective of their hydroxylation pattern, but petunia possesses a DFR that does not convert DHK into leucopelargonidin. In the 1980s and 1990s genetically engineered (GE)-petunias with orange flowers were created by introducing either a maize DFR encoded by the $A_1$ gene (Meyer et al., 1986; Elomaa et al., 1995) or a gerbera DFR (Elomaa et al., 1995).

The petunia belongs to the predominant balcony and bedding plants worldwide. A few years ago petunia varieties, showing a novel orange flower color, started to appear on the market and were swiftly adopted in private and public flower arrangements, in Europe and the US. Recently, the vast majority of them turned out to be genetically modified, after PCR-screening for the *35S*-promoter and the $A_1$ gene (Bashandy and Teeri, 2017; David, 2017; Servick, 2017).

We selected three varieties, released by breeders from three countries, for an-in-depth investigation of the presence and nature of a transgenic construct and its impact on the flavonoid metabolism. We show that they all carry the same construct, and that this can be traced back to the first GE-petunia (Meyer et al., 1986) with near absolute certainty. But surprisingly, the orange petunias were not characterized by a drastically changed DFR substrate specificity compared to common red and blue petunia flowers, as would have been expected. We aimed on elucidating this paradox and demonstrate that the orange petunia owe their color primarily to a rare biochemical background. We underpin this by flavonoid analyses together with enzyme assays and expression and transcriptome studies.

## MATERIALS AND METHODS

### Material

Flowers (stage 1: buds of 0.6–3 cm length, stage 2: buds of 3–5 cm length, stage 3: open flowers) of cv. Salmon Ray (Danziger, Moshav Mishmar Hashiva, Israel), cv. Viva Orange (Florensis, Ambacht, The Netherlands), and cv. Electric Orange (Selecta One, Stuttgart, Germany) were harvested in the summers 2015–2017. Non-transgenic control plants of *Petunia* × *hybrida* cv. BabyDoll were obtained from Selecta One, cvs. Corso Rot, Corso Blau and Blackberry were purchased from Austrosaat (Vienna, Austria). The plant material was harvested from balcony pots or garden beddings, shock-frozen and kept at −80°C until analysis. Images of the petunia varieties are found in **Figures 1**, **2** and Supplementary Figure S3.

Reference compounds (cyanidin, delphinidin, malvidin, pelargonidin, peonidin, petunidin, dihydromyricetin, dihydroquercetin, kaempferol, myricetin, and quercetin) were purchased from Extrasynthese (Genay, France), dihydrokaempferol from Sigma Aldrich (Vienna, Austria). Radiolabeled substrates were synthesized as previously described (Halbwirth et al., 2006).

### HPLC Analysis

For analyzing the flavonoid class/anthocyanidin type composition in the petals, sugar moieties were removed by acidic or enzymatic hydrolysis. 1 g plant material was extracted with 1 ml 2 M hydrochloric acid in methanol. For anthocyanin analysis, 40 µl of the supernatant after centrifugation were incubated with 160 µl 4 N HCl for 60 min at 95°C. For analysis of other flavonoids, 20 µl of the supernatant were subjected to enzymatic hydrolysis by 10 U Naringinase (Sigma-Aldrich,

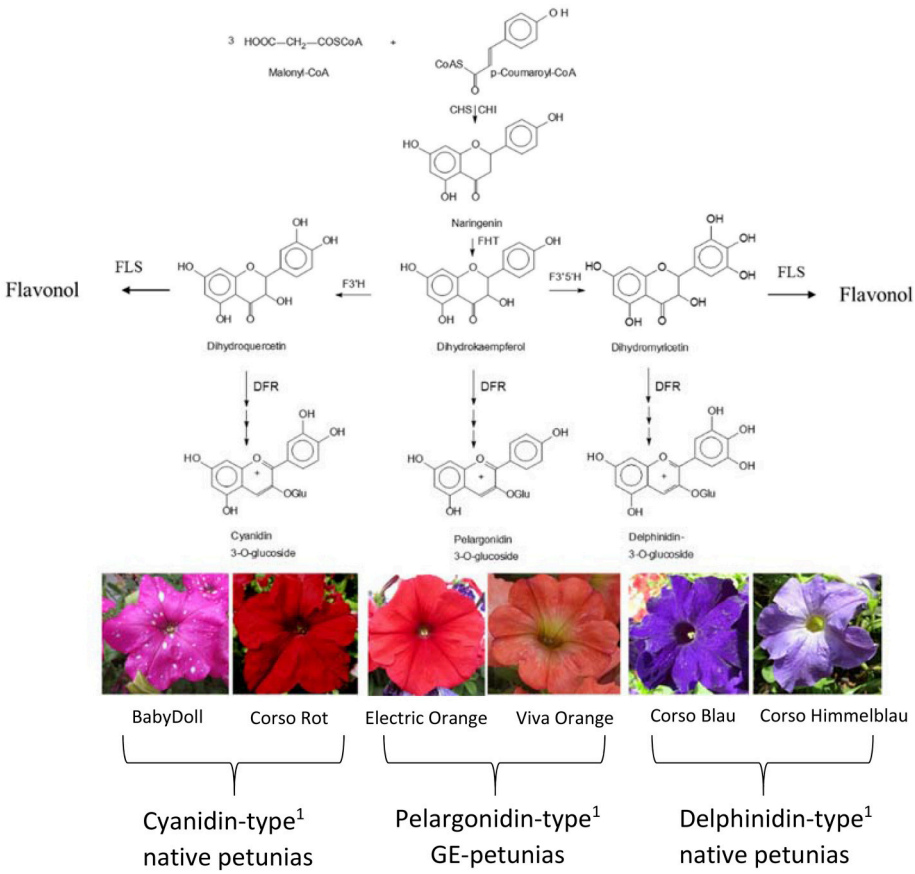


**FIGURE 1 |** Simplified flavonoid pathway demonstrating the influence of the B-ring hydroxylation pattern on the establishment of petunia flower color. [1]Petals contain prevalently the respective anthocyanidin type. CHS, Chalcone synthase; CHI, chalcone isomerase; DFR, dihydroflavonol 4-reductase; FHT, flavanone 3-hydroxylase; F3′H, flavonoid 3′-hydroxylase; F3′5′H, flavonoid 3′,5′-hydroxylase; FLS, flavonol synthase.

Vienna, Austria) and hydrolysed for 20 min at 40°C in 0.1 M McIlvaine buffer pH 4. After hydrolysis, solid compounds were removed by centrifugation, and 4 µl of the supernatants were injected after filtration by 0.2 µm syringe filters.

HPLC analysis was performed on a Thermo Scientific Dionex UltiMate® 3000 RSLC System with DAD-3000RS Photodiode Array Detector (Thermo Scientific, Germany) using an Acclaim™ column RSLC 120 C18, 2.2 µm, 120Å, 2.1 × 150 mm (Dionex Bonded Silica Products: No. 071399) operated at 25°C. For analysis of anthocyanidins, elution solvents were (A) 10% formic acid and (B) 10% formic acid/22.5% acetonitrile/22.5% methanol in water (v/v) using a slightly modified method from Thermo Scientific Application note 281 (gradient: −10 to 0 min 9% B, 0–30 min 9–90% B, 30–40 min 90% B; flow rate 0.2 ml/min). For analysis of other flavonoids, elution solvents were (A) 0.1% formic acid and (B) 0.1% formic acid in acetonitrile (gradient: −3 to 0 min 20% B, 0–15 min 20–53% B, 15–20 min 53–95% B; 20–30 min 95% B, 31–35 min 20% B; flow rate 0.2 ml/min). Anthocyanidins were detected at 520 nm, other flavonoids at 290 nm. All compounds were identified by retention times and comparison of their UV-VIS spectra from 190 to 800 nm. The concentrations were calculated from the peak areas of samples and standard lines obtained with the respective reference compounds. Methylated anthocyanidins are not listed separately (**Table 1**), but were included according to their number of hydroxy groups in the delphinidin type (petunidin, malvidin) or cyandin type (peonidin) anthocyanidins. Relative contents of anthocyanidin types (% Pg/Cy/Dp based pigments was calculated from the [µg/g] values in **Table 1**. Flavonoid class distribution (% anthocyandins/flavonols/dihydroflavonols) were calculated from the [µg/g] values in **Table 1** in relation to a mathematical total amount of flavonoids resulting from the three types.

## PCR, qPCR

Genomic DNA was obtained according to Lipp et al. (1999). mRNA was extracted with the µMACS mRNA isolation Kit (Miltenyi Biotec, Germany) and cDNA was synthesized as described (Thill et al., 2012). PCR and qPCR primers are listed in Supplementary Table S1. PCR was performed with the GoTaq DNA polymerase (Promega, Germany). Quantitative gene expression (at least in biological triplicates with three technical replications each) of *DFR*, $A_1$, *F3′H*, and *FLS* in comparison to the *actin* reference gene (Mallona et al., 2010)

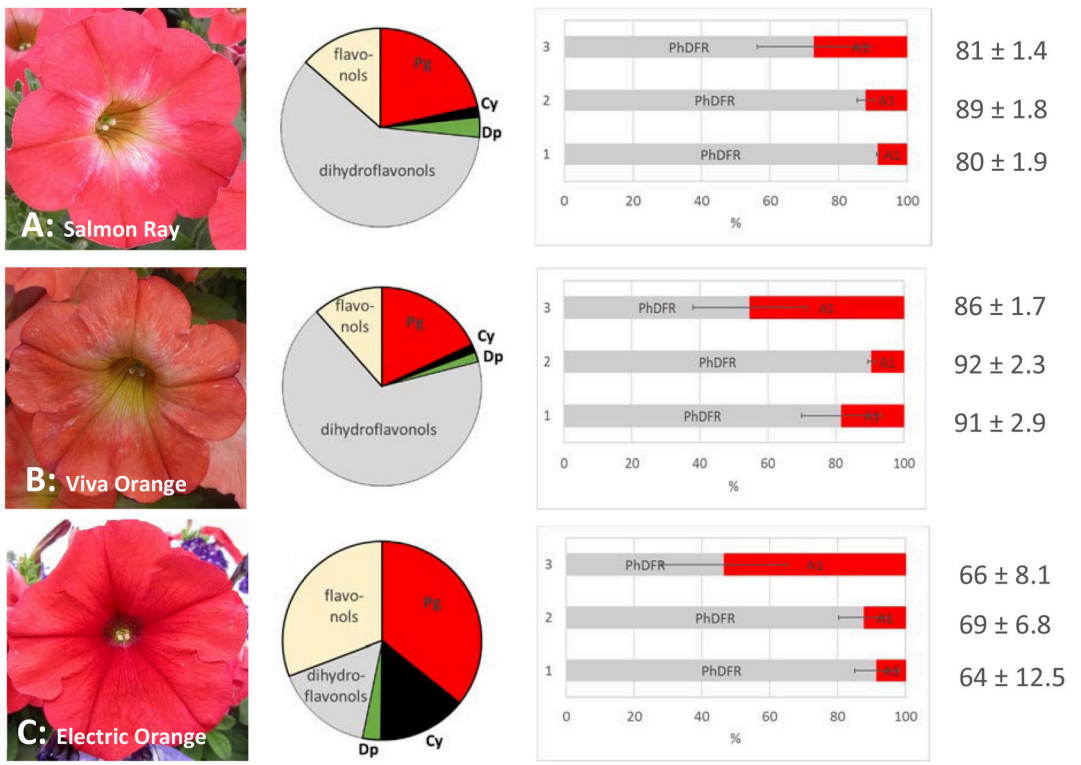


**FIGURE 2 |** Flavonoid content, *A1:PhDFR* gene expression ratio and relative pelargonidin content of flowers from *Petunia* × *hybrida* cv. Salmon Ray **(A)**, cv. Viva Orange **(B)**, and cv. Electric Orange **(C)**. Pie chart (bright red: pelargonidin (Pg), black: cyanidin (Cy), green: delphinidin (Dp), gray: dihydroflavonols, yellow: flavonols) of flavonoid contents (for absolute values see **Table 1**). Bar chart with the ratio of *A1:PhDFR* gene expression in % rel for each developmental stage (1: buds of 0.6–3 cm length, 2: buds of 3–5 cm length, 3: open flowers). Standard deviation (error bars) in $A_1$ and *PhDFR* gene expression ratios for each developmental stage are shown. Portions of pelargonidin based pigments of the anthocyanidins in total are given in % pelargonidin in the three stages of each cultivar.

were analyzed with a StepOnePlus system (Applied Biosystems, CA, USA) and the Luna® Universal qPCR Master Mix (New England Biolabs, Ipswich, UK). The relative expression ratio was calculated according to Pfaffl (2001). The efficiency of the PCR-reaction was determined on the basis of standard curves which were obtained by applying different DNA concentrations and calculated from the given slopes in the StepOne software according to equation $E = 10^{(-1/\text{slope})}$ (Pfaffl, 2001). All qPCR primers had an efficiency between 90 and 110% (for amplification efficiencies see Supplementary Table S1). The product specificity was confirmed by melting curve analysis and gel electrophoresis. Sequencing of PCR products was done by a commercial supplier (Microsynth, Vienna, Austria).

## Transcriptome Analysis

Plant material was harvested in summer 2016 and shock-frozen with liquid nitrogen. Preparation of rRNA, depleted RNA, random-primed cDNA and Illumina PE sequencing (50 million 150 bp, paired-end reads) was performed by a commercial supplier (vertis AG, Freising, Germany) on an Illumina NextSeq 500 system using 2 × 150 bp read length.

The random tagged prime RNA-seq data was first analyzed with the common NGS (next generation sequencing) analysis tools: First, the entire rRNA database provided by the tool was analyzed with sortmerna (v 2.1; Kopylova et al., 2012). From the remaining reads, the low-quality reads (below 20 quality score) were trimmed using trimmomatic (v 0.36) (Bolger et al., 2014) and the parameters TRAILING:20 AVGQUAL:20 SLIDINGWINDOW:5:20 MINLEN:75. Reads were mapped against the available *Petunia axillaris* genome (Bombarely et al., 2016), in which we incorporated the sequence of $A_1$ (NCBI CAA28734) to allow a quantification of the transgene expression. FPKM (Fragments Per Kilobase of transcript per Million mapped reads) were obtained using the method for quantification of RNA expression RSEM (v 1.3.0) (Li and Dewey, 2011).

## Recombinant DFR

The DFR cDNA clone of *P. hybrida* was synthesized by GeneCust Europe (Dudelange, Luxembourg) based on the sequence available in the database (NCBI X15537). The $A_1$ cDNA clone (NCBI CAA28734) from maize was provided by Udo Wienand

**TABLE 1 |** Flavonoid composition ([μg/g FW] and % rel) of methanolic extracts of three orange flowering petunias after acidic and enzymatic hydrolysis in comparison to the non-GE cultivars Corso Rot (red), Corso Blau (blue) and BabyDoll (pink with white dots).

| Pigment composition after acidic or enzymatic hydrolysis* | | Salmon ray | Viva Orange | Electric Orange | Corso Rot | Corso Blau | BabyDoll |
|---|---|---|---|---|---|---|---|
| Total anthocyanidins** | [μg/g FW] | 684.6 ± 299.6 | 522.7 ± 2.1 | 684.6 ± 299.6 | 552.0 ± 44.7 | 737.5 ± 194.4 | 959.3 ± 148.4 |
| Pelargonidin type | [μg/g FW] | 555.5 ± 193.4 | 448.5 ± 93.0 | 474.6 ± 314.2 | n.d. | n.d. | n.d. |
| Cyanidin type | [μg/g FW] | 43.0 ± 32.0 | 32.7 ± 7.3 | 191.7 ± 74.2 | 521.8 ± 45.0 | n.d. | 853.7 ± 123.8 |
| Delphinidin type | [μg/g FW] | 86.0 ± 15.7 | 41.5 ± 3.8 | 36.9 ± 43.9 | 30.3 ± 14.4 | 737.5 ± 194.4 | 105.6 ± 24.6 |
| Total dihydroflavonols | [μg/g FW] | 1,538.9 ± 1,040.6 | 1,680.2 ± 88.8 | 212.4 ± 47.8 | 455.0 ± 66.9 | n.d. | 188.2 ± 32.3 |
| Dihydrokaempferol (DHK) | [μg/g FW] | 1,502.4 ± 1,040.6 | 1,652.5 ± 88.1 | 179.9 ± 34.0 | n.d. | n.d. | n.d. |
| Dihydroquercetin (DHQ) | [μg/g FW] | 36.5 ± 29.5 | 27.8 ± 10.6 | 32.5 ± 26.2 | 455.0 ± 66.9 | n.d. | 188.2 ± 32.3 |
| Dihydromyricetin (DHM) | [μg/g FW] | n.d. | n.d. | n.d. | n.d. | n.d. | n.d. |
| Total flavonols | [μg/g FW] | 348.8 ± 276.2 | 284.1 ± 130.5 | 408.53 ± 190.6 | 857.2 ± 189.6 | 1,458.3 ± 42.4 | 1,942.1 ± 232.4 |
| Kaempferol | [μg/g FW] | 298.3 ± 205.3 | 284.1 ± 130.5 | 180.3 ± 27.7 | n.d. | n.d. | 168.9 ± 30.5 |
| Quercetin | [μg/g FW] | 50.5 ± 71.4 | n.d. | 228.1 ± 164.2 | 857.2 ± 189.6 | 1,407.1 ± 38.5 | 1,773.0 ± 199.9 |
| Myricetin | [μg/g FW] | n.d. | n.d. | n.d. | n.d. | 51.2. ± 3.9 | n.d. |
| Dihydroflavonols | % | 57 ± 4.1 | 68 ± 4.1 | 17 ± .1.5 | 29 ± .6.5 | n.d. | 6 ± .1.3 |
| Flavonols | % | 12 ± 2.7 | 11 ± 4.9 | 41 ± 2.1 | 33 ± 4.8 | 66 ± 5.1 | 63 ± .5.1 |
| Anthocyanidins** | % | 31 ± 6.4 | 21 ± 1.2 | 42 ± 3.7 | 32 ± 7.9 | 34 ± 5.1 | 31 ± .6.4 |
| Pelargonidin type | % | 81 ± 1.4 | 86 ± 1.7 | 66 ± 8.1 | n.d. | n.d. | n.d. |
| Cyanidin type | % | 6 ± .2.2 | 6 ± .1.2 | 30 ± .8.3 | 95 ± .2.7 | n.d. | 11 ± .2.9 |
| Delphinidin type | % | 13 ± .2.2 | 8 ± .0.8 | 4 ± .3.1 | 5 ± .2.7 | 100 ± .2.7 | 89 ± .1.7 |

*Pictures of the cultivars are incorporated in **Figure 1**.*

**Average values and standard deviations were calculated from at least three biological replications collected at different sites. Large standard deviations of absolute values [μg/g fresh weight (FW)] partially result from the strong variation of flavonoid contents with external factors such as lighting conditions. But even from the same plants, flowers with divergent color intensity could be collected (details not shown). Despite this, the relative distribution [%] between the flavonoid classes (anthocyanins, dihydroflavonols, and flavonols) and within anthocyanidins (pelargonidin-, cyanidin-, delphinidin based pigments) was quite stable.*

***Methylated anthocyanidins are not shown separately, but were included according to their number of hydroxy groups in the delphinidin type (petunidin, malvidin) or cyandin type (peonidin) anthocyanidins.*

*n.d. not detected.*

(University of Hamburg, Germany). The cDNA clones were used for subcloning into the bacterial expression vector pGEX-6P-1 (GE Healthcare, Munich, Germany) for overexpression of the *DFRs* as GST-fusion proteins, as described previously (Gosch et al., 2014), using primers $A_1$DFR-FL, $A_1$DFR-FS, $A_1$DFR-RL, $A_1$DFR-RS, and PhDFR-FL, PhDFR-FS, PhDFR-RL, PhDFR-RS, respectively (Supplementary Table S2).

## Enzyme Assays

DFR assays with recombinant enzyme or preparations from flowers were performed as described previously (Gosch et al., 2014).

## Site Directed Mutagenesis

Mutants were generated by use of the Q5® Site-Directed Mutagenesis Kit (NewEngland Biolabs, Vienna, Austria). Primers were designed using the NEBase Changer™ provided at http://nebasechanger.neb.com. The sequences are given in Supplementary Table S2. The integrity of the constructs was confirmed by commercial sequencing (Microsynth, Vienna, Austria).

## Statistical Analysis

The statistical analysis of the qPCR data was performed using RStudio v 1.0.136 and R v 3.3.3 with the package "agricolae" (Ihaka and Gentleman, 1996; De Mendiburu, 2017). Shapiro-Wilk test was used for testing on normality (Razali and Wah, 2011). A Wilcoxon rank sum test was used for not normal distributed data and a paired *t*-test was used for normal distributed data, respectively. The correlation between pelargonidin content and the expression ratio of *PhDFR* was calculated using the Pearson correlation coefficient (Duncan, 1955). Group-wise comparison of gene expression between different developmental stages and varieties was calculated utilizing Duncan's new multiple range test (MRT) (Duncan, 1955). For all statistical significance tests, the significance level was set to 0.05 (5%).

# RESULTS

## Pigment Composition

We analyzed the pigment composition of three commercially available orange varieties. In all three, pelargonidin based pigments were the prevalent anthocyanins (pie chart in **Figure 2**, **Table 1**). Whereas cv. Salmon Ray and cv. Viva Orange contained more than 80% pelargonidin based pigments and only small amounts of cyanidin and delphinidin derivatives, cv. Electric Orange showed a relatively high content of cyanidin based pigments (30%), traces of delphinidin based pigments and 66%

pelargonidin based pigments. The anthocyanin pattern was relatively stable during flower development and varied only to a minor extent between buds of different size and fully developed flowers (**Figure 2** right). Common red, pink, or blue petunia varieties, which were analyzed as controls, accumulated cyanidin or delphinidin based pigments, depending on the color, but no pelargonidin based pigments could be detected (**Table 1**).

Besides anthocyanins, dihydroflavonols and flavonols were present in the petals (**Figure 2**, **Table 1**). In the orange cultivars Salmon Ray and Viva Orange, dihydroflavonols were the prevalent flavonoid class, with more than 55% of the total flavonoids, whereas relatively small amounts of flavonols (below 15%) could be found (**Table 1**, pie charts in **Figure 2**). As with the anthocyanins, cv. Electric Orange showed a somewhat different composition, with 41% flavonols and 17% dihydroflavonols. In the red cv. Corso Rot, concentrations of anthocyanins, dihydroflavonols and flavonols were almost equal, whereas the blue and pink cultivars contained more than 60% flavonols and no (cv. Corso Blau) or only traces of (cv. BabyDoll) dihydroflavonols (**Table 1**).

## Evidence for a Genetic Modification Event and Identification of the $A_1$ Source

We screened the varieties by PCR for sequences that would indicate the presence of a biotechnological construct. With specific primers for $A_1$, *nptII* and the *35S* promoter, PCR fragments could be amplified from genomic DNA of all three varieties (**Figure 3**), thereby confirming a genetic modification event. To illuminate the origin of the $A_1$ source, we analyzed the transgene present in the three orange varieties. Two $A_1$ constructs previously used to create orange GE-lines (Meyer et al., 1986; Elomaa et al., 1995) for scientific purposes are the most probable sources. Discrimination by PCR between these is possible (Table in **Figure 4**), based on the direction of the $A_1$ gene, which was either sense (Meyer et al., 1986) or antisense (Elomaa et al., 1995) to the *nptII* gene. All three orange petunia varieties showed an approximately 2.3 kb amplicon when PCR with genomic DNA as template and $A_1$ specific forward and *nptII* specific reverse primers was performed (**Figure 4**), as expected only for the construct of Meyer et al. (1986). We furthermore sequenced a 3.3 kb PCR product obtained from genomic DNA of the three

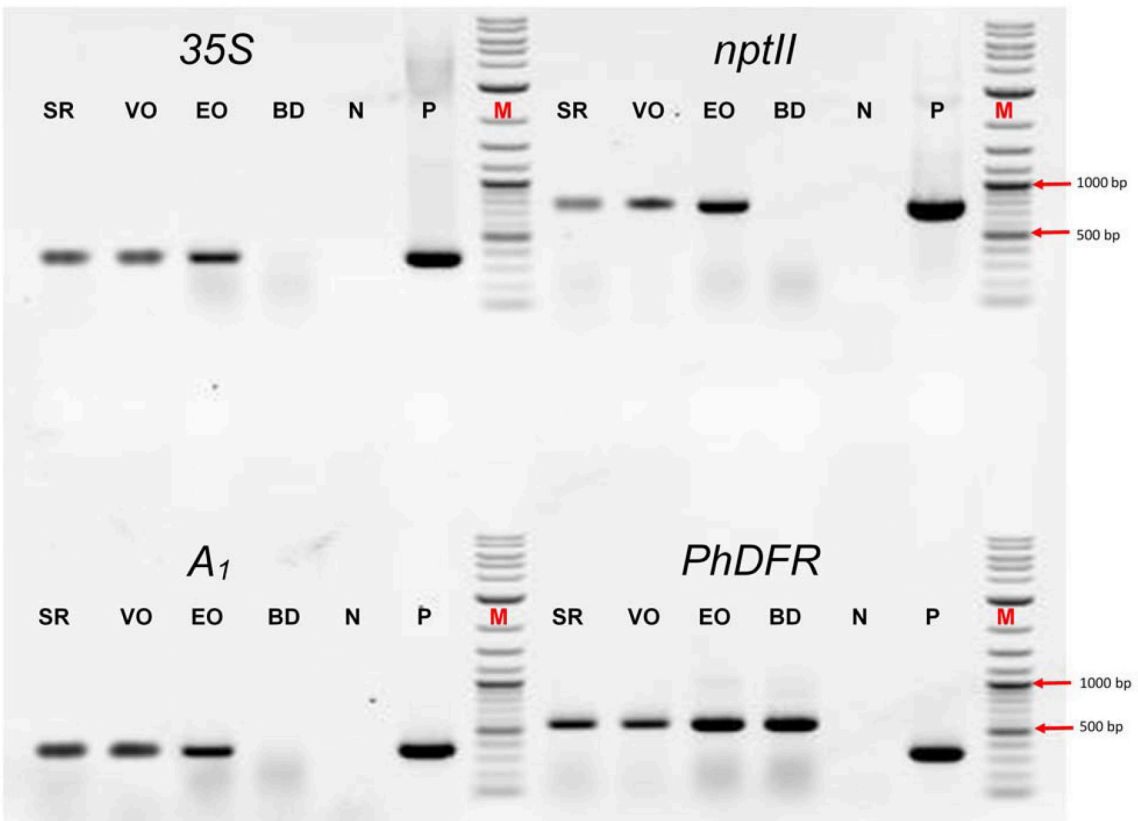


**FIGURE 3 |** PCR evaluation of genomic DNA of the three orange cultivars Salmon Ray (SR), Viva Orange (VO), and Electric Orange (EO) and the pink-white cultivar BabyDoll (BD) for the presence of specific DNA sequences. Water was used as negative control (N), and plasmids harboring the genes of interest as positive control (P) instead of genomic DNA. M: DNA marker 2-Log DNA Ladder; 1,000 and 500 bp fragments are marked with red arrows. *35S*: partial promoter sequence of the *35S* Cauliflower mosaic virus gene; *nptII*: partial coding sequence of the *nptII* selectable marker gene; $A_1$: partial coding sequence of the $A_1$ gene; *PhDFR*: partial coding sequence of the DFR of *Petunia* × *hybrida*. Primer sequences are provided in Supplementary Table S1. For genomic DNA, fragments of 365 bp (*35S*), 779 bp (*nptII*), 346 bp ($A_1$), and 565 bp (*PhDFR*) are expected. For *35S*, *nptII* and $A_1$, expected fragment sizes are identical for control plasmid. For *PhDFR*, a fragment of 337 bp for control plasmid DNA (cDNA clone) instead of 565 bp (genomic DNA) is expected.

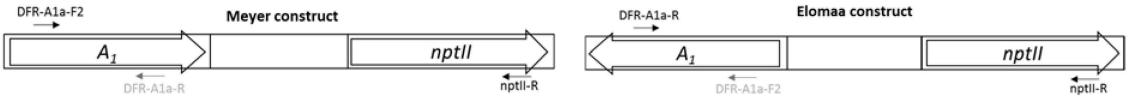


| | Primer 1 | Primer 2 | Amplicon expected for construct of | | Amplicon obtained with cDNA from three orange petunia varieties |
|---|---|---|---|---|---|
| | | | Meyer | Elomaa | |
| A | DFR-A1a-F2 | nptII-R | yes (2357 bp) | no | yes |
| B | DFR-A1a-R | nptII-R | no | yes | no |

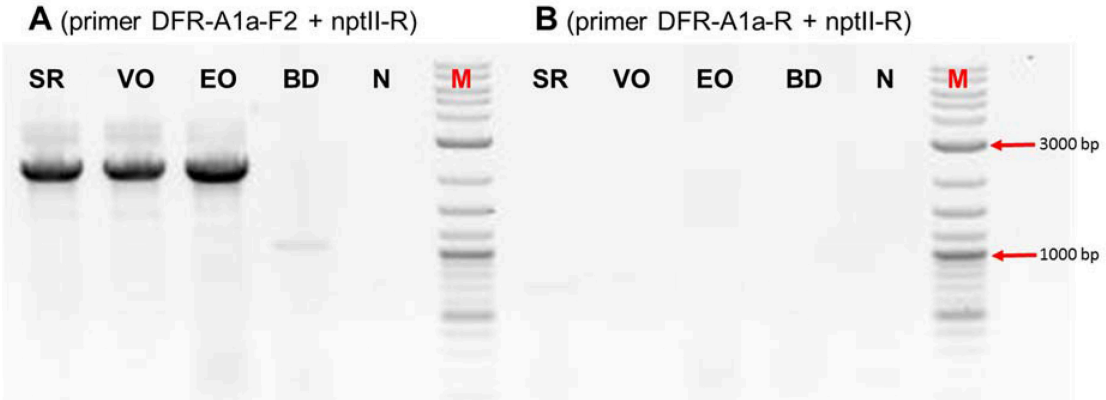


**FIGURE 4 |** PCR discrimination between the transformation plasmids of Meyer et al. (*A1* and *nptII* cloned in the sense orientation) and Elomaa et al. (*A1* and *nptII* cloned in the antisense direction). PCRs were performed with primer combinations **(A)** (primer DFR-*A1*a-F2 + *nptII*-R) and **(B)** (primer DFR-*A1*a-R + *nptII*-R) with genomic DNA of cvs. Salmon Ray (SR), Viva Orange (VO), Electric Orange (EO), and BabyDoll (BD). N, negative control in which genomic DNA is replaced by water; M, DNA marker 2-Log DNA Ladder; 3,000 and 1,000 bp fragments are marked with red arrows.

orange lines as templates using a *35S* promoter specific forward and an *OCS terminator* specific reverse primer.

All three amplicons showed identical sequences (Supplementary Figure S1) at the nucleotide level (NCBI MF521566). This included a partial sequence of the *35S* promoter (217 bp), followed by the restriction sites of *Xba*I and *Eco*RI, a 5′ untranslated region (UTR) of the $A_1$ cDNA clone of maize, the 1,074 bp full size $A_1$ cDNA clone, and an adjacent 3′ UTR with a 144 bp insertion consisting of the partial *Cin4-1* transposable element with a polyA stretch as present in the type 2 allele of $A_1$ described by Schwarz-Sommer et al. (1987a,b). After the polyA stretch, we identified an *Eco*RI and *Xba*I restriction site, a 226 bp t*35S* terminator flanked by an *Eco*RI restriction site, and a selection gene cassette including the p*NOS* promoter, *nptII* cDNA clone and t*OCS* terminator (1,402 bp fragment with only partial t*OCS*).

## DFR Substrate Specificity

Protein preparations obtained from the three orange petunia varieties were, surprisingly, not able to convert DHK under *in vitro* assay conditions, although they showed DFR activity with dihydromyricetin (DHM) as a substrate (**Table 2**). DHK conversion with enzyme preparation of the orange petunia petals could be observed neither in buds nor in petals. DHQ was not accepted either, with exception of the enzyme preparations from cv. Electric Orange, which converted DHQ to some extent, although at dramatically lower level than DHM (**Table 2**). Common blue and red petunias, which were used as controls, showed dihydroflavonol conversion levels that were almost comparable to those of the GE-petunia. High conversion rates were obtained with DHM as substrate, whereas DHK was not converted (**Table 2**). Conversion of DHQ was much lower than with DHM and lower than those observed with preparations from cv. Electric Orange. To exclude a false negative result, the integrity of DHK was confirmed with enzyme preparations from strawberry (**Table 2**) which possess a DFR showing high DHK substrate specificity (Miosic et al., 2014). Thus, the orange petunias showed the same lack of DHK acceptance under common DFR assay conditions as the blue and red flowering non-GE controls.

To shed further light on the substrate specificity of the maize DFR encoded by $A_1$, we heterologously expressed an $A_1$ cDNA clone as GST-fusion protein in *E. coli*. After removal of the GST-tag, the purified recombinant $A_1$ protein showed high substrate specificity, converting DHQ and DHM to a comparable extent, but no conversion of DHK could be observed during time spans sufficient to exhaust DHQ and DHM (**Table 2**). Even when incubation times with DHK were extended over night or up to 24 h at 4°C, no conversion of DHK to leucopelargonidin could be observed *in vitro*. Kinetic data indicate a comparable substrate specificity for DHM ($K_m$ 3.1 µM, $V_{max}$ 1.0 × $10^{-3}$ µM/s; $k_{cat}$ 0.87 $s^{-1}$; $k_{cat}/K_m$ 0.28 $s^{-1}µM^{-1}$) and DHQ ($K_m$

**TABLE 2 |** Specific DFR activity with DHK, DHQ, and DHM as substrate using enzyme preparations from petals of petunia cultivars and with recombinant DFR from maize and petunia.

| Enzyme source | $A_1$ present | Specific activity [nmol/g protein] measured with substrate | | |
|---|---|---|---|---|
| | | DHK | DHQ | DHM |
| Salmon Ray buds/open flowers | Yes | –/–* | –/– | 1.96/1.94 |
| Electric Orange buds/open flowers | Yes | –/–* | 0.13/0.12 | 1.96/1.96 |
| Viva Orange buds/open flowers | Yes | –/–* | –/– | 1.96/1.96 |
| BabyDoll | No | –/–* | –/– | 1.96/1.93 |
| Corso Rot | No | –/–* | 0.01/– | 1.96/1.94 |
| Corso Blau | No | –/–* | 0.03/– | 1.96/1.96 |
| Control reaction (strawberry) | No | 1.96 | 0.25 | 0 |
| recombinant $A_1$ protein | | – | 0.33 | 0.55 |
| Recombinant wild type *Ph*DFR (137L, 138D)** | | – | – | 1.47 |
| Recombinant *Ph*DFR mutant (137V, 138D)** | | – | – | 1.52 |
| Recombinant *Ph*DFR mutant (137V, 138N)** | | | 1.41 | 1.14 |
| Recombinant *Ph*DFR mutant (137L, 138N)** | | – | 1.48 | 1.48 |

*Enzyme preparations from strawberry fruits were used as control to demonstrate integrity of the DHK and DHQ substrates.*
**DHK conversion was not observed even if incubation time was extended to 24 h at 4°C; **Numbering according to the deduced amino acid sequence of $A_1$ as shown in Supplementary Figure S2; –: below detection level.*

2.9 μM, $V_{max}$ 1.25 × $10^{-3}$ μM/s; $k_{cat}$ 0.70 $s^{-1}$; $k_{cat}/K_m$ 0.24 $s^{-1}\mu M^{-1}$).

To compare the substrate specificities of the DFRs of maize and *Petunia* × *hybrida,* studies were also performed with recombinant *Petunia* × *hybrida* DFR (*Ph*DFR). Purified recombinant, *Ph*DFR showed no DHQ or DHK conversion and thus, a clear specificity for DHM (**Table 2**), which was also confirmed by the kinetic data ($K_m$ 1.3 μM; $V_{max}$ 0.5 × $10^{-3}$ μM/s; $k_{cat}/K_m$ 2.14 $s^{-1}$; $k_{cat}/K_m$ 1.6 $s^{-1}$ $\mu M^{-1}$). Amino acid sequence identity between *Ph*DFR and $A_1$ is only 54%. Particularly the region presumably determining substrate specificity shows a difference in positions 132–134 (amino acid numbering according *Ph*DFR). To investigate whether the striking difference in the DHQ acceptance between the two recombinant DFRs is based on this region as suggested (Johnson et al., 2001), we created mutants with altered amino acids (**Table 2**). Whereas an exchange of the leucine with a valine in position 137 did not result in increased DHQ conversion, the exchange of aspartic acid with asparagine in position 138 raised DHQ conversion from zero to levels equaling those of DHM.

## Gene Expression in the Orange Petunia Varieties

The transcriptomes of orange (cv. Salmon Ray), red (cv. Corso Rot) and black (cv. Blackberry) petunias were analyzed for differences in their gene expression pattern with respect to the phenotype. We particularly focused on the genes involved in color formation (Bombarely et al., 2016). The three varieties did not provide a uniform picture (Supplementary Figure S3). Whereas cv. Salmon Ray showed lower gene expressions in many of the structural genes of the flavonoid pathway, but not of the phenylpropanoid pathway, most of the structural genes in the early and late flavonoid pathway seemed to be up-regulated in the two other varieties. However, an increased *DFR:FLS* expression ratio was observed in the red and in all three orange cultivars compared to the black. This was further examined by quantitative real-time PCR.

Quantitative real-time PCR performed with primers discriminating between the DFRs from maize ($A_1$) and petunia (*PhDFR*) (Supplementary Table S1), showed that *PhDFR* expression strongly dominated over $A_1$expression (**Figure 2**, bar charts) in developing buds of the orange varieties, despite being under the control of the strong, constitutive p*35S* promoter. $A_1$/*PhDFR* expression ratios of approximately 1 could only be observed in open flowers. The qPCR studies also confirmed that the three orange petunia varieties had a low expression of *F3'H* and *FLS* and thus a very high *DFR:FLS* expression ratio during the flower life cycle (**Figure 6**). There was, however, no statistically significant correlation between the $A_1$/*PhDFR* expression ratios and the pelargonidin-type anthocyanidin concentration in the petals (**Figure 2**).

# DISCUSSION

The DFR of petunia has ever been the role model for studies on DFR substrate specificity, and the resulting lack of orange flower color in petunia has always been the best example for the complex mechanisms of color establishment in flowers. The creation of an orange petunia by a transgenic approach in the 1980s at the Max Planck Institute for Plant Breeding Research in Cologne, Germany was a further landmark in the field of flower color research and the subsequent field trial attracted attention far beyond the horticultural community. Thus, the fact that petunia does not naturally possess orange flower color, and the underlying biochemical reason, has been established knowledge for a few decades (Meyer et al., 1986, 1992; Johnson et al., 1999, 2001). Therefore, the appearance of orange petunia varieties on the European market attracted the interest of scientists familiar with anthocyanin flower color. As they were not declared as genetically modified plants, which would have been compulsory if a transgenic breeding method had been used, they were apparently a result of classical breeding. Recent research demonstrated, however, that the vast majority of the commercially available orange petunia varieties, but not all, are genetically engineered and harbor the $A_1$ cDNA clone from *Zea mays* (Bashandy and Teeri, 2017). Despite the general consensus that the transgenic construct most probably derived from the first scientific GE-petunia (Meyer et al., 1986), it always remained unmentioned that there was a second scientific petunia (Elomaa et al., 1995), which was constructed with the same GE-elements, which could have been a possible source of the putatively unintentionally escaped $A_1$ cDNA clone. Our data unequivocally demonstrate, however, that of these two possible

known sources, an unintentional release of the construct of the Elomaa et al. (1995) can indeed be excluded.

In an independent approach we analyzed three varieties released by breeders from three countries, The Netherlands, Israel and Germany. All three amplicons showed identical sequences (Supplementary Figure S1) at the nucleotide level (NCBI MF521566), demonstrating that a single $A_1$ source had entered breeding programmes worldwide. The sequence we obtained was in line with NCBI KY964325 (Bashandy and Teeri, 2017). There is, however, an overlap, as our primers started 699 bp downstream at the 5′-end, but provided an additional 375 bp stretch at the 3′-end.

Our sequencing results identified with near absolute certainty the transformation construct of Meyer et al. (1986) as the $A_1$ source, based on the following characteristics (**Figure 5**, Supplementary Figure S1): the same arrangement of *35S* promoter, $A_1$, *35S* terminator, *nopaline synthase* (*NOS*) promoter, *nptII, octopine synthase (OCS)* terminator, and the restriction sites used for the p35A1 plasmid construction, as described for the Meyer et al. (1986) construct, was identified (**Figure 5**). Pre-eminently, the transgene found in the three orange petunia varieties contains the $A_1$ type 2 allele previously used for plasmid p35A1 construction (Meyer et al., 1986), which includes, at the 3′-end, an additional segment from the non-viral transposable *Cin4-1* sequence (Schwarz-Sommer et al., 1987a). In addition, in the transition zone between the *35S* promoter and the $A_1$ gene, parts of the untranslated sequences of the 5′ flanking region, described previously (Schwarz-Sommer et al., 1987b), are present. This rules out other potential, as yet unidentified, sources, as it is unlikely that a putative third, yet unknown construct would harbor this special $A_1$ allele, particularly as the transposable element does not add any functional advantage with respect to color formation.

Unexpectedly, the orange petunias showed the same lack of DHK acceptance under common DFR assay conditions as the blue and red flowering non-GE controls. Concordantly, the orange petals accumulate large amounts of DHK derivatives (**Table 1**) that have not been ultimately converted to pelargonidin-based pigments. Such elevated dihydroflavonol levels were not found in common petunia varieties with a high F3′5′H activity, as this favors creation of delphinidin based pigments. Likewise, in the absence of F3′5′H activity, accumulated DHK and DHQ can be converted to flavonols, if FLS is active in the petals, as is the case in the red variety (**Table 1**). The low substrate specificity for DHK was surprising, given the fact that $A_1$ had been introduced to explicitly enable conversion of DHK and thus, formation of pelargonidin based pigments. Much better color effects had been achieved by transformation with an unspecific gerbera *DFR* (Elomaa et al., 1995), thereby already pointing to a low substrate specificity of the maize DFR for DHK, although observed effects were rather attributed to the instability of monocotyledonous cDNA in the dicotyledonous petunia (Elomaa et al., 1995). The low substrate specificity of the protein encoded by the $A_1$ gene was confirmed with recombinant maize DFR obtained by heterologous expression in *E. coli*.

Only low expression rates were observed for the $A_1$ gene, which is in accordance with findings of epigenetic downregulation effects in GE-petunia (Linn et al., 1990; Meyer and Heidmann, 1994; Meyer, 1998). $A_1$ gene expression generally remained below the rates measured for the *PhDFR*. Highest expression was found in fully developed flowers, where an $A_1$/*PhDFR* ratio of up to 1 could be measured. Despite this, the content of pelargonidin-based pigments remained surprisingly unchanged during flower development (**Figure 2**). There was, however, no statistically relevant correlation between the pelargonidin-based pigment concentration and the $A_1$ gene expression. Moreover, we never observed DHK conversion with enzyme preparations of the orange petunia petals independently of a high (open flowers) or low $A_1$/*PhDFR* (buds) expression ratio, raising the question, if, besides the maize DFR, the petunia DFR could also contribute to pelargonidin-precursor production.

To determine how the orange coloration may occur at all, if a poorly expressed non-petunia *DFR*, with an additionally low substrate specificity for DHK, was present in GE-petunia petals, we compared the transcriptomes of the three orange varieties (cvs. Salmon Ray, Viva Orange, Electric Orange), red (cv. Corso Rot) and black (cv. Blackberry) petunias (Supplementary Figure S3) and analyzed the genes particularly involved in color formation (Bombarely et al., 2016). An increased *DFR:FLS* expression ratio in the red and orange cultivars was observed, compared to the black, which was confirmed by qPCR (**Figure 6**) and by the relatively small amounts of flavonols found in the petals of orange varieties (**Table 1**).

Apparently, the establishment of orange petunia flower color can occur only in the absence of interfering F3′H and FLS activities (**Figure 6**). Considering the low substrate specificity of both *Ph*DFR and $A_1$ protein for DHK, sufficient


**FIGURE 5 |** Schematic representation of the transgenic insert found in the three GE-petunia varieties cvs. Salmon Ray, Viva Orange and Electric Orange (NCBI MF521566) p*35S*, promoter sequence of the *35S* Cauliflower mosaic virus gene; $A_1$, coding sequence of the $A_1$ gene; *Cin4-1*, partial *Cin4-1* transposable element present in type 2 allele of $A_1$ according to Schwarz-Sommer et al. (1987a,b); t*35S*, terminator sequence of the *35S* Cauliflower mosaic virus gene; p*NOS*, promoter sequence of the nopaline synthase gene; *nptII*, coding sequence of the neomycine phosphotransferase II selectable marker gene; t*OCS*, terminator sequence of the octopine synthase gene. Positions of primers are marked by arrows. Primer sequences are provided in Supplementary Table S1.

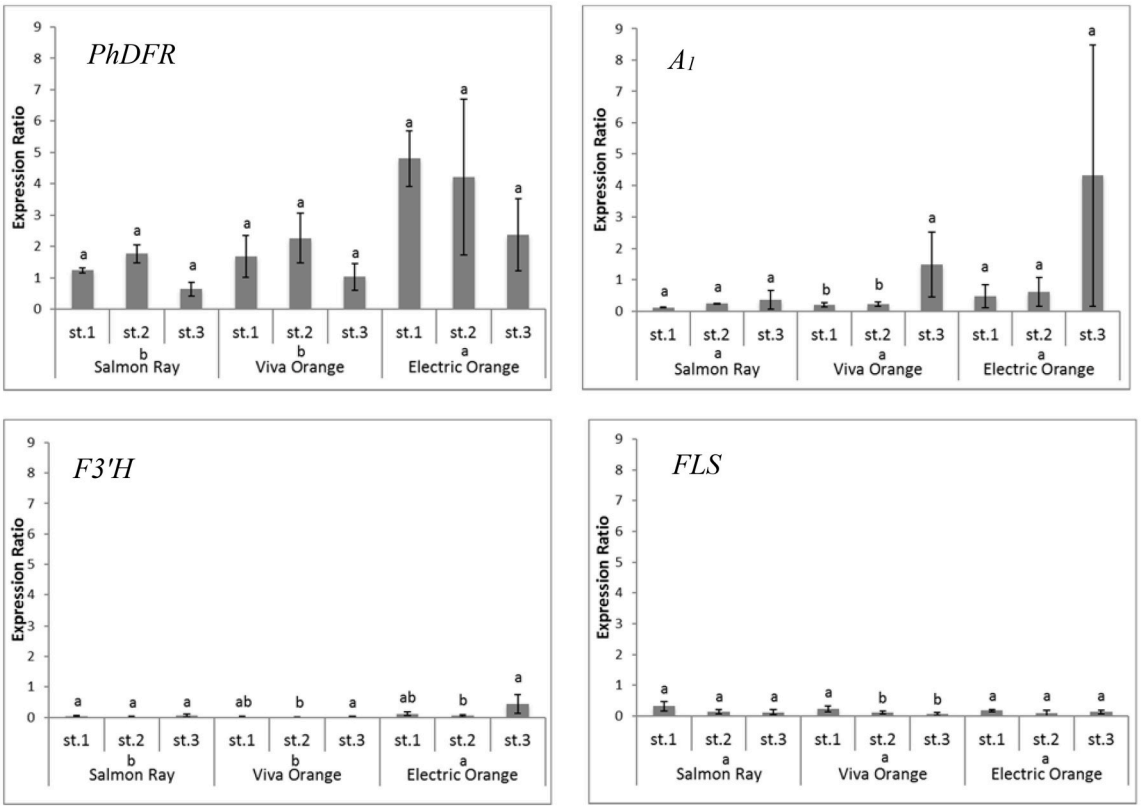


**FIGURE 6 |** Quantitative gene expression of *PhDFR*, $A_1$, *F3′H* and *FLS*, normalized to *actin* in three developmental stages (st. 1: buds of 0.6–3 cm length, st. 2: buds of 3–5 cm length, st. 3: open flowers) of orange petunia flowers in three varieties (cvs. Salmon Ray, Viva Orange, Electric Orange). Average values were calculated from at least three biological replications collected at different sites. Error bars show standard deviation. Different letters above bars denote statistical difference according to Duncan test ($p < 0.05$) between the developmental stages separately for each variety. Different letters above cultivar names denote statistical difference according to Duncan test ($p < 0.05$) between the three varieties in general calculated from pooled stages.

leucopelargonidin precursor for pelargonidin-type flowers will be synthesized (i) very slowly over a long time, (ii) only if no other dihydroflavonol precursor is present (absent or low F3′H and F3′5′H activity), and (iii) if the accumulating DHK is not redirected by a highly active FLS toward flavonols. In the same way, cyanidin-based red flowering petunia varieties occur naturally, despite the fact that *Ph*DFR shows stringent specificity for DHM as substrate (**Table 2**). The red cultivar used as a control accumulates a substantial amount of dihydroflavonols, however, thereby confirming the low *FLS* expression and elevated *DFR:FLS* expression ratio in the red cultivars already indicated by the transcriptome analysis. Considering the DFR substrate specificity of petunia for DHM, increased flavonol formation, at the expense of anthocyanin accumulation, and thus, only a pale color, would be expected in the case of a highly active petunia FLS. The elaborate creation of transgenic petunia and the current global commotion surrounding the escaped $A_1$ gene seem to be a great cause, in comparison to the relatively small color effects attained by the use of the inefficient maize DFR.

American and European authorities unambiguously stated that the GE-petunia is not harmful to consumers and environment. It is still unknown, how plants harboring the $A_1$ construct of Meyer et al. (1986) entered classical breeding programmes. Nefarious use of GE-plants is unlikely, due to foreseeable troubles when plants inevitably attract attention. There are, however, several scenarios how the GE-petunia could have escaped. After its creation at the Max Planck Institute for Plant Breeding Research in Cologne (Meyer et al., 1986), and the contentious field trial in Germany in 1990, the plants were kept in several institutions, and were also used for breeding purposes (Oud et al., 1995; Servick, 2017), followed by field trials in the US. Currently, the most favored explanation (Servick, 2017) seems to be that during a chain of company fusions the GE-background of orange petunias was forgotten, and the lines could therefore enter new breeding programmes. Our results demonstrate why the presence of the $A_1$ does not result in orange phenotypes in a common biochemical petunia background, which facilitates undetected dispersion. Thus, the original GE-petunia (Meyer et al., 1986) or progenies thereof, created by classical breeding (Oud et al., 1995) or—less likely—by escaped pollen, in the field or in the greenhouse, could have infiltrated classical breeding chains, unless it re-emerged as orange petunia in a rare event of a proper genetic background. The large spectrum of undeclared GE-petunia varieties can be explained by the use of early orange varieties as parent plants in classical breeding attempts for further orange varieties by other companies and by the use of non-orange

breeding material harboring an unrecognized $A_1$. The fact that a single construct was found so far in the orange petunia varieties, as opposed to plural different constructs, points at a single event in the breeding chain rather than at multiple parallel events.

In the current debate, it was iterated that real orange petunia flower colors cannot occur naturally (David, 2017). Some few petunia varieties, however, show a pattern of red and yellow pigments that, at a glance, might be mistaken for orange (Bashandy and Teeri, 2017). But even minor mutations in the active site of the DFR can result in higher DHK specificity, as demonstrated by the existing patent for a DHK specific DFR (Johnson et al., 2001). A spontaneous mutation occurring in a suitable background, although unlikely, could indeed provide a naturally orange-flowering petunia. This could also be achieved by cutting-edge genome editing methods causing a targeted mutation, which can currently not be distinguished from mutations induced by well accepted methods such as mutation via chemicals or radiation. It remains to be seen how the escaped GE-petunias will influence the current debate about the classification of genome editing as a genetic engineering method, and on biotech patents in general, which was provoked by the recent barley patents obtained by large brewing companies.

## AVAILABILITY OF DATA AND MATERIALS

All data supporting the findings is contained in the manuscript and its supplementary files. Transcriptome data are available at the Short Read Archive of the International Nucleotide Sequence Database Collaboration: SAMN07988829 (*Petunia* × *hybrida* cv. Blackberry), SAMN07988830 (*Petunia* × *hybrida* cv. Corso Rot), SAMN07988831 (*Petunia* × *hybrida* cv. Viva Orange), SAMN07988832 (*Petunia* × *hybrida* cv. Electric Orange), SAMN07988833 (*Petunia* × *hybrida* cv. Salmon Ray).

## AUTHOR CONTRIBUTIONS

HH, CH-G, and KS: Conceived the research and wrote the manuscript; SM, DN, BR, BW, RP, RL, and LE: conducted the experiments; TR and KO: analyzed the data. All authors approved the manuscript.

## FUNDING

We acknowledge funding by the Austrian Science Fund (FWF) P 28134-B25 and from the European Union's Horizon 2020 research and innovation program under the Marie Skłodowska-Curie grant agreement No 675657.

## SUPPLEMENTARY MATERIAL

The Supplementary Material for this article can be found online at: https://www.frontiersin.org/articles/10.3389/fpls.2018.00149/full#supplementary-material

## REFERENCES

Bashandy, H., and Teeri, T. H. (2017). Genetically engineered orange petunias on the market. *Planta* 246, 277–280. doi: 10.1007/s00425-017-2722-8

Bolger, A. M., Lohse, M., and Usadel, B. (2014). Trimmomatic: a flexible trimmer for Illumina sequence data. *Bioinformatics* 30, 2114–2120. doi: 10.1093/bioinformatics/btu170

Bombarely, A., Moser, M., Amrad, A., Bao, M., Bapaume, L., Barry, C. S., et al. (2016). Insight into the evolution of the Solanaceae from the parental genomes of *Petunia hybrida*. *Nat. Plants* 2:16074. doi: 10.1038/nplants.2016.74

David, M. (2017). U.S. flower sellers rush to destroy illegal GE petunias. *Sci. Post. Plants Anim. Sci. Policy*. doi: 10.1126/science.aal1200

De Mendiburu, F. (2017). *Agricolae: Statistical Procedures for Agricultural Research*. R package version 1.2-8. Available online at: https://CRAN.R-project.org/package=agricolae.

Duncan, D. B. (1955). Multiple range and multiple F tests. *Biometrics* 11, 1–42. doi: 10.2307/3001478

Elomaa, P., Helariutta, Y., Kotilainen, M., Teeri, T. H., Griesbach, R. J., and Seppänen, P. (1995). Transgene inactivation in *Petunia hybrida* is influenced by the properties of the foreign gene. *Mol. Gen. Genet.* 248, 649–656. doi: 10.1007/BF02191704

Gosch, C., Nagesh, K. M., Thill, J., Miosic, S., Plaschil, S., Milosevic, M., et al. (2014). Isolation of Dihydroflavonol 4-Reductase cDNA Clones from Angelonia × angustifolia and Heterologous Expression as GST Fusion Protein in *Escherichia coli*. *PLoS ONE* 9:e107755. doi: 10.1371/journal.pone.0107755

Halbwirth, H. (2010). The creation and physiological relevance of divergent hydroxylation patterns in the flavonoid pathway. *Int. J. Mol. Sci.* 11, 595–621. doi: 10.3390/ijms11020595

Halbwirth, H., Kahl, S., Jager, W., Reznicek, G., Forkmann, G., and Stich, K. (2006). Synthesis of ($^{14}$C)-labeled 5-deoxyflavonoids and their application in the study of dihydroflavonol/leucoanthocyanidin interconversion by dihydroflavonol 4-reductase. *Plant Sci.* 170, 587–595. doi: 10.1016/j.plantsci.2005.10.013

Ihaka, R., and Gentleman, R. (1996). R: a language for data analysis and graphics. *J. Comput. Graph. Stat.* 5, 299–314.

Johnson, E. T., Ryu, S., Yi, H., Shin, B., Cheong, H., and Choi, G. (2001). Alteration of a single amino acid changes the substrate specificity of dihydroflavonol 4-reductase. *Plant J.* 25, 325–333. doi: 10.1046/j.1365-313x.2001.00962.x

Johnson, E. T., Yi, H., Shin, B., Oh, B. J., Cheong, H., and Choi, G. (1999). Cymbidium hybrida dihydroflavonol 4-reductase does not efficiently reduce dihydrokaempferol to produce orange pelargonidin-type anthocyanins. *Plant J.* 19, 81–85. doi: 10.1046/j.1365-313X.1999.00502.x

Kopylova, E., Noé, L., and Touzet, H. (2012). SortMeRNA: fast and accurate filtering of ribosomal RNAs in metatranscriptomic data. *Bioinformatics* 28, 3211–3217. doi: 10.1093/bioinformatics/bts611

Li, B., and Dewey, C. N. (2011). RSEM: accurate transcript quantification from RNA-Seq data with or without a reference genome. *BMC Bioinformatics* 12:323. doi: 10.1186/1471-2105-12-323

Linn, F., Heidmann, I., Saedler, H., and Meyer, P. (1990). Epigenetic changes in the expression of the maize A1 gene in *Petunia hybrida*: role of numbers of integrated gene copies and state of methylation. *Mol. Gen. Genet.* 222, 329–336. doi: 10.1007/BF00633837

Lipp, M., Brodmann, P., Pietsch, K., Pauwels, J., Anklam, E., Borchers, T., et al. (1999). IUPAC collaborative trial study of a method to detect genetically modified soy beans and maize in dried powder. *J. AOAC Int.* 82, 923–928.

Mallona, I., Lischewski, S., Weiss, J., Hause, B., and Egea-Cortines, M. (2010). Validation of reference genes for quantitative real-time PCR during leaf and flower development in *Petunia hybrida*. *BMC Plant Biol.* 10:4. doi: 10.1186/1471-2229-10-4

Meyer, P. (1998). Stabilities and instabilities in transgene expression. *Trans. Plant Res.* 263–275.

Meyer, P., and Heidmann, I. (1994). Epigenetic variants of a transgenic petunia line show hypermethylation in transgene DNA: an indication for specific recognition of foreign DNA in transgenic plants. *Mol. Gen. Genet.* 243, 390–399.

Meyer, P., Heidmann, I., Forkmann, G., and Saedler, H. (1986). A new petunia flower colour generated by transformation of a mutant with a maize gene. *Nature* 330, 677–678. doi: 10.1038/330677a0

Meyer, P., Linn, F., Heidmann, I., Meyer, H., Niedenhof, I., and Saedler, H. (1992). Endogenous and environmental factors influence 35S promoter methylation of a maize A1 gene construct in transgenic petunia and its colour phenotype. *Mol. Gen. Genet.* 231, 345–352. doi: 10.1007/BF00292701

Miosic, S., Thill, J., Milosevic, M., Gosch, C., Pober, S., Molitor, C., et al. (2014). Dihydroflavonol 4-reductase genes encode enzymes with contrasting substrate specificity and show divergent gene expression profiles in Fragaria Species. *PLoS ONE* 9:e112707. doi: 10.1371/journal.pone.0112707

Oud, J. S., Schneiders, H., Kool, A. J., and Van Grinsven, M. Q. (1995). Breeding of transgenic orange *Petunia hybrida* varieties. *Euphytica* 84, 175–181. doi: 10.1007/BF01681809

Petit, P., Granier, T., d'estaintot, B. L., Manigand, C., Bathany, K., Schmitter, J. M., et al. (2007). Crystal structure of grape Dihydroflavonol 4-Reductase, a Key Enzyme in Flavonoid Biosynthesis+. *J. Mol. Biol.* 368, 1345–1357. doi: 10.1016/j.jmb.2007.02.088

Pfaffl, M. W. (2001). A new mathematical model for relative quantification in real-time RT–PCR. *Nucleic Acids Res.* 29:e45. doi: 10.1093/nar/29.9.e45

Razali, N. M., and Wah, Y. B. (2011). Power comparisons of shapiro-wilk, kolmogorov-smirnov, lilliefors and Anderson-darling tests. *J. Stat. Model. Anal.* 2, 21–33.

Schwarz-Sommer, Z., Leclercq, L., Göbel, E., and Saedler, H. (1987a). Cin4, an insert altering the structure of the A1 gene in Zea mays, exhibits properties of nonviral retrotransposons. *EMBO J.* 6:3873.

Schwarz-Sommer, Z., Shepherd, N., Tacke, E., Gierl, A., Rohde, W., Leclercq, L., et al. (1987b). Influence of transposable elements on the structure and function of the A1 gene of Zea mays. *EMBO J.* 6:287.

Servick, K. (2017). The strange case of the orange petunias. *Science* 356:792. doi: 10.1126/science.356.6340.792

Tanaka, Y., Brugliera, F., and Chandler, S. (2009). Recent progress of flower colour modification by biotechnology. *Int. J. Mol. Sci.* 10, 5350–5369. doi: 10.3390/ijms10125350

Tanaka, Y., Brugliera, F., Kalc, G., Senior, M., Dyson, B., Nakamura, N., et al. (2010). Flower color modification by engineering of the flavonoid biosynthetic pathway: practical perspectives. *Biosci. Biotechnol. Biochem.* 74, 1760–1769. doi: 10.1271/bbb.100358

Thill, J., Miosic, S., Ahmed, R., Schlangen, K., Muster, G., Stich, K., et al. (2012). 'Le Rouge et le Noir': a decline in flavone formation correlates with the rare color of black dahlia (*Dahlia variabilis* hort.) flowers. *BMC Plant Biol.* 12:225. doi: 10.1186/1471-2229-12-225

Winkel-Shirley, B. (2001). Flavonoid biosynthesis. a colorful model for genetics, biochemistry, cell biology, and biotechnology. *Plant Physiol.* 126:485. doi: 10.1104/pp.126.2.485

**Conflict of Interest Statement:** The authors declare that the research was conducted in the absence of any commercial or financial relationships that could be construed as a potential conflict of interest.

frontiers in Plant Science

ORIGINAL RESEARCH
published: 30 January 2018
doi: 10.3389/fpls.2018.00041

# Epigenetic Variance, Performing Cooperative Structure with Genetics, Is Associated with Leaf Shape Traits in Widely Distributed Populations of Ornamental Tree *Prunus mume*

*Kaifeng Ma[1], Lidan Sun[1], Tangren Cheng[1], Huitang Pan[1], Jia Wang[1] and Qixiang Zhang[1,2]**

*[1] Beijing Key Laboratory of Ornamental Plants Germplasm Innovation and Molecular Breeding, National Engineering Research Center for Floriculture, Beijing Laboratory of Urban and Rural Ecological Environment, Key Laboratory of Genetics and Breeding in Forest Trees and Ornamental Plants of Ministry of Education, School of Landscape Architecture, Beijing Forestry University, Beijing, China, [2] Beijing Advanced Innovation Center for Tree Breeding by Molecular Design, Beijing Forestry University, Beijing, China*

Increasing evidence shows that epigenetics plays an important role in phenotypic variance. However, little is known about epigenetic variation in the important ornamental tree *Prunus mume*. We used amplified fragment length polymorphism (AFLP) and methylation-sensitive amplified polymorphism (MSAP) techniques, and association analysis and sequencing to investigate epigenetic variation and its relationships with genetic variance, environment factors, and traits. By performing leaf sampling, the relative total methylation level (29.80%) was detected in 96 accessions of *P. mume*. And the relative hemi-methylation level (15.77%) was higher than the relative full methylation level (14.03%). The epigenetic diversity ($I^* = 0.575$, $h^* = 0.393$) was higher than the genetic diversity ($I = 0.484$, $h = 0.319$). The cultivated population displayed greater epigenetic diversity than the wild populations in both southwest and southeast China. We found that epigenetic variance and genetic variance, and environmental factors performed cooperative structures, respectively. In particular, leaf length, width and area were positively correlated with relative full methylation level and total methylation level, indicating that the DNA methylation level played a role in trait variation. In total, 203 AFLP and 423 MSAP associated markers were detected and 68 of them were sequenced. Homologous analysis and functional prediction suggested that the candidate marker-linked genes were essential for leaf morphology development and metabolism, implying that these markers play critical roles in the establishment of leaf length, width, area, and ratio of length to width.

**Keywords: DNA methylation, molecular marker, genetic/epigenetic diversity, genetic/epigenetic structure, environmental factors, association analysis, *Prunus mume***

OPEN ACCESS

***Edited by:***
*Raquel Sánchez-Pérez, University of Copenhagen, Denmark*

***Reviewed by:***
*Xiang Gao, Northeast Normal University, China*
*Hongjun Liu, Shandong Agricultural University, China*

***Correspondence:**
*Qixiang Zhang*
*zqxbjfu@126.com*

***Specialty section:***
*This article was submitted to Plant Biotechnology, a section of the journal Frontiers in Plant Science*

***Received:*** *04 September 2017*
***Accepted:*** *09 January 2018*
***Published:*** *30 January 2018*

***Citation:***
*Ma K, Sun L, Cheng T, Pan H, Wang J and Zhang Q (2018) Epigenetic Variance, Performing Cooperative Structure with Genetics, Is Associated with Leaf Shape Traits in Widely Distributed Populations of Ornamental Tree Prunus mume. Front. Plant Sci. 9:41. doi: 10.3389/fpls.2018.00041*

## INTRODUCTION

*Prunus mume* Sieb. et Zucc. ($2n = 2x = 16$), also known as mei, was domesticated in China more than 3,000 years ago as an ornamental plant and fruit tree (Zhang et al., 2012). Its distribution is centered around the borders of northwestern Yunnan Province, southwestern Sichuan Province, and southeastern Tibet Autonomous Region (Bao, 1993; Bao and Chen, 1994). The wild form of

*P. mume* can also be found across a wide region south of Changjiang River (Zhang et al., 2010). Genetic diversity, population structure, and genetic linkage mapping analyses on *P. mume* have investigated the molecular markers that support the hypothesis that the genetic diversity center of the species is southwest China (Yang et al., 2007). A high-density linkage map of *P. mume* was constructed and used to detect quantitative trait loci (QTLs) (Sun et al., 2014), and specific-locus amplified fragment sequencing (SLAF-seq) marker located on linkage group 7 was associated with branch weeping (Zhang J. et al., 2015; Zhang et al., 2017). Molecular identification also proved that fruiting mei and Japanese flowering mei originated in different locations (Shen et al., 2011). Importantly, the complete genome sequence of *P. mume* is now available (Zhang et al., 2012), and this has provided new sights into the genetics of this species. However, little is known about the variation or regulation mechanisms involved in epigenetics in *P. mume*.

In eukaryotes, genetic variation and epigenetic variation both play important roles in determining phenotypic characteristics by regulating gene expression (Massicotte et al., 2011; Mirouze and Paszkowski, 2011; Heyn et al., 2013). Increasing evidence has revealed that epigenetic modifications, such as patterns of DNA methylation (Dubrovina and Kiselev, 2016), histone modifications (Thorstensen et al., 2011), histone variants (Chen et al., 2011), and small RNAs (Heo et al., 2013), can be passed from one generation to the next via mitosis or meiosis, or can change either spontaneously or in response to external signals (Pérez et al., 2006; Fang and Chao, 2007; Becker and Weigel, 2012; Geoghegan and Spencer, 2012; Li et al., 2017). And the variations in the epigenome are of utmost importance during development and in response to changing environmental conditions (Feng et al., 2010; Feng and Jacobsen, 2011; Schmitz and Ecker, 2012; Nicotra et al., 2015).

DNA methylcytosine, which suppresses transposable elements (Lisch and Bennetzen, 2011), changes flower symmetry (Cubas et al., 1999), and influences fruit ripening (Manning et al., 2006; Seymour et al., 2008), is a widely studied and common epigenetic feature in plant genomes (Bennetzen and Zhu, 2011). Methylcytosine, which comprises 6–30% of the total cytosine in a genome (Chen and Li, 2004), generally occurs in the symmetrical sequence CG, but can also be found in CHG or CHH (H = A, T, or C) sequences (Gruenbaum et al., 1981; Lister et al., 2008). Methylcytosine also gives rise to epialleles that are potentially reversible and often exist in metastable states (Vaughn et al., 2007; Foerster et al., 2011), which provides the opportunity for uncovering epigenetic diversity and structure within or between populations (Liu et al., 2012; Ma et al., 2013; Foust et al., 2016) and epigenetic linkage mapping (Zhang et al., 2008; Long et al., 2011), and as well as increases the efficiency of breeding programs and achieving crop improvement (Manning et al., 2006; Seymour et al., 2008). However, compared with the application of population genetics that has revealed how genetic diversity, structure and linkage/association analysis can be performed (Fisher et al., 2013; Ye et al., 2015; Du et al., 2016), the significance of variation in epigenetic states at the population level presents a complex challenge and remains largely unexplored (Richards, 2008; Cao et al., 2011). This difference exists because epialleles as a cause of phenotypic variance are more difficult to identify than genetic variation associated with DNA mutations (Chodavarapu et al., 2012).

Herein, in order to investigate epigenetic indices of diversity and structure, as well as the relationships between epigenetic variants and genetic variations, environmental factors, and traits, we used the amplified fragment length polymorphism (AFLP) and methylation-sensitive amplified polymorphism (MSAP) techniques together with multivariate statistics and association analysis, as well as short fragment sequencing to search for markers in the *P. mume* genome. We also explored the function of candidate marker-linked genes based of the sequences of candidate markers. Our results will help breeders to understand and use epigenetic variation to accelerate the improvement of *P. mume* plants.

# MATERIALS AND METHODS

## Plant Material and DNA Isolation

Three groups of two people each collected and measured leaf samples from 1a branches of 96 accessions of *P. mume*. The leaves were snap-frozen in liquid nitrogen for DNA extraction and genotyping. Thirty leaves of each genotype from the three populations were harvested with three replications and this collection was performed in the main areas where wild plants of *P. mume* are distributed, namely, southwest China and southeast China, as well as sites where they are cultivated (**Figure 1**), on 11–21 September 2013. Leaf shape traits, including length, width, area, and ratio of length to width, were measured using a portable laser leaf area meter (CI-202, CID Bio-Science, Inc., United States) and tested using one-way analysis of variance (ANOVA). The geographic coordinates and altitude were recorded using a handheld GPS (UniStrong, Co., Ltd., China) (Supplementary Table 1). Plant materials were ground in liquid nitrogen and total DNA was isolated using the CTAB method, detected using a NanoVue UV/visible spectrophotometer (GE Healthcare Limited, Sweden), and stored at −80°C (Ma et al., 2013).

## Meteorological Data

Meteorological data, including average, lowest, and highest daily temperatures, average and minimum daily relative humidity, total daily precipitation, and total daily sunshine time, between 01 September 2012, and 31 August 2013, were acquired from a Chinese meteorological data sharing service[1]. Parameters of annual and monthly average temperatures, average daily lowest and average daily highest temperatures, average relative humidity, average minimum relative humidity, total precipitation, and total sunshine time, were then calculated (Supplementary Table 1).

## Detection of Genetic Markers

To detect genetic markers, an AFLP technique including digestion with the combination of restriction endonucleases

[1]http://www.cma.gov.cn/2011qxfw/2011qsjgx/

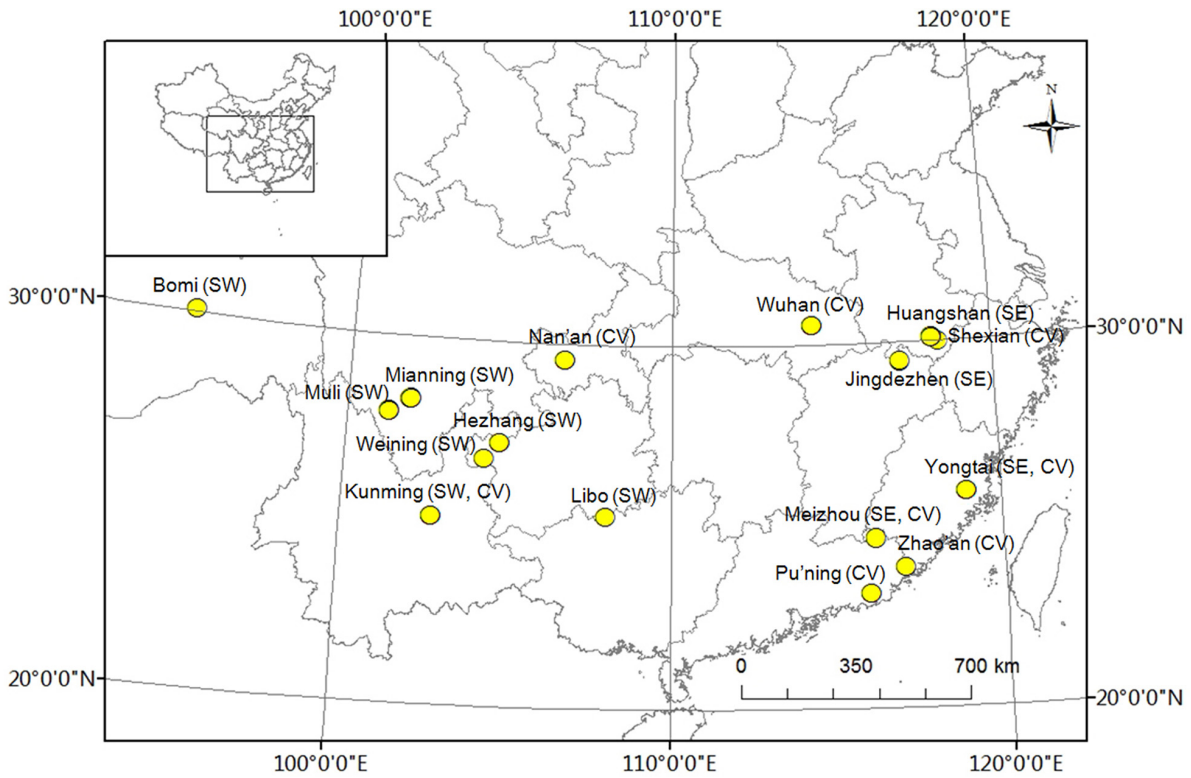


**FIGURE 1 |** Distribution of experimental *Prunus mume* samples. 'SW' represents samples collected in southwest China, 'SE' represents samples collected in southeast China, and 'CV' represents cultivated varieties.

*Eco*RI and *Mse*I, ligation, and pre- and selective-amplification was adopted, in accordance with the work of Vos et al. (1995). The 15 fluorescently labeled primer pairs used for *Eco*RI/*Mse*I enzyme combination AFLP selective-amplifications were shown in Supplementary Table 2. Instead of silver staining, a fluorescent capillary electrophoresis detection method (Beijing Microread Gene Technology, Co., Ltd., Beijing, China) that is more sensitive, faster, and safer was used to resolve the selective amplification products. Marker bands were revealed by GeneMarker V1.7.1 and transformed into a binary character matrix with "0" for absence and "1" for presence (Ma et al., 2013).

## Detection of Genomic Methylation Markers

The MSAP marker detection procedure was adapted from Ma et al. (2013) and was similar to the AFLP technique described above, except for the double digestion with the restriction endonuclease combinations *Eco*RI/*Hpa*II and *Eco*RI/*Msp*I and the use of corresponding adapters and fluorescently labeled primers instead of *Eco*RI/*Mse*I. The 15 fluorescently labeled primer pairs used for the MSAP selective amplifications with the *Eco*RI/*Hpa*II and *Eco*RI/*Msp*I enzyme combinations were shown in Supplementary Table 3. Epigenetic bands generated from GeneMarker V1.7.1 were transformed into a binary character matrix with "0" for absence and "1" for presence.

## Statistical Analysis of Diversity, Methylcytosine Level, and Structure

Environmental factors included geographic coordinates and meteorological information, and the annual (01 September 2012 to 31 August 2013) and monthly (01 August 2013 to 31 August 2013) values of which were estimated using the daily data downloaded from the database of a Chinese meteorological data sharing service (Supplementary Table 1). These data were transformed in ADE-4 software as:

$$x_{ij} \mapsto (x_{ij} - m_j)/s_j \text{ with}$$

$$m_j = \sum_i p_i x_{ij} \text{ and } s_j = \sqrt{\sum_i p_i (x_{ij} - m_j)^2}$$

where $x_{ij}$ represents the value of the $i$th and $j$th columns and $p_i$ represents the $i$th row weight (Thioulouse et al., 1996).

The AFLP markers were used to investigate genetic diversity and structure. These genetic markers were analyzed using STRUCTURE v.2.3.4 software to detect uniformity within each population based on Bayesian clustering (Evanno et al., 2005). Genetic diversity ($I$, Shannon's information index; $h$, genetic diversity; $uh$, unbiased genetic diversity) was estimated using GenAlEx 6.5 (Peakall and Smouse, 2012), the genetic differentiation coefficient was calculated as $G_{ST} = (h_{total} - h_{pop})/h_{total}$ and the gene flow was estimated as $Nm = (1 - G_{ST})/4 G_{ST}$ (McDermott and McDonald, 1993; Bussell, 1999).

The among-population variances were also structured and maximized using a between-group eigenanalysis, namely, between-group principal component analysis (BPCA)-PCA among groups based on the PCA among individuals (Parisod and Christin, 2008). Based on Euclidean distances, this method can divide the genetic variance into within- and between-population components, enabling $\beta_{ST}$, equal to the ratio of the inertia between populations to the total inertia and analogous to the *F*-statistic, to be obtained (Parisod et al., 2005). The significance of differences among populations was determined by a Romesburg randomization test (9999 permutations) in ADE-4 software (Thioulouse et al., 1996).

The MSAP markers were used to calculate epigenetic variance and the "0, 1" matrix was transformed and redefined. Four patterns of methylation were defined according to the emerging bands: (i) present in both *Eco*RI/*Hpa*II and *Eco*RI/*Msp*I (1,1), non-methylation; (ii) absent in *Eco*RI/*Hpa*II but present in *Eco*RI/*Msp*I (0,1), full methylation; (iii) present in *Eco*RI/*Hpa*II but absent in *Eco*RI/*Msp*I (1,0), hemi-methylation; and (iv) absent in both *Eco*RI/*Hpa*II and *Eco*RI/*Msp*I (0,0), uninformative methylation. We defined an additional pattern of methylation as, (v) total methylation, the summation of full methylation and hemi-methylation (Ma et al., 2012; Ci et al., 2015).

The methylation/non-methylation levels were defined as the ratio of the number of bands with one pattern to the total number of bands in one genotype or population. These methylation/non-methylations are relative because only 5′-CCGG sites, not all methylcytosine residues, can be detected using MASP. Within each population, relative full methylation and hemi-methylation levels, and relative total methylation and non-methylation levels were compared by Wilcoxon's rank-sum test. Among populations, the relative total methylation and non-methylation levels, and relative full methylation and hemi-methylation levels were both examined using a Kruskal–Wallis *H* test (Lira-Medeiros et al., 2010).

Scoring epiloci with (i) non-methylation and (iv) uninformative methylation as "0," and epiloci with (ii) full methylation and (iii) hemi-methylation as "1," we reconstructed a methylation-sensitive polymorphism (MSP) profile and calculated the epigenetic diversity (*I**, Shannon's information index; *h**, epigenetic diversity; *uh**, unbiased epigenetic diversity) by using GenAlEx 6.5 (Foust et al., 2016). Significant differences in epigenetic diversity among populations were detected by the Kruskal–Wallis *H* test. The epigenetic differentiation coefficient was calculated as $G_{ST}^* = (h_{total}^* - h_{pop}^*)/h_{total}^*$ (McDermott and McDonald, 1993; Bussell, 1999).

Based on the MSP profile, we determined the epigenetic variance and structure among populations using a between-group eigenanalysis, similar to the method described above. The contributions of epigenetic and genetic profiles to variance of the structured population were evaluated using a symmetrical co-inertia analysis. The test of significant differences in epigenetic and genetic structures was performed by 9999 Monte Carlo permutations in ADE-4 software (Thioulouse et al., 1996). Similarly, a cooperative structure with matching information between the epigenetic matrix and environmental factors was also established according to the processes of ADE-4.

## Association Analysis and Sequencing of the Candidate Markers

To investigate the correlation between relative methylation level and phenotype, we performed a linear correlation analysis (Ma et al., 2012), as well as an association analysis using an MLM model within the software package TASSEL 2.1 (Bradbury et al., 2007). Parameters of membership probability (Q-matrix) and pairwise kinship (K-matrix), which were used to evaluate the effects of population genetic structure and relatedness between each pair of individuals, were estimated based on 1,864 AFLP markers following the operating processes of the STRUCTURE v.2.3.4 and TASSEL 2.1 software packages, respectively. Epimarker association analysis was performed similarly to genetic marker association using the same Q-matrix and K-matrix, but with the four epigenotype patterns: (i) non-methylation, (ii) full methylation, (iii) hemi-methylation, and (iv) uninformative site.

The products generated from the AFLP and MSAP selective amplifications were monitored using polyacrylamide gel electrophoresis (PAGE) and silver staining techniques as described by Bassam et al. (1991), respectively. Candidate markers were recycled based on the PAGE results, and reamplified, transformed, and cloned (Ma et al., 2012). Positive clones were detected using the selective-amplification protocol described above, and sequenced at Ruibiotech Co., Ltd. (Beijing, China). Sequences homology analysis and function prediction were performed using the NCBI[2] and JGI[3] databases.

# RESULTS

## Genetic Diversity and Structure

We used an AFLP technique with 15 selective primer-pair combinations to detect polymorphic sites in the *P. mume* genome. A total of 1,864 polymorphic markers were detected out of 2,254 total bands (Supplementary Table 2). The genetic diversity of each of the 96 accessions was calculated and showed a high level of genetic diversity, as evaluated globally by Shannon's diversity index ($I = 0.484$), and Nei's gene diversity index ($h = 0.319$). However, the gene diversity index ($h$) among the three populations, measured as 0.305 (cultivated population), 0.291 (wild population in southwest China), and 0.293 (wild population in southeast China), did not differ significantly ($P = 0.105$). This might be caused by a downward bias produced by related or inbred individuals within the accessions (Degiorgio et al., 2010). Therefore, another parameter, the gene unbiased diversity ($uh = 0.322$) that showed a significant difference ($P = 0.006$) among the populations, was introduced. A low genetic differentiation coefficient ($G_{ST} = 0.044$) and high gene flow ($Nm = 5.432$) of the cultivated population indicated there was strong gene exchange among the cultivated individuals,

[2]https://www.ncbi.nlm.nih.gov/

[3]https://phytozome.jgi.doe.gov/pz/portal.html

possibly a result of selective breeding from objective traits. In contrast, the high $G_{ST}$ and low $Nm$ of wild types indicated a high level of population differentiation and low gene exchange, respectively (**Table 1**).

Genetic structure was analyzed first using a Bayesian clustering test ($K = 3$, Ln Pr(X|K) $= -83680.1$), which showed that the 96 accessions could be divided into three populations that were significantly separated from each other (**Figure 2A**). Then, the same molecular profile was used for eigenanalysis (BPCA-PCA among groups based on the PCA among individuals), which, as expected, produced the same division (**Figure 2B**). According to eigenanalysis, the molecular genetic variation based on each individual, and visualized as a two-dimensional plot produced by PCA using the first two principal components (F1 = 65.69%, F2 = 34.31%), could be divided into two parts, namely, between (inertia = 17.95) and within (inertia = 279.39) populations ($P < 0.001$), similar to $F$-statistics. These results verified the reliability of the classification of the 96 accessions into three populations.

## Relative Genomic Methylation Levels

The MSAP approach identified methylation sites by double digestion of total DNA with *Eco*RI/*Hpa*II or *Eco*RI/*Msp*I. A total of 2,849 markers which ranged in length from 59 to 712 bp and had 2,810 polymorphic sites were identified (Supplementary Table 3). Only 5′-CCGG sites, not all methylcytosines, were identified in the whole genome. Therefore, the methylation and non-methylation levels in the genome of *P. mume* are relative and were classified as relative full methylation (14.03%), relative hemi-methylation (15.77%), relative total methylation (29.80%), relative non-methylation (31.83%), and uninformative sites (38.37%). The results showed that relative hemi-methylation was significant higher than relative full methylation ($P = 0.005$), but the difference between the relative total methylation level and relative non-methylation level was not significant (**Table 2**). These results suggested that different patterns of DNA methylation levels may play important roles within the *P. mume* genome.

A significant difference in relative total methylation among the three populations was detected by Kruskal–Wallis $H$ test ($P = 0.021$) (**Table 2** and Supplementary Figure 1). In addition, the relative total methylation level of the cultivated plants was higher than the relative total methylation levels of the wild plants in the southwest and southeast China populations (Supplementary Figure 1). In each population, no significant difference was detected between relative hemi-methylation and full methylation levels, or no significant difference was found between relative total methylation and non-methylation levels indicating the environmental plasticity of DNA methylation levels (Supplementary Figure 1).

## Epigenetic Diversity and Its Comparison with Genetic Diversity

Based on the MSAP markers of each individual, the three parameters, Shannon's diversity index ($I^*$), epigenetic diversity index ($h^*$) and epi-gene unbiased diversity ($uh^*$), were assessed and showed that the epigenetic diversity was significant difference among the three populations ($P < 0.001$). Compared with the results obtained using the genetic information, all three parameters were higher ($I^* > I$, $h^* > h$, $uh^* > uh$) although they showed similar tendencies (**Tables 1**, **3**). Together with the parameters $I$ and $h$ displayed no significant differences among the three populations, the results indicated that the epigenetic diversity ($I^*$ and $h^*$) of *P. mume* was high with a low epigenetic differentiation coefficient ($G_{ST}{}^* = 0.033$) and was easily affected by the environment (or cultivation). Further, the epigenetic diversity index of the wild population in southwest China was lower than the epigenetic diversity index of the wild population in southeast China. A high epigenetic differentiation coefficient (0.064) was obtained for the wild population in southwest China (**Table 3**), and this phenomenon occurred within epigenetic markers, indicating that high epigenetic variation was present in the population of southwest China.

## Epigenetic Structure and Its Relationships with Genetic Structure, and Environment

Based on the MSP profile, a between-group analysis was carried out and the epigenetic variance was visualized in a two-dimensional plot based on the first two principal components explaining 100% of the variance, which was separated into between- (inertia = 13.79) and within-group components (inertia = 538.24). The analysis revealed that the 96 accessions of *P. mume* significantly separated into three populations based on epigenetic markers ($P < 0.001$) (**Figure 2C**), which was similar to the result based on genetic markers. Thus, the population division based on epigenetic

**TABLE 1 |** The genetic diversity, differentiation coefficient and gene flow across the three populations[a].

| Populations | Number | *Na* | *Ne* | *I* | *h* | *uh* | $G_{ST}$ | *Nm* |
|---|---|---|---|---|---|---|---|---|
| Cultivated population | 59 | 1.967 | 1.506 | 0.466 | 0.305 | 0.310 | 0.044 | 5.432 |
| Wild population in southwest China | 23 | 1.852 | 1.485 | 0.442 | 0.291 | 0.304 | 0.089 | 2.559 |
| Wild population in southeast China | 14 | 1.776 | 1.490 | 0.444 | 0.293 | 0.316 | 0.081 | 2.836 |
| Mean | 32 | 1.865 | 1.494 | 0.451 | 0.296 | 0.310 | — | — |
| Total | 96 | 2 | 1.535 | 0.484 | 0.319 | 0.322 | 0.071 | 3.271 |

[a] *The significance of differences among populations was analyzed by Kruskal–Wallis H test (I, chi-square = 4.230, df = 2, P = 0.121; h, chi-square = 4.505, df = 2, P = 0.105; uh, chi-square = 10.299, df = 2, P = 0.006).*

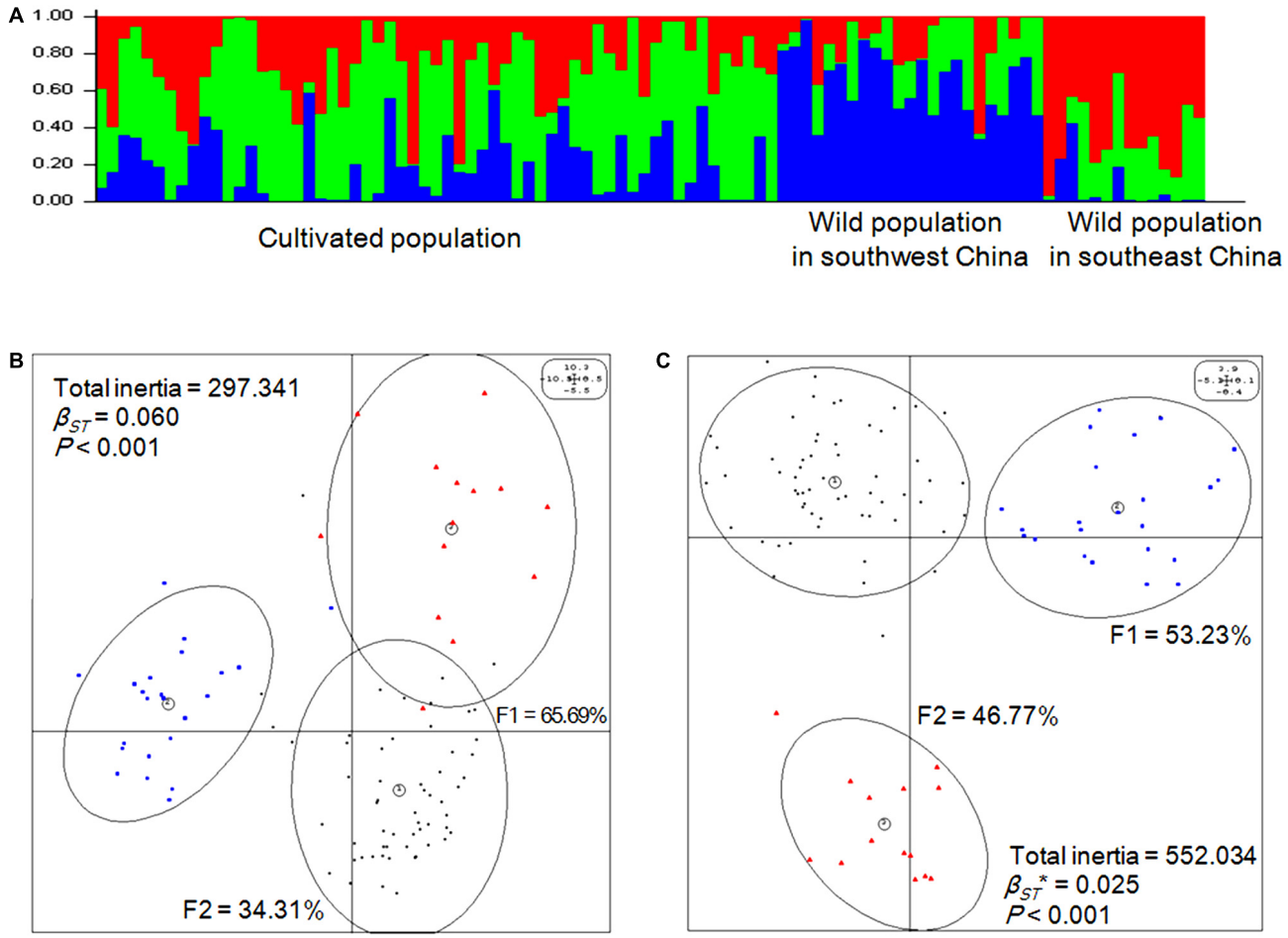


**FIGURE 2 |** Genetic and epigenetic structures of *Prunus mume*. **(A)** Genetic populations were detected using STRUCTURE (v.2.3.4) software [$K$ = 3, Ln Pr(X| K) = −83680.1] based on Bayesian clustering. **(B)** Eigenanalysis among the three populations of *P. mume* using principal component analysis (PCA) values generated from genetic covariance matrices based on the AFLP profile. F1 and F2 values show the contributions of the first two principal components summarizing the total variance of each data set. $\beta_{ST}$ was calculated by between-group PCA (BPCA) for genetic profiles and tested with Romesburg randomization permutations. Numbers within circles represent the populations: (1) cultivated population, each individual genotype is represented by a small dark circle; (2) wild population in southwest China, each individual genotype is represented by a blue quadrate; (3) wild population in southeast China, each individual genotype is represented by a red triangle. **(C)** Eigen analysis among the three populations of *P. mume* using PCA values generated from epigenetic covariance matrices based on the methylation-sensitive polymorphism (MSP) profile. $\beta_{ST}$* was calculated by BPCA for epigenetic profiles and tested with Romesburg randomization permutations. Numbers within circles represent the populations: (1) cultivated population, each individual epigenotype is represented by a small dark circle; (2) wild population in southwest China, each individual epigenotype is represented by a blue quadrate; (3) wild population in southeast China, each individual epigenotype is represented by a red triangle.

markers was consistent with population division based on genetic markers.

Next, the relationships between epigenetic structure and genetic structure, and environmental factors were revealed by co-inertia analysis, respectively. The markers and environment factors were transformed into multi-dimensional spatial based on Euclidean distance (Thioulouse et al., 1996), to reveal the distribution of MSAP marker within the spatial constitution of AFLP, and environmental factors. The space matching information of epigenetic and genetic markers was visualized using the first two principal components explaining 12.11% of the co-inertia, which revealed notable cooperativity ($P < 0.001$) in their structures (**Figure 3A**). The relationship between epigenetic structure and environmental factors also exhibited cooperativity ($P < 0.001$), and the first two principal components in the profiles explained 48.90 and 19.36% of the co-inertia, respectively (**Figure 3B**). These results indicated that the epigenetic structure shared common units and performed cooperativity with both the genetic structure, and environmental structure.

## Leaf Shape Traits and Linear Correlation, Association Analyses

The leaf shape traits (including leaf length, 6.24 ± 1.51 cm; width, 3.80 ± 0.84 cm; area, 16.85 ± 6.51 $cm^2$; and ratio of length to width, 1.65 ± 0.18) displayed normal distribution and

significant differences among the three populations (**Figure 4A**). Linear correlation analysis (two-tailed) showed that the relative full methylation level and relative total methylation level were positively correlated with leaf length, width, and area, but the relative uninformative loci were negatively correlated with leaf length, width, and area (**Figure 4B**). These results suggested that DNA methylation levels were correlated with positive regulation of leaf phenotype.

Next, we performed an association analysis to examine the relationship between molecular markers and leaf shape traits based on an MLM model within the Tassel 2.1 software package (Bradbury et al., 2007). In total, 113 multi-function and 90 trait-specific associated genetic markers were detected. Among these 203 AFLP markers, 109, 105, 62, and 105 (explaining 1.69–8.73% of variation) were significantly associated with leaf length, width, area, and ratio of length to width, respectively (**Figure 5A** and Supplementary Table 4). As shown in **Figure 5B**, 423 MASP markers, including 181 multi-function and 242 trait-specific markers, were associated with phenotype. Among them, 188, 164, 168 and 175 MSAP markers (explaining 1.76–15.42% of variance) were associated with leaf length, width, area, and ratio of leaf length to width, respectively. Among these markers, 46, 43, 13, and 140 were trait-specific and associated with leaf length, width, area, and ratio of leaf length to width, respectively (**Figure 5B** and Supplementary Table 5). These associated genetic/epigenetic markers provide important molecular evidence that can be used to reveal the gene regulation of complex quantitative traits of leaf.

## Function Prediction of the Linkage Genes

The candidate markers were sequenced following the PAGE and silver staining processes (Supplementary Figure 2) to predict the functions of the linkage genes. A total of 38 AFLP and 30 MSAP markers associated with leaf traits (explaining 1.70–8.73% and 3.45–6.61% of the traits variation, respectively) were sequenced successfully (Supplementary Data 1). Homology analysis (Supplementary Table 6) showed that one candidate maker-linked gene was origin from chloroplast [*PmcpGENE-1* (MSAP-2258)] and two were from mitochondria [*PmMatR* (AFLP-1128) and *PmmtGENE-1* (MSAP-2046)]. Five maker-linked genes were transcription factor genes [*PmTCP1* (AFLP-1113), *PmMatR* (AFLP-1128), *PmmTERF5* (AFLP-1475), *PmGATA5-LIKE* (MSAP-2025), and *PmTIFY4B-LIKE* (AFLP-2491)]; four maker-linked genes encoded chloroplast proteins [*PmCGS* (AFLP-950), *PmmTERF5* (AFLP-1475), *PmQS* (MSAP-1679), *PmPPR* (MSAP-1954)]; and three makers linked genes encoded mitochondria proteins [*PmLBD1-LIKE* (AFLP-305), *PmSHM2* (AFLP-512), *PmMatR* (AFLP-1128)] (Supplementary Table 6).

Importantly, as displayed in Supplementary Table 6, these marker-linked genes were enriched in the following GO terms: leaf development [*PmLBD1-LIKE*(AFLP-305)], glycine hydroxymethyltransferase activity [*PmSHM2* (AFLP-512)], RNA splicing [*PmMatR*(AFLP-1128)], signal transduction [*PmCaMBPs* (AFLP-543)], transporter activity [*PmNPF6.1* (MSAP-2230)], ATP binding [*PmTCP1* (AFLP-1113)],

**TABLE 2 |** Relative genomic methylation/non-methylation levels in the three populations of *Prunus mume*.

| | Mean | *SD* | CV (%) | Min | Max | Significant difference among populations[a] | | |
|---|---|---|---|---|---|---|---|---|
| | | | | | | $\chi^2$ | *df* | *P*-value |
| Hemi-methylation[b] | 15.77 | 3.41 | 21.62 | 7.72 | 27.69 | 4.586 | 2 | 0.101 |
| Full methylation[b] | 14.03 | 3.56 | 25.35 | 7.69 | 24.29 | 3.466 | 2 | 0.177 |
| Total methylation[b] | 29.80 | 4.33 | 14.53 | 17.97 | 40.75 | 7.732 | 2 | 0.021 |
| Non-methylation[b] | 31.83 | 7.11 | 22.35 | 18.85 | 59.50 | 1.189 | 2 | 0.552 |
| Uninformative locus | 38.37 | 6.11 | 15.93 | 18.74 | 49.84 | 5.240 | 2 | 0.073 |

[a]*The significance of differences among the three populations was examined by Kruskal–Wallis H test.* [b]*Significant difference between relative hemi-methylation and full methylation levels was examined by Wilcoxon's rank-sum test (Z = −2.817, df = 1, P = 0.005). Significant difference between relative total methylation and non-methylation levels was examined by Wilcoxon's rank-sum test (Z = −1.678, df = 1, P = 0.093).*

**TABLE 3 |** Epigenetic diversity and differentiation coefficient among the three populations[a,b].

| Populations | Number | *Na** | *Ne** | *I** | *h** | *uh** | $G_{ST}$* |
|---|---|---|---|---|---|---|---|
| Cultivated population | 59 | 1.992 | 1.683 | 0.570 | 0.389 | 0.396 | 0.004 |
| Wild population in southwest China | 23 | 1.959 | 1.634 | 0.545 | 0.368 | 0.385 | 0.064 |
| Wild population in southeast China | 14 | 1.925 | 1.680 | 0.560 | 0.383 | 0.413 | 0.025 |
| Mean | 32 | 1.958 | 1.666 | 0.558 | 0.380 | 0.398 | — |
| Total | 96 | 2 | 1.690 | 0.575 | 0.393 | 0.397 | 0.033 |

[a]*Among-population significance test of parameters, I* (chi-square = 65.890, df = 2, P < 0.001), h* (chi-square = 69.279, df = 2, P < 0.001), and uh* (chi-square = 217.872, df = 2, P < 0.001), was carried out by Kruskal–Wallis H test.* [b]*Comparison of diversity parameters between genetic and epigenetic levels was carried out by Kruskal–Wallis H test (I*, chi-square = 254.628, df = 1, P < 0.001; h*, chi-square = 254.628, df = 1, P < 0.001; uh*, chi-square = 254.628, df = 1, P < 0.001).*

NAD biosynthetic process [*PmPEPC-LIKE* (MSAP-2760)], *S*-adenosylmethionine-dependent methyltransferase activity [*PmPMT7* (AFLP-1834)], and transcription factor activity. These genes may be essential for plant morphology, development, and energy metabolism in *P. mume*.

# DISCUSSION

Many epimutations have been revealed to influence phenotypes in plants (Cubas et al., 1999; Manning et al., 2006; Seymour et al., 2008) and advances have been made in the emerging subfield of population epigenetics, which addresses questions about the prevalence and importance of epigenetic variation in the natural world (Richards, 2008). However, little is known about epialleles at the population level and their mechanism of inheritance in relation to genetics; that is, whether it occurs randomly or non-randomly (Massicotte et al., 2011; Becker and Weigel, 2012), whether epialleles can be retained or revert to their original state in response to changes in the environment or selection, and what substantial functions do they perform. In this study, we aimed to uncover the relationships between epigenetics and genetics, environment, and leaf shape traits, in the ornamental tree *P. mume* on basis of: (i) Leaves from 96 accessions were harvested from the 1a branches on 11–21 September 2013, and meteorological data were collected from 01 September 2012 to 31 August 2013 that overlapped with the main growth period of 1a branches and leaves, to minimize statistical errors. (ii) The sample individuals widely distributed in China were separated into three populations by a Bayesian clustering test using AFLP markers within STRUCTURE v.2.3.4. (iii) Leaf traits, important elements for biomass, displayed normal distribution and were examined significant different among the three populations.

## Cooperativity of Epigenetic and Genetic Structures Were Determined

Wild *P. mume* is distributed across a wide stretch of mainland China and little is presently known about the epigenetic diversity or structure in the wild population, although the parameters of genetic diversity and structure are well known in cultivated varieties (Yang et al., 2007; Shen et al., 2011; Sun et al., 2014; Zhang J. et al., 2015; Zhang et al., 2017). In this study, we used cultivated plants and wild individuals from southwest and southeast China to reveal the genetic and epigenetic diversity in this species. We showed that the genetic diversity of 96 accessions was lower than the epigenetic diversity, and that the epigenetic diversity differed significantly among the three populations, which suggested that epigenetics might contribute more than genetics to variation among populations, although some information on the epigenetic diversity represented by the pattern of total methylcytosine was missed by summing hemi-methylation and full methylation based on MSAP markers. The gene flow parameter showed strong gene exchange for the cultivated population, as expected, during artificial domestication and selection based on AFLP markers. Our findings indicated that the epigenetic diversity was not quite consistent with the genetic diversity.

We also investigated the genetic and epigenetic structures among the three populations of *P. mume* and used statistical analyses to reveal that the genetic $\beta_{ST}$ value (0.060) was higher than the epigenetic one (0.025), which suggested that the genetic variation resulted more strongly from population grouping than from epigenetic variation. This result is similar to findings reported previously for populations of two salt marsh perennials (Foust et al., 2016); however, opposite results were obtained in oak populations (Platt et al., 2015). Thus, the controversy over whether epigenetic changes are dependent on genetic variation remains. At a genome-wide scale, genetic and epigenetic variance were found to perform as one synergistic structure based on AFLP and MSAP markers, as revealed using co-inertia analysis. Further, the AFLP and MSAP markers, which provided a genome-wide snapshot of epigenetic and genetic variations, had a similar spatial distribution. The existence of a link between epigenetic and genetic variations is still unclear because information about the heredity of epigenetic loci and their relationship with genetic loci has been obtained only for a few populations. One perspective is that DNA methylation could be a source of random variation in natural populations (Massicotte et al., 2011). In contrast, Becker and Weigel (2012) suggested that DNA methylation patterns do not fluctuate randomly from one generation to the next, but neither are they completely stable. To resolve these issues, we believe that sequencing epiloci and determining of the rules regarding the presence or absence of a link between epigenetic and genetic variations offer the best approach.

## Linear Correlations between Relative Methylcytosine Levels and Leaf Traits

The patterns and levels of methylcytosine are considered to differ among different plants, within a single species at different developmental stages, and in different environments (Messeguer et al., 1991; Xiong et al., 1999; Hauben et al., 2009). The relative methylcytosine levels in the *P. mume* genome were calculated as the ratio of the number of patterns to the total bands. The relative total methylation level was 29.80%, and the relative total methylation levels differed significantly among the three populations. In perennial woody plant *Populus tomentosa* genomes, relative methylcytosine levels were 26.57% (natural populations) and 17.86% (F1 population) (Ma et al., 2012, 2013), and in *Populus simonii*, the relative methylcytosine level was 26.61% (Ci et al., 2015). In the model plant *Arabidopsis thaliana*, 32.4% of cytosines were found to be methylated in a genome-wide survey, including 24% CG methylation, 6.7% CHG methylation, and 1.7% CHH methylation (Jacobsen, 2011). Accordingly, a high level of methylcytosine is present in the genomes of higher plants.

Evidence has shown that an increase or decrease of DNA methylation level may affect gene expression and result in various phenotypic changes, and genes methylated in transcribed regions are highly expressed and constitutively active (Zhang et al., 2008). We found that leaf length, width, and area of *P. mume* were

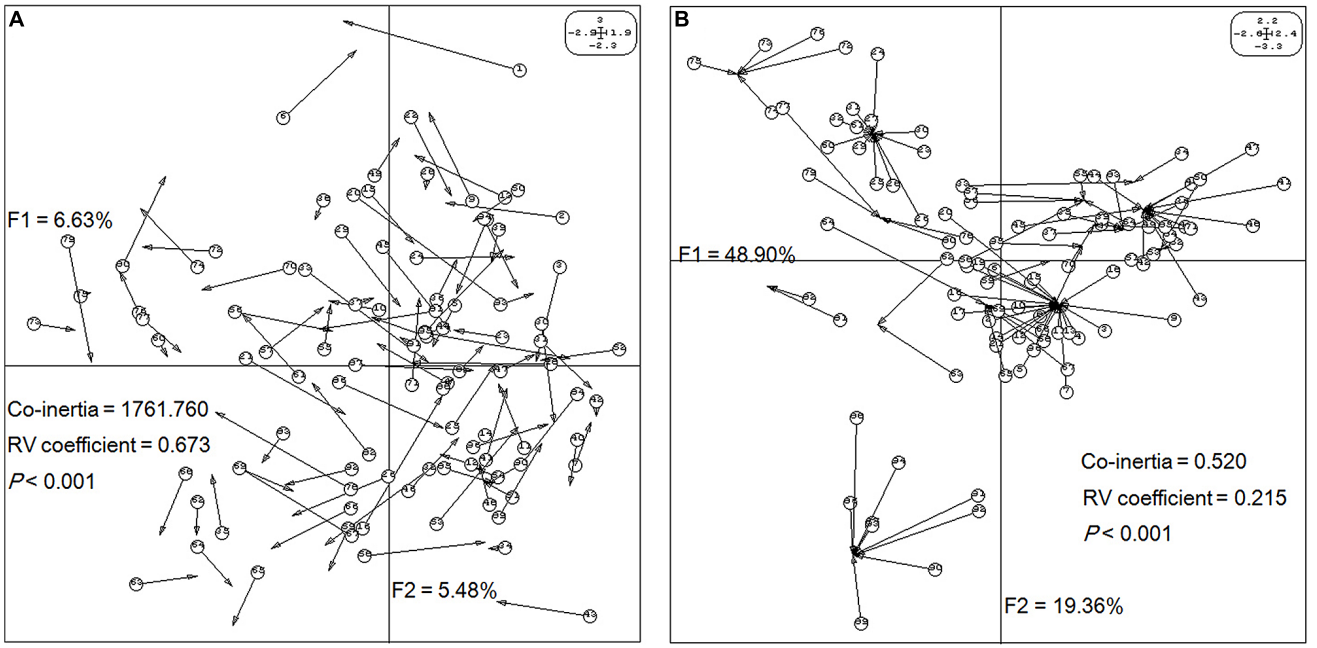


**FIGURE 3 |** Structure matching analysis of *Prunus mume* based on genetic variables, epigenetic variables, and environmental variables. F1 and F2 values show the contributions of the first two principal components summarizing the total variance of each data set. **(A)** Co-inertia analysis of *P. mume* using principal component analysis (PCA) scores based on a methylation-sensitive polymorphism (MSP) covariance matrix (epigenetic variables) and AFLP covariance matrix (genetic variables). Each arrow positions an individual by its epigenetic variables (arrow start and number in a circle) and its genetic variables (arrow end). **(B)** Co-inertia analysis of *P. mume* using PCA scores based on a MSP covariance matrix (epigenetic variables) and environmental covariance matrix (environmental variables). Each arrow positions an individual by its epigenetic variables (arrow start and number in a circle) and its environmental variables (arrow end).

positively correlated with relative full and total methylation levels, which is similar to the previous finding that DNA methylation was positively correlated with growth traits and photosynthetic characteristics in poplar (Gourcilleau et al., 2010; Ma et al., 2012; Ci et al., 2015).

## Both Alleles and Epialleles Induce Variety of Leaf Traits

Linkage and association analyses are mature statistical techniques that are used to understand genetic markers and their function for molecular-assisted selective breeding in hybridization and natural populations (Ci et al., 2015; Ye et al., 2015). In *P. mume*, 120 simple sequence repeats (SSRs) and 1,484 single nucleotide polymorphisms (SNPs) that explaining 3–12% of the phenotypic variance of growth and leaf traits were detected (Sun et al., 2014). And by using SLAF-seq and whole-genome re-sequencing techniques, Zhang J. et al. (2015) and Zhang et al. (2017) successfully constructed a high-density genetic map for an F1 population and located a region on linkage group 7 that was strongly responsible for the weeping trait, and its functional effect was also analyzed. In poplar, although they ignored actual genetic relationships between individuals or metastable property of epigenetics in populations, Ma et al. (2012) and Ci et al. (2015) provided a new strategy for identifying epimarkers linked or associated with traits. However, the parameters relevant to both of the genetic and epigenetic markers were also ignored. We compared the uniformity of genetic and epigenetic structures and found they gave a cooperative structure that could be used to consider the genetic relationship, but not intergenerational relationships, between individuals of wild and cultivated *P. mume*. Therefore, the Q-matrix and K-matrix parameters generated from the AFLP markers were shared by both genetic and epigenetic associations, thereby avoiding errors caused by epigenetic changeability in structured populations for the first time. In total, 203 genetic and 423 epigenetic markers associated with leaf shape traits were detected, and 38 and 30 of them were sequenced, respectively.

Homology analysis and function prediction indicated that the variations in leaf traits were induced by both allelic and epiallelic candidate genes that participate in morphological development, metabolism, stress defense, signal transduction, and molecular transport, and encode transcription factors. Some unannotated sequences were also found. Some of the candidate genes, including some that encode organellar protein and methyltransferase activity protein, are discussed below.

Plant-specific *LATERAL ORGAN BOUNDARIES DOMAIN (LBD)* is a key regulator of plant organ development. *ASYMMETRIC LEAVES1* (*AS1*) and *AS2*, two members of *LBD*, are required for the development of normal leaf polarity formation and shape, and for the repression of *KNOX* genes in the leaf (Semiarti et al., 2001; Lin et al., 2003; Xu et al., 2003). Ectopic expression of *LBD1-LIKE* gene leads to alterations in the size and morphology of leaves (Shuai et al., 2002; Evans, 2007). Thereby, the candidate marker-linked gene *PmLBD1-LIKE*

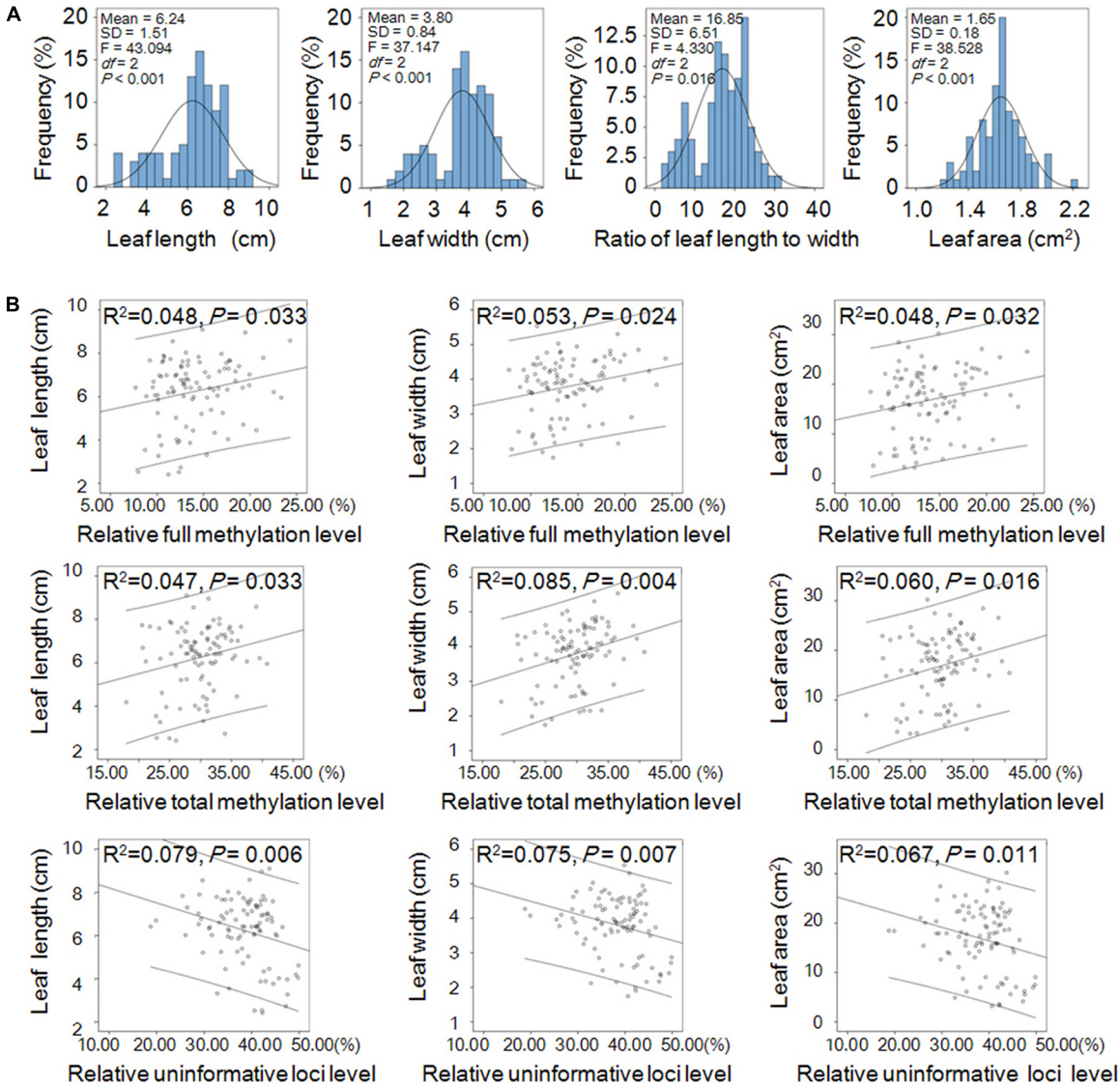


**FIGURE 4 |** Leaf shape traits and their linear correlations with relative DNA methylation levels in *Prunus mume*. **(A)** Frequency distribution of the shape traits including leaf length, width, area, and ratio of length to width of *P. mume* and one-way ANOVA ($P < 0.05$) among the three populations. **(B)** Linear correlations between leaf shape traits and relative DNA methylation levels. Abscissa and ordinate represent relative methylation/uninformative loci levels, and leaf phenotype, respectively. The 95% prediction limits are shown within the hyperbolas in each graph.

may participate in leaf development. Interestingly, one of the marker-linked genes, *PmPMT7*, was predicted to encode an *S*-adenosylmethionine-dependent methyltransferase activity protein, which has been found to be located in the Golgi, for DNA methylation (Santi et al., 1983; Nikolovski et al., 2012). The detection of *PmPMT7* among the marker-linked genes suggests that the encoded methyltransferase may regulate the variation of genomic methylation producing phenotypic variants of *P. mume*.

Three of the marker-linked genes encode the transcription factors PmmTERF5, PmTIFY4B-LIKE and PmGATA5-LIKE, which respond to stress, perform roles in regulating chloroplast homeostasis, leaf size and shape, and plant height (Bi et al., 2005; White, 2006; Kleine, 2012; Robles et al., 2012; Chung and Sunter, 2014). The transcription termination factor (mTERF) was first detected in human mitochondrial (Kruse et al., 1989) and then characterized in *A. thaliana* in both mitochondria and chloroplasts (Babiychuk et al., 2011). In plant, it plays important roles in affecting communication among chloroplasts, mitochondria, and the nucleus and leading to changes in the steady-state concentration of nuclear gene transcripts (Meskauskiene et al., 2009; Quesada et al., 2011; Romani et al., 2015). The *mda1* (*mTERF defective in Arabidopsis1*, *mterf5*) mutants exhibited altered chloroplast morphology and plant growth, and reduced pigmentation of cotyledons, leaves, stems and sepals (Robles et al., 2012). Similarly, *mterf4* (*bsm, rug2*) and *mterf9* showed defective chloroplast development,

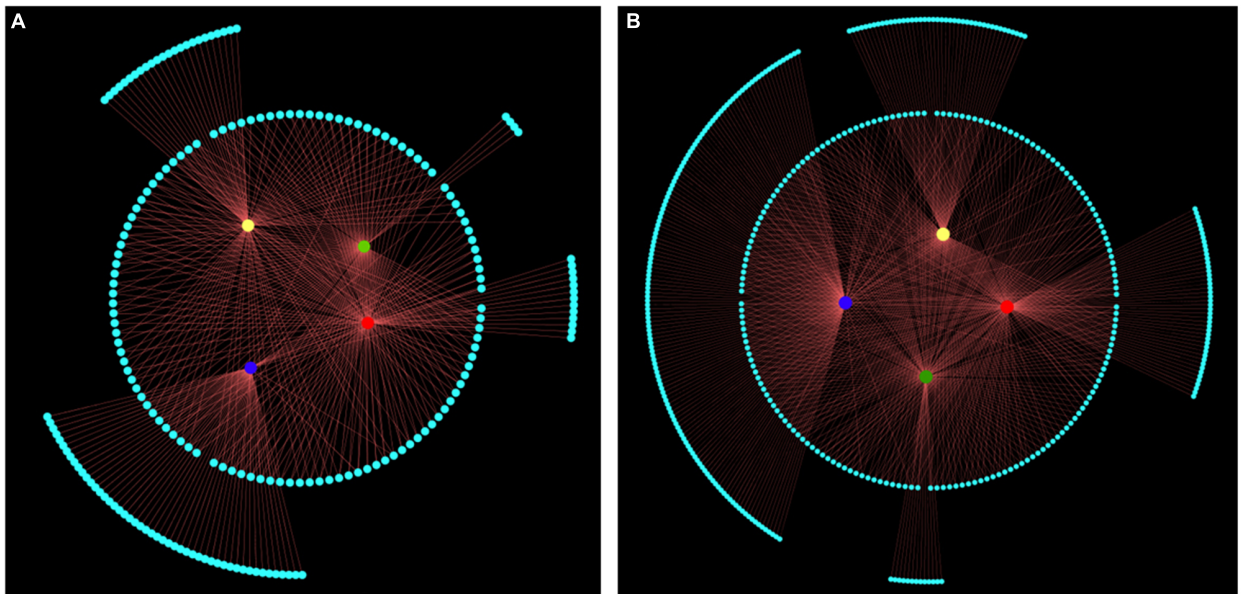


**FIGURE 5 |** All significant associated markers represented by structural networks ($P < 0.05$). Nodes in the innermost circle represent leaf length (red), width (yellow), area (green), and ratio of leaf length to width (blue). Nodes with gray color in the middle circle represent multi-function associated markers. Nodes with gray color in the outermost circle represent trait-specific associated markers. Edge size represents ratio of variant explained by associated markers, which explained 1.69-15.42% of leaf shape traits variance. **(A)** The 203 genetic markers associated with leaf length (total/trait-specific associated markers, 109/13), width (105/24), area (105/4), and ratio of leaf length to width (62/49). **(B)** The 495 epigenetic markers associated with leaf length (188/46), width (164/43), area (168/13), and ratio of leaf length to width (175/140).

which is likely to cause paleness, stunted growth, reduced mesophyll cell numbers and abnormalities in leaf development (Babiychuk et al., 2011; Quesada et al., 2011; Robles et al., 2015). And *mterf6-1* mutant, a defect in photosynthesis, is associated with reduced levels of photosystem subunits causing seedling lethality (Romani et al., 2015). The plant specific transcription factor TIFY, is classified into four subfamilies as TIFY, PPD, JAZ and ZML according to the different domain architectures (Yan et al., 2007; Melotto et al., 2008; Bai et al., 2011). Ye et al. (2009) identified 20 *TIFY* genes in rice genomes and found most of them were predominantly expressed in leaf and they displayed tempo-spatial expression patterns, suggesting that expression and function vary by stage of plant growth and development. And Zhang Z. et al. (2015) described that transcription of maize genes *ZmTIFY4*, *5*, *8*, *26,* and *28* was induced, while transcription of *ZmTIFY16*, *13*, *24*, *27*, *18,* and *30* was suppressed in response to drought stress. In *Arabidopsis*, deletion of the *PEAPOD* (*PPD*) locus increases leaf lamina size and results in dome-shaped rather than flat leaves (White, 2006). While AtTIFY4B with three domains (PPD, TIFY, and CCT_2) conserved between homologs from different plant species takes part in host defense against geminiviruses (Chung and Sunter, 2014). Similarly, *AtGATA5-LIKE*, regulating chlorophyll synthesis carbon and nitrogen metabolism, affects leaf blade extension (Reyes et al., 2004; Bi et al., 2005). Therefore, we considered that the candidate marker-linked genes *PmmTERF5*, *PmTIFY4B-LIKE* and *PmGATA5-LIKE* may take part in the development of leaf shape traits of *P. mume*.

*TCP1*, encoding a TCP transcription factor and containing a basic helixloop-helix (bHLH) domain, may play roles in regulating flower organ symmetry and dwarfed plants (Cubas et al., 2001; Koyama et al., 2010). It was also found that the activation tagged locus, *tcp1-1D*, can suppress the defective phenotypes of *bri1-5* resulted in dwarfed transgenic plants similar to typical *BR* deficient mutants, or signaling defective mutants (An et al., 2011). And the promoter of *TCP1* is active in the cotyledonary petioles and the distal part of the expanding leaves, as well as the midrib region and the petiole (Guo et al., 2010). It seems that *PmTCP1* may regulate the growth of leaves of *P. mume*.

Other candidate marker-linked genes were also detected. *PmSHM2* and *PmPEPC-LIKE* may encode proteins involved in core metabolic functions of mitochondria (Heazlewood et al., 2004; Engel et al., 2011), and play crucial roles in modulating the balance of carbon and nitrogen metabolism, respectively (Shi et al., 2015). *PmCaMBPS* may play a role in response to environmental stimuli (Snedden and Fromm, 1998; Zielinski, 1998; Bouché et al., 2005) and *PmNPF6.1* may encode a protein that transports a wide variety of substrates (Leran et al., 2014).

## Relationships between Epigenetics and Environment, and Artificial Cultivation

Epigenetics plays an important role in regulating gene expression and can be shaped by the environment, which provides insight into processes that function at the population level. Studies have revealed a correlation of environmental factors with epigenetic variances (Lira-Medeiros et al., 2010; Foust et al., 2016)

and an association with adaptive phenotypic plasticity (Nicotra et al., 2010, 2015; Ci et al., 2015). Our results showed there was a cooperative structure between epimarkers and environmental factors, suggesting that epigenetic variance could be induced through environmental shifts affecting the population of *P. mume*, a species that has been cultivated for more than 3,000 years. We used the cultivated individuals to detect the variance of epimarkers with the aim of discovering the relationship between epigenetic and breeding. According to recent studies, epigenetic variation could have a major role in improving breeding efficiency and strategies for crop improvement (Manning et al., 2006; Seymour et al., 2008; Mirouze and Paszkowski, 2011; Springer, 2013). It has also been proposed that epimutations associated with beneficial traits could be selected and stably inherited from one generation to the next mitotically and/or meiotically, free from environmental impact, as described by Cubas et al. (1999). With the significant variation between wild and cultivated populations in terms of epigenetic diversity and structure, and candidate epiallele which plays essential roles in the formation of trait variation, we suggest the epigenetic variation could be reconstructed and selected across the domestication and cultivation processes and it has significant meaning for molecular breeding.

## CONCLUSION

This study was established with the aim of investigating the relationships between epigenetic variance, and genetic variance, environment factors, and traits of *P. mume* using molecular markers, multivariable statistics, association analysis, as well as sequencing approaches. We found that epigenetic diversity was greater than genetic diversity in the three populations studied. The epigenetic structure and genetic structure, and environmental factors performed the similarly statistical units, respectively. It suggested that epigenetic variance was affected by both genetics and the environment. Importantly, linear correlation analysis showed that leaf traits were positively correlated with both relative full methylation and total methylation levels. After association analysis, cloning, and sequencing, 68 AFLP and MSAP candidate marker sequences were obtained, and their annotations indicated that some of these marker-linked genes were essential for leaf morphology development and metabolism. Our results imply that these markers may play critical roles in the establishment of leaf length, width, area, and ratio of length to width. These findings are significant for molecular-assisted selection (MAS) for ornamental plant improvement.

## AUTHOR CONTRIBUTIONS

KM and QZ designed the experiments. LS, TC, HP, and JW collected the plant materials and measured leaf traits. KM performed and analyzed the molecular markers test. KM and QZ wrote the manuscript. LS, TC, HP, and JW provided suggestions for revision.

## FUNDING

This work was supported by the Fundamental Research Funds for the Central Universities (Nos. BLX2013010 and 2016ZCQ02), the National Natural Science Foundation of China (No. 31501787), and the Special Fund for Beijing Common Construction Project.

## SUPPLEMENTARY MATERIAL

The Supplementary Material for this article can be found online at: https://www.frontiersin.org/articles/10.3389/fpls.2018.00041/full#supplementary-material

## REFERENCES

An, J., Guo, Z., Gou, X., and Li, J. (2011). *TCP1* positively regulates the expression of *DWF4* in *Arabidopsis thaliana*. *Plant Signal. Behav.* 6, 1117–1118. doi: 10.4161/psb.6.8.15889

Babiychuk, E., Vandepoele, K., Wissing, J., Garcia-Diaz, M., De-Rycke, R., Akbari, H., et al. (2011). Plastid gene expression and plant development require a plastidic protein of the mitochondrial transcription termination factor family. *Proc. Natl. Acad. Sci. U.S.A.* 108, 6674–6679. doi: 10.1073/pnas.1103442108

Bai, Y., Meng, Y., Huang, D., Qi, Y., and Chen, M. (2011). Origin and evolutionary analysis of the plant-specific TIFY transcription factor family. *Genomics* 98, 128–136. doi: 10.1016/j.ygeno.2011.05.002

Bao, M. (1993). The germplasm resources and exploitation of *Prunus mume* in partial area of Sichuan, Yunnan and Tibet of China. *J. Huazhong Agric. Univ.* 12, 498–501.

Bao, M., and Chen, J. (1994). Studies on the variation and distribution of *Prunus mume* Sieb et Zucc. *Acta Hortic. Sin.* 21, 81–86.

Bassam, B. J., Caetanoanolles, G., and Gresshoff, P. M. (1991). Fast and sensitive silver staining of DNA in polyacrylamide gels. *Anal. Biochem.* 196, 80–83. doi: 10.1016/0003-2697(91)90120-I

Becker, C., and Weigel, D. (2012). Epigenetic variation: origin and transgenerational inheritance. *Curr. Opin. Plant Biol.* 15, 562–567. doi: 10.1016/j.pbi.2012.08.004

Bennetzen, J. L., and Zhu, J. (2011). Epigenetics of the epigenome. *Curr. Opin. Plant Biol.* 14, 113–115. doi: 10.1016/j.pbi.2011.03.015

Bi, Y., Zhang, Y., Signorelli, T., Zhao, R., Zhu, T., and Rothstein, S. J. (2005). Genetic analysis of *Arabidopsis* GATA transcription factor gene family reveals a nitrate-inducible member important for chlorophyll synthesis and glucose sensitivity. *Plant J.* 44, 680–692. doi: 10.1111/j.1365-313X.2005.02568.x

Bouché, N., Yellin, A., Snedden, W. A., and Fromm, H. (2005). Plant-specific calmodulin-binding proteins. *Annu. Rev. Plant Biol.* 56, 435–466. doi: 10.1146/annurev.arplant.56.032604.144224

Bradbury, P. J., Zhang, Z., Kroon, D., Casstevens, T. M., Ramdoss, Y., and Buckler, E. S. (2007). TASSEL: software for association mapping of complex traits in diverse samples. *Bioinformatics* 23, 2633–2635. doi: 10.1093/bioinformatics/btm308

Bussell, J. D. (1999). The distribution of random amplified polymorphic DNA (RAPD) diversity amongst populations of *Isotoma petraea* (Lobeliaceae). *Mol. Ecol.* 8, 775–789. doi: 10.1046/j.1365-294X.1999.00627.x

Cao, J., Schneeberger, K., Ossowski, S., Gunther, T., Bender, S., Fitz, J., et al. (2011). Whole-genome sequencing of multiple *Arabidopsis thaliana* populations. *Nat. Genet.* 43, 956–963. doi: 10.1038/ng.911

Chen, T., and Li, E. (2004). Structure and function of eukaryotic DNA methyltransferases. *Curr. Top Dev. Biol.* 60, 55–89. doi: 10.1016/S0070-2153(04)60003-2

Chen, X., Hu, Y., and Zhou, D. (2011). Epigenetic gene regulation by plant Jumonji group of histone demethylase. *Biochim. Biophys. Acta* 1809, 421–426. doi: 10.1016/j.bbagrm.2011.03.004

Chodavarapu, R. K., Feng, S., Ding, B., Simon, S. A., Lopez, D., Jia, Y., et al. (2012). Transcriptome and methylome interactions in rice hybrids. *Proc. Natl. Acad. Sci. U.S.A.* 109, 12040–12045. doi: 10.1073/pnas.1209297109

Chung, H. Y., and Sunter, G. (2014). Interaction between the transcription factor AtTIFY4B and begomovirus AL2 protein impacts pathogenicity. *Plant Mol. Biol.* 86,185–200. doi: 10.1007/s11103-014-0222-9

Ci, D., Song, Y., Du, Q., Tian, M., Han, S., and Zhang, D. (2015). Variation in genomic methylation in natural populations of *Populus simonii* is associated with leaf shape and photosynthetic traits. *J. Exp. Bot.* 67, 723–737. doi: 10.1093/jxb/erv485

Cubas, P., Coen, E., and Zapater, J. M. M. (2001). Ancient asymmetries in the evolution of flowers. *Curr. Biol.* 11, 1050–1052. doi: 10.1016/S0960-9822(01)00295-0

Cubas, P., Vincent, C., and Coen, E. (1999). An epigenetic mutation responsible for natural variation in floral symmetry. *Nature* 401, 157–161. doi: 10.1038/43657

Degiorgio, M., Jankovic, I., and Rosenberg, N. A. (2010). Unbiased estimation of gene diversity in samples containing related individuals: exact variance and arbitrary ploidy. *Genetics* 186, 1367–1387. doi: 10.1534/genetics.110.121756

Du, Q., Gong, C., Wang, Q., Zhou, D., Yang, H., Pan, W., et al. (2016). Genetic architecture of growth traits in *Populus* revealed by integrated quantitative trait locus (QTL) analysis and association studies. *New Phytol.* 209, 1067–1082. doi: 10.1111/nph.13695

Dubrovina, A. S., and Kiselev, K. V. (2016). Age-associated alterations in the somatic mutation and DNA methylation levels in plants. *Plant Biol.* 18, 185–196. doi: 10.1111/plb.12375

Engel, N., Ewald, R., Gupta, K. J., Zrenner, R., Hagemann, M., and Bauwe, H. (2011). The presequence of *Arabidopsis* serine hydroxymethyltransferase SHM2 selectively prevents import into mesophyll mitochondria. *Plant Physiol.* 157, 1711–1720. doi: 10.1104/pp.111.184564

Evanno, G., Regnaut, S., and Goudet, J. (2005). Detecting the number of clusters of individuals using the software STRUCTURE: a simulation study. *Mol. Ecol.* 14, 2611–2620. doi: 10.1111/j.1365-294X.2005.02553.x

Evans, M. M. (2007). The indeterminate gametophyte1 gene of maize encodes a LOB domain protein required for embryo sac and leaf development. *Plant Cell* 19, 46–62. doi: 10.1105/tpc.106.047506

Fang, J., and Chao, C. (2007). Methylation-sensitive amplification polymorphism in date palms (*Phoenix dactylifera* L.) and their off-shoots. *Plant Biol.* 9, 526–533. doi: 10.1055/s-2007-964934

Feng, S., and Jacobsen, S. E. (2011). Epigenetic modifications in plants: an evolutionary perspective. *Curr. Opin. Plant Biol.* 14, 179–186. doi: 10.1016/j.pbi.2010.12.002

Feng, S., Jacobsen, S. E., and Reik, W. (2010). Epigenetic reprogramming in plant and animal development. *Science* 330, 622–627. doi: 10.1126/science.1190614

Fisher, M. C., Rellstab, C., Tedder, A., Zoller, S., Gugerli, F., Shimizu, K. K., et al. (2013). Population genomic footprints of selection and associations with climate in natural populations of *Arabidopsis halleri* from the Alps. *Mol. Ecol.* 22, 5594–5607. doi: 10.1111/mec.12521

Foerster, A. M., Dinh, H. Q., Sedman, L., Wohlrab, B., and Mittelsten, S. O. (2011). Genetic rearrangements can modify chromatin features at epialleles. *PLOS Genet.* 7:e1002331. doi: 10.1371/journal.pgen.1002331

Foust, C. M., Preite, V., Schrey, A. W., Alvarez, M., Robertson, M. H., Verhoeven, K. J. F., et al. (2016). Genetic and epigenetic differences associated with environmental gradients in replicate populations of two salt marsh perennials. *Mol. Ecol.* 25, 1639–1652. doi: 10.1111/mec.13522

Geoghegan, J. L., and Spencer, H. G. (2012). Population-epigenetic models of selection. *Theor. Popul. Biol.* 81, 232–242. doi: 10.1016/j.tpb.2011.08.001

Gourcilleau, D., Bogeat-Triboulot, M., Thiec, D. L., Lafonplacette, C., Delaunay, A., Elsoud, W. A., et al. (2010). DNA methylation and histone acetylation: genotypic variations in hybrid poplars, impact of water deficit and relationships with productivity. *Ann. For. Sci.* 67:208. doi: 10.1051/forest/2009101

Gruenbaum, Y., Naveh-Many, T., Cedar, H., and Razin, A. (1981). Sequence specificity of methylation in higher plant DNA. *Nature* 292, 860–862. doi: 10.1038/292860a0

Guo, Z., Fujioka, S., Blancaflor, E. B., Miao, S., Gou, X., and Li, J. (2010). TCP1 modulates brassinosteroid biosynthesis by regulating the expression of the key biosynthetic gene *DWARF4* in *Arabidopsis thaliana*. *Plant Cell* 22, 1161–1173. doi: 10.1105/tpc.109.069203

Hauben, M., Haesendonckx, B., Standaert, E., Katrien, V. D. K., Azmi, A., Akpo, H., et al. (2009). Energy use efficiency is characterized by an epigenetic component that can be directed through artificial selection to increase yield. *Proc. Natl. Acad. Sci. U.S.A.* 106, 20109–20114. doi: 10.1073/pnas.0908755106

Heazlewood, J. L., Tontifilippini, J., Gout, A. M., Day, D. A., Whelan, J., and Millar, A. H. (2004). Experimental analysis of the *Arabidopsis* mitochondrial proteome highlights signaling and regulatory components, provides assessment of targeting prediction programs, and indicates plant-specific mitochondrial proteins. *Plant Cell* 16, 241–256. doi: 10.1105/tpc.016055

Heo, J. B., Lee, Y., and Sung, S. (2013). Epigenetic regulation by long noncoding RNAs in plants. *Chromosome Res.* 21, 685–693. doi: 10.1007/s10577-013-9392-6

Heyn, H., Moran, S., Hernando-Herraez, I., Sayols, S., Gomez, A., Sandoval, J., et al. (2013). DNA methylation contributes to natural human variation. *Genome Res.* 23, 1363–1372. doi: 10.1101/gr.154187.112

Jacobsen, S. E. (2011). Establishing, maintaining and modifying DNA methylation patterns in plants and animals. *Nat. Rev. Genet.* 11, 204–220. doi: 10.1101/gr.154187.112

Kleine, T. (2012). *Arabidopsis thaliana* mTERF proteins: evolution and functional classification. *Front. Plant Sci.* 3:233. doi: 10.3389/fpls.2012.00233

Koyama, T., Sato, F., and Ohmetakagi, M. (2010). A role of TCP1 in the longitudinal elongation of leaves in *Arabidopsis*. *Biosci. Biotechnol. Biochem.* 74, 2145–2147. doi: 10.1271/bbb.100442

Kruse, B., Narasimhan, N., and Attardi, G. (1989). Termination of transcription in human mitochondria: identification and purification of a DNA binding protein factor that promotes termination. *Cell* 58, 391–397. doi: 10.1016/0092-8674(89)90853-2

Leran, S., Varala, K., Boyer, J. C., Chiurazzi, M., Crawford, N. M., Danielvedele, F., et al. (2014). A unified nomenclature of NITRATE TRANSPORTER 1/PEPTIDE TRANSPORTER family members in plants. *Trends Plant Sci.* 19, 5–9. doi: 10.1016/j.tplants.2013.08.008

Li, S., Xia, Q., Wang, F., Yu, X., Ma, J., Kou, H., et al. (2017). Laser irradiation-induced DNA methylation changes are heritable and accompanied with transpositional activation of *mPing* in rice. *Front. Plant Sci.* 8:363. doi: 10.3389/fpls.2017.00363

Lin, W., Shuai, B., and Springer, P. S. (2003). The *Arabidopsis LATERAL ORGAN BOUNDARIES-Domain* Gene *ASYMMETRIC LEAVES2* functions in the repression of *KNOX* gene expression and in adaxial-abaxial patterning. *Plant Cell* 15, 2241–2252. doi: 10.1105/tpc.014969

Lira-Medeiros, C. F., Parisod, C., Fernandes, R. A., Mata, C. S., Cardoso, M. A., and Ferreira, P. C. G. (2010). Epigenetic variation in mangrove plants occurring in contrasting natural environment. *PLOS ONE* 5:e10326. doi: 10.1371/journal.pone.0010326

Lisch, D., and Bennetzen, J. L. (2011). Transposable element origins of epigenetic gene regulation. *Curr. Opin. Plant Biol.* 14, 156–161. doi: 10.1016/j.pbi.2011.01.003

Lister, R., O'Malley, R. C., Tonti-Filippini, J., Gregory, B. D., Berry, C. C., Millar, A. H., et al. (2008). Highly integrated single-base resolution maps of the epigenome in *Arabidopsis*. *Cell* 133, 523–536. doi: 10.1016/j.cell.2008.03.029

Liu, S., Sun, K., Jiang, T., Ho, J. P., Liu, B., and Feng, J. (2012). Natural epigenetic variation in the female great roundleaf bat (*Hipposideros armiger*) populations. *Mol. Genet. Genomics* 287, 643–650. doi: 10.1007/s00438-012-0704-x

Long, Y., Xia, W., Li, R., Wang, J., Shao, M., Feng, J., et al. (2011). Epigenetic QTL mapping in *Brassica napus*. *Genetics* 189, 1093–1102. doi: 10.1534/genetics.111.131615

Ma, K., Song, Y., Jiang, X., Zhang, Z., Li, B., and Zhang, D. (2012). Photosynthetic response to genome methylation affects the growth of Chinese white poplar. *Tree Genet. Genomes* 8, 1407–1421. doi: 10.1007/s11295-012-0527-2

Ma, K., Song, Y., Yang, X., Zhang, Z., and Zhang, D. (2013). Variation in genomic methylation in natural populations of Chinese white poplar. *PLOS ONE* 8:e63977. doi: 10.1371/journal.pone.0063977

Manning, K., Tor, M., Poole, M., Hong, Y. G., Thompson, A., King, G. J., et al. (2006). A naturally occurring epigenetic mutation in a gene encoding an SBP-box transcription factor inhibits tomato fruit ripening. *Nat. Genet.* 38, 948–952. doi: 10.1038/ng1841

Massicotte, R., Whitelaw, E. S., and Angers, B. (2011). DNA methylation: a source of random variation in natural populations. *Epigenetics* 6, 421–427. doi: 10.4161/epi.6.4.14532

McDermott, A. J., and McDonald, B. A. (1993). Gene flow in plant pathosystems. *Annu. Rev. Phytopathol.* 31, 353–373. doi: 10.1146/annurev.py.31.090193.002033

Melotto, M., Mecey, C., Niu, Y., Chung, H. S., Katsir, L., Yao, J., et al. (2008). A critical role of two positively charged amino acids in the Jas motif of Arabidopsis JAZ proteins in mediating coronatine- and jasmonoyl isoleucine-dependent interactions with the COI1 F-box protein. *Plant J.* 55, 979–988. doi: 10.1111/j.1365-313X.2008.03566.x

Meskauskiene, R., Wursch, M., Laloi, C., Vidi, P., Coll, N. S., Kessler, F., et al. (2009). A mutation in the *Arabidopsis* mTERF-related plastid protein SOLDAT10 activates retrograde signaling and suppresses 1O2-induced cell death. *Plant J.* 60, 399–410. doi: 10.1111/j.1365-313X.2009.03965.x

Messeguer, R., Ganal, M. W., Steffens, J. C., and Tanksley, S. D. (1991). Characterization of the level, target sites and inheritance of cytosine methylation in tomato nuclear DNA. *Plant Mol. Biol.* 16, 753–770. doi: 10.1007/BF00015069

Mirouze, M., and Paszkowski, J. (2011). Epigenetic contribution to stress adaptation in plants. *Curr. Opin. Plant Biol.* 14, 267–274. doi: 10.1016/j.pbi.2011.03.004

Nicotra, A. B., Atkin, O. K., Bonser, S. P., Davidson, A. M., Finnegan, E. J., Mathesius, U., et al. (2010). Plant phenotypic plasticity in a changing climate. *Trends Plant Sci.* 15, 684–692. doi: 10.1016/j.tplants.2010.09.00

Nicotra, A. B., Segal, D. L., Hoyle, G. L., Schrey, A. W., Verhoeven, K. J. F., and Richards, C. L. (2015). Adaptive plasticity and epigenetic variation in response to warming in an Alpine plant. *Ecol. Evol.* 5, 634–647. doi: 10.1002/ece3.1329

Nikolovski, N., Rubtsov, D. V., Segura, M. P., Miles, G. P., Stevens, T. J., Dunkley, T. P., et al. (2012). Putative glycosyltransferases and other plant Golgi apparatus proteins are revealed by LOPIT proteomics. *Plant Physiol.* 160, 1037–1051. doi: 10.1104/pp.112.204263

Parisod, C., and Christin, P. A. (2008). Genome wide association to fine scale ecological heterogeneity within a continuous population of *Biscutella laevigata* (Brassicaceae). *New Phytol.* 178, 436–447. doi: 10.1111/j.1469-8137.2007.02361.x

Parisod, C., Trippi, C., and Galland, N. (2005). Genetic variability and founder effect in the pitcher plant *Sarracenia purpurea* (Sarraceniaceae) in populations introduced into Switzerland: from inbreeding to invasion. *Ann. Bot.* 95, 277–286. doi: 10.1093/aob/mci023

Peakall, R., and Smouse, P. E. (2012). GenAlEx 6.5: genetic analysis in Excel. Population genetic software for teaching and research-an update. *Bioinformatics* 28, 2537–2539. doi: 10.1093/bioinformatics/bts460

Pérez, J. E., Nirchio, M., Alfonsi, C., and Muñoz, C. (2006). The biology of invasions: the genetic adaptation paradox. *Biol. Invasion* 8, 1115–1121. doi: 10.1007/s10530-005-8281-0

Platt, A., Gugger, P., and Sork, V. (2015). Genome-wide signature of local adaptation linked to variable CpG methylation in oak populations. *Mol. Ecol.* 24, 3823–3830. doi: 10.1111/mec.13230

Quesada, V., Sarmiento-Mañús, R., González-Bayón, R., Hricová, A., Pérez-Marcos, R., Graciá-Martínez, E., et al. (2011). *Arabidopsis RUGOSA2* encodes an mTERF family member required for mitochondrion, chloroplast and leaf development. *Plant J.* 68, 738–753. doi: 10.1111/j.1365-313X.2011.04726.x

Reyes, J. C., Muro-Pastor, M. I., and Florencio, F. J. (2004). The GATA family of transcription factors in Arabidopsis and rice. *Plant Physiol.* 134, 1718–1732. doi: 10.1104/pp.103.037788

Richards, E. J. (2008). Population epigenetics. *Curr. Opin. Genet. Dev.* 18, 221–226. doi: 10.1016/j.gde.2008.01.014

Robles, P., Micol, J. L., and Quesada, V. (2012). *Arabidopsis* MDA1, a nuclear-encoded protein, functions in chloroplast development and abiotic stress responses. *PLOS ONE* 7:e42924. doi: 10.1371/journal.pone.0042924

Robles, P., Micol, J. L., and Quesada, V. (2015). Mutations in the plant-conserved MTERF9 alter chloroplast gene expression, development and tolerance to abiotic stress in *Arabidopsis thaliana*. *Physiol. Plant.* 154, 297–313. doi: 10.1111/ppl.12307

Romani, I., Manavski, N., Morosetti, A., Tadini, L., Maier, S., Kuhn, K., et al. (2015). mTERF6, a member of the *Arabidopsis* mitochondrial transcription termination factor family is required for maturation of chloroplast tRNAIle (GAU). *Plant Physiol.* 169, 627–646. doi: 10.1104/pp.15.00964

Santi, D. V., Garrett, C., and Barr, P. J. (1983). On the mechanism of inhibition of DNA-cytosine methyltransferases by cytosine analogs. *Cell* 33, 9–10. doi: 10.1016/0092-8674(83)90327-6

Schmitz, R. J., and Ecker, J. R. (2012). Epigenetic and epigenomic variation in *Arabidopsis thaliana*. *Trends Plant Sci.* 17, 149–154. doi: 10.1016/j.tplants.2012.01.001

Semiarti, E., Ueno, Y., Tsukaya, H., Iwakawa, H., Machida, C., and Machida, Y. (2001). The *ASYMMETRIC LEAVES2* gene of *Arabidopsis thaliana* regulates formation of a symmetric lamina, establishment of venation and repression of meristem-related homeobox genes in leaves. *Development* 128, 1771–1783.

Seymour, G. B., Poole, M., Manning, K., and King, G. J. (2008). Genetics and epigenetics of fruit development and ripening. *Curr. Opin. Plant Biol.* 11, 58–63. doi: 10.1016/j.pbi.2007.09.003

Shen, Y., Ding, X., Wang, F., Cai, B., Gao, Z., and Zhang, Z. (2011). Analysis of genetic diversity in Japanese apricot (*Prunus mume* Sieb et Zucc) based on REMAP and IRAP molecular markers. *Sci. Hortic.* 132, 50–58. doi: 10.1016/j.scienta.2011.10.005

Shi, J., Yi, K., Liu, Y., Xie, L., Zhou, Z., Chen, Y., et al. (2015). Phosphoenolpyruvate carboxylase in *Arabidopsis* leaves plays a crucial role in carbon and nitrogen metabolism. *Plant Physiol.* 167, 671–681. doi: 10.1104/pp.114.254474

Shuai, B., Reynaga-Peña, C. G., and Springer, P. S. (2002). The *LATERAL ORGAN BOUNDARIES* gene defines a novel, plant-specific gene family. *Plant Physiol.* 129, 747–761. doi: 10.1104/pp.010926

Snedden, W. A., and Fromm, H. (1998). Calmodulin, calmodulin-related proteins and plant responses to the environment. *Trends Plant Sci.* 3, 299–304. doi: 10.1016/S1360-1385(98)01284-9

Springer, N. M. (2013). Epigenetics and crop improvement. *Trends Genet.* 29, 241–247. doi: 10.1016/j.tig.2012.10.009

Sun, L., Wang, Y., Yan, X., Cheng, T., Ma, K., Yang, W., et al. (2014). Genetic control of juvenile growth and botanical architecture in an ornamental woody plant, *Prunus mume* Sieb. et Zucc. as revealed by a high-density linkage map. *BMC Genet.* 15:S1. doi: 10.1186/1471-2156-15-S1-S1

Thioulouse, J., Chessel, D., Doldec, S., and Olivier, J. (1996). Ade-4: a multivariate analysis and graphical display software. *Stat. Comput.* 7, 75–83. doi: 10.1023/A:1018513530268

Thorstensen, T., Grini, P. E., and Aalen, R. B. (2011). SET domain proteins in plant development. *Biochim. Biophys. Acta* 1809, 407–420. doi: 10.1016/j.bbagrm.2011.05.008

Vaughn, M. W., Tanurdžic, M., Lippman, Z. B., Jiang, H., Carrasquillo, R., Rabinowicz, P. D., et al. (2007). Epigenetic natural variation in *Arabidopsis thaliana*. *PLOS Biol.* 5:e174. doi: 10.1371/journal.pbio.0050174

Vos, P., Hogers, R., Bleeker, M., Reijans, M., van de Lee, T., Hornes, M., et al. (1995). AFLP: a new technique for DNA fingerprinting. *Nucleic Acids Res.* 23, 4407–4414. doi: 10.1093/nar/23.21.4407

White, D. W. (2006). *PEAPOD* regulates lamina size and curvature in *Arabidopsis*. *Proc. Natl. Acad. Sci. U.S.A.* 103, 13238–13243. doi: 10.1073/pnas.0604349103

Xiong, L., Xu, C., Maroof, M. A., and Zhang, Q. (1999). Patterns of cytosine methylation in an elite rice hybrid and its parental lines, detected by a methylation-sensitive amplification polymorphism technique. *Mol. Genet. Genomics* 261, 439–446. doi: 10.1007/s004380050986

Xu, L., Xu, Y., Dong, A., Sun, Y., Pi, L., Xu, Y., et al. (2003). Novel *as1* and *as2* defects in leaf adaxial-abaxial polarity reveal the requirement for *ASYMMETRIC LEAVES1* and *2* and *ERECTA* functions in specifying leaf adaxial identity. *Development* 130, 4097–4107. doi: 10.1242/dev.00622

Yan, Y., Stolz, S., Chételat, A., Reymond, P., Pagni, M., Dubugnon, L., et al. (2007). A downstream mediator in the growth repression limb of the jasmonate pathway. *Plant Cell* 19, 2470–2483. doi: 10.1105/tpc.107.050708

Yang, C., Zhang, J., Yan, X., and Bao, M. (2007). Genetic relatedness and genetic diversity of ornamental mei (*Prunus mume* Sieb. et Zucc.) as analysed by AFLP markers. *Tree Genet. Genomes* 4, 255–262. doi: 10.1007/s11295-007-0106-0

Ye, H., Du, H., Tang, N., Li, X., and Xiong, L. (2009). Identification and expression profiling analysis of TIFY family genes involved in stress and phytohormone responses in rice. *Plant Mol. Biol.* 71, 291–305. doi: 10.1007/s11103-009-9524-8

Ye, M., Jiang, L., Mao, K., Wang, Y., Wang, Z., and Wu, R. (2015). Functional mapping of seasonal transition in perennial plants. *Brief. Bioinform.* 16, 526–535. doi: 10.1093/bib/bbu025

Zhang, J., Zhang, Q., Cheng, T., Yang, W., Pan, T., Zhong, J., et al. (2015). High-density genetic map construction and identification of a locus controlling weeping trait in an ornamental woody plant (*Prunus mume* Sieb. et Zucc.). *DNA Res.* 22, 183–191. doi: 10.1093/dnares/dsv003

Zhang, Z., Li, X., Yu, R., Han, M., and Wu, Z. (2015). Isolation, structural analysis, and expression characteristics of the maize *TIFY* gene family. *Mol. Genet. Genomics* 290, 1849–1858. doi: 10.1007/s00438-015-1042-6

Zhang, J., Zhao, K., Hou, D., Cai, J., Zhang, Q., Cheng, T., et al. (2017). Genome-wide discovery of DNA polymorphisms in Mei (*Prunus mume* Sieb. et Zucc.), an ornamental woody plant, with contrasting tree architecture and their functional relevance for weeping trait. *Plant Mol. Biol. Rep.* 35, 37–46. doi: 10.1007/s11105-016-1000-4

Zhang, Q., Chen, W., Sun, L., Zhao, F., Huang, B., Yang, W., et al. (2012). The genome of *Prunus mume*. *Nat. Commun.* 3, 1318–1318. doi: 10.1038/ncomms2290

Zhang, Q., Wu, G., Zhao, Y., Lv, Y., Cheng, T., and Luo, L. (2010). Distribution of resources of wild mei (*Prunus mume* Sieb et Zucc) flower in Anhui, Jiangxi, Sichuan and Yunnan provinces of China. *J. Beijing For. Univ.* 32, 8–13.

Zhang, X., Shiu, S. H., Cal, A., and Borevitz, J. O. (2008). Global analysis of genetic, epigenetic and transcriptional polymorphisms in *Arabidopsis thaliana* using whole genome tiling arrays. *PLOS Genet.* 4:e1000032. doi: 10.1371/journal.pgen.1000032

Zielinski, R. E. (1998). Calmodulin and calmodulin-binding proteins in plants. *Annu. Rev. Plant Biol.* 49, 697–725. doi: 10.1146/annurev.arplant.49.1.697

**Conflict of Interest Statement:** The authors declare that the research was conducted in the absence of any commercial or financial relationships that could be construed as a potential conflict of interest.

frontiers in Plant Science

ORIGINAL RESEARCH
published: 30 October 2018
doi: 10.3389/fpls.2018.01587

# Expression Profiles of Phosphoenolpyruvate Carboxylase and Phosphoenolpyruvate Carboxylase Kinase Genes in *Phalaenopsis*, Implications for Regulating the Performance of Crassulacean Acid Metabolism

*Chia-Yun Ping[1], Fure-Chyi Chen[2], Teen-Chi Cheng[2], Huey-Ling Lin[3], Tzong-Shyan Lin[1], Wen-Ju Yang[1]* and Yung-I Lee[4,5]**

[1] Department of Horticulture and Landscape Architecture, National Taiwan University, Taipei, Taiwan, [2] Department of Plant Industry, National Pingtung University of Science and Technology, Pingtung, Taiwan, [3] Department of Horticulture, National Chung Hsing University, Taichung, Taiwan, [4] Department of Biology, National Museum of Natural Science, Taichung, Taiwan, [5] Department of Life Sciences, National Chung Hsing University, Taichung, Taiwan

*Phalaenopsis* is one of the most important potted plants in the ornamental market of the world. Previous reports implied that crassulacean acid metabolism (CAM) orchids at their young seedling stages might perform $C_3$ or weak CAM photosynthetic pathways, but the detailed molecular evidence is still lacking. In this study, we used a key species in white *Phalaenopsis* breeding line, *Phalaenopsis aphrodite* subsp. *formosana*, to study the ontogenetical changes of CAM performance in *Phalaenopsis*. Based on the investigations of rhythms of day/night $CO_2$ exchange, malate contents and phosphoenolpyruvate carboxylase (PEPC) activities, it is suggested that a progressive shift from $C_3$ to CAM occurred as the protocorms differentiated the first leaf. To understand the role of phosphoenolpyruvate carboxylase kinase (PEPC kinase) in relation to its target PEPC in CAM performance in *Phalaenopsis*, the expression profiles of the genes encoding *PEPC* (*PPC*) and *PEPC kinase* (*PPCK*) were measured in different developmental stages. In *Phalaenopsis*, two *PPC* isogenes were constitutively expressed over a 24-h cycle similar to the housekeeping genes in all stages, whereas the significant day/night difference in *PaPPCK* expression corresponds to the day/night fluctuations in PEPC activity and malate level. These results suggest that the *PaPPCK* gene product is most likely involved in regulation of CAM performance in different developmental stages of *Phalaenopsis* seedlings.

**Keywords: CAM rhythm, orchid, photosynthesis transition, phosphoenolpyruvate carboxylase, phosphoenolpyruvate carboxylase kinase**

OPEN ACCESS

***Edited by:***
*Swee-Suak Ko,*
*Academia Sinica, Taiwan*

***Reviewed by:***
*Daniel Wood,*
*The University of Sheffield, United Kingdom*
*Wim van Ieperen,*
*Wageningen University & Research, Netherlands*

****Correspondence:***
*Wen-Ju Yang*
*wendy@ntu.edu.tw*
*Yung-I Lee*
*leeyungi@hotmail.com*

***Specialty section:***
*This article was submitted to Plant Evolution and Development, a section of the journal Frontiers in Plant Science*

***Received:*** *31 January 2018*
***Accepted:*** *12 October 2018*
***Published:*** *30 October 2018*

***Citation:***
*Ping C-Y, Chen F-C, Cheng T-C, Lin H-L, Lin T-S, Yang W-J and Lee Y-I (2018) Expression Profiles of Phosphoenolpyruvate Carboxylase and Phosphoenolpyruvate Carboxylase Kinase Genes in Phalaenopsis, Implications for Regulating the Performance of Crassulacean Acid Metabolism. Front. Plant Sci. 9:1587. doi: 10.3389/fpls.2018.01587*

## INTRODUCTION

*Phalaenopsis*, an epiphytic orchid, is regarded as an obligate crassulacean acid metabolism (CAM) plant because of its succulent leaf with large and highly vacuolated mesophyll cells. Previous studies have indicated that mature plants of *Phalaenopsis* fixed $CO_2$ and stored as malate inside the vacuoles at night (Endo and Ikusima, 1989; Ota et al., 1991; Cui et al., 2004; Guo and Lee, 2006). However, it has been reported that CAM orchids at their protocorm or young seedling stages might perform $C_3$ or weak CAM pathways (Goh et al., 1984). For instance, no significant day/night changes in the titratable acidity were observed during the protocorm development of *Dendrobium taurinum* (Hew and Khoo, 1980). Chen and Lee (2002) reported that *in vitro* young seedlings of *Phalaenopsis* absorbed more $CO_2$ during the light than in the dark. In addition, the *in vitro* young seedlings of *Phalaenopsis* exhibited the carbon isotopic values ($\delta^{13}C$) of −21.4‰ to −19.5‰, suggesting a weak CAM photosynthetic pathway (Lo, 2008). These findings imply that an alteration of the photosynthetic pathway from $C_3$ to CAM occurred at the early developmental stage of CAM orchids; however, definite proof has not yet been illustrated.

CAM is a water-preserving photosynthetic pathway adaptive in arid environments, in which stomata are closed during the daytime and opened at night In CAM plants, phosphoenolpyruvate carboxylase (PEPC, EC 4.1.1.31) serves as the key enzyme that fixes $CO_2$ to phosphoenolpyruvate (PEP) in the cytosol during the nighttime (Osmond and Holtum, 1981; Chollet et al., 1996; Vidal and Chollet, 1997; Nimmo, 2000; Borland et al., 2014), and produces oxaloacetic acid (OAA) stored in the vacuole through the formation of malic or citric acids. In the daytime, decarboxylation of these organic acids increases internal $CO_2$ concentration enabling CAM plants to maintain high rates of photosynthesis as the stomata are closed (Winter and Smith, 1996). This feature is an important strategy for the survival of plants in the dry habitat (Silvera et al., 2009; Rodrigues et al., 2013).

Most plants contain several PEPC isoforms encoded by a small gene family that are related to specific physiological functions (Gehrig et al., 1995; Gehrig et al., 2001). In facultative CAM plants, such as the common ice plant (*Mesembryanthemum crystallinum*) and *Kalanchoe* species, the CAM-specific PEPC isoform is induced to fulfill the primary carboxylation and carbon flux while switches to CAM pathway (Cushman et al., 1989; Gehrig et al., 1998). The PEPC isoforms, in addition to a CAM-specific isoform, is important for anapleurotic "housekeeping" or tissue-specific functional roles (Gehrig et al., 1998). Changes in PEPC activity are regulated by phosphorylation of a serine residue of PEPC at night that increases the catalytic activity of PEPC, and reduces the inhibitory effect on PEPC of its allosteric inhibitor, malate (Nimmo G. A. et al., 2001; Taybi et al., 2004). The phosphorylation state of PEPC is catalyzed by PEPC kinase, encoded by *PPCKs* (Chollet et al., 1996; Vidal and Chollet, 1997; Nimmo H. G. et al., 2001). In the common ice plant, the expression of CAM-specific *PPC* and *PPCK* are both induced during the induction of CAM (Cushman et al., 1989; Li and Chollet, 1994; Taybi et al., 2000). In *Clusia minor*, a $C_3$-CAM intermediate species, the increased expression of PEPC kinase plays an interesting role in regulating CAM performance (Borland and Griffiths, 1997). Altogether, examining the relationship between the expression of CAM-specific *PPC* and *PPCK* could be a great strategy to illustrate the developmental changes in CAM orchids.

In orchids, protocorms are tuber-shaped structures derived from germinating embryos (Arditti, 1992). The protocorm is a transitional structure, which subsequently produces the shoot and roots, resulting in the formation of a young seedling. If the protocorms or young seedlings of *Phalaenopsis* perform $C_3$ type metabolism, the developmental stage from which the plants onset the shift from $C_3$ to CAM is of interested. To elucidate the progression from $C_3$ to CAM photosynthetic pathway in *Phalaenopsis*, we investigated the expression of *PPC* and *PPCK* genes, the profiles of day/night $CO_2$ exchange, malate contents and the PEPC activity of different developmental stages. During the past decade, commercial production of *Phalaenopsis* as potted flowering plants has increased massively in the world (Griesbach, 2000; U.S. Department of Agriculture [USDA], 2017). A better understanding the regulation in CAM performance will provide insights into the micropropagation and cultivation of *Phalaenopsis*.

## MATERIALS AND METHODS

### Plant Materials

The mature plants of *Phalaenopsis aphrodite* subsp. *formosana* were maintained in a greenhouse with the pad-and-fan cooling system at National Museum of Natural Science, Taichung, Taiwan. To ensure good pod set and seed quantity, flowers at anthesis were hand-pollinated immediately. Mature seeds were harvested at 150 days after pollination for *in vitro* cultures. For *in vitro* seed germination, we used the 1/4-strength macro-elements (i.e., $KNO_3$, $NH_4NO_3$, $KH_2PO_4$, $MgSO_4{\cdot}7H_2O$ and $CaCl_2{\cdot}2H_2O$) and full-strength micro-elements (i.e., $FeSO_4{\cdot}7H_2O$, $Na_2{\cdot}EDTA$, $MnSO_4{\cdot}4H_2O$, $ZnSO_4{\cdot}7H_2O$, $CuSO_4{\cdot}5H_2O$, KI, $CoCl_2{\cdot}6H_2O$, $H_3BO_3$, $NaMoO_4{\cdot}2H_2O$) of Murashige and Skoog (MS) medium (Murashige and Skoog, 1962), supplemented with 10 $g{\cdot}L^{-1}$ sucrose (Sigma–Aldrich Co., St. Louis, MO, United States), 1 $g{\cdot}L^{-1}$ peptone (Merck KGaA, Darmstadt, Germany) and 2.2 $g{\cdot}L^{-1}$ Gelrite (Sigma–Aldrich Co.). The pH value of the media was adjusted to 5.7 with 1 N KOH prior to autoclaving at 121°C and 1.2 $kg{\cdot}cm^{-2}$ for 15 min. When the first true leaf and root emerged, the developing protocorms were subcultured onto the culture medium containing 1/2-strength macro-elements and full-strength micro-elements of MS medium, supplemented with 10 $g{\cdot}L^{-1}$ sucrose, 1 $g{\cdot}L^{-1}$ peptone and 2.2 $g{\cdot}L^{-1}$ Gelrite. The cultures were placed at the growth chamber at 30 $\mu mol{\cdot}m^{-2}{\cdot}s^{-1}$ (daylight fluorescent tube FL-20D/18, 20W, China Electric Co., Taipei) and 26 ± 2°C with a 12-h daylength (0600 to 1800 h). Different developmental stages were shown and described in **Figure 1**.

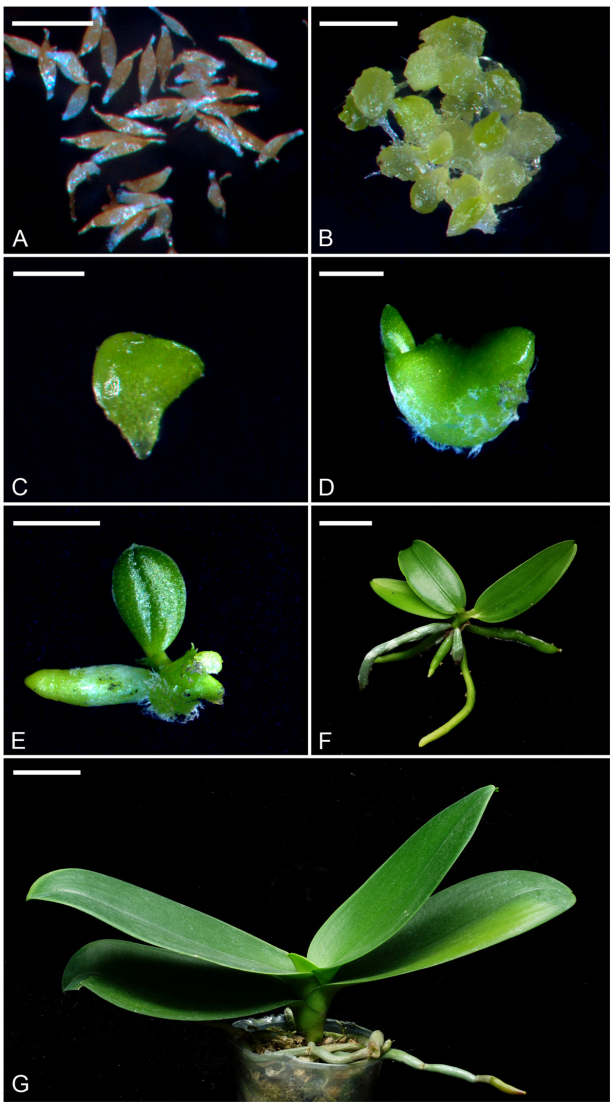


**FIGURE 1 |** The seeds, protocorms and seedlings of *P. aphrodite* subsp. *formosana* at different developmental stages (stage 0 to stage 6). **(A)** Stage 0: mature seeds. Bar = 0.25 mm. **(B)** Stage 1: the embryo swelled and turned green after 2 weeks of culture. Bar = 1 mm. **(C)** Stage 2: the protocorm of diameter 1–3 mm could be observed after 4 weeks of culture. Bar = 2 mm. **(D)** Stage 3: the protocorm with a shoot apical meristem could be observed after 6 weeks of culture. Bar = 4 mm. **(E)** Stage 4: the protocorm had differentiated the first true leaf and root after 10 weeks of culture. Bar = 1 cm. **(F)** Stage 5: the seedling at the time for taking out of flasks after 32 weeks of culture. Bar = 2 cm. **(G)** Stage 6: a 3-year-old mature seedling represented the mature stage that was planted in a 9 cm pot with sphagnum moss. Bar = 4 cm.

## Measurement of Diurnal $CO_2$ Exchange

Since developing protocorms (the stages 1–3) were too small to measure the photosynthetic rate using LI-COR's portable photosynthesis systems, we measured the changes of $CO_2$ concentrations within the culture tubes for representing their photosynthetic profiles. For obtaining the diurnal $CO_2$ change curves *in vitro*, one gram of protocorms were inoculated onto the culture medium in a culture tube (120 mm tall × 13 mm with 11 mm inside diameter) sealed with the aluminum foil. The cultures were placed in the growth room at 30 $\mu mol \cdot m^{-2} \cdot s^{-1}$ (daylight fluorescent tube FL-20D/18, 20W, China Electric Co., Taipei) and 26 ± 2°C with a 12-h daylength (0600 to 1800 h). The air within the sealed culture tube was collected by a 1-mL syringe every 2 h during a 24-h period, and the $CO_2$ concentration was determined by IR-analyzer (UNOR 610, Maihak AG, Hamburg, Germany). Each data point was measured by the accumulation of $CO_2$ concentration for 2 h within the culture tube. Before the first measurement, the aluminum foil was removed from the culture tube to balance the $CO_2$ concentration from ambient air for 5 min, then the culture tube was sealed with a rubber stopper for 2 h. After each measurement, the rubber stopper was opened to balance the $CO_2$ concentration from ambient air. Three replications were performed in each stage, and each replicate contained the measurement of three tubes. The empty tubes without protocorms were used for $CO_2$ measurements (340 ppm) for calibration.

After the leaf differentiation (stages 4, 5, and 6), gas exchange parameters were measured on the middle part of the top second leaf of a plant by a portable Infra Red Gas Analyzer (LI-COR 6400, LI-COR, Lincoln, NE, United States) with a 2 $cm^2$ leaf chamber every 2 h during a 24-h period. Photosynthetic responses were measured at leaf temperature of 30 ± 2.5°C with 350 $\mu mol \cdot mol^{-1}$ $CO_2$ supplied at a flow rate of 200 $\mu mol \cdot s^{-1}$. In the stages of 4 and 5, young seedlings grown in flasks (six seedlings per flask) were take out and the roots were wrapped in the moistened sphagnum moss for measurements. The leaf in the stage 4 was too small to fit a 2 $cm^2$ leaf chamber, and the lead area was estimated by LI-3100C Area Meter for correction of leaf area measurement according to the LI-6400 manual. In the stage 6, 3-year old seedlings grown in the greenhouse were measured. In these experiments, the cultures and seedlings were placed at the growth chamber at 30 $\mu mol \cdot m^{-2} \cdot s^{-1}$ (daylight fluorescent tube FL-20D/18, 20W, China Electric Co., Taipei) with a 12-h daylength (0600 to 1800 h). The sampled leaf was placed in the leaf chamber for 20 min before the data readings were recorded. The environmental conditions in the leaf chambers were controlled as close to those in the growth chamber as possible to reduce the variations between the sampled leaves. In this study, the completely randomized design was used, and the measurements were performed with three replications, and each replication represented the average of six seedlings of each stage.

## Measurement of Malate Levels

About 0.2 g tissue from developing protocorms or leaves at each stage was sampled every 2 h during a 24-h period. In stage 5 and 6, the middle part of the top second leaf of a plant was collected for measurement. The samples were ground in a mortar with 5 mL of distilled water. The crude extracts were heated at 90°C water bath for 30 min, then cooled at room temperature. The malate content of the cooled extract was measured according to the method of Möllering and Malt (1974). The concentration of malate was determined using standard curves. For the analysis of

titratable acidity, 4 mL of the supernatant was titrated with 0.01 N NaOH solution to the end point of pH value at 8.3. The amount of NaOH was used to calculate the concentration of the titratable acid, expressed as micromoles $H^+$ per gram fresh weight. In this study, the completely randomized design was used, and the measurements were performed with three replications, and each replication represented the average of six seedlings of each stage. The significantly different by *t*-test between day and night in the same stage were indicated by asterisk ($P < 0.05$).

## Assay of PEPC Activity

PEPC was extracted from developing protocorms and leaves of 0.1 g of each stage were sampled every 2 h during a 24-h period. In stage 5 and 6, the middle part of the top second leaf of a plant was collected for measurement. The sample was homogenized with 1.5 ml extraction buffer (50 mM Tris-HCl, pH 7.0, 10 mM $MgCl_2$, 1 mM EDTA, 5 mM DTT, 2.5% PVPP and 10% glycerol) according to the method of Ku et al. (1999). The homogenate was centrifuged at 17709 × *g* for 15 min at 4°C. PEPC activity of the supernatant was measured according to Krömer et al. (1996). Protein concentration was determined by using Bio-Rad protein assay reagent (Bradford, 1976). In this study, the completely randomized design was used, and the measurements were performed with three replications, and each replication represented the average of six seedlings of each stage. Significantly differences between day and night in the same stage, as identified by a *t*-test, were indicated by asterisks ($P < 0.05$).

### Cloning of cDNAs of *PaPPCK* of *P. aphrodite* subsp. *formosana*

Total RNA was extracted from the leaves of seedlings at stage 5 using RNeasy Plant Mini Kit (Qiagen, Hilden, Germany) and modified as Gehrig et al. (2000). For the double-stranded cDNA synthesis, 1 μg RNA was reverse-transcribed using the SuperScript™ III kit (Invitrogen, Carlsbad, CA, United States) according to the manufacturer's instruction. The synthesized cDNA fragments and the *PaPPCK* degenerate primers designed from the conserved amino acid sequences in the expressed sequence tag (EST) library of *Phalaenopsis* (FC Chen, unpublished) were used in PCR experiments. The amplified fragment containing the partial sequence of *PaPPCK* that showed high sequence similarity to PPCK was identified by using a blastx algorithm in a BLAST search against the NCBI database (National Center for Biotechnology Information, GenBank). The internal gene-specific primers were designed from the partial sequence of *PaPPCK* for 5′ and 3′ rapid amplified cDNA ends (RACE) using SMART™ RACE cDNA amplification kit (Clontech, Palo Alto, CA, United States). The full-length cDNA for *PaPPCK* was obtained by PCR amplification using the PaPPCK-F and PaPPCK-R primers. All the primers used were listed in **Supplementary Table S1**.

## Real-Time PCR Analysis

Real-time PCR was performed using ABI PRISM 7300 Sequence Detection System (Applied Biosystems, Waltham, MA, United States) with SYBR Green PCR Master Mix (Applied Biosystems) for time-course transcript measurements. Seeds (stage 0), protocorms (stages 1–3) or the top second leaves of seedlings at different stages (stages 4–6) were collected every 2 h for total RNA isolation and cDNA synthesis. The condition of real-time PCR was 95°C for 10 min, then 40 cycles of amplification (95°C for 15 s, 60°C for 1 min, 72°C for 30 s). The real-time PCR experiments were repeated at least three times. The gene-specific primers for real-time PCR for two *PPC* genes and one *PaPPCK* gene were designed using the Primer Express 2.0 (Applied Biosystems). The *Actin* gene of *P. aphrodite* subsp. *formosana* was used for normalization. All the primers used were listed in **Supplementary Table S1**.

## Reverse-Transcription PCR Assay

For total RNA isolation and cDNA synthesis, the top second leaf of mature plants of *P. aphrodite* subsp. *formosana* were collected every 2 h at the growth chamber at 30 $\mu mol \cdot m^{-2} \cdot s^{-1}$ (daylight fluorescent tube FL-20D/18) with a 12-h daylength (0600 to 1800 h). Primers specific for two PEPC isogenes, i.e., *PPC1* (PEQU07008) and *PPC2* (PEQU14315) in RT-PCR amplification were designed using Primer3 Input (v. 0.4.0)[1]. The condition for amplification was one cycle of 94°C for 5 min; 35 cycles of 95°C for 30 s, 55°C for 30 s, and 72°C for 30 s; and a final elongation at 72°C for 5 min. The *Actin* gene of *P. aphrodite* subsp. *formosana* was used as the positive control.

## Phylogenetic Analysis

The PaPPCK sequence was analyzed by using a BLASTX algorithm in a BLAST search against the NCBI database to find the closest sequence matches in the database. Multiple alignments of amino acid sequences was performed using the ClustalW program (Thompson et al., 1994) in BioEdit Ver. 7.0.0 (Hall, 1999). Phylogenetic relationships were estimated using MEGA Ver. 4 with Neighbor-joining (NJ) analysis. The scale bar indicates a genetic distance for 0.1 amino acid substitutions per site. Every branch was supported by bootstrap analysis for 1000 replications (values of more than 70% are shown below the branches). Calcium-dependent protein kinase (CDPKs) sequences were used as the outgroup. Accession numbers of genes used for alignment and phylogenetic analyses in this study were listed in **Supplementary Table S2**.

# RESULTS

## Photosynthetic Characteristics at Different Developmental Stages

In developing protocorms, higher $CO_2$ concentrations within culture tubes were detected during the dark period than the light period, indicating the lack of CAM expression (**Figure 2A**). By stage 4, only a small amount of net $CO_2$ assimilation were detected during the light period, but no net $CO_2$ assimilation was detected during the dark period (**Figure 2B**). The typical net $CO_2$ assimilation rhythm of CAM was first observed by stage 5, which showed a major net $CO_2$ assimilation during the dark period.

[1] http://primer3.ut.ee

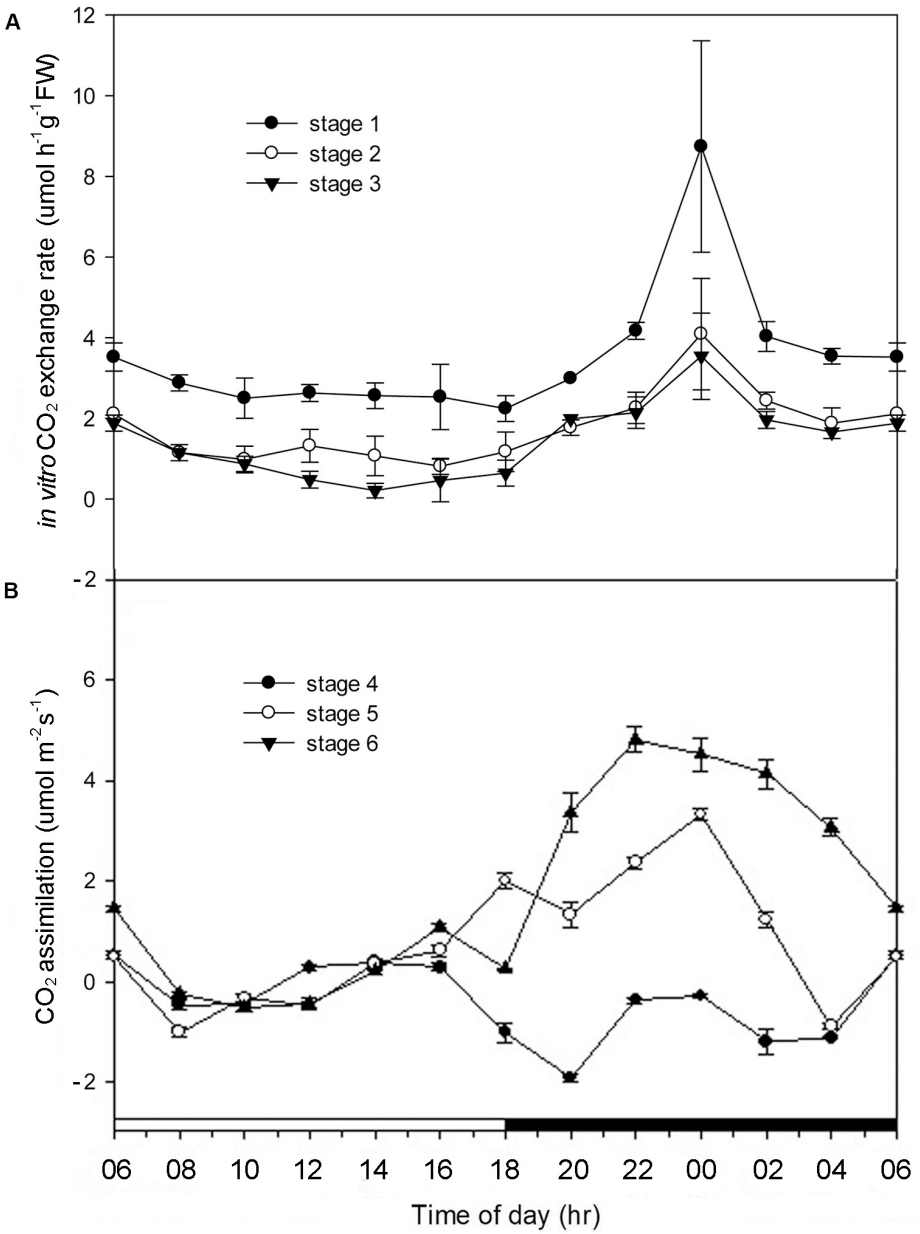


**FIGURE 2 |** Alterations of $CO_2$ exchange rate in *Phalaenopsis* at different developmental stages. **(A)** $CO_2$ exchange rate of *Phalaenopsis* in culture tubes measured by IR-analyzer from stages 1 to 3 during a 24-h period. **(B)** $CO_2$ assimilation of *Phalaenopsis* at stages 4–6 measured by LI-COR's portable photosynthesis system during a 24-h period. Error bars represent standard error (SE) for three independent replications with the 3 mean of three culture tubes. The black bar on the *x*-axis represent the dark period.

## Malate Contents and PEPC Activities at Different Developmental Stages

From stages 0 to 2, no diurnal differences in the malate contents were observed. By stage 3, the noteworthy diurnal fluctuations in the malate contents first appeared, and the diurnal fluctuations were becoming noticeable as the seedlings becoming mature (stages 4–6) (**Figure 3A**). In developing protocorms and seedlings, the diurnal fluctuations in PEPC activity were similar to those in malate contents (**Figure 3B**).

## Characterization of PEPC Isoforms in *Phalaenopsis*

The whole genome sequence dataset of *Phalaenopsis equestris* revealed two isoforms of *PPC* (i.e., PEQU07008 and PEQU14315) occurred in its genome (Cai et al., 2015), while only one copy of *PPC* (AJ300742) was found in the EST library of *P. aphrodite* subsp. *formosana* (previously known as *P. amabilis*) (Tsai et al., 2013). In this study, molecular phylogenetic analysis indicated that PEQU07008 and AJ300742 were nested in *PPC1* clade (the

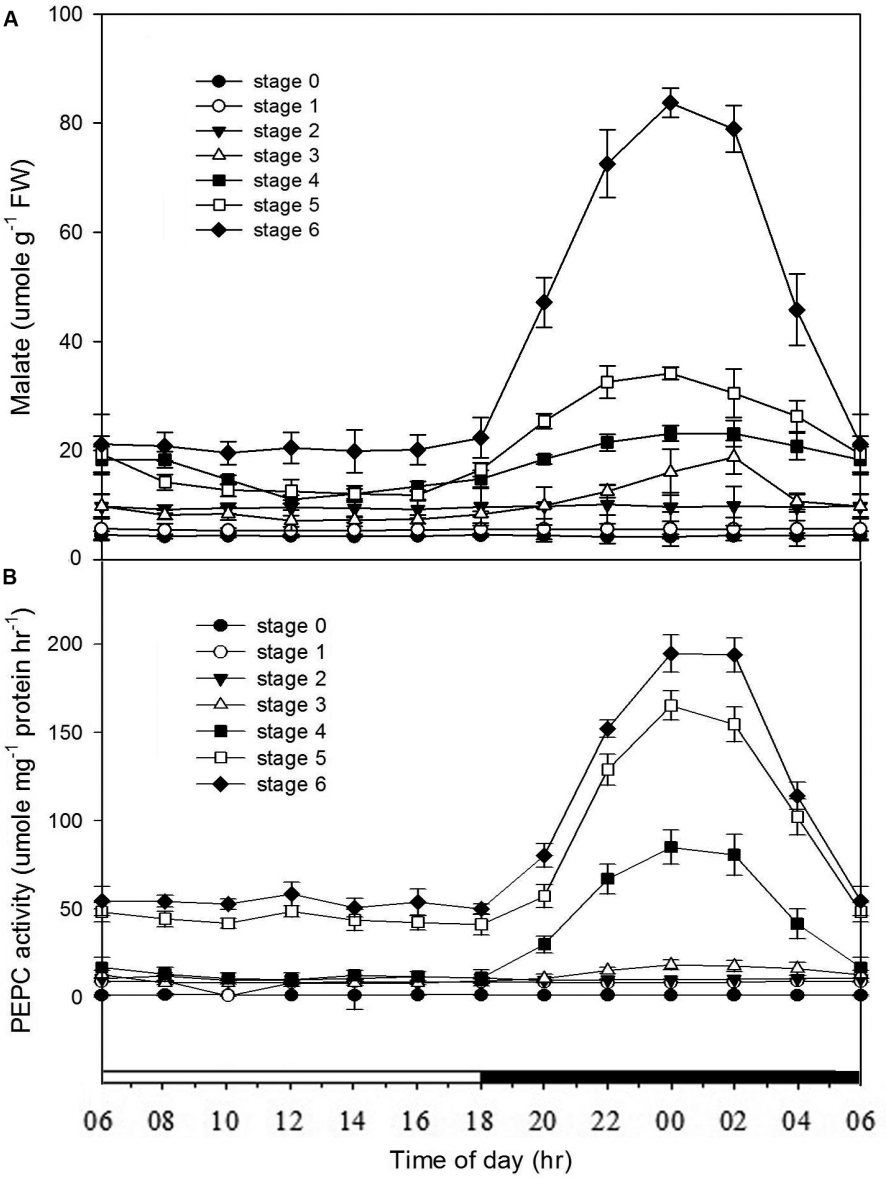


**FIGURE 3 |** Changes of malate contents and PEPC activities in *Phalaenopsis* at different developmental stages. Day/night changes in **(A)** malate content and **(B)** PEPC activity in different developmental stages (stages 0–6). Malate and PEPC activity were detected in the mature seed (stage 0), the enlarged embryo (stage 1), the protocorm (stages 2 and 3) and the different developmental ages of leaf (stages 4–6). Error bars represent standard error (SE) for three independent replications with the mean of six samples.

CAM-related), while PEQU14315 was nested in *PPC2* clade (the anapleurotic) (**Supplementary Figure S1**).

## Isolation and Characterization of *PaPPCK* cDNA

Full-length of *PaPPCK* cDNA was successfully cloned from *P. aphrodite* subsp. *formosana* using a combination of RT-PCR and RACE strategies. The GenBank accession numbers of *PaPPCK* sequence was 2100748. The cDNA contains an open reading frame of 843 bp, flanked by 5′- and 3′-untranslated sequences of 35 and 233 bp, respectively. The cDNA of *PaPPCK* encodes a protein of 281 amino acids that demonstrates 61∼64%, 61%, and 57% sequence identity to three rice PPCKs, ice plant PPCK, and *Kalanchoe fedtschenkoi* PPCK, respectively (**Supplementary Figure S2**). The molecular phylogenetic analysis among PaPPCK and several other PPCK orthologs revealed that PaPPCK clustered with the same group of monocots (**Figure 4**).

## Expression and Abundance of *PPC* Isogenes and *PaPPCK*

To gain the further insight into the relationships among the $CO_2$ assimilation, malate content, PEPC activity and gene expression

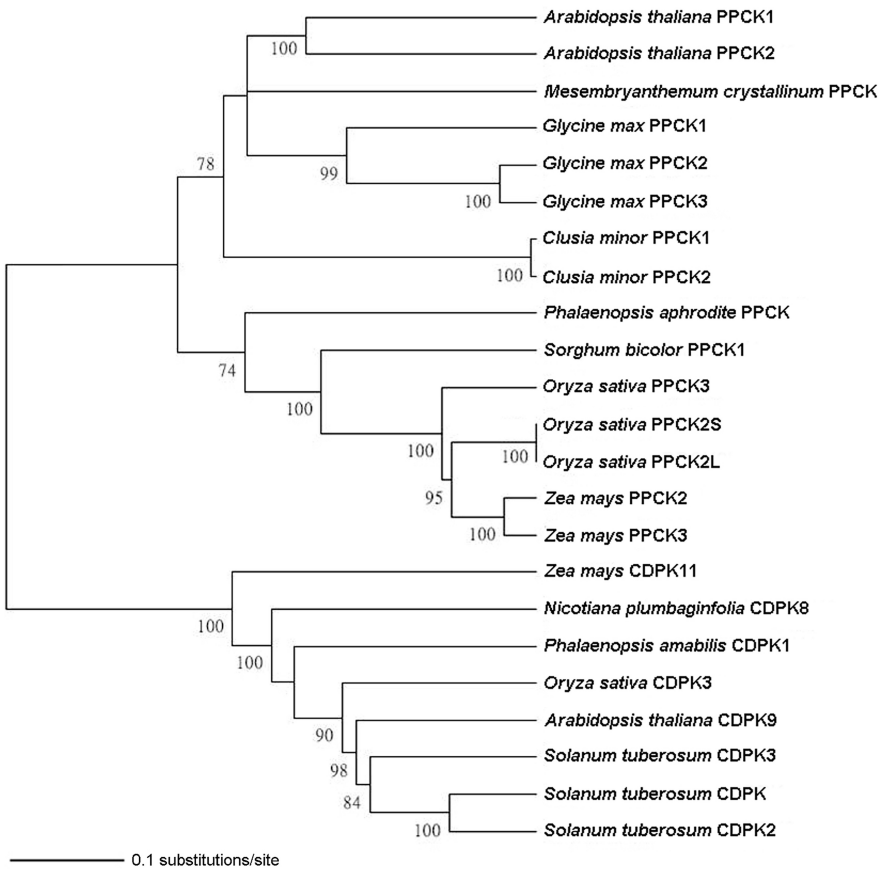


**FIGURE 4 |** Phylogenetic analysis of the PaPPCK protein. The phylogenetic relationship is conducted using Neighbor-Joining with 1000 bootstrap replicates (bootstrap values < 70% are not shown). The scale bar indicates a genetic distance for 0.1 amino acid substitutions per site. Calcium-dependent protein kinase (CDPKs) sequences are used as the outgroup. The accession numbers of genes are given in **Supplementary Table S2**.

patterns at different developing stages, the mRNA levels of *PPC* and *PaPPCK* were analyzed every 2 h over a 24 h period by quantitative real-time PCR analysis (**Figure 5**). As expressions of *PPC* isogenes in different developmental stages were measured, no obvious day/night fluctuations was observed, and their expressions were constitutive and rather constant. From stages 4 to 6, the expression pattern of *PaPPCK* showed a typical diurnal/nocturnal rhythm.

## DISCUSSION

In *Phalaenopsis*, the nocturnal $CO_2$ uptake was not observed until stage 5 (**Figure 2**). During stages 1–3, no obvious depletion of $CO_2$ *in vitro* was detected, and the increase of $CO_2$ concentration within the culture tubes from light to dark periods may reflect the elevated respiration rate of high-energy requirements in developing protocorms (**Figure 2A**). Differences between day/night malate and PEPC activity was first observed at stage 3 and the breadth of day/night fluctuation enlarged as the seedlings developed (**Figure 3**). These results implied a progressive shift from $C_3$ to CAM as the protocorms differentiated the first leaf in *Phalaenopsis* (from stages 3–5). The age-dependent expression of CAM has been reported in a number of plants. In *M. crystallinum*, CAM performance is modulated ontogenetically by a genetic developmental program, although high salinity could rapidly induce CAM expression in young plants (Cushman et al., 1990; Cushman and Bohnert, 1996). Several CAM species, such as *Ananas comosus, Kalanchoe fedtschenkoi*, *Peperomia*, and *Clusia* species, have demonstrated that a progression from $C_3$ to CAM occurred as the leaves becoming matured (Jones, 1975; Holthe et al., 1987; Zotz and Winter, 1996; Vaasen et al., 2006; Winter et al., 2008). During the transitional phase from $C_3$ to CAM, the photosynthetic features (e.g., no significant nocturnal $CO_2$ uptake but having malate accumulation in the stage 4 seedlings) were similar to CAM-cycling in which plants kept their stomata closed and accumulation organic acids by recapturing the respiratory $CO_2$ during the night (Holthe et al., 1987; Ting et al., 1996). CAM-cycling strategy allows the maintenance of photosynthetic capacity as well as water saving during drought or in the dry season (Harris and Martin, 1991). In *Phalaenopsis*, upon germination, the embryo first develops into a protocorm

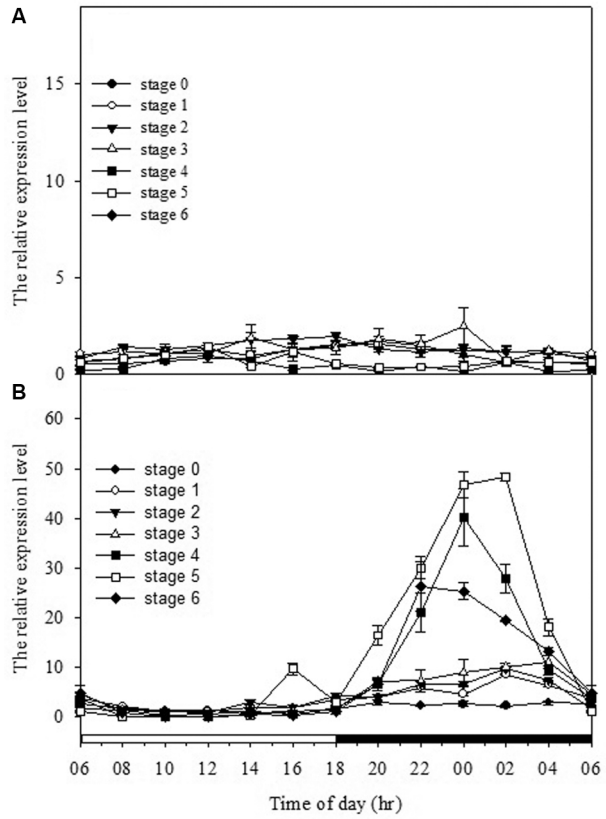


**FIGURE 5 |** Day/night changes in levels of **(A)** *PPC1* (AJ300742) and **(B)** *PaPPCK* (2100748) in different developmental stages (stages 0–6). Relative transcript levels are measured by real-time PCR with *Actin* gene of *P. aphrodite* subsp. *formosana* as loading control. Error bars represent standard error (SE) for three independent replications. The black bar on the *x*-axis represents the dark period.

before forming a plantlet. Since the differentiation of first root takes about 8 weeks after germination to uptake water efficiently, CAM-cycling may help protocorms to tolerate water deficit.

Previous reports have shown that the performance of CAM could be transcriptionally regulated at the mRNA amounts of PEPC as plants became mature or in response to stress conditions (Cushman et al., 1990; Haasg-Kerwer et al., 1992; Borland et al., 1996). To determine if the ontogenetic difference in CAM performance in *Phalaenopsis* was reflected by differences in the expression of *PPC* transcripts, we measured the expression and abundance of two *PPC* isogenes in different developmental stages. In orchids, molecular phylogenetic analysis of *PPC* genes indicated that *PPCs* can be separated into two clades that reflected their different functions, i.e., the CAM-related *PPC1* and the anapleurotic function *PPC2*, respectively (Silvera et al., 2014; Deng et al., 2016). Our previous study (Ping et al., 2010) as well as the results in this study demonstrated that both *PPC1* (the CAM-related) and *PPC2* (the anapleurotic) expressed in all developmental stage regardless of the time point (**Figure 5** and **Supplementary Figure S3**), suggesting that the day/night rhythm of PEPC activity is not likely controlled at the abundance of both *PPC* transcripts but another factor.

In addition to the transcriptional control of PEPC activity, the posttranslational control by PEPC kinase also plays an important role in CAM performance (Hartwell et al., 1999; Taybi et al., 2004). The activation of PEPCs in CAM is regulated through a reversible phosphorylation by PEPC kinase (Vidal and Chollet, 1997; Nimmo, 2000, 2003). PEPC kinase is encoded by a small gene family involved in a variety of functions for the precise regulation of PEPC activity (Sullivan et al., 2004; Fukayama et al., 2006; Shenton et al., 2006). In *Phalaenopsis*, so far only one gene encoding PEPC kinase has been found. In general, *PaPPCK* increases its expression levels as the seedlings grew up. High levels of *PaPPCK* transcripts were detected during the dark period and extremely low amounts during the light period, particularly in the plants of stage 3 (**Figure 5B**). In stage 5, the increased magnitudes of malate accumulation and PEPC activity were not as high as the level of *PaPPCK* expression (**Figures 3**, 5). The existence of a protein inhibitor of PEPC kinase may provide an additional layer of control over malate accumulation by PEPC activity (Nimmo G. A. et al., 2001). Indeed, the apparent day/night difference in *PaPPCK* expression corresponds to day/night fluctuations in PEPC activity and malate levels. In *C. minor*, a $C_3$-CAM intermediate species, CAM performance is also achieved through the shift in *PPCK* expression (Borland and Griffiths, 1997). In facultative CAM species, e.g., *K. fedtschenkoi* and *M. crystallinum*, the phosphorylation of PEPC is primarily controlled by the abundance of the *PPCK* transcript, and hence facilitates the nocturnal $CO_2$ uptake (Hartwell et al., 1999; Taybi et al., 2000). It is known that PPCK contains a protein kinase domain without regulatory regions indicated that its activity appears to be controlled primarily at the level of expression (Nimmo H. G. et al., 2001; Nimmo, 2003). In *Phalaenopsis*, the distinctive expression pattern of *PaPPCK* leads us propose that PaPPCK likely plays a critical role in regulating the phosphorylation state of PEPC during the night to CAM performance.

## CONCLUSION

Our results demonstrated a progressive shift from $C_3$ to CAM as the protocorms differentiated the first leaf in *Phalaenopsis* seedlings by measuring the profiles of day/night $CO_2$ exchange, malate contents, PEPC activity and the expression of *PPC* isogenes and *PaPPCK*. Notably, in *Phalaenopsis* seedlings, the day/night fluctuations in PEPC activity and the expression of *PaPPCK* as well as $CO_2$ uptake was coincident well along the developing stages. Since *PPC* isogenes were constitutively expressed over a 24-h cycle, *PaPPCK* may be involved in regulating CAM performance in *Phalaenopsis*.

## AUTHOR CONTRIBUTIONS

Y-IL conceived the study. Y-IL, F-CC, T-SL, and W-JY designed the study. C-YP, F-CC, and T-CC performed molecular analyses. C-YP performed qPCR and biochemical experiments.

C-YP and H-LL performed photosynthesis analyses. C-YP, Y-IL, W-JY, and F-CC wrote the paper. All the authors read and approved the final manuscript.

## ACKNOWLEDGMENTS

This work was supported by the grant [98SB-05.01-ST-01(5)] from the Council of Agriculture, Executive Yuan, ROC to W-JY; from National Museum of Natural Science, Taiwan, to Y-IL.

## SUPPLEMENTARY MATERIAL

The Supplementary Material for this article can be found online at: https://www.frontiersin.org/articles/10.3389/fpls.2018.01587/full#supplementary-material

**Figure S1 |** Phylogenetic analysis of PEPC amino acid sequences using Neighbor-joining method described above in the phylogenetic analysis. The other sequences of PEPC obtained from GenBank were added to the analysis by referring to Deng et al. (2016). The *PEPC* genes from *Phalaenopsis* are denoted by arrows. Branch numbers indicated bootstrap support (1000 replicates). Bootstrap values < 70% were not shown.

**Figure S2 |** Alignment of deduced PaPPCK amino acid sequence with PPCKs. The accession numbers of genes were given in **Supplementary Table S2**. Black and shadow represented identities and similarities respectively. At, *Arabidopsis thaliana*; Ft, *Flaveria trinervia*; Kf, *Kalanchoë fedtschenkoi*; Mc, common ice plant; Os, rice; Pa, *Phalaenopsis aphrodite*; Sb, *Sorghum bicolor*; Zm, maize.

**Figure S3 |** Day/night changes in levels of transcripts for two *PEPC* genes, i.e., *PPC1* (PEQU07008 and AJ300742), *PPC2* (PEQU14315), and *Actin* as control for equal RNA input and RT-PCR conditions in mature leaves of *P. aphrodite* subsp. *formosana*.

**Table S1 |** Primer pairs used in this study.

**Table S2 |** PPCK and CDPK sequences used for conducting the amino acid alignment and phylogenetic analysis.

## REFERENCES


Arditti, J. (1992). *Fundamentals of Orchid Biology*. New York, NY: John Wiley& Sons.

Borland, A. M., and Griffiths, H. (1997). A comparative study on the regulation of C3 and C4 carboxylation processes in the constitutive crassulacean acid metabolism (CAM) plant Kalanchoë daigremontiana and the C3-CAM intermediate Clusia minor. *Planta* 201, 368–378. doi: 10.1007/s004250050079

Borland, A. M., Griffiths, H., Maxwell, C., Fordham, M. C., and Broadmeadow, M. S. J. (1996). CAM induction in *Clusia minor* L. during the transition from wet to dry season in Trinidad: the role of organic acid speciation and decarboxylation. *Plant Cell Environ.* 19, 655–664. doi: 10.1111/j.1365-3040.1996.tb00400.x

Borland, A. M., Hartwell, J., Weston, D. J., Schlauch, K. A., Tschaplinski, T. J., Tuskan, G. A., et al. (2014). Engineering crassulacean acid metabolism to improve water-use efficiency. *Trends Plant Sci.* 19, 327–338. doi: 10.1016/j.tplants.2014.01.006

Bradford, M. M. (1976). A rapid and sensitive method for the quantitation of microgram quantities utilizing the principle of protein-dye binding. *Anal. Biochem.* 72, 248–254. doi: 10.1006/abio.1976.9999

Cai, J., Liu, X., Vannest, K., Proost, S., Tsai, W. C., Liu, K. W., et al. (2015). The genome sequence of the orchid *Phalaenopsis equestris*. *Nat. Genet.* 47, 65–72. doi: 10.1038/ng.3149

Chen, Y. I., and Lee, N. (2002). Diurnal rhythm of carbon dioxide, ethylene and organic acid concentration in *Phalaenopsis amabilis* var. *formosana* plantlets cultured in vitro. *J. Chin. Soc. Hortic. Sci.* 48, 157–166.

Chollet, R., Vidal, J., and O'Leary, M. H. (1996). Phosphoenolpyruvate carboxylase: a ubiquitous, highly regulated enzyme in plants. *Annu. Rev. Plant Physiol. Mol. Biol.* 47, 273–298. doi: 10.1146/annurev.arplant.47.1.273

Cui, Y. Y., Pandey, D. M., Hahn, E. J., and Paek, K. Y. (2004). Effect of drought on physiological aspects of crassulacean acid metabolism in *Doritaenopsis*. *Plant Sci.* 167, 1219–1226. doi: 10.1016/j.plantsci.2004.06.011

Cushman, J. C., and Bohnert, H. J. (1996). "Transcription activation of CAM genes during development and environmental stress," in *Crassulacean acid Metabolism: Biochemistry, Ecophysiology and Evolution*, eds K. Winter and J. A. C. Smith (New York, NY: Springer-Verlag), 135–158.

Cushman, J. C., Meyer, G., Michalowski, C. B., Schmitt, J. M., and Bohnert, H. J. (1989). Salt stress leads to differential expression of two isogenes of phosphoenolpyruvate carboxylase during crassulacean acid metabolism induction in the common ice plant. *Plant Cell* 1, 715–725. doi: 10.2307/3868962

Cushman, J. C., Michalowski, C. B., and Bohnert, H. J. (1990). Developmental control of crassulacean acid metabolism inducibility by salt stress in the common ice plant. *Plant Physiol.* 94, 1137–1142. doi: 10.1104/pp.94.3.1137

Deng, H., Zhang, L. S., Zhang, G. Q., Zheng, B. Q., Liu, Z. J., and Wang, Y. (2016). Evolutionary history of PEPC genes in green plants: implications for the evolution of CAM in orchids. *Mol. Phylogenet. Evol.* 94, 559–564. doi: 10.1016/j.ympev.2015.10.007

Endo, M., and Ikusima, I. (1989). Diurnal rhythm and characteristics of photosynthesis and respiration in the leaf and root of a Phalaenopsis plant. *Plant Cell Physiol.* 30, 43–47. doi: 10.1093/oxfordjournals.pcp.a077715

Fukayama, H., Tamai, T., Taniguchi, Y., Sullivan, S., Miyao, M., and Nimmo, H. G. (2006). Characterization and functional analysis of phosphoenolpyruvate carboxylase kinase genes in rice. *Plant J.* 47, 258–268. doi: 10.1111/j.1365-313x.2006.02779.x

Gehrig, H., Faist, K. V., and Kluge, M. (1998). Identification of phosphoenolpyruvate carboxylase isoforms in leaf, stem and roots of the obligate CAM plant *Vanilla planifolia* Salib (Orchidaceae): a physiological and molecular approach. *Plant Mol. Biol.* 38, 1215–1223. doi: 10.1023/a:1006006331011

Gehrig, H., Heute, V., and Kluge, M. (2001). New partial sequences of phosphoenolpyruvate carboxylase as molecular phylogenetic markers. *Mol. Phylogenet. Evol.* 20, 262–274. doi: 10.1006/mpev.2001.0973

Gehrig, H., Taybi, T., Kluge, M., and Brulfert, J. (1995). Identification of multiple PEPC isogenes in leaves of the facultative crassulacean acid metabolism (CAM) plant *Kalanchoë blossfeldiana* Poelln. cv. *Tom Thumb*. *FEBS Lett.* 377, 399–402. doi: 10.1016/0014-5793(95)01397-0

Gehrig, H., Winter, K., Cushman, J., Borland, A., and Taybi, T. (2000). An improved RNA isolation method for succulent plant species rich in polyphenols and polysaccharides. *Plant Mol. Biol. Rep.* 18, 369–376. doi: 10.1007/bf02825065

Goh, C. J., Wara-Aswapati, O., and Avadhami, P. N. (1984). Crassulacean acid metabolism in young orchid leaves. *New Phytol.* 96, 519–526. doi: 10.1111/j.1469-8137.1984.tb03585.x

Griesbach, R. J. (2000). Potted phalaenopsis orchid production: history, present status, and challenges for the future. *Horttechnology* 10:429.

Guo, W. J., and Lee, N. (2006). Effect of leaf and plant age, and day/night temperature on net CO2 uptake in *Phalaenopsis amabilis* var. *formosa*. *J. Am. Soc. Hortic. Sci.* 131, 320–326.

Haasg-Kerwer, A., Haag-Kerwer, A., Franco, A. C., and Luttge, U. (1992). The effects of temperature and light on gas exchange and acid accumulation in the C3-CAM plant *Clusia minor* L. *J. Exp. Bot.* 43, 345–352. doi: 10.1093/jxb/43.3.345

Hall, T. A. (1999). BioEdit: a user-friendly biological sequence alignment editor and analysis program for Windows 95/98/NT. *Nucleic Acids Symp. Ser.* 41, 95–98.

Harris, F. S., and Martin, C. E. (1991). Correlation between CAM-cycling and photosynthetic gas exchange in five species of *Talinum* (Portulacaceae). *Plant Physiol.* 96, 1118–1124. doi: 10.1104/pp.96.4.1118

Hartwell, J., Gill, A., Nimmo, G. A., Wilkins, M. B., Jenkins, G. I., and Nimmo, H. G. (1999). Phosphoenolpyruvate carboxylase kinase is a novel protein kinase regulated at the level of expression. *Plant J.* 20, 1–10. doi: 10.1046/j.1365-313x.1999.00609.x

Hew, C. S., and Khoo, S. I. (1980). Photosynthesis of young orchid seedlings. *New Phytol.* 86, 349–357. doi: 10.1111/j.1469-8137.1980.tb01675.x

Holthe, P. A., Sternberg, L. D. S. L., and Ting, I. P. (1987). Developmental control of CAM in Peperomia scandens. *Plant Physiol.* 84, 743–747. doi: 10.1104/pp.84.3.743

Jones, M. B. (1975). The effect of leaf age on leaf resistance and CO2 exchange of the CAM plant *Bryophyllum fedtschenkoi*. *Planta* 123, 91–96. doi: 10.1007/bf00388063

Krömer, S., Gardeström, P., and Samuelsson, G. (1996). Regulation of the supply of cytosolic oxaloacetate for mitochondrial metabolism via phosphoenolpyruvate carboxylase in barley leaf protoplasts. I. The effect of covalent modification on PEPC activity, pH response, and kinetic properties. *BBA* 1289, 343–350. doi: 10.1016/0304-4165(95)00164-6

Ku, M. S. B., Agarie, S., Nomura, M., Fukayama, H., Tsuchida, H., Ono, K., et al. (1999). High-level expression of maize phosphoenolpyruvate carboxylase in transgenic rice plants. *Nat. Biotechnol.* 17, 76–80. doi: 10.1038/5256

Li, B., and Chollet, R. (1994). Salt induction and the partial purification/characterization of phosphoenolpyruvate carboxylase protein-serine kinase from an inducible crassulacean-acid-metabolism (CAM) plant, *Mesembryanthemum crystallinum* L. *Arch. Biochem. Biophys.* 314, 247–254. doi: 10.1006/abbi.1994.1437

Lo, S. C. (2008). Identification of native Phalaenopsis photosynthetic characteristics. *Res. Bull. Taitung District Agric. Improve. Station* 18, 15–44.

Möllering, H., and Malt, L. (1974). *Methoden der Enzymatischen Analyse*, ed. H. U. Bergmeyer (Weinheim: Verlag Chemie Press), 1636–1639.

Murashige, T., and Skoog, F. (1962). A revised medium for rapid growth and bioassays with tobacco tissue cultures. *Physiol. Plant.* 15, 473–497. doi: 10.1111/j.1399-3054.1962.tb08052.x

Nimmo, G. A., Wilkins, M. B., and Nimmo, H. G. (2001). Partial purification and characterization of a protein inhibitor of phosphoenolpyruvate carboxylase kinase. *Planta* 213, 250–257. doi: 10.1007/s004250000501

Nimmo, H. G., Fontaine, V., Hartwell, J., Jenkins, G. I., Nimmo, G. A., and Wilkins, M. B. (2001). PEP carboxylase kinase is a novel protein kinase controlled at the level of expression. *New Phytol.* 151, 91–97. doi: 10.1046/j.1469-8137.2001.00155.x

Nimmo, H. G. (2000). The regulation of phosphoenolpyruvate carboxylase in CAM plants. *Trends Plant Sci.* 5, 75–80. doi: 10.1016/s1360-1385(99)01543-5

Nimmo, H. G. (2003). Control of the phosphorylation of phosphoenolpyruvate carboxylase in higher plants. *Arch. Biochem. Biophys.* 414, 189–196. doi: 10.1016/s0003-9861(03)00115-2

Osmond, C. B., and Holtum, J. A. M. (1981). "Crassulacean acid metabolism," in *The Biochemistry of Plants: A Comprehensive Treatise*, Vol. 8, eds M. D. Hatch and N. K. Boardman (London: Academic), 283–328.

Ota, K., Morioka, K., and Yamamoto, Y. (1991). Effects of leaf age, inflorescence, temperature, light intensity and moisture conditions on CAM photosynthesis in Phalaenopsis. *Engei Gakkai Zasshi* 60, 125–132. doi: 10.2503/jjshs.60.125

Ping, C. Y., Lee, Y. I., Lin, T. S., Yang, W. J., and Lee, G. C. (2010). Crassulacean acid metabolism in *Phalaenopsis aphrodite* var. *formosa* during different developmental stages. *Acta Hortic.* 878, 71–77. doi: 10.17660/actahortic.2010.878.7

Rodrigues, M. A., Matiz, A., Cruz, A. B., Matsumura, A. T., Takahashi, C. A., Hamachi, L., et al. (2013). Spatial patterns of photosynthesis in thin- and thick-leaved epiphytic orchids: unravelling C3-CAM plasticity in an organ-compartmented way. *Ann. Bot.* 112, 17–29. doi: 10.1093/aob/mct090

Shenton, M., Fontaine, V., Hartwell, J., Marsh, J. T., Jenkins, G. I., and Nimmo, H. G. (2006). Distinct patterns of control and expression amongst members of the PEP carboxylase kinase gene family in C4 plants. *Plant J.* 48, 45–53. doi: 10.1111/j.1365-313x.2006.02850.x

Silvera, K., Santiago, L. S., Cushman, J. C., and Winter, K. (2009). Crassulacean acid metabolism and epiphytism linked to adaptive radiations in the Orchidaceae. *Plant Physiol.* 149, 1838–1847. doi: 10.1104/pp.108.132555

Silvera, K., Winter, K., Rodriguez, B. L., Albion, R. L., and Cushman, J. C. (2014). Multiple isoforms of phosphoenolpyruvate carboxylase in the Orchidaceae (subtribe Oncidiinae): implications for the evolution of crassulacean acid metabolism. *J. Exp. Bot.* 65, 3623–3636. doi: 10.1093/jxb/eru234

Sullivan, S., Jenkins, G. I., and Nimmo, H. G. (2004). Roots, cycles and leaves. Expression of the phosphoenolpyruvate carboxylase kinase gene family in soybean. *Plant Physiol.* 135, 2078–2087. doi: 10.1104/pp.104.042762

Taybi, T., Nimmo, H. G., and Borland, A. M. (2004). Expression of phosphoenolpyruvate carboxylase and phosphoenolpyruvate carboxylase kinase genes. Implications for genotypic capacity and phenotypic plasticity in the expression of crassulacean acid metabolism. *Plant Physiol.* 135, 587–598. doi: 10.1104/pp.103.036962

Taybi, T., Patil, S., Chollet, R., and Cushman, J. C. (2000). A minimal serine/threonine protein kinase circadianly regulates phosphoenolpyruvate carboxylase activity in CAM induces leaves of the common ice plant. *Plant Physiol.* 123, 1471–1482. doi: 10.1104/pp.123.4.1471

Thompson, J. D., Higgins, D. G., and Gibson, T. J. (1994). CLUSTAL W: improving the sensitivity of progressive multiple sequence alignments through sequence weighting, position specific gap penalties and weight matrix choice. *Nucleic Acids Res.* 22, 4673–4680. doi: 10.1093/nar/22.22.4673

Ting, I. P., Patel, A., Kaur, S., Hann, J., and Walling, L. (1996). "Ontogenetic development of crassulacean acid metabolism as modified by water stress in *Peperomia*," in *Crassulacean acid Metabolism: Biochemistry, Ecophysiology, and Evolution*, eds K. Winter and J. A. C. Smith (New York, NY: Springer-Verlag), 204–215.

Tsai, W. C., Fu, C. H., Hsiao, Y. Y., Huang, Y. M., Chen, L. J., Wang, M., et al. (2013). OrchidBase 2.0: comprehensive collection of Orchidaceae floral transcriptomes. *Plant Cell Physiol.* 54:e7. doi: 10.1093/pcp/pcs187

U.S. Department of Agriculture [USDA] (2017). *Floriculture Crops 2016 Summary*. Washington, DC: U.S. Dept. Agr.

Vaasen, A., Begerow, D., and Hampp, R. (2006). Phosphoenolpyruvate carboxylase genes in C3, crassulacean acid metabolism (CAM) and C3/CAM intermediate species of the genus Clusia: rapid reversible C3/CAM switches are based on the C3 housekeeping gene. *Plant Cell Environ.* 29, 2113–2123. doi: 10.1111/j.1365-3040.2006.01583.x

Vidal, J., and Chollet, R. (1997). Regulatory phosphorylation of C4 PEP carboxylase. *Trends Plant Sci.* 2, 230–237. doi: 10.1016/S1360-1385(97)89548-9

Winter, K., Garcia, M., and Holtum, J. A. M. (2008). On the nature of facultative and constitutive CAM: environmental and developmental control of CAM expression during early growth of Clusia, Kalanchoe, and Opuntia. *J. Exp. Bot.* 59, 1829–1840. doi: 10.1093/jxb/ern080

Winter, K., and Smith, A. P. C. (1996). *Crassulacean Acid Metabolism. Biochemistry, Ecophysiology and Evolution*. Heidelberg: Springer-Verlag. doi: 10.1007/978-3-642-79060-7

Zotz, G., and Winter, K. (1996). "Seasonal changes in daytime versus nighttime CO2 fixation of *Clusia uvitana* in situ," in *Crassulacean Acid Metabolism: Biochemistry, Ecophysiology, and Evolution*, eds K. Winter and J. A. C. Smith (New York, NY: Springer-Verlag), 312–323.

**Conflict of Interest Statement:** The authors declare that the research was conducted in the absence of any commercial or financial relationships that could be construed as a potential conflict of interest.

frontiers in Plant Science

ORIGINAL RESEARCH
published: 25 April 2018
doi: 10.3389/fpls.2018.00552

# Immunolocalization and Changes of Hydroxyproline-Rich Glycoproteins During Symbiotic Germination of *Dendrobium officinale*

*Yuan-Yuan Li[1†], Xiao-Mei Chen[1†], Ying Zhang[1], Yu-Hsiu Cho[2], Ai-Rong Wang[1], Edward C. Yeung[3], Xu Zeng[1], Shun-Xing Guo[1*] and Yung-I Lee[2,4*]*

[1] Institute of Medicinal Plant Development, Chinese Academy of Medical Sciences and Peking Union Medical College, Beijing, China, [2] Biology Department, National Museum of Natural Science, Taichung, Taiwan, [3] Department of Biological Sciences, University of Calgary, Calgary, AB, Canada, [4] Department of Life Sciences, National Chung Hsing University, Taichung, Taiwan

OPEN ACCESS

**Edited by:**
Swee-Suak Ko,
Academia Sinica, Taiwan

**Reviewed by:**
Raffaella Balestrini,
Consiglio Nazionale delle Ricerche (CNR), Italy
Miguel Angel Flores-Vergara,
North Carolina State University, United States

***Correspondence:**
Shun-Xing Guo
sxguo1986@163.com
Yung-I Lee
leeyungi@hotmail.com;
leeyungi@mail.nmns.edu.tw

[†] These authors have contributed equally to this work.

**Specialty section:**
This article was submitted to Plant Evolution and Development, a section of the journal Frontiers in Plant Science

**Received:** 05 January 2018
**Accepted:** 09 April 2018
**Published:** 25 April 2018

**Citation:**
Li Y-Y, Chen X-M, Zhang Y, Cho Y-H, Wang A-R, Yeung EC, Zeng X, Guo S-X and Lee Y-I (2018) Immunolocalization and Changes of Hydroxyproline-Rich Glycoproteins During Symbiotic Germination of Dendrobium officinale. Front. Plant Sci. 9:552. doi: 10.3389/fpls.2018.00552

Hydroxyproline-rich glycoproteins (HRGPs) are abundant cell wall components involved in mycorrhizal symbiosis, but little is known about their function in orchid mycorrhizal association. To gain further insight into the role of HRGPs in orchid symbiosis, the location and function of HRGPs were investigated during symbiotic germination of *Dendrobium officinale*. The presence of JIM11 epitope in developing protocorms was determined using immunodot blots and immunohistochemical staining procedures. Real-time PCR was also employed to verify the expression patterns of genes coding for extensin-like genes selected from the transcriptomic database. The importance of HRGPs in symbiotic germination was further investigated using 3,4-dehydro-L-proline (3,4-DHP), an inhibitor of HRGP biosynthesis. In symbiotic cultures, immunodot blots of JIM11 signals were moderate in mature seeds, and the signals became stronger in swollen embryos. After germination, signal intensities decreased in developing protocorms. In contrast, in asymbiotic cultures, JIM11 signals were much lower as compared with those stages in symbiotic cultures. Immunofluorescence staining enabled the visualization of JIM11 epitope in mature embryo and protocorm cells. Positive signals were initially localized in the larger cells near the basal (suspensor) end of uninfected embryos, marking the future colonization site of fungal hyphae. After 1 week of inoculation, the basal end of embryos had been colonized, and a strong signal was detected mostly at the mid- and basal regions of the enlarging protocorm. As protocorm development progressed, the signal was concentrated in the colonized cells at the basal end. In colonized cells, signals were present in the walls and intracellularly associated with hyphae and the pelotons. The precise localization of JIM11 epitope is further examined by immunogold labeling. In the colonized cells, gold particles were found mainly in the cell wall and the interfacial matrix near the fungal cell wall. Four extensin-like genes were verified to be highly up-regulated in symbiotically germinated protocorms as compared to asymbiotically germinated ones. The 3,4-DHP treatment inhibited the accumulation of HRGPs and symbiotic seed germination. In these protocorms, fungal

hyphae could be found throughout the protocorms. Our results indicate that HRGPs play an important role in symbiotic germination. They can serve as markers for fungal colonization, establishing a symbiotic compartment and constraining fungal colonization inside the basal cells of protocorms.

**Keywords: *Dendrobium*, immunolocalization, hydroxyproline-rich glycoproteins, mycorrhiza, symbiotic germination**

## INTRODUCTION

Plant cell walls are composed of polysaccharides and other polymers that provide the protoplasm with structural support and protection (Taiz and Zeiger, 2010). In addition to carbohydrate polymers, plant cell walls also contain structural proteins, e.g., hydroxyproline-rich glycoproteins (HRGPs), proline-rich proteins (PRPs), glycine-rich proteins and arabinogalactan-proteins (AGPs) that modify the physical and chemical characteristics of cell wall in response to various developmental and environmental signals (Cassab, 1998). HRGPs occur in plant cell walls as a major protein component (Berger et al., 1994; Cassab, 1998). Extensins are cell wall proteins belonging to the superfamily of HRGPs, and they are known to participate in many processes during plant growth and development, such as pollen recognition and fertilization (Wu et al., 2001), cell division and differentiation (Ruiz-Avila et al., 1992), cell adhesion (Cassab, 1998), cessation of the cell growth (Cassab and Varner, 1987), and zygotic and somatic embryo development (Ruiz-Avila et al., 1991; Xu et al., 2011). Furthermore, HRGPs are involved in the interactions between plants and microorganisms, such as resistance to pathogens (Xie et al., 2011) and symbiotic associations (Balestrini et al., 1997). In the legume-rhizobium symbiosis, HRGPs are found to accumulate mainly in the walls of infected cells and in peribacteroid membranes surrounding groups of bacteroides (Benhamou et al., 1991; Rae et al., 1992), suggesting a crucial role in nodule development.

Endomycorrhizas, e.g., arbuscular mycorrhizas, ericoid mycorrhizas and orchid mycorrhizas, are characterized by intracellular hyphae growth and demonstrate a great diversity of infection patterns (Gianinazzi-Pearson, 1996; Peterson and Massicotte, 2004). In arbuscular mycorrhizas, the intracellular haustoria-like structures, known as arbuscules are formed by Glomeromycota, while in orchid mycorrhizas, intracellular hyphae coils, known as pelotons are produced by fungal species mostly belonging to Basidiomycetes, and these fungal hyphae are eventually digested by orchid cells (Smith and Read, 2008; Dearnaley and Cameron, 2017). During arbuscular mycorrhizal symbiosis, the arbuscules form an important symbiotic interface for nutrient exchange, and HRGPs have been located in the interfacial zone in addition to that in the peripheral walls of the host cells (Bonfante-Fasolo et al., 1991; Balestrini et al., 1994; Balestrini and Bonfante, 2005). These results suggest that HRGPs play a role in symbiotic associations, e.g., the formation of an interfacial compartment (Balestrini and Bonfante, 2014).

In the natural environment, germination of orchid seeds depends on appropriate mycorrhizal associations for nutrient supplies, e.g., carbohydrates and essential minerals (Smith and Read, 2008; Rasmussen and Rasmussen, 2009). Recent studies have revealed the occurrence of bidirectional nutrient transfer in orchid protocorms. Developing protocorm receives carbon and minerals nutrients, e.g., P and N from a mycorrhizal fungus (Cameron et al., 2006, 2007; Bougoure et al., 2013; Kuga et al., 2014) and returns $NH_4^+$ to its fungal partners (Fochi et al., 2017). In the mycorrhizal protocorm, nodulin-like genes were notably up-regulated, suggesting a role in carbon flow (Perotto et al., 2014). During symbiotic germination, nutrients are transported from the fungal hyphae to protocorm cells through the interfacial zone and the plasma membrane of orchid cells. There has been extensive research on the changes of nutrient reserves, organelles, plasma membrane, fungal structures and the organization of cytoskeleton in symbiotic germination of orchids (Smith, 1967; Peterson and Currah, 1990; Uetake et al., 1992; Peterson et al., 1998). Although cell wall remodeling is crucial during symbiotic interactions, until now, there is little information available on the distribution and the role of plant cell wall proteins during orchid symbiotic germination.

In this study, we investigate the distribution and the possible role of HRGPs on symbiotic germination of *Dendrobium officinale*. *D. officinale* has been used in the nobile-type dendrobium breeding and its dry stems are used in traditional Chinese medicine with a broad range of therapeutic effects (Pharmacopoeia Committee of People's Republic of China, 2005). In our previous studies, we have developed an efficient symbiotic germination culture protocol of *D. officinale* to inoculate seeds with fungal strains (*Tulasnella* sp.) isolated by the *in situ* seed baiting technique (Wang et al., 2011; Tan et al., 2014). This procedure provides an ideal system for investigating the interactions between orchid seeds and their mycorrhizal fungal partners (Zhao et al., 2013; Chen et al., 2017). To gain a better insight into the possible functions of HRGPs in symbiotic germination of orchids, it is essential to determine their distribution and to study their biological function during symbiotic interaction. In this study, immunolocalization of JIM 11 epitope was performed to investigate the distribution of HRGPs during symbiotic germination of *D. officinale*. The JIM11 epitope, which recognizes specific arabinosylation motifs of HRGPs has been successfully used to localize extensins during embryo development of monocots, i.e., *Musa* (Xu et al., 2011) and *Phalaenopsis* (Lee et al., 2013). For the study of HRGP function, an inhibitor of HRGP biosynthesis, 3,4-dehydro-L-proline (3,4-DHP), was applied to alter the contents of HRGPs in cell walls of orchid embryos to identify any significant consequences of altering HRGPs on symbiotic germination.

# MATERIALS AND METHODS

## Symbiotic Germination

*Dendrobium officinale* plants were cultivated in the greenhouse at the Menghai experimental station, Institute of Medicinal Plant Development, Chinese Academy of Medical Sciences and Peking Union Medical College, Xishuangbanna, Yunnan, China. The flowers were pollinated by hand, and the capsules were collected just prior to dehiscence at 180 days after pollination. The capsules were surface sterilized with 1% sodium hypochlorite solution for 20 min in the laboratory. After surface sterilization, the capsules were cut open, and the seeds were taken out and placed onto the surface of 2 cm × 2 cm sections of nylon cloth within a 9 cm diameter Petri dish containing 20 mL sterile oatmeal agar (OMA: oat 2.5 g $L^{-1}$, agar 12 g $L^{-1}$, the pH measured at 5.2 prior to autoclaving). The OMA medium was autoclaved at 101.33 kPa and 121°C for 20 min. About 100 seeds were sown onto each nylon cloth section, with four nylon cloth sections per Petri dish. The mycorrhizal fungal isolate (*Tulasnella* S6 strain) was incubated on fresh Potato Dextrose Agar (PDA: infusion from potato 200 g $L^{-1}$, dextrose 20 g $L^{-1}$, agar 15 g $L^{-1}$, the pH measured at 5.6 prior to autoclaving) in darkness at 25°C for 10 days, then the actively growing mycelia from the colony margin were severed and used as the fungal inoculum. Each seed-containing plate was inoculated with five pieces (0.5 $cm^3$) of fungal inoculum, the plates without fungal inoculum served as the control. Plates were sealed with PARAFILM®. Thirty replicate plates were maintained in the growth room under a 12/12-h photoperiod at 30 μmol $m^{-2}$ $s^{-1}$ (daylight fluorescent tubes FL-20D/18, 20 W). The plates were observed and recorded under a dissecting stereomicroscope every week after inoculation. Seed germination and the growth of protocorms were scored as defined by Stewart et al. (2003). Germination was defined as emergence of the embryo from the seed coat, i.e., stage 2.

## Asymbiotic Germination

After surface sterilization, the capsules were cut open, and the seeds were taken out and placed onto 20 ml modified Murashige and Skoog (MS) medium (Murashige and Skoog, 1962) in a 9 cm diameter Petri dish. The modified MS medium contained 1/2 strength of macroelements with full strength of microelements, 2 mg $L^{-1}$ glycine, 0.5 mg $L^{-1}$ niacin, 0.5 mg $L^{-1}$ pyridoxine HCl, 0.1 mg $L^{-1}$ thiamine, and 100 mg $L^{-1}$ myo-inositol, 20 g $L^{-1}$ sucrose, and 7 g $L^{-1}$ agar. The pH was adjusted to 5.7 before autoclaving at 101.33 kPa and 121°C for 20 min. The cultures were maintained in the growth room under a 12/12-h photoperiod at 30 μmol $m^{-2}$ $s^{-1}$ as described above. After seed germination, developing protocorms were collected for the immunofluorescence labeling and real-time PCR experiments.

## Histological Study

The seeds and mycorrhizal protocorms were fixed in a solution of 2.5% glutaraldehyde and 1.6% paraformaldehyde in 0.05 M phosphate buffer (pH 6.8) for 4 h at room temperature. After fixation, the samples were dehydrated using an ethanol series, and embedded in Technovit 7100 (Kulzer and Co., Germany) as described by Yeung and Chan (2015). Serial, 3 μm-thick sections were cut with glass knives using a Reichert-Jung 2040 Autocut rotary microtome. These sections were stained with Periodic acid–Schiff's reaction for total insoluble carbohydrates, and counterstained with either 0.05% (w/v) toluidine blue O (TBO) in benzoate buffer for general histology or 1% (w/v) amido black 10B in 7% acetic acid for protein (Yeung, 1984). The sections were examined and the images were captured digitally using a CCD camera attached to a light microscope (Axio Imager A1, Carl Zeiss AG). More than 100 different protocorms of each developmental stage were studied.

## Identification of Extensin-Like Genes From Expressed Sequence Tags Database

Four putative genes coding for extensin-like genes were selected from the expressed sequence tags database (Chen et al., 2017), and were compared with the NCBI non-redundant protein database (Nr) using BLASTX after translating DNA sequences into the respective amino acid sequences. The GenBank accession numbers were KX906493, KX906494, KX906495, and KX906496.

## RNA Extraction and Real-Time PCR

Total RNA was extracted from mature seeds, symbiotically and asymbiotically germinated protocorms using RNeasy Plant Mini Kit (Qiagen, Hilden, Germany) according to the manufacturer's instructions. RNA samples were treated with RQ1 DNase (Invitrogen, United States) to remove DNA remnants, then underwent synthesis of the first cDNA strand by using the Prime Script RT reagent Kit (TaKaRa Bio, Japan). Primers for real-time PCR were designed by using Primer Premier 5.0 (Premier Biosoft, India) and the actin gene was used as an internal quantification standard (**Supplementary Table S1**). Each real-time PCR experiment contained 7.5 μL of SYBR Premix Ex Taq II (TaKaRa Bio), 1.5 μL of cDNA, and 0.3 μL primers, and water was added to 15 μL. For each real-time PCR, each sample was analyzed in three biological replicates with three technical replicates using the Light Cycler 480 II Real-Time PCR System (Roche, Switzerland) with its relative quantification program. The parameters of reactions were consisted of an initial denaturation at 95°C for 30 s, then 40 cycles of 95°C for 5 s, and 60°C for 30 s. The $2^{-\Delta\Delta Ct}$ method was used for evaluating gene expression. The data were statistically analyzed using ANOVA followed by Fisher's protected least significant difference test.

## Immunodot Blot Assay of HRGPs

A set of JIM antibodies (JIM 11, JIM 12, JIM13, JIM14, JIM15, JIM16, and JIM20) was obtained from PlantProbes (Leeds, United Kingdom) to test the presence of HRGPs. In a preliminary survey using the immunodot blot assay, JIM 11 gave the most intense staining in the zygotic embryo. To evaluate if JIM11 recognized an epitope of extensin, another monoclonal antibody to extensin, LM1 (Smallwood et al., 1995) from PlantProbes, was also tested. JIM11 staining mirrored that of LM1 (**Supplementary Figure S1**), confirming that JIM11 recognized extensin. Therefore, we used JIM11 as the cell wall

marker in the experiment of immunofluorescence labeling of HRGPs. The procedure for immunodot blot assay of HRGPs has been described by Lee et al. (2013). Briefly, samples of equal fresh weight (200 mg) were collected and ground into fine powders in liquid nitrogen. Proteins were extracted using 0.7 mL extraction buffer [100 mM Tris, 900 mM sucrose, 10 mM ethylene diamine-tetra-acetic acid (EDTA), 100 mM KCl and 0.4% (v/v) mercapto-ethanol, pH 8.8] and 0.7 mL of Tris-saturated phenol (pH 8.8). After centrifugation at 8,000 rpm for 5 min at 4°C, the supernatant was collected for protein precipitation. The proteins were precipitated by the addition of five volumes of 0.1 M ammonium acetate (in 100% methanol) to the phenol phase, and left at −20°C overnight. The precipitate was centrifuged at 16,000 × *g* for 20 min at 4°C. The pellet was dissolved in rehydration buffer [8 M urea, 2% CHAPS, 2% Triton X-100, 50 mM 1,4-dithiothreitol (DTT)]. Samples were boiled at 96°C for 5 min and were equally spotted on a nitrocellulose membrane by a micropipette (as 5 μL drops). The membrane was air-dried for 1 h and blocked in PBS buffer containing 5% (w/v) milk powder and 0.5% BSA for 1 h, followed by labeling with the primary monoclonal antibodies, JIM11 and LM1. The primary antibodies were diluted 1:1000 in PBS containing 1% BSA. After three washes with PBST (PBS buffer containing 0.2% Tween 20) for 10 min, the membrane was probed with a 1:2500 dilution of the secondary antibody, horseradish peroxidase (HRP)-conjugated anti-rat IgG at room temperature for 1 h. After the final wash with PBST, the detection of signal was performed by adding chemiluminescent HRP substrate (WBKL S0500, Millipore, Billerica, MA, United States) and captured by a luminescent image analyzer, LAS-4000 (FUJIFILM, Japan). Three biological replicates have been performed in the assay of immunodot blot of HRGPs.

## Immunofluorescence Labeling of JIM11

For immunofluorescence labeling of HRGPs, samples were collected and fixed in 4% (v/v) paraformaldehyde in stabilizing buffer MSTB [50 mM piperazine-N, N′-bis(2-ethanesulfonic acid) (PIPES), 5 mM $MgSO_4.7H_2O$, 5 mM ethylene glycol-bis(2-aminoethylether)-*N, N, N′, N′*-tetraacetic acid (EGTA), pH 6.9] and left overnight at 4°C. Samples were dehydrated in an ethanol series (30, 50, 70, 90, and 100%) and placed in pure acetone. The samples were infiltrated gradually with a graded series of 100% acetone to Technovit 8100 (3:1, 1:1, and 1:3; Kulzer and Co., Wehrheim, Germany), followed by two changes of pure Technovit 8100 (Yeung and Chan, 2015). The resin was polymerized at 4°C and 3 μm thick sections were cut, placed on a drop of water on a slide and dried at room temperature. Sectioned samples were rehydrated in PBS, pH 7.3, for 5 min followed by blocking in a 2% bovine serum albumin (BSA) in PBS for 5 min. The sections were labeled with primary monoclonal antibody, JIM11, and left overnight at 4°C. The primary antibodies were diluted 1:20 in PBS containing 1% BSA. After washing in PBS three times (5 min each time), sections were incubated with a 1:20 dilution of the secondary antibody (anti-rat IgG-FITC, F6258, Sigma) in PBS containing 1% BSA for 1 h in the dark, followed by three washes in PBS (10 min each time). For quenching the tissue autofluorescence, the sections were stained with 0.01% TBO in PBS for 1 min. After washing in PBS three times (5 min each), sections were mounted in medium containing an anti-fade mounting reagent (VECTASHIELD® Mounting Medium, Vector Laboratories, Inc., Burlingame, CA, United States) before observation. Controls were prepared by incubating with the blocking solution instead of the primary antibodies. The sections were examined and the images were captured using a LSM510 META confocal laser-scanning microscope (Carl Zeiss AG). For FITC detection, the 488 nm laser was used for excitation, and the emission filter was set to detect in the 500–530 nm range. To detect the autofluorescence, the 488 nm laser was also used for excitation, and the emission filter in the 565–615 nm range was used for detection. Three biological replicates have been performed in the experiment of immunofluorescence labeling, and more than thirty different protocorms were observed in each replicate.

## Immunogold Observation

Symbiotic protocorms at stage 3 were collected and fixed by high-pressure freezing fixation in a high-pressure freezer (Leica EM PACT2). The fixed protocorms were subjected to freeze substitution in ethanol (containing 0.2% glutaraldehyde and 0.1% uranyl acetate) in a Leica Automatic Freeze-Substitution System, then embedded in London Resin White methacrylate resin (London Company, Basingstoke, United Kingdom). Ultrathin sections (70–90 nm) were cut with a diamond knife on a Leica Reichert Ultracut S (Leica Microsystems GmbH[1]) and placed on formvar-coated nickel grids. For transmission electron microscopy (TEM) observation, the immunological staining was performed as previously described (Van Aelst and Van Went, 1992) with minor modifications. The sections were incubated in 3% normal goat serum and 0.5% BSA in PBST for 10 min at room temperature. Grids were then transferred to another drop of PBST containing the JIM11 antibody (1:200) and 0.5% BSA for 1 h at room temperature. After washing thoroughly with PBST, the sections were then treated for 20 min at room temperature with goat anti-mouse colloid gold conjugates (18 nm; RPN422 Auro-Probe EMGAR G18, Amersham), diluted 1:20 in PBST. After a further wash with PBST and distilled water, the sections were counterstained with uranyl acetate, followed by lead citrate. Controls were made to confirm the specificity of the immunological staining procedure, including (1) the incubation with pre-immune mouse IgG (Vector Laboratories, Inc.) and (2) the incubation with colloidal gold-conjugated anti-mouse IgG, omitting the first antibody. A Philip CM 100 transmission electron microscope (FEI Company[2]) at 80 kV was used for observation. At least three protocorms and more than 30 sections for each time point were examined.

## Treatment With 3,4-Dehydro-L-Proline (3,4-DHP)

The role of HRGPs in the symbiotic germination of *D. officinale* was investigated using 3,4-DHP, an inhibitor of prolyl hydroxylase to alter the structure of HRGPs in cell walls

[1]http://www.leica-microsystems.com/

[2]http://www.feicompany.com

(Xu et al., 2011). In symbiotic germination, 200 μM of 3,4-DHP (Sigma-Aldrich Co.) was added to the OMA medium with fungal inoculum. Plates without 3,4-DHP treatment were used as controls. The seed germination experiments were processed as described above. Germination was defined as emergence of the embryo from the seed coat. After 3 weeks of culture, the germination percentage was calculated as the percentage of the number of seeds germinated among the total countered number of seeds with embryos. At the same time, the expression of JIM11 antigen in 3,4-DHP-treated cultures was examined by fluorescence labeling as described above. Experiments were performed using a completely randomized design. Twelve plate replicates were examined for each treatment. The data were analyzed statistically using ANOVA followed by Fisher's protected least significant difference test.

# RESULTS

## Symbiotic Germination

In the first week of inoculation, the embryos had absorbed water and became slightly swollen, but the seed coats remained intact (stage 0) (**Figure 1A**). After 1 week of inoculation, most embryos had become swollen and some embryos began to turn light-green (stage 1) (**Figure 1B**). After 2 weeks of inoculation, the embryos continued to swell and then ruptured the seed coat (stage 2) (**Figure 1C**). After 3 weeks of inoculation, more than 70% of inoculated seeds had germinated. The embryos developed further and resulted in the formation of green protocorms (stage 3). At this stage, a shoot tip became visible at one end of a protocorm, and numerous rhizoids formed at the opposite end (**Figure 1D**).

## Histological Study

Before the invasion by fungal hyphae, the uninfected embryos, covered by a thin layer of seed coat, were only ten to eleven cells long and six to seven cells wide (**Figure 2A**). A gradient of cell size was observed in the embryos with smaller cells located at the chalazal end. Within the embryo cells, protein and lipid bodies were present. In the first week of inoculation, embryos became slightly swollen due to the uptake of water, and the fungal hyphae congregated at the suspensor end of the embryos (**Figure 3A**). At this time, storage products, i.e., protein and lipid bodies began to break down, while starch grains appeared and tended to congregate near the nuclei. After 1 week of inoculation, the embryos had enlarged by vacuolization and the storage products, i.e., protein and lipid bodies had

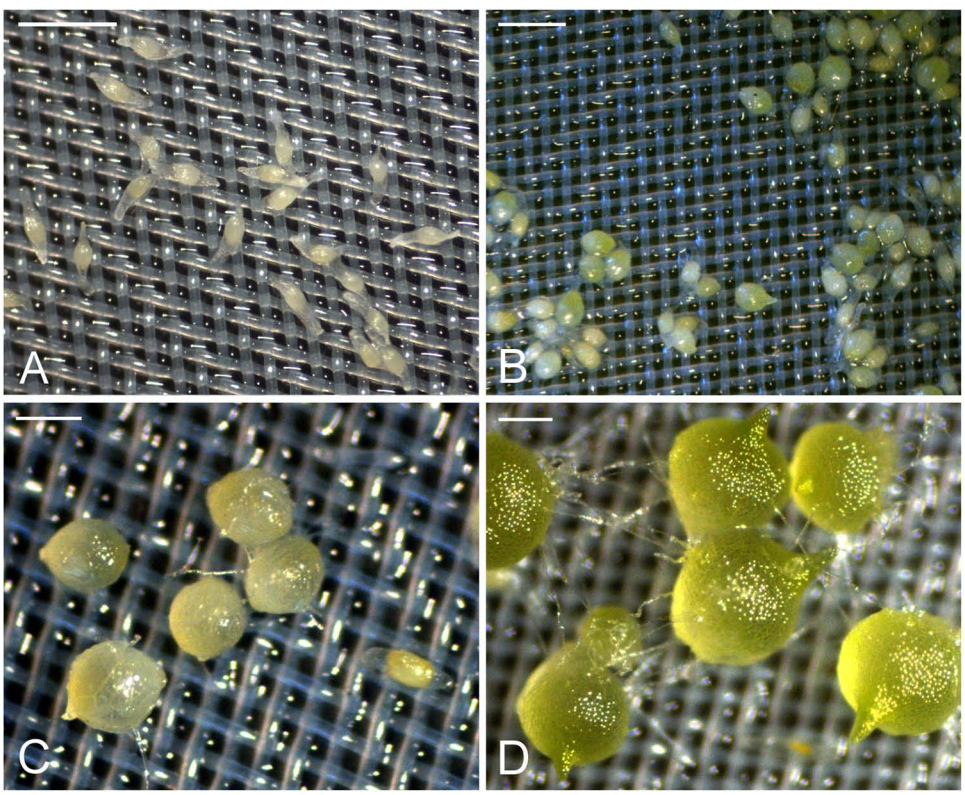


**FIGURE 1 |** The successive developmental stages of *D. officinale* from seed germination to protocorm formation in symbiotic culture. **(A)** Stage 0, the embryos enclosed by the intact seed coats in the first week of inoculation. Scale bar = 0.5 mm. **(B)** Stage 1, swollen seeds after 1 week of inoculation. Scale bar = 0.5 mm. **(C)** Stage 2, globular protocorm rupturing the seed coat after 2 weeks of inoculation. Scale bar = 1 mm. **(D)** Stage3, green protocorm with the shoot tip and rhizoids after 3 weeks of inoculation. Scale bar = 1 mm.

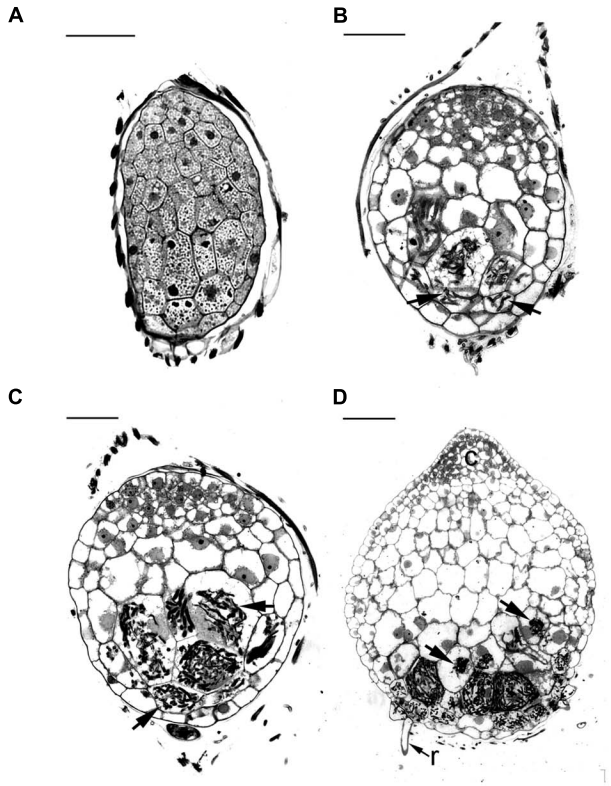


**FIGURE 2 |** Light micrographs of sections showing the successive developmental stages of *D. officinale* from seed germination to protocorm formation in symbiotic culture. **(A)** Stage 0, the uncolonized embryo covered by a thin seed coat in the first week of inoculation. The embryo cells filled with storage products, such as protein and lipid bodies. Scale bar = 50 μm. **(B)** Stage 1, the infected embryo after 1 week of inoculation. Fungal hyphae have colonized the embryo and formed the pelotons (arrows) within embryo cells. Larger vacuoles make the embryo cells expand and the storage nutrients disappear from most embryo cells. Scale bar = 50 μm. **(C)** Stage 2, the enlarged embryo with the rupture of the seed coat after 2 weeks of inoculation. The pelotons (arrows) locate in outer cortical cells and inner cortical cells of the spherical protocorm. Scale bar = 50 μm. **(D)** Stage3, protocorm with the first crest and rhizoids after 3 weeks of inoculation. At this stage, the pelotons (arrows) are digested in the inner cortical cells. c, crest; r, rhizoid. Scale bar = 100 μm.

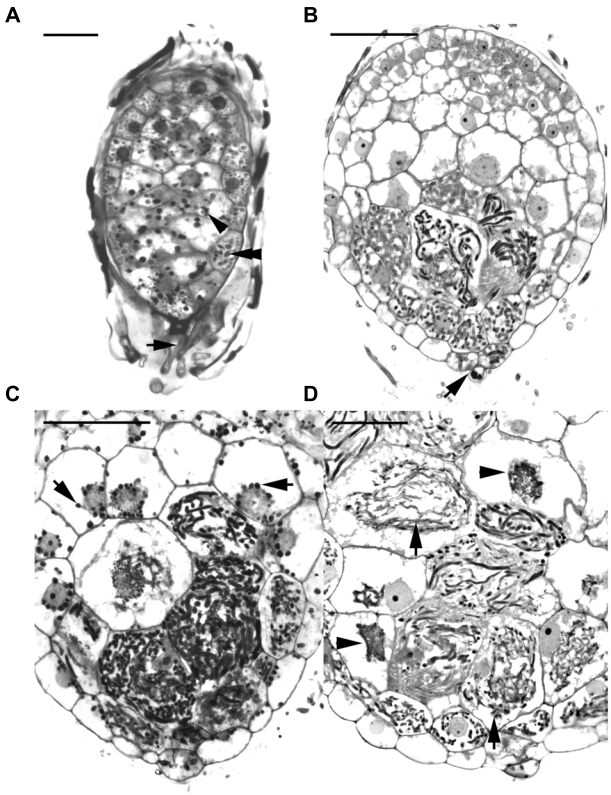


**FIGURE 3 |** Longitudinal sections of developing protocorms from symbiotic cultures showing the cells with the development and degeneration of fungal hyphae. **(A)** In the first week of inoculation, the embryo has become slightly swollen, and the fungal hyphae (arrow) have just touched the suspensor end of embryo. Within the embryo cells, the protein bodies are degenerating (double arrowhead), and the starch grains appear (arrowhead). Scale bar = 50 μm. **(B)** Fungal hyphae have penetrated the embryo through the suspensor end (arrow) and colonized the middle and basal cortical cells of the enlarged embryo at stage 1. Scale bar = 50 μm. **(C)** In a developing protocorm at stage 2, the peloton hyphae are primarily found in the middle and basal cortical cells. In the infected cortical cells, starch grains were depleted, while in the top portion of the protocorm, chloroplasts had appeared and starch grains (arrows) were noticeable within the cytoplasm. Scale bar = 50 μm. **(D)** As the protocorm further grows up (stage3), there are a number of collapsing peloton hyphae (arrows) and degenerated hyphal clumps (arrowheads) in the cortical cells. Scale bar = 50 μm.

disappeared from most cells (**Figure 2B**). At this stage, fungal hyphae had penetrated the embryos through their suspensor end. The large, basal cells of the swollen embryos became colonized by hyphae (**Figure 3B**). Cell divisions occurred at the apical (chalazal) end of the embryos, generating a zone of meristematic cells. After 2 weeks of inoculation, the embryos continued to enlarge, rupturing the seed coat. This resulted in the formation of spherical protocorms (**Figure 2C**). The mycorrhizal hyphae were found mainly in the outer and inner cells at the basal (suspensor) end of the protocorms (**Figure 3C**). After 3 weeks of inoculation, protocorms developed further with the formation of the first crest at the apical end and the rhizoids at the basal end (**Figure 2D**). At this stage, collapsing peloton hyphae and degenerated hyphal clumps were present in the basal cells of developing protocorms (**Figure 3D**). During symbiotic germination, mycorrhizal hyphae were confined to the basal end of the protocorm and not present in the developing shoot pole.

## Expression Patterns of *D. officinale* Extensin-Like Genes

From the RNA-seq database of the symbiotic protocorm (Chen et al., 2017), we selected sequences coding four different extensin-like proteins (**Table 1**), i.e., *Unigene5337*, *CL9853*, *CL493.contig2* and *Unigene4313*. Real-time PCR of these four genes performed to verify their expression in mature seeds and symbiotically and asymbiotically germinated stage 3 protocorms (**Figure 4**). The four extensin-like genes showed low expression levels in

**TABLE 1 |** *D. officinale* extensin-like genes investigated by real-time PCR.

| Sequence code | GenBank accession | Blastx result | Reference gene accession | Query coverage | *E*-value | Conserved domain |
|---|---|---|---|---|---|---|
| CL9853.contig1 | KX906495 | Extensin2 like protein | XP_008791833 | 52% | 7.00E-50 | Pollen proteins Ole e I like (pfam01190) |
| Unigene4313 | KX906494 | Extensin2 like isoform X1 | XP_012481562 | 46% | 0.030 | Extensin_2 (pfam04554) |
| Unigene5337 | KX906496 | LLR extensin like protein | XP_019707248 | 78% | 0 | Leucine-rich repeat (pfam13855) |
| CL493.contig2 | KX906493 | Extensin like | XP_020242813 | 88% | 0.007 | – |

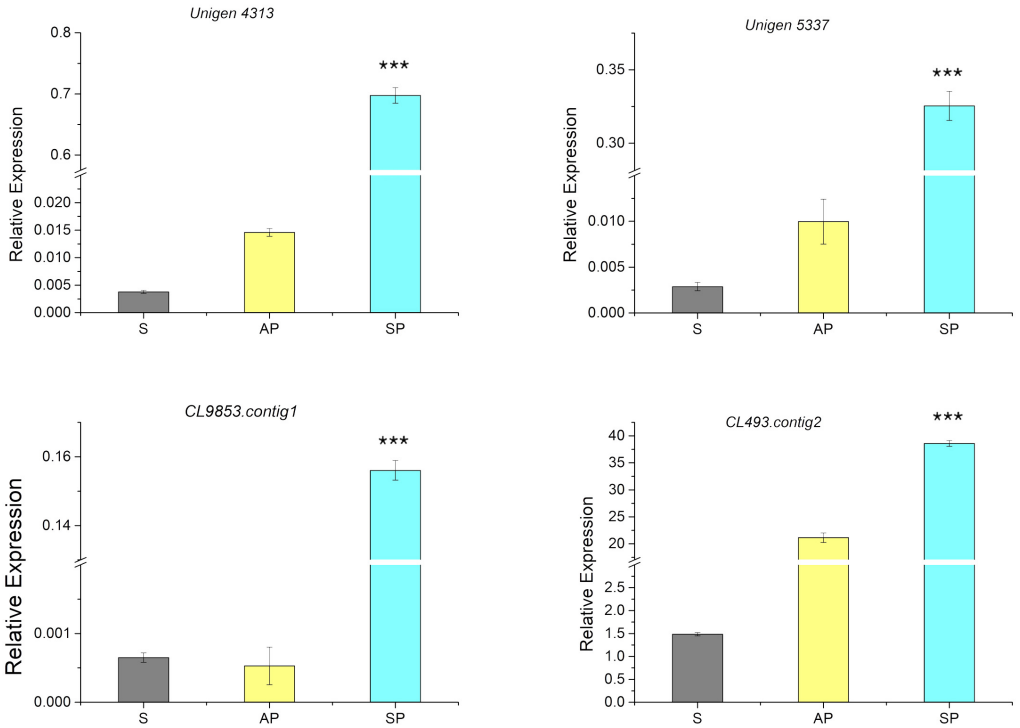


**FIGURE 4 |** Expression of genes coding for extensin-like genes in the mature seeds (S), symbiotically (SP), and asymbiotically (AP) germinated protocorms measured by real-time PCR. ***Indicates significant difference at $P < 0.001$ probability.

mature seeds and asymbiotically germinated protocorms (except for *CL493.contig2*), while high expression levels were detected in symbiotically germinated protocorms.

## Immunodot Blot, Immunofluorescence, and Immunogold Localization of JIM11 Epitope in Symbiotic Germination

For the assay of immunodot blot in the symbiotic cultures, a moderate intensity of JIM11 staining could be observed in the mature seeds. The signal of JIM11 in swollen embryos (stage 1) was relatively high, while the signal intensities in the developing protocorms decreased after germination (stages 2 and 3). On the contrary, in asymbiotic cultures, the signals of JIM11 in swollen embryos and developing protocorms were much lower as compared with those stages in symbiotic cultures (**Figure 5**).

Since dot blot results represented the total contents of JIM11 from protocorms at different stages of germination, a qualitative comparative overview of immunolabeling of JIM11 epitope was carried out and the result is summarized in **Table 2**. In the uninfected seeds, conspicuous fluorescence signals of JIM11 epitope were observed, with a stronger signal in the larger cells near the basal (suspensor) end, and weaker signals at the apical (chalazal) end of the embryos (**Figure 6A**). After 1 week of inoculation, the basal end of embryos had been infected by the hyphae, and a strong signal was detected mostly at the middle and basal cells of enlarging embryos (**Figure 6B**). Fluorescent signals could also be found in adjacent uninfected cells in the basal end of protocorms, while no signal was detected in cells of the future shoot pole (**Figure 6B**). As protocorm continued to develop, the signal was concentrated mainly in the colonized cortical cells at the basal end. In the infected cells, the signals were present in the

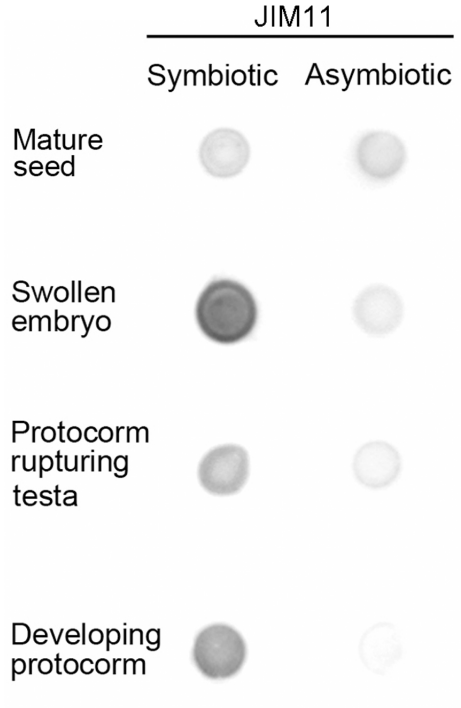


**FIGURE 5 |** Semi-quantitative analysis by immunodot blots of the relative abundance of JIM11 epitope in extracts prepared from the mature seeds and developing protocorms in the symbiotic and asymbiotic cultures.

**TABLE 2 |** The intensity evaluation of immunofluorescence labeling with JIM11 antibody during the formation of protocorm of *D. officinale* in symbiotic culture.

| Developmental stages | Embryo regions | JIM11 signal intensity |
|---|---|---|
| Stage 0 | Apical region | – |
| | Middle region | ++ |
| | Basal region | ++ |
| Stage 1 | Apical region | – |
| | Middle region | +++ |
| | Basal region | ++++ |
| Stage 2 | Apical region | – |
| | Middle region | + |
| | Basal region | +++ |
| Stage 3 | Apical region | – |
| | Middle region | + |
| | Basal region | +++ |

*Increasing intensity was evaluated as: – (no signal); ±(very weak); + (weak); ++ (intermediate); +++ (strong); ++++ (very strong).*

walls and intracellularly associated with hyphae and the pelotons (**Figures 6C,D**). In the negative staining control, no signal can be detected in the embryo after incubation without the primary antibody of JIM11 (**Supplementary Figure S2**).

In order to determine the precise localization of JIM11 epitope within the infected cells of symbiotic protocorms at stage 3, the immunogold staining was used. No immunogold particles were detected in the cell wall at the apical part of protocorm (**Figure 7A**). Immunogold particles were observed in the colonized cortical cells at the basal part of protocorm, particularly where they were deposited in the protocorm cell wall (**Figure 7B**). A few immunogold particles were observed in the interfacial matrix near the fungal cell wall (**Figure 7B**), as well as around the collapsed fungal hyphae (**Figure 7C**). The control with the incubation with pre-immune mouse IgG or the omission of JIM11 antibody showed no immunogold particles in any infected cells (**Figure 7D**).

## Effect of 3,4-DHP on Symbiotic Germination

To evaluate the effect of 3,4-DHP on symbiotic germination, 3,4-DHP was added to the OMA medium with fungal inoculum. After 3 weeks of culture, a remarkable decreased in germination percentage was observed as compared with the untreated control culture (**Table 3**). To evaluate the effect of 3,4-DHP on the distribution and localization of HRGPs in developing protocorms during symbiotic germination, immunolabeling with JIM11 antibody was carried out on seeds cultured on the symbiotic germination medium supplemented with 3,4-DHP. After 3 weeks of culture, very low expression of the JIM11 epitope was detected in the ungerminated embryos treated with 3,4-DHP (**Figure 8A**). With the 3,4-DHP treatment, only a few embryos enlarged and reached stage 1 (**Table 3**), and a very weak labeling with the JIM11 antibody was observed in the walls of basal region of protocorms (**Figure 8B**). In the ungerminated protocorm, severe fungal invasion could be commonly observed (**Figure 8C**). The hyphae could be found throughout the entire protocorm and a well-defined zone of meristematic cells located at the future shoot pole was absent.

# DISCUSSION

In orchids, the establishment of seedlings requires the formation of protocorms. The protocorm is a post-embryonic structure from which a shoot and a root subsequently differentiate (Arditti and Krikorian, 1996). In symbiotic germination, compatible fungi colonize orchid seeds and provide nutrients for the formation of protocorms (Rasmussen, 1995; Peterson et al., 1996; Selosse and Martos, 2014).

Hydroxyproline-rich glycoproteins are abundant cell wall components with different functions (Berger et al., 1994; Cassab, 1998). They have been shown to involve in symbiotic interactions (Berry et al., 2002; Olsson et al., 2002; Rathbun et al., 2002) and in plant defense (Davies et al., 1997; Raggi, 2000). In this study, the results of immunodot blot analysis indicate that HRGPs are present in mature seeds and mycorrhizal protocorms of *D. officinale*. The immunofluorescence signals of JIM11 epitopes are primarily present in the suspensor end of uncolonized and colonized embryos (**Figure 6**). Four extensin-like genes are up-regulated supporting the immunolocalization studies (**Figure 4**).

Successful penetration of fungal hyphae into protocorms is a key step in establishing mycorrhizal association. The presence of

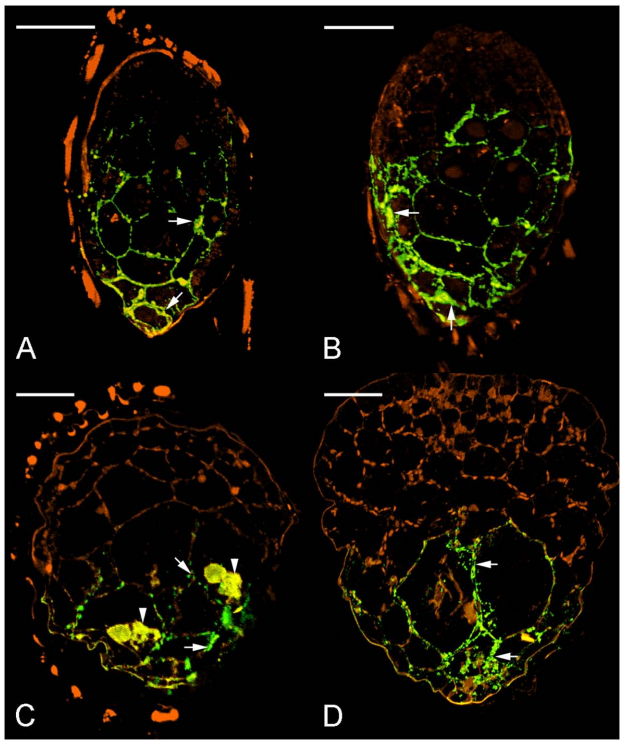


**FIGURE 6 |** Immunofluorescence localization of JIM11 epitope during symbiotic seed germination of *D. officinale*. **(A)** The uncolonized embryo with strong signals of JIM11 epitope (green color, excitation 488 nm and emission 500–530 nm). The signals (arrows) are present mainly in the walls of the middle and basal regions of the embryo. The orange color indicates the autofluorescence (excitation 488 nm and emission 565–615 nm). Scale bar = 50 μm. **(B)** After 1 week of inoculation, the infected embryo showing strong signals of JIM11 epitope (arrows) in the walls of the middle and basal regions of the swollen embryo. Scale bar = 50 μm. **(C)** After 2 weeks of inoculation, the enlarged embryo with the rupture of the seed coat showing prominent signals of JIM 11 epitope in the pelotons (arrowheads) and the walls of colonized cells (arrows) in the basal protocorm. Scale bar = 50 μm. **(D)** After 3 weeks of inoculation, the signals of JIM 11 epitope (arrows) are mainly observed in the walls of colonized cells of the developing protocorm. Scale bar = 100 μm.

JIM11 epitope at the suspensor end of the embryo may serve as a possible recognition site of fungal colonization. Previous reports have indicated that the suspensor end of an orchid embryo is one of the main sites for the penetration of fungal hyphae (Peterson and Currah, 1990; Rasmussen, 1990). In this study, by 5 days after inoculation, fungal hyphae have reached the suspensor end of *Dendrobium* embryo (**Figure 3A**) and have penetrated into the basal parenchyma cells through the degenerated suspensor after 1 week of inoculation (**Figure 3B**). It is well established in orchid embryos, a distinct cuticle is present over the entire embryo proper surface but is absent from the suspensor cell wall (Yeung et al., 1996; Lee et al., 2006; Lee and Yeung, 2010). Although the suspensor has degenerated as the seed matured, the presence of primary wall not covered by a cuticle makes the suspensor end a vulnerable or a predetermined site for fungal penetration.

The signals for JIM11 epitope become stronger in the *Dendrobium* protocorms as colonization begin to take hold (**Figure 6**). On the contrary, as compared to asymbiotic germination control, JIM11 epitope signals remain weak upon germination (**Supplementary Figure S3**). In parsley, the expression of HRGP transcripts is much higher in mycorrhizal roots than those in the uncolonized control (Franken and Gnadinger, 1994). In maize root, the activation of HRGP transcripts is induced by arbuscular mycorrhizal fungi, and this response is restricted to mycorrhizal tissues (Balestrini et al., 1997). In this study, four extensin-like genes are up-regulated primarily in symbiotically germinated protocorms (**Figure 4**). This result supports the work by Balestrini et al. (1997) and Xie et al. (2011) that extensin-like genes are involved in the interactions between plants and microorganisms, and symbiotic association. More importantly, the up-regulation of extensin-like genes corroborates the fluorescent staining patterns of JIM11. Our results suggest that mycorrhizal colonization may induce *de novo* synthesis of HRGPs in basal cells of *Dendrobium* protocorms in preparation for the colonization process.

During symbiotic germination, fungal colonization is restricted to the basal portion (suspensor end) of a protocorm (**Figures 2B–D**). Fluorescent signals of JIM11 epitope are primarily located in the walls and in association with the hyphae and the pelotons of colonized cells. It is important to note that fluorescent signals can also be found in adjacent uncolonized cells of a protocorm, while no signals are detected in the apical end (**Figures 6B–D**, **7A**). The accumulation of HRGPs in the intracellular interfaces between hyphae and peri-fungal host membrane has been reported in various plant/arbuscular mycorrhizal fungus combinations (Bonfante-Fasolo et al., 1991; Bonfante, 2001; Balestrini and Bonfante, 2005). In this study, the precise localization of JIM11 epitope within symbiotic protocorms is further examined by immunoelectron microscopy. In the colonized cells, immunogold particles were primarily observed in the cell wall as well as the interfacial matrix near the fungal cell wall (**Figure 7B**). The formation of plant-fungal interfaces is crucial for establishing the partnership in mutualistic relationships that allows a two-way exchange of signal molecules and nutrients (Smith and Smith, 1990). Our results suggest that HRGPs are integral parts of the interface that is essential for the establishment of symbiotic association between orchid protocorms and mycorrhizal fungi.

Furthermore, it is noteworthy that the cross-linking of HRGPs such as extensin through peroxidation plays an important role in strengthening of plant cell wall (Jackson et al., 2001). In pathogenic interactions, the rapid insolubilization of extensin is an essential component of the plant's primary defensive reaction to microbial attack (Lamb and Dixon, 1997). But these defense responses seem to be weakly or transiently activated as compared to pathogenic interactions. In arbuscular mycorrhizal symbiosis, the penetration of fungal hyphae induces HRGPs-encoding genes in mycorrhizal tissues (Balestrini et al., 1997). In the legume-rhizobium symbiosis, the expression of extensin genes in root hairs and nodules has been proposed to remodel plant cell wall architecture and to limit the bacterial

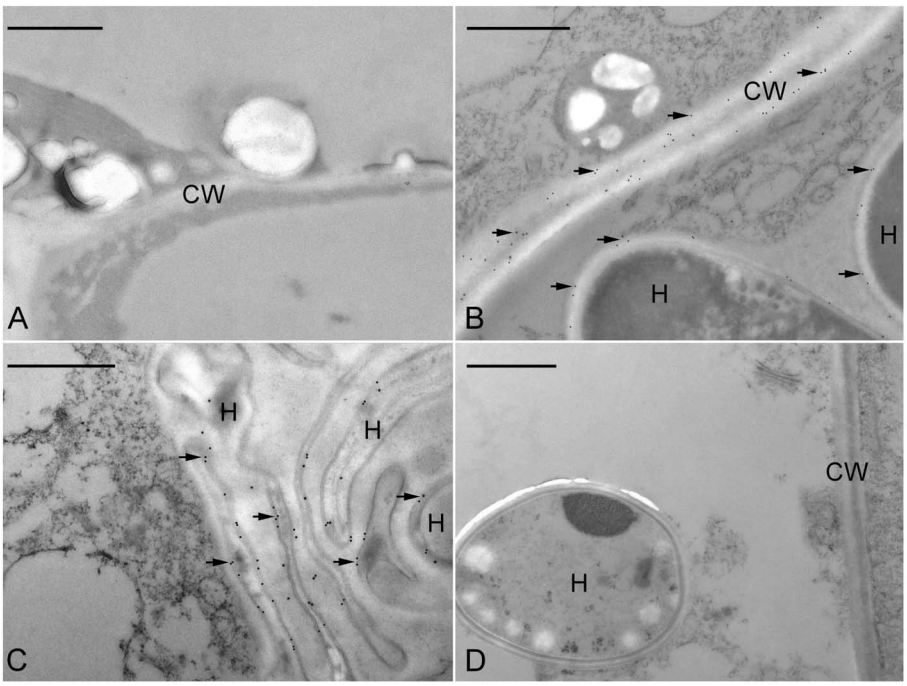


**FIGURE 7 |** Immunogold staining of JIM11 epitope in the symbiotic protocorms of *D. officinale*. **(A)** In the apical portion of the protocorm, no immunogold particles were observed. Scale bar = 1 μm. **(B)** TEM of a basal portion of protocorm cell with fungal hyphae (H). Labeling occurred in the host cell wall (CW) and the interfacial matrix (arrowhead) or fungal cell wall. Scale bar = 1 μm. **(C)** TEM of a portion of protocorm cell with collapsed fungal hyphae (H). Scale bar = 1 μm. **(D)** The control staining. Thin sections were incubated with the mouse pre-immune IgG instead of JIM11 antibody. Immunogold particles were absent in these treatments. Scale bar = 1 μm.

**TABLE 3 |** Effect of 3,4-DHP on symbiotic seed germination of *D. officinale*.

| Treatment | Germination | Developmental stages | | | |
|---|---|---|---|---|---|
| | (%) | 0 | 1 | 2 | 3 |
| Control | 92.9[a] | 0 | 7.1 | 20.4 | 72.5 |
| 200 μM 3,4-DHP | 1.8[b] | 61.8 | 36.4 | 1.8 | 0 |

*Means having the same letter in a column are not significantly different at 5% level by Fischer's protected LSD test. Data were scored after 3 weeks of culture. Germination was defined as emergence of the embryo from the seed coat, i.e., stage 2.*

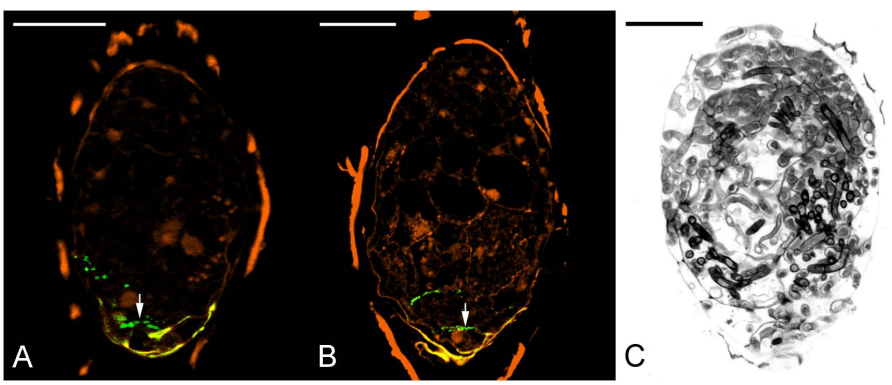


**FIGURE 8 |** The effect of 3,4-DHP on the localization of JIM11 epitope during symbiotic seed germination of *D. officinale*. **(A)** After 3 weeks of inoculation, most embryos did not enlarge, and weak signals of JIM11 epitope (arrow) are observed in the walls of basal end of the embryo. Scale bar = 50 μm. **(B)** After 3 weeks of inoculation, the infected embryo showing weak signals of JIM11 epitope (arrow) in the walls of basal end of the swollen embryo. Scale bar = 50 μm. **(C)** Most seeds in the treatment with 3,4-DHP are unable to germinate, and the severe fungal invasion in the ungerminated seeds could be commonly observed. Scale bar = 50 μm.

growth in infection thread (Arsenijevic-Maksimovic et al., 1997; Wisniewski et al., 2000). In this study, the extensin-like genes are highly up-regulated in the symbiotic protocorms as compared to the asymbiotic protocorms (**Figure 4**), and JIM11 epitope are localized in the cells containing fungal hyphae (**Figures 6**, **7**). The results from our studies indicated that HRGPs may be essential for limiting the fungal spread inside the protocorms and modulating the accommodation process of the mycorrhizal fungi inside the basal cells of protocorms, allowing the formation of a shoot apical meristem at the apical end of protocorm.

It is clear in this study that HRGPs are not present in the rapidly dividing cells where the shoot apical meristem will subsequently develop. Since HRGPs may serve to strengthen cell walls, their absence will not hinder rapid cell division leading to SAM formation. It is interesting to note that HRGPs are present in the maize root meristem cell walls (Balestrini et al., 1994). Their presence may serve to protect the root meristem from infection, enabling the continual growth of the root. Future studies will further our insight into the role of HRGPs in meristem development and function in orchids.

The importance of HRGPs is clearly demonstrated by 3,4-DHP treatment. In symbiotic cultures treated with 3,4-DHP, little JIM11 epitopes were present in these colonized embryo cells (**Figures 8A,B**), and severe fungal invasion was observed (**Figure 8C**). The absence of HRPGs alters the internal regulatory process resulting in the uncontrolled growth of the hyphae, leading to developmental arrest and death of protocorms. Judging from the inhibitor studies, HRPGs may have a defensive role to play as they serve to separate the colonized cells from apical cells destined to form the shoot apical meristem.

## CONCLUSION

In conclusion, this is the first report that shows the accumulation of HRGPs as recognized by JIM11 epitope, in the mycorrhizal protocorm in response to colonization by symbiotic fungi. The treatment with 3,4-DHP inhibits symbiotic germination and the accumulation of HRGPs in colonized cells of seeds. The presence of HRGPs in the basal region of protocorm appears to be essential for the establishment of a symbiotic relationship between *D. officinale* and *Tulasnella*. With the accomplishment in genome sequencing of *D. officinale* (Yan et al., 2015), future molecular genetics studies will provide new insight into the regulatory process for orchid symbiosis.

## AUTHOR CONTRIBUTIONS

Y-IL and S-XG conceived the study. Y-IL, S-XG, X-MC, Y-YL, and A-RW designed the study. XZ performed sequence analyses. Y-YL and YZ performed qPCR experiments. Y-IL, Y-YL, and EY performed histological and immunohistochemical studies. Y-HC and Y-YL performed immunodot blots experiments. Y-IL, S-XG, EY, and Y-YL wrote the paper. All authors read and approved the final manuscript.

## FUNDING

This work was supported by grants from the Innovation Fund for Medical Sciences (CIFMS) (2017-I2M-3-013) to X-MC; from the National Natural Science Foundation of China (No.81573526) to S-XG; from National Museum of Natural Science, Taiwan, to Y-IL; and from the Natural Sciences and Engineering Research Council of Canada to EY.

## ACKNOWLEDGMENTS

We would like to thank Dr. Mei-Chu Chung in Institute of Plant and Microbial Biology, Academia Sinica, Taipei, Taiwan (IPMB), and Dr. Wann-Neng Jane and Miss Mei-Jane Fang (Plant Cell Biology Core Lab, IPMB) for the uses of transmission electron microscopy and confocal laser-scanning microscope.

## SUPPLEMENTARY MATERIAL

The Supplementary Material for this article can be found online at: https://www.frontiersin.org/articles/10.3389/fpls.2018.00552/full#supplementary-material

**FIGURE S1 |** Semi-quantitative analysis by immunodot blots of the relative abundance of LM1 epitope in extracts prepared from the mature seeds and developing protocorms in the symbiotic and asymbiotic cultures.

**FIGURE S2 |** In the negative control of immunofluorescence localization of JIM11 epitope, no signal can be detected in the enlarged embryo after incubation without the primary antibody of JIM11. Scale bar = 50 μm.

**FIGURE S3 |** In the asymbiotic germination culture, **(A)** after 3 days of culture, the signals of JIM11 epitope (green color) were located in the walls of the middle and basal regions of the imbibed embryo, scale bar = 50 μm; **(B)** after 2 weeks of culture, a few signals of JIM11 epitope were located in the wall of the basal region of the swollen embryo, scale bar = 50 μm; after 3 and 4 weeks of culture, in the enlarged embryo with the rupture of the seed coat, scale bar = 50 μm **(C)**, and the developing protocorm, scale bar = 100 μm **(D)**, the signals of JIM 11 epitope only remained in the surface of the basal protocorms.

**TABLE S1 |** The primers used in the quantitative PCR analyses.

## REFERENCES

Arditti, J., and Krikorian, D. (1996). Orchid micropropagation: the path from laboratory to commercialization and an account of several unappreciated investigators. *Bot. J. Linn. Soc.* 122, 183–241. doi: 10.1111/j.1095-8339.1996.tb02073.x

Arsenijevic-Maksimovic, I., Broughton, W. J., and Krause, A. (1997). Rhizobia modulate root-hair-specific expression of extensin genes. *Mol. Plant Microbe Interact.* 10, 95–101. doi: 10.1094/mpmi.1997.10.1.95

Balestrini, R., and Bonfante, P. (2005). The interface compartment in arbuscular mycorrhizae: a special type of plant cell wall? *Plant Biosyst.* 139, 8–15. doi: 10.1080/11263500500056799

Balestrini, R., and Bonfante, P. (2014). Cell wall remodeling in mycorrhizal symbiosis: a way towards biotrophism. *Front. Plant Sci.* 5:237. doi: 10.3389/fpls.2014.00237

Balestrini, R., Jose-Estanyol, M., Puigdomenech, P., and Bonfante, P. (1997). Hydroxyproline-rich glycoprotein mRNA accumulation in maize root cells colonized by an arbuscular mycorrhizal fungus as revealed by in situ hybridization. *Protoplasma* 198, 36–42. doi: 10.1007/bf01282129

Balestrini, R., Romera, C., Puigdomenech, P., and Bonfante, P. (1994). Location of a cell wall hydroxyproline-rich glycoprotein, cellulose and β-1,3 glucans in apical and differentiated regions of maize mycorrhizal roots. *Planta* 195, 201–209. doi: 10.1007/bf00199680

Benhamou, N., Lafontaine, P. J., Mazau, D., and Esquerré-Tugayé, M. T. (1991). Differential accumulation of hydroxyproline-rich glycoproteins in bean root nodule cells infected with a wild-type strain or a $C_4$-dicarboxylic acid mutant of *Rhizobium leguminosarum* bv. *phaseoli*. *Planta* 184, 457–467. doi: 10.1007/bf00197893

Berger, F., Taylor, A., and Brownlee, C. (1994). Cell fate determination by the cell wall in early *Fucus* development. *Science* 263, 1421–1423. doi: 10.1126/science.263.5152.1421

Berry, A. M., Rasmussen, U., Bateman, K., Huss-Danell, K., Lindwall, S., and Bergman, B. (2002). Arabinogalactan proteins are expressed at the symbiotic interface in root nodules of *Alnus* spp. *New Phytol.* 155, 469–479. doi: 10.1046/j.1469-8137.2002.00466.x

Bonfante, P. (2001). "At the interface between mycorrhizal fungi and plants: the structural organization of cell wall, plasma membrane and cytoskeleton," in *Fungal Associations*, eds K. Esser, and B. Hock (Berlin: Springer), 45–61.

Bonfante-Fasolo, P., Tamagnone, L., Peretto, R., Esquerré-Tugayé, M. T., Mazau, D., Mosiniak, M., et al. (1991). Immunocytochemical location of hydroxyproline rich glycoproteins at the interface between a mycorrhizal fungus and its host plants. *Protoplasma* 165, 127–138. doi: 10.1007/bf01322283

Bougoure, J., Ludwig, M., Brundrett, M., Cliff, J., Clode, P., Kilburn, M., et al. (2013). High-resolution secondary ion mass spectrometry analysis of carbon dynamics in mycorrhizas formed by an obligately myco-heterotrophic orchid. *Plant Cell Environ.* 39, 1223–1230. doi: 10.1111/pce.12230

Cameron, D. D., Johnson, I., Leake, J. R., and Read, D. J. (2007). Mycorrhizal acquisition of inorganic phosphorus by the green-leaved terrestrial orchid *Goodyera repens*. *Ann. Bot.* 99, 831–834. doi: 10.1093/aob/mcm018

Cameron, D. D., Leake, J. R., and Read, D. J. (2006). Mutualistic mycorrhiza in orchids: evidence from plant–fungus carbon and nitrogen transfers in the green-leaved terrestrial orchid *Goodyera repens*. *New Phytol.* 171, 405–416. doi: 10.1111/j.1469-8137.2006.01767.x

Cassab, G. I. (1998). Plant cell wall proteins. *Annu. Rev. Plant Physiol. Mol. Biol.* 49, 281–309. doi: 10.1146/annurev.arplant.49.1.281

Cassab, G. I., and Varner, J. E. (1987). Immunolocalization of extensin in developing soybean seed coats by immunogold-silver staining and tissue printing on nitrocellulose paper. *J. Cell Biol.* 105, 2581–2588. doi: 10.1083/jcb.105.6.2581

Chen, J., Liu, S. S., Kohler, A., Yan, B., Luo, H. M., Chen, X. M., et al. (2017). iTRAQ and RNA-Seq analyses provide new insights into regulation mechanism of symbiotic germination of *Dendrobium officinale* seeds (Orchidaceae). *J. Proteome Res.* 16, 2174–2187. doi: 10.1021/acs.jproteome.6b00999

Davies, H. A., Daniels, M. J., and Dow, J. M. (1997). Induction of extracellular matrix glycoproteins in *Brassica* petioles by wounding and in response to *Xanthomonas campestris*. *Mol. Plant Microbe Interact.* 10, 812–820. doi: 10.1094/mpmi.1997.10.7.812

Dearnaley, J. D., and Cameron, D. D. (2017). Nitrogen transport in the orchid mycorrhizal symbiosis-further evidence for a mutualistic association. *New Phytol.* 213, 10–12. doi: 10.1111/nph.14357

Fochi, V., Chitarra, W., Kohler, A., Voyron, S., Singan, V. R., Lindquist, E. A., et al. (2017). Fungal and plant gene expression in the *Tulasnella calospora-Serapias vomeracea* symbiosis provides clues about nitrogen pathways in orchid mycorrhizas. *New Phytol.* 213, 365–379. doi: 10.1111/nph.14279

Franken, P., and Gnadinger, F. (1994). Analysis of parsley arbuscular endomycorrhiza: infection development and mRNA levels of defence-related genes. *Mol. Plant Microbe Interact.* 7, 612–620. doi: 10.1094/MPMI-7-0612

Gianinazzi-Pearson, V. (1996). Plant cell responses to arbuscular mycorrhizal fungi: getting to the roots of the symbiosis. *Plant Cell* 8, 1871–1883. doi: 10.1105/tpc.8.10.1871

Jackson, P. A., Galinha, C. I., Pereira, C. S., Fortunato, A., Soares, N. C., Amancio, S. B., et al. (2001). Rapid deposition of extensin during the elicitation of grapevine callus cultures is specifically catalyzed by a 40-kilodalton peroxidase. *Plant Physiol.* 127, 1065–1076. doi: 10.1104/pp.010192

Kuga, U., Sakamoto, N., and Yurimoto, H. (2014). Stable isotope imaging reveals that both live and degenerating fungal pelotons transfer carbon and nitrogen to orchid protocorms. *New Phytol.* 202, 594–605. doi: 10.1111/nph.12700

Lamb, C., and Dixon, R. A. (1997). The oxidative burst in plant disease resistance. *Annu. Rev. Plant Physiol. Mol. Biol.* 48, 251–275. doi: 10.1146/annurev.arplant.48.1.251

Lee, Y. I., Hsu, S. T., and Yeung, E. C. (2013). Orchid protocorm-like bodies are somatic embryos. *Am. J. Bot.* 100, 2121–2131. doi: 10.3732/ajb.1300193

Lee, Y. I., and Yeung, E. C. (2010). The osmotic property and fluorescent tracer movement of developing orchid embryos of *Phaius tankervilliae* (Aiton) Bl. *Sex. Plant Reprod.* 23, 337–341. doi: 10.1007/s00497-010-0143-y

Lee, Y. I., Yeung, E. C., Lee, N., and Chung, M. C. (2006). Embryo development in the lady's slipper orchid, *Paphiopedilum delenatii* with emphases on the ultrastructure of the suspensor. *Ann. Bot.* 98, 1311–1319. doi: 10.1093/aob/mcl222

Murashige, T., and Skoog, F. (1962). A revised medium for rapid growth and bio assays with tobacco tissue cultures. *Physiol. Plant.* 15, 473–479. doi: 10.1111/j.1399-3054.1962.tb08052.x

Olsson, P. A., Kjellbom, P., and Rosendahl, L. (2002). *Rhizobium* colonization induced changes in membrane-bound and soluble hydroxyproline-rich glycoprotein composition in pea. *Physiol. Plant.* 114, 652–660. doi: 10.1034/j.1399-3054.2002.1140420.x

Perotto, S., Rodda, M., Benetti, A., Sillo, F., Ercole, E., Rodda, M., et al. (2014). Gene expression in mycorrhizal orchid protocorms suggests a friendly plant–fungus relationship. *Planta* 239, 1337–1349. doi: 10.1007/s00425-014-2062-x

Peterson, R. L., and Currah, R. S. (1990). Synthesis of mycorrhizae between protocorms of *Goodyera repens* (Orchidaceae) and *Ceratobasidium cereale*. *Can. J. Bot.* 68, 1117–1125. doi: 10.1139/b90-141

Peterson, R. L., Kuga, Y., and Zelmer, C. (1998). Fungal symbioses with orchid protocorms. *Symbiosis* 25, 29–55.

Peterson, R. L., and Massicotte, H. B. (2004). Exploring structural definitions of mycorrhizas, with emphasis on nutrient-exchange interfaces. *Can. J. Bot.* 82, 1074–1088. doi: 10.1139/b04-071

Peterson, R. L., Uetake, Y., Bonfante, P., and Faccio, A. (1996). The interface between fungal hyphae and orchid protocorm cells. *Can. J. Bot.* 74, 1861–1870. doi: 10.1139/b96-223

Pharmacopoeia Committee of People's Republic of China (2005). *Pharmacopoeia of the People's Republic of China*, Vol. 1. Beijing: People's Medical Publishing House.

Rae, A. L., Bonfante-Fasolo, P., and Brewin, N. J. (1992). Structure and growth of infection threads in the legume symbiosis with *Rhizobium leguminosarum*. *Plant J.* 2, 385–395. doi: 10.1111/j.1365-313x.1992.00385.x

Raggi, V. (2000). Hydroxyproline-rich glycoprotein accumulation in tobacco leaves protected against *Erysiphe cichoracearum* by potato virus Y infection. *Plant Pathol.* 49, 179–186. doi: 10.1046/j.1365-3059.2000.00442.x

Rasmussen, H. N. (1990). Cell differentiation and mycorrhizal infection in *Dactylorhiza majalis* (Rchb. f.) Hunt & Summerh. (Orchidaceae) during germination *in vitro*. *New Phytol.* 116, 137–147. doi: 10.1111/j.1469-8137.1990.tb00519.x

Rasmussen, H. N. (1995). *Terrestrial Orchids-From Seed to Mycotrophic Plant*. Cambridge: Cambridge University Press. doi: 10.1017/CBO9780511525452

Rasmussen, H. N., and Rasmussen, F. N. (2009). Orchid mycorrhiza: implications of a mycophagous life style. *OIKOS* 118, 334–345. doi: 10.1111/j.1600-0706.2008.17116.x

Rathbun, E. A., Naldrett, M. J., and Brewin, N. J. (2002). Identification of a family of extensin-like glycoproteins in the lumen of *Rhizobium*-induced infection threads in pea root nodules. *Mol. Plant Microbe Interact.* 15, 350–359. doi: 10.1094/mpmi.2002.15.4.350

Ruiz-Avila, L., Burgess, S. R., Stiefel, V., Ludevid, M. D., and Puigdomènech, P. (1992). Accumulation of cell wall hydroxyproline-rich glycoprotein mRNA is

an early event in maize embryo cell differentiation. *Proc. Natl. Acad. Sci. U.S.A.* 89, 2414–2418. doi: 10.1073/pnas.89.6.2414

Ruiz-Avila, L., Ludevid, M. D., and Puigdomènech, P. (1991). Differential expression of a hydroxyproline-rich cell-wall protein gene in embryonic tissues of *Zea mays* L. *Planta* 184, 130–136. doi: 10.1007/bf00208246

Selosse, M. A., and Martos, F. (2014). Do chlorophyllous orchids heterotrophically use mycorrhizal fungal carbon? *Trends Plant Sci.* 19, 683–685. doi: 10.1016/j.tplants.2014.09.005

Smallwood, M., Martin, H., and Knox, J. P. (1995). An epitope of rice threonine- and hydroxyproline-rich glycoprotein is common to cell wall and hydrophobic plasma-membrane glycoporoteins. *Planta* 196, 510–522. doi: 10.1007/BF00203651

Smith, S. E. (1967). Carbohydrate translocation in orchid mycorrhizas. *New Phytol.* 66, 371–378. doi: 10.1111/j.1469-8137.1967.tb06016.x

Smith, S. E., and Read, D. J. (2008). *Mycorrhizal Symbiosis*, 3rd Edn. San Diego, CA: Academic Press.

Smith, S. E., and Smith, F. A. (1990). Structure and function of the interfaces in biotrophic symbioses as they relate to nutrient transport. *New Phytol.* 114, 1–38. doi: 10.1111/j.1469-8137.1990.tb00370.x

Stewart, S. L., Zettler, L. W., Minso, J., and Brown, P. M. (2003). Symbiotic germination and reintroduction of *Spiranthes brevilabris* Lindley, an endangered orchid native to Florida. *Selbyana* 24, 64–70.

Taiz, L., and Zeiger, E. (2010). *Plant Physiology*, 5th Edn. Sunderland, MA: Sinauer Association.

Tan, X. M., Wang, C. L., Chen, X. M., Zhou, Y. Q., Wang, Y. Q., Luo, A. X., et al. (2014). In vitro seed germination and seedling growth of an endangered epiphytic orchid, *Dendrobium officinale*, endemic to China using mycorrhizal fungi (*Tulasnella* sp.). *Sci. Hortic.* 165, 62–68. doi: 10.1016/j.scienta.2013.10.031

Uetake, Y., Kobayashi, K., and Ogoshi, A. (1992). Ultrastructural changes during the symbiotic development of *Spiranthes sinensis* (Orchidaceae) protocorms associated with binucleate *Rhizoctonia anastomosis* group C. *Mycol. Res.* 96, 199–209. doi: 10.1016/s0953-7562(09)80966-0

Van Aelst, A. C., and Van Went, J. L. (1992). Ultrastructural immuno-localization of pectins and glycoproteins in *Arabidopsis thaliana* pollen grains. *Protoplasma* 168, 14–19. doi: 10.1007/BF01332646

Wang, H., Fang, H. Y., Wang, Y. Q., Duan, L. S., and Guo, S. X. (2011). In situ seed baiting techniques in *Dendrobium officinale* Kimura et Migo and *Dendrobium nobile* Lindl.: the endangered Chinese endemic *Dendrobium* (Orchidaceae). *World. J. Microbiol. Biotechnol.* 27, 2051–2059. doi: 10.1007/s11274-011-0667-9

Wisniewski, J. P., Rathbun, E. A., Knox, J. P., and Brewin, N. J. (2000). Involvement of diamine oxidase and peroxidase in insolubilization of the extracellular matrix: implications for pea nodule initiation by *Rhizobium leguminosarum*. *Mol. Plant Microbe Interact.* 13, 413–420. doi: 10.1094/mpmi.2000.13.4.413

Wu, H., De Graaf, B., Mariani, C., and Cheung, A. Y. (2001). Hydroxyproline-rich glycoproteins in plant reproductive tissues: structure, functions and regulation. *Cell. Mol. Life Sci.* 58, 1418–1429. doi: 10.1007/pl00000785

Xie, D., Ma, L., Šamaj, J., and Xu, C. (2011). Immunohistochemical analysis of cell wall hydroxyproline-rich glycoproteins in the roots of resistant and susceptible wax gourd cultivars in response to *Fusarium oxysporum* f. sp. *Benincasae* infection and fusaric acid treatment. *Plant Cell Rep.* 30, 1555–1569. doi: 10.1007/s00299-011-1069-z

Xu, C. X., Takáč, T., Burbach, C., Menzel, D., and Šamaj, J. (2011). Developmental localization and the role of hydroxyproline rich glycoproteins during somatic embryogenesis of banana (*Musa* spp. AAA). *BMC Plant Biol.* 11:38. doi: 10.1186/1471-2229-11-38

Yan, L., Wang, X., Liu, H., Tian, Y., Lian, J., Yang, R., et al. (2015). The genome of *Dendrobium officinale* illuminates the biology of the important traditional Chinese orchid herb. *Mol. Plant* 8, 922–934. doi: 10.1016/j.molp.2014.12.011

Yeung, E. C. (1984). "Histological and histochemical staining procedures," in *Cell Culture and Somatic Cell Genetics of Plants: Laboratory Procedures and Their Applications*, Vol. 1, ed. I. K. Vasil (Orlando, FL: Academic Press), 689–697.

Yeung, E. C., and Chan, C. K. W. (2015). "The glycol methacrylate embedding resins – Technovit 7100 and 8100," in *Plant Microtechniques and Protocols*, eds E. C. Yeung, C. Stasolla, B. Q. Huang, and M. J. Sumner (Cham: Springer), 67–82.

Yeung, E. C., Zee, S. Y., and Ye, X. L. (1996). Embryology of Cymbidium sinense: Embryo development. *Ann. Bot.* 78, 105–110. doi: 10.1006/anbo.1996.0101

Zhao, M. M., Zhang, G., Zhang, D. W., Hsiao, Y. Y., and Guo, S. X. (2013). ESTs analysis reveals putative genes involved in symbiotic seed germination in *Dendrobium officinale*. *PLoS One* 8:e72705. doi: 10.1371/journal.pone.0072705

**Conflict of Interest Statement:** The authors declare that the research was conducted in the absence of any commercial or financial relationships that could be construed as a potential conflict of interest.

frontiers in Plant Science

ORIGINAL RESEARCH
published: 17 July 2018
doi: 10.3389/fpls.2018.01043

# Increased Expression of 9-*Cis*-Epoxycarotenoid Dioxygenase, *PtNCED1*, Associated With Inhibited Seed Germination in a Terrestrial Orchid, *Phaius tankervilliae*

*Yung-I. Lee[1,2], Ming-Chuan Chen[1], Li Lin[3], Mei-Chu Chung[4]* and Wei-Ming Leu[3,5]**

[1] Department of Biology, National Museum of Natural Science, Taichung, Taiwan, [2] Department of Life Sciences, National Chung Hsing University, Taichung, Taiwan, [3] Institute of Biotechnology, National Chung Hsing University, Taichung, Taiwan, [4] Institute of Plant and Microbial Biology, Academia Sinica, Taipei, Taiwan, [5] Advanced Plant Biotechnology Center, National Chung Hsing University, Taichung, Taiwan

The phytohormone abscisic acid (ABA) is involved in regulating seed dormancy and germination. A crucial step of ABA biosynthesis in higher plants is the oxidative cleavage of *cis*-epoxycarotenoids by 9-*cis*-epoxycarotenoid dioxygenase (NCED). Seed development in orchids is unusual because the embryos are minute in size, without obvious histodifferentiation, and lack endosperm. To understand the regulation of ABA biosynthesis in orchid seeds, we isolated and characterized a full-length cDNA encoding an NCED homolog, *PtNCED1*, from developing seeds of an ornamental orchid, *Phaius tankervilliae*. Germination percentage was high at 90 days after pollination (DAP), when a globular embryo proper with a degenerating suspensor was evident. After 90 DAP, seed maturation was accompanied by a decrease in water content and a concomitant increase in ABA content and *PtNCED1* mRNA level along with a marked decrease in germination percentage. Mature seeds pretreated with NaOCl solution lowered ABA content and improved seed germination. Moreover, after seed germination, developing protocorms could respond to dehydration stress. Dehydration of protocorms stimulated an increase in *PtNCED1* level along with ABA content. Our results provide evidence of the involvement of *PtNCED1* in regulating endogenous ABA content in developing seeds and protocorms. The accumulation of endogenous ABA content in orchid seeds may have a critical role in seed dormancy and the protocorm response to water stress after seed germination.

**Keywords: abscisic acid, orchid, seed development, 9-*cis*-epoxycarotenoid dioxygenase, germination**

OPEN ACCESS

***Edited by:***
*Akira Kanno,*
*Tohoku University, Japan*

***Reviewed by:***
*Zhong Chen,*
*Nanyang Technological University, Singapore*
*Kiyoshi Mashiguchi,*
*Tohoku University, Japan*

****Correspondence:***
*Mei-Chu Chung*
*bomchung@gate.sinica.edu.tw*
*Wei-Ming Leu*
*wmleu@nchu.edu.tw*

***Specialty section:***
*This article was submitted to Plant Evolution and Development, a section of the journal Frontiers in Plant Science*

***Received:*** *30 January 2018*
***Accepted:*** *27 June 2018*
***Published:*** *17 July 2018*

***Citation:***
*Lee Y-I, Chen M-C, Lin L, Chung M-C and Leu W-M (2018) Increased Expression of 9-Cis-Epoxycarotenoid Dioxygenase, PtNCED1, Associated With Inhibited Seed Germination in a Terrestrial Orchid, Phaius tankervilliae. Front. Plant Sci. 9:1043. doi: 10.3389/fpls.2018.01043*

## INTRODUCTION

Orchids produce numerous tiny seeds within a capsule. At the time of capsule maturity, an orchid seed contains an undifferentiated globular-shaped embryo covered by a thin testa without endosperm (Arditti and Ghani, 2000). In the natural environment, mycorrhizal fungi are required for successful germination and establishment of seedlings (Rasmussen, 1995), whereas in asymbiotic cultures in the absence of mycorrhizal fungi, the addition of soluble sugars and mineral nutrients are needed for germination and seedling establishment (Knudson, 1922). After

germination, orchid embryos first show a temporary tubercle structure called a protocorm from which a shoot and a root differentiate to form a seedling (Yeung, 2017).

*Phaius tankervilliae* is a terrestrial species, known as "nun" orchid, and is native to the lowland forest in tropical Asia. It is a popular ornamental orchid used as a potted plant or garden plant (Moir, 1983). In general, seeds of terrestrial orchids are considered more difficult to germinate than those of epiphytic orchids (Arditti et al., 1982). The reasons for the poor germination may relate to the impermeable seed coat (Veyret, 1969; Lee et al., 2005) and/or the accumulation in mature seeds of inhibitory substances, such as phenolics (Kako, 1976) and abscisic acid (ABA) (Van Waes and Debergh, 1986; Van der Kinderen, 1987). NaOCl solution treatment of mature seeds significantly improved germination percentage, which indicates the removal of germination inhibitors (Van Waes and Debergh, 1986; Lee et al., 2007). In a recent study, mature seeds of *Cypripedium formosanum* showed high endogenous ABA content, and reducing the ABA content by fluridone application improved seed germination (Lee et al., 2015). These results indicate that ABA has a regulatory role in embryo development and seed dormancy of orchids.

The phytohormone ABA plays a crucial role in regulating the signaling networks associated with adaptation to stressful environments and physiological processes including stomatal movement and seed dormancy (Nambara and Marion-Poll, 2005). In higher plants, enzymes involved in biosynthesis of ABA and the pivotal role of ABA during transition from seed maturation to germination has been studied in great detail (Yan and Chen, 2017). ABA is *de novo* synthesized from carotenoids in plastids. The oxidative cleavage of 9-*cis*-epoxycarotenoids by the 9-*cis*-epoxycarotenoid dioxygenase (NCED) to produce xanthoxin is the first committed and also the rate-limiting step for ABA biosynthesis. Xanthoxin is subsequently exported from the plastids to cytosol and be converted to ABA via abscisic aldehyde (Nambara and Marion-Poll, 2005). In *Arabidopsis*, because the enzymes acting before or after NCED are all encoded by a single locus, the five-membered NCED gene family may play a spatio-temporal regulatory role in ABA biosynthesis (Iuchi et al., 2001; Tan et al., 2003; Frey et al., 2012).

In *Arabidopsis*, *AtNCED6* is expressed specifically in endosperm and *AtNCED9* in both embryo and endosperm. Genetic analysis of mutants suggested that *AtNCED6* and *AtNCED9* are essential for inducing and maintaining seed dormancy (Lefebvre et al., 2006). However, little is known about the roles of NCEDs for ABA biosynthetic activities in seed germination and protocorm development of orchids. To date, only a quantitative proteomic study of the symbiotic germination of *Oncidium* orchid detected an induced accumulation of NCED proteins, thus suggesting that ABA may promote the development of arbuscules in root cortical cells (Valadares et al., 2014). The basic knowledge of seed physiology in terrestrial orchids would benefit mass propagation to meet commercial needs in ornamental plant markets.

To gain further understanding of the role and regulation of ABA during seed development and germination in *P. tankervilliae*, we cloned and characterized a new gene encoding an NCED homolog, *PtNCED1*. In this study, we aimed to (1) analyze and characterize *PtNCED1* from *P. tankervilliae* seeds, (2) investigate the associations among water content, ABA content and *PtNCED1* transcript level and seed germination percentage, (3) investigate the effect of pretreating seeds with NaOCl solution on ABA content and seed germination, and (4) investigate the effect of dehydration treatment of protocorms on *PtNCED1* and ABA levels. The results demonstrate that the expression of *PtNCED1* plays an important role in regulating ABA content in orchid seed and protocorm development.

# MATERIALS AND METHODS

## Plant Material

The plants of *P. tankervilliae* were cultivated in a greenhouse at the National Museum of Natural Science, Taichung, Taiwan. The flowers were manually pollinated at anthesis in March. In each experiment, capsules were randomly collected at regular intervals of 15 days from 45 to 120 days after pollination (DAP).

## Histology

The developing seeds were fixed in a solution of 2.5% glutaraldehyde and 1.6% paraformaldehyde in 0.1 M phosphate buffer (pH 6.8) for 4 h at room temperature. After fixation, the samples were dehydrated with an ethanol series and embedded in Technovit 7100 (Kulzer & Co., Germany) as described (Yeung and Chan, 2015). Sections of 3-μm thick were cut with glass knives by using a Reichert-Jung 2040 Autocut rotary microtome. Sections were stained with periodic acid-Schiff (PAS) reaction for total insoluble carbohydrates, and counterstained with 0.05% (w/v) toluidine blue O in benzoate buffer for general histology or 1% (w/v) amido black 10B in 7% acetic acid for protein (Yeung, 1984). Sections were examined and captured digitally by using a CCD camera attached to a light microscope (Axio Imager A1, Carl Zeiss AG). More than 100 capsules were used for the study of seed development and more than 600 different protocorms of each developmental stage were observed.

## Cloning of *PtNCED1* From *P. tankervilliae*

An RNA-Seq dataset was generated from developing seeds (90 DAP) of *P. tankervilliae* on an Illumina Hiseq 2000 platform. The raw data were cleaned by removing reads containing adapter and low-quality reads, yielding c. 53 million cleaned reads (i.e., ∼26 M paired-end reads, read length 100 bp). FASTQ sequence files were deposited at the National Center for Biotechnology Information (NCBI) under BioProject PRJNA445551 and sequence read archive (SRA) database SRP139691. The clean reads were assembled by using the Trinity method (Grabherr et al., 2011) with optimized *k*-mer length of 25 into 45688 contigs and deposited in the Transcriptome Shotgun Assembly (TSA) database at the NCBI under accession number GGMF01000000. We used the AtNCED6 and 9 protein sequences (encoded by AT3G24220 and AT1G78390, respectively) as queries to perform tBLASTn searches among the RNA-Seq dataset. Only one contig (Contig1245, or GGMF01001196 in the TSA database) was found to encode an NCED-like sequence. We named it as *PtNCED1* and

deposited it in the NCBI with accession number MH105783 (see details in "Results" section).

## Southern Hybridization Analysis

About 100 μg genomic DNA was isolated from approximately 1.5 g seeds of *P. tankervilliae* by the CTAB method. For each enzyme digestion, approximately 20 μg genomic DNA was used. Samples were resolved on 1% agarose gel, blotted onto a nylon membrane, then probed with a $^{32}$P-labeled *PtNCED1* cDNA fragment. The cDNA fragment was PCR-amplified by using NCED-8, 9 primers (Supplementary Table S1) with p32H-NCED (see below) as a template. Isotope labeling was performed according to Amersham Megaprime DNA labeling systems (GE Healthcare Life Sciences, Marlborough, MA, United States). Hybridization and probe stripping were performed as described (Wang et al., 2011).

## Phylogenetic Analyses

Sequences of all NCED/CCD members in the genome of *Arabidopsis* and rice were retrieved from TAIR[1] and RGAP[2], respectively. Other representative members of NCED/CCD from various species were obtained from the NCBI. Multiple alignments of amino acid sequences involved use of the NCBI Constraint-based Multiple Alignment Tool (COBALT[3], Papadopoulos and Agarwala, 2007). The phylogenetic tree was constructed by the Neighbor-Joining method with protein distance estimated by the Grishin correction method.

## Transient Overexpression of *PtNCED1* in Tobacco Leaves

For overexpressing PtNCED1 in plant cells, the *PtNCED1* cDNA fragment was amplified by RT-PCR with NCED-8, 9 primers (Supplementary Table S1), digested by PstI and BamHI restriction endonucleases, then subcloned into the pEpyon32H binary vector (C.-H. Yang, unpublished data) to produce the p32H-NCED plasmid. The pEpyon32H vector contains the mGFP5 reporter gene (Haseloff, 1999) under control of a 2x35S CaMV promoter. For overexpressing the PtNCED1-mGFP5 fusion protein (abbreviated as PtNCED1-GFP), a plasmid similar to p32H-NCED was constructed but using a primer that does not contain a stop codon (NCED-10, Supplementary Table S1) instead of the NCED-9 primer. After sequencing confirmation, both plasmids were transformed into *Agrobacterium* strain C58C1. Agroinfiltration was performed according to Cheng et al. (2010) on leaves of 4-week-old *Nicotiana benthamiana*. After transient expression for 3 days under a 16/8-h photoperiod at 25 ± 2°C, the subcellular distribution of PtNCED1-GFP was visualized by confocal microscopy (Olympus, IX81; Software, FV1000). Wavelengths of excitation/emission for chlorophyll and GFP were 470/633 and 488/510 nm, respectively. Furthermore, content of endogenous ABA was measured in agroinfiltrated tobacco leaves as described below.

[1]https://www.arabidopsis.org/

[2]http://rice.plantbiology.msu.edu/

[3]https://www.ncbi.nlm.nih.gov/tools/cobalt/re_cobalt.cgi

## Real-Time PCR

Total RNA was extracted from developing seeds by using the RNeasy Plant Mini Kit (Qiagen, Hilden, Germany) according to the manufacturer's instructions. RNA samples were treated with RQ1 DNase (Invitrogen, United States) to remove DNA remnants, then synthesis of the first cDNA strand involved using the PrimeScript RT reagent Kit (TaKaRa Bio, Japan). The *Ptactin-7-like* gene (Contig62, or GGMF01000062 in the TSA database, also deposited in the NCBI with accession number MH124736) was used as an internal quantification standard. Primers for real-time PCR were designed by using Premier 5.0 (Premier Biosoft, India, Supplementary Table S1) and each real-time PCR experiment involved 7.5 μL of SYBR Premix Ex Taq II (TaKaRa Bio), 1.5 μL cDNA, and 0.3 μL primers, and water was added to 15 μL. Each sample was analyzed in three biological replicates with three technical replicates by using the LightCycler 480 II Real-Time PCR System (Roche, Switzerland) with its relative quantification program. The parameters of reactions were an initial denaturation at 95°C for 30 s, then 40 cycles of 95°C for 5 s, and 60°C for 30 s. The $2^{-\Delta\Delta C_t}$ method was used for evaluating gene expression.

## *In Vitro* Germination

After surface sterilization, seeds were removed from capsules and placed onto 20 ml culture medium in a 9-cm diameter Petri dish. The culture medium for seed germination is the modified Murashige and Skoog (MS) medium (Murashige and Skoog, 1962) which contained 1/4 strength of macroelements with full strength microelements (2 mg glycine, 0.5 mg niacin, 0.5 mg pyridoxine HCl, 0.1 mg thiamine, 100 mg myo-inositol, 20 g sucrose and 6 g agar per liter). The pH was adjusted to 5.7 before autoclaving at 102 kPa and 121°C for 20 min. The cultures were maintained in the growth room under light (20 $\mu molm^{-2}$ $s^{-1}$) with a 12/12-h photoperiod at 25 ± 2°C. Experiments were performed in a randomized design and repeated three times. Twelve replicates (plates) were used for each treatment, with a minimum of 200 seeds per plate. Each plate was examined monthly by using a stereomicroscope (Carl Zeiss AG, Germany), and germination percentage was scored after 120 days of culture. Germination was defined as emergence of the embryo from the testa.

## Measurement of Water Content of Developing Seeds

Three capsules were randomly collected at intervals of 15 days from 45 to 120 DAP. Seeds of 0.1 g at different developmental stages were dissected carefully from the placenta and then dried at 70°C for 48 h. The water content was estimated as the percentage of water loss: fresh weight minus dry weight, to its fresh weight.

## Measurement of the Endogenous ABA Level

The procedure for endogenous ABA measurement was described in detail by Lee et al. (1993). In this study, samples for ABA measurement had three replicates, including seeds at each

developing stage, or for seed pretreatments, protocorm for water stress experiments, and the agroinfiltrated tobacco leaves for transient overexpression of *PtNCED1*. In each replicate, seeds of 20 mg, protocorms of 100 mg and tobacco leaves of 700 mg were homogenized with mortar and pestle in a 1.5-mL Eppendorf tube containing the extraction solution (80% methanol and 2% glacial acetic acid). For estimating extraction efficiency, an internal standard, 166.5 Bq DL-[G-$^3$H]-ABA (Amersham Biosciences, Buckinghamshire, United Kingdom) was added to the Eppendorf tube during the extraction procedure. Extraction was carried out at 4°C with shaking for 48 h in darkness. Extracts were filtered through filter paper (Whatman No. 1), and then further rinsed twice with extraction solution. The filtrates were dried in vacuo at 30°C then resuspended in 100% methanol. A solution of 0.2 M $(NH_4)_2HPO_4$ was subsequently added and the samples were allowed to stand for 10 min at 4°C until ammonium salts formed. In order to remove pigments, phenolics and polar compounds, extracts were first passed through a polyvinylpyrrolidone (PVP) column, then a C18 cartridge (Waters, Milford, MA, United States). ABA trapped in the C18 cartridge was then eluted with 55% methanol. Eluates of 100 μl of each extraction were subjected to scintillation counting to determine ABA recovery, and the average recovery ranged from 70 to 76%. The eluates were dried in vacuo and resuspended in Tris-buffered saline (50 mM Tris-HCl, 10 mM NaCl, 1 mM $MgCl_2$, 15mM $NaN_3$, pH 7.5) and stored at −20°C for enzyme-linked immunosorbent assay (ELISA). ABA was quantified by ELISA according to Walker-Simmons (1987) using a Phytodetek® ABA ELISA kit (Agdia, Elkhart, IN, United States). ABA levels are expressed as ng/mg fresh mass.

## Pretreatments With NaOCl Solution and the Application of Exogenous ABA on Seed Germination

For evaluating the effect of sodium hypochlorite solution, mature seeds at 120 DAP were collected and soaked in 0.5% NaOCl solution with two drops of a wetting agent Tween 20 (Sigma-Aldrich Co. St. Louis, MO, United States) for 10 or 20 min. For the control, seeds were soaked only in water. After treatments, seeds were rinsed three times with sterilized water and then placed on the culture medium or analyzed for ABA content. To examine the effect of exogenous ABA on seed germination, the mature seeds at 120 DAP which were pretreated with 0.5% NaOCl solution for 20 min were inoculated on the culture medium with the supplement of 0.0003, 0.0037, 0.0378, or 0.3787 μM (these concentrations were equal to 0.1, 1, 10, or 100 ng/mL) (±)−ABA (A1049, Sigma-Aldrich Co.). The culture medium without ABA supplement was used as control. ABA solution was filter-sterilized and added to the medium after autoclaved sterilization. The germination percentage was scored after 50 days of culture.

## Water Stress Experiments in Protocorms

Protocorms of about 2 mm in diameter were dehydrated by placing onto a 9-cm diameter Petri dish containing MS medium (as described above) supplemented with 10% polyethylene glycol (PEG) 6000 (Sigma-Aldrich Co.) for 24 and 48 h. Cultures were placed under light (20 $\mu molm^{-2}$ $s^{-1}$) with a 12/12-h photoperiod at 25 ± 2°C. The control non-stressed protocorms were kept in the MS medium without the addition of PEG 6000 and under the same conditions as dehydrated protocorms for 24 and 48 h. Each sample was analyzed in three biological replicates and repeated three times. Each biological replicate (Petri dish) contained at least 30 protocorms.

## Statistical Analysis

Except for measurement of ABA content in the *PtNCED1* transiently expressed tobacco leaves in which an unpaired Student's *t*-test was applied, all other statistical analyses were carried out with SAS statistical software version 8.2 (SAS Institute, Cary, NC, United States). The data were analyzed using analysis of variance (ANOVA) in combination with Fisher's protected least significant difference test at $P < 0.05$. Data were arsine-transformed before performing ANOVA.

# RESULTS

## Histological Observations of Seed Development

This study confirmed the earlier study by Ye et al. (1997) and documented clearly the time course of changes during embryo development. Fertilization occurred approximately 40 DAP (**Figure 1A**). From 45 to 60 DAP, the zygote and proembryo were observed within the capsules (**Figures 1B,C**). The zygote appeared as a highly polarized cell with a nucleus toward the chalazal end, and a prominent vacuole toward the micropylar end. Inside the endosperm cavity, the polar nuclei and one of the sperm nuclei formed the endosperm complex; these nuclei disintegrated rapidly as the embryo developed. However, endosperm was finally degenerated in the seed. In the early globular stage (75 DAP), the suspensor cell had enlarged with the process of vacuolation (**Figure 1D**). Within the developing embryo proper, starch granules began to accumulate and tended to congregate around the nucleus of the cell. At 90 DAP, the mitotic activity seemed to have ceased within the embryo proper and the suspensor started to degenerate (**Figure 1E**). At the same time, protein and lipid bodies were formed and accumulated within the embryo proper. At 105 DAP, the mature embryo filled with storage products was only six cells long and five to six cells wide without differentiation of apical meristem and cotyledon (**Figure 1F**). The seed coat was derived from the outer integument, which was only two cells thick. During early embryo development, the outer seed coat was highly vacuolated (**Figure 1A**). As the seed matured, a secondary wall was added to the radial and inner tangential walls of the outer layer. At maturity, the cells of seed coat became dehydrated and compressed into a thin layer (**Figure 1F**). Moreover, the dehydrated seed coat stained blue green with toluidine blue O, indicating the presence of phenolic compounds in the walls.

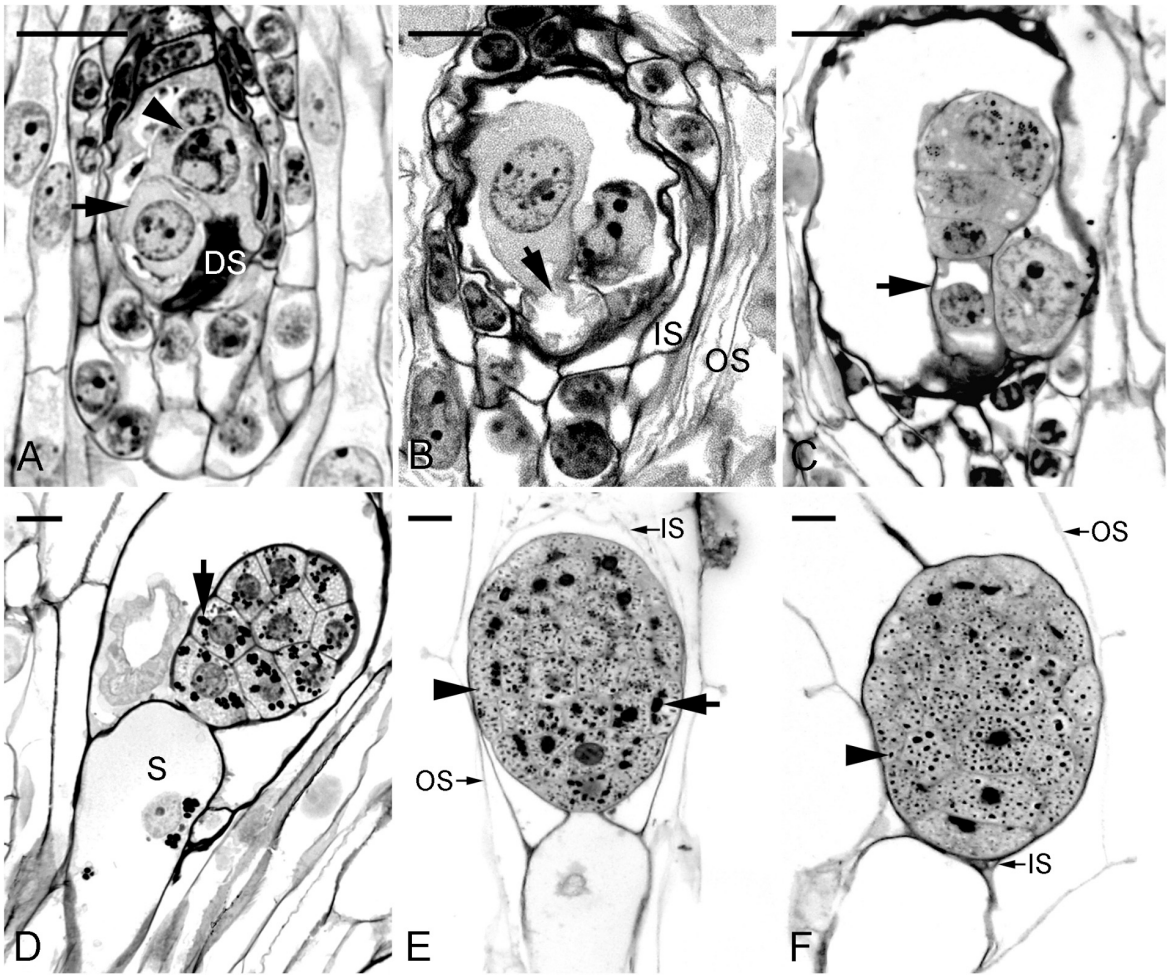


**FIGURE 1 |** Light micrographs showing the embryo of *Phaius tankervilliae* at different stages of development. **(A)** A zygote (arrow) after fertilization at 40 days after pollination (DAP). In this species, the endosperm fails to develop, and the polar-chalazal complex (arrowhead) includes the chalazal nuclei and the polar nuclei. DS, degenerated synergid. **(B)** Elongated zygote at 45 DAP. Before the first cell division, the zygote is highly polarized with a nucleus located toward the chalazal end and a prominent vacuole (arrow) occupying the micropylar end. IS, the inner seed coat; OS, the outer seed coat. **(C)** Longitudinal section through a proembryo at 60 DAP. Vacuoles begin to enlarge at the suspensor cell (arrow). **(D)** Longitudinal section through a globular embryo with an enlarged single-celled suspensor (S) at 75 DAP. A number of starch grains (arrow) are present in the cells of the embryo proper. **(E)** Longitudinal section through a near-mature embryo at 90 DAP. At this stage, the suspensor has degenerated. Many starch grains (arrow) and protein bodies (arrowhead) are present in the cells of the embryo proper. The inner seed coat (IS) is dehydrating and compressing. **(F)** Longitudinal section through a mature embryo at 105 DAP. At this stage, the suspensor has degenerated. At maturity, the embryo is enveloped by the shriveled IS and the OS. Starch grains have disappeared and protein bodies (arrowhead) of various sizes are observed within the embryo proper. Although lipids could not be preserved in Historesin, plentiful translucent vesicles within the cytoplasm of embryo proper indicate the deposition of lipid bodies. Scale bar = 20 μm.

## Isolation and Characterization of *PtNCED1* From *P. tankervilliae*

To examine roles of ABA in seed and protocorm development in *P. tankervilliae,* we isolated a gene encoding NCED, the key enzyme for ABA biosynthesis in seeds. Because *AtNCED6* and *9* were known to be expressed predominantly during seed development and play key roles in regulating seed development and dormancy in *Arabidopsis* (Lefebvre et al., 2006), we looked for their homolog in the RNA-Seq dataset of *P. tankervilliae* by a tBLASTn search. Among 45688 assembled contigs, only one contig (Contig1245) was found to encode polypeptide that shares high sequence similarity with AtNCED6 or 9. The second similar subject found (Contig941, or GGMF01000904 in the TSA database) encodes polypeptide which share higher similarity to AtCCD1 than to AtNCED6 and 9, so was named as PtCCD1 in this study. Contig1245 contains a full-length open reading frame of 1830 nt with 257 and 487 nt as the 5′ and 3′-UTR, respectively. We named the deduced amino acid sequence as PtNCED1. PtNCED1 showed high sequence similarity (77–81%) with AtNCED2, 3, 5, and 9 but only 70% similarity with AtNCED6 (Supplementary Table S2).

A BLASTp search of the NCBI database revealed that PtNCED1 contains a highly conserved RPE65 domain for catalytic activity of the carotenoid cleavage dioxgenases (CCDs)

and shares the highest sequence similarity (92%) with an NCED from *Dendrobium catenatum*. PSORT[4] predicted a chloroplast stroma localization for PtNCED1. A transit peptide (1–53 amino acids of PtNCED1) was detected by ChloroP analysis (Emanuelsson et al., 1999). Sequence alignments for PtNCED1 with AtNCED6 and 9 together with the predicted transit peptide are in Supplementary Figure S1.

The NCED/CCD gene family has 8–9 members in both *Arabidopsis* and rice. To determine which member was most related to PtNCED1, we constructed a phylogenetic tree using the full-length protein sequences of NCED/CCD from various species. Located in the NCED clade, PtNCED1 shared the highest sequence similarity with NCEDs from orchids including *Oncidium* (Chiou et al., 2010), *D. catenatum*, and *Phalaenopsis equestris* (**Figure 2**). These orchid NCEDs are sister to NCEDs from rice and maize, then to a clade constituted by NCEDs from dicotyledon, and finally grouped with AtNCED6 to form the NCED clade. Of note, all NCED members are highly conserved (sharing >74% sequence similarity with each other) while sequences in most CCD members are quite divergent from each other. The putative PtCCD1 was most similar to the *Oncidium* CCD (Chiou et al., 2010) and grouped within the CCD clade.

To examine the copy number of *PtNCED1* gene in *P. tankervilliae*, we performed genomic Southern analysis. Three restriction enzymes KpnI, EcoRI and BglI possessing cutting sites on the probe, each generated 2–3 prominent bands, and HindIII, which has no expected site on the probe region, showed only a single band (**Figure 3**). Because a high stringency wash (5% SDS, 65°C, then 1% SDS, 65°C) was carried out after hybridization, we concluded that no other genes sharing high sequence similarity with *PtNCED1* existed in *P. tankervilliae*. Nevertheless, some very faint bands detected in the KpnI and BglI-digested lanes still implicated the less-related NCED members. Moreover, a 1- and 1.3-kb band appeared in the KpnI- and EcoRI-digested lanes, respectively, which agrees with its length in the cDNA probe, therefore suggesting that *PtNCED1* is likely an intronless gene.

## Subcellular Localization of PtNCED1 in Chloroplasts

Because NCED catalyzes the committed step for *de novo* synthesis of ABA, which occurs in plastids, we examined the subcellular localization of PtNCED1 by fusion with GFP and transient expression in tobacco leaves by agroinfiltration. On confocal microscopy, the free GFP proteins were distributed in the cytosol of mesophyll cells, whereas PtNCED1-GFP predominantly co-localized with chlorophyll in chloroplasts (**Figure 4**). Thus, PtNCED1 is mainly located in chloroplasts, most likely in the stroma as predicted by PSORT.

## Analysis of Enzyme Activity for PtNCED1

To verify that PtNCED1 has NCED activity, we used agroinfiltrated tobacco leaves to overproduce PtNCED1 protein. ABA level was increased approximately 3- and 12-fold with overexpression of PtNCED1-GFP fusion protein and PtNCED1, respectively, as compared with the vector control (**Figure 5**). Therefore, PtNCED1 has NCED activity. The lower amounts of ABA produced by PtNCED1-GFP than PtNCED1 implies that GFP fusion may disturb the protein-folding and/or enzyme activity of PtNCED1 or, alternatively, decrease the protein abundancy.

## Effect of the Timing of Seed Collection on Germination

Germination was not observed in immature seeds at 45 and 60 DAP but thereafter increased to a maximum of 47.4% at 90 DAP (**Figure 6A**). However, as the seeds approached maturity, from 105 to 120 DAP, the germination percentage progressively decreased.

## Changes in Water Content in Developing Seeds

The water content of seeds collected from 45 to 75 DAP was more than 90% of the fresh weight (**Figure 6B**). During this period, the capsules were green and seeds were white and moist and still attached to the placenta. By 90 DAP, the seeds began to turn yellowish white with a sharp drop in water content. After 105 DAP, the seeds had turned yellow and became dry and free from the placenta, which allowed them to be readily shaken onto the medium. The water content of mature seeds (120 DAP) was estimated at 12.8%.

## Changes in Endogenous ABA Content and *PtNCED1* Level in Developing Seeds

During the early stages of seed development, from 45 to 60 DAP, the ABA content was maintained at low levels (0.43–0.44 ng/mg fresh weight) (**Figure 6C**). After 75 DAP, ABA content increased rapidly, with peak content (6.81 ng/mg fresh weight) at 120 DAP and continual increase from 105 to 120 DAP. Hence, the seeds of *P. tankervilliae* maintained a high ABA content for a prolonged period until the capsules split. Similar to changes in ABA content in developing seeds of *P. tankervilliae* (**Figure 6D**), the expression of *PtNCED1* was low during the early stage of seed development (45–60 DAP) but progressively increased from 70 DAP to peak at 105 DAP, then declined slightly when seeds matured.

## Effect of NaOCl Pretreatment and Exogenous ABA Application on Seed Germination

Soaking mature seeds with the 0.5% NaOCl solution for 10 or 20 min greatly increased seed germination percentage more than threefold, reaching >72% (**Figure 7A**). A substantial decrease of endogenous ABA content from 6.24 to 1.81 ng/mg fresh weight improved seed germination (**Figure 7B**), suggesting an effect by ABA removal. Moreover, applying a relatively low concentration of ABA (0.0037 μM, i.e., 1 ng/mL) in the culture medium was sufficient to suppress the germination of mature seeds pretreated with 0.5% NaOCl solution for 20 min (**Figure 7C**).

[4]https://psort.hgc.jp/

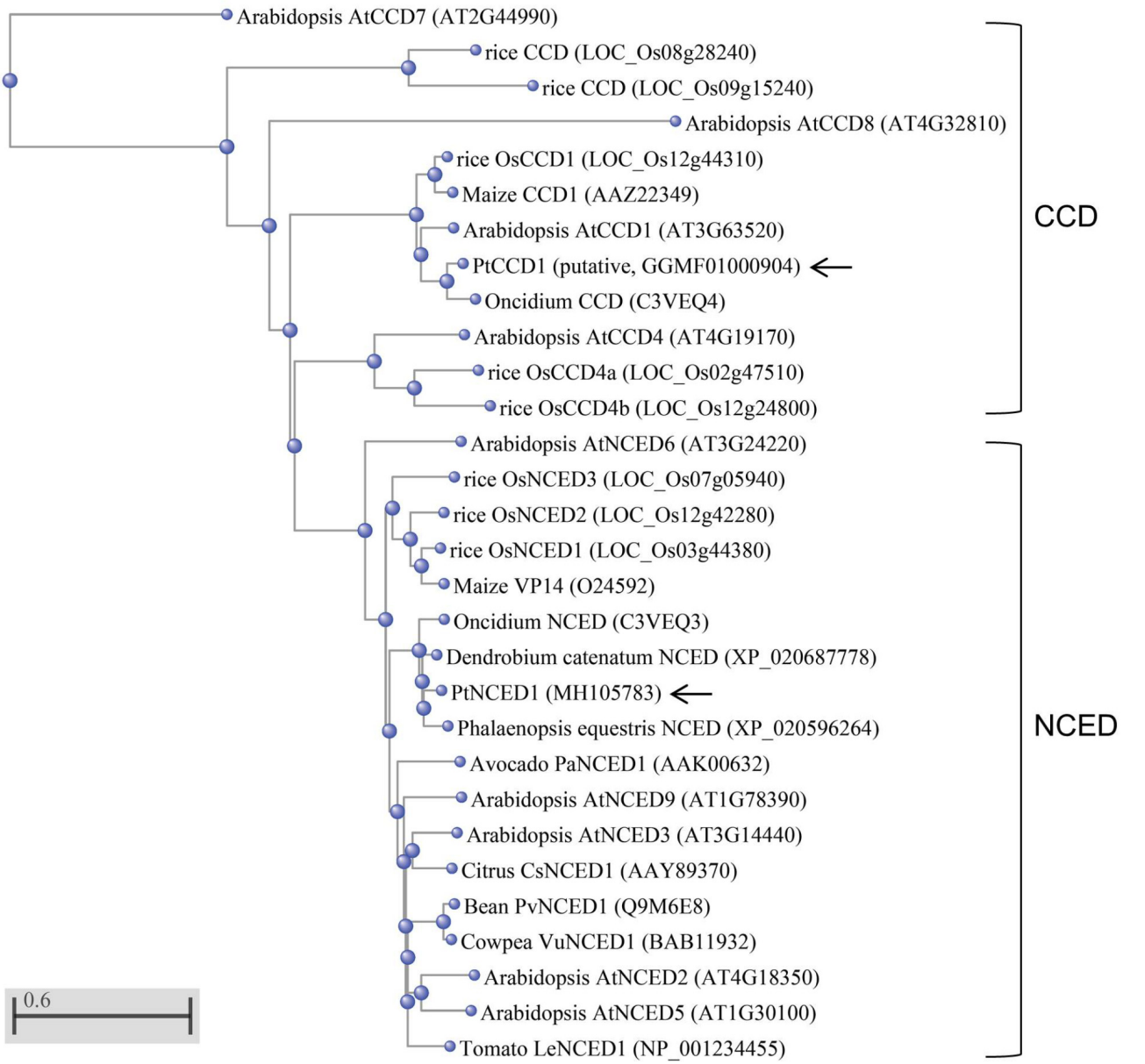


**FIGURE 2 |** Phylogenetic analysis of PtNCED1 and other plant NCEDs and CCDs. The PtNCED1 protein sequence was aligned with the full-length NCED/CCD members from various species by using the COBALT program with Neighbor Joining as tree method in the NCBI. The scale bar indicates a genetic distance for 0.6 amino acid substitutions per site. Of note, members with very dissimilar sequences (>0.5) may only be accurate in grouping but not in genetic distance. Shown in bracket are the locus names for Arabidopsis and rice, obtained from TAIR (https://www.arabidopsis.org/) and MSU (http://rice.plantbiology.msu.edu/), respectively, and the accession numbers for other species, obtained from the NCBI. For rice, members of CCD and NCED follow the names given in Tan et al. (2003). PtNCED1 and PtCCD1 obtained in this study are denoted by arrows.

## Changes in *PtNCED1* Level and ABA Content in Response to Dehydration in Protocorms

To examine whether the *PtNCED1* level could be induced by dehydration in protocorms, we quantified *PtNCED1* level in water-stressed protocorms and showed a 5.7- and 7.3-fold increase after dehydration for 24 and 48 h, respectively (**Figure 8A**). In agreement, ABA content increased from 0.2 to 1.15, then from 0.24 to 1.62 ng/mg fresh weight after dehydration (**Figure 8B**).

## DISCUSSION

As consistent with our previous studies on other orchids (Lee et al., 2007, 2015), here we found that ABA accumulates during embryo development of *P. tankervilliae*, and we demonstrate

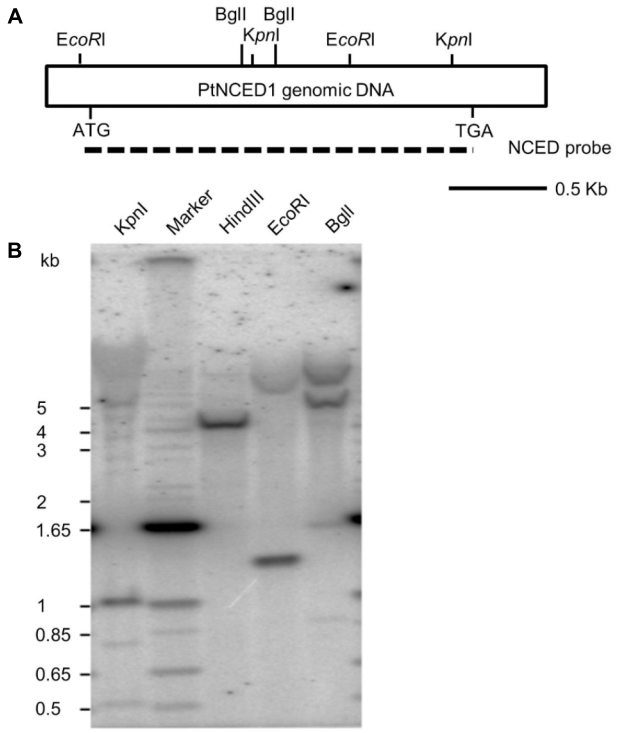


**FIGURE 3 |** Southern hybridization of the *PtNCED1* gene. **(A)** Schematic depiction of the cDNA fragment of *PtNCED1* with *Eco*RI, *Bgl*I and *Kpn*I endonuclease sites shown. Dashed line indicates the open reading frame region used as a probe. **(B)** Southern blot analysis. Each lane was loaded with 20 μg genomic DNA from *P. tankervilliae* digested by the indicated restriction enzyme. The DNA markers are indicated on the left.

for the first time that the key gene *PtNCED1* involved in ABA biosynthesis is indeed present in orchid. *PtNCED1* shares common characteristics with the known *AtNCEDs* and *OsNCEDs*. This work clearly indicates that orchids can synthesize ABA during embryogenesis and protocorm development.

## Characteristics of the Sole *PtNCED1* Transcript in Developing Seeds of *P. tankervilliae*

In *Arabidopsis*, each of *AtNCED* genes has its specific function — *AtNCED3* in abiotic stress response (Iuchi et al., 2001), *AtNCED5* in plant disease susceptibility (Fan et al., 2009), *AtNCED2* and *AtNCED3* in determining root growth direction (Tan et al., 2003), and *AtNCED6* and *AtNCED9* in seed development and dormancy (Lefebvre et al., 2006). Nevertheless, searching of the RNA-Seq dataset which we constructed from the developing seeds (90 DAP) of *P. tankervilliae* revealed only contig1245 encoding for a full-length NCED, together with other 6–7 contigs encoding for either full-length or truncated CCDs (data not shown). The lack of NCED isoforms may be due to the unique feature of seed development in orchids, e.g., the absence of endosperm and the rudimentary embryo (**Figure 1**). Moreover, as *AtNCED6* is expressed only in endosperm while *AtNCED9* in both embryo and endosperm (Lefebvre et al., 2006), it is not surprising that PtNCED1 is obviously closer to AtNCED9 than to AtNCED6 in phylogenetic analysis (**Figure 2**).

Although the two subfamilies NCED and CCD both possess the RPE65 domain and share significant protein sequence similarity with each other, their gene structures are very different. Most *CCD* genes contain multiple introns (5–13), whereas the *NCED* genes in *Arabidopsis* and rice are all intronless. Southern hybridization analysis confirmed that none intron existed in *PtNCED1* (**Figure 3**). To examine whether all sequenced *NCED* genes are intronless, we performed a tBLASTn search of the AtNCED6 protein sequence in the NCBI RefSeq Genome Database. Even by restricting the search targets to species distantly related to *Arabidopsis*, such as moss and algae, only intronless *NCED* genes were found, for example, NC_037277.1 from *Physcomitrella patens* (taxid:3218) and NC_009356.1 from *Ostreococcus lucimarinus* (taxid:242159).

In ABA biosynthesis, NCED is the key enzyme that cleaves an epoxycarotenoid precursor to form xanthoxin within plastids (Nambara and Marion-Poll, 2005). We examined the subcellular localization of PtNCED1 by fusion with a GFP protein tag. In accordance with the predicted transit peptide located on the N-terminal 1–53 amino acid region of PtNCED1 (Supplementary Figure S1), almost all PtNCED1-GFP signals were detected within chloroplasts (**Figure 4**). Moreover, examination of the transiently overexpressed PtNCED1 in agroinfiltrated tobacco leaves revealed a significant change in ABA content, approximately 3- and 12-fold increase for PtNCED1-GFP and non-fused PtNCED1, respectively (**Figure 5**). These analyses demonstrated the functionality of the cloned *PtNCED1* gene.

## Roles of *PtNCED1* and ABA Content in Developing Seeds of *P. tankervilliae*

In seed development, the spatio-temporal regulation of *NCED* genes is particularly important for control of ABA levels, which affect dormancy and germination (Nambara and Marion-Poll, 2005; Lefebvre et al., 2006). In this study, *PtNCED1* level continued to increase rapidly from 75 to 105 DAP and was maintained at this high level until the capsule split (120 DAP). This finding was associated with increased ABA content and decreased water content in developing seeds of *P. tankervilliae* (**Figure 6**). A similar change of ABA accumulation has been observed in other terrestrial orchids: *Calanthe tricarinata* (Lee et al., 2007) and *C. formosanum* (Lee et al., 2015). In response to desiccation as the seeds approaching maturity, dehydration and NCED upregulation usually act synergistically in enhancing ABA content in seeds (Lefebvre et al., 2006). ABA is involved in inducing the storage protein accumulation, the acquisition of desiccation tolerance and the regulation of seed dormancy (Karssen et al., 1983; Rivin and Grudt, 1991; McCarty, 1995; Kagaya et al., 2005). In most plants, ABA content usually peaks during the mid-stage of seed development, then declines as the seed approaches maturation (Goldbach and Michael, 1976; King, 1976; Kawakami et al., 1997). Different from most plants, orchid seeds maintain a high level of ABA at maturity

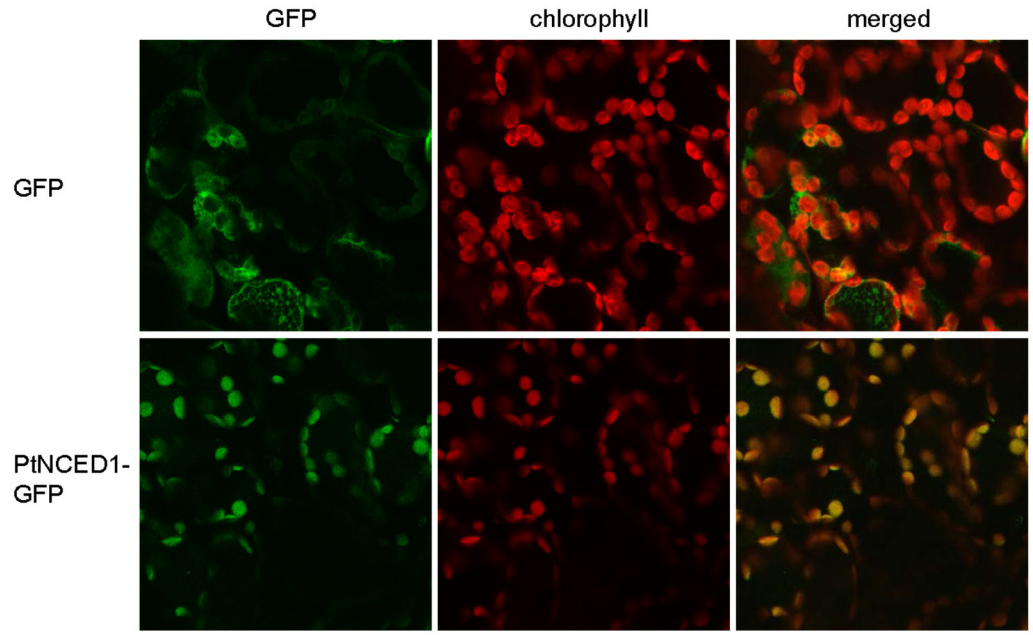


**FIGURE 4 |** Subcellular localization of PtNCED1 in chloroplasts. *Nicotiana benthamiana* leaves were agroinfiltrated to express the GFP protein or the PtNCED1-GFP fusion protein for 3 days. The signal for GFP is shown in green, the autofluorescence of chlorophyll is red, and the co-localized signal is yellow.

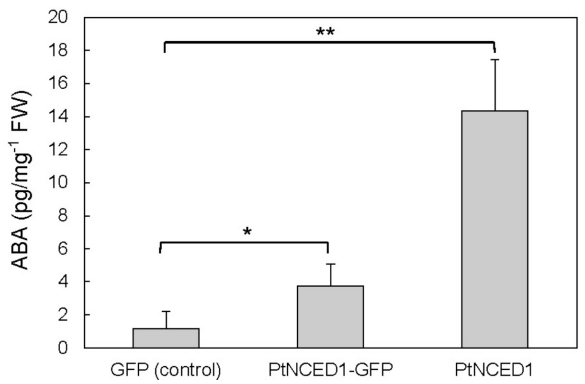


**FIGURE 5 |** Abscisic acid content in the *PtNCED1* transiently expressed tobacco leaves. The materials were the same as in **Figure 4**. *N. benthamiana* leaves were agroinfiltrated to express the GFP, PtNCED1-GFP, or PtNCED1 protein for 3 days. Data are mean ± SD from three biological replicates. Significant difference was set at $P \leq 0.05$ (*) and $P \leq 0.01$ (**) by unpaired Student's *t*-test.

(Van der Kinderen, 1987; Lee et al., 2007, 2015). Because the structure of orchid seed is simple, with a globular-like embryo housed within a thin seed coat and no endosperm, the embryo has little protection against seed desiccation as the seed matures. Maintaining a high ABA content may serve to protect the embryo under unfavorable germination conditions.

In developing seeds of *P. tankervilliae*, the endogenous ABA content keep increasing while approaching maturity. Pretreating mature seeds with 0.5% NaOCl solution for 10 and 20 min improved seed germination significantly to 72.2% and reduced endogenous ABA content (**Figures 7A,B**). Similar results of diminishing ABA contents in mature seeds have been observed in the pretreatment of hypochlorite solutions in *Dactylorhiza maculata* (Van Waes and Debergh, 1986) and *C. tricarinata* (Lee et al., 2007). Since NaOCl is an oxidizing agent, the endogenous ABA in seeds could be demolished through oxidation. In addition, different hypochlorites, e.g., $Ca(OCl)_2$ and NaOCl have been used to scarify the seed coat that make the seed coat more hydrophilic and permeable (Lee, 2011; Barsberg et al., 2013). The increase in seed coat permeability may facilitate ABA leaching from mature seeds, and thus improved the germinability. In *C. formosanum*, the application of fluridone, an ABA synthesis inhibitor of developing seeds, reduced endogenous ABA content in mature seeds and improved the germination of mature seeds (Lee et al., 2015). In this study, the application of a small amount of exogenous ABA at 0.0037 μM was sufficient to inhibit the germination of immature seeds (**Figure 7C**), indicating that seed germination of *P. tankervilliae* is highly sensitive to a small amount of increase in ABA level. Together, these results confirm that ABA plays an important role in inducing and maintaining seed dormancy of orchids.

Upon seed germination, the orchid embryo first develops into a protocorm before forming a plantlet (Yeung, 2017). Under natural conditions, a protocorm without an active root system may be exposed to water stress under conditions of rainfall fluctuations. The *de novo* ABA biosynthesis induced by dehydration is an important avoidance/adaptation mechanism in response to stress (Lefebvre et al., 2006). In *Arabidopsis*, *AtNCED3* level has been shown to increase rapidly in response to dehydration, and transgenic plants overexpressing *AtNCED3*

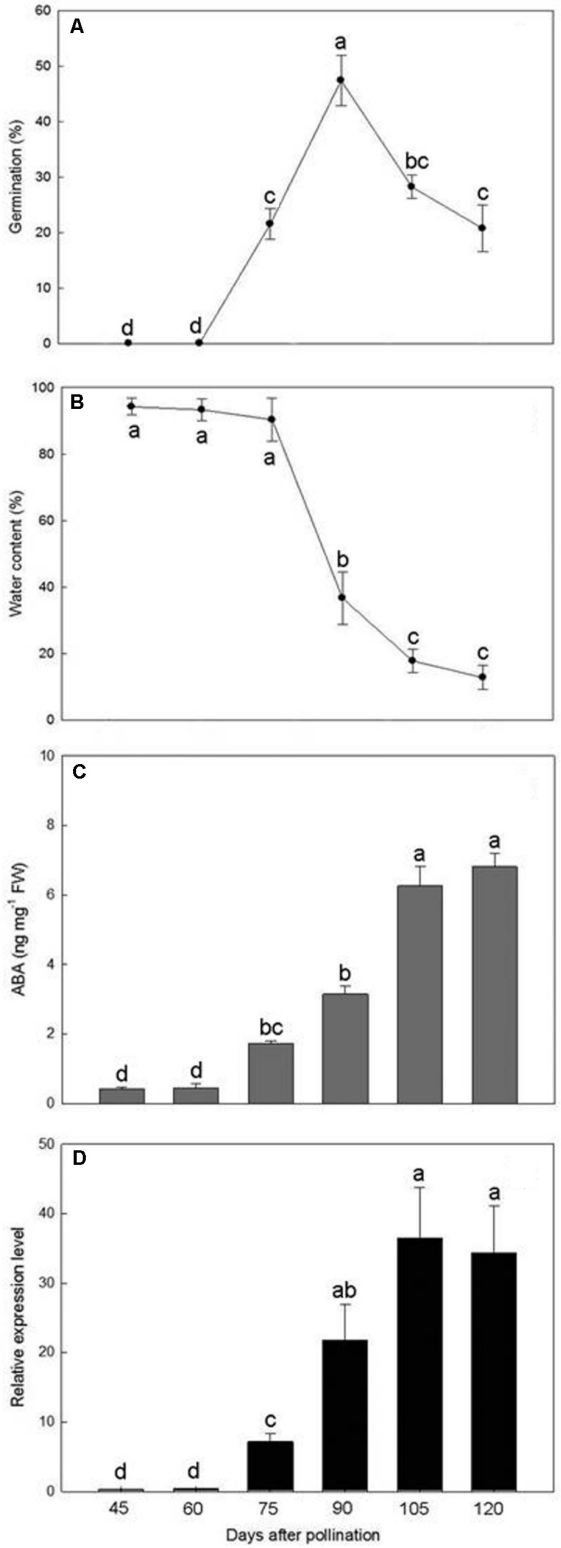


**FIGURE 6 |** Changes in germination percentage **(A)**, water content **(B)**, ABA content **(C)**, and *PtNCED1* transcript level **(D)** in developing seeds. Data are mean ± SD from three biological replicates. Bars labeled with the same letter are not significantly different at $P \leq 0.05$ by Fischer's protected LSD test.

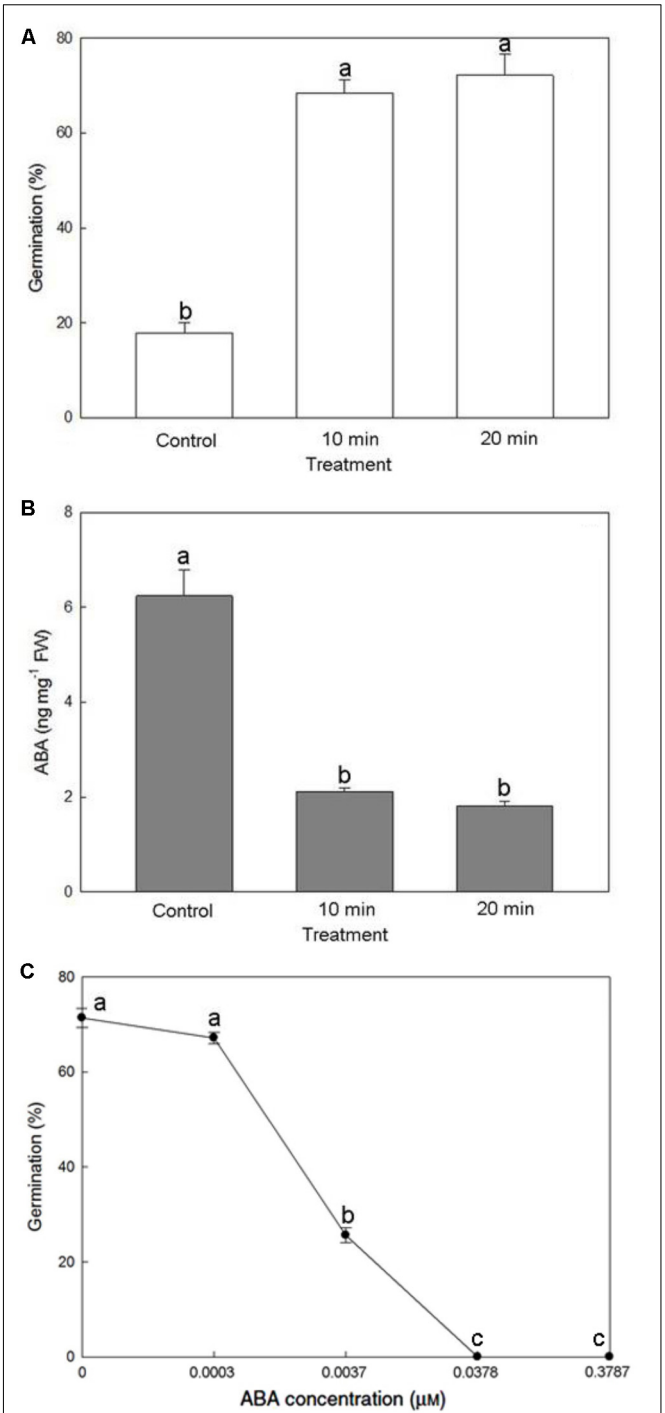


**FIGURE 7 |** Effect of NaOCl pretreatment on seed germination **(A)** and endogenous ABA content within the mature seeds **(B)**, and effect of exogenous ABA application on seed germination after the NaOCl pretreatment **(C)**. Bars labeled with the same letter are not significantly different at $P \leq 0.05$ by Fischer's protected LSD test.

showed enhanced stress tolerance (Iuchi et al., 2001). In leaves of avocado and citrus, specific NCED isoforms, *PaNCED1* and *CsNCED1*, respectively, were required to adjust ABA content

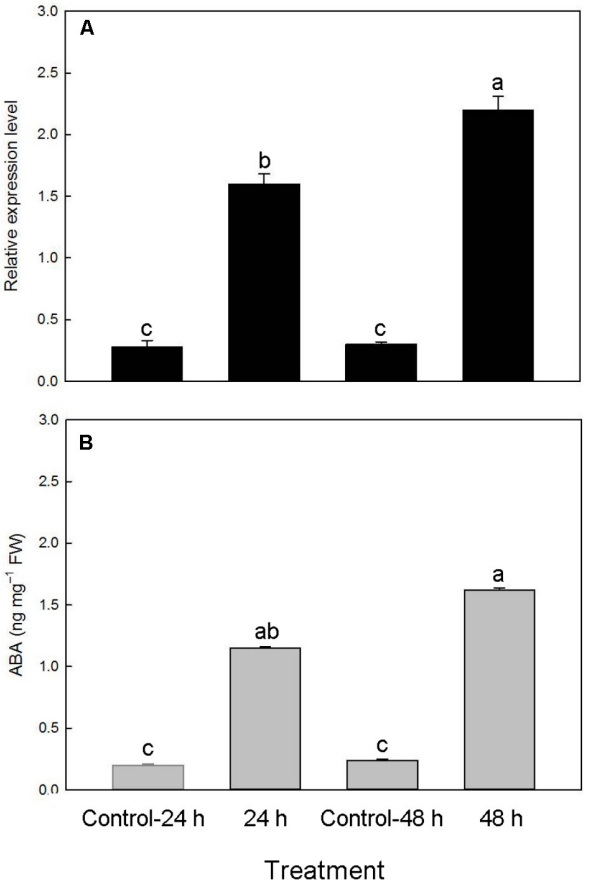


**FIGURE 8 |** Changes in accumulation of *PtNCED1* transcripts **(A)** and ABA content **(B)** in response to dehydration in protocorms. 10% PEG 6000 was used for dehydration treatments for 24 and 48 h. Bars labeled with the same letter are not significantly different at $P \leq 0.05$ by Fischer's protected LSD test.

in response to drought stress (Chernys and Zeevaart, 2000; Rodrigo et al., 2006). In this study, we demonstrated that orchid protocorms can upregulate *PtNCED1* level, which leads to greater accumulation of ABA content in response to dehydration (**Figure 8**).

## *In Silico* Search of Genes Involved in ABA Biosynthesis and Catabolism in *P. tankervilliae*

In our TSA dataset, the *de novo* assembled ∼26M paired-end reads may contain a representative capture of the transcriptomes of developing seeds in *P. tankervilliae*. We were curious to have an overview for the gene members involved in ABA biosynthesis and catabolism. Therefore we used protein sequences of enzymes from *Arabidopsis* (Endo et al., 2014; Yan and Chen, 2017) as queries and performed tBLASTn against our RNA-Seq dataset in NCBI (TSA database, choosing *P. tankervilliae* as organism). For the ABA biosynthetic pathway, contigs encoding enzymes that shared 83, 78, 78, and 66% sequence similarity with ABA 1, 4, 2, and 3 were all found (Supplementary Table S3). However, contig corresponding the AAO3, an enzyme required for the last step conversion of *abscisic aldehyde* to ABA (Endo et al., 2014), was absent in our dataset. Instead, xanthine dehydrogenase (XDH) was revealed to share the highest sequence similarity (∼48%) with AAO3 (and also AAO1, 2, and 4). Although AAO3 and XDH both are molybdenum cofactor (MoCo)-containing enzymes and belong to the big oxidoreductase family, XDH has been characterized as a strict dehydrogenase but not an oxidase (Hesberg et al., 2004), therefore unlikely to substitute the role of AAOs. Interestingly, searching of the Transcriptomics Resource for the Orchid Family database (Orchidstra 2.0[5]) revealed that many orchids do not express AAO-like transcripts (data not shown). In the whole genome-sequenced orchid species, e.g., *P. equestris* (Cai et al., 2015) and *Apostasia shenzhenica* (Zhang et al., 2017), no AAO-like genes were found either. It would be interesting to examine whether minor routes, possibly via xanthoxic acid or abscisic alcohol as describe by Endo et al. (2014), may provide shunt pathways for ABA biosynthesis after the production of xanthoxin in orchids.

As the seed matured, ABA is converted into an inactive compound, 8′-OH-ABA, by CYP707A in most plants. In *Arabidopsis*, CYP707A1 and CYP707A2 play distinct roles for ABA degradation in the seed development and maturation/germination stages, respectively (Okamoto et al., 2006; Matilla et al., 2015; Yan and Chen, 2017). As two contigs encoding CYP707A-like proteins were found in our dataset (Supplementary Table S3), it would be worthy to investigate their gene expression profiles during seed development of orchids in future studies.

From the *in silico* analysis, we found an analogy between *P. tankervilliae* and other plants in the ABA metabolic pathway. Particularly, it is noted that the contig encoding *PtNCED1* possess an extremely high raw reads (16069) compared with other contigs (808–5074). This data indicates an abundancy of the *PtNCED1* transcripts in the developing seeds of *P. tankervilliae*, again implicates its critical roles there.

## CONCLUSION

In a terrestrial orchid, *P. tankervilliae*, we identified and characterized a 9-*cis*-epoxycarotenoid dioxygenase gene, *PtNCED1*. *PtNCED1* gene expression was increased in developing seeds and in water-stressed protocorms in a pattern consistent with the accumulation of ABA content. Pretreatments for improving germination of mature seeds could lower ABA content in seeds. These data suggest that *PtNCED1* is directly involved in ABA content regulation in seed dormancy and water stress responses in orchid protocorms.

## AUTHOR CONTRIBUTIONS

Y-IL, Me-CC, and W-ML conceived the study. Y-IL and W-ML designed the study. LL and Mi-CC performed the

[5]http://orchidstra2.abrc.sinica.edu.tw/orchidstra2/index.php

molecular experiments. Y-IL performed histological study and hormone measurement experiments. Y-IL, W-ML, and Me-CC wrote the paper. All authors read and approved the final manuscript.

## FUNDING

This work was supported by grants from National Museum of Natural Science, Taiwan, ROC to Y-IL; from Academia Sinica, Taiwan, ROC to Me-CC; and from the Ministry of Education, Taiwan, ROC under the ATU plan to W-ML. This work was also financially supported (in part) by the Advanced Plant Biotechnology Center from The Featured Areas Research Center Program within the framework of the Higher Education Sprout Project by the Ministry of Education (MOE) in Taiwan to W-ML.

## ACKNOWLEDGMENTS

We thank Professor Edward C. Yeung of the Department of Biological Sciences, University of Calgary, Canada, for the histological study and commenting on the manuscript.

## SUPPLEMENTARY MATERIAL

The Supplementary Material for this article can be found online at: https://www.frontiersin.org/articles/10.3389/fpls.2018.01043/full#supplementary-material

## REFERENCES

Arditti, J., Clements, M. A., Fast, G., Hadley, G., Nishimura, G., and Ernst, R. (1982). "Orchid seed germination and seedling culture. A manual," in *Orchid Biology: Reviews and Perspectives, II*, ed. J. Arditti (New York, NY: Cornell University Press), 243–370.

Arditti, J., and Ghani, A. K. A. (2000). Numerical and physical properties of orchid seeds and their biological implications. *New Phytol.* 145, 367–421. doi: 10.1046/j.1469-8137.2000.00587.x

Barsberg, S., Rasmussen, H. N., and Kodahl, N. (2013). Composition of *Cypripedium calceolus* (Orchidaceae) seeds analyzed by attenuated total reflectance IR spectroscopy: in search of understanding longevity in the ground. *Am. J. Bot.* 100, 2066–2073. doi: 10.3732/ajb.1200646

Cai, J., Liu, X., Vanneste, K., Proost, S., Tsai, W. C., Liu, K. W., et al. (2015). The genome sequence of the orchid Phalaenopsis equestris. *Nat. Genet.* 47, 65–72. doi: 10.1038/ng.3149

Cheng, S. F., Huang, Y. P., Wu, Z. R., Hu, C. C., Hsu, Y. H., and Tsai, C. H. (2010). Identification of differentially expressed genes induced by Bamboo mosaic virus infection in *Nicotiana benthamiana* by cDNA-amplified fragment length polymorphism. *BMC Plant Biol.* 10:286. doi: 10.1186/1471-2229-10-286

Chernys, J. T., and Zeevaart, J. A. D. (2000). Characterization of the 9-*cis*-epoxycarotenoid dioxygenase gene family and the regulation of abscisic acid biosynthesis in avocado. *Plant Physiol.* 124, 343–354. doi: 10.1104/pp.124.1.343

Chiou, C. Y., Pan, H. A., Chung, Y. N., and Yeh, K. W. (2010). Differential expression of carotenoid-related genes determines diversified carotenoid coloration in floral tissues of Oncidium cultivars. *Planta* 232, 937–948. doi: 10.1007/s00425-010-1222-x

Emanuelsson, O., Nielsen, H., and Heijne, G. V. (1999). ChloroP, a neural network-based method for predicting chloroplast transit peptides and their cleavage sites. *Protein Sci.* 8, 978–984. doi: 10.1110/ps.8.5.978

Endo, A., Okamoto, M., and Koshiba, T. (2014). "ABA biosynthetic and catabolic pathways," in *Abscisic Acid: Metabolism, Transport and Signaling*, ed. D. P. Zhang (Dordrecht: Springer), doi: 10.1007/978-94-017-9424-4_2

Fan, J., Hill, L., Crooks, C., Doerner, P., and Lamb, C. (2009). Abscisic acid has a key role in modulating diverse plant-pathogen interactions. *Plant Physiol.* 150, 1750–1761. doi: 10.1104/pp.109.137943

Frey, A., Effroy, D., Lefebvre, V., Seo, M., Perreau, F., Berger, A., et al. (2012). Epoxycarotenoid cleavage by NCED5 fine-tunes ABA accumulation and affects seed dormancy and drought tolerance with other NCED family members. *Plant J.* 70, 501–512. doi: 10.1111/j.1365-313x.2011.04887.x

Goldbach, H., and Michael, G. (1976). Abscisic acid content of barley grains during ripening as affected by temperature and variety. *Crop Sci.* 16, 797–799. doi: 10.2135/cropsci1976.0011183x001600060015x

Grabherr, M. G., Hass, B. J., Yassour, M., Levin, J. Z., Thompson, D. A., Amit, I., et al. (2011). Full-length transcriptome assembly from RNA-Seq data without a reference genome. *Nat. Biotechnol.* 29, 644–652. doi: 10.1038/nbt.1883

Haseloff, J. (1999). GFP variants for multispectral imaging of living cells. *Methods Cell Biol.* 58, 139–151. doi: 10.1016/S0091-679X(08)61953-6

Hesberg, C., Hänsch, R., Mendel, R. R., and Bittner, F. (2004). Tandem orientation of duplicated xanthine dehydrogenase genes from *Arabidopsis thaliana*: differential gene expression and enzyme activities. *J. Biol. Chem.* 279, 13547–13554. doi: 10.1074/jbc.M312929200

Iuchi, S., Kobayashi, M., Taji, T., Naramoto, M., Seki, M., Kato, T., et al. (2001). Regulation of drought tolerance by gene manipulation of 9-*cis*-epoxycarotenoid dioxygenase, a key enzyme in abscisic acid biosynthesis in *Arabidopsis*. *Plant J.* 27, 325–333. doi: 10.1046/j.1365-313x.2001.01096.x

Kagaya, Y., Okuda, R., Ban, A., Toyoshima, R., Tsutsumida, K., Usui, H., et al. (2005). Indirect ABA-dependent regulation of seed storage protein genes by FUSCA3 transcription factor in *Arabidopsis*. *Plant Cell Physiol.* 46, 300–311. doi: 10.1093/pcp/pci031

Kako, S. (1976). "Study on the germination of seeds of *Cymbidium goeringii*," in *Seed Formation and Sterile Culture of Orchids*, ed. H. Torigata (Tokyo: Tokyo Seibundoshinkosha), 174–237.

Karssen, C. M., Brinkhorst-van, der Swan, D. L. C., Breekland, A. E., and Koornneef, M. (1983). Induction of dormancy during seed development by endogenous abscisic acid: studies on abscisic-acid deficient genotypes of *Arabidopsis thaliana* (L.) Heynh. *Planta* 157, 158–165. doi: 10.1007/bf00393650

Kawakami, N., Miyake, Y., and Noda, K. (1997). ABA insensitivity and low ABA levels during seed development of non-dormant wheat mutants. *J. Exp. Bot.* 48, 1415–1421. doi: 10.1093/jxb/48.7.1415

King, R. W. (1976). Abscisic acid in developing wheat grains and its relationship to grain growth and maturation. *Planta* 132, 43–51. doi: 10.1007/bf00390329

Knudson, L. (1922). Nonsymbiotic germination of orchid seeds. *Bot. Gaz.* 73, 1–25. doi: 10.1086/332956

Lee, T. M., Lur, H. S., and Chu, C. (1993). Role of abscisic acid in chilling tolerance of rice (*Oryza sativa* L.) seedings. I. Endogenous abscisic acid levels. *Plant Cell Environ.* 16, 481–490. doi: 10.1111/j.1365-3040.1993.tb00895.x

Lee, Y. I. (2011). "In vitro culture and germination of terrestrial Asian orchid seeds," in *Plant Embryo Culture; Methods and Protocols, Methods in Molecular Biology*, eds T. A. Thorpe and E. C. Yeung (Berlin: Springer Science), 53–62. doi: 10.1007/978-1-61737-988-8_5

Lee, Y. I., Chung, M. C., Yeung, E. C., and Lee, N. (2015). Dynamic distribution and the role of abscisic acid during seed development of a lady's slipper orchid, *Cypripedium formosanum*. *Ann. Bot.* 116, 403–411. doi: 10.1093/aob/mcv079

Lee, Y. I., Lee, N., Yeung, E. C., and Chung, M. C. (2005). Embryo development of *Cypripedium formosanum* in relation to seed germination *in vitro*. *J. Am. Soc. Hortic. Sci.* 130, 747–753.

Lee, Y. I., Lu, C. F., Chung, M. C., Yeung, E. C., and Lee, N. (2007). Developmental changes in endogenous abscisic acid levels and asymbiotic seed germination of a terrestrial orchid, *Calanthe tricarinata* Lindl. *J. Am. Soc. Hortic. Sci.* 132, 246–252.

Lefebvre, V., North, H., Frey, A., Sotta, B., Seo, M., Okamoto, M., et al. (2006). Functional analysis of *Arabidopsis* NCED6 and NCED9 genes indicates that ABA synthesized in the endosperm is involved in the induction of seed dormancy. *Plant J.* 45, 309–319. doi: 10.1111/j.1365-313x.2005.02622.x

Matilla, A. J., Carrillo-Barral, N., and Rodriguez-Gacio, M. D. C. (2015). An update on the role of NCED and CYP707A ABA metabolism genes in seed dormancy induction and the response to after-ripening and nitrate. *J. Plant Growth Regul.* 34, 274–293. doi: 10.1007/s00344-014-9464-7

McCarty, D. R. (1995). Genetic-control and integration of maturation and germination pathways in seed development. *Annu. Rev. Plant Physiol. Plant Mol. Biol.* 46, 71–93. doi: 10.1146/annurev.arplant.46.1.71

Moir, A. M. (1983). *The Garden Watcher*. Honolulu, HI: University of Hawaii Press.

Murashige, T., and Skoog, F. (1962). A revised medium for rapid growth and bioassays with tobacco tissue cultures. *Physiol. Plant.* 15, 473–497. doi: 10.1111/j.1399-3054.1962.tb08052.x

Nambara, E., and Marion-Poll, A. (2005). Abscisic acid biosynthesis and metabolism. *Annu. Rev. Plant Biol.* 56, 165–185. doi: 10.1146/annurev.arplant.56.032604

Okamoto, M., Kuwahara, A., Seo, M., Kushiro, T., Asami, T., Hirai, N., et al. (2006). CYP707A1 and CYP707A2, which encode abscisic acid 8(-hydroxylases, are indispensable for proper control of seed dormancy and germination in *Arabidopsis*. *Plant Physiol.* 141, 97–107. doi: 10.1104/pp.106.079475

Papadopoulos, J. S., and Agarwala, R. (2007). COBALT: constraint-based alignment tool for multiple protein sequences. *Bioinformatics* 23, 1073–1079. doi: 10.1093/bioinformatics/btm076

Rasmussen, H. N. (1995). *Terrestrial Orchids – From Seed to Mycotrophic Plant*. Cambridge: Cambridge University Press. doi: 10.1017/CBO9780511525452

Rivin, C. J., and Grudt, T. (1991). Abscisic acid and the development regulation of embryo storage proteins in maize. *Plant Physiol.* 95, 358–365. doi: 10.1104/pp.95.2.358

Rodrigo, M. J., Alquezar, B., and Zacarias, L. (2006). Cloning and characterization of two 9-*cis*-epoxycarotenoiddioxygenase genes, differentially regulated during fruit maturation and under stress conditions, from orange (*Citrus sinensis* L. Osbeck). *J. Exp. Bot.* 57, 633–643. doi: 10.1093/jxb/erj048

Tan, B. C., Joseph, L. M., Deng, W. T., Liu, L., Li, Q. B., Cline, K., et al. (2003). Molecular characterization of the *Arabidopsis* 9-*cis* epoxycarotenoid dioxygenase gene family. *Plant J.* 35, 44–56. doi: 10.1046/j.1365-313X.2003.01786.x

Valadares, R. B. S., Perotto, S., Santos, E. C., and Lambais, M. R. (2014). Proteome changes in *Oncidium sphacelatum* (Orchidaceae) at different trophic stages of symbiotic germination. *Mycorrhiza* 24, 349–360. doi: 10.1007/s00572-013-0547-2

Van der Kinderen, G. (1987). Abscisic acid in terrestrial orchid seeds: a possible impact on their germination. *Lindleyana* 2, 4–87.

Van Waes, J. M., and Debergh, P. C. (1986). In vitro germination of some Western European orchids. *Physiol. Plant.* 67, 253–261. doi: 10.1111/j.1399-3054.1986.tb02452.x

Veyret, Y. (1969). La structure des semences des *Orchidaceae* et leur aptitude a la germination *in vitro* en cultures pures. *Travaux du Laboratoire de La Jaysinia, MuseUum Nationale D'Histroire Naturelle*, Paris Fascicle 3, 89–98.

Walker-Simmons, M. (1987). ABA levels and sensitivity in the developing embryos of sprouting and susceptible cultivars. *Plant Physiol.* 84, 61–66. doi: 10.1104/pp.84.1.61

Wang, C. W., Chen, W. C., Lin, L. J., Lee, C. T., Tseng, T. H., and Leu, W. M. (2011). OIP30, a RuvB-like DNA helicase 2, is a potential substrate for the pollen-predominant OsCPK25/26 in rice. *Plant Cell Physiol.* 52, 1641–1656. doi: 10.1093/pcp/pcr094

Yan, A., and Chen, Z. (2017). The pivotal role of abscisic acid signaling during transition from seed maturation to germination. *Plant Cell Rep.* 36, 689–703. doi: 10.1007/s00299-016-2082-z

Ye, X. L., Zee, S. Y., and Yeung, E. C. (1997). Suspensor development in the nun orchid, Phaius tankervilliae. *Int. J. Plant Sci.* 158, 704–712. doi: 10.1086/297482

Yeung, E. C. (1984). "Histological and histochemical staining procedures," in *Cell Culture and Somatic Cell Genetics of Plants: Laboratory Procedures and Their Applications*, Vol. 1, ed. I. K. Vasil (Orlando, FL: Academic Press), 689–697.

Yeung, E. C. (2017). A perspective on orchid seed and protocorm development. *Bot. Stud.* 58:33. doi: 10.1186/s40529-017-0188-4

Yeung, E. C., and Chan, C. K. W. (2015). "The glycol methacrylate embedding resins – Technovit 7100 and 8100," in *Plant Microtechniques and Protocols*, eds E. C. T. Yeung, C. Stasolla, B. Q. Huang, and M. J. Sumner (New York, NY: Springer), 67–82.

Zhang, G. Q., Liu, K. W., Li, Z., Lohaus, R., Hsiao, Y. Y., Niu, S. C., et al. (2017). The Apostasia genome and the evolution of orchids. *Nature* 549, 379–383. doi: 10.1038/nature23897

**Conflict of Interest Statement:** The authors declare that the research was conducted in the absence of any commercial or financial relationships that could be construed as a potential conflict of interest.

The reviewer KM and handling Editor declared their shared affiliation.

frontiers in Plant Science

METHODS
published: 24 July 2018
doi: 10.3389/fpls.2018.01035

# Embryogenic Callus as Target for Efficient Transformation of *Cyclamen persicum* Enabling Gene Function Studies

*Svenja Ratjens, Samuel Mortensen, Antje Kumpf, Melanie Bartsch and Traud Winkelmann**

*Institute of Horticultural Production Systems, Leibniz Universität Hannover, Hanover, Germany*

*Cyclamen persicum* is an ornamental plant with economic relevance in many parts of the world. Moreover, it can be regarded as an applied model for somatic embryogenesis, since transcriptomic, proteomic, and metabolomic comparisons have revealed insights into this regeneration process on the molecular level. To enable gene function analyses, the aim of this study was to establish an efficient *Agrobacterium tumefaciens*-mediated genetic transformation protocol for *C. persicum*. For the first time, embryogenic callus cultures were used as a target material. The advantages of embryogenic callus are the defined and known genotype compared to seedlings, the high regeneration potential and the stability of the regenerated plants. *A. tumefaciens* strains EHA105 and LBA4404 were most efficient for transformation, resulting in transformation efficiencies of up to 43 and 20%, respectively. In regenerated plants, the presence of the transgenes was verified by PCR, Southern hybridization, and a histochemical GUS assay. The protocol was applied successfully to two *C. persicum* genotypes. Moreover, it served to transfer two reporter constructs, the auxin-responsive promoter DR5 driving the *gus* gene and the redox sensor roGFP2_Orp1, to the *C. persicum* genotypes, allowing the localization of high auxin concentrations and reactive oxygen species in order to study their roles in somatic embryogenesis in the future. For success in transformation, we regard the following factors as important: highly embryogenic cell lines, the use of Silwet® L-77 as a surfactant during co-culture, a genotype-specific appropriate selection schedule with hygromycin, and *A. tumefaciens* strains EHA105 and LBA4404.

**Keywords: *Agrobacterium tumefaciens*, auxin, DR5 promoter, embryogenic callus, ornamental plant, redox sensor roGFP2_Orp1, somatic embryogenesis**

OPEN ACCESS

***Edited by:***
*Mariana Mondragón-Palomino, University of Regensburg, Germany*

***Reviewed by:***
*Katsutomo Sasaki, Institute of Vegetable and Floriculture Science, NARO, Japan*
*Trine (Anne Kathrine) Hvoslef-Eide, Norwegian University of Life Sciences, Norway*

****Correspondence:***
*Traud Winkelmann*
*Traud.winkelmann@zier.uni-hannover.de*

***Specialty section:***
*This article was submitted to Plant Biotechnology, a section of the journal Frontiers in Plant Science*

***Received:*** *29 March 2018*
***Accepted:*** *26 June 2018*
***Published:*** *24 July 2018*

***Citation:***
*Ratjens S, Mortensen S, Kumpf A, Bartsch M and Winkelmann T (2018) Embryogenic Callus as Target for Efficient Transformation of Cyclamen persicum Enabling Gene Function Studies. Front. Plant Sci. 9:1035. doi: 10.3389/fpls.2018.01035*

## INTRODUCTION

Cyclamen (*Cyclamen persicum* Mill.) is an ornamental crop of high economic relevance in temperate regions, mainly of Europe and Japan (Schwenkel, 2001). Commercially, it is propagated via seeds, but interest exists in vegetative propagation due to the costs of manual emasculation and pollination, and despite $F_1$ hybrid breeding programs, the remaining inhomogeneity in some cultivars. Clonal propagation for multiplication of the parental genotypes of $F_1$ hybrid cultivars and for mass propagation of selected superior plants can only be achieved by employing *in vitro* culture techniques. Among these, somatic embryogenesis in particular was proposed to be an efficient method of vegetative propagation and has been introduced for cyclamen by several groups (e.g., Wicart et al., 1984; Otani and Shimada, 1991; Kiviharju et al., 1992; Kreuger et al., 1995;

Takamura et al., 1995; Schwenkel and Winkelmann, 1998; Winkelmann, 2010, reviewed by Jalali et al., 2012). Although this technique is in principle applicable to a wide range of genotypes (Winkelmann and Serek, 2005; Winkelmann, 2010), different genotype-dependent efficiencies and problems such as asynchronous development (Rode et al., 2011), precocious germination, lack of desiccation tolerance, or the absence of a growth arrest connected to maturation (Schmidt et al., 2006) have been assigned to somatic embryogenesis in cyclamen. Thus, a better understanding of the molecular and physiological control of the regeneration pathway is needed. Insights have been gained from comparisons of somatic and zygotic embryos on the transcriptomic (Hoenemann et al., 2010), proteomic (Winkelmann et al., 2006a; Bian et al., 2010; Rode et al., 2011; Mwangi et al., 2013), and metabolomic (Winkelmann et al., 2015) levels. These analyses have shown that somatic embryos are less well protected from stress than zygotic embryos are and that they lack seed storage proteins.

The key prerequisite for testing the candidate genes identified in the abovementioned comparative approaches for their functional roles in somatic embryogenesis is an efficient transformation protocol allowing overexpression, knock-down via RNA interference and knock-out using CRISPR-Cas approaches. Genetic transformation of cyclamen via *Agrobacterium tumefaciens* was first reported by Aida et al. (1999). Since then, only a very few reports of *A. tumefaciens*-mediated transformation have been published (**Table 1**), most of them based on adventitious shoot formation from etiolated seedlings. Seedlings, however, have the disadvantage of unknown genetic constitution in this allogamous species. When comparing the regeneration pathways organogenesis (adventitious shoot formation) and somatic embryogenesis in *C. persicum*, somatic embryogenesis stands out due to the high number of regenerated plants and their true-to-typeness in many genotypes (Schwenkel and Winkelmann, 1998). Moreover, single or only few cells give rise to the formation of somatic embryos, thus reducing the risk of chimeras. Additionally, due to the easy scalability and the less hands-on time, embryogenic cultures are a highly suitable target material for *A. tumefaciens*-mediated transformation allowing genetic studies in a clonal offspring.

In the pioneering works of Aida et al. (1999) and Boase et al. (2002), relatively high transformation efficiencies of 19 and 15.3% were obtained, defined as the number of GUS (β-glucuronidase)-positive, blue-stained shoots at six and two and a half months after transformation, respectively. Somatic embryos were the targets of transformation in only one study, and plants were regenerated via secondary somatic embryogenesis; however, this method had a low transformation efficiency of only 0.7% (Terakawa et al., 2008). When comparing hygromycin (5 $mgL^{-1}$) and kanamycin (100 $mgL^{-1}$) for selection of transgenic shoots in cyclamen, Aida et al. (1999) observed clearly higher transformation efficiencies with hygromycin. Consequently, all selection approaches (**Table 1**) in recent studies have used hygromycin as the selective agent, whereas in the early report of Boase et al. (2002), kanamycin was the selective agent. Genes of interest that have been successfully transferred to *C. persicum* include genes that modify flower color (Boase et al., 2010); flower shape (ruffled petals: Tanaka et al., 2011); fatty acid composition, providing heat tolerance (Kai et al., 2012); and floral organs (double flowers: Tanaka et al., 2013, see also **Table 1**).

The objective of this study was to establish an efficient *A. tumefaciens*-mediated transformation protocol for *C. persicum* using embryogenic callus as a target material. This transformation system will provide a base for gene function analyses. Moreover, the first genes of interest were transferred to cyclamen: a *DR5*::*gus* (Ulmasov et al., 1997a,b) construct to visualize auxin sensitivity and the *roGFP2_Orp1* redox sensor (Gutscher et al., 2009; Schwarzländer et al., 2016) to localize hydrogen peroxide. From subsequent analyses of their expression patterns, we expect insights into the roles of auxin response and reactive oxygen species (ROS) distribution during somatic embryogenesis.

# MATERIALS AND METHODS

## Plant Material

Two *C. persicum* genotypes representing different genetic backgrounds were included in the study: Genotype 56/2 refers to one plant of the large-flowered commercial $F_1$ hybrid cultivar 'Maxora Light Purple' (breeder: Varinova BV, Berkel en Rodenrijs, Netherlands), whereas genotype 3145 represents one plant of the mini-type commercial $F_1$ hybrid cultivar 'Zanetto Light Pink' (breeder: Syngenta Flowers, Enkhuizen, Netherlands).

### Induction of Embryogenic Callus Cultures

The protocols for somatic embryogenesis in *C. persicum* have been described in detail previously (Schwenkel and Winkelmann, 1998; Winkelmann et al., 1998; Winkelmann, 2010). Embryogenic callus was induced from unpollinated ovules on propagation medium [half-strength MS (Murashige and Skoog, 1962) medium containing 9.05 μM 2,4-dichlorophenoxyacetic acid and 3.94 μM 2iP (6-(γ,γ-dimethylallylamino)purine) and 4 $gL^{-1}$ Gelrite (Duchefa, Haarlem, Netherlands), pH 5.5-5.6] and propagated for 2–3 years by monthly subculture. At each subculture, callus samples were plated on differentiation medium (see section "Regeneration of Plants via Somatic Embryogenesis") to check the embryogenesis of the line. The lines developing the highest number of embryos were selected for propagation. All cultures were kept at a temperature of 24°C in darkness.

### Regeneration of Plants via Somatic Embryogenesis

Somatic embryos differentiated within 4 weeks after plating of 200–300 mg embryogenic callus on plant growth regulator-free differentiation medium [half-strength MS medium solidified with 4 $gL^{-1}$ Gelrite (Duchefa), pH 5.5–5.6]. The developing embryos were picked and transferred to fresh differentiation medium of the same composition for germination. After another 4 weeks or when the cotyledons had reached a length of 1–2 cm, the plantlets were transferred to light (16 h photoperiod provided by fluorescent tubes at 30–50 $\mu molm^{-2}s^{-1}$) and subcultured

**TABLE 1 |** Overview of published reports on genetic transformation of *Cyclamen persicum*.

| Regeneration pathway | Target material (explants) | Pre-culture | *Agrobacterium tumefaciens* strain | Transferred genes | Selection | Transformation efficiency | Reference |
|---|---|---|---|---|---|---|---|
| Adventitious shoot formation | Etiolated petioles | 6 days | AGL-0, LBA4404 | *gusA*int, *hpt* & *npt*II | 5 $mgL^{-1}$ hyg or 100 $mgL^{-1}$ kan | 9–19% (AGL-0); 0–2.5% (LBA4404) | Aida et al., 1999 |
| Adventitious shoot formation | Etiolated hypocotyl segments | 1–8 days | LBA4404, EHA105 | *npt*II, *gusA*int | 50 $mgL^{-1}$ kan | 15.3% (LBA4404); 2.3% (EHA105) | Boase et al., 2002 |
| Secondary somatic embryogenesis | Somatic embryos | 3 months | LBA4404 | *gusA*int, *hpt* | 5 $mgL^{-1}$ hyg | 0.7% $hyg^R$ calluses | Terakawa et al., 2008 |
| Adventitious shoot formation | Etiolated hypocotyl segments | 1–8 days | EHA105 | *CpF3′5′H hpt* | 5 $mgL^{-1}$ hyg (12 days); 20 $mgL^{-1}$ hyg (65 days); 15 $mgL^{-1}$ hyg (thereafter) | Not indicated | Boase et al., 2010 |
| Adventitious shoot formation | Etiolated petioles regenerated from leaf explants | – | LBA4404 | *CpTCP-SRDX, hpt* | 5 $mgL^{-1}$ hyg | 53% | Tanaka et al., 2011 |
| Adventitious shoot formation | Etiolated petioles of seedlings | 6 days | EHA105 | *CpFAD7*, *hpt* | 10 $mgL^{-1}$ hyg | Not indicated | Kai et al., 2012 |
| Adventitious shoot formation | Etiolated petioles regenerated from leaf explants | – | GV3101, LBA4404 | *CpAG1-SRDX, CpAG2-SRDX, hpt* | 5 $mgL^{-1}$ hyg | Not indicated | Tanaka et al., 2013 |
| Somatic embryogenesis | Embryogenic callus | 10 days | LBA4404, EHA105, GV2260, GV3101, AGL-1 | *hpt, gusAint, DR5::gus, roGFP2_Orp1,* | 5–10 $mgL^{-1}$ hyg (14 days), 10–20 $mgL^{-1}$ (thereafter) sensitivity depends on genotype | 43% (EHA105), 20% (LBA4404) | Ratjens et al., this study |

*gusAint, reporter gene gusA containing an intron; hpt, hygromycin (hyg) phosphotransferase gene; nptII, neomycin phosphotransferase gene conferring kanamycin (kan) resistance; CpF3′5′H, flavonoid 3′5′-hydroxylase of Cyclamen persicum; CpFAD7, omega-3 fatty acid desaturase of Cyclamen persicum; CpTCP-SRDX, Cyclamen persicum TCP transcription factor – repressor; CpAG-SRDX, Cyclamen persicum AGAMOUS – repressor; $hyg^R$, hygromycin-resistant cells growing on hygromycin-containing medium; DR5, synthetic auxin response element; roGFP2_Orp1, redox-sensitive green fluorescent protein biosensor version 2 integrated with a yeast peroxidase gene.*

every 4 to 8 weeks until plants with well-developed tubers and 2–3 leaves could be transferred to greenhouse conditions.

## *Agrobacterium tumefacien* Strains and Vectors

In the first series of experiments, four *A. tumefaciens* strains were compared, all based on the chromosomal background of C58: the octopine type GV2260 (McBride and Summerfelt, 1990), the nopaline type GV3101 (Holsters et al., 1980) and the succinamopine types EHA105 (Hood et al., 1993), and AGL-1 (Lazo et al., 1991). The transformation protocol was established by comparing the four strains all harboring the vector pCAMBIA1301[1] (gene bank accession number: AF234297.1) carrying T-DNA consisting of the *hygromycin phosphotransferase* (*hpt*) gene under the control of the *CaMV35S* promoter and the β-*glucuronidase* (*gusA*, originally *uidA* of *Escherichia coli,* hereafter termed *gus*) gene with an intron of the *catalase* gene from *Ricinus communis* under control of the 35S promoter.

The vector pCAMBIA1380_DR5::GUS was obtained by cloning the *DR5::gus* sequence from the pGEM®-T-DR5::GUS plasmid (kindly provided by Günther Scherer, Ulmasov et al., 1997b) via restriction with *Eco*RI und *Sal*I into the plasmid pCAMBIA1380[1] (gene bank accession number: AF234301.1). This vector was transformed into the *A. tumefaciens* strains EHA105, GV2260, and the TiAch5 strain LBA4404 (Hellens et al., 2000).

The plasmid with the integrated gene construct *roGFP2_Orp1* within the vector pH2GW7_c-roGFP2_LR_Orp1 (vector sequence: gene bank accession number FN398078.1, roGFP2: Hanson et al., 2004, yeast Orp1: gene ID: 854855, cloning strategy described in Scuffi et al., 2018) was kindly provided by Markus Schwarzländer (University of Bonn, now University of Münster). The plasmid used was 11187 bp in size and contained, in addition to the $H_2O_2$ sensing gene, the streptomycin-spectinomycin resistance gene *Sm/SpR* on the vector backbone and the *hpt* gene within the T-DNA; the *roGFP2_Orp1* and *hpt* genes were both under the control of the *CaMV35S* promoter (Schwarzländer et al., 2016). The vector was electroporated into the *A. tumefaciens* strains EHA105, GV2260, and LBA 4404.

## Hygromycin Sensitivity Test

Embryogenic cells were used as the target material for *A. tumefaciens*-mediated transformation. To identify concentrations suitable for the selection of transgenic cells, the sensitivity of the embryogenic callus to hygromycin and kanamycin was tested. Because even concentrations of 200 $mgL^{-1}$ kanamycin could not consistently inhibit callus growth, we decided to use hygromycin as the selective agent in the transformation experiments. To identify suitable concentrations for the selection of transgenic cells, callus lines

[1]www.cambia.org

of the two *C. persicum* genotypes 56/2 and 3145 were grown on propagation medium containing 0, 5, 10, 15, or 20 $mgL^{-1}$ hygromycin. Five replicates (6 cm Petri dishes) with 100 ± 10 mg embryogenic callus were prepared individually, and the whole experiment was repeated once. After 4 weeks, the callus fresh mass was recorded and expressed as a percentage of the initial mass plated.

## Transformation Protocol

### Preparation of the *Agrobacterium tumefaciens* Culture

Bacterial glycerine stock cultures were regularly tested for the presence of the transformation vector by colony PCR, and only positive colonies were selected for inoculation in 10 mL YEB medium (5 $gL^{-1}$ peptone, 5 $gL^{-1}$ yeast extract, 5 $gL^{-1}$ beef extract, 5 $gL^{-1}$ sucrose, 0.493 $gL^{-1}$ $MgSO_4$, pH: 7.2) and the respective antibiotics (50 $mgL^{-1}$ kanamycin; 50 $mgL^{-1}$ rifampicin; for strain GV2260, 25 $mgL^{-1}$ carbenicillin; for LBA4404, 10 $mgL^{-1}$ streptomycin). After overnight culture at 28°C and 160 rpm, the suspensions were diluted 1:10 with an amendment of 50 $mgL^{-1}$ acetosyringone after reaching an $OD_{600}$ of 1.0. After the dilution reached an $OD_{600}$ of 0.4–0.6, the bacteria were pelleted (3000 rpm, 10 min) and resuspended in liquid differentiation medium (see section "Regeneration of Plants via Somatic Embryogenesis") at an $OD_{600}$ of 0.5. This solution was supplemented with 50 $mgL^{-1}$ acetosyringone and 0.03% Silwet® L-77 and used for transformation.

### Transformation of Embryogenic Cells

Three portions of 100 ± 10 mg embryogenic cells were plated in a thin layer in five to ten 6 cm Petri dishes containing 10 mL propagation medium (see section "Regeneration of Plants via Somatic Embryogenesis"), resulting in 15 to 30 replicates. These cells were subjected to a preculture of 10 days at 24°C in darkness. Thereafter, 300 µL of the transformation solution (see section "Preparation of the *Agrobacterium tumefaciens* Culture") was pipetted on top of the cells of each replicate. After 2 days co-culture under the same culture conditions, the cells were washed by overlaying each replicate with 200 µl liquid propagation medium with 500 $mgL^{-1}$ cefotaxime and pipetting this solution up and down several times. The cells of each replicate were then transferred to fresh propagation medium containing 500 $mgL^{-1}$ cefotaxime in individual Petri dishes and cultured at 24°C in darkness for 10 days.

### Selection of Transgenic Cells and Plant Regeneration

Ten days after co-culture, the cells were transferred to proliferation medium containing 500 $mgL^{-1}$ cefotaxime and 5 $mgL^{-1}$ hygromycin for selection. After 2 weeks, the cells were subcultured, and the selection pressure was increased to 10 $mgL^{-1}$ hygromycin. Thereafter, every 4 weeks, the cultures were evaluated for growth and color and subcultured by plating them in thin layers. After three subcultures, cefotaxime was no longer added to the medium, because no outgrowth of bacteria was observed.

Starting from the second subculture after co-culture, cell proliferation of the putative transgenic cells was obvious. Thus, at the third subculture, parts of these actively growing cells were transferred to differentiation medium with 500 $mgL^{-1}$ cefotaxime and 10 $mgL^{-1}$ hygromycin, on which globular somatic embryos became visible after 3 weeks. After 4 to 5 weeks, torpedo stage embryos were singulated and further cultured on fresh medium of the same composition. Within 4 weeks, still in darkness at 24°C, most of the somatic embryos germinated and were then transferred to light (see section "Regeneration of Plants via Somatic Embryogenesis") and to differentiation medium containing 5 $mgL^{-1}$ hygromycin and 2.9 µM indole acetic acid (IAA) to promote root growth.

## Molecular Analyses of Transformed Regenerants

### Extraction of Genomic DNA

DNA was extracted from callus, somatic embryos or leaf material using the NucleoSpin® Plant II kit following the manufacturer's instructions (Macherey-Nagel, Düren, Germany). The purified DNA was eluted in a volume of 100 µL elution buffer, and its concentration and purity were determined spectrophotometrically (Nanodrop, Peqlab, Erlangen, Germany).

### Amplification of Transgenes via PCR

A multiplex PCR was used to amplify fragments of the *hpt* and *gus* genes. One 25 µL reaction contained 10 ng genomic DNA, 1 µL of each primer (Supplementary Table 1) at a concentration of 10 $pmol\mu L^{-1}$, 0.75 µL dNTPs (10 mM), buffer (Williams et al., 1990), and 1U Taq polymerase (DNA Cloning Service, Hamburg, Germany). The protocol used for the multiplex PCR was as follows: initial denaturation at 94°C for 3 min; 15 cycles of 94°C for 45 s, 65°C for 45 s, 72°C for 70 s; 25 cycles of 94°C for 45 s, 58°C for 45 s, 72°C for 70 s; final elongation at 72°C for 7 min. To test for residual agrobacteria, PCR amplification of chromosomal DNA [*PicA* (Plant inducible chromosomal A) gene] was performed as described in Winkelmann et al. (2006b). PCR products were separated in a 1% agarose gel with 1 $\mu gL^{-1}$ ethidium bromide for visualization of the bands at 300 nm.

For the transgenes *DR5::gus* and *roGFP2_Orp1*, separate PCRs were performed with the following thermocycler program: initial denaturation at 94°C, 3 min; 40/35 (for *DR5::gus* and *roGFP2_Orp1*, respectively) cycles of 94°C for 45 s, $T_A$ (Supplementary Table 1) for 45 s, 72°C for 70 s for *DR5::gus* and for 45 s for *roGFP2_Orp1*; and finally 72°C for 7 min.

### Southern Hybridization

Approximately 3 µg of genomic DNA from different transgenic plants and untransformed control plants was digested with 30 U *Hin*dIII overnight at 37°C before adding a further 10 U *Hin*dIII and incubating for 24 h. Following the report of Sriskandarajah et al. (2007), the DNA fragments were separated in 1% agarose gels and blotted onto a nylon membrane. The *hpt* probe, with a size of 578 bp, was digoxigenin-labeled using the DIG DNA Labeling Mix (Roche Applied Science Co., Mannheim, Germany) according to the manufacturer's instructions. Plasmid DNA served as a positive control. All steps, including hybridization, washing and detection, were carried out as described in Sriskandarajah et al. (2007).

## GUS Assay

The histochemical GUS assay was carried out according to Jefferson (1987) for callus as well as somatic embryos and the leaf tissue of the regenerated plantlets. From 200 to 600 μL of the GUS staining buffer was placed into 2 mL reaction tubes containing the plant material. Infiltration of the tissue was promoted by evacuation at 200 mbar for 30–60 min. After incubation at 37°C for 16 h, the samples were bleached and fixed by immersion in increasing concentrations of ethanol (30–98%) before being evaluated under a stereomicroscope. Six weeks after co-culture, samples of all embryogenic callus replicates of the first series of transformation experiments were tested for GUS expression. *DR5*::*gus* transgenic somatic embryos were submitted to the GUS assay weekly after the transfer of embryogenic cells to differentiation medium.

## Statistical Analysis

The relative increase in callus fresh mass during the 4 weeks of culture in each hygromycin treatment was compared to that of the corresponding control. The data was log-transformed and statistically analyzed using the software R, version 3.4.2, by Dunnett's test at $p < 0.05$.

# RESULTS

## Selection Based on Hygromycin Sensitivity

On the hygromycin-free control medium, embryogenic callus of the genotypes 56/2 and 3145 grew quickly, resulting in tenfold and eightfold fresh mass after 4 weeks of culture, respectively (**Figure 1**). For genotype 56/2, the lowest tested concentration of 5 $mgL^{-1}$ hygromycin completely inhibited callus growth. The cells of genotype 3145 were much less sensitive and showed an increase in fresh mass of 600% on medium with 5 $mgL^{-1}$ hygromycin (**Figure 1**); even at 10 $mgL^{-1}$ hygromycin, cell proliferation occurred, although at a much lower level (82%) and with pronounced browning (**Figure 1**). Thus, for genotype 3145, selection should use 15–20 $mgL^{-1}$ hygromycin, whereas for genotype 56/2, selection starting with 5 $mgL^{-1}$ hygromycin (and after 2 weeks increasing to 10 $mgL^{-1}$) is recommended.

## Comparison of Different *Agrobacterium tumefaciens* Strains

The aim of the first series of transformation experiments was to identify *A. tumefaciens* strains that are most efficient in transforming the embryogenic cells of *C. persicum*. In the first 2 weeks of selection, using a hygromycin concentration of 5 $mgL^{-1}$, only a small percentage of calluses of genotype 56/2 stopped growing, and depending on the *A. tumefaciens* strain, between 67 and 89% of the calluses were transferred to fresh propagation medium with 10 $mgL^{-1}$ hygromycin (**Figure 2**). After 4 weeks of culture at the higher hygromycin selection level, a clear reduction in viable calluses was recorded, although in strain EHA105, more than 50% of the calluses were still actively growing. At this time point, the first GUS assay revealed similar results for the different *A. tumefaciens* strains, although at a lower overall level (**Figure 2**, inlay). Interestingly, the GUS assay reflected the percentages of transformed calluses after 18 weeks very well. At the end of each subculture period, areas of actively growing cells among the dead brown cells were observed, and these living cells were then subcultured (**Figure 3**, photo selection). Further culture passages reduced the number of hygromycin-resistant and thus putatively transgenic calluses, until 18 weeks after start of selection, when a stable percentage was reached. The *A. tumefaciens* strain EHA105 resulted in the highest transformation rate of 42.6% followed by strain GV2260 with 6.7%, while no transformed calluses could be obtained with strains AGL-1 or GV3101 (**Figure 2**). The transformation rate for EHA105 was based on the highest replicate number, but from the standard deviation, the high variability between experiments becomes obvious. Although we tried to keep all handling of callus lines consistent, there is always variation among the Petri dishes from which callus was taken as starting material. This variation concerned callus color, consistency, embryogenesis, and growth rates. Lines with a high embryogenic potential were found to give rise to high transformation rates.

Ten weeks after the start of selection (= approximately 12 weeks after transformation), portions of actively growing embryogenic callus were plated on differentiation medium containing 10 $mgL^{-1}$ hygromycin. Somatic embryos developed in high numbers within 4 weeks (**Figure 3**, photo differentiation), which were singulated and cultured for another 4 weeks on the same medium in Petri dishes before being transferred to larger vessels (250 mL) in light. Only 4% of the separated somatic embryos could be converted into plantlets on the differentiation medium with 10 $mgL^{-1}$ hygromycin. However, from 1 g of embryogenic callus, 200 somatic embryos could be generated, on average. Root growth was inhibited on the hygromycin-containing medium compared to that of non-transformed control plants, but this effect was overcome by the addition of 2.9 μM IAA to the medium and reducing the hygromycin concentration to 5 $mgL^{-1}$.

## Verification of Transgenic Plants

Integration of the transgenes was tested by a multiplex PCR allowing the simultaneous testing of the presence of both the *hpt* and *gus* genes (**Figure 4A**). In most plants that were regenerated from the transformation experiments, both genes were detected; only a few plants did not show a signal for the *gus* gene but had a clear band for the *hpt* gene (plants number 3 and 11 in **Figure 4A**). All DNA samples were also subjected to PCR to detect *A. tumefaciens* DNA and thus residual agrobacteria, but all were found to be negative in the *PicA* PCR (Supplementary Figure 1).

The expression of the *gus* gene was proven in histochemical GUS assays. In callus cells sampled 6 weeks after the start of selection, GUS staining was already observed (**Figure 2**), and likewise, tests of somatic embryos and leaves revealed the deep blue coloration of the tissues, although to different extents (**Figures 5D–F**). The non-transgenic controls mostly did not show any blue color; however, in a few cells, a faint blue staining

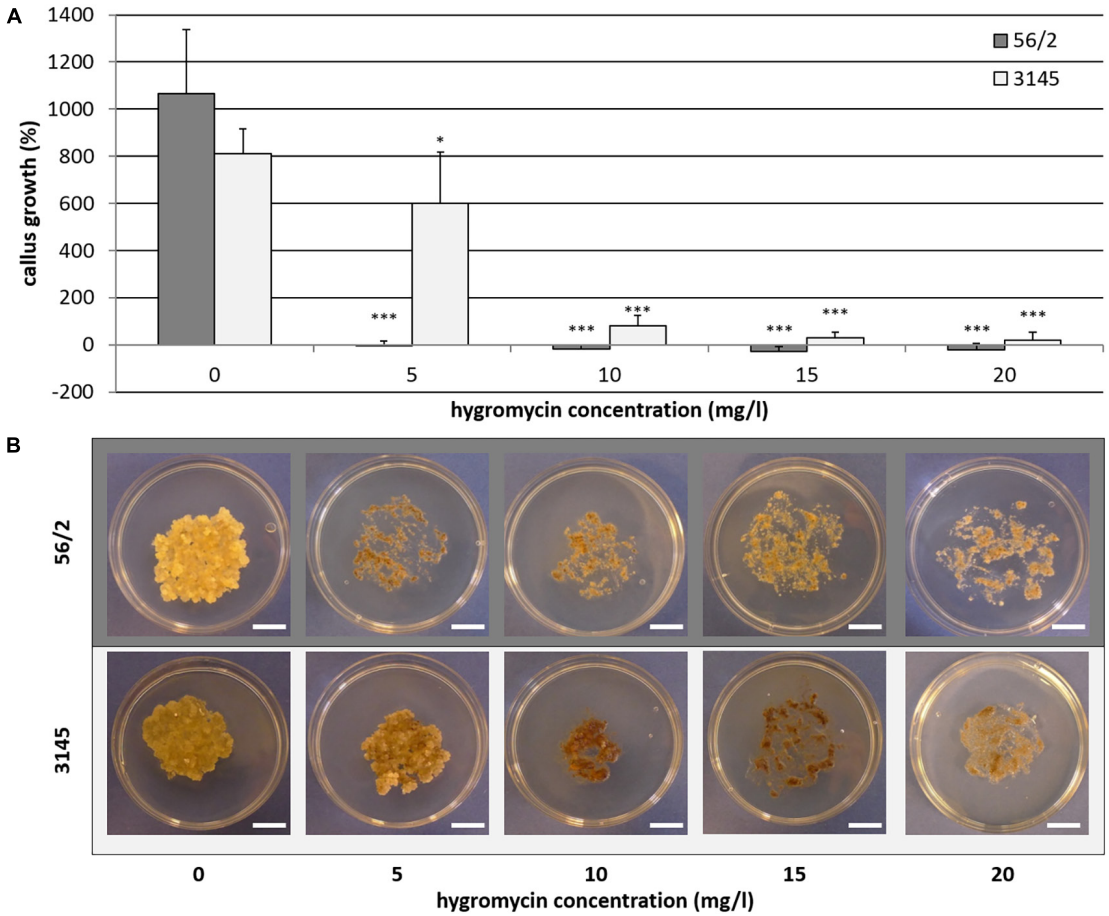


**FIGURE 1 |** Genotype-dependent hygromycin sensitivity of *Cyclamen persicum*. **(A)** Callus growth as relative increase of fresh mass after 4 weeks on propagation medium, error bar = SD, asterisks indicate significant differences between the treatments and the corresponding control by Dunnett's test (*$p \leq 0.05$ and ***$p \leq 0.001$), $n = 5$. **(B)** Callus cultures after 4 weeks on propagation medium under selective conditions, bars = 1 cm.

was observed (**Figures 5A–C**), which could be distinguished from the intense staining in the GUS-positive cells.

From the transformation experiments mentioned in the section "Comparison of Different *Agrobacterium tumefaciens* Strains," 217 hygromycin-resistant plants were obtained overall, 38 of which were subjected to GUS assays and multiplex PCR (Supplementary Table 2). None of these 38 tested plants was found to test negative for all three parameters. Most of the plants (29, 76.3%) consistently tested positive for all traits. Four plants were found to contain *hpt* but lack the *gus* gene, and five plants gave contradictory results when the GUS assay was compared to the PCR amplification of the *gus* gene (Supplementary Table 2). Among these five plants, two were GUS positive but did not show positive signals in the *gus* PCR. Overall, these data indicated that the GUS assay gave valid results and that hygromycin selection was efficient.

A small subsample of four plants was submitted to a Southern hybridization analysis, which proved the integration of single copies of the *hpt* gene (**Figure 4B**, lanes 5–8). The four plants were obtained from calluses grown in different Petri dishes and from two different transformation experiments. Consequently, the different sizes of the hybridization signals indicate them to be independent transgenic events.

## *DR5*::*gus* Transgenic *C. persicum*

A first application of the transformation protocol was the transfer of the *gus* gene under the auxin-responsive promoter DR5. This set of transformation experiments included, in addition to the previously tested *A. tumefaciens* strains EHA105 and GV2260, the strain LBA4404 and consisted of three experimental replications with 10 Petri dishes each. At the end of the fourth culture passage after the start of selection, 50% of the calluses were actively growing on propagation medium with 10 $mgL^{-1}$ hygromycin when transformed with EHA105 and LBA4404, whereas this percentage was much lower (26%) for strain GV2260. However, due to a longer first selection phase on 5 $mgL^{-1}$ hygromycin (4 weeks instead of 2 weeks), the percentages of GUS-positive calluses better reflected the transformation efficiencies at this time point, which were 20% for LBA4404 and 7% for EHA105. Seventeen callus lines were randomly selected for molecular verification via PCR; nine of them were positive for the hpt gene, but only five were positive for the *gus* gene. Via Southern

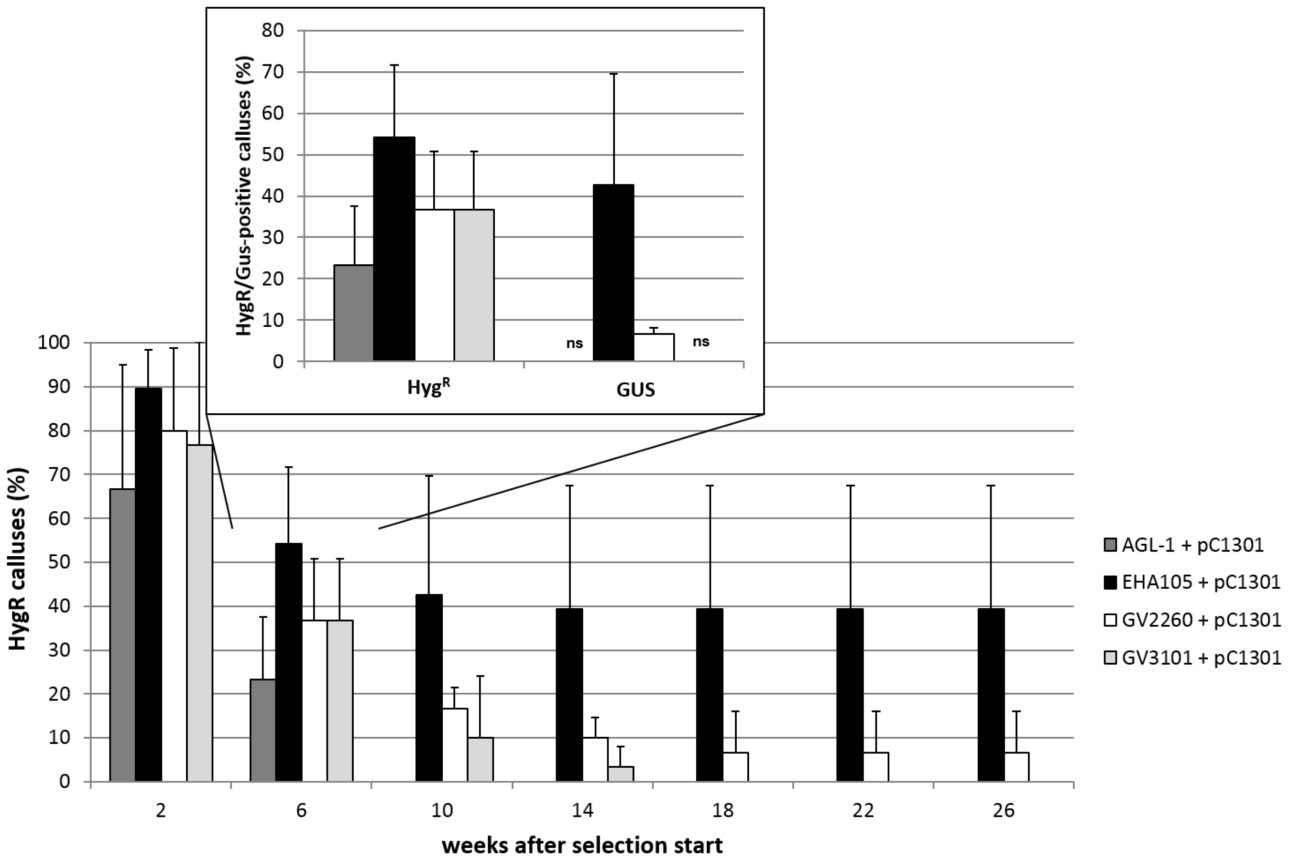


**FIGURE 2 |** Transformation success for the different *A. tumefaciens* strains in terms of percentage of hygromycin-resistant ($Hyg^R$) calluses over time for genotype 56/2. Inset shows percentages of $Hyg^R$ calluses and GUS-positive (GUS) calluses 6 weeks after the start of selection. ns, no signal in GUS assay, pC1301, pCAMBIA1301. Replicate numbers: $n = 30$ for AGL-1, GV2260, and GV3101, $n = 72$ for EHA105. Whiskers indicate standard deviations between experiments.

hybridization, three plants (two obtained from transformation with LBA4404 and one with EHA105) were shown to carry single copies of the *hpt* gene due to independent transgenic events (**Figure 4B**, lanes 2–4).

*DR5*::*gus* transgenic cells, somatic embryos and germinated embryos were analyzed in a histochemical GUS assay (**Figures 5G–L**). While the embryogenic cells were mostly stained intensely blue (**Figure 5G**), comparable to *35S*::*gus* transgenic lines (**Figure 5D**), in somatic embryos, GUS expression was mainly observed in the lower parts of the tubers and the root and the shoot poles (**Figures 5H,I**). This differential localization of the stain could be first observed 2 weeks after transfer to the differentiation medium. Germinated somatic embryos showed blue coloration in the tubers, the root tips, the root parenchyma, and later, the cotyledons (**Figure 5J**). Interestingly, the first analyses of malformed somatic embryos revealed that they either expressed only very low GUS activity or were completely stained blue (**Figures 5K,L**).

## *roGFP2_Orp1* Transgenic *C. persicum*

The aims of the third and final series of transformation experiments were (i) to test the transformation protocol with a second *C. persicum* genotype and (ii) to produce transgenic cyclamen carrying the redox sensor construct *roGFP2_Orp1*, which will enable hydrogen peroxide localization within living cells. Therefore, embryogenic callus of the genotypes 56/2 and 3145 was transformed following the established protocol, with the only alteration being doubled hygromycin concentrations for the selection of genotype 3145. The vector pH2GW7_c-roGFP2_LR_Orp1 was tested in the three *A. tumefaciens* strains EHA105, GV2260, and LBA4404. The protocol could be successfully applied in genotype 3145 (**Table 2**). All strains resulted in comparable transformation efficiencies of 3–5%, estimated as the percentage of hygromycin-resistant calluses 18 weeks after the start of selection. Transgenic plants were regenerated from the hygromycin-resistant calluses, and a first batch of 16 plants was tested for the presence of the transgenes by PCR. For all 16 plantlets, the bacterial gene *PicA* was not amplified, whereas all contained the *hpt* gene and all except one also carried the *roGFP2_Orp1* gene. Transformation efficiencies were much lower than those in the previous experiments (**Table 2**). Especially for genotype 56/2, only with the strain LBA4404 were three out of 180 calluses found to grow on selection medium after 18 weeks, corresponding to a transformation efficiency of only 1.7%. A first observation under the fluorescence microscope revealed the

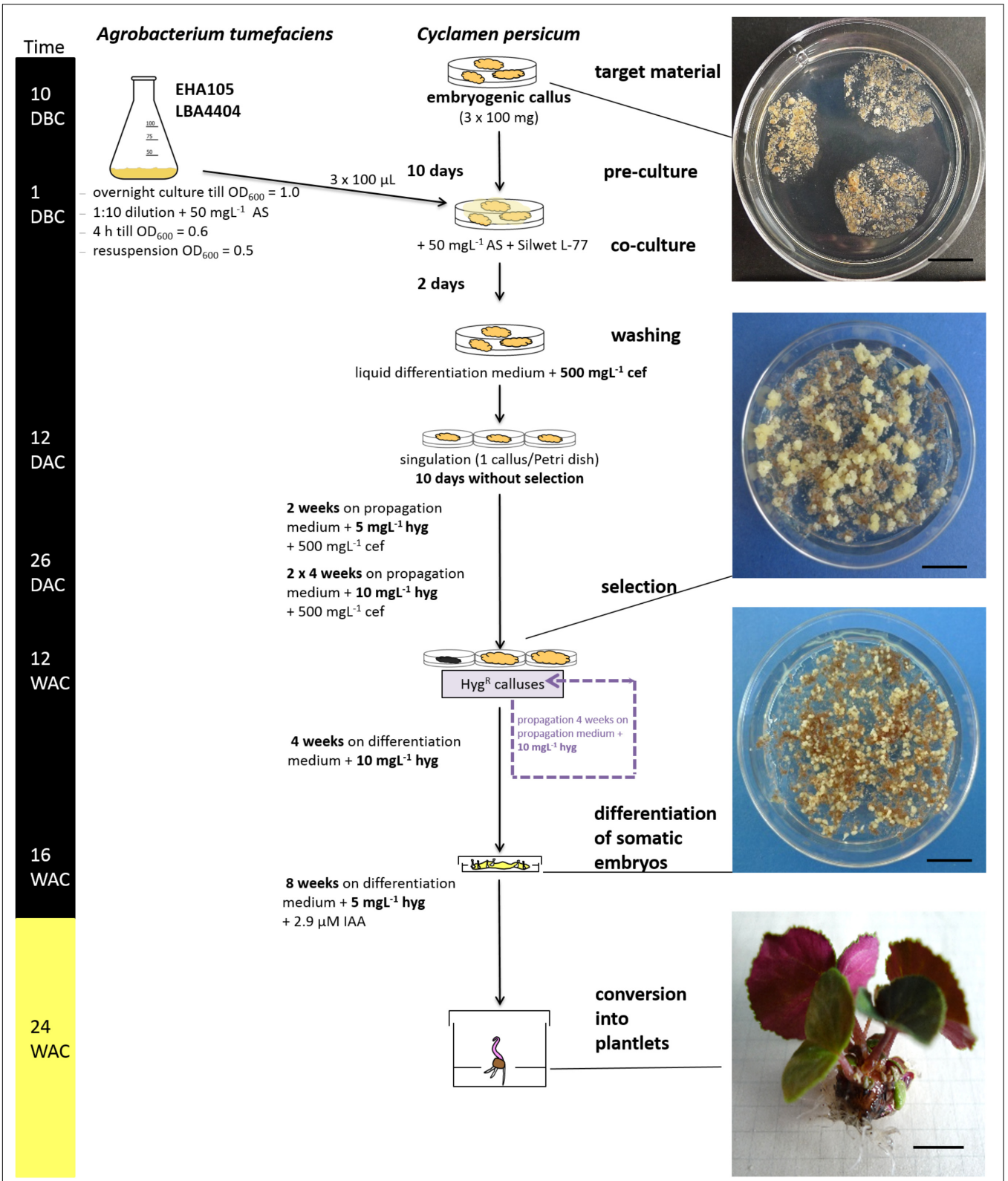


**FIGURE 3 |** Overview of the validated transformation protocol for *C. persicum*. AS, acetosyringone; hyg, hygromycin; cef, cefotaxime; DBC, days before co-culture; DAC, days after co-culture; WAC, weeks after co-culture. Black bar = culture in darkness, yellow bar = culture under 16 h light. Size standards in photos represent 1 cm.

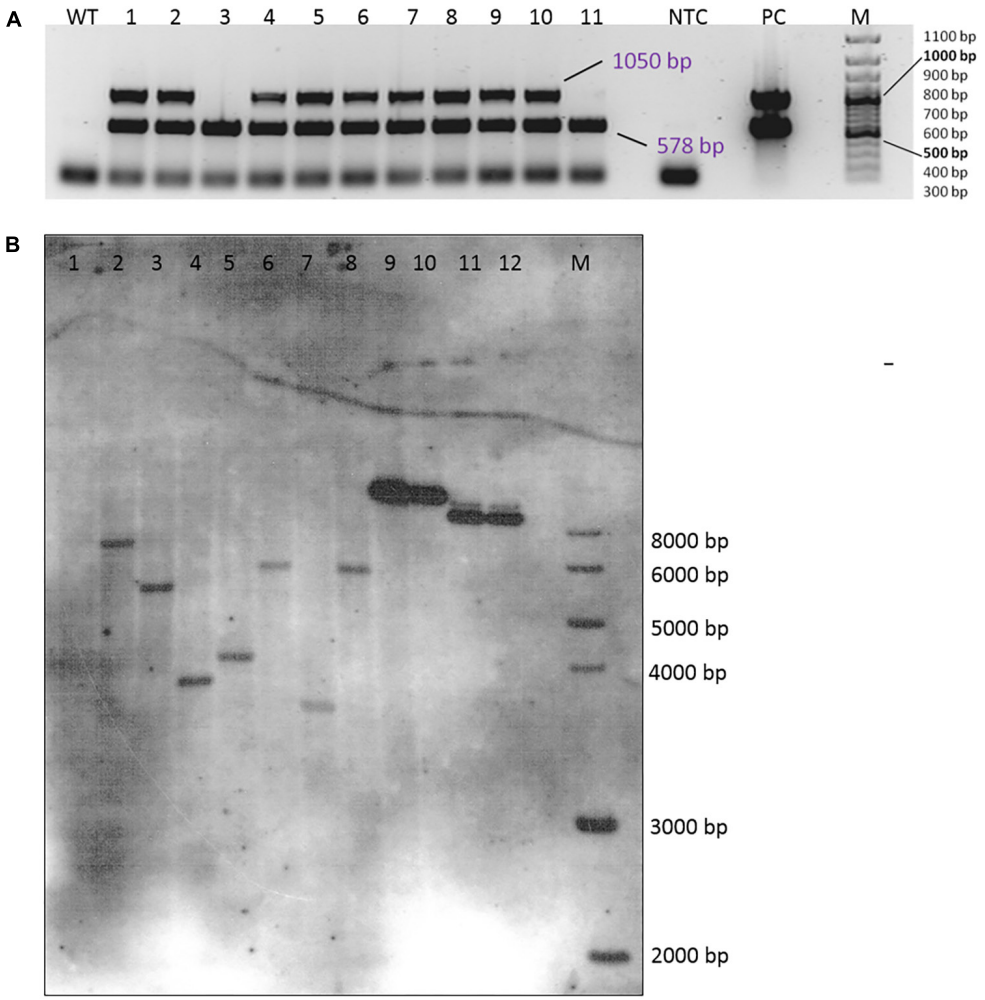


**FIGURE 4 |** Verification of transgenic plants. **(A)** Multiplex PCR amplification of the *hpt* (578 bp) and the *gus* (1050 bp) gene fragments from DNA isolated from the leaves of 11 independent transgenic plants (genotype 56/2, EHA105 + pCAMBIA1301). WT, wild-type 56/2, DNA of a non-transformed plant; NTC, no template control ($H_2O$); PC, EHA 105 + pCAMBIA1301; M = 100 bp size standard. **(B)** Southern hybridization of DNA from wild-type and transgenic plants of genotype 56/2 from different transformation experiments. The DNA was digested with *Hin*dIII and probed with a DIG-labeled *hpt* amplicon. 1 = WT, 2–3 = transformed with LBA4404 + pCAMBIA1380_DR5::GUS, 4: transformed with EHA105 + pCAMBIA1380_DR5::GUS, 5–8 = transformed with EHA105 + pCAMBIA1301, 9: 0.5 ng pCAMBIA1301, 10: 0.2 ng pCAMBIA1301, 11: 0.5 ng pCAMBIA1380_DR5::GUS, 12: 0.2 ng pCAMBIA1380_DR5::GUS, M: 1 kb DNA Ladder (New England Biolabs, Inc., Ipswich, MA, United States).

typical GFP fluorescence, which was strongest in meristematic cells (Supplementary Figure 2).

## DISCUSSION

### Hygromycin Sensitivity in *C. persicum* Is Genotype-Dependent

To select transgenic cells from among untransformed cells in embryogenic callus, hygromycin was chosen as a selective agent after trials with kanamycin had revealed a high tolerance in *C. persicum* embryogenic cells. This result is in agreement with those of earlier transformation studies that used seedlings as starting material and selected transgenic regenerants with 5–20 $mgL^{-1}$ hygromycin (**Table 1**; Aida et al., 1999; Terakawa et al., 2008; Boase et al., 2010; Kai et al., 2012). The selection scheme established in this study started 10 days after co-culture with a concentration of 5 $mgL^{-1}$, which was doubled after 4 weeks of culture. For the later phase of the root growth of transgenic plants *in vitro*, the concentration was again lowered to 5 $mgL^{-1}$. Applying this selection scheme, transgenic plants were repeatedly generated, and thus, the balance was kept between stringent selection preventing chimeras and escapes on the one hand, and overly harsh selection resulting in rapid death of untransformed cells, which can also kill transformed cells due to their degradation products, on the other hand.

An interesting observation was the divergent sensitivity of the two genotypes under investigation (**Figure 1**). In consequence, it seems recommendable to define different selection schedules

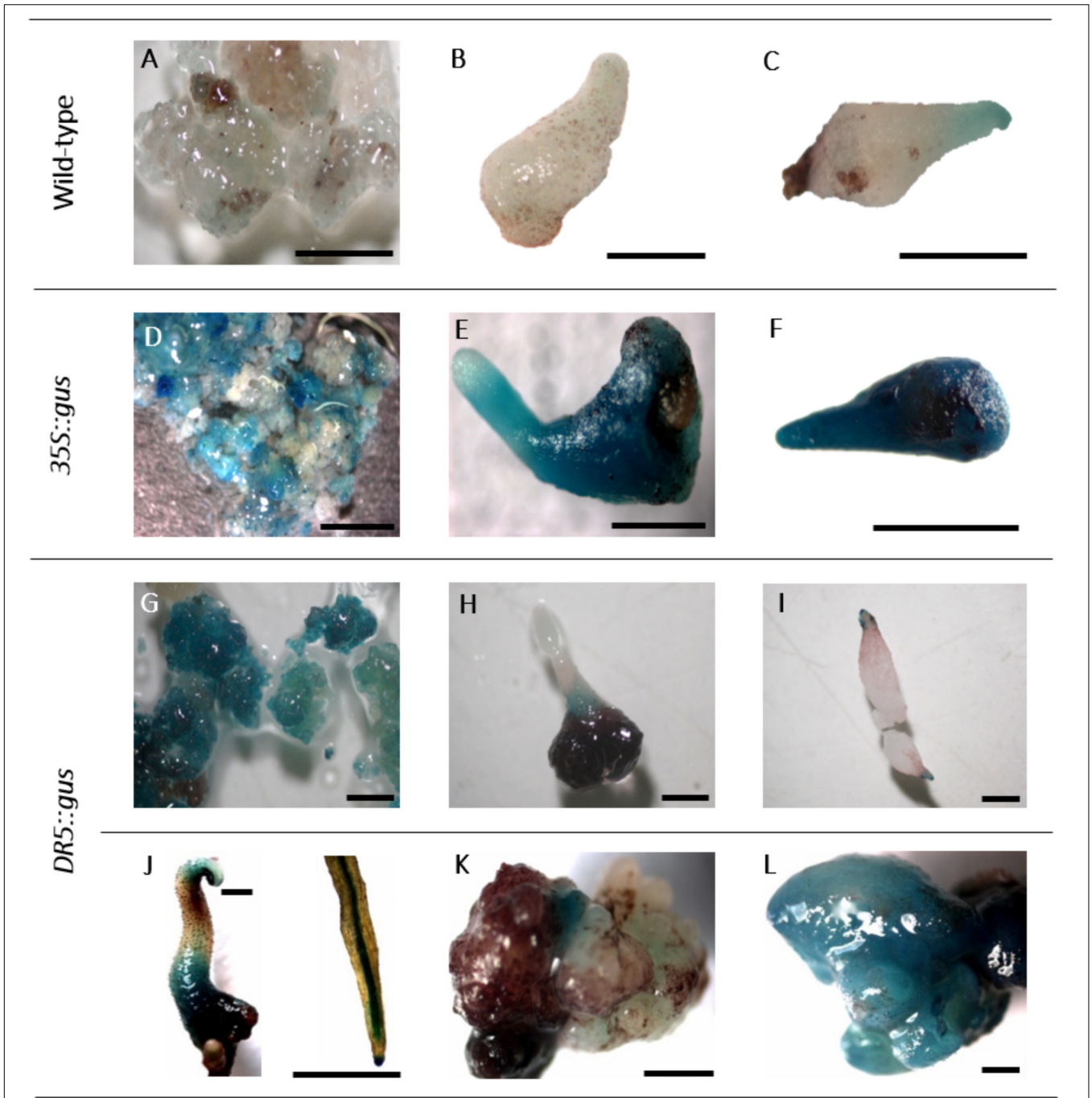


**FIGURE 5 |** Histochemical GUS assay. **A–C**: non-transgenic lines of genotype 56/2: **A**: embryogenic callus, **B,C**: somatic embryos. **D–F**: *35S*::*gus* transgenic lines of genotype 56/2: **D**: embryogenic callus, **E,F**: somatic embryos. **G–L**: *DR5*::*gus* transgenic lines of genotype 56/2: **G**: embryogenic callus, **H,I**: somatic embryos, **J**: germinated somatic embryo and close-up of a root, **K,L**: malformed somatic embryos. Bars represent 1 mm.

and concentrations for different *C. persicum* genotypes. For genotype 3145, a doubling of the hygromycin concentrations was employed in the transformation experiments with the *roGFP2_Orp1* gene. The reasons for the differences in sensitivity are unknown thus far but could involve uptake and detoxification mechanisms. In rice, Sultana et al. (2014) also reported genotypic differences in the reaction to hygromycin: the growth of embryogenic callus in three genotypes was inhibited at 40–47 $mgL^{-1}$ hygromycin, whereas for germination of somatic embryos, even greater genotypic differences were observed for the inhibitory concentrations (32–62 $mgL^{-1}$). This result confirms that genotypes and developmental phases differ in

**TABLE 2 |** Results of three transformation experiments to transfer the *roGFP2_Orp1* gene into the *C. persicum* genotypes 56/2 and 3145.

| Genotype | *A. tumefaciens* strain | Number of calluses transformed | $Hyg^R$ calluses 18 weeks after start of selection | | No. of plants submitted to PCR | No. of plants testing positive by PCR for | |
|---|---|---|---|---|---|---|---|
| | | | Number | Percentage | | *hpt* | *roGFP2_Orp1* |
| 56/2 | EHA105 | 60 | 0 | 0 | 0 | – | – |
| | GV2260 | 30 | 0 | 0 | 0 | – | – |
| | LBA4404 | 180 | 3 | 1.7 | 0 | – | – |
| 3145 | EHA105 | 60 | 3 | 5.0 | 0 | – | – |
| | GV2260 | 30 | 1 | 3.3 | 5 | 5 | 5 |
| | LBA4404 | 75 | 4 | 5.3 | 11 | 11 | 10 |

*The experiments included a comparison of the three A. tumefaciens strains EHA105, GV2260, and LBA4404.*

their hygromycin sensitivity and demonstrates variation between species.

## Transformation Efficiencies Depend on the *Agrobacterium tumefaciens* Strain

When preparing the *A. tumefaciens* solutions for genetic transformation experiments, it was observed that strain EHA105, in approximately 50% of the colonies tested from plated glycerine stocks, had lost the plasmid pCAMBIA1301. Thus, it was essential to prove the presence of the transformation vector in the starting material before preparing the transformation solution, by colony PCR.

The transformation solution was supplemented with 0.03% Silwet® L-77, a detergent that is commonly used in the floral dip transformation protocol for *Arabidopsis thaliana* (Clough and Bent, 1998) but has also been shown to improve transformation efficiencies in wheat (Cheng et al., 1997).

In a series of four transformation experiments, the transformation efficiency, expressed as percentage of hygromycin-resistant calluses (**Figure 2**), varied greatly among the four *A. tumefaciens* strains used. The most efficient strain was EHA105 (42.6% transformation efficiency), followed by GV2260, while GV3101 and AGL-1 did not result in calluses growing in the presence of hygromycin 18 weeks after start of selection. EHA105 is a hypervirulent *A. tumefaciens* strain that also, in previous studies, was found to be suitable and efficient for the transformation of embryogenic cultures, for instance those of banana (Ganapathi et al., 2001), *Vitis vinifera* (Lopez-Perez et al., 2008), and *Citrus sinensis* (Dutt and Grosser, 2010). If previous work in *C. persicum* is considered (**Table 1**), the majority of studies successfully used strains EHA105 or LBA4404. A comparison of strains EHA105 and LBA4404 was included in the three transformation experiments transferring the *DR5*::*gus* gene. There, we found much lower transformation efficiencies overall, most likely due to insufficient selection pressures in weeks three and four (see section "*DR5*::*gus* Transgenic *C. persicum*"), but higher values of 20% for strain LBA4404. The differences between single experimental replications were most likely caused by uncontrollable physiological differences in the callus lines.

The transformation efficiencies (max. 42.6%) achieved in this series of experiments were high compared to those in most previous studies in *C. persicum* (**Table 1**): Aida et al. (1999) and Boase et al. (2002) reported 19 and 15.3% transformation efficiencies in the best variants, respectively. Only Tanaka et al. (2011) reached even higher values of 55% transformed explants.

## Confirmation of Transgenic Plants

Plants regenerated from the transformation experiments were analyzed by GUS assays and PCR for the presence of the *gus* and *hpt* genes. Residual agrobacteria were not detected in any of the plants, showing that the washing and thin plating on cefotaxime-containing medium were sufficient to fully suppress bacterial growth. Almost all regenerants (95%) contained the *hpt* gene, indicating successful selection. In addition, the results of the GUS assay and the *gus* PCR had high congruence (87%, Supplementary Table 2). Since the results of the GUS assay carried out 6 weeks after the start of selection resembled the final transformation efficiencies after 18 weeks (expressed as hygromycin-resistant calluses in **Figure 2**), a GUS assay allows an early estimation of the transformation efficiency. In four plants, only the *hpt* gene, but not the *gus* gene, was detected. On the T-DNA of the plasmid pCAMBIA1301, the *gus* gene is located close to the right border, where integration into the plant genome starts (Hellens et al., 2000). It is therefore not probable that these four plants were the result of incomplete incorporation of the T-DNA or deletions, which have been described to occur mainly at the left border (Li et al., 2007). Instead, the spectrophotometric measurements of the DNA extracts of these four plants revealed low absorption ratios ($A_{230}/A_{260}$), and thus, these extracts were contaminated with phenols and/or polysaccharides. One explanation for the missing band for the *gus* gene could be a higher sensitivity of the *gus* primers to these impurities.

By Southern hybridization, it was proven that single copies of the transgene (in this case *hpt*) were integrated (**Figure 4B**) and that different plants represented independent transgenic events. Further analyses of the other transgenes (*gus* and *DR5*::*gus*) and of a higher number of plants will allow the estimation of frequencies of single copy events for the genes of interest.

The histochemical GUS assay allowed early identification of transformed cells and clearly indicated the typical deep blue coloration in callus cells (**Figure 5D**). However, in a few samples

of non-transformed callus cells as well as somatic embryos, a faint but clear blue tone was also observed (**Figures 5A,C**). Residual agrobacteria as the cause of these blue shades can be excluded, because the intron-containing *gus* gene version was used, which only be spliced by eukaryotic cells. Moreover, the *PicA* PCR was negative in all tested DNA samples. According to Jefferson (1987), blue background signals can occur when long incubation times are chosen, as in the present study. Furthermore, intrinsic GUS-like activities have been reported in other plants previously (Hu et al., 1990; Taylor, 1997). However, the faint coloration of the controls allowed them to be distinguished from the deep blue color and sharp localization of transgenic GUS-expressing cells.

When callus cells were subjected to GUS assays, they turned out to be mixtures of GUS-positive and GUS-negative cells, even within one cell aggregate (**Figure 5D**). This result can be explained by either a chimeric structure of the callus lines, including transgenic cells and escapes; an inhomogeneous infiltration of the GUS staining solution; or low expression levels of the *gus* gene in some cells. In principle, the 35S promoter controlling *gus* gene expression seemed to be active in *C. persicum* callus cells (**Figure 5D**), somatic embryos (**Figures 5E,F**) and the young leaves of regenerated plants (not shown).

## *DR5*::*gus* Transgenic Cyclamen Allow Visualization of Auxin Gradients

Transgenic cyclamen plants were generated carrying the *DR5::gus* construct. From the auxin-responsive element DR5, which was found naturally in the promoters of auxin-responsive genes, Ulmasov et al. (1997a, b) developed the synthetic DR5 promoter that was used in our study. They combined seven repeats of the DR5 motif with a fragment of the *Cauliflower mosaic virus* 35S promoter and the translation-enhancing omega sequence of *Tobacco mosaic virus*. In the *DR5::gus* construct, this synthetic promoter, being efficiently activated by auxin, controls the expression of the *gus* gene in order to visualize auxin in tissues. The *DR5::gus* gene has been used in a wide range of plant species to visualize auxin distribution in different organs and different developmental processes, for instance *A. thaliana* (Kurczynska et al., 2007), *Pisum sativum* (DeMason and Polowick, 2009), poplar (Chen et al., 2013), or strawberry (Estrada-Johnson et al., 2017). Moreover, it has become a widely used tool in fundamental research of auxin homeostasis and signaling (e.g., Deng et al., 2016; Lin et al., 2016). In *DR5::gus* transgenic *A. thaliana*, Kurczynska et al. (2007) observed overall high auxin concentrations in globular somatic embryos, but a differentiation in embryos in the heart stage, with elevated concentrations in the protoderm and the root and shoot poles. Cotyledonary somatic embryos expressed GUS activity mainly in the roots, vascular tissue, and parenchyma cells of the hypocotyl (Kurczynska et al., 2007). Using the *DR5::gus* approach and comparing somatic to zygotic *A. thaliana* embryos, Bassuner et al. (2007) found striking similarities in the mature embryos of both types. Both accumulated auxin in the tips of the roots and cotyledons. Interestingly, malformed *A. thaliana* somatic embryos often lacked the auxin signals detected by DR5::gus in their roots (Nowak et al., 2012).

For *C. persicum*, we performed the first analyses of the *DR5::gus* transgenic somatic embryos and could observe a more or less uniform blue coloration during the first week of differentiation, until the globular stage. Beginning in the second week, an auxin gradient, with higher GUS expression first in the root pole and later at the tip of the developing cotyledon, was seen (**Figures 5H,I**). Comparable to *A. thaliana*, in later stages, the root tips and root parenchyma cells, as well as the hypocotyl-derived tubers, showed blue signals. Malformed somatic embryos were either lacking GUS activity or were more or less fully stained (**Figures 5K,L**).

An auxin gradient is needed to establish polarity and pattern formation in early embryogenesis (Möller and Weijers, 2009). Since somatic embryogenesis protocols often involve high auxin concentrations in the induction phase, the establishment of an auxin gradient is based on controlled efflux as well as polar auxin transport, as discussed for Norway spruce somatic embryos (Hakman et al., 2009). Future studies in *C. persicum* could focus on more detailed time-line analyses of auxin distribution in *DR5::gus* transgenic lines, a comparison of somatic and zygotic embryos and the response of auxin distribution to exogenously applied plant growth regulators. *DR5::gfp* transgenic plants would help to overcome the limitations of the histochemical GUS assay and would allow auxin localization in living cells.

Although the GUS staining pattern reflected the expected auxin distribution well, a proof for the functionality, i.e., auxin sensitivity of the *DR5::gus* construct in *C. persicum* still is required. First trials to achieve this evidence were undertaken by incubating *DR5::gus* transgenic *C. persicum* roots in naphthalene acetic acid (NAA) at 50 μM for 24 h, as also used in previous studies (Ulmasov et al., 1997b; Estrada-Johnson et al., 2017). The GUS staining was observed in root tips and vascular tissue, but was not different from the water incubated control roots. However, in petioles, a deeper blue staining of the vasculature and blue coloration at the cut surfaces was observed after an incubation at 100 μM NAA for 2 h (Supplementary Figure 3). Thus, like previously reported for *DR5::gus* transgenic poplar (Chen et al., 2013), it will be obviously necessary to identify the appropriate type of auxin, its concentration and the duration of application in a organ-specific way in order to demonstrate the response of the promoter GUS construct in *C. persicum*.

## *roGFP2_Orp1* Transgenic Cyclamen as a Basis for ROS Localization

In the process of somatic embryogenesis, stress plays an important role (Karami and Saidi, 2010). Upon stress, plants produce ROS, which have a dual role in stress response and development. In high concentrations, ROS are toxic and will cause cell death, whereas in low concentrations, they act as important signal molecules for developmental processes (Mittler et al., 2011; Kocsy et al., 2013). Furthermore, the ROS signaling pathway is linked to plant hormone signaling, as shown in cotton somatic embryogenesis, where auxin signaling was shown to be regulated by ROS homeostasis (Zhou et al., 2016). Due to rapidly

acting detoxification systems, ROS detection is not trivial, and fluorescent protein redox sensors such as roGFP2_Orp1 offer the great advantage of localization of ROS, in this case $H_2O_2$, in living cells (Schwarzländer et al., 2016). The emitted light wavelengths of the roGFP2 protein differ between the oxidized and reduced state and thus allow ratiometric imaging using confocal laser scanning microscopy (Schwarzländer et al., 2016).

To better understand the role of ROS in the process of somatic embryogenesis in comparison to zygotic embryogenesis, the redox sensor gene *roGFP2_Orp1* was transferred to *C. persicum* in this study. By PCR, it could be shown that the *roGFP2_Orp1* gene was present in plantlets regenerated from transformation experiments of genotype 3145 with *A. tumefaciens* strains GV2260 and LBA4404 (**Table 2**). Thereby, it was shown that the established transformation protocol could be successfully transferred to another genotype of a distinct gene pool and to another vector system. Differentiation of additional plants from the hygromycin-resistant calluses is in progress. All 16 regenerated plantlets were positive by PCR for the *hpt* gene, and only one plant was negative in the PCR testing for the *roGFP2_Orp1* gene. Again, the DNA of the negative sample (for roGFP2_Orp1) had a low A230/A260 ratio when analyzed spectrophotometrically, pointing to a possible inhibition of the PCR by polyphenols or polysaccharides. The reasons for the low transformation efficiencies most likely can be found in the different vector system, the larger size of the transferred DNA and the status of the plant material. Under fluorescent light, the functionality of the roGFP2 protein was proven, but testing the functionality of the redox sensing awaits labor-intensive studies under a confocal laser scanning microscope.

## CONCLUSION

An efficient transformation protocol for *C. persicum* starting from embryogenic callus has been established and successfully used to transfer genes of interest into different genotypes. This protocol does not depend on seedlings, which have genetic variability and the value of which has not been tested when used for transformation. Instead it is based on the regeneration via somatic embryogenesis starting from explants of adult plants which is highly efficient and connected to low percentages of aberrations in some genotypes (Schwenkel and Winkelmann, 1998). Embryogenic callus can be induced in the vast majority of genotypes (Winkelmann and Serek, 2005), although in different percentages. Additionally, the maintenance of embryogenic cultures differs between genotypes, with approximately 10–20% of the genotypes being easy to maintain. This fact may limit the applicability of the established transformation system for commercial breeders, if transgenic cyclamen would be accepted by the public. However, our intention is to use this transformation system for gene functional analyses, hence a set of two to three genotypes with different genetic backgrounds that are stably propagated as embryogenic cultures is sufficient. For success in transformation, we regard the following factors as important: highly embryogenic cell lines, the use of Silwet® L-77 as a surfactant during co-culture, an appropriate selection schedule with hygromycin, and *A. tumefaciens* strains EHA105 and LBA4404. Because somatic embryos develop from few or even single cells within embryogenic callus cultures, we assume a low risk of chimeric regenerants, but this must be proven in further studies.

Applying the protocol established here, if a lower efficiency of 10% is taken as a basis for calculation, 100 callus portions of 100 mg would be needed to generate 10 independent transgenic lines. After 14 weeks (**Figure 3**) on selection medium (2 weeks with 5 $mgL^{-1}$ hygromycin and two passages of 4 weeks with 10 $mgL^{-1}$ hygromycin), the surviving embryogenic callus lines can be plated on differentiation medium. After 4 weeks, 50 somatic embryos should be picked per line to obtain two transgenic plants per event, on average.

## AUTHOR CONTRIBUTIONS

SR performed major parts of the experimental work and data analysis and revised the manuscript. SM and AK performed parts of the experimental work and data analysis and revised the manuscript. MB conceived and designed the experiments and the manuscript structure. TW contributed to the experimental design and wrote the manuscript.

## ACKNOWLEDGMENTS

The kind provision of the DR5 promoter by Günther Scherer and of the plasmid pH2GW7:c-roGFP2-Orp1 by Markus Schwarzländer and Thomas Nietzel is highly acknowledged. The authors thank Bärbel Ernst, Ewa Schneider, and Friederike Schröder for their excellent technical assistance; Rena Becker, Björn Heinemann, Christine Weber, and Katharina Wellpott for their help in the lab; colleagues from the section Floriculture of our institute for their help with the Southern hybridization; and Bunlong Yim for his support in performing the statistical tests.

## SUPPLEMENTARY MATERIAL

The Supplementary Material for this article can be found online at: https://www.frontiersin.org/articles/10.3389/fpls.2018.01035/full#supplementary-material

## REFERENCES

Aida, R., Hirose, Y., Kishimoto, S., and Shibata, M. (1999). *Agrobacterium tumefaciens*–mediated transformation of *Cyclamen persicum* Mill. *Plant Sci.* 148, 1–7. doi: 10.1016/S0168-9452(99)00072-2

Bassuner, B. M., Lam, R., Lukowitz, W., and Yeung, E. C. (2007). Auxin and root initiation in somatic embryos of *Arabidopsis*. *Plant Cell Rep.* 26, 1–11. doi: 10.1007/s00299-006-0207-5

Bian, F., Zheng, C., Qu, F., Gong, X., and You, C. (2010). Proteomic analysis of somatic embryogenesis in *Cyclamen persicum* Mill. *Plant Mol. Biol. Rep.* 28, 22–31. doi: 10.1007/s11105-009-0104-5

Boase, M. R., Lewis, D. H., Davies, K. M., Marshall, G. B., Patel, D., Schwinn, K. E., et al. (2010). Isolation and antisense suppression of flavonoid 3′,5′-hydroxylase modifies flower pigments and color in cyclamen. *BMC Plant Biol.* 10:107. doi: 10.1186/1471-2229-10-107

Boase, M. R., Marshall, G. B., Peters, T. A., and Bendall, M. J. (2002). Long-term expression of the gusA reporter gene in transgenic cyclamen produced from etiolated hypocotyls explants. *Plant Cell Tissue Organ Cult.* 70, 27–39. doi: 10.1023/A:1016001124197

Chen, Y., Yordanov, Y. S., Ma, C., Strauss, S., and Busov, V. B. (2013). DR5 as a reporter system to study auxin response in *Populus*. *Plant Cell Rep.* 32, 453–463. doi: 10.1007/s00299-012-1378-x

Cheng, M., Fry, J. E., Pang, S., Zhou, H., Hironaka, C. M., Ducan, D. R., et al. (1997). Genetic transformation of wheat mediated by *Agrobacterium tumefaciens*. *Plant Physiol.* 115, 971–980. doi: 10.1104/pp.115.3.971

Clough, S. J., and Bent, A. F. (1998). Floral dip: a simplified method for *Agrobacterium*-mediated transformation of *Arabidopsis thaliana*. *Plant J.* 16, 735–743. doi: 10.1046/j.1365-313x.1998.00343.x

DeMason, D. A., and Polowick, P. L. (2009). Patterns of DR5::*GUS* expression in organs of pea (*Pisum sativum* L.). *Int. J. Plant Sci.* 170, 1–11. doi: 10.1086/593046

Deng, K., Yu, L., Zheng, X., Zhang, K., Wang, W., Dong, P., et al. (2016). Target of rapamycin is a key player for auxin signaling transduction in *Arabidopsis*. *Front. Plant Sci.* 7:291. doi: 10.3389/fpls.2016.00291

Dutt, M., and Grosser, J. W. (2010). An embryogenic suspension cell culture system for *Agrobacterium*-mediated transformation of citrus. *Plant Cell Rep.* 29, 1251–1260. doi: 10.1007/s00299-010-0910-0

Estrada-Johnson, E., Csukasi, F., Pizarro, C. M., Vallarino, J. G., Kiryakova, Y., Vioque, A., et al. (2017). Transcriptomic analysis in strawberry fruits reveals active auxin biosynthesis and signaling in the ripe receptacle. *Front. Plant Sci.* 8:889. doi: 10.3389/fpls.2017.00889

Ganapathi, T. R., Higgs, N. S., Balint-Kurti, P. J., Arntzen, C. J., May, G. D., and Van Eck, J. M. (2001). *Agrobacterium*-mediated transformation of embryogenic cell suspension of the banana cultivar Rasthali (AAB). *Plant Cell Rep.* 20, 157–162. doi: 10.1007/s002990000287

Gutscher, M., Sobotta, M., Wabnitz, G. H., Ballikaya, S., Meyer, A. J., Samstag, Y., et al. (2009). Proximity-based protein thiol oxidation by $H_2O_2$-scavenging peroxidases. *J. Biol. Chem.* 284, 31532–31540. doi: 10.1074/jbc.M109.059246

Hakman, I., Hallberg, H., and Palovaara, J. (2009). The polar auxin transport inhibitor NPA impairs embryo morphology and increases the expression of an auxin efflux facilitator protein PIN during *Picea abies* somatic embryo development. *Tree Physiol.* 29, 483–496. doi: 10.1093/treephys/tpn048

Hanson, G. T., Aggeler, R., Oglesbee, D., Cannon, M., Capaldi, R. A., Tsien, R. Y., et al. (2004). Investigating mitochondrial redox potential with redox-sensitive Green Fluorescent Protein indicators. *J. Biol. Chem.* 279, 13044–13053. doi: 10.1074/jbc.M312846200

Hellens, R., Mullineux, P., and Klee, H. (2000). Technical focus: a guide to *Agrobacterium* binary Ti vectors. *Trends Plant Sci.* 5, 446–451. doi: 10.1016/S1360-1385(00)01740-4

Hoenemann, C., Richardt, S., Krueger, K., Zimmer, A. D., Hohe, A., and Rensing, A. S. (2010). Large impact of the apoplast on somatic embryogenesis in *Cyclamen persicum* offers possibilities for improved developmental control *in vitro*. *BMC Plant Biol.* 2010:77. doi: 10.1186/1471-2229-10-77

Holsters, M., Silva, B., Van Vliet, F., Genetello, C., De Block, M., Dhaese, P., et al. (1980). The functional organization of the nopaline *Agrobacterium tumefaciens* plasmid pTiC58. *Plasmid* 3, 212–230. doi: 10.1016/0147-619X(80)90110-9

Hood, E. E., Gelvin, S. B., Melchers, L. S., and Hoekema, A. (1993). New *Agrobacterium* helper plasmids for gene transfer to plants. *Transgenic Res.* 2, 208–218. doi: 10.1007/BF01977351

Hu, C., Chee, P. P., Chesney, R. H., Zhou, J. H., Miller, P. D., and O'Brien, W. T. (1990). Intrinsic GUS-like activities in seed plants. *Plant Cell Rep.* 9, 1–5. doi: 10.1007/BF00232123

Jalali, N., Naderia, R., Shahi-Gharahlara, A., and Teixeira da Silva, J. A. (2012). Tissue culture of *Cyclamen* spp. *Sci. Hortic.* 137, 11–19. doi: 10.1016/j.scienta.2012.01.015

Jefferson, R. A. (1987). Assaying chimeric genes in plants: the GUS gene fusion system. *Plant Mol. Biol. Rep.* 5, 387–405. doi: 10.1007/BF02667740

Kai, H., Hirashima, K., Matsuda, O., Ikegami, H., Winkelmann, T., Nakahara, T., et al. (2012). Thermotolerant cyclamen with reduced acrolein and methyl vinyl ketone. *J. Exp. Bot.* 63, 4143–4150. doi: 10.1093/jxb/ers110

Karami, O., and Saidi, A. (2010). The molecular basis for stress-induced acquisition of somatic embryogenesis. *Mol. Biol. Rep.* 37, 2493–2507. doi: 10.1007/s11033-009-9764-3

Kiviharju, E., Tuominen, U., and Tormalä, T. (1992). The effect of explant material on somatic embryogenesis of *Cyclamen persicum* Mill. *Plant Cell Tissue Organ Cult.* 28, 187–194. doi: 10.1007/BF00055516

Kocsy, G., Tari, I., Vankova, R., Zechmann, B., Gulyas, Z., Poor, P., et al. (2013). Redox control of plant growth and development. *Plant Sci.* 211, 77–91. doi: 10.1016/j.plantsci.2013.07.004

Kreuger, M., Postma, E., Brouwer, Y., and Van Holst, G. J. (1995). Somatic embryogenesis of *Cyclamen persicum* in liquid medium. *Physiol. Plant.* 94, 605–612. doi: 10.1111/j.1399-3054.1995.tb00974.x

Kurczynska, E. U., Gaj, M., Ujczak, A., and Mazur, E. (2007). Histological analysis of direct somatic embryogenesis in *Arabidopsis thaliana* (L.) Heynh. *Planta* 226, 619–628. doi: 10.1007/s00425-007-0510-6

Lazo, G. R., Stein, P. A., and Ludwig, R. A. (1991). A DNA transformation competent *Arabidopsis* genomic library in *Agrobacterium*. *Biotechnology* 9, 963–967. doi: 10.1038/nbt1091-963

Li, G., Zhou, Z., Liu, G., Zheng, F., and He, C. (2007). Characterization of T-DNA insertion patterns in the genome of rice blast fungus *Magnaporthe oryzae*. *Curr. Genet.* 51, 233–243. doi: 10.1007/s00294-007-0122-5

Lin, X. Y., Ye, Y. Q., Fan, S. K., Jin, C. W., and Zheng, S. J. (2016). Increased sucrose accumulation regulates iron-deficiency responses by promoting auxin signaling in Arabidopsis plants. *Plant Physiol.* 170, 907–920. doi: 10.1104/pp.15.01598

Lopez-Perez, A.-J., Velasco, L., Pazos-Navarro, M., and Daauza, M. (2008). Development of highly efficient genetic transformation protocols from table grape Sugraone and Crimson Seedless at low *Agrobacterium* density. *Plant Cell Tissue Organ Cult.* 94, 189–199. doi: 10.1007/978-1-61779-558-9_19

McBride, K. E., and Summerfelt, K. R. (1990). Improved binary vectors for *Agrobacterium*-mediated plant transformation. *Plant Mol. Biol.* 14, 269–276. doi: 10.1007/BF00018567

Mittler, R., Vanderauwera, S., Suzuki, N., Miller, G., Tognetti, V. B., Vandepoele, K., et al. (2011). ROS signaling: the new wave? *Trends Plant Sci.* 16, 300–309. doi: 10.1016/j.tplants.2011.03.007

Möller, B., and Weijers, D. (2009). Auxin control of embryo patterning. *Cold Spring Harb. Perspect. Biol.* 1:a001545. doi: 10.1101/cshperspect.a001545

Murashige, T., and Skoog, F. (1962). A revised medium for rapid growth and bio assays with tobacco tissue cultures. *Physiol. Plant.* 15, 473–497. doi: 10.1111/j.1399-3054.1962.tb08052.x

Mwangi, J. W., Rode, C., Colditz, F., Haase, C., Braun, H. P., and Winkelmann, T. (2013). Proteomic and histological analyses of endosperm development in *Cyclamen persicum* as a basis for optimization of somatic embryogenesis. *Plant Sci.* 20, 52–65. doi: 10.1016/j.plantsci.2012.11.004

Nowak, K., Wojcikowska, B., Szyrajew, K., and Gaj, M. D. (2012). Evaluation of different embryogenic systems for production of true somatic embryos in *Arabidopsis*. *Biol. Plant.* 56, 401–408. doi: 10.1007/s10535-012-0063-9

Otani, M., and Shimada, T. (1991). Somatic embryogenesis and plant regeneration from *Cyclamen persicum* Mill. leaf cultures. *Plant Tissue Cult. Lett.* 8, 121–123. doi: 10.5511/plantbiotechnology1984.8.121

Rode, C., Gallien, S., Heintz, D., van Dorsselaer, A., Braun, H. P., and Winkelmann, T. (2011). Enolases: storage compounds in seeds? Evidence from a proteomic comparison of zygotic and somatic embryos of *Cyclamen persicum* Mill. *Plant Mol. Biol.* 75, 305–319. doi: 10.1007/s11103-010-9729-x

Schmidt, T., Ewald, A., Seyring, M., and Hohe, A. (2006). Comparative analysis of cell cycle events in zygotic and somatic embryos of *Cyclamen persicum* indicates strong resemblance of somatic embryos to recalcitrant seeds. *Plant Cell Rep.* 25, 643–650. doi: 10.1007/s00299-006-0130-9

Schwarzländer, M., Dick, T. P., Meyer, A. J., and Morgan, B. (2016). Dissecting redox biology using fluorescent protein sensors. *Antioxid. Redox Signal.* 24, 680–712. doi: 10.1089/ars.2015.6266

Schwenkel, H. G. (2001). "Introduction: botany, economic importance, cultivars, micropropagation of *C. persicum*," in *Reproduction of Cyclamen persicum Mill. Through Somatic Embryogenesis using Suspension Culture Systems*, ed. H. G. Schwenkel (Luxembourg: European Communities), 3–7.

Schwenkel, H. G., and Winkelmann, T. (1998). Plant regeneration via somatic embryogenesis from ovules of *Cyclamen persicum* Mill. *Plant Tissue Cult. Biotechnol.* 4, 28–34.

Scuffi, D., Nietzel, T., Di Fino, L. M., Meyer, A. J., Lamattina, L., Schwarzländer, M., et al. (2018). Hydrogen sulfide increases production of NADPH oxidase-dependent hydrogen peroxide and phospholipase D-derived phosphatidic acid in guard cell signaling. *Plant Physiol.* 176, 2532–2542. doi: 10.1104/pp.17.01636

Sriskandarajah, S., Mibus, H., and Serek, M. (2007). Transgenic *Campanula carpatica* plants with reduced ethylene sensitivity showing specific expression of etr1-1 in flowers and buds. *Plant Cell Rep.* 26, 805–813. doi: 10.1007/s00299-006-0291-6

Sultana, S., Ho, C. L., Namasivayam, P., and Napis, S. (2014). Genotypic differences in response to hygromycin effect on untransformed calli death and rice germination. *Bangladesh Rice J.* 18, 38–43. doi: 10.3329/brj.v18i1-2.23001

Takamura, T., Miyajima, I., and Matsuo, E. (1995). Somatic embryogenesis of *Cyclamen persicum* Mill. 'Anneke' from aseptic seedlings. *Plant Cell Rep.* 15, 22–25. doi: 10.1007/BF01690246

Tanaka, Y., Oshima, Y., Yamamura, T., Sugiyama, M., Mitsuda, N., Ohtsubo, N., et al. (2013). Multi-petal cyclamen flowers produced by AGAMOUS chimeric repressor expression. *Sci. Rep.* 3:2642. doi: 10.1038/srep02641

Tanaka, Y., Yamamura, T., Oshima, Y., Mitsuda, N., Koyama, T., Ohme-Takagi, M., et al. (2011). Creating ruffled flower petals in *Cyclamen persicum* by expression of the chimeric cyclamen TCP repressor. *Plant Biotechnol.* 28, 141–147. doi: 10.5511/plantbiotechnology.10.1227a

Taylor, C. B. (1997). Promoter fusion analysis: an insufficient measure of gene expression. *Plant Cell* 9, 273–275. doi: 10.1105/tpc.9.3.273

Terakawa, T., Yamamura, T., and Murayama, T. (2008). Improvement of regeneration and transformation system for *Cyclamen persicum* using somatic embryo culture. *Plant Biotechnol.* 25, 77–80. doi: 10.5511/plantbiotechnology.25.77

Ulmasov, T., Hagen, G., and Guilfoyle, T. J. (1997a). ARF1, a transcription factor that binds to auxin response elements. *Science* 276, 1865–1868.

Ulmasov, T., Murfett, J., Hagen, G., and Guilfoyle, T. J. (1997b). Aux/IAA proteins repress expression of reporter genes containing natural and highly active synthetic auxin response elements. *Plant Cell* 9, 1963–1971.

Wicart, G., Mouras, A., and Lutz, A. (1984). Histological study of organogenesis and embryogenesis in *Cyclamen persicum* tissue cultures: evidence for a single organogenetic pattern. *Protoplasma* 119, 159–167. doi: 10.1007/BF01288870

Williams, J. G. K., Kubelik, A. R., Livak, K. J., Rafalski, J. A., and Tingey, S. V. (1990). DNA polymorphisms amplified by arbitrary primers are useful as genetic markers. *Nucleic Acids Res.* 18, 6531–6535. doi: 10.1093/nar/18.22.6531

Winkelmann, T. (2010). "Clonal propagation of *Cyclamen persicum* via somatic embryogenesis," in *Protocols for In vitro Propagation of Ornamental Plants. Methods in Molecular Biology*, Vol. 589, eds S. M. Jain and S. J. Ochatt (Berlin: Springer), 281–290.

Winkelmann, T., Heintz, D., van Dorsselaer, A., Serek, M., and Braun, H.-P. (2006a). Proteomic analyses of somatic and zygotic embryos of *Cyclamen persicum* Mill. reveal new insights into seed and germination physiology. *Planta* 224, 508–519.

Winkelmann, T., Kaviani, K., and Serek, M. (2006b). *Agrobacterium*-mediated transformation of pelargonium (*Pelargonium zonale* hybrids and *Pelargonium peltatum* hybrids). *Acta Hortic.* 725, 737–745. doi: 10.17660/ActaHortic.2006.725.103

Winkelmann, T., Hohe, A., and Schwenkel, H. G. (1998). Establishing embryogenic suspension cultures in *Cyclamen persicum* 'Purple Flamed'. *Adv. Hortic. Sci.* 12, 25–30.

Winkelmann, T., Ratjens, S., Bartsch, M., Rode, C., Niehaus, K., and Bednarz, H. (2015). Metabolite profiling of somatic embryos of *Cyclamen persicum* in comparison to zygotic embryos, endosperm, and testa. *Front. Plant Sci.* 6:597. doi: 10.3389/fpls.2015.00597

Winkelmann, T., and Serek, M. (2005). Genotypic differences in callus formation and regeneration of somatic embryos in *Cyclamen persicum* MILL. *Euphytica* 144, 109–116. doi: 10.1007/s10681-005-5038-x

Zhou, T., Yang, X., Guo, K., Deng, J., Xu, J., Gao, W., et al. (2016). ROS homeostasis regulates somatic embryogenesis via the regulation of auxin signaling in cotton. *Mol. Cell. Proteom.* 15, 2108–2124. doi: 10.1074/mcp.M115.049338

**Conflict of Interest Statement:** The authors declare that the research was conducted in the absence of any commercial or financial relationships that could be construed as a potential conflict of interest.

frontiers in Plant Science

METHODS
published: 22 June 2018
doi: 10.3389/fpls.2018.00843

# A Protoplast Transient Expression System to Enable Molecular, Cellular, and Functional Studies in *Phalaenopsis* orchids

*Hsiang-Yin Lin[1,2], Jhun-Chen Chen[1,2] and Su-Chiung Fang[1,2]**

[1] Biotechnology Center in Southern Taiwan, Academia Sinica, Tainan, Taiwan, [2] Agricultural Biotechnology Research Center, Academia Sinica, Taipei, Taiwan

The enigmatic nature of the specialized developmental programs of orchids has fascinated plant biologists for centuries. The recent releases of orchid genomes indicate that orchids possess new gene families and family expansions and contractions to regulate a diverse suite of developmental processes. However, the extremely long orchid life cycle and lack of molecular toolkit have hampered the advancement of orchid biology research. To overcome the technical difficulties and establish a platform for rapid gene regulation studies, in this study, we developed an efficient protoplast isolation and transient expression system for *Phalaenopsis aphrodite*. This protocol was successfully applied to protein subcellular localization and protein–protein interaction studies. Moreover, it was confirmed to be useful in delineating the PaE2F/PaDP-dependent cell cycle pathway and studying auxin response. In summary, the established orchid protoplast transient expression system provides a means to functionally characterize orchid genes at the molecular level allowing assessment of transcriptome responses to transgene expression and widening the scope of molecular studies in orchids.

**Keywords: protoplast, *Phalaenopsis aphrodite*, orchid, transient expression, gene regulation**

OPEN ACCESS

***Edited by:***
*Mariana Mondragón-Palomino, University of Regensburg, Germany*

***Reviewed by:***
*Guangdong Wang, Nanjing Agricultural University, China*
*Gian Pietro Di Sansebastiano, University of Salento, Italy*
*Vidhu Sankar Babu, Manipal Academy of Higher Education, India*

***Correspondence:**
*Su-Chiung Fang*
*scfang@gate.sinica.edu.tw*

***Specialty section:***
*This article was submitted to Plant Biotechnology, a section of the journal Frontiers in Plant Science*

***Received:*** *27 February 2018*
***Accepted:*** *30 May 2018*
***Published:*** *22 June 2018*

***Citation:***
*Lin H-Y, Chen J-C and Fang S-C (2018) A Protoplast Transient Expression System to Enable Molecular, Cellular, and Functional Studies in Phalaenopsis orchids. Front. Plant Sci. 9:843. doi: 10.3389/fpls.2018.00843*

## INTRODUCTION

Orchidaceae represent one of the largest angiosperm families comprising more than 25,000 species that are grown in a wide range of habitats including rainforest, grassland, and even mangrove swamp and low arctic tundra. Orchids have distinct morphological and physiological characteristics such as the co-evolution of pollinators and distinct floral structure (Waterman and Bidartondo, 2008), lack of cotyledon development during embryogenesis (Kull and Arditti, 2002), formation of pollen dispersal units (pollinia) (Pacini and Hesse, 2002), and unique growth and development coupled with mycotrophic strategies (Rasmussen, 2002). These unique developmental programs or strategies have drawn the attention of many evolutionary and plant biologists. Additionally, the wide use of certain orchids as medicinal plants indicates that orchids may have a repertoire of secondary metabolites whose functionality still remains to be explored. (Kong et al., 2003; Bulpitt et al., 2007; Bory et al., 2008). Despite the enormous interest in understanding the molecular mechanisms of the specialized developmental or physiological programs in orchids, the lack of a robust molecular toolkit hampers the advancement of orchid biology.

Recent efforts using next generation sequencing have started to unravel the complexity of the orchid genome and transcriptome atlas (Rao et al., 2014; Cai et al., 2015; Fang et al., 2016; Zhang et al., 2016, 2017; Chao et al., 2017). Progress in the development of tools for manipulation and analysis of cellular processes has promoted research in various orchid species (Yu et al., 2001; Liau et al., 2003; Hsu et al., 2011; Lu et al., 2012; Chen and Fang, 2016; Chen et al., 2016; Hsing et al., 2016). However, studies of orchid gene functions and genetic networks are highly challenging because of a lack of mutant collections and the large amounts of time needed to obtain transgenic orchids.

Protoplast transient expression systems have been widely used to study gene regulation, protein localization, protein–protein interactions, and cell signaling pathways in response to hormones, environmental cues, and pathogen-derived elicitors in model systems (Sheen, 2001; Fraiture et al., 2014). Because of their versatility and ability to detect cell-autonomous responses, protoplast transient expression systems have also been developed and applied to many non-model plants whose transformation platforms are not yet available or for which regeneration of transgenic plants is difficult (Nyman and Wallin, 1992; Hirata et al., 2012; Bu et al., 2014; Lin Y.C. et al., 2014; Kidokoro et al., 2015; Muchero et al., 2015; Kanofsky et al., 2016; Lu et al., 2016; Nanjareddy et al., 2016; Thevenin et al., 2016; Shen et al., 2017; Wang et al., 2017). In addition, protoplast-based transient expression systems allow the study of immediate transcriptome responses to expression of the genes of interest and provide an alternative means to characterize and analyze the cellular functions and regulatory networks of such genes.

The protoplast system has also been used to investigate and discover signaling transduction pathways in various plants (Sheen, 2001; Asai et al., 2002; Baena-Gonzalez et al., 2007; Müller and Sheen, 2008; Boudsocq et al., 2010; Fraiture et al., 2014). Even though protoplast isolation has been reported in *Phalaenopsis* orchids, the requirement of callus induction for protoplast preparation makes the procedure difficult to implement (Kobayashi et al., 1993; Shrestha et al., 2007). A recent study reported a protoplast-based transient gene expression protocol in a *Phalaenopsis* hybrid cultivar (Li et al., 2018). Inconveniently, this protocol requires young leaves of shoots induced from flower nodal buds that may not be readily available in different *Phalaenopsis* cultivars. Also, the transfection efficiency is below 50%, a minimum threshold (Yoo et al., 2007) required to obtain reliable and repeatable data for molecular studies. Furthermore, the protoplast transient expression protocol and its broad usage for functional genomics studies have not been rigorously tested. To simplify the protoplast preparation procedure and establish a system for rapid gene regulation studies for orchids, here an optimized petal-based protoplast isolation and transient expression protocol was established. This protoplast transient expression system worked successfully in investigating subcellular localization of proteins and protein–protein interaction. In addition, our results demonstrate its amenability for studies of transcription activity of PaE2F3/PaDP transcription factors and auxin response. Taken together, development of an orchid protoplast transient expression assay provides a versatile experimental platform to enable molecular, cellular, and functional studies of orchids. Because experimental settings and empirical experience are provided, the testing parameters may easily be adjusted for different orchid species.

# MATERIALS AND METHODS

## Plant Materials and Growth Conditions

Tetraploid *Phalaenopsis aphrodite* subsp. *formosana* (m1663) plants in 3.5-inch pots were purchased from Chain Port Orchid Nursery (Ping Tung, Taiwan). Plants were grown and maintained as previously described (Chen and Fang, 2016). Under flowering inductive conditions [alternating 12 h light (23°C)/12 h dark (18°C) cycles], the floral stalks (∼0.5 to 1 cm long) became visible approximately 2 months after treatment. The first open flower appeared approximately 3–4 months after treatment.

## Protoplast Isolation

Fully open flower petals were used for protoplast isolation. Petal protoplasts were successfully isolated from petals collected 1–15 days after full bloom. Orchid petals were cut into 0.5–1.0-mm strips using a fresh sharp razor blade. The petal strips were transferred to a petri dish containing freshly prepared enzyme solution. The enzyme solution was made as follows: 1% (w/v) cellulase R-10 (Yakult Pharmaceutical), 0.25% (w/v) macerozyme R-10 (Yakult Pharmaceutical), 0.7 M (or otherwise described in the Results) mannitol (Sigma), 20 mM KCl (Sigma), and 20 mM MES (pH 5.7, Sigma) were warmed up to 55°C for 10 min to enhance enzyme solubility and to inactivate DNase and protease. The enzyme solution was allowed to cool to room temperature before 10 mM $CaCl_2$ and 0.1% BSA (Sigma cat #A7906) were added. The enzyme mixture was then filtered and sterilized by 0.45 μm Millex-HP filter (Millipore). The petal strips were then completely submerged in the enzyme mixture and allowed to digest without agitation in the dark for approximately 16 h (or as described in the section "Results"). Carbenicillin was added to a final concentration of 50 μg/ml to avoid bacterial contamination. Adding carbenicillin during the protoplast preparation is strongly recommended for petals collected from the greenhouse.

After digestion, the enzyme mixture was gently agitated to release the protoplasts and the protoplast/enzyme suspension was diluted with equal volume of wash and incubation solution (WI-0.7) that contained 0.7 M mannitol (or as described in the section "Results"), 20 mM KCl, and 4 mM MES (pH 5.7). The protoplast/enzyme solution was then filtered through a 100-μm nylon mesh (BD Falcon) to remove tissue debris. (Note: the mesh is normally kept in 95% ethanol and rinsed with WI-0.7 solution before use). The flow-through was then centrifuged at 200 *g* for 2 min in a desktop centrifuge (Eppendorf 5810R) to pellet the protoplasts. The acceleration ramp was set to 2 and deceleration ramp was set to 0. The supernatant was removed and the pellet was gently resuspended in 3 ml WI-0.7 solution. The protoplast suspension was washed gently one more time with 3 ml WI-0.7 solution. The cell concentration was measured using a hemocytometer. The protoplast suspension was kept on ice for 30 min. The protoplast suspension was briefly centrifuged at 200 *g*

to pellet protoplasts. WI-0.7 solution was carefully removed and the pellet was resuspended in pre-chilled MMG-0.7 solution (0.7 M mannitol, 15 mM $MgCl_2$, and 4 mM MES, pH5.7) to obtain a cell concentration of approximately $1.0 \times 10^6$/ml. Based on our protocol, 20 ml of enzyme solution can digest up to 20 orchid petals (10 flowers) and yield 5 ml of $\sim 1.0 \times 10^6$/ml protoplasts before transfection. Approximately $1.0 \times 10^6$ cells (from 4 petals) are required for each RNA preparation.

## DNA-PEG-Calcium Transfection

A modified PEG-mediated protoplast transfection protocol (Yoo et al., 2007) was used. Orchid protoplasts were adjusted to a final concentration of $\sim 0.5–2 \times 10^5$ cells/ml with MMG-0.7 solution. Twenty microliters of 10 to 20 μg plasmid DNA was mixed with 200 μl protoplasts ($\sim 1–4 \times 10^4$ cells) in MMG-0.7 solution and an equal volume (220 μl) of freshly prepared PEG-calcium transfection solution was added. PEG-calcium transfection solution (40% w/v PEG4000, 0.6 M mannitol, and 0.1 M $CaCl_2$) was prepared as follows: PEG4000 (Fluka, cat. no. 81240) and mannitol were first dissolved in water by heating up to 60°C for approximately 10–20 min. After the solution was cooled down to room temperature, $CaCl_2$ was added. The DNA-PEG-calcium-protoplast solution was mixed gently and incubated at room temperature for 6–10 min. After transfection, the transfected protoplast mixture was immediately diluted with 2–3 ml of WI-0.7 solution and centrifuged at 200 *g* for 2 min. Then the supernatant was carefully removed. The transfected protoplasts were washed one more time with 2–3 ml of WI-0.7 solution followed by centrifugation. The protoplasts were gently resuspended in 1 ml WI-0.7 solution. The protoplast mixture was carefully removed and the transfected protoplasts were incubated in WI-0.7 solution in 12-well tissue culture plates or Eppendorf tubes pre-rinsed with 1% BSA solution for the desired amount of time before further analysis. It is recommended that $\sim 1 \times 10^6$ cells/ml are used and the amount of plasmid DNA is scaled up if transfected protoplasts need to be harvested for RNA or protein extraction.

For hormone treatment, transfected protoplast cells were treated with 1 μM 1-naphthaleneacetic acid (NAA), 100 nM *trans*-zeatin, 50 μM gibberellic acid 3 ($GA_3$), or 100 μM abscisic acid (ABA) (Müller and Sheen, 2008) for 2 h before microscopic observation. Fluorescence images were photographed on a LSM 710 Confocal Microscope (Zeiss) or Zeiss Axio Scope A1 microscope equipped with an AxioCam HRc camera.

## Protoplast Viability Test

Propidium iodide (PI) was dissolved in 0.65 M mannitol to make 0.5 mg/ml stock solution. Fluorescein diacetate (FDA) was dissolved in acetone to make 5 mg /ml stock solution. A total of 20 μl of PI and 20 μl FDA stock solutions were added in 1 ml 0.65 M mannitol as the staining solution (this has to be made fresh). For staining, 10 μl of staining solution was added into 20 μl of isolated protoplast cells and incubated at room temperature for 1–2 min. The living protoplast cells (green, stained with FDA) and dead cells (red, stained with PI) were visualized and photographed by LSM 710 confocal microscope (Zeiss). Five to twelve snapshots were taken for each sample. For viability measurement, at least 150 protoplast cells were examined from each sample. Viability was measured as green cells/green + red cells × 100%. These experiments were repeated at least three times.

## RNA Isolation and Quantitative RT-PCR

The transfected protoplasts were flash frozen in liquid nitrogen and stored in a freezer at −80°C. RNA was isolated using RNA extraction reagent (3-Zol, MDBio, Inc.) according to the manufacturer's instructions. To remove DNA, total RNA was treated with RNase-free DNase (Qiagen) followed by RNeasy column purification (Qiagen) according to the manufacturer's instruction.

RNA (0.4 to 1 micrograms) was reverse transcribed in the presence of a mixture of oligo dT and random primers (9:1 ratio) using the GoScript Reverse Transcription System (Promega) as described previously (Lin H.Y. et al., 2014). Ten microliters of quantitative RT-PCR reaction contained 2.5 μl of 1/20 diluted cDNA, 0.2 μM of primers, and 5 μl of 2X KAPA SYBR FAST master mix (KAPA Biosystems). Real-time RT-PCR was carried out using a Bio-Rad CFX96 (Bio-Rad). The following program was used for amplification: 95°C for 1 min, 40 cycles of 95°C for 5 s, and 58°C for 20 s. PCR was performed in triplicate, and the experiments were repeated with RNA isolated from three independent samples. Fold change in expression was calculated as $2^{-\Delta\Delta CT}$. A melting curve of each PCR was examined to ensure no spurious products were present. Primer pairs used for quantitative PCR are listed in Supplementary Table S1. Because expression level of ubiquitin (*PaUBI1*) remained relatively constant across the tissues examined (Lin H.Y. et al., 2014), it was used as an internal control.

# RESULTS

## Protoplast Isolation

Petal protoplast isolation has been reported in *Dendrobium* orchid (Hu et al., 1998). We therefore chose petals of *Phalaenopsis aphrodite* as our starting materials. The release and integrity of petal protoplasts was visually inspected in cellulose- and macerozyme-containing enzyme solution adjusted to different osmotic conditions (in 0.4 M, 0.6 M, 0.7 M, or 0.8 M mannitol). Protoplasts were successfully released from petal tissues and remained intact after overnight (∼16 h) enzyme digestion (**Figure 1A**) regardless of the concentrations of mannitol tested (**Figure 1B**). To survey the viability of the petal protoplasts, PI and FDA, which mark dead and live cells, respectively (Huang et al., 1986), were used to stain the isolated protoplasts. Petal tissue digested with enzymes for 16 h gave a better yield than that digested for only 8 h (**Table 1**). Moreover, the protoplast viability was not compromised after 16 h of digestion (**Table 1**). Approximately 90–94% of protoplasts were viable after resuspension in WI buffer supplemented with various concentrations of mannitol (**Table 2** and **Figure 1C**). More than 80% of protoplasts remained viable after resuspension in MMG-0.6 and MMG-0.7 solution (**Table 2** and **Figure 1D**). Approximately 75.3% and 77.5% of protoplast cells prepared

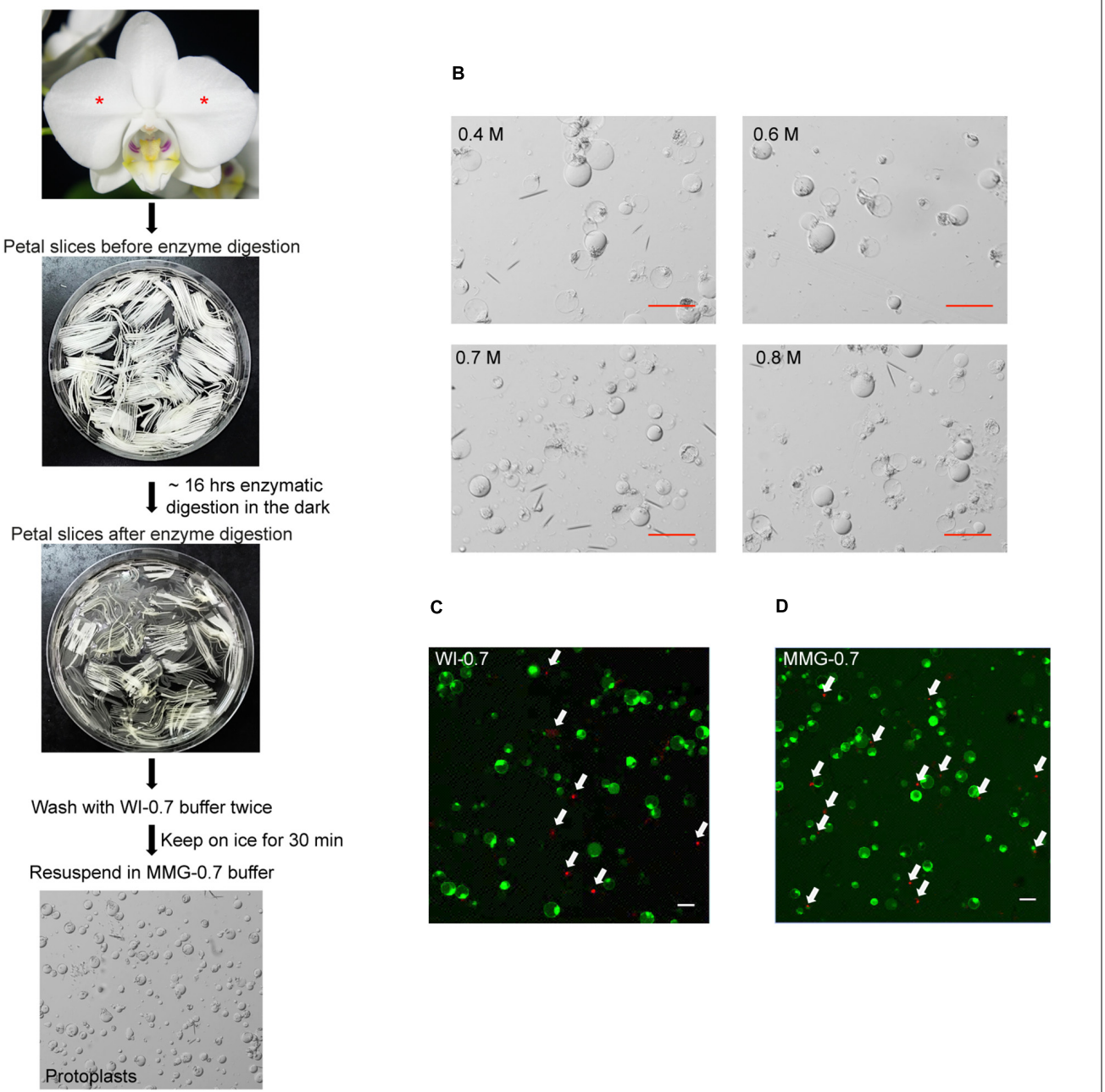


**FIGURE 1 |** Isolation of protoplasts from petals of *P. aphrodite*. **(A)** A flowchart showing the procedure of protoplast isolation. Asterisks mark the petals used for protoplast isolation. **(B)** Protoplast morphology remained intact in enzyme solution supplemented with 0.4 M, 0.6 M, 0.7 M, or 0.8 M mannitol. **(C)** A snapshot of cell viability test after resuspending cells in WI-0.7 solution. **(D)** A snapshot of cell viability test after resuspending cells in MGG-0.7 solution. White arrows indicate the dead cells stained by PI. Red and white scale bars, 50 μm.

in 0.6 M and 0.7 M mannitol-based solution, respectively, remained viable after the transfection procedure (**Table 2**). Even though there was no drastic difference in cell viability with preparation in 0.6 M or 0.7 M mannitol-based buffer, 0.7 M mannitol seemed to work slightly better in protecting cells during the transient expression procedure. Therefore, 0.7 M mannitol was chosen for the rest of the experiments. Under this condition, the yield of viable protoplasts from one petal after transfection was estimated to be approximately $1.9 \times 10^5$ cells [$2.5 \times 10^5$ cells (number of protoplast cells per petal) $\times$ 77.5% (viability of transfected protoplast prepared in 0.7 M mannitol condition)]. The size of petal protoplasts was

**TABLE 1 |** Effect of duration of enzyme digestion on protoplast yield and viability.

| Digestion duration in enzyme solution supplemented with 0.7 M mannitol | Protoplast Yield ($\times 10^5$ cells/ petal) | Viability (%) |
|---|---|---|
| 8 h | 2.2 ± 0.4 | 89.1 ± 3.3 |
| 16 h | 6.1 ± 0.5 | 90.1 ± 2.4 |

**Standard deviations were derived from three independent experiments.*

**TABLE 2 |** Effect of mannitol concentration on protoplast viability during the isolation procedure.

| After enzyme digestion and resuspension in WI based buffer | Viability (%) |
|---|---|
| 0.4 M | 90.7 ± 5.7 |
| 0.6 M | 91.6 ± 4.5 |
| 0.7 M | 91.1 ± 6.1 |
| 0.8 M | 94.1 ± 2.1 |
| **After washing and resuspension in MMG based buffer** | **Viability (%)** |
| 0.4 M | 77.3 ± 10.5 |
| 0.6 M | 81.1 ± 8.2 |
| 0.7 M | 81.3 ± 0.4 |
| 0.8 M | 73.9 ± 9.2 |
| **After transfection** | **Viability (%)** |
| 0.4 M | 66.6 ± 2.6 |
| 0.6 M | 75.3 ± 4.2 |
| 0.7 M | 77.5 ± 2.4 |
| 0.8 M | 67.9 ± 12.4 |

**Standard deviations were derived from at least three independent experiments.*

calculated and it ranged from 20 to 50 μm in diameter with an average of approximately 34 ± 7.1 μm in diameter (Supplementary Datasheet S1). These results demonstrated the feasibility of using orchid protoplasts for further molecular biology analyses.

Leaves are readily accessible and mesophyll protoplast cells have been successfully isolated from leaf tissues of various plant species (Sheen, 2001; Chen et al., 2006; Yoo et al., 2007; Mazarei et al., 2008; Lung et al., 2011; Masani et al., 2014; Nanjareddy et al., 2016; Shen et al., 2017). Therefore, we also tested the conditions for mesophyll protoplast preparation. The youngest fully expanded leaves were used for this test. Similarly, different osmotic conditions of enzyme solution (in 0.4 M, 0.6 M, 0.7 M, or 0.8 M mannitol) were tested and the integrity of leaf mesophyll protoplasts during enzyme digestion was inspected under a microscope over time. Unlike petal protoplasts, the integrity of mesophyll protoplasts declined quickly over time. For the cells that retained relative integrity, the interior content of protoplasts including chloroplasts was gradually concentrated and pushed to one side of the cell (Supplementary Figure S1A). Mesophyll protoplast cells started to rupture after 2 h of incubation in enzyme solution (Supplementary Figure S1B). The cell integrity was completely disrupted after transfection (Supplementary Figure S1C).

## Protoplast Transient Expression System Enables Subcellular Localization and Bimolecular Fluorescence Complementation Studies

To test whether petal protoplasts were suitable for subcellular localization studies, nuclear and plasma membrane markers were transformed into protoplasts by PEG-mediated transformation (see Methods). As expected, nuclear marker mCherry-VirD2NLS (Lee et al., 2008), which carries the nuclear localization signal, started to appear in the nucleus 4 h after transfection (**Figure 2A**) and accumulated in almost all the inspected nuclei 20 h after transfection (**Figure 2B**). Unlike biolistic transient assay where cells with fluorescence signals were sparsely distributed on the petal due to uneven spraying of the gold particles (Supplementary Figure S2), the majority of protoplasts (>80%, Supplementary Datasheet S2) had fluorescence signals, indicating protoplast-based transfection is relatively homogenous and enables broader molecular and biochemical analyses of the transgene-encoded protein product (**Figure 2B**). This transfection efficiency is almost equivalent or better than protoplast transfection efficiency reported in the model systems (Yoo et al., 2007; Wu et al., 2009; Faraco et al., 2011). In addition, the plasma membrane marker aquaporin AtPIP2a-YFP (Nelson et al., 2007) was correctly targeted to the plasma membrane (**Figure 2C**). These experiments demonstrated that *Phalaenopsis* orchid protoplasts are suitable for protein localization studies.

The application of petal protoplasts to bimolecular fluorescence complementation (BIFC) analysis for protein–protein interaction study was also tested. Cyclin-dependent kinases (CDKs) are central cell-cycle regulators whose activities are regulated by physical interaction with the cell-cycle phase specific cyclins (CYCs) (Morgan, 2007). To test the feasibility of using orchid protoplasts for protein–protein interaction studies, the construct containing the *PaCDKA* gene fused N-terminal half of the *EYFP* (*N-(nEYFP)-CDKA1*) was co-transfected with a construct containing *PaCYCD3;1* fused to a C-terminal half of the *EYFP* (*N-cEYFP-CYCA3;1*). The direct interaction of PaCDKA and PaCYCD3;1 scored by the presence of yellow fluorescence was verified by confocal microscopy (**Figure 3A** and Supplementary Figure S3A). As a negative control, the construct containing *N-(nEYFP)-CDKA1* was co-transfected with only the C-terminal half of the EYFP (*N-cEYFP*) construct. No fluorescence was detected when the *N-cEYFP* construct was co-transfected with the *N-(nEYFP)-CDKA1* construct (**Figure 3B** and Supplementary Figure S3B). This is consistent with biolistic-based BIFC assay in petal cells (Lin H.Y. et al., 2014).

## PaE2F3/PaDP2 Activates Expression of S- and G2-Phase Cell Cycle Genes

The cell division cycle is fundamental for the growth of organisms (Hall et al., 2004). In plants, cell cycle genes are duplicated and diverged to accommodate complex developmental programs (Gutierrez, 2016). Our previous study showed that expression of the core cell cycle genes is coordinately regulated from ovule development to embryogenesis during sexual reproduction

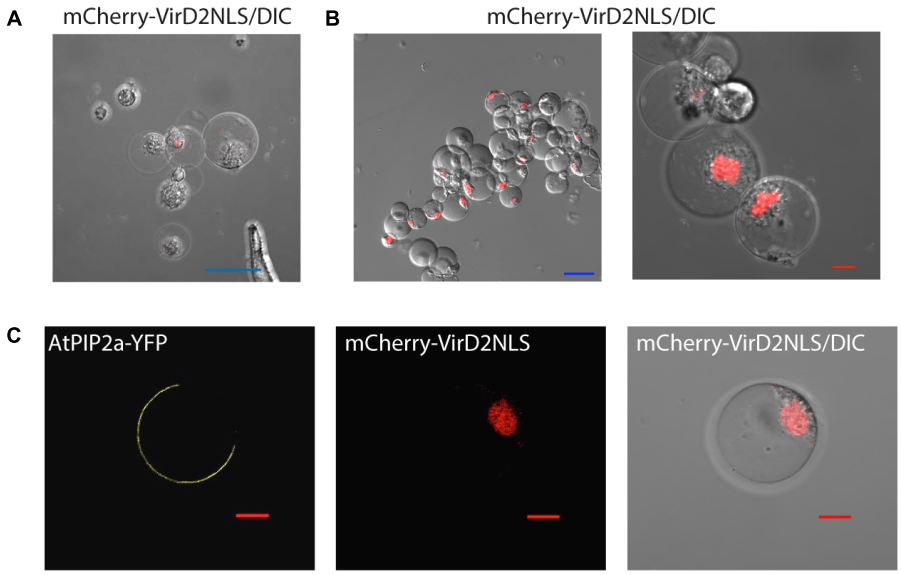


**FIGURE 2 |** Subcellular localization of protein markers. **(A)** Nuclear localization of mCherry-VirD2NLS marker 4 h after transfection. **(B)** The vast majority of cells expressed the nuclear marker 20 h after transfection. **(C)** Plasma membrane localization of AtPIP2a-YFP aquaporin marker. Note that the protoplasts were co-transfected with AtPIP2a-YFP and mCherry-VirD2NLS markers. Blue scale bar, 50 μm; red scale bar, 10 μm. DIC, differential interference contrast image of cells superimposed with the fluorescence marker.

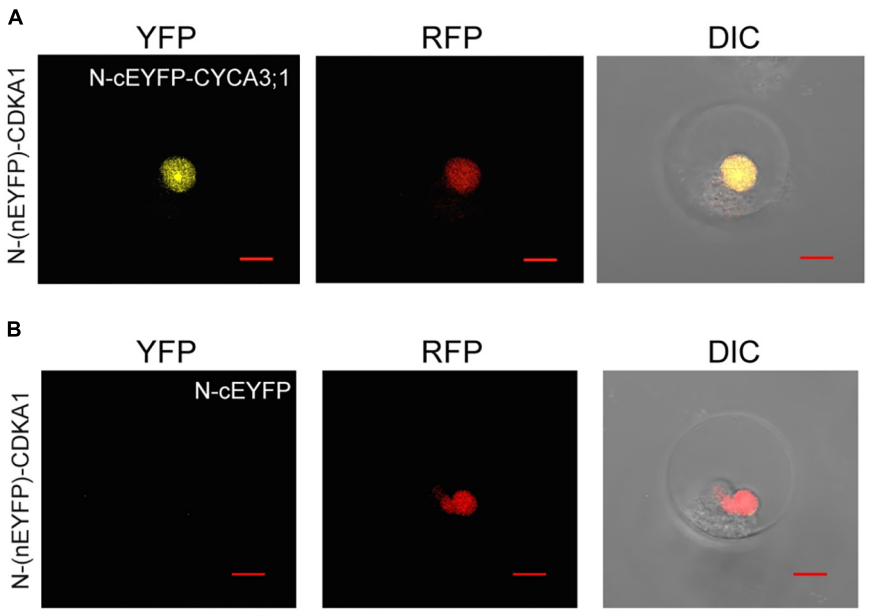


**FIGURE 3 |** Protein–protein interactions of CDKA1/CYCA3;1 proteins visualized using BiFC. **(A)** The BiFC signal was detected in protoplast cells co-transfected with *N-(nEYFP)-CDKA1* and *N-cEYFP-CYCA3;1* constructs. **(B)** No signal was detected in protoplast cells co-transfected with *N-(nEYFP)-CDKA1* and *N-cEYFP* constructs. mCherry-VirD2NLS was used as a nuclear marker. DIC, differential interference contrast images of cells superimposed with YFP and RFP channels. Scale bar, 10 μm.

in *P. aphrodite* (Lin H.Y. et al., 2014). Moreover, transcripts associated with cell cycle-associated biological processes, such as DNA replication initiation, cell division, and regulation of the cell cycle are strongly enriched in interior ovary tissues 30–40 days after pollination (DAP) when ovules are developing (Fang et al., 2016). Among the enriched cell cycle regulators identified, *PaE2F3* encodes an evolutionarily conserved transcription factor that heterodimerizes with the DP protein to control G1/S transition as cells enter the division cycle. Being the cell cycle activator, E2F/DP transcription factor is reported to activate

genes involved in DNA replication and mitotic functions (Ishida et al., 2001; Ramirez-Parra et al., 2003; Fung and Poon, 2005; Vandepoele et al., 2005; Dante et al., 2014). Furthermore, overexpression of *Arabidopsis* E2F (AtE2Fb) and its dimerization partner AtDPa is sufficient to activate downstream cell cycle genes and drive cell proliferation in differentiated tissues (De Veylder et al., 2002; Rossignol et al., 2002; Magyar et al., 2005; Sozzani et al., 2006). To investigate the potential targets of PaE2F3, the expression levels of selected cell cycle regulators enriched simultaneously in ovary tissues at 30–40 DAP (**Table 3**) were analyzed in protoplast cells co-transfected with *PaE2F3* and its interaction partner *PaDP1* or *PaDP2* (Lin H.Y. et al., 2014).

After transfection, overexpression of *PaE2F3* and *PaDP1* was verified by quantitative RT-PCR analysis (**Figure 4A**). Overexpression of *PaE2F3* and *PaDP1* resulted in an increase in expression levels of *PaPCNA1* in three independent experiments (**Figure 4A**), but did not have significant effects on expression of *PaCYCB2;1*, *PaCYCA1:1*, *PaCYCA2:3*, *PaCYCA3:2*, *PaCYCB1:1*, and *PaCYCD1:3* (Supplementary Figure S4A). Because *PaCYCB1;2* mRNA could not be reliably detected in transfected protoplast cells, it was omitted from further analysis.

For protoplast cells transfected with *PaE2F3* and *PaDP2* constructs, accumulation of *PaE2F3* and *PaDP2* mRNAs was also verified by quantitative RT-PCR analysis (**Figure 4B**). Overexpression of *PaE2F3* and *PaDP2* up-regulated expression of *PaPCNA1* and *PaCYCB2;1* (**Figure 4B**) but did not have significant effects on accumulation of *PaCYCA1:1*, *PaCYCA2:3*, *PaCYCA3:2*, *PaCYCB1:1*, and *PaCYCD1:3* (Supplementary Figure S4B). Activation of *PaPCNA1* and *PaCYCB2;1* by co-overexpression of *PaE2F3* and *PaDP2* was validated in three independent experiments (**Figure 4B**). Hence, our data provide evidence that *PaPCNA1* and *PaCYCB2;1* are the potential targets of PaE2F3.

## The *DR5v2* Reporter Is Responsive to Auxin in *Phalaenopsis* Protoplasts

To assess the potential of using *Phalaenopsis* protoplasts to investigate the hormone response, the auxin reporter *DR5v2* (Liao et al., 2015) was transfected into the petal protoplasts. While treatment with a synthetic auxin, NAA, resulted in accumulation of GFP and ntdTomato florescent proteins in the nuclei, only the background signal was detected in the absence of NAA treatment (**Figure 5A** and Supplementary Figure S5). Furthermore, treatment with trans-zeatin, GA, or ABA had no effect on accumulation of GFP and ntdTomato florescent proteins in the transfected protoplasts (**Figure 5B** and Supplementary Figure S5). Taken together, these results demonstrated that *DR5v2* reporter responds to the auxin signal in petal protoplasts and suggests the potential of using *DR5v2* reporter to map the auxin regulatory pathway in *Phalaenopsis* orchids.

# DISCUSSION

Protoplast transient expression systems are a powerful tool for studying the molecular mechanisms underlying signal transduction pathways. Here, we described a streamlined protocol for petal protoplast isolation and polyethylene glycol-calcium transfection for *P. aphrodite* (**Figure 1A**) and demonstrated its feasibility for analyses of protein subcellular localization and protein–protein interaction. Moreover, our reported transfection efficiency (> 80%) is significantly improved in comparison to the transfection efficiency of *Phalaenopsis* protoplasts reported recently (Li et al., 2018). The ability to isolate large numbers of viable protoplasts (**Table 1**), high transfection efficiency, and high numbers of viable transfected cells (**Table 2**) enable

**TABLE 3 |** Comparative transcript abundances of cell cycle genes in reproductive tissues of *P. aphrodite* by RNA-sequencing analysis.

| | | FPKM values | | | | | | | | | | |
|---|---|---|---|---|---|---|---|---|---|---|---|---|
| **Transcript ID** | **Annotation** | **30/40 DAP** | **50/60 DAP** | **70/80 DAP** | **90/100/120 DAP** | **140/160 DAP** | **180/200 DAP** | **PLB** | **Protocorm** | **Young leaves** | **Stalk buds** | **Floral stalks** |
| **E2Fs and DPs** | | | | | | | | | | | | |
| orchid.id113590.tr318945 | PaE2F1 | 6.7 | 4.3 | 2.9 | 7.8 | 2.2 | 1.5 | 5.0 | 7.0 | 3.8 | 3.0 | 3.7 |
| orchid.id117614.tr38827 | PaE2F2 | 3.1 | 1.4 | 1.5 | 1.5 | 1.3 | 2.0 | 0.3 | 2.5 | 1.1 | 0.7 | 0.9 |
| orchid.id1949.tr77229 | PaE2F3 | 14.2 | 6.4 | 2.7 | 1.8 | 5.5 | 4.8 | 3.2 | 5.2 | 3.4 | 3.4 | 4.6 |
| orchid.id42993.tr191185 | PaE2F4 | 1.3 | 0.9 | 1.3 | 0.9 | 0.8 | 0.5 | 1.7 | 2.6 | 2.8 | 2.4 | 2.9 |
| orchid.id113906.tr107393 | PaDP1 | 53.0 | 48.1 | 54.5 | 60.2 | 32.4 | 37.7 | 47.5 | 41.7 | 38.6 | 43.1 | 42.6 |
| orchid.id123685.tr127191 | PaDP2 | 4.4 | 4.5 | 3.1 | 3.4 | 3.0 | 3.0 | 1.2 | 1.4 | 3.1 | 1.9 | 2.8 |
| **Cell cycle genes enriched at 30/40 DAP** | | | | | | | | | | | | |
| orchid.id130751.tr142269 | PaPCNA1 | 44.1 | 27.2 | 4.9 | 3.9 | 11.1 | 5.7 | 38.1 | 22.2 | 18.0 | 15.4 | 28.7 |
| orchid.id93462.tr632091 | PaCYCA1;1 | 22.2 | 16.3 | 0.4 | 2.0 | 6.9 | 4.5 | 5.3 | 25.9 | 17.7 | 0.2 | 7.8 |
| orchid.id104694.tr178804 | PaCYCA2;3 | 20.3 | 12.0 | 1.8 | 1.8 | 7.6 | 15.1 | 7.5 | 9.2 | 9.2 | 6.0 | 8.5 |
| orchid.id119353.tr176450 | PaCYCA3:2 | 11.3 | 6.3 | 1.4 | 0.2 | 0.4 | 0.1 | 2.8 | 5.1 | 4.3 | 2.6 | 7.0 |
| orchid.id130531.tr130848 | PaCYCB1;1 | 27.5 | 22.3 | 1.1 | 2.4 | 1.8 | 0.1 | 1.7 | 3.2 | 11.5 | 14.9 | 31.9 |
| orchid.id3686.tr138153 | PaCYCB1;2 | 4.2 | 5.7 | 0.2 | 0.2 | 0.0 | 0.0 | 0.1 | 0.2 | 3.2 | 0.0 | 2.1 |
| orchid.id100343.tr56122 | PaCYCB2;1 | 34.8 | 26.1 | 0.2 | 1.2 | 0.8 | 0.0 | 2.8 | 4.2 | 8.9 | 0.3 | 12.5 |
| orchid.id121744.tr208045 | PaCYCD1;3 | 7.7 | 6.0 | 1.9 | 0.6 | 0.6 | 0.6 | 0.6 | 0.3 | 5.2 | 0.2 | 2.8 |

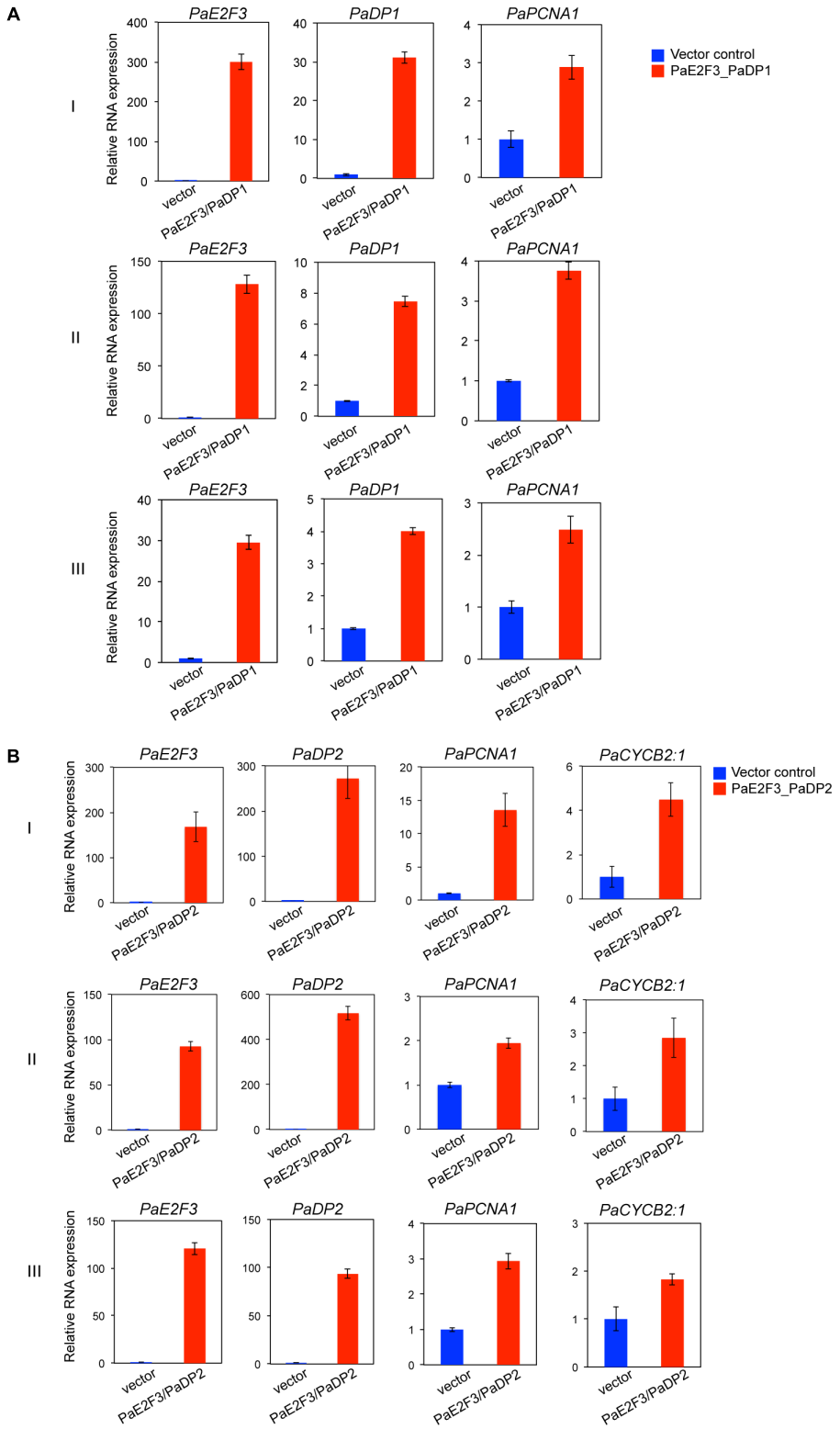


**FIGURE 4 |** Overexpression of PaE2F3 and PaDP2 up-regulates expression of the specific cell cycle genes. **(A)** Validation of expression of *PaE2F3* and *PaDP2* mRNAs in protoplast cells co-transfected with the *PaE2F3* and *PaDP2* constructs. **(B)** Relative expression levels of *PaPCNA1* and *PaCYCB2:1* in protoplast cells co-transfected with the *PaE2F3* and *PaDP2* constructs. Protoplasts transfected with the empty vectors were used as a negative control. Expression levels of the indicated genes from protoplasts transfected with the empty vectors (vector) were arbitrarily set to be one. Three independent experiments I, II, and III are shown.

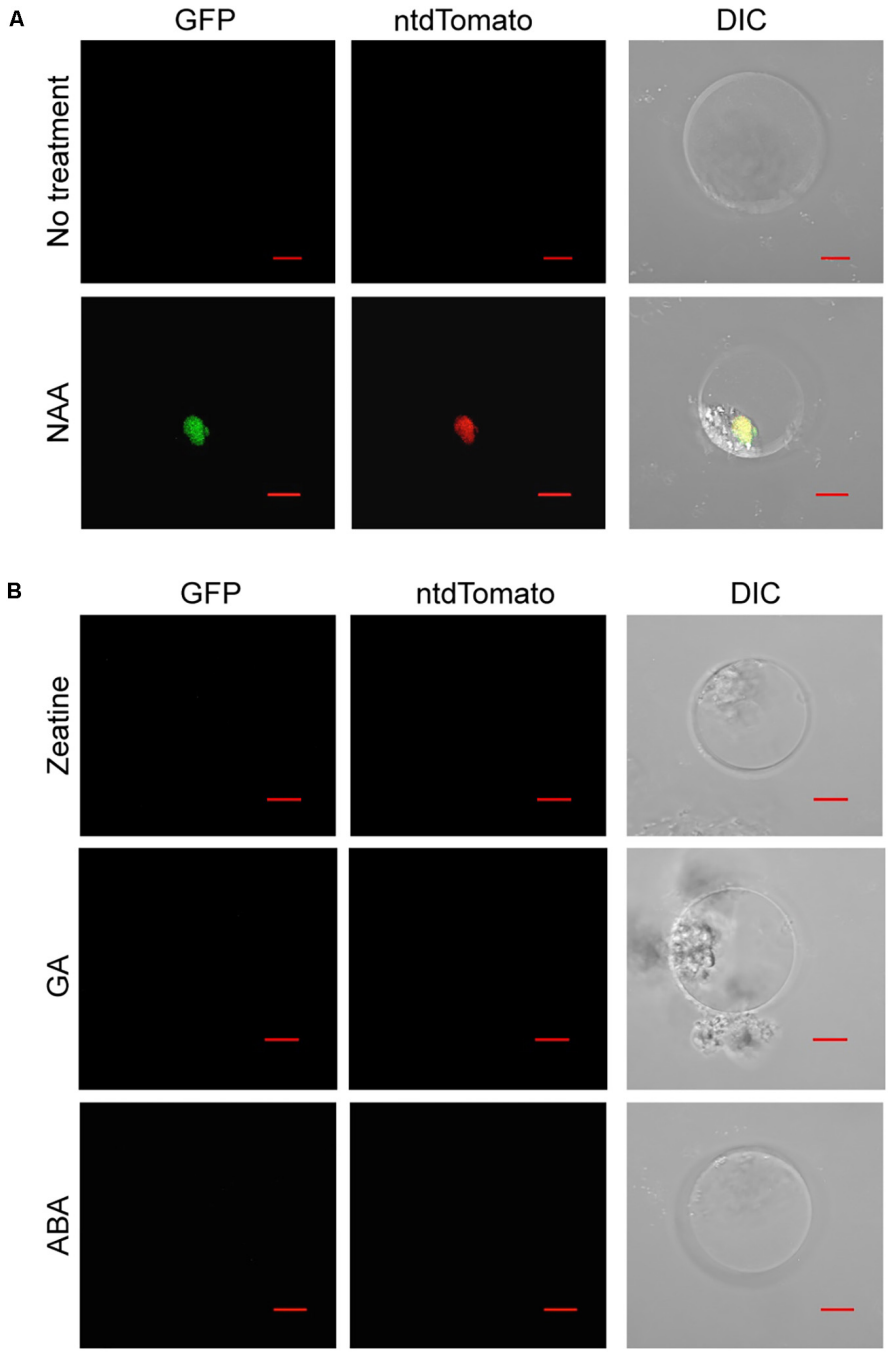


**FIGURE 5 |** Auxin activates the *DR5v2* reporter in *Phalaenopsis* protoplast transient expression assay. **(A)** NAA activated *DR5v2* reporter. **(B)** Zeatin, GA, and ABA did not activate *DR5v2* reporter. DIC, differential interference contrast images of cells superimposed with GFP and ntdTomato signals. Scale bar, 10 μm.

construction of a hierarchical gene regulatory pathway and studies of hormone responses. Hence, this protocol provides a useful platform for in-depth studies of gene functions and molecular networks that were previously difficult in *Phalaenopsis* orchids. Recently, protoplast transient expression systems have been extended to studies on dissection of miRNA pathways (Martinho et al., 2015), protein-DNA binding (Lee et al., 2017), microbe-associated molecular patterns-triggered immunity (Fraiture et al., 2014; Kanofsky et al., 2016), ribonuclease-mediated mRNA decay (Hayashi et al., 2016), and auxin-mediated transcriptional regulatory networks (Wehner et al., 2017). It is therefore conceivable that our established protocol may be applied to diverse aspects of orchid biology studies.

## Co-expression of *PaE2F3*/*PaDP1* and *PaE2F3*/*PaDP2* Induce Expression of *PaPCNA1*

PaE2F3 has been shown to interact with PaDP1 and PaDP2 in yeast two-hybrid and petal transient expression assays (Lin H.Y. et al., 2014). As proof-of-principle for gene regulation study, we found that transient overexpression of *PaE2F3*/*PaDP2* transcription factor was capable of up-regulating expression of *PaPCNA1* and *PaCYCB2;1* that are co-expressed with *PaE2F3* in ovary tissues of *P. aphrodite*. Transient overexpression of *PaE2F3*/*PaDP1* transcription factor, on the other hand, only up-regulated expression of *PaPCNA1* and did not seem to have a significant effect on the expression of the other genes tested. It is possible that PaE2F3 interacts with different partners to regulate both overlapping and distinct sets of cell cycle genes in *P. aphrodite*.

It is not surprising to see that co-expression of *PaE2F3* and *PaDPs* induced accumulation of *PaPCNA1* mRNA because PCNA, which is required for DNA replication in both plant and animal systems, is identified as the direct downstream target of E2F/DP protein (Yamaguchi et al., 1995; Egelkrout et al., 2002; Kosugi and Ohashi, 2002; Vandepoele et al., 2005). It is intriguing to discover that PaE2F3/PaDP2 transcription factor induced accumulation of B-type cyclin, *PaCYCB2;1*, which is normally considered to be an M phase gene (Van Leene et al., 2011). The functional roles of E2F/DP at the G2-M checkpoint and mitotic activity have been reported in animals (Ren et al., 2002; Li et al., 2012). In *Arabidopsis*, E2Fa-DPa transcription factor has been reported to regulate G2-M phase gene *CDKB1;1* to control stomatal development (Boudolf et al., 2004). Our findings illustrate a potential PaE2F3/PaDP2-mediated cross talk between the G1-S and G2-M stages in ovary development of *P. aphrodite* and support the role of E2F in G2-M phase. It will be interesting to investigate how PaE2F3/PaDP2 regulates expression of *PaCYCB2;1* to coordinate the cell cycle progression in *Phalaenopsis* orchids. Taken together, our data demonstrate the possibility of using the orchid protoplast transient expression system to quickly screen for potential E2F/DP downstream targets in developing ovary tissues.

## The Auxin Reporter *DR5v2* Is Functional in *Phalaenopsis* Orchids

Auxin is reported to play important roles in orchid development (Arditti et al., 1971; Tsavkelova et al., 2007; Novak and Whitehouse, 2013; Novak et al., 2014). However, it is not clear how auxin responses are regulated to coordinate specialized orchid developmental programs. *DR5v2* reporter assay provides evidence that petal protoplasts may be potentially conducive to dissecting the auxin response pathway of *Phalaenopsis* orchids. In addition, the orchid protoplast transient expression system could be used to assess the transcriptional responses of auxin signaling molecules or regulatory components.

## Orchid Protoplasts: One for All?

In addition to *Phalaenopsis* orchids, petal protoplasts have successfully been used for gene functional studies in petunia and rose (Faraco et al., 2011; Hirata et al., 2012) supporting the general applicability of the petal system. However, conceivable limitations of the petal protoplast transient expression system may exist. It is reported that protoplasts retain their differentiation state and gene expression program within the time frame of transient expression experiments (Faraco et al., 2011; Lin Y.C. et al., 2014). Accordingly, protoplasts with the right cellular context providing the ideal gene expression program may be required to address tissue- or context-specific questions. It is possible that petal protoplasts are not suitable to analyze light- and sugar-dependent responses of the photosynthetic genes. In such cases, results should be interpreted with caution. It is presently difficult to isolate active protoplasts from mature leaf tissues, the most used source for protoplast isolation. During the attempts to isolate mesophyll protoplasts, protoplasts collapsed hours after isolation regardless the mannitol concentration tested. It is not clear why leaf mesophyll protoplasts are sensitive to the isolation procedure. Generally, protoplasts rupture in hypotonic solution and collapse in hypertonic solution (Ohshima and Toyama, 1989). It is possible that the cell wall of mesophyll cells releases phytotoxic factors that poison the isolated protoplasts (Hahne and Lorz, 1988). The presence of abundant calcium oxalate crystals may also contribute to the damage to protoplasts. The establishment of orchid protoplast transient expression protocols for different tissue types in the future may be important to address tissue- or context-specific questions.

Protoplast-based high-throughput systems have been established for dissection of signaling pathways, analysis of transcription factor functions, and identification of kinase-associated phosphoisoforms (Wehner et al., 2011; Zhang et al., 2015; Dory et al., 2016; Wehner et al., 2017). Therefore, the orchid protoplast transient expression system provides a molecular tool to characterize functions of proteins identified from open reading frames from recently released transcriptome datasets (Cai et al., 2015; Fang et al., 2016; Chao et al., 2017) and potentially allows discovery and/or validation of hierarchical gene regulatory networks. In summary, the protocol presented here will enable in-depth studies of the molecular networks governing the unique developmental processes and hormone regulating pathways in orchids and provide an alternative method to conduct functional genomic studies in *Phalaenopsis* orchids.

## AUTHOR CONTRIBUTIONS

S-CF wrote the manuscript and designed the experiments. H-YL developed the protoplast isolation and transfection system. J-CC maintained the orchid plants and did the RT-PCR experiments. All authors read and approved the final manuscript.

## FUNDING

This work was supported by the Innovative Translational Agricultural Research Grants (to S-CF); and in part by a grant

(to S-CF) from the Biotechnology Center in Southern Taiwan, Academia Sinica.

## ACKNOWLEDGMENTS

We thank Dr. Dolf Weijers for sharing the DR5v2 construct, Dr. Choun-Sea Lin for sharing the subcellular localization constructs; the AS-BCST Greenhouse and Confocal Microscopy Core Facilities for core services; Mr. Chin-Lin Chung and Ms. Yen-Ling Lin for critical reading of the manuscript; and Ms. Miranda Loney for English editing.

## SUPPLEMENTARY MATERIAL

The Supplementary Material for this article can be found online at: https://www.frontiersin.org/articles/10.3389/fpls.2018.00843/full#supplementary-material

## REFERENCES

Arditti, J., Jeffrey, D. C., and Flick, B. H. (1971). Post-pollination phenomena in orchid flowers. 3. Effects and interactions of auxin, kinetin or gibberellin. *New Phytol.* 70, 1125–1141. doi: 10.1111/j.1469-8137.1971.tb04595.x

Asai, T., Tena, G., Plotnikova, J., Willmann, M. R., Chiu, W. L., Gomez-Gomez, L., et al. (2002). MAP kinase signalling cascade in *Arabidopsis* innate immunity. *Nature* 415, 977–983. doi: 10.1038/415977a

Baena-Gonzalez, E., Rolland, F., Thevelein, J. M., and Sheen, J. (2007). A central integrator of transcription networks in plant stress and energy signalling. *Nature* 448, 938–942. doi: 10.1038/nature06069

Bory, S., Grisoni, M., Duval, M. F., and Besse, P. (2008). Biodiversity and preservation of vanilla: present state of knowledge. *Genet. Resour. Crop Evol.* 55, 551–571. doi: 10.1007/s10722-007-9260-3

Boudolf, V., Vlieghe, K., Beemster, G. T., Magyar, Z., Torres Acosta, J. A., Maes, S., et al. (2004). The plant-specific cyclin-dependent kinase CDKB1;1 and transcription factor E2Fa-DPa control the balance of mitotically dividing and endoreduplicating cells in *Arabidopsis*. *Plant Cell* 16, 2683–2692. doi: 10.1105/tpc.104.024398

Boudsocq, M., Willmann, M. R., McCormack, M., Lee, H., Shan, L., He, P., et al. (2010). Differential innate immune signalling via $Ca^{2+}$ sensor protein kinases. *Nature* 464, 418–422. doi: 10.1038/nature08794

Bu, Y., Zhao, M., Sun, B., Zhang, X., Takano, T., and Liu, S. (2014). An efficient method for stable protein targeting in grasses (*Poaceae*): a case study in *Puccinellia tenuiflora*. *BMC Biotechnol.* 14:52. doi: 10.1186/1472-6750-14-52

Bulpitt, C. J., Li, Y., Bulpitt, P. F., and Wang, J. (2007). The use of orchids in Chinese medicine. *J. R. Soc. Med.* 100, 558–563. doi: 10.1258/jrsm.100.12.558

Cai, J., Liu, X., Vanneste, K., Proost, S., Tsai, W. C., Liu, K. W., et al. (2015). The genome sequence of the orchid *Phalaenopsis equestris*. *Nat. Genet.* 47, 65–72. doi: 10.1038/ng.3149

Chao, Y. T., Yen, S. H., Yeh, J. H., Chen, W. C., and Shih, M. C. (2017). Orchidstra 2.0-a transcriptomics resource for the orchid family. *Plant Cell Physiol.* 58, 1–13. doi: 10.1093/pcp/pcw220

Chen, J. C., and Fang, S. C. (2016). The long pollen tube journey and in vitro pollen germination of *Phalaenopsis* orchids. *Plant Reprod.* 29, 179–188. doi: 10.1007/s00497-016-0280-z

Chen, S., Tao, L., Zeng, L., Vega-Sanchez, M. E., Umemura, K., and Wang, G. L. (2006). A highly efficient transient protoplast system for analyzing defence gene expression and protein-protein interactions in rice. *Mol. Plant Pathol.* 7, 417–427. doi: 10.1111/j.1364-3703.2006.00346.x

Chen, T. K., Yang, H. T., Fang, S. C., Lien, Y. C., Yang, T. T., and Ko, S. S. (2016). Hybrid-Cut: an improved sectioning method for recalcitrant plant tissue samples. *J. Vis. Exp.* 117:54754. doi: 10.3791/54754

Dante, R. A., Larkins, B. A., and Sabelli, P. A. (2014). Cell cycle control and seed development. *Front. Plant Sci.* 5:493. doi: 10.3389/fpls.2014.00493

De Veylder, L., Beeckman, T., Beemster, G. T., de Almeida Engler, J., Ormenese, S., Maes, S., et al. (2002). Control of proliferation, endoreduplication and differentiation by the *Arabidopsis* E2Fa-DPa transcription factor. *EMBO J.* 21, 1360–1368. doi: 10.1093/emboj/21.6.1360

Dory, M., Doleschall, Z., Nagy, S. K., Ambrus, H., Mészáros, T., Barnabás, B., et al. (2016). Kinase-associated phosphoisoform assay: a novel candidate-based method to detect specific kinase-substrate phosphorylation interactions in vivo. *BMC Plant Biol.* 16:204. doi: 10.1186/s12870-016-0894-1

Egelkrout, E. M., Mariconti, L., Settlage, S. B., Cella, R., Robertson, D., and Hanley-Bowdoin, L. (2002). Two E2F elements regulate the proliferating cell nuclear antigen promoter differently during leaf development. *Plant Cell* 14, 3225–3236. doi: 10.1105/tpc.006403

Fang, S. C., Chen, J. C., and Wei, M. J. (2016). Protocorms and protocorm-like bodies are molecularly distinct from zygotic embryonic tissues in Phalaenopsis aphrodite. *Plant Physiol.* 171, 2682–2700. doi: 10.1104/pp.16.00841

Faraco, M., Di Sansebastiano, G. P., Spelt, K., Koes, R. E., and Quattrocchio, F. M. (2011). One protoplast is not the other! *Plant Physiol.* 156, 474–478. doi: 10.1104/pp.111.173708

Fraiture, M., Zheng, X., and Brunner, F. (2014). An *Arabidopsis* and tomato mesophyll protoplast system for fast identification of early MAMP-triggered immunity-suppressing effectors. *Methods Mol. Biol.* 1127, 213–230. doi: 10.1007/978-1-62703-986-4_17

Fung, T. K., and Poon, R. Y. (2005). A roller coaster ride with the mitotic cyclins. *Semin. Cell Dev. Biol.* 16, 335–342. doi: 10.1016/j.semcdb.2005.02.014

Gutierrez, C. (2016). 25 Years of cell cycle research: What's ahead? *Trends Plant Sci.* 21, 823–833. doi: 10.1016/j.tplants.2016.06.007

Hahne, G., and Lorz, H. (1988). Release of phytotoxic factors from plant-cell walls during protoplast isolation. *J. Plant Physiol.* 132, 345–350. doi: 10.1016/S0176-1617(88)80118-4

Hall, M. N., Raff, M., and Thomas, G. (2004). *Cell Growth - Control of Cell Size*. Cold Spring Harbor, NY: John Inglis.

Hayashi, S., Wakasa, Y., Ozawa, K., and Takaiwa, F. (2016). Characterization of IRE1 ribonuclease-mediated mRNA decay in plants using transient expression analyses in rice protoplasts. *New Phytol.* 210, 1259–1268. doi: 10.1111/nph.13845

Hirata, H., Ohnishi, T., Ishida, H., Tomida, K., Sakai, M., Hara, M., et al. (2012). Functional characterization of aromatic amino acid aminotransferase involved in 2-phenylethanol biosynthesis in isolated rose petal protoplasts. *J. Plant Physiol.* 169, 444–451. doi: 10.1016/j.jplph.2011.12.005

Hsing, H. X., Lin, Y. J., Tong, C. G., Li, M. J., Chen, Y. J., and Ko, S. S. (2016). Efficient and heritable transformation of *Phalaenopsis* orchids. *Bot. Stud.* 57:30. doi: 10.1186/s40529-016-0146-6

Hsu, C. T., Liao, D. C., Wu, F. H., Liu, N. T., Shen, S. C., Chou, S. J., et al. (2011). Integration of molecular biology tools for identifying promoters and genes abundantly expressed in flowers of *Oncidium* Gower Ramsey. *BMC Plant Biol.* 11:60. doi: 10.1186/1471-2229-11-60

Hu, W. W., Wong, S. M., Loh, C. S., and Goh, C. J. (1998). Synergism in replication of cymbidium mosaic potexvirus (CymMV) and odontoglossum ringspot tobamovirus (ORSV) RNA in orchid protoplasts. *Arch. Virol.* 143, 1265–1275. doi: 10.1007/s007050050374

Huang, C. N., Cornejo, M. J., Bush, D. S., and Jones, R. L. (1986). Estimating viability of plant protoplasts using double and single staining. *Protoplasma* 135, 80–87. doi: 10.1007/Bf01277001

Ishida, S., Huang, E., Zuzan, H., Spang, R., Leone, G., West, M., et al. (2001). Role for E2F in control of both DNA replication and mitotic functions as revealed from DNA microarray analysis. *Mol. Cell. Biol.* 21, 4684–4699. doi: 10.1128/MCB.21.14.4684-4699.2001

Kanofsky, K., Lehmeyer, M., Schulze, J., and Hehl, R. (2016). Analysis of microbe-associated molecular pattern-responsive synthetic promoters with the parsley protoplast system. *Methods Mol. Biol.* 1482, 163–174. doi: 10.1007/978-1-4939-6396-6_11

Kidokoro, S., Watanabe, K., Ohori, T., Moriwaki, T., Maruyama, K., Mizoi, J., et al. (2015). Soybean DREB1/CBF-type transcription factors function in heat and drought as well as cold stress-responsive gene expression. *Plant J.* 81, 505–518. doi: 10.1111/tpj.12746

Kobayashi, T., Kameya, T., and Ichihashi, S. (1993). Plant regeneration from protoplasts derived from callus of *Phalaenopsis*. *Plant Tissue Cult. Lett.* 10, 267–270. doi: 10.5511/plantbiotechnology1984.10.267

Kong, J. M., Goh, N. K., Chia, L. S., and Chia, T. F. (2003). Recent advances in traditional plant drugs and orchids. *Acta Pharmacol. Sin.* 24, 7–21.

Kosugi, S., and Ohashi, Y. (2002). E2F sites that can interact with E2F proteins cloned from rice are required for meristematic tissue-specific expression of rice and tobacco proliferating cell nuclear antigen promoters. *Plant J.* 29, 45–59. doi: 10.1046/j.1365-313x.2002.01196.x

Kull, T., and Arditti, J. (2002). *Orchid Biology Reviews and Perspectives.* London: Kluwer Academic Publishers. doi: 10.1007/978-94-017-2500-2

Lee, J. H., Jin, S., Kim, S. Y., Kim, W., and Ahn, J. H. (2017). A fast, efficient chromatin immunoprecipitation method for studying protein-DNA binding in *Arabidopsis* mesophyll protoplasts. *Plant Methods* 13:42. doi: 10.1186/s13007-017-0192-4

Lee, L. Y., Fang, M. J., Kuang, L. Y., and Gelvin, S. B. (2008). Vectors for multi-color bimolecular fluorescence complementation to investigate protein-protein interactions in living plant cells. *Plant Methods* 4:24. doi: 10.1186/1746-4811-4-24

Li, J. L., Liao, X. Z., Zhou, S. S., Liu, S., Jiang, L., and Wang, G. D. (2018). Efficient protoplast isolation and transient gene expression system for *Phalaenopsis* hybrid cultivar 'Ruili Beauty'. *In Vitro Cell. Dev. Biol. Plant* 54, 87–93. doi: 10.1007/s11627-017-9872-z

Li, Y., Zhang, D. Y., Ren, Q., Ye, F., Zhao, X., Daniels, G., et al. (2012). Regulation of a novel androgen receptor target gene, the cyclin B1 gene, through androgen-dependent E2F family member switching. *Mol. Cell. Biol.* 32, 2454–2466. doi: 10.1128/MCB.06663-11

Liao, C. Y., Smet, W., Brunoud, G., Yoshida, S., Vernoux, T., and Weijers, D. (2015). Reporters for sensitive and quantitative measurement of auxin response. *Nat. Methods* 12, 207–210. doi: 10.1038/nmeth.3279

Liau, C. H., You, S. J., Prasad, V., Hsiao, H. H., Lu, J. C., Yang, N. S., et al. (2003). *Agrobacterium tumefaciens*-mediated transformation of an *Oncidium* orchid. *Plant Cell Rep.* 21, 993–998. doi: 10.1007/s00299-003-0614-9

Lin, H. Y., Chen, J. C., Wei, M. J., Lien, Y. C., Li, H. H., Ko, S. S., et al. (2014). Genome-wide annotation, expression profiling, and protein interaction studies of the core cell-cycle genes in *Phalaenopsis* aphrodite. *Plant Mol. Biol.* 84, 203–226. doi: 10.1007/s11103-013-0128-y

Lin, Y. C., Li, W., Chen, H., Li, Q., Sun, Y. H., Shi, R., et al. (2014). A simple improved-throughput xylem protoplast system for studying wood formation. *Nat. Protoc.* 9, 2194–2205. doi: 10.1038/nprot.2014.147

Lu, H. C., Hsieh, M. H., Chen, C. E., Chen, H. H., Wang, H. I., and Yeh, H. H. (2012). A high-throughput virus-induced gene-silencing vector for screening transcription factors in virus-induced plant defense response in orchid. *Mol. Plant Microbe Interact.* 25, 738–746. doi: 10.1094/MPMI-10-11-0266

Lu, X., Kracher, B., Saur, I. M., Bauer, S., Ellwood, S. R., Wise, R., et al. (2016). Allelic barley MLA immune receptors recognize sequence-unrelated avirulence effectors of the powdery mildew pathogen. *Proc. Natl. Acad. Sci. U.S.A.* 113, E6486–E6495. doi: 10.1073/pnas.1612947113

Lung, S. C., Yanagisawa, M., and Chuong, S. D. (2011). Protoplast isolation and transient gene expression in the single-cell C4 species, *Bienertia sinuspersici*. *Plant Cell Rep.* 30, 473–484. doi: 10.1007/s00299-010-0953-2

Magyar, Z., De Veylder, L., Atanassova, A., Bakó, L., Inzé, D., and Bögre, L. (2005). The role of the *Arabidopsis* E2FB transcription factor in regulating auxin-dependent cell division. *Plant Cell* 17, 2527–2541. doi: 10.1105/tpc.105.033761

Martinho, C., Confraria, A., Elias, C. A., Crozet, P., Rubio-Somoza, I., Weigel, D., et al. (2015). Dissection of miRNA pathways using *Arabidopsis* mesophyll protoplasts. *Mol. Plant* 8, 261–275. doi: 10.1016/j.molp.2014.10.003

Masani, M. Y., Noll, G. A., Parveez, G. K., Sambanthamurthi, R., and Prufer, D. (2014). Efficient transformation of oil palm protoplasts by PEG-mediated transfection and DNA microinjection. *PLoS One* 9:e96831. doi: 10.1371/journal.pone.0096831

Mazarei, M., Al-Ahmad, H., Rudis, M. R., and Stewart, C. N. Jr. (2008). Protoplast isolation and transient gene expression in switchgrass, *Panicum virgatum* L. *Biotechnol. J.* 3, 354–359. doi: 10.1002/biot.200700189

Morgan, D. O. (2007). *The Cell Cycle: Principles of Control.* London: New Science Press Ltd.

Muchero, W., Guo, J., DiFazio, S. P., Chen, J. G., Ranjan, P., Slavov, G. T., et al. (2015). High-resolution genetic mapping of allelic variants associated with cell wall chemistry in *Populus*. *BMC Genomics* 16:24. doi: 10.1186/s12864-015-1215-z

Müller, B., and Sheen, J. (2008). Cytokinin and auxin interaction in root stem-cell specification during early embryogenesis. *Nature* 453, 1094–1097. doi: 10.1038/nature06943

Nanjareddy, K., Arthikala, M. K., Blanco, L., Arellano, E. S., and Lara, M. (2016). Protoplast isolation, transient transformation of leaf mesophyll protoplasts and improved *Agrobacterium*-mediated leaf disc infiltration of *Phaseolus vulgaris*: tools for rapid gene expression analysis. *BMC Biotechnol.* 16:53. doi: 10.1186/s12896-016-0283-8

Nelson, B. K., Cai, X., and Nebenfuhr, A. (2007). A multicolored set of in vivo organelle markers for co-localization studies in *Arabidopsis* and other plants. *Plant J.* 51, 1126–1136. doi: 10.1111/j.1365-313X.2007.03212.x

Novak, D. S., Luna, L. J., and Gamage, R. N. (2014). Role of auxin in orchid development. *Plant Signal. Behav.* 9:e972277. doi: 10.4161/psb.32169

Novak, S. D., and Whitehouse, G. A. (2013). Auxin regulates first leaf development and promotes the formation of protocorm trichomes and rhizome-like structures in developing seedlings of *Spathoglottis plicata* (Orchidaceae). *AoB Plants* 5:pls053. doi: 10.1093/aobpla/pls053

Nyman, M., and Wallin, A. (1992). Transient gene expression in strawberry (*Fragaria x ananassa* Duch.) protoplasts and the recovery of transgenic plants. *Plant Cell Rep.* 11, 105–108. doi: 10.1007/BF00235264

Ohshima, M., and Toyama, S. (1989). Studies on culture of cells and tissues of crop plants: 1. Survey on enzymatic isolation and culture of rice leaf sheath protoplasts. *Jpn. J. Crop Sci.* 58, 103–110. doi: 10.1626/jcs.58.103

Pacini, E., and Hesse, M. (2002). Types of pollen dispersal units in orchids, and their consequences for germination and fertilization. *Ann. Bot.* 89, 653–664. doi: 10.1039/aob/mcf138

Ramirez-Parra, E., Frundt, C., and Gutierrez, C. (2003). A genome-wide identification of E2F-regulated genes in *Arabidopsis*. *Plant J.* 33, 801–811. doi: 10.1046/j.1365-313X.2003.01662.x

Rao, X., Krom, N., Tang, Y., Widiez, T., Havkin-Frenkel, D., Belanger, F. C., et al. (2014). A deep transcriptomic analysis of pod development in the vanilla orchid (*Vanilla planifolia*). *BMC Genomics* 15:964. doi: 10.1186/1471-2164-15-964

Rasmussen, H. N. (2002). Recent developments in the study of orchid mycorrhiza. *Plant Soil* 244, 149–163. doi: 10.1023/A:1020246715436

Ren, B., Cam, H., Takahashi, Y., Volkert, T., Terragni, J., Young, R. A., et al. (2002). E2F integrates cell cycle progression with DNA repair, replication, and G(2)/M checkpoints. *Genes Dev.* 16, 245–256. doi: 10.1101/gad.949802

Rossignol, P., Stevens, R., Perennes, C., Jasinski, S., Cella, R., Tremousaygue, D., et al. (2002). AtE2F-a and AtDP-a, members of the E2F family of transcription factors, induce *Arabidopsis* leaf cells to re-enter S phase. *Mol. Genet. Genomics* 266, 995–1003. doi: 10.1007/s00438-001-0624-7

Sheen, J. (2001). Signal transduction in maize and *Arabidopsis* mesophyll protoplasts. *Plant Physiol.* 127, 1466–1475. doi: 10.1104/pp.010820

Shen, Y., Meng, D., McGrouther, K., Zhang, J., and Cheng, L. (2017). Efficient isolation of *Magnolia* protoplasts and the application to subcellular localization of *MdeHSF1*. *Plant Methods* 13:44. doi: 10.1186/s13007-017-0193-3

Shrestha, B. R., Tokuhara, K., and Mii, M. (2007). Plant regeneration from cell suspension-derived protoplasts of *Phalaenopsis*. *Plant Cell Rep.* 26, 719–725. doi: 10.1007/s00299-006-0286-3

Sozzani, R., Maggio, C., Varotto, S., Canova, S., Bergounioux, C., Albani, D., et al. (2006). Interplay between *Arabidopsis* activating factors E2Fb and E2Fa in cell cycle progression and development. *Plant Physiol.* 140, 1355–1366. doi: 10.1104/pp.106.077990

Thevenin, J., Xu, W., Vaisman, L., Lepiniec, L., Dubreucq, B., and Dubos, C. (2016). The *Physcomitrella patens* system for transient gene expression assays. *Methods Mol. Biol.* 1482, 151–161. doi: 10.1007/978-1-4939-6396-6_10

Tsavkelova, E. A., Cherdyntseva, T. A., Botina, S. G., and Netrusov, A. I. (2007). Bacteria associated with orchid roots and microbial production of auxin. *Microbiol. Res.* 162, 69–76. doi: 10.1016/j.micres.2006.07.014

Van Leene, J., Boruc, J., De Jaeger, G., Russinova, E., and De Veylder, L. (2011). A kaleidoscopic view of the *Arabidopsis* core cell cycle interactome. *Trends Plant Sci.* 16, 141–150. doi: 10.1016/j.tplants.2010.12.004

Vandepoele, K., Vlieghe, K., Florquin, K., Hennig, L., Beemster, G. T., Gruissem, W., et al. (2005). Genome-wide identification of potential plant E2F target genes. *Plant Physiol.* 139, 316–328. doi: 10.1104/pp.105.066290

Wang, H., Nicolay, B. N., Chick, J. M., Gao, X., Geng, Y., Ren, H., et al. (2017). The metabolic function of cyclin D3-CDK6 kinase in cancer cell survival. *Nature* 546, 426–430. doi: 10.1038/nature22797

Waterman, R. J., and Bidartondo, M. I. (2008). Deception above, deception below: linking pollination and mycorrhizal biology of orchids. *J. Exp. Bot.* 59, 1085–1096. doi: 10.1093/jxb/erm366

Wehner, N., Hartmann, L., Ehlert, A., Bottner, S., Onate-Sanchez, L., and Droge-Laser, W. (2011). High-throughput protoplast transactivation (PTA) system for the analysis of *Arabidopsis* transcription factor function. *Plant J.* 68, 560–569. doi: 10.1111/j.1365-313X.2011.04704.x

Wehner, N., Herfert, J., Droge-Laser, W., and Weiste, C. (2017). High-throughput protoplast trans-activation (PTA) screening to define transcription factors in auxin-mediated gene regulation. *Methods Mol. Biol.* 1569, 187–202. doi: 10.1007/978-1-4939-6831-2_16

Wu, F. H., Shen, S. C., Lee, L. Y., Lee, S. H., Chan, M. T., and Lin, C. S. (2009). Tape-*Arabidopsis* Sandwich - a simpler *Arabidopsis* protoplast isolation method. *Plant Methods* 5:16. doi: 10.1186/1746-4811-5-16

Yamaguchi, M., Hayashi, Y., and Matsukage, A. (1995). Essential role of E2F recognition sites in regulation of the proliferating cell nuclear antigen gene promoter during *Drosophila* development. *J. Biol. Chem.* 270, 25159–25165. doi: 10.1074/jbc.270.42.25159

Yoo, S. D., Cho, Y. H., and Sheen, J. (2007). *Arabidopsis* mesophyll protoplasts: a versatile cell system for transient gene expression analysis. *Nat. Protoc.* 2, 1565–1572. doi: 10.1038/nprot.2007.199

Yu, H., Yang, S. H., and Goh, C. J. (2001). *Agrobacterium*-mediated transformation of a *Dendrobium* orchid with the class 1 *knox* gene *DOH1*. *Plant Cell Rep.* 20, 301–305. doi: 10.1007/s002990100334

Zhang, G. Q., Liu, K. W., Li, Z., Lohaus, R., Hsiao, Y. Y., Niu, S. C., et al. (2017). The *Apostasia* genome and the evolution of orchids. *Nature* 549, 379–383. doi: 10.1038/nature23897

Zhang, G. Q., Xu, Q., Bian, C., Tsai, W. C., Yeh, C. M., Liu, K. W., et al. (2016). The *Dendrobium catenatum* Lindl. genome sequence provides insights into polysaccharide synthase, floral development and adaptive evolution. *Sci. Rep.* 6:19029. doi: 10.1038/srep19029

Zhang, Y., Lee, C. W., Wehner, N., Imdahl, F., Svetlana, V., Weiste, C., et al. (2015). Regulation of oncogene expression in T-DNA-transformed host plant cells. *PLoS Pathog.* 11:e1004620. doi: 10.1371/journal.ppat.1004620

**Conflict of Interest Statement:** The authors declare that the research was conducted in the absence of any commercial or financial relationships that could be construed as a potential conflict of interest.

# Advantages of publishing in Frontiers

**OPEN ACCESS**
Articles are free to read for greatest visibility and readership

**FAST PUBLICATION**
Around 90 days from submission to decision

**HIGH QUALITY PEER-REVIEW**
Rigorous, collaborative, and constructive peer-review

**TRANSPARENT PEER-REVIEW**
Editors and reviewers acknowledged by name on published articles

**Frontiers**
Avenue du Tribunal-Fédéral 34
1005 Lausanne | Switzerland

**Visit us:** www.frontiersin.org
**Contact us:** info@frontiersin.org | +41 21 510 17 00

**REPRODUCIBILITY OF RESEARCH**
Support open data and methods to enhance research reproducibility

**DIGITAL PUBLISHING**
Articles designed for optimal readership across devices

**FOLLOW US**
@frontiersin

**IMPACT METRICS**
Advanced article metrics track visibility across digital media

**EXTENSIVE PROMOTION**
Marketing and promotion of impactful research

**LOOP RESEARCH NETWORK**
Our network increases your article's readership